



In vitro Modelling of High-risk ALL Fusions Uncovers Genomic Alterations and Non-canonical Signalling Pathways as a Mode of TKI-resistance – Implications for Targeted Therapy

Kartini Asari

Leukaemia Research Laboratory
Cancer Theme
South Australian Health & Medical Research Institute
SAHMRI

&

Adelaide Medical School
Faculty of Health & Medical Sciences
The University of Adelaide
Adelaide, South Australia

A thesis submitted to The University of Adelaide
in candidature for the degree of Doctor of Philosophy 2018

THIS PAGE INTENTIONALLY LEFT BLANK.

ACKNOWLEDGEMENTS

The hardest part of being a young scientist is the transition between having a passion for technicality as a wet-lab RA, into the development of philosophical ideas that channel towards the daily discoveries. This PhD journey would not have been possible without the encouragement, passion, faith, contribution and support of so many people.

I would like to thank my supervisors Professor Deborah White, Dr. Sue Heatley and Dr. Tamara Leclercq for their mentorship, expertise and patience. Deb, thank you for teaching me the ropes of developing high-level research ideas – I have learnt so much in our field through your experience. I cannot thank you enough for this PhD opportunity – it has added so much more meaning into my life. Sue, thank you very much for your constant moral support, especially when times were tough. You made me realise that I never walk alone on this journey. Tam, thank you for being so supportive of my studies even though you were away on maternity leave while the bulk of my experiments occurred (and returning just in time as I was thesis-writing!). You are one of the most passionate people around – thank you for looking out for me and liaising with the administrative matters when they arose.

Sincere thanks to Professor Timothy Hughes for all the scientific insights during our leukaemia laboratory meetings. Tim, seeing your passion for science and medicine is highly inspiring; I'm constantly reminded of how our little discoveries can potentially add up to bigger ideas one day.

Thank you also to our collaborators both overseas and locally, for the scientific discussions, resources and development of ideas. I'd like to acknowledge Professor Charles Mullighan and Dr. Kathryn Roberts, whose provision of fusion constructs were essential for this thesis. Thank you, Dr. Chung Kok (bioinformatics in **Chapter 3** & teaching me how to code in R), Dr. Stephen Fitter (for teaching me the ropes of molecular cloning) and Professor Andrew Zannettino (for providing the viral backbones). Dr. Sriganesh Srihari (CHAT network analysis in **Chapter 6** and network biology pathway discussions), Dr. Max Moldovan, A/Prof. David Lynn (on using InnateDB & Cytoscape), Dr. Kelly Quek and Dr. Jiyuan An (for 1st pass mRNA-seq analysis), your guidances were truly appreciated. I would also like to acknowledge the support of the ALL team at SAHMRI (Dr. Barbara McClure, Dr.

David Yeung, Dr. Eva Nievergall, Dr. Teresa Sadras, Dr. Laura Eadie and Kate Galbraith), the ACRF flow and laser-scanning cytometry facility (Dr. Randall Grose) and David Gunn genomics core facility (Mark Van Der Hoek). Folks, your technical expertise are remarkable. Heartfelt thanks to A/Prof Charles Chuah, for inspiring my early days in leukaemia research whilst in Singapore.

I am really grateful to have known so many great people throughout the course of my PhD – sincere appreciation goes to all members of the Leukaemia Research Laboratory, and people I have met from the Cancer Theme, SAHMRI and the Adelaide Medical School. Each and every one of you has made my PhD journey more vibrant – I couldn't have asked for a better scientific environment. Special mentions to Jenny, Stephanie, Phuong, Ilaria, Jarrad and most importantly, Verity Saunders. Thank you also to the funding bodies for providing me with the support in undertaking this research.

To my lab buddies Liu, Ben, Kate, Heather and Nadia, thanks heaps for the friendship throughout this journey! I have been so lucky to know each of you – thank you for making this PhD experience a lot more entertaining. Heartfelt thanks to Sissy, for being there for me and the great conversations about the essence of life and philosophy. Thank you so much Melody, for the compassionate listening ear and constantly reminding me of how there's light at the end of the tunnel. You have given me the strength to keep going, even though we're living on opposite sides of the globe! Thank you, Heidi, Catherine and Andrea, for being such great inspirations – I am so proud of how far we've come. To Trev, Nate, Elyse Bell, Susan & Lisa Christo – thank you for inspiring me with your diverse walks of life.

This phase of my life would not have been possible if it wasn't for the understanding, love, patience and support of my beloved family. Mami (Hadijah Adnan) & Papa (Asari Rafie), thank you so much for the upbringing, love and guidance throughout my childhood. Your hard work and sacrifices have moulded me into who I am today – my life would have been very different otherwise. To my siblings, Siti Mariam (+ Roy Iryan), Karmila (+ Helmi) and Riyanto, thank you for all the memorable times we shared and for being there for me always. Though life may take us through different journeys, I will always cherish the moments we spent together. Thank you for all your encouragement, love, patience and open-mindedness whenever life throws surprises our way. I love all of you heaps, always.

Major appreciation to my grandpa (Yai – Hj. Adnan Md Yatim) and grandma (Nenek – Almarhumah Hjh. Tumyah Sarbini) for all the amazing doa's, as well as my late paternal grandparents (Almarhum Rafie Hj. Salleh & Almarhumah Saimah Hj. Ali) for being great role models. Thank you to my extended family, especially those who truly believed in me. *Matur nuwun* & *khàawp-khun mâak ná khâ*.

None of this would have been possible if it wasn't for the support of *il mio amore*, Dr. Gerard. Thank you for often offering to help with my PhD, being equally happy to accept my refusals, and always allowing me to be the woman that I am. You have been a great mentor and my pillar of strength. I'll always love you and shall embrace wherever life takes us next. I'm truly blessed to have known your lovely family – *grazie mille* for all the love, understanding of my thesis-writing phase and accommodating my dietary preferences (especially when I'm least expecting), it really touches my heart.

Many thanks to you, the reader of this thesis. Most importantly and with gratitude, I'd like to thank the childhood leukaemia patients and their parents – this research is dedicated to you and I hope this work will bring us closer towards a world free of cancer.

THIS PAGE INTENTIONALLY LEFT BLANK.

DECLARATION

I certify that this work contains no material which has been accepted for the award of any other degree or diploma in my name, in any university or other tertiary institution and, to the best of my knowledge and belief, contains no material previously published or written by another person, except where due reference has been made in the text. In addition, I certify that no part of this work will, in the future, be used in a submission in my name, for any other degree or diploma in any university or other tertiary institution without the prior approval of the University of Adelaide and where applicable, any partner institution responsible for the joint-award of this degree.

I give permission for the digital version of my thesis to be made available on the web, via the University's digital research repository, the Library Search and also through web search engines, unless permission has been granted by the University to restrict access for a period of time.

Kartini Asari

January 2018

CONFERENCE ABSTRACTS & PRESENTATIONS

Asari K, Sadras T, Leclercq T, Srihari S, Fitter S, An J, Zannettino A, Lynn D, Hughes T, Kok CH, Heatley S, White D. *In vitro* Modelling of TKI Therapy in Ph-like ALL Reveals Novel Genomic Alterations Associated with Treatment Resistance. *Australian and New Zealand Children's Haematology/Oncology Group (ANZCHOG) Annual Scientific Meeting.* Hilton Hotel Adelaide, June 2017. **Oral Presentation**, Medical Stream.

Asari K, Sadras T, Leclercq T, Srihari S, Fitter S, An J, Zannettino A, Lynn D, Hughes T, Kok CH, Heatley S, White D. *In vitro* Modelling of TKI Therapy in Ph-like ALL Reveals Novel Genomic Alterations Associated with Treatment Resistance. *Australian Society for Medical Research (ASMR) SA Scientific Meeting*. Adelaide Convention Centre, June 2017. **Oral Presentation**, Cancer Session.

Asari K, Heatley S, Sadras T, Leclercq T, Fitter S, Kok CH, Zannettino A, Hughes T, White D. *In vitro* Modeling of Ph-like ALL Fusions Identifies Novel Kinase-domain Mutations as Mode of TKI-Resistance - Implications for Targeted Therapy. *American Society of Hematology Annual Meeting.* San Diego Convention Centre, CA USA, December 2016. **Poster Presentation**.

Asari K, Heatley S, Leclercq T, Fitter S, Zannettino A, Hughes T, White D. Point Mutations in TKI-resistant Ph-like Acute Lymphoblastic Leukaemia via *In Vitro* Modelling: - Implications for Targeted Therapeutic Approaches. *Haematology Association Australia (HAA) Annual Scientific Meeting.* Melbourne Convention Centre, November 2016. **Oral Presentation**, Combined HSANZ / ASTH Presidential Symposium.

Asari K, Heatley S, Sadras T, Leclercq T, Fitter S, Kok CH, Zannettino A, Hughes T, White D. Point Mutations in TKI-resistant Ph-like Acute Lymphoblastic Leukaemia via *In Vitro* Modelling: - Implications for Targeted Therapeutic Approaches. *EMBL Australia Postgraduate Symposium.* SAHMRI Adelaide, November 2016. **Oral Presentation**, Cancer Session.

Asari K, Heatley SL, Sadras T, Leclercq T, Fitter S, Kok CH, Zannettino A, Hughes TP, White DL. *In vitro* Modelling of Ph-like ALL Fusions Identifies Novel Kinase-domain Mutations as Mode of TKI-Resistance - Implications for Targeted Therapy. *10th Florey International Postgraduate Research Conference, Faculty of Health & Medical Sciences, The University of Adelaide*. National Wine Centre of Australia, September 2016. **Poster Presentation**. Awarded the Adelaide Medical School Prize.

Asari K, Heatley S, Leclercq T, Grose R, Fitter S, Kok CH, Zannettino A, Hughes T, White D. Investigating Modes of Therapeutic Resistance via *In Vitro* Modelling of TKI-resistant High-Risk Philadelphia-chromosome-positive and Philadelphia-chromosome-like Acute Lymphoblastic Leukaemia. *Australian Society for Medical Research (ASMR) SA Scientific Meeting*. Adelaide Convention Centre, June 2016. **Poster Presentation**.

Asari K, Heatley S, Leclercq T, Fitter S, Zannettino A, Hughes T, White D. *In vitro* Modelling of Therapeutic Resistance to Elucidate Mechanisms of TKI-Resistant High-Risk ALL. *New Directions in Leukaemia Research (NDLR) Biennial Meeting*, Noosa QLD March 2016. **Poster Presentation**.

Asari K, Heatley S, Leclercq T, Fitter S, Zannettino A, Hughes T, White D. *In-vitro* Modelling of Therapeutic Resistance to Elucidate Mechanisms of TKI-Resistant High-Risk ALL. *Haematology Association Australia (HAA) Annual Scientific Meeting.* Adelaide Convention Centre, October 2015. **Oral Presentation**.

Asari K, Heatley S, Leclercq T, Fitter S, Zannettino A, Hughes T, White D. *In-vitro* Modelling of Therapeutic Resistance to Elucidate Mechanisms of TKI-Resistant High-Risk ALL. *Florey International Postgraduate Research Conference, Faculty of Health Sciences, The University of Adelaide*. National Wine Centre of Australia, September 2015. **Poster Presentation**. Shortlisted as a Finalist for the Adelaide Research & Innovation Pty Ltd (ARI) Prize. Awarded the School of Medicine Prize.

Asari K, Heatley S, Leclercq T, Fitter S, Zannettino A, Hughes T, White D. *In-vitro* Modelling of Therapeutic Resistance to Elucidate Mechanisms of TKI-Resistant High-Risk ALL. *SAHMRI Research Showcase.* SAHMRI Adelaide, September 2015. **Poster Presentation**.

Asari K, Heatley S, Leclercq T, Fitter S, Zannettino A, Hughes T, White D. *In-vitro* Modelling of Therapeutic Resistance to Elucidate Mechanisms of TKI-Resistant High-Risk ALL. *Blood Club Translational Research Meeting.* SAHMRI Adelaide, June 2015. **Oral Presentation**.

Asari K, Heatley S, Leclercq T, Grose R, Fitter S, Zannettino A, Hughes T, White D. Investigating Drug Sensitivity and Modes of Therapeutic Resistance in High-Risk Philadelphia-chromosome-like Acute Lymphoblastic Leukaemia (Ph-Like ALL). *Australian Society for Medical Research (ASMR) SA Scientific Meeting*. National Wine Centre of Australia, June 2015. **Oral Presentation**, Cancer Session.

Asari K, Heatley S, Nievergall A, Dang P, Sadras T, Mullighan C, Hughes T, White D. Investigating Modes of Therapeutic Resistance in High-Risk Ph-like ALL. *Florey International Postgraduate Research Conference, Faculty of Health Sciences, The University of Adelaide*. National Wine Centre of Australia, September 2014. **Poster Presentation**.

ACHIEVEMENTS, AWARDS & SCHOLARSHIPS

Beat Cancer Project Travel Grant 2016

Support for early-career researchers to attend an international conference in the field of cancer research. Awarded on the basis of the submitted abstract entitled: "*In vitro* Modeling of Ph-like ALL Fusions Identifies Novel Kinase-domain Mutations as Mode of TKI-Resistance - Implications for Targeted Therapy", for attendance of the 58th American Society of Haematology Meeting (ASH), San Diego CA USA, December 2016. Value: $1500

Presidential Symposium, HAA Melbourne 2016

For the abstract entitled "Point Mutations in TKI-resistant Ph-like Acute Lymphoblastic Leukaemia via In Vitro Modelling: - Implications for Targeted Therapeutic Approaches". As part of the top four abstracts selected based on quality and merit of research, invited for an oral presentation in the combined HSANZ / ASTH Presidential Symposium session at the Haematology Association Australia (HAA) Annual Scientific Meeting, Melbourne 2016.

Beat Cancer Project Top-up Scholarship 2016

Top-up scholarship from the Cancer Council, awarded to applicants in receipt of a PhD scholarship and based on merit of research. Value: $5000

President of the Health Sciences Postgraduate Association (HeSPA) 2016/17

As part of the HeSPA committee, a voluntary postgraduate student network initiated by the Higher Degree in Research (HDR) committee. The HeSPA committee serves as a panel for planning & strategising of career-development activities (i.e. seminars & workshops) for all postgraduate students within the Faculty of Health Sciences, The University of Adelaide.

Adelaide Medical School Prize 2016

For poster presentation of the abstract entitled "*In vitro* Modelling of Ph-like ALL Fusions Identifies Novel Kinase-domain Mutations as Mode of TKI-Resistance - Implications for Targeted Therapy". *10th Florey International Postgraduate Research Conference, Faculty of Health & Medical Sciences, The University of Adelaide*. National Wine Centre of Australia, September 2016. Value: $200

Statewide Super Research Scholarship, SAHMRI 2016

Support for outstanding early career health and medical research students to conduct ground-breaking nationally and internationally competitive research in South Australia. Competitive grant awarded based on merit and research proposal. Value: $10,000

School of Medicine Prize 2015

For poster presentation of the abstract entitled "*In-vitro* Modelling of Therapeutic Resistance to Elucidate Mechanisms of TKI-Resistant High-Risk ALL". *Florey International Postgraduate Research Conference, Faculty of Health & Medical Sciences, The University of Adelaide*. National Wine Centre of Australia, September 2015. Value: $200

Finalist for the Adelaide Research & Innovation Pty Ltd (ARI) Prize 2015

Shortlisted as a finalist for the Adelaide Research & Innovation Pty Ltd (ARI) prize for the project with the most commercial potentiell, based on the abstract entitled "In-vitro Modelling of Therapeutic Resistance to Elucidate Mechanisms of TKI-Resistant High-Risk ALL". Florey International Postgraduate Research Conference, Faculty of Health & Medical Sciences, The University of Adelaide. National Wine Centre of Australia, September 2015

Melissa White Memorial PhD Scholarship, The University of Adelaide 2014-2017

Support for the educational and professional development of researchers and other professionals undertaking a PhD. The award is to support research in South Australia into the causes, treatment and care of people with leukaemia and related blood disorders, and is awarded on the merits of the applicant and project proposal. Value: Annual living allowance & study fees as per the Australian Postgraduate Award guidelines, The University of Adelaide.

TABLE OF CONTENTS

ACKNOWLEDGEMENTS ..... **III**
DECLARATION ..... **VII**
CONFERENCE ABSTRACTS & PRESENTATIONS ..... **VIII**
ACHIEVEMENTS, AWARDS & SCHOLARSHIPS ..... **X**
TABLE OF CONTENTS ..... **XII**
LIST OF FIGURES, TABLES & APPENDICES ..... **XVIII**
ABBREVIATIONS ..... **XXIII**
ABSTRACT ..... **XXVIII**
CHAPTER 1 – INTRODUCTION **1**
1.1. ACUTE LYMPHOBLASTIC LEUKAEMIA 2
1.1.1. Clinical Features of ALL *2*
1.1.2. Genomic Alterations in Childhood ALL *3*
1.1.3. Ph+ and Ph-like High-risk ALL *8*
1.1.4. Ph-like or BCR-ABL1-like ALL *8*
1.2. AN OVERARCHING PERSPECTIVE OF PH-LIKE ALL 10
1.2.1. Alterations Affecting the Jak Signalling Pathway *10*
1.2.2. Alterations Involving Abl-class Signalling Pathways *14*
1.2.3. Alterations Involving Other Signalling Mechanisms *18*
1.2.4. Summary of Alterations in Ph-like ALL *20*
1.3. THERAPEUTIC OPTIONS IN HIGH-RISK ALL 22
1.3.1. Chemotherapy in Acute Lymphoblastic Leukaemia *22*
1.3.2. Use of Tyrosine Kinase Inhibitor (TKI) as Targeted Therapy *24*
1.3.3. Anecdotal Use of TKI in Ph-like ALL *28*
1.4. TKI-RESISTANCE 30
1.4.1. Mechanisms of TKI-resistance in Abl kinase *30*
1.4.2. Mechanisms of TKI-resistance in Jak kinase *38*
1.4.3. Case of TKI relapse in Ph-like ALL *38*
1.5. CONCLUDING REMARKS 40
1.6. RESEARCH HYPOTHESIS 42
1.7. RESEARCH AIMS & OBJECTIVES 42
CHAPTER 2 – MATERIALS & METHODS **43**
2.1. COMMONLY USED REAGENTS & BUFFERS 44
2.2. CELL CULTURE MEDIA & SOLUTIONS 52
2.3. INHIBITORS 54
2.3.1. Imatinib (STI-571) *54*

2.3.2. Dasatinib (BMS-354825) *54*
2.3.3. Ponatinib (AP24534) *54*
2.3.4. Ruxolitinib (INCB018424) *54*
2.3.5. BMS-911543 ..... *54*
2.4. COMMON BUFFERS & SOLUTIONS FOR PROTEIN ASSAYS 55
2.4.1. 1x Phosphate-buffered saline (1x PBS) *55*
2.4.2. 1x Tris-buffered saline (1x TBS) *55*
2.4.3. 1x Tris-buffered saline + 0.1% Tween-20 (1x TBST) *55*
2.4.4. 1x SDS-PAGE gel running buffer *55*
2.4.5. 1x Western blotting transfer buffer *55*
2.4.6. 1x Laemmli's buffer for cell lysis & CrkL protein stabilisation *56*
2.4.7. 1% Triton™ X-100 cell lysis buffer *56*
2.4.8. 10% APS (10% ammonium persulfate) *56*
2.4.9. Buffer A (for use in 14% resolving gel) *56*
2.4.10. Buffer B (for use in 5% stacking gel) *56*
2.4.11. Polyacrylamide gel components specific for Hoefer SE260 system *57*
2.4.12. Ponceau S staining solution *57*
2.4.13. PVDF membrane blocking buffer (5% BSA) *57*
2.5. COMMON BUFFERS & SOLUTIONS FOR FLOW CYTOMETRY ANALYSIS 58
2.5.1. 1x Binding buffer for 'Annexin-V / 7-AAD (7-AminoActinomycin-D)' assay *58*
2.5.2. 1x Binding buffer for phospho-flow assay *58*
2.5.3. Methanol permeabilisation solution for phospho-flow assay *58*
2.5.4. Flow cytometry fixative (FACS fix) *58*
2.6. MOLECULAR BIOLOGY REAGENTS 59
2.6.1. dNTP set (N=A, T, C, G) *59*
2.6.2. LB Broth *59*
2.6.3. LB Agar *59*
2.6.4. 1x Tris-acetate EDTA (1x TAE) buffer *59*
2.6.5. 1% Agarose gel for DNA electrophoresis *59*
2.7. GENERAL CELL CULTURE TECHNIQUES 60
2.7.1. Subculturing of cell lines *60*
2.7.2. Cryopreservation of cell lines *61*
2.7.3. Cell washout protocol prior to drug treatment assays *61*
2.8. ANNEXIN-V-PE/7-AAD EXCLUSION ASSAY 62
2.8.1. Drug treatment of cells for Annexin-V-PE/7-AAD cell-death assay *62*
2.8.2. Annexin-V-PE/7-AAD exclusion staining protocol *62*
2.9. PHOSPHOFLOW ASSAY 64
2.9.1. Drug treatment of cells for phosphoflow assay *64*

2.9.2. Preparation of cells for phosphoflow assay 64
2.10. PROTEIN ELECTROPHORESIS 66
2.10.1. Drug treatment of cells 66
2.10.2. Preparation of protein lysates 66
2.10.3. Protein assay 66
2.10.4. Preparation of protein samples for SDS-PAGE gel electrophoresis 67
2.10.5. SDS-PAGE protein electrophoresis 67
2.10.6. Western blotting 67
2.10.7. Stripping of PVDF membranes for re-probing of other proteins of interest 68
2.10.8. Densitometry analysis 68
2.11. CRKL (SURROGATE FOR BCR-ABL KINASE ACTIVITY) ASSAY 70
2.11.1. TKI-treatment of cells for CrkL analysis 70
2.11.2. Preparation of protein lysates for SDS-PAGE gel electrophoresis 70
2.11.3. Resolution of CrkL protein via SDS-PAGE gel electrophoresis 70
2.11.4. Western transfer and blotting of CrkL protein 71
2.11.5. p-CrkL IC_{50} 71
2.12. GENERATION OF BA/F3 PH-LIKE ALL STABLE CELL LINES 72
2.12.1. Transformation of competent cells for amplification of Ph-like ALL fusion gene plasmids 74
2.12.2. Long-term storage of transformed bacterial cells 75
2.12.3. Extraction and purification of plasmid DNA 75
2.12.4. Molecular cloning of Ph-like ALL fusion genes 75
2.12.5. Generation of viral particles via transfection of HEK-293T cells 80
2.12.6. Retroviral transduction of Ba/F3 parental wildtype pro-B cells 80
2.12.7. Confirmation of incorporation of Ph-like ALL fusion constructs in Ba/F3 cells 81
2.13. ANALYSIS OF TKI-SENSITIVITY PRIOR TO GENERATION OF TKI-RESISTANCE 81
2.14. GENERATION OF TKI-RESISTANT CELLS VIA DOSE-ESCALATION OF TKI 82
2.15. GENOMIC STUDIES 83
2.15.1. RNA extraction of TRIzol® samples 83
2.15.2. cDNA synthesis 83
2.15.3. DNA extraction by phenol-chloroform 84
2.15.4. Polymerase chain reaction (PCR) and Sanger sequencing 85
2.15.5. Long PCR for kinase-domain sequencing 86
2.15.6. Breakpoint sequencing of Ph-like ALL constructs 88
2.15.7. Generic PCR with AmpliTaq Gold™ enzyme 89
2.15.8. Transcriptomic sequencing (mRNA-seq) 90
2.15.9. Real-time Quantitative PCR (RQ-PCR) 91
2.15.10. Comprehensive RQ-PCR Primer List 92

2.16. BIOINFORMATICS ANALYSIS 95
2.16.1. Differential expression analysis of SUP-B15 Ph+ ALL lines 95
2.16.2. Differential expression analysis of Ba/F3 Ph-like ALL lines 95
2.16.3. Hierarchical clustering, heatmap and volcano plots via R studio 95
2.16.4. Pathway analysis via InnateDB 96
2.16.5. Network analysis via Cytoscape 96
2.17. STATISTICAL ANALYSIS 96

CHAPTER 3 – TKI-RESISTANCE IN IMMORTALISED SUP-B15 PH+ ALL CELLS IS MEDIATED BY A BCR-ABL INDEPENDENT MECHANISM 99
3.1. INTRODUCTION 100
3.2. APPROACH 102
3.3. RESULTS 104
3.3.1. Investigation of p-CrkL activity in low-dose TKI-resistant SUP-B15 cell lines 104
3.3.2. SUP-B15 30 nM dasatinib/ponatinib-resistant SUP-B15 cells demonstrate no increase in p-Bcr-Abl or p-CrkL IC_{50}, despite abrogation of cleaved PARP cell death marker expression 112
3.3.3. Analysis of Erk phosphorylation via western blotting indicates an increased phosphorylation in the 50 nM intermediate TKI-resistant cell lines 122
3.3.4. Highly-resistant SUP-B15 cell lines do not demonstrate increased p-CrkL IC_{50} 126
3.3.5. mRNA sequencing data suggests increased expression of BCR-ABL1 independent signalling, in TKI-resistant SUP-B15 cell lines 130
3.3.6. Identification of RAS mutations in the TKI-resistant SUP-B15 cell lines 142
3.4. DISCUSSION 150

CHAPTER 4 – TKI-RESISTANCE IN *RANBP2-ABL1* CELL LINES IS MEDIATED BY CLINICALLY-RELEVANT POINT MUTATIONS AND NON-CANONICAL SIGNALLING 163
4.1. INTRODUCTION 164
4.2. APPROACH 166
4.3. RESULTS 167
4.3.1. Ba/F3 cells transduced with RANBP2-ABL1 Ph-like ALL fusion gene demonstrates kinase-independent survival capacity 167
4.3.2. Ba/F3 RANBP2-ABL1 cells are sensitive to clinically-available TKIs 188
4.3.3. Imatinib and dasatinib-resistant Ba/F3 RANBP2-ABL1 cells are more tolerant to TKI compared to control lines 198
4.3.4. Ba/F3 RANBP2-ABL1 cells develop resistance to imatinib and dasatinib through the acquirement of the clinically-significant ABL1-T315I mutation (targetable by ponatinib) 207

4.3.5. Secondary dose-escalation of Ba/F3 RANBP2-ABL1 imatinib and dasatinib-resistant ABL1-T315I cells in ponatinib results in highly-resistant line 212
4.3.6. Secondary dose-escalation of Ba/F3 RANBP2-ABL1 imatinib and dasatinib-resistant ABL1-T315I cells leads to the acquirement of compound mutations..... 224
4.3.7. Ba/F3 RANBP2-ABL1 cells dose-escalated to ponatinib as first-line therapy are cross-resistant to first and second generation Abl TKIs 228
4.3.8. Clinically-relevant ABL1-E255K mutation identified in ponatinib-resistant Ba/F3 RANBP2-ABL1 cells, but no corresponding fusion protein..... 233
4.3.9. RQ-PCR confirms mRNA expression of Ba/F3 RANBP2-ABL1 fusion gene, despite lack of detectable fusion protein..... 236
4.3.10. Identification of a C-terminal deletion in ponatinib-resistant Ba/F3 RANBP2-ABL1 cells 240
4.3.11. Identification of non-canonical signalling pathways in ponatinib-resistant Ba/F3 RANBP2-ABL1 cells..... 246
4.4. DISCUSSION 254
4.4.1. Modelling of RANBP2-ABL1 Ph-like ALL 254
4.4.2. T315I as a mechanism of imatinib and dasatinib resistance in RANBP2-ABL1 Ph-like ALL..... 255
4.4.3. Compound mutations as a mechanism of TKI-resistance in cells exposed to ponatinib as secondary therapy..... 256
4.4.4. Ponatinib as first-line therapy results in genetic aberrations and activation of alternative signalling pathways..... 258

CHAPTER 5 – TKI-RESISTANCE IN A *SSBP2-CSF1R* CELL LINE IS ATTRIBUTABLE TO AN ACCUMULATION OF GENETIC ALTERATIONS..... 271
5.1. INTRODUCTION 272
5.2. APPROACH 274
5.3. RESULTS 275
5.3.1. Ba/F3 cells transduced with SSBP2-CSF1R demonstrate kinase-independent survival capacity..... 275
5.3.2. Ba/F3 SSBP2-CSF1R cells are sensitive to clinically-available TKIs 294
5.3.3. Generation of imatinib-resistance in Ba/F3 SSBP2-CSF1R cells results in an acquired novel point mutation..... 300
5.3.4. Imatinib-resistant Ba/F3 SSBP2-CSF1R L785M cells were sensitive to other TKIs..... 311
5.3.5. Generation of dasatinib-resistance in Ba/F3 SSBP2-CSF1R cells results in the accumulation of multiple genetic alterations 314
5.4. DISCUSSION 328

CHAPTER 6 – MECHANISMS OF TKI-RESISTANCE IN BA/F3 CELLS HARBOURING THE *PAX5-JAK2* PH-LIKE ALL FUSION....339
6.1. INTRODUCTION....340
6.2. APPROACH....342
6.3. RESULTS....344
6.3.1. Ba/F3 PAX5-JAK2 Ph-like ALL cells are sensitive to Jak-specific TKIs....344
6.3.2. TKI-resistant Ba/F3 PAX5-JAK2 cell lines are cross-resistant to ruxolitinib and BMS-911543 (Jak2i) compared to DMSO control cells....346
6.3.3. Identification of a JAK2-Y931C kinase-domain mutation in TKI-resistant Ba/F3 PAX5-JAK2 cell lines....353
6.3.4. Ruxolitinib-resistant Ba/F3 PAX5-JAK2 Y931C cells demonstrate a higher proliferation rate compared to DMSO control cells....356
6.3.5. mRNA sequencing identifies non-canonical signalling pathways associated with ruxolitinib-resistance in Ba/F3 PAX5-JAK2 cell line....360
6.4. DISCUSSION....376
CHAPTER 7 – FINAL DISCUSSION....395
7.1. INTRODUCTION....396
7.2. MAJOR FINDINGS....397
7.2.1. TKI-resistance in Ph+ ALL is attributable to RAS mutations....397
7.2.2. TKI-resistance in Ph-like ALL varies according to the fusion gene present and the applied TKI....398
7.3. OVERALL SUMMARY & FUTURE DIRECTIONS....405
REFERENCES....411

LIST OF FIGURES, TABLES & APPENDICES

Figure 1.1 – Hierarchy of B-cell development. B-cell maturation is a complex process, involving a cascade of events. 5
Figure 1.2 – Estimated frequency of genomic subtypes in childhood ALL. 7
Table 1.1 – Alterations involving the Jak/Stat signalling pathway identified in Ph-like ALL. 13
Table 1.2 – Abl-class kinase alterations identified in Ph-like ALL. 17
Table 1.3 – Other classes of kinase alterations identified in Ph-like ALL. 18
Figure 1.3 – Representation of types of pathways that may alter in Ph-like ALL 21
Figure 1.4 – Molecular structure of imatinib (STI-571; Glivec). 25
Figure 1.5 – Molecular structure of ruxolitinib (INCB-018424; Jakafi). 27
Figure 1.6 – Mutations in the Abl kinase domain of BCR-ABL1 in CML patients treated with TKIs 31
Figure 1.7 – Molecular structures of second-generation Abl-kinase inhibitors nilotinib and dasatinib. 33
Figure 1.8 – Molecular structure of ponatinib (AP-24534; Iclusig). 35
Table 1.4 – Clinical studies of TKI as first-line therapy in the treatment of Ph+ ALL. Patients were administered imatinib, nilotinib or dasatinib in-combination with chemotherapy upon diagnosis of Ph+ ALL. TKI induced complete haematological and cytogenetic responses for a minimum of 2 years, prior to subsequent relapse. 36
Table 2.1 – Common reagents 44
Table 2.2 – List of Western blotting antibodies 48
Table 2.3 – List of phospho-flow antibodies 51
Table 2.4 – Polyacrylamide gel reagents for CrkL electrophoresis 57
Table 2.5 – Cell culture seeding densities 60
Table 2.6 – Volume of reagents for Annexin-V-PE/7-AAD staining solution 62
Table 2.7 – Volume of antibodies for phosphoflow staining 65
Figure 2.1 – Generation of Ph-Ba/F3 Ph-like ALL stable cell lines via retroviral transduction 73
Table 2.8 – Strategies for sub-cloning of Ph-like ALL fusion genes 76
Figure 2.2 – Vector maps for pCR®-Blunt II-TOPO® (top panel) and pRuf-iG2 (bottom panel). 77
Table 2.9 – Volume of reagents used for molecular cloning of Ph-like ALL fusions 78
Table 2.10 – Incubation conditions for molecular cloning 79
Table 2.11 – Primer sequences for the amplification of kinase domains within fusion genes in Ba/F3 Ph-like ALL cell lines 86
Table 2.12 – Volume of components for 'Long PCR' master mix 86
Table 2.13 – Sequencing primers utilised for kinase domain mutation analysis in Ba/F3 Ph-like ALL cell lines 87
Table 2.14 – Primer sequences for breakpoints of Ph-like ALL fusion genes 88
Table 2.15 – Volume of reagents for 'Phusion PCR' master mix 88
Table 2.16 – Primer sequences for confirmation of RAS mutations 89
Table 2.17 – Volume of reagents for 'AmpliTaq Gold™ PCR' master mix 89
Table 2.18 – Volume of reagents for SYBR® Green RQ-PCR master mix 91

Table 2.19 – Primers used for RQ-PCR of RANBP2-ABL1 fusion gene in Ba/F3 cells 92
Table 2.20 – Primers used for validation of SUP-B15 Ph+ ALL mRNA-seq data (dasatinib-resistant line)..... 92
Table 2.21 – Primers used for validation of SUP-B15 mRNA-seq via RQ-PCR (ponatinib-resistant line)..... 93
Table 2.22 – Primers used for validation of Ba/F3 Ph-like ALL mRNA-seq data..... 93
Figure 3.1 – Dasatinib and ponatinib p-CrkL IC_{50} in control and low-dose TKI-resistant SUP-B15 cells. 105
Figure 3.2 – Dasatinib and ponatinib p-CrkL IC_{50} of 20 nM intermediate TKI-resistant cell lines suggest Bcr-Abl is not the driver of TKI-resistance..... 109
Figure 3.3 – 30 nM dasatinib-resistant cells do not demonstrate any increased Bcr-Abl activity, despite an abrogation of cell death 114
Figure 3.4 – 30 nM ponatinib-resistant cells indicate no increased Bcr-Abl activity, despite abrogation of cell death 118
Figure 3.5 – TKI-resistant cells demonstrate increased p-Erk expression compared to DMSO control cells..... 123
Figure 3.6 – Highly-resistant SUP-B15 cell lines do not demonstrate an increased p-CrkL IC_{50} compared to DMSO control cells. 127
Figure 3.7 – mRNA-seq heatmap of SUP-B15 TKI-sensitive and 200 nM TKI-resistant cell lines 132
Figure 3.8 – Validation of mRNA-seq data in DMSO control and dasatinib-resistant SUP-B15 cell lines 135
Figure 3.9 – Validation of mRNA-seq data in DMSO control and ponatinib-resistant SUP-B15 cell lines 139
Figure 3.10 – Alignment of mRNA sequencing data reveals presence of a KRAS-G12S mutation in dasatinib-resistant SUP-B15 cells as confirmed by Sanger sequencing of genomic DNA 143
Figure 3.11 – Alignment of mRNA sequencing data revealed an NRAS-G12S mutation in ponatinib-resistant SUP-B15 cells as confirmed by Sanger sequencing of genomic DNA 147
Figure 3.12 – Schematic representation of TKI-resistance in dasatinib and ponatinib-resistant SUP-B15 Ph+ ALL cells..... 157
Appendix 3.1..... 158
Appendix 3.2..... 159
Appendix 3.3..... 160
Appendix 3.4..... 161
Figure 4.1 – Isolation of RANBP2-ABL1 Ph-like ALL fusion gene from pCR®-Blunt II-TOPO® plasmids 170
Figure 4.2 – PCR confirms presence of RANBP2-ABL1 fusion gene in molecularly-cloned pRuf-iG2 retroviral vector 173
Figure 4.3 – GFP expression in HEK-293T cells retrovirally-transfected with pRuf-iG2 RANBP2-ABL1 in parallel with the empty vector 177
Figure 4.4 – Ba/F3 cells successfully transduced with pRuf-iG2 constructs express GFP positivity 181

Figure 4.5 – Ba/F3 cells transduced with pRuf-iG2 RANBP2-ABL1 express the fusion gene and protein. 184
Figure 4.6 – Ba/F3 cells containing the RANBP2-ABL1 Ph-like fusion gene demonstrate IL-3 independent growth. 186
Figure 4.7 – Ba/F3 pRuf-iG2 RANBP2-ABL1 cells are sensitive to the second-generation TKI dasatinib 190
Figure 4.8 – Ba/F3 RANBP2-ABL1 cells are sensitive to Abl-kinase specific TKIs, as indicated by reduction in p-CrkL and p-Stat5 via phosphoflow 192
Figure 4.9 – Ba/F3 RANBP2-ABL1 cells exhibit decrease in downstream phospho-protein expression when treated with Abl-specific TKI by western blotting analysis 194
Figure 4.10 – Ba/F3 RANBP2-ABL1 cells are sensitive to Abl-kinase targeted TKI 197
Figure 4.11 – Confirmation of imatinib and dasatinib resistance in dose-escalated Ba/F3 RANBP2-ABL1 cells via cell death assay 200
Figure 4.12 – Imatinib and dasatinib-resistant Ba/F3 RANBP2-ABL1 cells maintain p-Ranbp2-Abl1 in the presence of TKI 202
Figure 4.13 – Imatinib and dasatinib-resistant Ba/F3 RANBP2-ABL1 cells demonstrate increased phosphorylated CrkL (p-CrkL) IC_{50} compared to TKI-sensitive cells 204
Figure 4.14 – Identification of the ABL1-T315I kinase-domain mutation as a cause of TKI-resistance 208
Figure 4.15 – Ba/F3 RANBP2-ABL1 imatinib and dasatinib-resistant ABL1-T315I lines are sensitive to the third generation TKI ponatinib 210
Figure 4.16 – Re-escalation of imatinib-resistant Ba/F3 RANBP2-ABL1 T315I cells in ponatinib confers greater resistance to ponatinib 214
Figure 4.17 – Ponatinib-resistant ABL1-T315I cells demonstrate a higher phospho-Ranbp2-Abl1 IC_{50} compared to parental lines. 217
Figure 4.18 – Ponatinib-resistant ABL1-T315I cell lines demonstrate increased phosphorylated CrkL (p-CrkL) IC_{50} compared to parental lines. 221
Figure 4.19 – Ponatinib-resistant ABL1-T315I Ba/F3 RANBP2-ABL1 cells found to harbour compound mutations 225
Figure 4.20 – Ba/F3 RANBP2-ABL1 cells resistant to ponatinib as first-line therapy exhibits cross-resistance to first and second generation Abl TKIs. 230
Figure 4.21 – Ba/F3 RANBP2-ABL1 cells dose-escalated in ponatinib (as first-line treatment) exhibit an ABL1-E255K mutation, however, the fusion protein was undetectable via western blotting 235
Figure 4.22 – RQ-PCR confirms expression of RANBP2-ABL1 fusion gene 238
Figure 4.23 – Ba/F3 RANBP2-ABL1 ponatinib-resistant cells comprise of a C-terminal deletion in its Ph-like ALL fusion gene 241
Figure 4.24 – Ba/F3 RANBP2-ABL1 ponatinib-resistant cells demonstrate no marked increase in p-CrkL IC_{50} compared to TKI-sensitive line 244
Figure 4.25 – Clustering of mRNA-seq data confirms difference in gene expression between Ba/F3 RANBP2-ABL1 DMSO control and ponatinib-resistant cell lines 248

Figure 4.26 – Validation of mRNA-seq differentially-expressed genes in ponatinib-resistant compared to DMSO control Ba/F3 RANBP2-ABL1 cells, via RQ-PCR 250
Figure 4.27 – Pathway enrichment analysis of mRNA-seq data uncovers association of non-canonical pathways in TKI-resistance 252
Figure 4.28 – Schematic representations of TKI-resistance in Ba/F3 RANBP2-ABL1 Ph-like ALL cells 265
Appendix 4.1 – mRNA-seq and RQ-PCR readouts of Ba/F3 RANBP2-ABL1 ponatinib-resistant cells 267
Appendix 4.2A – Upregulated gene set in Ba/F3 RANBP2-ABL1 ponatinib-resistant line 268
Appendix 4.2B – Downregulated gene set in Ba/F3 RANBP2-ABL1 ponatinib-resistant line 269
Figure 5.1 – Isolation of SSBP2-CSF1R fusion gene from pCR®-Blunt II-TOPO® plasmids 277
Figure 5.2 – Confirmation of molecularly-cloned SSBP2-CSF1R Ph-like ALL fusion gene in pRuf-iG2 retroviral vector 279
Figure 5.3 – GFP expression in HEK-293T cells transfected with pRuf-iG2 constructs 283
Figure 5.4 – GFP positivity of Ba/F3 cells successfully transduced with pRuf-iG2 SSBP2-CSF1R 286
Figure 5.5 – Ba/F3 cells transduced with pRuf-iG2 SSBP2-CSF1R expresses both the fusion gene and the protein. 290
Figure 5.6 – Ba/F3 cells containing the SSBP2-CSF1R fusion gene demonstrate IL-3 independent survival and proliferation. 292
Figure 5.7 – Clinically-available tyrosine kinase inhibitors induce cell death in Ba/F3 SSBP2-CSF1R cells 295
Figure 5.8 – Phosphoflow analysis of TKI-treatment in Ba/F3 SSBP2-CSF1R cells reveals sensitivity to Abl-kinase inhibitors. 296
Figure 5.9 – Western immunoblotting of TKI-sensitivity in Ba/F3 SSBP2-CSF1R cells 298
Figure 5.10 – Investigation of TKI resistance in Ba/F3 SSBP2-CSF1R cells via Annexin-V/7-AAD cell death analysis 302
Figure 5.11 – Investigation of TKI resistance in Ba/F3 SSBP2-CSF1R cells via p-Ssbp2-Csf1r western blotting analysis 304
Figure 5.12 – Identification of the CSF1R-L785M kinase-domain mutation as probable cause of imatinib-resistance 306
Figure 5.13 – CSF1R-L785M is a novel kinase-domain mutation 309
Figure 5.14 – Imatinib-resistant Ba/F3 SSBP2-CSF1R cells are similarly sensitive to second and third generation Abl-kinase inhibitors as naïve control cells. 312
Figure 5.15 – Dasatinib-resistant Ba/F3 SSBP2-CSF1R cells are tolerant of dasatinib and imatinib but not ponatinib 316
Figure 5.16 – Dasatinib-resistant Ba/F3 SSBP2-CSF1R cells exhibit a truncation in the CSF1R 3' partner gene 318
Figure 5.17 – Identification of genetic deletion spanning the SSBP2-CSF1R breakpoint region in dasatinib-resistant cells 320
Figure 5.18 – Identification of a CSF1R-A652V mutation in dasatinib-resistant Ba/F3 SSBP2-CSF1R cells 322

Figure 5.19 – CSF1R-A652V identified in dasatinib-resistant Ba/F3 SSBP2-CSF1R cells is a novel kinase-domain mutation 325
Figure 5.20 – Investigation of p-Ssbp2-Csf1r in dasatinib-resistant Ba/F3 SSBP2-CSF1R cells reveal a truncation in protein band size and unchanged p-Csf1r dasatinib IC_{50}. 326
Figure 5.21 – Visualisation of the L785 residue in imatinib-bound Csf1r 331
Figure 5.22 – Schematic diagram of TKI-resistance in Ba/F3 SSBP2-CSF1R Ph-like ALL cells 335
Appendix 5.1 336
Figure 6.1 – Ba/F3 PAX5-JAK2 cells are sensitive to the Jak-specific inhibitors ruxolitinib and BMS-911543 345
Figure 6.2 – Annexin-V/7-AAD cell death exclusion assay confirms Jaki-resistance in Ba/F3 PAX5-JAK2 ruxolitinib and BMS-911543 resistant cell lines 348
Figure 6.3 – Western blotting of p-Stat5 (direct downstream partner of Jak2 activity) indicates an increased pStat5 IC_{50} in ruxolitinib and BMS-911543 resistant Ba/F3 PAX5-JAK2 cell lines, compared to DMSO control 350
Figure 6.4 – Sanger sequencing uncovers a JAK2-Y931C kinase-domain mutation in ruxolitinib and BMS-911543 resistant Ba/F3 PAX5-JAK2 cell lines 354
Figure 6.5 – Ba/F3 PAX5-JAK2 ruxolitinib-resistant cells demonstrate a higher proliferation rate compared to DMSO control cell line 358
Figure 6.6 – Hierarchical clustering and heatmap of mRNA-seq data confirms close association and significantly differentially-expressed genes between biological replicates of Ba/F3 PAX5-JAK2 TKI-sensitive and resistant cell lines 364
Figure 6.7 – Volcano plot of differentially-expressed genes and validation of mRNA-seq data via RQ-PCR in Ba/F3 PAX5-JAK2 ruxolitinib-resistant and DMSO control cells 367
Figure 6.8 – Pathway enrichment analysis of differentially-expressed genes identifies noncanonical signalling pathways in ruxolitinib-resistance 370
Figure 6.9 – Network analysis of ruxolitinib-resistant PAX5-JAK2 cells reveals a close association between Jak/Stat and cancer signalling gene sets in ruxolitinib-resistant PAX5-JAK2 cells 372
Figure 6.10 – Network analysis of contextually-relevant hubs associated with TKI-resistance in Ba/F3 PAX5-JAK2 ruxolitinib-resistant cell line 374
Figure 6.11 – Schematic representation of TKI-resistance in Ba/F3 PAX5-JAK2 Ph-like ALL cells 385
Appendix 6.1- Western blotting of p-Jak2 (Y1007/1008) in Ba/F3 PAX5-JAK2 cell lines 386
Appendix 6.2 389
Appendix 6.3A 390
Appendix 6.3B 391
Figure 7.1 – Schematic summary of TKI-resistance in SUP-B15 Ph+ ALL and Ba/F3 Ph-like ALL cell lines identified in this study 408

ABBREVIATIONS

ABCB1/ABCG2	ATP binding cassette (ABC) transporter proteins B1 and G2
ABL1	Abelson murine leukaemia viral oncogene homolog 1
ABL2	Abelson murine leukaemia viral oncogene homolog 2
ALL	acute lymphoblastic leukaemia
APS	ammonium persulfate
ATF7IP	activating transcription factor 7-interacting protein 1
ATP	adenosine triphosphate
BCR	breakpoint cluster region, RhoGEF and GTPase activating protein
BCR-ABL1	breakpoint cluster region-Abelson kinase fusion gene
Bcr-Abl	breakpoint cluster region-Abelson kinase fusion transcript/protein
BLNK	B-cell linker
bp	base pairs
C	Celsius
CAR	chimeric antigen receptor
CCyR	complete cytogenetic response
CD	cluster of differentiation
cDNA	complementary deoxyribonucleic acid
CENPC	centromere protein C
CHO	Chinese hamster ovary
CHR	complete haematologic response
CML	chronic myeloid leukaemia
CrkL	CT10 regulator of kinase-like
CRLF2	cytokine receptor like factor 2
CSF1R	colony-stimulating factor 1 receptor
Csf1r	colony stimulating factor 1 receptor
DABCO	1,4-diazabicyclo[2.2.2]octane
DAS	dasatinib
ddNTP	dideoxynucleotide triphosphate
DEPC	diethyl pyrocarbonate
DMEM	Dulbecco's Modified Eagle Medium
DMSO	dimethyl sulfoxide
DNA	deoxyribonucleic acid

dNTP	deoxynucleotide triphosphates
DNTT	DNA nucleotidylexotransferase
DTT	dithiothreitol
EBF1	early B cell factor 1
EPOR	erythropoietin receptor
ETV6	ETS variant 6
FACS	fluorescence activated cell sorting
FBS	foetal bovine serum
FGFR1	fibroblast growth factor receptor 1
FIP1L1	factor interacting with PAPOLA and CPSF1
FISH	fluorescence in situ hybridisation
FLT3	fms related tyrosine kinase 3
FOXP1	Forkhead box P1
FW	forward
g	gram
GATAD2A	GATA zinc finger domain containing 2A
GAPDH	glyceraldehyde 3-phosphate dehydrogenase
GOLGA5	golgin A5
GUS-β	beta-glucuronidase
HBSS	Hanks Balanced Salt Solution
HCl	hydrochloric acid
HMBOX1	homeobox containing 1
IC50	inhibitory concentration 50%
IgG	immunoglobulin G
IGH	immunoglobulin heavy locus
IGK	immunoglobulin kappa locus
IL2Rβ	interleukin 2 receptor subunit beta
IL7R	interleukin 7 receptor
IM	Imatinib mesylate
IMDM	Iscove's Modified Dulbecco's Medium
JAK1	Janus kinase 1
JAK2	Janus kinase 2
JAK3	Janus kinase 3
kb	Kilobase
KD	kinase domain
kDa	Kilo Dalton

L	Litre
LAIR1	leukocyte associated immunoglobulin like receptor 1
LSM14	LSM family member 14
Lyn	tyrosine-protein kinase Lyn
M	Molar (Moles per litre)
MCR	major cytogenetic response
MDR	multidrug resistance
MEF2D	myocyte enhancer factor 2D
mL	milli Litre
mM	milli molar (10-3 Molar)
MMR	major molecular response
mRNA	messenger ribonucleic acid
MYB	MYB proto-oncogene, transcription factor
MYH9	myosin heavy chain 9
NCOR1	nuclear receptor corepressor 1
NCS	newborn calf serum
NHEJ	non-homologous end-joining
NIL	nilotinib
nM	nano molar (10^-9 Molar)
NTRK3	neurotrophic receptor tyrosine kinase 3
NUP153	nucleoporin 153
NUP214	nucleoporin 214
OCT-1	organic cation transporter 1
OFD1	oral-facial-digital syndrome 1
P-loop	phosphate binding loop
P-value	probability value
P2RY8	purinergic receptor P2Y8
PAG1	phosphoprotein membrane anchor with glycosphingolipid microdomains 1
PAX5	paired box 5
PBS	phosphate buffered saline
PCM1	pericentriolar material 1
PCR	polymerase chain reaction
PDGFRα	platelet-derived growth factor receptor-like-α
PDGFRβ	platelet-derived growth factor receptor-like-β
PFA	paraformaldehyde

Ph	Philadelphia chromosome
PI3-K	phosphatidylinositol-3-kinase
PPFIBP1	PPFIA binding protein 1
PVDF	polyvinylidene fluoride
RANBP2	RAN binding protein 2 / nucleoporin 358 (Nup358)
RCF	relative centrifugal force (also abbreviated as ‘x g’)
RCSD1	RCSD domain containing 1
RFX3	regulatory factor X3
RNA	ribonucleic acid
RPMI	Roswell Park Memorial Institute (-1640 medium)
RT	room temperature
RQ-PCR	real-time quantitative polymerase chain reaction
RV	reverse
SD	standard deviation
SDS-PAGE	sodium dodecyl sulphate polyacrylamide gel electrophoresis
SEM	standard error of the mean
SFPQ	splicing factor proline and glutamine rich
SH	Src homology domain
SH2B3	SH2B adaptor protein 3
SMARCA4	SWI/SNF related, matrix associated, actin dependent regulator of chromatin, subfamily A, member 4
SMU1	suppressor of mec-8 and unc-52 protein homolog
SN	supernatant
SNX2	sorting nexin 2
SNX29	sorting nexin 29
SPTAN1	spectrin alpha, non-erythrocytic 1
Src	proto-oncogene tyrosine-protein kinase Src
SSBP2	single-stranded DNA binding protein 2
SSC	saline-sodium citrate buffer
STRN	striatin 3
TBL1XR1	transducin beta like 1 x-linked receptor 1
TBS	tris buffered saline
TBST	tris buffered saline with 0.1% Tween® 20
TERF2	telomeric repeat binding factor 2
THADA	thyroid adenoma associated
TKI	tyrosine kinase inhibitor

TNIP1	TNFAIP3 interacting protein 1
TPR	ubiquitin specific peptidase 25
Tris	tris(hydroxymethyl)aminomethane
TYK2	tyrosine kinase 2
USP25	ubiquitin specific peptidase 25
UV	ultra violet
ZBTB46	zinc finger BTB domain containing 46
ZC3HAV1	zinc finger CCCH-type antiviral protein 1
ZEB2	zinc finger e-box binding homeobox 2
ZMIZ1	zinc finger MIZ domain-containing protein
ZMYM2	zinc finger MYM-type containing 2
ZMYND8	zinc finger MYND-type containing 8
ZNF274	zinc finger protein 274
ZNF340	zinc finger protein 340
µg	micro gram (10^-6 gram)
µM	micro molar (10^-6 Molar)

ABSTRACT

Treatment-resistant acute lymphoblastic leukaemia (ALL) remains a significant clinical issue. Genomic profiling has identified a subtype of high-risk ALL termed Philadelphia-chromosome-like (Ph-like) ALL that is associated with accumulation of kinase-activating fusion genes and poor outcome. Studies have demonstrated the kinases encoded by Ph-like ALL fusion genes are targetable *in vitro* and *in vivo* by tyrosine kinase inhibitors (TKI), though it is known through CML and Ph+ ALL studies, that TKI-resistance is likely, leading to relapse and/or progression. Therefore, there is an urgent need to identify drivers of potential TKI-resistance in the Ph-like ALL setting. This study aims to model TKI-resistance in high-risk Ph+ and Ph-like ALL in order to understand the underlying mechanisms and inform future therapeutic strategies that may overcome resistance, thereby improving patient outcomes.

In this thesis, Ba/F3 cells expressing Ph-like ALL fusion genes were generated by retroviral transduction of fusions identified in primary Ph-like ALL samples, while Ph+ ALL was modelled using the immortalised cell line SUP-B15. TKI-resistance was generated through long-term exposure (~6-12 months) of cells to increasing concentration of TKI (imatinib, dasatinib, ponatinib or ruxolitinib – depending on fusion kinase). TKI-resistant Ba/F3 Ph-like ALL cells were found to acquire the clinically-reported *ABL1*-T315I, *ABL1*-G250E/T315I and *JAK2*-Y931C kinase domain mutations associated with drug resistance. Interestingly, a novel *CSF1R*-L785M mutation and a previously unreported *ABL1*-L302H/T315I compound mutation were identified, with these mutations predicted to alter drug binding.

Importantly, next-generation transcriptomic sequencing uncovered the association of non-canonical signalling pathways in TKI-resistant high-risk ALL cells. In ruxolitinib-resistant *JAK2*-Y931C Ba/F3 cells, mRNA-seq pathway analysis revealed the involvement of glycolytic metabolism and G-protein coupled receptor signal transduction pathways as potential modes of TKI-resistance. Transcriptomic analysis also uncovered a *KRAS* and *NRAS* mutation in dasatinib and ponatinib-resistant SUP-B15 Ph+ ALL cells respectively, resulting in upregulation of mitogen-activated protein kinase (MAPK) cell survival signalling cascades. Together these findings represent attractive targets for future studies into parallel treatment

modalities that may inhibit the development of, or overcome established treatment resistance in ALL.

Overall this thesis has demonstrated that TKI-resistance in high-risk Ph-like and Ph+ ALL can be attributed to clinically-relevant point-mutations and the involvement of key alternative signalling mechanisms which override TKI sensitivity. This knowledge is critical towards potentially informing future management of patients who relapse on first-line TKI therapies, as well as the prospective development of combinatorial treatments that target critical fusion kinase and parallel signalling pathways likely contributing to the emergence of treatment resistance, in high-risk ALL and other diseases of similar treatment-resistant modalities.

THIS PAGE INTENTIONALLY LEFT BLANK.

CHAPTER 1 –

INTRODUCTION

1.1. Acute Lymphoblastic Leukaemia

1.1.1. Clinical Features of ALL

Acute lymphoblastic leukaemia (ALL) is characterised by maturation arrest of lymphoid lineage cells which leads to an accumulation of immature blast cells in the blood and bone marrow. Affecting both children and adults, ALL has a peak prevalence in children, occurring between the ages of 3 to 5 years[7]. ALL can be diagnosed by the presence of recurring karyotypic alterations in a patient sample, such as chromosomal translocations and aneuploidy as ascertained by cytogenetic identification[8,9].

Depending on genomic subtype, ALL can be a highly treatable disease in children, often resulting in a 5-year event-free survival of approximately 90%, due to advancement in modern medicine[10]. Despite the high rate of achieving a favourable outcome, ALL remains the most common form of cancer in childhood[11,12]. In adults, the disease has a significantly worse prognosis, which is attributed to an increased accumulation of chromosomal alterations[10,13]. Chemotherapy (in-combination with targeted therapy, depending on subtype) is currently the mode of therapy however treatment resistance remains a major cause of clinical relapse, leading to mortality[14,15].

Two main types of ALL exist – B-cell and T-cell lineage ALL – however for purpose of this thesis, B-ALL will be the focus of study. In ALL, a patient's age and white cell count predicts prognosis, and these features are used to sub-classify ALL as 'standard-risk' or 'high-risk', based on the Children's Oncology Group (COG) classification criteria[7,16]. 'Standard risk' (two thirds of childhood B-ALL cases) is defined as patients with a white-cell count of less than $5x10^4/\mu L$ and between the

ages of 1-10 years. 'High-risk' ALL (a third of childhood B-ALL cases) is defined by white-cell counts of more than $5x10^4/\mu L$ at diagnosis, with poorer prognosis with increasing age (≥10 yrs). Infants below the age of 1 are a unique group, often with worse outcomes[17].

Patients with ALL clinically present with symptoms such as fatigue due to anaemia, infection resulting from neutropenia and bruising/bleeding due to thrombocytopenia[7]. The infiltration of leukaemic cells into medullary and extramedullary sites are also not uncommon in ALL[7].

1.1.2. Genomic Alterations in Childhood ALL

The precise cause of ALL is unknown, though development has been associated with the accumulation of genomic alterations. A genome-wide analysis by Mullighan *et al*. in 2007 identified a 40% occurrence of alterations (structural rearrangements, deletions, mutations and insertions) in transcription factors essential for the development and differentiation of B-cells[18]. Specifically, alterations in *PAX5* were identified as most common, occurring at a rate of 31.7% in the patients with B-ALL. Focal deletions in *EBF1*, a gene important for the determination of B cell identity, were also discovered[18]. Mullighan and colleagues further identified deletions in *IKZF1* that were found to be associated with poor prognosis[19], and *IKZF1* alterations are now a hallmark of high-risk B-ALL[20].

PAX5, also known as B-cell specific activator protein (BSAP), is critical for establishing B cell differentiation, controlling B-cell lineage commitment and identity[14,21,22]. *PAX5* promotes the expression of genes specific for B-cell development and accounts for approximately 25% of gene changes that occur as lymphoid progenitors mature from pro-B to pre-B cells via the V_H-to-D_HJ_H

recombination (a key step in B-cell differentiation)[18]. As *PAX5* is important in the normal maturation and development of B-cells, genetic alterations including mutations and deletions of *PAX5* can result in susceptibility to developing B-ALL[23,24]. Mutations of *PAX5* are found in B-ALL, with over 30% of patients affected by somatic alterations[18,25,26]. The occurrence of germline *PAX5* mutations has also been reported in a minority of patients, based on recent studies[21,27].

The transcription factor *EBF1* induces expression of genes that are integral to B-cell differentiation in multipotent progenitors[24]. The expression of *PAX5* is partly induced by *EBF1*, at an early step in the commitment of cells to the B-cell lineage[28-30]. Therefore, alterations in *EBF1* likely induce leukaemogenesis through dysregulation of B cell development in a way akin to that driven by alterations in *PAX5* [31,32].

IKZF1, which encodes Ikaros (a zinc finger transcription factor), is essential for the commitment of cells to the lymphoid lineage through repression of key myeloid genes[33,34]. Ikaros has also been shown to act as a mediator in the maturation of large to small pre-B cells, through interleukin-7 signalling[35]. A key regulator in the development of the immunoglobulin heavy chain locus, Ikaros also determines the fate of B-cell commitment [36].

B-cell development is a complex process, involving a controlled sequence of events (**Figure 1.1**). An alteration in any of the genes that regulate this process (i.e. *IKZF1*, *EBF1* or *PAX5*) can result in an abnormal B lymphocyte maturation process, leading to aberrant cell development and cancer.

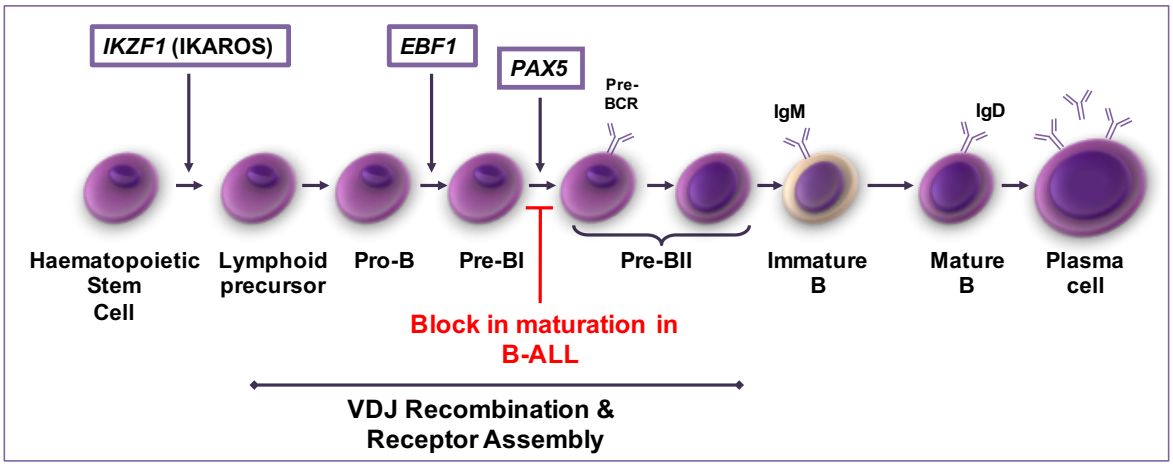


Figure 1.1 – Hierarchy of B-cell development. B-cell maturation is a complex process, involving a cascade of events.

Alterations in genes including *IKZF1*, *EBF1* and *PAX5* contribute to a blockade of B-cell maturation, resulting in B-ALL. Adapted and modified from Bernt & Hunger *Front Oncol* 2014[14].

Recent use of high resolution genomic approaches has enabled further elucidation and stratification of alterations involved in ALL, with B-cell lineage ALL in children exhibiting a wider diversity of genetic alterations compared to that of T-cell lineage ALL (**Figure 1.2**)[37,38]. This includes chromosomal alterations such as *TEL-AML1* (erythroblast transformation-specific (*ETS*) variant 6 (*ETV6*)-runt-related transcription factor 1 (*RUNX1*)) t(12;21) fusion that represents 22% of childhood cases, hyperdiploidy (>50 chromosomes) as seen in 20% of childhood ALL, and MLL-rearrangements (6% of patients)[8,9]. Alterations involving double homeobox 4 (*DUX4*) and erythroblast transformation-specific (*ETS*) related gene (*ERG*) deregulation, zinc finger protein 384 (*ZNF384*)-rearrangements as well as the complex intrachromosomal amplification of chromosome 21 (also known as iAMP21) have also been identified[39-46].

Additional alterations described in ALL include the *BCR-ABL1* fusion (Philadelphia (Ph) chromosome) and *BCR-ABL1*-like (Ph-like) ALL. Patients with these subsets of disease exhibit poor response to treatment/outcomes (Figure 1.2)[47,48].

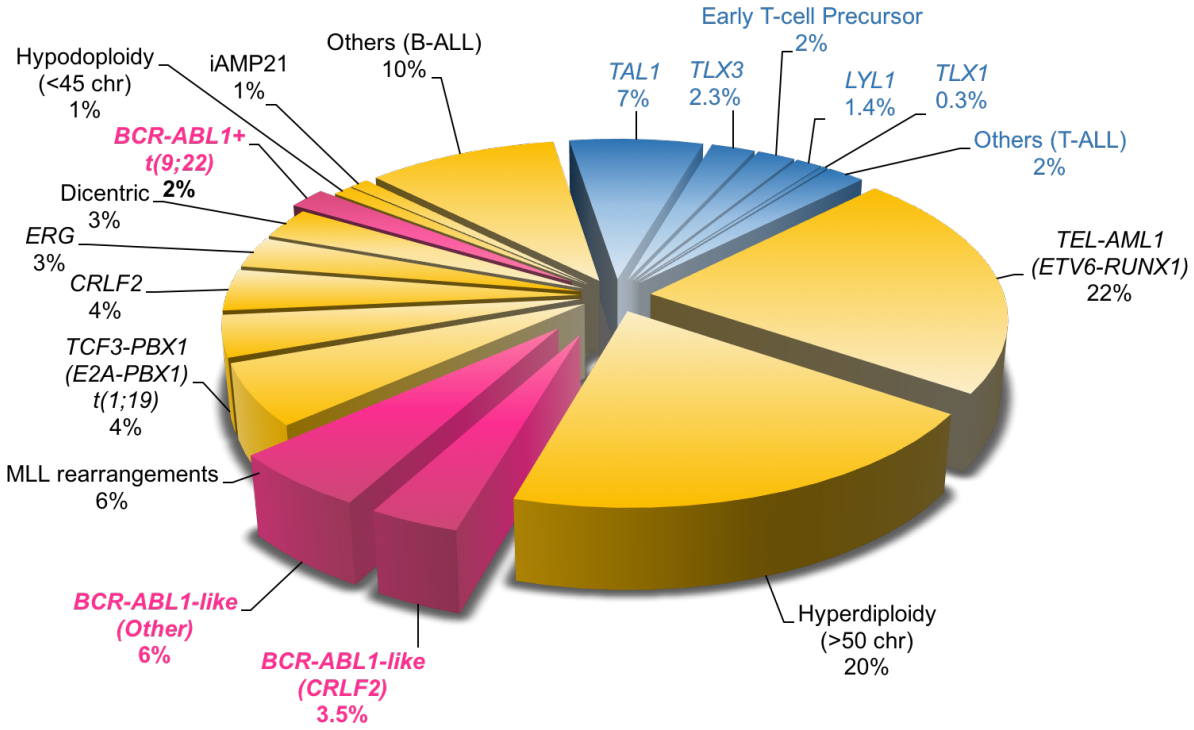


Figure 1.2 – Estimated frequency of genomic subtypes in childhood ALL.

Pie chart depicts genomic alterations in childhood B-ALL (pink and yellow sections) and T-ALL (blue sections). Pink slices: frequency of 'breakpoint cluster region – Abelson murine leukaemia viral oncogene homolog 1' (*BCR-ABL1*) also known as Philadelphia chromosome positive (Ph+) ALL), and, *BCR-ABL1*-like (Ph-like) high-risk B-ALL subtypes, which are of main interest in this thesis. Yellow: other B-ALL subtypes; Blue: T-ALL subtypes. *TAL1*: transcription factor 1, erythroid differentiation factor; *TLX3*: t-cell leukaemia homeobox 3; *LYL1*: lymphoblastic leukaemia associated haematopoiesis regulator 1; *TLX1*: T-cell leukaemia homeobox 1; *CRLF2*: cytokine receptor like factor 2; *MLL* myeloid/lymphoid mixed lineage leukaemia; *TCF3*: transcription factor 3; *E2A*: *E2A* immunoglobulin enhancer-binding factors E12/E47; *PBX1*: Pre-B-cell leukaemia transcription factor 1; iAMP21: intrachromosomal amplification of chromosome 21. Adapted & modified from Mullighan *Hematology Am Soc Hematol Educ Program* 2012[47]

1.1.3. Ph+ and Ph-like High-risk ALL

The Philadelphia chromosome is a hallmark of chronic myeloid leukaemia (CML) and Ph+ ALL, caused by a chromosomal translocation of chromosomes 9 and 22 t(9;22)(q34.1;q11.2)[49]. This results in the formation of a fusion gene, *BCR-ABL1* which translates the Bcr-Abl oncoprotein. This leads to oligomerisation of the Abl kinase domain, autophosphorylation and presentation of phosphotyrosine residues that serve as suitable binding sites for proteins containing Src homology 2 (SH2) domains such as CrkL, Erk1/2 and Stat5[50-52]. The resulting constitutively active phosphorylation of downstream cell proliferation and anti-apoptotic proteins, including signal transducer and activator of transcription 5 (Stat5), protein kinase B (Akt) and extracellular signal-regulated kinase (Erk), ultimately leads to aberrant cell proliferation, leukaemogenesis and disease[53-56].

Classified as a high-risk subtype of ALL, Ph+ ALL was found to be associated with a high frequency of *IKZF1* deletions (83.7% of Ph+ ALL leukaemic samples)[20], in a study first described by Mullighan and colleagues in 2008. *IKZF1* deletions were associated with poorer outcome, due to subsequent haploinsufficiency and complete loss of *IKZF1* expression essential for B-cell commitment[36,57].

1.1.4. Ph-like or *BCR-ABL1*-like ALL

In 2009, two groups of investigators – Mullighan *et al*. at the St Jude's Children's Research Hospital and the Children's Oncology Group (COG/SJCRH)[19] and Den Boer *et al*. at the Dutch Childhood Oncology Group and German Cooperative ALL (DCOG/COALL)[58] – independently identified a subgroup of B-ALL with a gene expression profile similar to Ph+ ALL, but without the *BCR-ABL1* oncogene. In both studies, *IKZF1* deletions were detected in a subset of Philadelphia-chromosome-

negative paediatric high-risk B-ALL (39% by in the DCOG/COALL cohort[58] and 28.6% in the COG/SJCRH cohort[19]). The deletions in *IKZF1* resulted in a distinct gene expression signature where an upregulation of genes related to cell-adhesion, cytoskeletal regulation and survival were observed[59]. Depending on the gene expression profiling platform utilised in the above studies, this subset of ALL was subsequently termed 'Ph-like ALL' (SJCRH/COG)[60-62], or '*BCR-ABL1*-like' ALL (DCOG/COALL cohort)[58,63], a focus of study in this thesis. In the COG/SJCRH cohort, two platforms – a Prediction of Microarray Analysis (PAM) RNA-seq classifier comprising of 257 gene probe sets[64,65] and 384-well low-density microarray (LDA) cards [66-68] – were utilised for the identification of Ph-like ALL. In the DCOG/COALL cohort, a hierarchical clustering based on 110 gene probe sets predicting the major ALL subtypes was utilised for *BCR-ABL1*-like ALL (the terminology utilised by Den Boer and colleagues for this cohort)[57,58,69,70]. The discrepancy between the frequency of Ph-like ALL / *BCR-ABL1*-like ALL in both cohorts were further attributed to the type of gene expression signature utilised, as well as the ethnicity of patients in both cohorts (mostly European in DCOG/COALL, while a mix of European and Hispanic ethnicities in the SJCRH/COG cohort)[63,71].

Ph-like ALL/*BCR-ABL1*-like ALL has since been associated with poor prognosis. The disease affects patients across all ages (childhood, adolescents, and adults)[67,70,72] – however is more prevalent with increasing age[62]. In a recent review by Pui and colleagues[62], the incidence of Ph-like ALL proportionately increases with age – 12% childhood B-ALL cases, 21% in adolescent cases (16 to 20 years of age) and 20-24% of adult Ph-like ALL cases above the age of 40[62]. The 5-year overall survival of Ph-like ALL is 72.8% (SD±4.8%) in children, 65.8% (±7.1%) in adolescent and 25.8% (±9.9%) in young adults[73].

Roberts *et al*.[64] assessed the genomic signatures of Ph-like ALL samples using the Recognition of Outliers by Sampling Ends (ROSE) (methods derived from Harvey *et al*., 2010[74]) and PAM algorithms[75], and where no significant alterations can be found, whole genome sequencing (WGS – a form of next-generation sequencing) was further performed[48,62,64,76]. These studies uncovered cytokine and kinase-activating genomic lesions in Ph-like ALL[64,73]. Studies further defining the alterations that underpin disease development in Ph+ and Ph-like ALL have highlighted specific classes of signalling pathways that will be discussed in the following section.

1.2. An Overarching Perspective of Ph-like ALL

The genomic lesions identified in Ph-like ALL involve 3 main classes of signalling pathways – 1) Jak-signalling i.e. *JAK* fusions and mutations, *CRLF2*-rearrangements, and, *EPOR* truncations; 2) *ABL* family fusions, and, 3) alterations involving other kinases (i.e. *NTRK3* and *RAS*)[73,77]. Although various alterations within each signalling class have been identified to date, new alterations are still being discovered as Ph-like ALL is an emerging field. Overarchingly, these alterations converge on cytokine receptor and kinase signalling pathways, which will be further explored.

1.2.1. Alterations Affecting the Jak Signalling Pathway

In Ph-like ALL, alterations in genes fundamental to the Jak signalling pathway have been identified. A key example is *CRLF2*, alterations of which are a hallmark of deregulated Jak-signalling. Crlf2 is a Jak-binding cytokine receptor[78], forming a heterodimeric complex with IL-7Rα (interleukin-receptor 7 α) upon activation by its ligand TSLP (thymic stromal lymphopoietin) [79-81]. This results in the activation of

Stat5 through Jak, which subsequently leads to cell proliferation and the activation of immunological responses[46,82,83].

Rearrangements of *CRLF2* identified in Ph-like ALL include the *P2RY8-CRLF2* and *IGH-CRLF2* fusions. A result of a recurring interstitial deletion in the pseudoautosomal region 1 (*PAR1*) of sex chromosomes X and Y (del(X)(p22.33p22.33), or, del(Y)(p11.32p11.32), the joining of *P2RY8* (purinergic receptor P2Y8) to *CRLF2* leads to an activated production of its transcript[44-46,84](**Table 1.1**). The *P2RY8-CRLF2* rearrangement has been identified in *7% of* individuals with B-progenitor ALL and 53% of individuals with ALL associated with Down syndrome[81,82,85]. The *IGH-CRLF2* rearrangement is a result of the translocation of the immunoglobulin binding locus to *CRLF2* t(X;14)(p22;q32) or t(Y;14)(p11; q32), occurring in 0.8% of 5% childhood ALL cases[81]. While *P2RY8-CRLF2* has been associated with younger age, the *IGH-CRLF2* was detected more frequently in older patients and patients of Hispanic ethnicity[82,86]. A *CRLF2*–F232C point mutation which permits homodimerisation and activation of its receptor, has also been reported[46].

In high-risk B-ALL cases that lack the *MLL*, *TCF3*, *TEL* or *BCR-ABL1* rearrangements, *CRLF2* is overexpressed in 15% of these patients[46]. In Ph-like ALL, 50% of patients were found to possess a *CRLF2* rearrangement, with concomitant *JAK1*/*JAK2* mutations (primarily, *JAK2*-R683G) identified in half of these patients (P<0.001)[82,85,86]. Comparisons between *CRLF2*-overexpressing B-ALL and Ph+ ALL further uncovered a common transcriptional signature, where an enrichment of genes involved in cytokine receptor and JAK/STAT signalling[60,82] was observed.

JAK alterations in Ph-like ALL comprise a multitude of subtypes, including chromosomal translocations, deletions and the acquirement of fusion genes. *JAK* rearrangements occur in approximately 7% of Ph-like ALL cases[62]. Genes encoding fusion kinases involving Jak signalling pathways include *JAK2,* tyrosine kinase 2 (*TYK2*) and the interleukin-2 receptor β (*MYH9-IL2Rβ*) (**Table 1.1**)[60].

Studies investigating the role of Crlf2 in the development of Ph-like ALL demonstrate that retroviral transduction of cytokine-dependant B-progenitor Ba/F3 murine cells with wildtype *CRLF2* and mutant *JAK2*-R683G *or JAK2*-R683S resulted in cytokine (interleukin-3 (IL-3)) independent growth. These cells also demonstrated sensitivity to JAK inhibitor I and K252a (a protein kinase C inhibitor)[46]. Ph-like ALL cases with Crlf2-rearrangements/Jak mutations may therefore be targeted using Jak inhibitors (i.e. ruxolitinib, momelotinib), potentially improving treatment outcomes.

A rearrangement in an additional member of the Jak signalling pathway, *EPOR*, has also been identified in Ph-like ALL (**Table 1.1**). Rearrangements in *EPOR*, which encodes the erythropoietin receptor, occurs in approximately 5% of Ph-like ALL cases[62]. The frequency of *EPOR* rearrangements in Ph-like ALL is highest in young adults (9%), compared to that of children (5%), adolescents (3%) and adults (1%)[62]. *EPOR* rearrangements include *IGH/IGK-EPOR* translocations and cryptic insertions[64,73], as well as deletions in the EPOR c-terminus, resulting in a loss of regulatory residues for downstream JAK/STAT signalling[77]. As such, this is another signalling mechanism that can potentially be targeted using currently-available TKI as an attractive clinical approach, which will be discussed in section **1.3.2**.

Table 1.1 – Alterations involving the Jak/Stat signalling pathway identified in Ph-like ALL.

Adapted from Roberts 2017[60]

Genes associated with JAK/STAT signalling	Number of fusion partners	Fusion partner genes	Potential TKI	Type of alteration	Method of identification
CRLF2	2	*IGH, P2RY8*	Jak, PI3K/mTOR or Tyk2 inhibitors	Translocation (IGH)	FISH
				Fusion to promoter (P2RY8)	Flow cytometry
JAK2	20	*ATF7IP, BCR, EBF1, ETV6, GOLGA5, HMBOX1, OFD1, PAX5, PCM1, PPFIBP1, RFX3, SMU1, SNX29, SSBP2, STRN3, TERF2, TPR, USP25, ZNF274, ZBTB46,*		In-frame fusion	FISH
					RT-PCR
					Transcriptome sequencing
EPOR	4	*IGH, IGK, LAIR1, THADA*		Cryptic rearrangement	Transcriptome sequencing
TYK2	3	*MYB, SMARCA4, ZNF340*		In-frame fusion	RT-PCR
					Transcriptome sequencing
IL2RB	1	*MYH9*		Rearrangement	Transcriptome sequencing
JAK1	0	N/A		Sequence mutation	Sanger sequencing
					Exome sequencing
JAK3	0	N/A		Sequence mutation	Sanger sequencing
					Exome sequencing
IL7R	0	N/A		Indel mutation	Sanger sequencing
					Exome sequencing
SH2B3	0	N/A		Sequence mutation	Sanger sequencing
				Focal deletions	Genome sequencing

Abbreviations: *ATF7IP*: activating transcription factor 7-interacting protein 1; *BCR*: Breakpoint cluster region, RhoGEF and GTPase activating protein; *CRLF2*: cytokine receptor like factor 2; *EBF1*: early B cell factor 1;; *EPOR*: erythropoietin receptor; *ETV6*: ETS Variant 6; *GOLGA5*: golgin A5; *HMBOX1*: homeobox containing 1; *IGH*: immunoglobulin heavy locus; *IGK*: immunoglobulin kappa locus, *IL2Rβ*: interleukin 2 receptor subunit beta; *IL7R*: interleukin 7 receptor; *JAK1*: Janus kinase 1; *JAK2*: Janus kinase 2; *JAK3* Janus kinase 3; *LAIR1*: leukocyte associated immunoglobulin like receptor 1; *MYB*: MYB proto-oncogene, transcription factor; *MYH9*: myosin heavy chain 9; *OFD1*: oral-facial-digital syndrome 1; *P2RY8*: purinergic receptor P2Y8; *PAX5*: paired box 5; PCM1: pericentriolar material 1; *PPFIBP1*: PPFIA binding protein 1; *RFX3*: regulatory factor X3; *SH2B3*: SH2B adaptor protein 3; SMARCA4: SWI/SNF related, matrix associated, actin dependent regulator of chromatin, subfamily A, member 4; *SMU1*: suppressor of mec-8 and unc-52 protein homolog; *SNX29*: sorting nexin 29; *SSBP2*: Single stranded DNA binding protein 2; *STRN*: striatin 3; *TERF2*: telomeric repeat binding factor 2; *THADA*: thyroid adenoma associated; *TPR*: ubiquitin specific peptidase 25; *TYK2*: tyrosine kinase 2; *USP25*: ubiquitin specific peptidase 25; *ZBTB46*: zinc finger BTB domain containing 46; *ZNF274*: zinc finger protein 274; *ZNF340*: zinc finger protein 340. Abbreviations are listed here for ease of thesis examination.

1.2.2. Alterations Involving Abl-class Signalling Pathways

In-addition to the identification of alterations involving Jak/Stat signalling, modifications of genes involving the Abl kinase signalling have also been identified in Ph-like ALL. These fusion kinases mimic the characteristics of the *BCR-ABL1* oncogene gene by activating similar downstream signal transduction pathways including phosphoinositide 3-kinase (Pi3k) and Stat [64,73,87-89]. Fusion partner genes encoding kinases involved in Abl-class signalling discovered to date in Ph-like ALL include the Abelson murine leukaemia viral oncogene homolog 1 *(ABL1)*, platelet-derived growth factor receptor-like-α (*PDGFR*α), platelet-derived growth factor receptor-like-β (*PDGFR*β) and colony-stimulating factor 1 receptor (*CSF1R*) (**Table 1.2**). These signalling pathways are associated with cell survival and proliferation. Therefore, the presence of a genomic alteration can result in dysregulation (activation) of downstream signalling cascades, leading to aberrant cell growth and cancer.

Abl-class fusions are known to occur in 12.6% of Ph-like cases and are common in children[39,73]. These cases are predicted to respond to Abl kinase inhibitors such as imatinib and the dual Abl/Src kinase inhibitor dasatinib[73]. Importantly, separate anecdotal cases by Weston[90] and Lengline[91] demonstrated that in patients whose leukaemic cells harboured the *EBF1-PDGFR*β fusion, the administration of imatinib (an Abl kinase inhibitor) in-conjunction with chemotherapy successfully reduced disease burden, improving treatment outcome.

As such, the use of Abl kinase inhibitors appears to be a promising approach in the treatment of Ph-like ALL patients harbouring this class of fusion. The use of Abl kinase inhibitors such as imatinib, however, have been associated with the development of clinical relapse, due to treatment resistance. These mechanisms

will be further explored in section **1.4.1**, which will discuss the implications of Abl TKI therapy.

THIS PAGE INTENTIONALLY LEFT BLANK.

Table 1.2 – Abl-class kinase alterations identified in Ph-like ALL.

Adapted from Roberts 2017[60]

Genes associated with Abl kinase signalling	Number of fusion partners	Fusion partner genes	Potential TKI	Type of alteration	Method of identification
ABL1	12	*CENPC, ETV6, FOXP1, LSM14, NUP214, NUP153, RCSD1, RANBP2, SNX2, SFPQ, SPTAN1, ZMIZ1*	Abl-kinase inhibitors (e.g. imatinib, dasatinib, nilotinib, ponatinib)[90-92]	In-frame fusion	FISH RT-PCR Transcriptome sequencing
ABL2	3	*PAG1, RCSD1, ZC3HAV1*		In-frame fusion	FISH RT-PCR Transcriptome sequencing
CSF1R	3	*MEF2D, SSBP2, TBL1XR1*		In-frame fusion	FISH RT-PCR Transcriptome sequencing
LYN	2	*NCOR1, GATAD2A*		In-frame fusion	RT-PCR Transcriptome sequencing
PDGFRα	1	*FIP1L1*		In-frame fusion	FISH RT-PCR Transcriptome sequencing
PDGFRβ	7	*ATF7IP, EBF1, ETV6, SSBP2, TNIP1, ZEB2, ZMYND8*		In-frame fusion	FISH RT-PCR Transcriptome sequencing

Abbreviations: *ABL1*: Abelson murine leukaemia viral oncogene homolog 1; *ABL2*: Abelson murine leukaemia viral oncogene homolog 2; *ATF7IP*: activating transcription factor 7-interacting protein 1; *CENPC*: centromere protein C; *CSF1R*: colony-stimulating factor 1 receptor; *EBF1*: early B cell factor 1; *ETV6*: ETS variant 6; *FIP1L1*: factor interacting with PAPOLA and CPSF1; *FOXP1*: Forkhead box P1; *GATAD2A*: GATA zinc finger domain containing 2A; *LSM14*: LSM family member 14; *LYN*: tyrosine-protein kinase Lyn; *MEF2D*: myocyte enhancer factor 2D; *NCOR1*: nuclear receptor corepressor 1; *NUP153*: nucleoporin 153; *NUP214*: nucleoporin 214; *PAG1*: phosphoprotein membrane anchor with glycosphingolipid microdomains 1; *PDGFRα:* platelet-derived growth factor receptor-like-α; *PDGFRβ:* platelet-derived growth factor receptor-like-β; *RANBP2*: RAN binding protein 2; *RCSD1*: RCSD domain containing 1; *SFPQ*: splicing factor proline and glutamine rich; *SNX2*: sorting nexin 2; *SPTAN1*: spectrin alpha, non-erythrocytic 1; *SSBP2*: single-stranded DNA binding protein 2; *TBL1XR1*: transducin beta like 1 x-linked receptor 1; *TNIP1:* TNFAIP3 interacting protein 1; *ZC3HAV1*: zinc finger CCCH-type antiviral protein 1; *ZEB2*: zinc finger e-box binding homeobox 2; *ZMIZ1:* zinc finger MIZ domain-containing protein; *ZMYND8*: zinc finger MYND-type containing 8; FISH: fluorescence in situ hybridisation; RT-PCR: reverse-transcription polymerase chain reaction

1.2.3. Alterations Involving Other Signalling Mechanisms

In addition to the discovery of alterations involving Abl-class fusion kinases and Jak/Stat signalling in *de novo* Ph-like ALL, alterations in other kinase-encoding fusion genes have also been identified using next-generation sequencing (**Table 1.3**). These include the identification of fusion genes such as *ETV6-NTRK3* (*ETV6* - neurotrophic receptor tyrosine kinase 3), also described in other cancers including breast and thyroid[93-97], *DNTT-BLNK* (DNA nucleotidylexotransferase - B-cell linker) as well as *ZYMY2-FLT3* (Zinc Finger MYM-Type Containing 2 – *FLT3*)[67]. The *FLT3* internal tandem duplication (ITD) commonly observed in AML, has also been identified in a Ph-like ALL setting[64].

Table 1.3 – Other classes of kinase alterations identified in Ph-like ALL.

Adapted from Roberts 2017[60]

Other signalling mechanisms	Number of fusion partners	Fusion partner genes	Potential TKI	Type of alteration	Method of identification
NTRK3	1	*ETV6*	TRK inhibitor	In-frame fusion	RT-PCR Transcriptome sequencing
FLT3	1	*ZMYM2*	FLT3 inhibitor	In-frame fusion	RT-PCR Transcriptome sequencing
FGFR1	1	*BCR*	FGFR inhibitor	In-frame fusion	RT-PCR Transcriptome sequencing
BLNK	1	*DNTT*	Unknown	In-frame fusion	RT-PCR Transcriptome sequencing

Abbreviations: *BCR*: Breakpoint cluster region, RhoGEF and GTPase activating protein; *BLNK*: B-cell linker; *DNTT*: DNA nucleotidylexotransferase; *ETV6*: ETS variant 6; *FGFR1*: fibroblast growth factor receptor 1; *FLT3*: fms related tyrosine kinase 3; *NTRK3*: neurotrophic receptor tyrosine kinase 3; *ZMYM2*: zinc finger MYM-type containing 2

Mutations in Ras signalling pathways have also been implicated in Ph-like ALL, including *KRAS* and *NRAS* mutations, which have been identified in other malignancies[98-101]. *RAS* mutations are becoming increasingly important because in Ph-like ALL, 4% of cases possess Ras activating mutations including *KRAS*, *NRAS*, *NF1*, *PTPN11*, and *CBL*, which often predominate in relapsed leukaemic clonal cells[39,60,62]. In normal cells, controlled expression of RAS activates the mitogen-activated protein kinase (MAPK) and phosphoinositide 3-kinase / mammalian target of rapamycin / protein kinase B (PI3K/mTOR/AKT) signalling pathways, leading to cell growth and survival. In cancer however, mutations in this pathway results in uncontrolled cellular division and disease[102,103].

Also involved in the regulation of Ras signalling, *NF1* is a tumour suppressor gene which encodes neurofibromin 1, a negative regulator of RAS. Loss of *NF1* has been associated with a risk of developing certain cancers (i.e. melanoma, breast cancer, etc.)[104-106]. *PTPN11* encodes for SHP-2, a protein essential for the regulation of RAS/MAPK signalling pathway and mutations of *PTPN11* have been reported in juvenile myelomonocytic leukaemia, myeloproliferative disorders and ALL[107-109]. Mutations in *RAS* have therefore been associated with poorer prognosis and the availability of MEK inhibitors (i.e. trametinib and selumetinib) that target downstream RAS signalling pathways, has been shown to be a promising therapeutic strategy[110,111].

1.2.4. Summary of Alterations in Ph-like ALL

Ph-like ALL is therefore a complex high-risk B-ALL subtype and with advances in next generation sequencing approaches (i.e. RNA-seq and WGS), the underlying alterations that drive this disease are now better defined. A schematic diagram of the 3 main classes described is depicted in **Figure 1.3**, where an overview of the downstream mechanisms is presented. Alterations in any of these pathways can contribute to a dysregulated downstream regulation of B-cell proliferation, survival and growth which ultimately results in an accumulation of leukaemic blast cells and presentation of disease. Hence, identifying suitable treatment approaches to target these pathways is vital for improved treatment of Ph-like ALL.

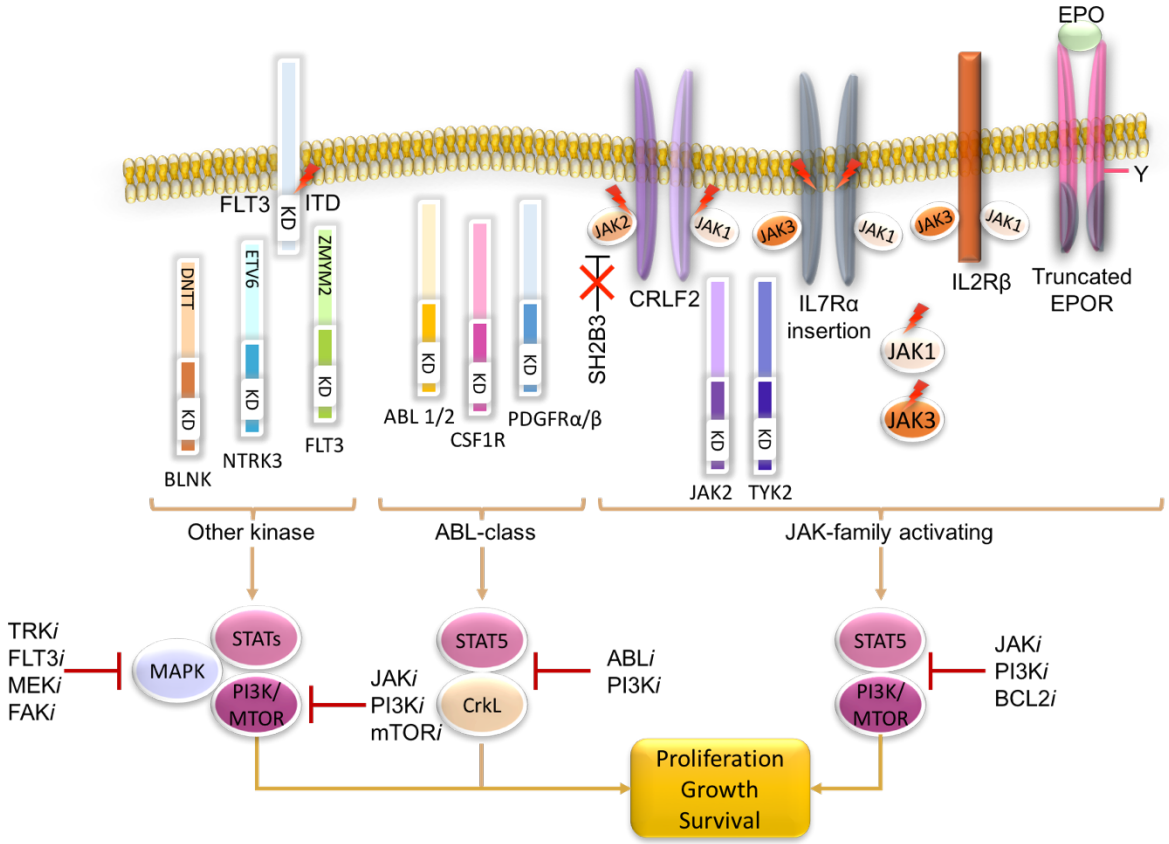


Figure 1.3 – Representation of types of pathways that may alter in Ph-like ALL.

This schematic diagram represents the major alterations involved in Ph-like ALL, including the Abl-class, Jak-family and other kinases involved, all converging into pathways that ultimately affect cell proliferation, growth and survival. Red lightning bolt represents activating mutations that can occur. KD: kinase domain; *BLNK*: B-cell linker, *NTRK3*: neurotrophic receptor tyrosine kinase 3; *FLT3*: fms related tyrosine kinase 3; ITD: internal tandem duplications; *SH2B3*: *SH2* B domain adapter protein 3; MEK: mechanistic target of rapamycin; mTOR: mammalian target of rapamycin *TYK2*: non-receptor tyrosine-protein kinase; FAK*i*: focal adhesion kinase inhibitor; *BCL2*: B-cell lymphoma 2. Adapted & modified from Roberts *Best Pract Res Clin Haematol* 2017[60] and Iacobucci & Mullighan *JCO* 2017[39]

1.3. Therapeutic Options in High-risk ALL

1.3.1. Chemotherapy in Acute Lymphoblastic Leukaemia

Most subtypes of ALL are currently treated with chemotherapy[112,113]. Chemotherapeutic regimes vary with respect to the type of ALL and severity of disease. Treatment for ALL can currently be stratified as 3 main stages: remission-induction, intensification (or consolidation) and continuation (or maintenance) therapy[112,113].

The remission-induction step aims to eradicate leukaemic cells with maximum efficiency. Here, patients are administered chemotherapy (e.g. vincristine, asparaginase, anthracycline) along with glucocorticoids (e.g. prednisolone, dexamethasone) as initial therapy. High-risk patients are typically prescribed a combination of four or more drugs[112,113].

Remission-induction is followed by the intensification (consolidation) stage, which aims to remove residual leukaemic cells[10,114]. This treatment may comprise of high dose methotrexate (an antifolate drug inhibiting DNA synthesis)[115] and/or vincristine/prednisolone[113], depending on the regimen. Allogeneic haematopoietic stem cell transplantation (HSCT) may be prescribed as alternative treatment, particularly in children and adults with very high-risk ALL[112,116]. HSCT involves the transplantation of cells from a matched related donor, matched unrelated donor or cord blood, and provides possible long-term disease-free survival [113].

The third phase of treatment (continuation/maintenance) lasts for approximately 2 years and is aimed of reducing recurrence of leukaemia. This therapy consists of weekly methotrexate and daily doses of mercaptopurine (an immunosuppressant)[116,117]. Along with the three main forms of treatment, central

nervous system (CNS) prophylaxis may be introduced to prevent any metastasis of leukaemic cells into the brain or nervous system[118].

Despite chemotherapy being effective at eradicating highly proliferative malignant cells, unlike small molecular inhibitors which can target specific pathways in cancer, chemotherapy lacks targeted efficacy. Chemotherapy is a highly aggressive form of therapy, often affecting normal cells that proliferate rapidly such as the hair and intestinal lining. Other complications of chemotherapy also include cardiac toxicity, suppression of the immune system, development of hypersensitivity to therapy (i.e. E.coli *L*-asparaginase)[119], vascular necrosis of the bone, neurocognitive impairment, impaired fertility[120] and endocrine complications[121,122].

In a Ph-like ALL / *BCR-ABL1*-like setting, therapeutic resistance to certain chemotherapeutic regiments have been observed[58]. In 2009, Den Boer and colleagues reported that *BCR-ABL1*-like ALL cells were found to be 73 times more resistant to L-asparaginase (p=0.001) and 1.6 times more resistant to daunorubicin (p=0.017) compared to other subtypes of precursor B-ALL[58]. The authors also noted no differences between the sensitivity of *BCR-ABL1*-like ALL and Ph+ ALL to vincristine and prednisolone, emphasising a need for better treatment approaches (i.e. more intensified therapy, or, precision medicine)[58].

1.3.2. Use of Tyrosine Kinase Inhibitor (TKI) as Targeted Therapy

To evade clinical relapse as a result of chemotherapeutic resistance, TKIs have been rationally designed and widely applied in the treatment of Ph+ neoplasms. As a form of targeted therapy, TKIs have revolutionised the way patients are treated in CML and Ph+ ALL. Imatinib (STI571/Glivec; **Figure 1.4)**, is a rationally designed first-generation TKI developed to overcome the Bcr-Abl oncoprotein[123,124]. Imatinib is a competitive inhibitor of Bcr-Abl, and functions by stabilising the inactive conformation of the adenosine triphosphate (ATP) binding site (known as the Asp-Phe-Gly-out; DFG-out conformation)[125] in the Abl kinase domain. This in turn results in an inhibition of downstream Bcr-Abl tyrosine kinase activity[126,127], affecting the activation of downstream PI3K and MAPK cell survival/growth pathways, in the presence of TKI[55]. TKIs are also known to have minimal adverse-effects (most common being nausea and diarrhoea)[128]. With remission rates averaging above 90% at 1 month after therapy, TKI-inhibition of the fusion protein is known to be effective in eradicating Ph+ cells, however, to a certain extent[114,129].

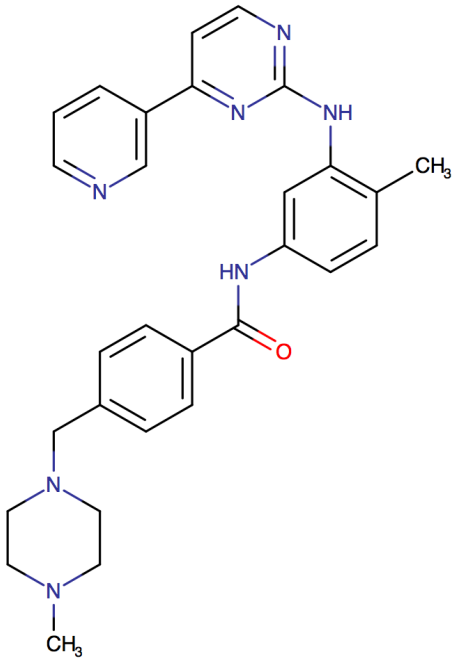


Figure 1.4 – Molecular structure of imatinib (STI-571; Glivec).

Chemical formula: $C_{29}H_{31}N_7O$. Molecular weight: 493.6027 g/mol. Molecular structure derived from DrugBank.ca[130]

The development of imatinib as a form of targeted therapy in inhibition of Abl kinase has enabled further generation of targeted therapies for other kinases, such as Jak[131]. Ruxolitinib (**Figure 1.5**) was the first FDA-approved Jak inhibitor[132], designed as a form of targeted therapy in myeloproliferative neoplasms (MPN), including polycythaemia vera (PV), primary myelofibrosis (MF) and essential thrombocytopenia (ET)[133]. In MPN, the well-described *JAK2*-V617F point mutation in the pseudokinase (autoinhibitory/regulatory) domain of Jak2[134-136] have been associated with spontaneous downstream Stat5 activation and subsequent disease[137].

Ruxolitinib was designed to inhibit the Jak2 kinase domain[132,138-140] and has been demonstrated to be highly effective and selective (inhibiting Jak1 and Jak2 at 3.3 and 2.8 nM respectively, compared to 323nM in Jak3)[141] with low levels of toxicity[142,143]. The exact binding structure of ruxolitinib to Jak is unknown, however recent studies of a prototypical system using c-Src suggests that it competitively binds to the active conformation of Jak, as a type I inhibitor[144]. Clinical trials for ruxolitinib in the dynamics of chronic and acute leukaemias are currently in progress[145,146].

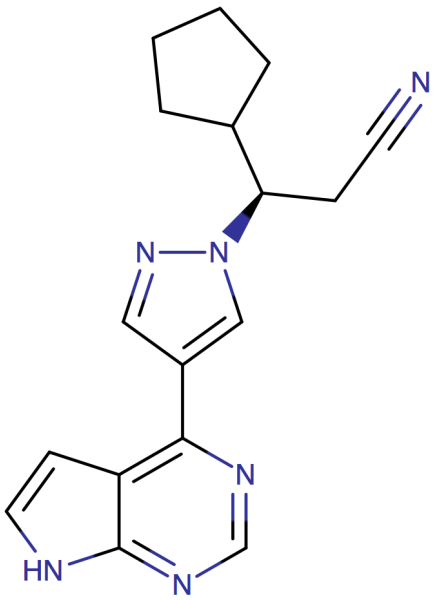


Figure 1.5 – Molecular structure of ruxolitinib (INCB-018424; Jakafi).

Chemical formula: $C_{17}H_{18}N_6$. Molecular weight: 306.365 g/mol. Molecular structure from DrugBank.ca[130]

In 2012, Roberts *et al*. discovered that Ba/F3 pro-B and Arf-/- pre-B cells transduced with *ABL*-class fusion genes first identified in Ph-like ALL responded favourably to the Abl kinase inhibitors imatinib and dasatinib, while cells transduced with a *BCR-JAK2* fusion were sensitive to ruxolitinib[64]. Subsequently in 2014, additional kinase alterations identified in Ph-like ALL were also shown to be targetable by currently available TKIs. In this study, cytokine-dependent Ba/F3 cells transformed with *ABL1*, *JAK2* and fusion genes involving other kinase pathways (i.e. *NTRK3*), resulted in cytokine independent survival and growth. These cells were however sensitive to TKIs, responding to dasatinib (Abl fusion), ruxolitinib (Jak fusion) and crizotinib (*NTRK3* fusion)[73]. Taken together, these indicate a promising approach for potential use of TKI-therapy and the value of modelling resistance in a Ph-like ALL setting.

1.3.3. Anecdotal Use of TKI in Ph-like ALL

Although Abl TKIs are presently used for the treatment of Ph+ ALL, their use in the Ph-like ALL setting has largely been anecdotal[90,91]. Ph-like ALL fusions involving *ABL* and *JAK*-class signalling are amenable to TKI therapy, with clinical trials involving dasatinib and ruxolitinib with chemotherapy recently initiated[147-149].

Anecdotally, clinical cases have demonstrated potential for TKI-use in treatment of Ph-like ALL, wherein patients with an *EBF1-PDGFRβ* fusion were administered imatinib, resulting in successful therapy evidenced by the reduction of blast counts, downregulation of *EBF1-PDGFRβ* expression[90,91] and the achievement of clinical remission [90].

TKI-use has also been documented in a 10-year-old paediatric patient whose leukaemic cells harboured the *ATF7IP-PDGFRβ* Ph-like ALL fusion. Initial

conventional therapy appeared ineffective, hence the patient was prescribed dasatinib as monotherapy. Three months after administration of dasatinib, PCR analysis revealed no evidence of disease. The patient maintained complete molecular remission for at least 12 months, suggesting that targeted TKI therapy during initial presentation of disease may promote treatment efficacy[150].

Taken together, these studies describe the potential for use for TKIs in precision medicine of Ph-like ALL. With targeted therapy, however, treatment resistance may arise. The following section further explores the mechanisms underpinning TKI-resistance, which will be a hallmark concept of this thesis.

1.4. TKI-resistance

1.4.1. Mechanisms of TKI-resistance in Abl kinase

Despite the promising use of TKIs and use of imatinib as the first TKI rationally-designed against Bcr-Abl, clinical responses in Ph+ ALL are brief, and resistance remains a common problem[14,151,152]. In CML, resistance is caused by a number of primary ('refractoriness' at the start of therapy) or secondary ('acquired resistance' after an initial response to treatment) resistant factors[153,154].

TKI-resistance is frequently caused by the presence of point mutations in the *ABL1* kinase domain, encoding mutations such as the *ABL1*-E255K, *ABL1*-Y253H and *ABL1*-T315I[155,156] (**Figure 1.6**). These mutations result in changes within the ATP-binding domain, leading to an abrogation of drug-binding and inhibition of downstream cellular survival and proliferation signals[124,153,157,158].

Other mechanisms of imatinib-resistance include overexpression of the fusion oncoprotein, or, presence of P-loop mutations that commonly reduce imatinib drug-binding[159,160]. Alterations in drug transport mechanism, namely a decrease in drug influx transporter OCT-1 (organic cation transporter, member 1), increase in drug efflux transporters ABCB1 (ATP-binding cassette, sub-family B, member 1) or ABCG2 (ATP-binding cassette, sub-family G, member 2) expression may also decrease intracellular concentrations of the TKI, reducing optimal drug efficacy[161-164].

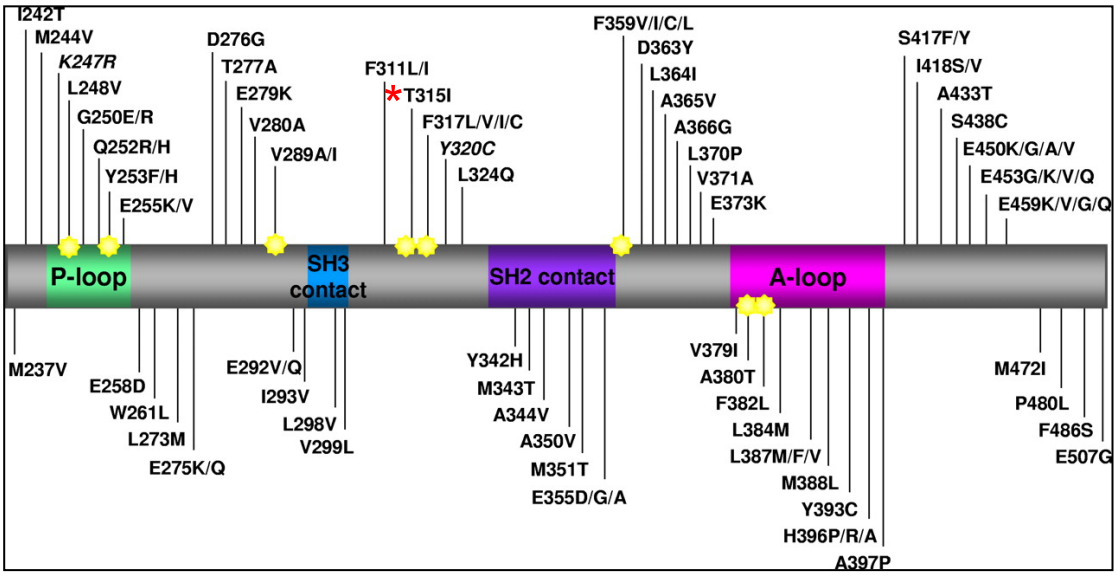


Figure 1.6 – Mutations in the Abl kinase domain of *BCR-ABL1* in CML patients treated with TKIs

These mutations are caused by amino acid substitutions that alter conformation of the drug-binding pocket, leading to the inability/reduction of imatinib drug binding and subsequent TKI resistance. Yellow stars indicate the amino acid residues predicted in imatinib-binding. The gatekeeper *ABL1*-T315I mutation is indicated with a red asterisk (*). P-loop: phosphate binding loop; SH2 contact and SH3 contact: contact regions with SH2 and SH3 domain-containing proteins; A-loop: activation loop. Adapted from Soverini *et al*., *Blood* 2011[165]

Second-generation Abl-kinase inhibitors have been designed to overcome imatinib-resistance[166]. These include nilotinib and dasatinib (**Figure 1.7**) that in *in vitro* studies are 20 and 325-fold more potent compared to imatinib, respectively[167]. Like imatinib, nilotinib binds to the inactive conformation of the Abl kinase, however, the slight difference in molecular structure (the condensed trifluoromethyl/imidazole phenyl group in nilotinib, compared a bulkier *N*-methylpiperazine in imatinib) allows for better selectivity and efficacy at well-tolerated doses[166,168,169].

Nilotinib also targets the Abelson-related gene kinase Arg (transcribed by the *ABL2* gene), Pdgfrβ and the Ephrin type-B receptor 4 precursor (EPHB4)[166]. In Bcr-Abl, the presence of certain kinase-domain mutations (i.e. *ABL1*-Y253H, *ABL1*-E255K and *ABL1*-E255V) a higher concentration of nilotinib is required in order to overcome these mutations[167,170].

Dasatinib is a highly potent inhibitor of Abl and Src family of tyrosine protein kinases[171]. Unlike imatinib and nilotinib, dasatinib inhibits Bcr-Abl *in vitro* and *in vivo* by preferentially binding to the active conformation of the Abl kinase domain[172,173]. The difference in drug-binding ('DFG-out' catalytically inactive motif in imatinib/nilotinib binding of Abl, in contrast to 'DFG-in' active conformation of Abl in dasatinib drug binding), enables dasatinib to overcome point mutations resistant to imatinib/nilotinib, that are present in the P-loop of the Abl kinase[172,173].

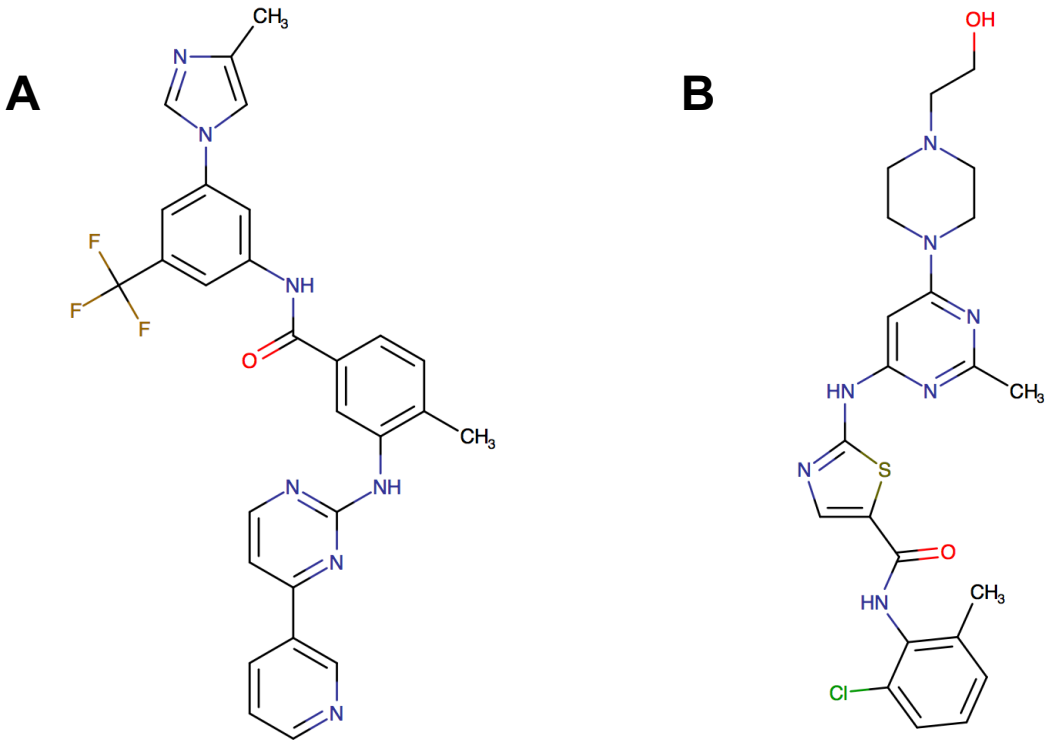


Figure 1.7 – Molecular structures of second-generation Abl-kinase inhibitors nilotinib and dasatinib.

A: Nilotinib (AMN-107; Tasigna); chemical formula: $C_{28}H_{22}F_3N_7O$; molecular weight: 529.5158 g/mol. **B**: Dasatinib (BMS-354825; Sprycel). Chemical formula $C_{22}H_{26}ClN_7O_2S$; Molecular weight: 488.006 g/mol. Molecular structures derived from DrugBank.ca[130]

Second-generation Abl-class TKIs may be effective at overcoming most point mutations (depending on binding site and efficacy), however, the *ABL1*-T315I mutation remains a clinical issue, resulting in poor outcome and relapse[174,175]. The likelihood of developing this mutation is further increased in advanced-phase CML and Ph+ ALL[176]. The *ABL1*-T315I mutation is caused by the base pair substitution of cytosine to thymine, resulting in the amino acid substitution of threonine to isoleucine at codon position 315 in the Abl protein[174,177]. First and second generation TKIs form a critical bond with the threonine at position 315, which is negated by the presence of the large isoleucine amino acid[174,177-179]. This substitution of threonine to isoleucine forms a stearic hindrance in the hydrophobic binding pocket where first and second generation TKIs would usually bind[177]. The *ABL1*-T315I mutation is currently resistant to all TKIs except ponatinib (**Figure 1.8**)[180-182]. Ponatinib overcomes the bulky stearic hindrance of *ABL1*-T315I by possessing a novel triple-bond linkage, allowing it to fit between the bulky isoleucine residue at position 315[178,183,184]. However, ponatinib resistance still occurs, through the development of compound mutations that decrease ponatinib drug binding, as well as through the activation of alternative signalling pathways such as Axl[185,186].

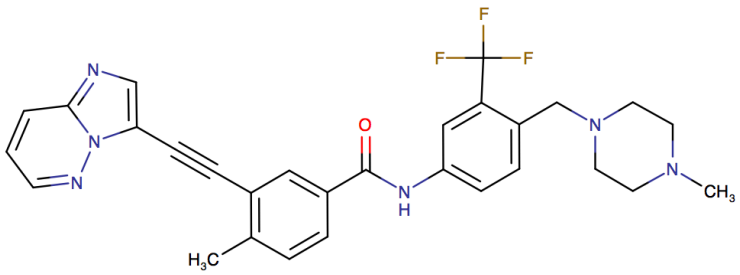


Figure 1.8 – Molecular structure of ponatinib (AP-24534; Iclusig).

Chemical formula: $C_{29}H_{27}F_3N_6O$; Molecular weight: 532.5595 g/mol. Molecular structure from DrugBank.ca[130]

Despite the availability of targeted therapy, drug resistance leading to relapse therefore remains a significant problem in Ph+ neoplasms, where TKIs are commonly applied[161,187,188]. Such evidence of TKI-relapse is also noted in other studies, whether patients were administered TKIs as a form of first-line therapy (**Table 1.4**), or following relapse after prior chemotherapy (**Table 1.5**)[189].

Although the use of Abl TKI therapy appears to be a promising approach in Ph-like ALL (as discussed above in section **1.3.3**), the mechanism of resistance in a Ph-like setting is not well-studied. Therefore, the development of treatment-resistant models of Ph-like ALL is imperative for the elucidation of therapeutic failure, which will be a central issue discussed in this thesis.

Table 1.4 – Clinical studies of TKI as first-line therapy in the treatment of Ph+ ALL. Patients were administered imatinib, nilotinib or dasatinib in-combination with chemotherapy upon diagnosis of Ph+ ALL. TKI induced complete haematological and cytogenetic responses for a minimum of 2 years, prior to subsequent relapse.

Study	Therapy	*n*	Response	Outcomes
Thomas 2004[190], 2008[191]	imatinib + chemotherapy (hyper-CVAD)	54	CHR-93% CMR-52%	3 yr DFS- 62% 3 yr OS -55%
Yanada 2006[192], 2008[193]	imatinib + chemotherapy (JALSG ALL202)	80	CHR-96%. CMR-71%	2 yr DFS-48.5% 2 yr OS -58.1%
Foa 2008[194]	dasatinib induction monotherapy	36	CHR-100%	OS 100% with 8.6 mth follow-up
Ravandi 2010[195]	dasatinib + chemotherapy (hyper-CVAD)	20	CHR-90% CCyR-82% CMR-47%	1 yr DFS- 48% 1 yr OS -74%

CHR: complete haematological response; CCyR: complete cytogenetic response; CMR: complete molecular response; DFS: disease-free survival; OS: overall survival. Adapted and modified from Gruber *et al*. *BJH* 2009[189]

Table 1.5 – Clinical studies of TKI treatment in Ph+ ALL following relapse to prior therapy. Patients were administered imatinib, nilotinib or dasatinib as a form of monotherapy upon relapse of Ph+ ALL. Although TKI induced complete haematological and cytogenetic responses, relapse is evident.

Study	Therapy	*n*	Response	Outcomes
Talpaz 2006[196]	dasatinib	10	CHR-70% MCyR-60% CCyR -30%	90% relapse med 4 m
Ottmann 2007[197] Porkka 2008[198]	dasatinib	46	CHR-35% MCyR-56% CCyR -54%	PFS 3.3 m 24 m OS-31%
Giles 2012[199]	nilotinib	31	CHR: 21% MCyR: 52% CCyR: 32%	OS 7.9 m 1 yr DFS – 35% 2 yr DFS – 10%

CHR: complete haematological response; CCyR: complete cytogenetic response; CMR: complete molecular response; DFS: disease-free survival; MCyR, major cytogenetic response; OS: overall survival. Adapted and modified from Gruber *et al*. *BJH* 2009[189]

1.4.2. Mechanisms of TKI-resistance in Jak kinase

Despite the effectiveness of ATP-competitive Jak inhibitors in overcoming cells harbouring the constitutively active *JAK2*-V617F mutation (pseudokinase JH2 domain of Jak2), the acquisition of point mutations in the kinase (JH1) domain can however lead to TKI resistance. Studies have demonstrated reduced binding of type I ATP-competitive inhibitors (i.e. ruxolitinib, BMS-911543, etc.) to cells expressing the *JAK2*-E864K, *JAK2*-Y931C and *JAK2*-G935R mutations[200-202].

In a study performed by Koppikar and colleagues[203], chronic exposure of cells to ruxolitinib was found to result in an increased stabilisation of the active Jak2 isoform (ruxolitinib binds to the active Jak2 conformation). This was accompanied by epigenetic changes, where increased H3K4me3 (a histone modification associated with active promoter transcription) was observed. The authors demonstrated that this leads to a further increase of *JAK2* mRNA and Jak2 protein expression, enabling heterodimerisation and transphosphorylation of Jak2 by its binding partners (i.e. Jak1 and Tyk2) and subsequent reduction in ruxolitinib sensitivity[203].

1.4.3. Case of TKI relapse in Ph-like ALL

In a clinical observation by Yeung *et al*, an 81-year-old patient diagnosed with Ph-like ALL was found to have the *ETV6-ABL1* fusion (detected via low-density array, DNA analysis and fluorescence *in situ* hybridisation)[92]. Further phosphoflow analysis determined cells to be sensitive to the Abl-TKI dasatinib, which was subsequently administered to the patient in-addition to chemotherapy. This led to a period of remission that lasted for approximately 9 months, prior to relapse. Subsequent analysis detected the presence of an *ABL1*-T315I kinase domain mutation, leading to a switch of therapeutic regime to ponatinib (a third-generation

Abl TKI) in-combination with high-dose dexamethasone and vincristine, to overcome the *ABL1*-T315I mutation. This treatment was efficacious for approximately 4 weeks, before *ABL1*-T315I was again detected, at which time the patient was palliated.

1.5. Concluding Remarks

Current literature provides an overview of the genomic alterations known in B-ALL, and the employment of modern next-generation sequencing (i.e. WGS, RNA-seq, etc.) has enabled the identification of a subtype termed 'Ph-like' ALL. Ph-like ALL, also known as *BCR-ABL1*-like ALL, has a similar gene expression profile as Ph+ ALL, where high frequencies of *IKZF1* deletions were also observed[20,65]. Further research into the genomic landscape of Ph-like ALL uncovered the presence of alterations involving cytokine and kinase-activating gene fusions, which are targetable by currently-available TKIs[64,73,204]. Presently, studies have shown that these fusion kinases are sensitive to clinically-available TKI *in vitro* and *in vivo*[73,98,204,205].

From studies of TKI-therapy in Ph+ neoplasms, however, relapse due to TKI-resistance remains a major issue. As the incorporation of TKI-therapy in Ph-like ALL appears to be a promising approach and clinical trials for targeting Ph-like ALL using currently-available therapies are currently in process[146,148,149], it is therefore highly important that we identify and understand the potential modes of resistance that can occur. This is because treatment resistance can vary between patients, depending on the kinase and TKI of choice. Therefore, an urgent need to identify and understand the mechanisms of TKI-resistance exists. This is critical for an ultimate purpose of overcoming and averting future relapse in a clinical setting.

This PhD thesis will therefore discuss the findings of *in vitro* modelling of various modes of TKI-resistance in high-risk Ph+ ALL (using an immortalised Ph+ ALL human cell line, SUP-B15) and Ph-like ALL (using fusion genes identified in Ph-like ALL patients, molecularly transformed into Ba/F3 pro-B lymphocytes). The discoveries in this thesis will significantly inform the mechanisms of TKI-resistance

that can potentially be implicated in clinics, providing knowledge which will be key towards contribution of future drug development for a high-risk cancer that currently lacks optimal therapy.

1.6. Research Hypothesis

I hypothesise that long-term exposure of Ph+ and Ph-like ALL cells to tyrosine kinase inhibitor targeted therapy will lead to the development TKI-resistance in a certain proportion of patients. This will be due to the selection for cells harbouring kinase domain alterations, historically known to affect drug-binding. As high-risk ALL is an aggressive disease, TKI-resistance in this setting will also be driven by alternative mechanisms of cell survival signalling, that are imperative towards the acquisition of highly-resistant cancer cells.

1.7. Research Aims & Objectives

Aim 1: To generate dasatinib and ponatinib-resistant SUP-B15 Ph+ ALL cell lines

Aim 2: To model Ba/F3 Ph-like ALL by retrovirally-transducing cells to express the patient-derived *RANBP2-ABL1* and *SSBP2-CSF1R* fusion genes

Aim 3: To generate TKI-resistance in Ba/F3 *RANBP2-ABL1*, *SSBP2-CSF1R* and *PAX5-JAK2* Ph-like ALL cell lines using the clinically-available TKIs imatinib, dasatinib, ponatinib (for *ABL1*/*CSF1R* fusions) and ruxolitinib (for *JAK2* fusion).

Aim 4: To identify and characterise canonical/noncanonical mechanisms of TKI-resistance using NGS (mRNA-seq) and bioinformatics approaches

CHAPTER 2 –

MATERIALS & METHODS

2.1. Commonly Used Reagents & Buffers

Table 2.1 – Common reagents

Category	Reagent	Supplier	Catalogue No.
General Chemicals	Acetic acid	Sigma-Aldrich	#320099 – 2.5 L
	CellTiter 96® AQ_{ueous} One Solution Cell Proliferation Assay (MTS)	Promega	G3582
	CellTiter-Blue® Cell Viability Assay	Promega	G8080
	DC™ Protein Assay Kit	Bio-Rad	#5000112
	Dulbecco's phosphate-buffered saline (DPBS) (10X), no calcium, no magnesium	Gibco	#14200-075
	Ethanol	Merck Millipore	#6-10107-2511
	Glycerol	Univar	#242 – 500 mL
	Glycine	Sigma-Aldrich	G8898 – 1 kg
	Hydrochloric acid (HCl, 35%)	Fisher Scientific	# 1100
	Isopropanol	Merck Millipore	#6-10224.2511
	Methanol	Chem-Supply	MA004-P
	Sodium chloride	Univar	#465 – 2.5 kg
	Tris (hydroxymethyl) aminomethane	Sigma-Aldrich	#252859 – 500 g
	β-mercaptoethanol	Aldrich	M6250 – 100 mL
Cell Culture Reagents	Fetal bovine serum (FBS), USA	Bovogen Biologicals Pty Ltd	SFBS-U
	Dimethyl sulfoxide	Merck Millipore	#1.02952.2500
	Dulbecco's Modified Eagle's Medium (DMEM)	Sigma-Aldrich	D5671
	Iscove's Modified Dulbecco's Medium (IMDM)	Sigma-Aldrich	I3390
	L-glutamine 200 mM	Sigma-Aldrich	G7513
	Lymphoprep	Axis Shield. Oslo Norway	#1114547
	Newborn Calf Serum (NCS)	Sigma-Aldrich	#13023C
	Penicillin/Streptomycin	Sigma-Aldrich	P4333 – 100 mL
	Roswell Park Memorial Institute (RPMI) 1640 Medium	Sigma-Aldrich	R0883
	Trypan blue 0.4%	Gibco	#15250-061, 100 mL
Flow Cytometry Assay	16% Paraformaldehyde, EM grade	Electron Microscopy Sciences	#15710

Category	Reagent	Supplier	Catalogue No.
Flow Cytometry Assay	7-Aminoactinomycin D (7AAD)	Life Technologies	A1310
	Annexin V Binding Buffer, 10X concentrate	BD Pharmingen	#556454
	Annexin-V-PE	BD Biosciences	#556421
	Calcium Chloride	Sigma-Aldrich	C1016 – 500 g
	Hanks' Balanced Salt solution (HBSS)	Sigma-Aldrich	H9394
	HEPES solution, 1 M, pH 7.0-7.6	Sigma-Aldrich	H0887
Reagents for SDS-PAGE / Western Blotting	0.1% bromophenol blue	Sigma-Aldrich	#114391
	10% Criterion™ TGX Stain-Free™ Protein Gel, 12+2 well, 45 µl	Bio-Rad	#5678033
	4–15% Criterion™ TGX™ Precast Midi Protein Gel, 18 well, 30 µl	Bio-Rad	#5671084
	40% Acrylamide/Bis Solution, 37.5:1	Bio-Rad	#1610148
	Ammonium Persulfate (APS)	Sigma-Aldrich	A9164
	BenchMark Prestained Protein Ladder	Invitrogen	#10748-010
	Bovine serum albumin	Sigma-Aldrich	A9418
	cOmplete™ Mini EDTA-Free Protease Inhibitor Cocktail Tablets	Roche	#04693159001
	Enhanced Chemifluorescence (ECF)™ Substrate for Western Blotting	GE Healthcare Amersham	#45-000-097
	Halt™ Phosphatase Inhibitor Cocktail	Thermo Fisher Scientific	#78420
	Ponceau S	Sigma-Aldrich	P3504 – 10 g
	Precision Plus Protein™ Kaleidoscope	Bio-Rad	#161-0375
	PVDF Immobilon®-P Membrane, 0.45 µm	Merck Millipore	IPVH00010
	SDS (Sodium Dodecyl Sulphate)	Sigma-Aldrich	L4509
	Sodium fluoride	Sigma-Aldrich	S7920
	Sodium (ortho) Vanadate (Na_3VO_4)	Sigma-Aldrich	S6508
	TEMED (N,N,N′,N′-Tetramethylethylenediamine)	Sigma-Aldrich	T7024
	Trans-Blot® Turbo™ RTA Midi LF PVDF Transfer Kit	Bio-Rad	#1704275
	Triton™ X-100	Sigma-Aldrich	T8532
	Tween-20	Sigma-Aldrich	P2287 – 500 mL
	Western blot recycling stripping buffer (10x)	Alpha Diagnostic International	#90101
	Whatman® cellulose chromatography papers	Thermo Scientific	WHA3030-917

Category	Reagent	Supplier	Catalogue No.
Genomics	100bp DNA Ladder	New England Biolabs	N3231s
	10x Blue Juice (Gel Loading Buffer)	Invitrogen	#10816-015
	1kb DNA ladder	New England Biolabs	N3232S
	6x DNA Loading Dye	Fermentas	R0611
	Agarose	Sigma-Aldrich	A6013 – 500 g
	AmpliTaq Gold DNA Polymerase	Thermo Fisher Scientific	N8080241
	Chloroform	Merck Millipore	#100776B
	Deoxynucleotide Set, 100 mM	Sigma-Aldrich	DNTP100-1KT
	DNA hydration solution	Qiagen	#158914
	EDTA Disodium Salt	Univar	AJA180 – 100 g
	ExoSAP-IT	Affymetrix	P/N 78201
	Expand Long Template PCR System	Roche	#11681834001
	Gel Loading Dye, Purple (6x), no SDS	New England Biolabs	B7025S
	GelRed™ Nucleic Acid Stain	Biotium	#41002
	Glycogen for molecular biology	Roche	#10 901 393 001
	Nuclease-free water (NF-H_2O)	Qiagen	#129117
	Paraformaldehyde powder, 95%	Fluka	#76240
	Phusion High-fidelity DNA Polymerase	New England Biolabs	M0530L
	Proteinase K	Roche	#03115887001
	Quantitect Reverse Transcription Kit	Qiagen	#205313
	RNAse A	Qiagen	#19101
	RT² SYBR® Green qPCR Mastermix	Qiagen	#330503
	TRIzol® reagent	Life Technologies	#15596-018
	Ultrapure™ Buffer Saturated Phenol	Invitrogen	#15515-039
	UltraPure™ Phenol:Chloroform:Isoamyl alcohol (25:24:1, v/v)	Invitrogen	#15593-031
Molecular Cloning	Ampicillin	Sigma-Aldrich	A5354
	DNA Polymerase I, Large (Klenow) Fragment	New England Biolabs	M0210S
	Kanamycin Sulfate	Gibco	#15160-054
	HindIII	New England Biolabs	R0104S
	Luria Broth Base (Miller's LB Broth Base®)	Invitrogen	#12795-084
	Not1	New England Biolabs	R0189S

Category	Reagent	Supplier	Catalogue No.
Molecular Cloning	Polybrene®	Santa Cruz Biotechnology	sc-134220
	Select Agar™	Invitrogen	#30391-023
	Shrimp Alkaline Phosphatase (rSAP)	New England Biolabs	M0371S
	SnaB1	New England Biolabs	R0130S
	Spe1	New England Biolabs	R0133S
	Subcloning Efficiency™ DH5α™ Competent Cells	Thermo Fisher Scientific	#18265017
	T4 DNA Ligase	New England Biolabs	M0202
	UltraClean 15 DNA Purification Kit	Mo Bio Laboratories, Inc.	#12100-300
	XbaI	New England Biolabs	R0145

Table 2.2 – List of Western blotting antibodies

Target	Antibody	Molecular Weight (kDa)	Species	Dilution	Cat #	Supplier
Abl Kinase Signalling	CrkL (c-20)	39	Rabbit	1:2000	sc-319	Santa Cruz
	Phospho-c-Abl (Y245)	135 (c-Abl); 190 (Bcr-Abl p190); 220 (Ranbp2-Abl1)	Rabbit	1:2000	#2861	Cell Signaling Technology
	Anti-Abl (c-, v-, Bcr-) clone 24-21	135 (c-Abl); 190 (Bcr-Abl p190); 220 (Ranbp2-Abl1)	Mouse	1:2000	MABT203	Merck Millipore
Jak/Stat Pathway	phospho-Stat5 (Y694)	90	Rabbit	1:2000	#9359	Cell Signaling Technology
	Stat5	90	Rabbit	1:2000	#9363	Cell Signaling Technology
	phospho-Jak2 (Tyr1007/1008)	125	Rabbit	1:2000	#3771	Cell Signaling Technology
	Jak2	125	Rabbit	1:2000	#3230	Cell Signaling Technology
PI3K/MAPK Pathway	p-Akt (Ser473)	60	Rabbit	1:2000	#9271	Cell Signaling Technology
	Akt	60	Rabbit	1:2000	#9272	Cell Signaling Technology
	p-Erk1/2 (p42/444 MAPK)	42/44	Rabbit	1:2000	#9101	Cell Signaling Technology
	Erk1/2	42/44	Rabbit	1:2000	#9102	Cell Signaling Technology
M-CSFR	Phospho-M-CSF Receptor (Tyr723) (49C10)	91 (SSBP2-CSF1R)	Rabbit	1:2000	#3155	Cell Signaling Technology
	Anti-MCSF Receptor	91 (SSBP2-CSF1R)	Rabbit	1:2000	ab37858	Abcam
RanBP2	RanBP2	358 (endogenous) 220 (Ranbp2-Abl1)	Rabbit	1:2000	PA1-082	Thermo Fisher Scientific
Cell Death Signalling	PARP	89, 116	Rabbit	1:2000	#9542	Cell Signaling Technology
	Cleaved PARP (Asp214) (D64E10) XP®	89	Rabbit	1:2000	#5625	Cell Signaling Technology

Target	Antibody	Molecular Weight (kDa)	Species	Dilution	Cat #	Supplier
Cell Death Signalling	Caspase-3	17, 19, 35	Rabbit	1:2000	#9662	Cell Signaling Technology
	Cleaved Caspase-3 (Asp175)	17, 19	Rabbit	1:2000	#9661	Cell Signaling Technology
Loading Control	β-actin (13E5)	45	Rabbit	1:2000	#4970	Cell Signaling Technology
	GAPDH (14C10)	37	Rabbit	1:2000	#2118	Cell Signaling Technology
	β-tubulin (9F3)	55	Rabbit	1:2000	#2128	Cell Signaling Technology
Secondary Antibodies	goat anti-rabbit IgG-AP	NA	Goat	1:10000	sc-2007	Santa Cruz
	goat anti-mouse IgG-AP	NA	Goat	1:10000	sc-2008	Santa Cruz
	donkey-anti-rabbit-IRDye®-680LT	NA	Donkey	1:10000	926-68023	Li-Cor
	donkey-anti-rabbit-IRDye®-800CW	NA	Donkey	1:10000	925-32213	Li-Cor
	donkey-anti-mouse-IRDye®-680LT	NA	Donkey	1:10000	925-68022	Li-Cor
	donkey-anti-mouse-IRDye®-800CW	NA	Donkey	1:10000	926-32212	Li-Cor

THIS PAGE INTENTIONALLY LEFT BLANK.

Table 2.3 – List of phospho-flow antibodies

Antibody	Clone	Isotype	Catalogue no.	Supplier
Anti-Phosphotyrosine 4G10-PE	4G10	IgG_{2b}, κ	FCMAB323PE	Merck Millipore™
Akt (pS473) - PE	M89-61	IgG_1, κ	561671	BD Phosflow™
CrkL (pY207)-PE	K30-391.50.80	IgG_{2a}, κ	560788	BD Phosflow™
Erk1/2 (pT202/pY204)-PE	20A	IgG_1	612566	BD Phosflow™
Stat5 (pY694)-PE	47	IgG_1, κ	612567	BD Phosflow™
IgG_1-PE	MOPC-21	IgG_1, κ	555749	BD Pharmingen™
IgG_{2a}-PE	DAK-GO5	IgG_{2a}, κ	X0950	DakoCytomation
IgG_{2b}-PE	27-35	IgG_{2b}, κ	555743	BD Pharmingen™

2.2. Cell Culture Media & Solutions

All cell culture media were stored at 4°C and preheated to 37°C in a water bath prior to use, unless otherwise stated.

Ba/F3 parental wildtype cell culture media
RPMI-1640 medium
2 mM *L*-glutamine
50 units/mL Penicillin
50 µg/mL Streptomycin
10% Foetal bovine serum (FBS)
5% WEHI-3B complete media (source of IL-3)

Ba/F3 IL-3 independent cell culture media
RPMI-1640 medium
2 mM *L*-glutamine
50 units/mL Penicillin
50 µg/mL Streptomycin
10% FBS

HEK-293T cell culture media
Dulbecco's Modified Eagle's Medium (DMEM)
2 mM *L*-glutamine
50 units/mL Penicillin
50 µg/mL Streptomycin
10% FBS

NIH-3T3 cell culture media
RPMI-1640 medium
2 mM *L*-glutamine
50 units/mL Penicillin
50 µg/mL Streptomycin
10% FBS

SUP-B15 Ph+ ALL cell culture media

RPMI-1640 medium
4 mM *L*-glutamine
50 units/mL Penicillin
50 µg/mL Streptomycin
20% FBS
0.05 mM β-mercaptoethanol

WEHI-3B cell culture media

RPMI-1640 medium
2 mM *L*-glutamine
50 units/mL Penicillin
50 µg/mL Streptomycin
10% FBS

CrkL IC_{50} media

90% Hanks' balanced salt solution (HBSS)
10% Newborn calf serum (NCS)

Cryoprotectant freezing solution

60% FBS
20% Cell culture media
20% Dimethyl sulfoxide (DMSO)

Solution was freshly made prior to cryopreservation of cells, and added 1:1 to cells that were resuspended in culture media. For more details, please refer to '**2.7.2** – Cryopreservation of cell lines'.

2.3. Inhibitors

2.3.1. Imatinib (STI-571)

MW: 589.71

Imatinib mesylate (Symansis, Shanghai, China) was dissolved in sterile Milli-Q® water to 10 mM, sterile filtered and stored at -80ºC. Serial dilutions were made in sterile Milli-Q® water immediately prior to use.

2.3.2. Dasatinib (BMS-354825)

MW: 488.01

Dasatinib (Symansis, Shanghai, China) was dissolved in DMSO to 10 mM and stored at 4ºC. Serial dilutions were made in sterile DMSO immediately prior to use.

2.3.3. Ponatinib (AP24534)

MW: 532.56

Ponatinib (Selleck Chemicals, Houston TX, USA) stock solutions was prepared at 10 mM in DMSO and stored at -20°C. Serial dilutions were made in sterile DMSO, immediately prior to use.

2.3.4. Ruxolitinib (INCB018424)

MW: 306.37

Ruxolitinib (Selleck Chemicals, Houston TX, USA) was dissolved to 10 mM in DMSO and stored at -20°C. Serial dilutions were made in sterile DMSO, immediately prior to use.

2.3.5. BMS-911543

MW: 432.52

BMS-911543 (Selleck Chemicals, Houston TX, USA) stock solutions were prepared at 50 and 10 mM in DMSO, and stored at -20°C. Serial dilutions were made in sterile DMSO, immediately prior to use.

2.4. Common Buffers & Solutions for Protein Assays

2.4.1. 1x Phosphate-buffered saline (1x PBS)

10 x PBS stock (Gibco #14200-075)

Diluted 1:10 in sterile Milli-Q® ultra-purified water

Solution was prepared and stored at 4°C.

2.4.2. 1x Tris-buffered saline (1x TBS)

20 mM Tris-HCL (pH 7.5)

150 mM NaCl

RO water

Solution was prepared and stored at room temperature (RT).

2.4.3. 1x Tris-buffered saline + 0.1% Tween-20 (1x TBST)

20 mM Tris-HCL (pH 7.5)

150 mM NaCl

0.1% Tween20

RO water

Solution was stored at RT and used within 2 weeks.

2.4.4. 1x SDS-PAGE gel running buffer

25 mM Tris

192 mM Glycine

0.1% SDS

RO water

Solution was prepared and stored at RT.

2.4.5. 1x Western blotting transfer buffer

25 mM Tris

192 mM glycine

20% methanol

RO water

Solution was prepared and stored at 4°C.

2.4.6. 1x Laemmli's buffer for cell lysis & CrkL protein stabilisation

50 mM TrisHCL, pH 6.8

2% SDS

10% Glycerol

5% β-mercaptoethanol

0.05% Bromophenol blue

1 mM Sodium vanadate

10 mM Sodium fluoride

Milli-Q® dH_2O

1x Laemmli's buffer was stored in 1 mL aliquots at -20ºC and thawed prior to use.

2.4.7. 1% Triton™ X-100 cell lysis buffer

1% Triton™ X-100

20 mM Tris-HCl, pH 8.2

150 mM NaCl

1 x protease & phosphatase inhibitors

Milli-Q® dH_2O

A stock solution (without inhibitors) was prepared and stored at 4°C, with protease and phosphatase inhibitors added directly prior to cell lysis.

2.4.8. 10% APS (10% ammonium persulfate)

1 g ammonium persulfate (APS)

10 mL Milli-Q® dH_2O

Solution was prepared and stored at -20°C.

2.4.9. Buffer A (for use in 14% resolving gel)

1.5 M Tris, pH 8.8

Milli-Q® dH_2O

Solution was prepared and stored at RT.

2.4.10. Buffer B (for use in 5% stacking gel)

0.5 M Tris pH 6.8

Milli-Q® dH_2O

Solution was prepared and stored at RT.

2.4.11. Polyacrylamide gel components specific for Hoefer SE260 system

Table 2.4 – Polyacrylamide gel reagents for CrkL electrophoresis

Components	Resolving gel (14% polyacrylamide)	Stacking gel (5% polyacrylamide)
Milli-Q® H2O	12.9 mL	6 mL
40% Acrylamide	9 mL	1.26 mL
1.5 M Tris Buffer A	7.5 mL	-
1.5 M Tris Buffer B	-	2.52 mL
10% SDS	300 µL	100 µL
10% APS	300 µL	100 µL
TEMED	8 µL	10 µL

Gels were freshly cast using the Hoefer SE260 system, prior to gel electrophoresis.

2.4.12. Ponceau S staining solution

0.5% w/v Ponceau S

5% acetic acid

Milli-Q® dH_2O

Solution was prepared and stored at RT.

2.4.13. PVDF membrane blocking buffer (5% BSA)

1x TBST

5% BSA

Solution was stored at 4°C and used within a week after preparation.

2.5. Common Buffers & Solutions for Flow Cytometry Analysis

2.5.1. 1x Binding buffer for 'Annexin-V / 7-AAD (7-AminoActinomycin-D)' assay

HBSS

10 mM HEPES

5 mM $CaCl_2$

Solution was freshly prepared and kept on ice.

2.5.2. 1x Binding buffer for phospho-flow assay

1x PBS

1% BSA

Solution was freshly prepared and kept on ice.

2.5.3. Methanol permeabilisation solution for phospho-flow assay

80% analytical grade methanol

20% Milli-Q® dH_2O

Solution was stored at -20^oC and used ice-cold for each application.

2.5.4. Flow cytometry fixative (FACS fix)

1x PBS

1% Formaldehyde

111 mM D-glucose

0.02% sodium azide

Solution was prepared at RT and stored at 4^oC.

2.6. Molecular Biology Reagents

2.6.1. dNTP set (N=A, T, C, G)

25 mM: 40 µL of each dNTP

5 mM: 1:5 dilution of 25 mM stock in 80 µL DEPC water

Solution was prepared and stored at -20°C

2.6.2. LB Broth

10 g Luria broth base

To 400 mL with Milli-Q® water

Solution was sterilised (autoclaved) and stored at RT.

2.6.3. LB Agar

10 g Luria broth base

6 g Select Agar™

To 400 mL with Milli-Q® water

Solution was sterilised (autoclaved) and stored at RT. Depending on antibiotic-resistance profile of plasmids, solidified LB agar stocks were heated to 100°C in a microwave oven and cooled to 37°C, prior to the addition of antibiotics (100 µg/µL ampicillin or 50 µg/µL kanamycin). Upon addition of antibiotics, LB agar solution was immediately aseptically transferred into sterile petri dishes and allowed to solidify at RT. LB agar plates were then carefully sealed using Parafilm M® (Bermis Inc., Neenah WI USA) and stored at 4°C for up to one week.

2.6.4. 1x Tris-acetate EDTA (1x TAE) buffer

40 mM Tris (pH 7.6)

20 mM acetic acid

1 mM EDTA

Milli-Q® water

Stored at RT.

2.6.5. 1% Agarose gel for DNA electrophoresis

1% agarose powder

0.01% GelRed™ nucleic acid stain

1x TAE buffer

Solution was freshly made prior to electrophoresis.

2.7. General Cell Culture Techniques

2.7.1. Subculturing of cell lines

Cells were analysed via Trypan blue exclusion (1:1 dilution) using an improved Neubauer haemocytometer (Marienfeld Superior GMBH & Co. KG, Germany), and percentage viability and density assessed using an Olympus CX41 microscope (Olympus Corporation, USA) under the 10x objective. In a biosafety class II cabinet (Esco Global, Singapore), cells were sub-cultured in 37^{o}C media (refer to '**2.2** – Cell Culture Media & Solutions') into T25, T75 or T150 culture flasks (Corning Inc., USA). Cells were sub-cultured at their recommended densities, depending on desired final volume (**Table 2.5**).

Table 2.5 – Cell culture seeding densities

Cell line	Cell type	Species	Recommended Live Cell Seeding Density
Ba/F3 IL-3 independent	Pro-B cells	Mouse	5×10^4 / mL
Ba/F3 parental wildtype	Pro-B cells	Mouse	1×10^5 / mL
HEK-293T	Embryonic kidney cells	Human	1×10^4 / cm^2
NIH-3T3	Fibroblasts	Mouse	5×10^3 / cm^2
SUP-B15 Ph+ ALL	B lymphoblasts	Human	5×10^5 / mL

2.7.2. Cryopreservation of cell lines

The desired number of cells (approximately 1 x 10^7 cells per sample) were collected into a 50 mL centrifuge tube and centrifuged at 1400 rpm (Heraus™ Multifuge™ 3SR, Thermo Fisher Scientific, USA) for 5 minutes (min) at RT. Supernatant was discarded and cells resuspended in 500 μL of culture media. An equal volume of ice-cold cryoprotectant solution (refer to '**2.2** – Cryoprotectant freezing solution') was then added onto the cell pellet in a dropwise fashion, with gentle agitation.

The suspension was immediately transferred into 1.5 mL ampoules (Nalgene Nunc International, Thermo Fisher Scientific, USA) and allowed to cool in a pre-chilled Mr. Frosty freezing container (Nalgene Nunc International, Thermo Fisher Scientific, USA) overnight, at a rate of -1°C per minute in a -80°C ultracool freezer (Haier Medical -86°C Ultra Low Temperature Freezer DW-86L828J, China). Ampoules were then transferred for long-term storage into liquid nitrogen (-196°C).

2.7.3. Cell washout protocol prior to drug treatment assays

TKI-resistant cells and parallel matched sensitive controls were incubated in TKI-free media based on an adaptation of technique established in our laboratory[206]. Cells were pelleted by centrifugation at 1,400 rpm for 5 min in a 50 mL centrifuge tube. The supernatant was discarded, and cells were resuspended in pre-warmed (37°C) TKI-free media. This step was repeated twice.

Because the specific amount of time required for complete washout of different drugs within resistant cell lines varies, the protocol was adjusted to incorporate an additional step of incubating cells in TKI-free media at 37°C in a humidified chamber overnight (5% CO_2), to ensure maximum drug washout. The following day (approximately 12 hr later), cells were pelleted at 1,400 rpm for 5 min in a 50 mL centrifuge tube and resuspended in pre-warmed (37°C) TKI-free media.

2.8. Annexin-V-PE/7-AAD Exclusion Assay

2.8.1. Drug treatment of cells for Annexin-V-PE/7-AAD cell-death assay

Following incubation of cells in TKI-free media overnight and analysis of cell viability and density using Trypan blue exclusion analysis, cells were adjusted to a final concentration of 5 x 10^4 / mL (Ba/F3 cells) or 5 x 10^5 / mL (SUP-B15 cells). Serial dilutions of TKI stocks were freshly prepared. For TKIs requiring DMSO as a solvent, stocks were prepared such that the final concentration of DMSO in cell culture was not more than 0.1% DMSO. Cells were exposed to differing concentrations of TKI (depending on the experimental set-up) in a 24-well plate and subsequently sub-cultured into 48-well plates, in technical triplicates. Cell culture plates were incubated at 37^{o}C in a humidified chamber (5% CO_2) for 72 hr prior to harvesting of cells for cell death analysis.

2.8.2. Annexin-V-PE/7-AAD exclusion staining protocol

Following drug exposure, 48-well tissue culture plates containing cells were centrifuged at 1,400 rpm for 5 min at RT. Upon completion of centrifugation, tissue culture media was gently decanted by inversion, followed by blotting onto a multi-fold towel (Kimberley-Clark Professional®, USA) to completely remove supernatant. Cells were resuspended in freshly-prepared ice-cold 1x binding buffer (HBSS + 1% HEPES + 5 mM $CaCl_2$), vortexed briefly (IKA® Vortex Genius 3 + plate adaptor) and samples transferred into a 96-well plate (Corning Inc., USA). Cells were then centrifuged at 1,400 rpm for 5 min at RT and the supernatant discarded as previously described. Annexin-V-PE/7-AAD staining solution was prepared and administered to samples according to the table below (**Table 2.6**).

Table 2.6 – Volume of reagents for Annexin-V-PE/7-AAD staining solution

Parameter	Annexin-V-PE	7-AAD	1x Binding Buffer
Unstained control	-	-	10 μL
Annexin-V single-stained control	0.5 μL	-	10 μL
7-AAD control single-stained control	-	0.1 μL	10 μL
Dual-stained control	0.5 μL	0.1 μL	10 μL
Experimental sample (per well)	0.5 μL	0.1 μL	10 μL

Cells were incubated in staining solution for 20 min on ice, in the dark, to allow binding of Annexin-V-PE and 7-AAD to apoptotic/apoptosing cells. Following staining, 200 μL of 1x binding buffer was added into each well. Control samples (unstained and single-stained) were analysed on the BD LSR Fortessa™ X-20 (BS Biosciences, USA) flow cytometer to define forward and side-scatter parameters, together with Annexin-V-PE (Ex_{max} 496 nm/Em_{max} 578 nm) and 7-AAD (Ex_{max} 488 nm/Em_{max} 647 nm) baseline fluorescence intensity gates. Experimental samples were acquired via the BD LSR FortessaTM X-20 high-throughput system (HTS), with compensation applied and data batch-analysed using FlowJo® software (FlowJo, LLC, USA).

2.9. Phosphoflow Assay

2.9.1. Drug treatment of cells for phosphoflow assay

Following overnight incubation of cells in TKI-free media (refer to '**2.7.3** – Cell washout protocol prior to drug treatment assays'), cells were analysed for viability/density using Trypan blue and adjusted to a final concentration of 1 x 10^6 / mL. Serial dilutions of TKI stocks were freshly prepared. For TKIs requiring DMSO as a solvent, stocks were prepared such that the final concentration of DMSO in cell culture was 0.1%. Cells were exposed to TKI in 1.7 mL microcentrifuge tubes (Axygen®, Corning Inc., USA) for 1 hr at 37^{o}C, in a humidified incubator (5% CO_2).

2.9.2. Preparation of cells for phosphoflow assay

Following the 1 hr drug-treatment, 100 μL of 16% paraformaldehyde (PFA) was added to each millilitre of sample. Cells were incubated in a 37^{o}C humidified chamber (5% CO_2) for 10 min, to allow fixation of intracellular phosphorylated proteins to occur. Cells were then centrifuged at 1,400 rpm for 5 min at RT in a microcentrifuge (Eppendorf™ #5424, Fisher Scientific, USA), and the supernatant discarded using a suction vacuum aspirator (Medi-Vac®, Cardinal Health Inc., USA). Cells were resuspended in 1 mL of ice-cold 1x PBS and then pelleted as previously described. The supernatant was discarded, and 80% ice-cold methanol was added in a drop-wise fashion, while vortexing (Stuart™ Scientific SA8 vortex mixer, Cole-Palmer, UK) at low speed (600 rpm) to allow resuspension and permeabilisation of cells. Samples were then stored at -20^{o}C overnight.

Following fixation and permeabilisation, cells were divided into a 96-well plate. Cells were pelleted by centrifugation at 1,400 rpm for 5 min at RT, and the supernatant discarded. Cells were resuspended in 1x phosphoflow buffer (1x PBS + 1% BSA), pelleted and the supernatant discarded. Antibodies were prepared according to the table below (**Table 2.7**). Cells were briefly vortexed and samples incubated in the dark, for 1 hr at RT. Following antibody incubation, 200 μL of 1x phosphoflow binding buffer was added and the cells were pelleted and supernatant discarded. Cells were resuspended in 200 μL ice-cold 1x PBS prior to flow cytometric analysis.

Table 2.7 – Volume of antibodies for phosphoflow staining

Parameters	Antibody	Volume per 5μL of 1x binding buffer (1x PBS + 1% BSA), in each well of a 96-well plate
Unstained control	NA	NA
Isotype control antibodies	IgG1-PE	0.125 μL
	IgG2a-PE	0.5 μL
	IgG2b-PE	0.125 μL
1° conjugated antibodies for phospho-proteins of interest	Akt (pS473) – PE, IgG1	0.5 μL
	Anti-phosphotyrosine 4G10-PE, IgG2b	0.25 μL
	CrkL (pY207)-PE, IgG2a	0.5 μL
	Erk1/2 (pT202/pY204)-PE, IgG1	0.5 μL
	Stat5 (pY694)-PE, IgG1	0.5 μL

Note: To minimise pipetting error, stock solutions (n+2) of each antibody plus binding buffer were prepared, prior to delivery of staining solution into each well (i.e. 10 wells of CrkL(pY207)-PE IgG2a = 6 μL antibody + 60μL binding buffer).

2.10. Protein Electrophoresis

2.10.1. Drug treatment of cells

Following overnight incubation of cells in TKI-free media (refer to '**2.7.3** – Cell washout protocol prior to drug treatment assays'), cells were analysed for viability and density by Trypan blue exclusion and adjusted to a final concentration of 1 x 10^6 / mL. Serial dilutions of TKI stocks were freshly prepared. For TKIs requiring DMSO as a solvent, stocks were prepared such that the final concentration of DMSO in cell culture was 0.1%. Cells were exposed to TKIs in 1.7 mL microcentrifuge tubes for 1 hr at 37^{o}C, in a humidified chamber (5% CO_2).

2.10.2. Preparation of protein lysates

Cells were washed in 1x ice-cold PBS via centrifugation at 550 x *g* for 5 min. The supernatant was aspirated and cells resuspended in 1% Triton-X lysis buffer (refer to '**2.4.7** – 1% TritonTM X-100 cell lysis buffer') at a volume of 100 μL per 1 x 10^7 cells. Cells were then frozen for a minimum of 1 hr at -80^{o}C, subsequently thawed on ice and centrifuged at 14,000 rpm in an ice-cold microcentrifuge for 10 min. The supernatant was collected and transferred into pre-labelled 1.7 mL microcentrifuge tubes as 'clarified protein lysate'.

2.10.3. Protein assay

Protein assays were performed using the Bio-Rad® DC Assay kit according to manufacturer's protocol. Briefly, 5 μL of 1:5 dilutions of clarified protein lysates, 1% Triton-X lysis buffer as well as protein standards comprising of BSA at concentrations of 0, 0.25, 0.5, 0.75, 1 and 1.5 μg/μL in water were aliquoted into wells of a 96 well plate, in duplicates. Twenty-five microlitres of Reagent A' (stock solution of 20 μL Reagent S per 1 mL of Reagent A) and 200 μL of Reagent B were added into each well, with gentle resuspension. Samples were incubated for 15 min at RT, and analysed via the Bio-Rad® iMark plate reader at an absorbance wavelength of 750 nm, measuring protein concentration. A standard curve was generated, using the formula ($y = mx + c$) such that y is the optical density reading, m is the gradient generated in the formula, x is the concentration of BSA (μg/μL) while c refers to the constant. Ensuring that the R^2 value of this standard curve is

as close to 1 as possible, the protein concentration in samples were then analysed according to this formula.

2.10.4. Preparation of protein samples for SDS-PAGE gel electrophoresis

In a fume cabinet (Laboratory Systems Group Pty Ltd., VIC, Australia), 2x or 4x Laemmli's loading buffer (depending on the volume of protein sample) was added to 20 μg of clarified protein lysate in 1.7 mL microcentrifuge tubes. Samples were then vortexed for 3-5 seconds and pulse centrifuged at high speed, prior to denaturation at 100°C on a dry block heater (Ratek Instruments Pty Ltd., Australia) for 10 min. Samples were again pulse centrifuged, vortexed and stored at -20°C.

2.10.5. SDS-PAGE protein electrophoresis

Bio-Rad® Criterion™ pre-cast gels were assembled in Bio-Rad® Criterion™ protein electrophoresis apparatus. 1x SDS-PAGE running buffer was added into both inner and outer tanks. Ten microlitres of Bio-Rad® Kaleidoscope protein ladder was added into the first lane and 20 μL of prepared protein samples (thawed on ice, boiled to 100°C and pulse centrifuged as previously described) were administered into each subsequent lane. An electrical current of 200 mA was applied for 35 min, allowing proteins to resolve.

2.10.6. Western blotting

After resolution of proteins via SDS-PAGE gel electrophoresis, proteins were transferred onto PVDF membrane (Immobilon® P, Merck Millipore, USA) using the Trans-Blot® Turbo™ semi-dry western apparatus (Run:Mixed setting; 1.3 A / 25 V for 7 min) or the Bio-Rad® Criterion™ wet transfer apparatus (400 mA for 60 min). Upon completion of protein transfer, Ponceau S staining was performed (refer to section **2.4.12** – Ponceau S staining solution) to observe the efficiency of protein transfer. Membranes were trimmed depending on sizes of proteins of interest, enabling simultaneous incubation of multiple blots in various antibody solutions. All incubations and membrane washes mentioned in the next steps were performed on a rocking platform (Ratek Instruments Pty Ltd., Australia) with gentle agitation unless otherwise specified. Membranes were incubated with blocking buffer (refer

to section **2.4.13** – PVDF membrane blocking buffer (5% BSA)) for 30 min at RT. Following overnight incubation at 4°C with primary antibodies (refer to **Table 2.2** – List of western blotting antibodies), the membranes were washed with 1x TBST for 3 x 5 min. Blots were then incubated in their respective secondary antibodies for 1 hr at RT. Membranes were washed in 1x TBST for 3 x 5 min and visualised on the Bio-Rad ChemiDoc® machine (if using enhanced chemifluorescence (ECF, GE Healthcare Amersham, USA) as a substrate for alkaline-phosphatase (AP) conjugated antibodies), or the LiCor Odyssey® fluorescent scanner (if using fluorescent-tagged antibodies).

2.10.7. Stripping of PVDF membranes for re-probing of other proteins of interest

PVDF membranes were incubated in 1x stripping buffer (Alpha Diagnostic International, San Antonio, TX, USA) by diluting 1:10 in Milli-Q water on a rocking platform for 5 min at RT. Blots were then placed in a 37°C humidified chamber for 15 min, followed by RT for 15 min with gentle agitation. Western blots were then washed in 1x TBST three times for 5 min and blocked in blocking buffer (5% BSA in 1x TBST) for 30 min at RT. Membranes were then re-probed as described above (refer section '**2.10.6** – Western blotting').

2.10.8. Densitometry analysis

Data from visualisation of western blots were analysed via the Bio-Rad® Image Lab ® software (for data from Bio-Rad® ChemiDoc™) or LiCor® ImageStudio™ (for data from LiCor® Odyssey™). The intensity of each band was recorded, and the corresponding background value measured and subtracted. Intensities of phosphorylated proteins were compared to their total counterparts, and a ratio (phospho-protein:total-protein) obtained. Values for samples were graphed to quantify changes seen.

THIS PAGE INTENTIONALLY LEFT BLANK.

2.11. CrkL (Surrogate for Bcr-Abl Kinase Activity) Assay

2.11.1. TKI-treatment of cells for CrkL analysis

To analyse the concentration of inhibitor required for 50% inhibition of CrkL (CrkL IC_{50}) drug treatment and subsequent western blotting were performed based on the methods of White *et al*. 2005[207]. Briefly, 2 x 10^5 cells were resuspended in 5 mL of CrkL IC_{50} media (HBSS + 10% newborn calf serum). Cells were exposed to various concentrations of TKI to a final concentration of 0.1% DMSO, in 10 mL yellow-capped centrifuge tubes (Starstedt AG & Co., Nümbrecht, Germany). Tubes were loosely capped and samples incubated at 37^{o}C with humidity and 5% CO_2 for 2 hr, with tubes rested sideways to enable maximum cell-to-drug contact. Following the incubation period, cells were harvested via centrifugation for 5 min at 1400 rpm and the supernatant discarded.

2.11.2. Preparation of protein lysates for SDS-PAGE gel electrophoresis

Cells were washed in 1x ice-cold PBS via centrifugation at 550 x *g* for 5 min. The supernatant was aspirated, and in a fume cabinet, cells were resuspended in 1x Laemmli's loading buffer with inhibitors (refer to section **2.4.6** – 1x Laemmli's buffer for cell lysis & CrkL protein stabilisation) at a volume of 20 μL per sample. Samples were then vortexed for 3-5 seconds and pulse centrifuged at high speed, prior to denaturation at 100^{o}C on a dry block heater for 10 min. Samples were again pulse centrifuged, vortexed and stored at -20^{o}C.

2.11.3. Resolution of CrkL protein via SDS-PAGE gel electrophoresis

SDS-PAGE gels (14% and 5% polyacrylamide for resolving and stacking gels respectively) were prepared according to components described in '**Table 2.4** – Polyacrylamide gel reagents for CrkL electrophoresis', on a gel casting apparatus (Hoefer Inc., USA). Gels were allowed to set prior to assembly in an SDS-PAGE gel electrophoresis apparatus with 1x SDS-PAGE running buffer added into both inner and outer tanks. Ten microlitres of Bio-Rad® Kaleidoscope protein ladder was administered into the first lane and 20 μL of prepared protein samples were loaded

into each subsequent lane. Current flow (for 2 gels: 40 mA for 45 min, then, 60 mA for 2 hr) was applied, allowing for proteins to resolve.

2.11.4. Western transfer and blotting of CrkL protein

Upon completion of SDS-PAGE gel electrophoresis, proteins were transferred onto a PVDF membrane in a Hoefer tank containing 1x western transfer buffer (Tris-glycine with 20% methanol in RO H_2O). Transfer at 65 mA was performed overnight at RT. PVDF membranes were then stained with Ponceau S (**2.4.12** – Ponceau S staining solution) and de-stained in Milli-Q® water to observe the efficiency of the transfer. All incubations and membrane washes in the following steps were performed on a rocking platform with gentle agitation unless otherwise specified. Membranes were incubated with blocking buffer (refer to '**2.4.13** – PVDF membrane blocking buffer (5% BSA)') for 30 min at RT, followed by anti-CrkL primary antibody for 2 hr at RT. This was followed by a 3 x 5 min wash with 1x TBST and subsequent incubation in anti-rabbit secondary antibody for 1 hr at RT. Membranes were washed in 1x TBST for 3 x 5 min and visualised on the Bio-Rad ChemiDoc® machine (if using ECF as a substrate for AP-conjugated antibodies), or the LiCor Odyssey® fluorescent scanner (if using fluorescent-tagged antibodies).

2.11.5. p-CrkL IC_{50}

Data from visualisation of western blots were analysed via the Bio-Rad® Image Lab ® software (for data from Bio-Rad® ChemiDoc™) or LiCor® ImageStudio™ (for data from LiCor® Odyssey™). As the CrkL primary antibody (Santa Cruz, USA) detects both unphosphorylated and phosphorylated CrkL (p-CrkL) between 37-39 kDa, the intensity of each band was analysed. The upper band is phosphorylated CrkL, whereas the lower band represents CrkL. The percentage of p-CrkL compared to total CrkL (sum of p-CrkL and CrkL) was determined, resulting in a ratio which was then graphed to generate a curve. The percentages of p-CrkL were normalised against the minimum and maximum test concentrations, with TKI concentration required to reduce p-CrkL by 50% defined as the IC_{50}.

2.12. Generation of Ba/F3 Ph-like ALL Stable Cell Lines

Ph-like ALL fusion genes in pCR®-Blunt II-TOPO® constructs were obtained under a Material Transfer Agreement (MTA) from our collaborators (Mullighan *et al*.) at St. Jude's Children's Research Hospital in Memphis, TN, USA[64,73]. The fusion genes *RANBP2-ABL1* and *SSBP2-CSF1R* were molecularly sub-cloned from pCR®-Blunt II-TOPO® constructs into pRuf-iG2, a mammalian-expressing retroviral-vector recipient backbone[208,209]. HEK-293T cells were transfected with fusion constructs to generate viral particles, followed by transduction into Ba/F3 parental cells (courtesy of Professor Andrew Zannettino and Dr. Stephen Fitter, The University of Adelaide). Transduced Ba/F3 cells were selected for green fluorescent protein (GFP) positivity via flow cytometry, followed by confirmation of interleukin-3 (IL-3) independence as being indicative of transformation. Ba/F3 cells expressing the Ph-like ALL fusion gene *PAX5-JAK2* were provided by Mullighan *et al*. A detailed description of these experimental approaches can be found in sections **2.12.1** – **2.12.7** and a schematic diagram is shown in **Figure 2.1**.

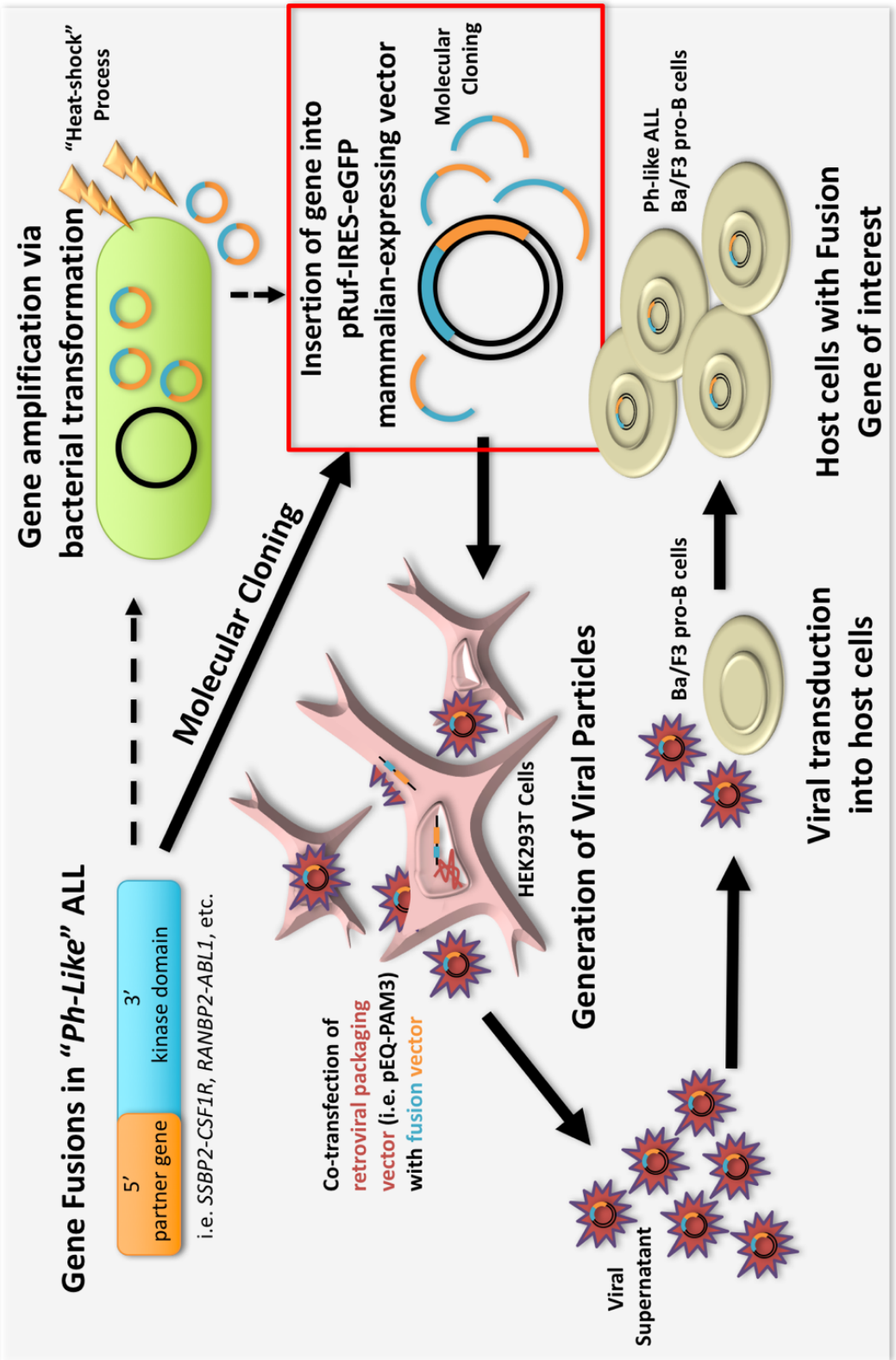


Figure 2.1 – Generation of Ph-Ba/F3 Ph-like ALL stable cell lines via retroviral transduction

2.12.1. Transformation of competent cells for amplification of Ph-like ALL fusion gene plasmids

The Ph-like ALL fusion constructs *RANBP2-ABL1* and *SSBP2-CSF1R* in the pCR®-Blunt II-TOPO® vector were expanded by bacterial transformation of DH5α™ competent cells (Thermo Fisher Scientific, USA) as per manufacturer's instructions. This included immediate thawing of competent cells on ice in a 1.7 mL microcentrifuge tube, followed by addition of 1 μL of fusion plasmid with gentle agitation of the tube to mix cells with plasmid DNA. Competent cells were incubated on ice for 30 min, allowing stabilisation of cells with plasmid DNA.

A 'heat-shock' process was then applied, where samples were incubated at 42ºC for 20 seconds on a dry block heater followed by immediate incubation on ice for 2 min. A volume of 500 μL of pre-warmed (37ºC) LB broth (without antibiotics) was added, and tubes incubated in a 37ºC bacterial orbital shaker (Ratek Instruments Pty Ltd., Australia) for 30 min, allowing competent cells to recover from the heat-shock process. Following this, cells prepared in pre-warmed LB broth at 3 dilutions (neat, 1:10 and 1:100), prior to culture on antibiotic-containing LB agar plates containing 50 μg/μL kanamycin and incubated overnight at 37ºC in a dry bacterial incubator (Ratek Instruments Pty Ltd., Australia).

The following day, single well-spaced colonies were carefully picked using a 200 μL sterile-autoclaved pipette tip and subsequently individually placed in 2 mL of LB broth containing 50 μg/μL kanamycin, in round-bottom polypropylene tubes (Falcon™, Fisher Scientific, USA). Competent cells were incubated in a bacterial orbital shaker for approximately 6 hr at 37ºC. Bacterial culture was further expanded by transferring a volume of 500 μL into a conical Erlenmeyer flask (Pyrex®, Corning Inc. USA) containing 100 mL of LB broth (with 50 μg/μL kanamycin). The conical flask was then incubated in an orbital shaker at 37ºC overnight, to achieve a log-phase culture and a further increase in the amount of plasmid DNA.

2.12.2. Long-term storage of transformed bacterial cells

Upon achievement of a confluent bacterial culture, competent cells were carefully decanted into 50 mL centrifuge tubes (Corning Inc., USA). Glycerol stocks of bacterial culture were made by diluting 500 μL of culture with 100% sterile glycerol to a final volume of 1 mL, and samples were stored in 2 mL screw-capped vials (Nalgene Nunc International, Thermo Fisher Scientific, USA) at -80°C. The remaining bacterial culture in 50 mL centrifuge tubes was then centrifuged at 3,000 x *g* for 20 min at RT, and the supernatant discarded with appropriate decontamination procedures in 8-12.5% sodium hypochlorite (Chem-Supply Pty Ltd, SA). The bacterial cell pellet, along with glycerol stocks, were stored at -80°C until extraction of plasmid DNA was required.

2.12.3. Extraction and purification of plasmid DNA

Extraction and purification of plasmid DNA was achieved using miniprep and midiprep kits (Qiagen, Hilden, Germany), depending on the starting volume of the bacterial culture. This was done according to the manufacturer's protocol using the alkaline lysis method, whereby key steps included resuspending bacterial cells in an isotonic buffer containing 1 μg/μL RNAse A, followed by cell lysis using a solution of 0.2 N NaOH and 1% SDS and neutralisation using a solution of 1M potassium acetate and 10 M acetic acid[210]. Plasmid DNA was precipitated using isopropanol (Merck Millipore, USA), washed in the presence of 70% ethanol and rehydrated in nuclease-free water (NF-H_2O).

2.12.4. Molecular cloning of Ph-like ALL fusion genes

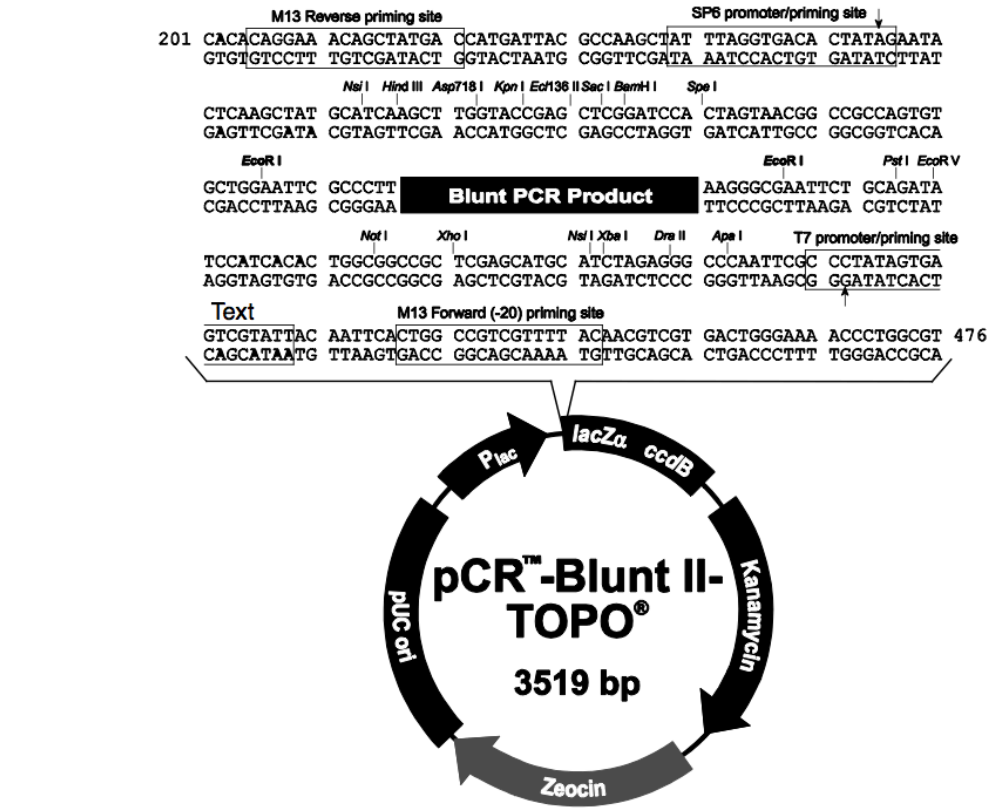
Ph-like ALL fusion genes in pCR®-Blunt II-TOPO® constructs required sub-cloning into a mammalian-compatible retroviral vector as the constructs are non-expressing in mammalian cells. *RANBP2-ABL1* and *SSBP2-CSF1R* were sub-cloned into the pRuf-iG2 vector, a mammalian-expressing retroviral vector courtesy of Professor Andrew Zannettino and Dr. Stephen Fitter (**Tables 2.8 – 2.10** and **Figure 2.2**).

Table 2.8 – Strategies for sub-cloning of Ph-like ALL fusion genes

Sub-cloning strategy	Fusion gene	
	SSBP2-CSF1R	***RANBP2-ABL1***
Preparation of insert (pCR®-Blunt II-TOPO® donor construct)	1. Perform restriction digest with HindIII & XbaI 2. Perform Klenow endfill 3. Gel purify with UltraClean® DNA purification kit (MoBio Inc., USA) and confirm purity of insert using agarose gel electrophoresis	1. Perform restriction digest with NotI & SpeI 2. Perform Klenow endfill 3. Gel purify and confirm purity of insert using agarose gel electrophoresis
Preparation of vector backbone (pRuf-iG2 recipient construct)	1. Perform restriction digest with SnaBI 2. Dephosphorylate 5' and 3' ends with rSAP 3. Gel purify and confirm purity of vector backbone using agarose gel electrophoresis	

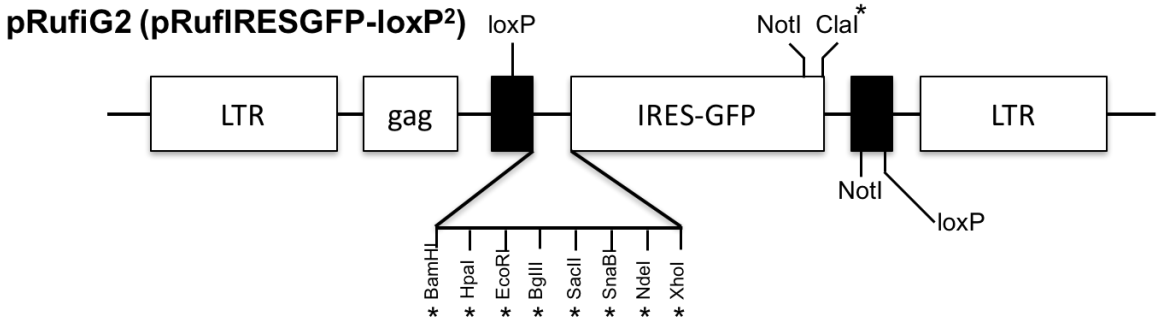
The isolated Ph-like ALL fusion gene insert (from pCR®-Blunt II-TOPO® construct) and vector backbone (pRuf-iG2) were ligated using T4 DNA ligase (New England Biolabs® Inc., USA). As this was blunt-end cloning, the correct orientation of the insert was further confirmed using the sequencing primers RCF-1 (TTG GGG GAC TCT GCT GAC CAC) and IRES-rv (ACA CCG GCC TTA TTC CAA G). The vector maps[208,209], are shown in '**Figure 2.2** – Vector maps for pCR®-Blunt II-TOPO® and pRuf-iG2'.

Donor vector



Taken from Invitrogen, Life Technologies 2014

Recipient vector



Legend: LTR – Long Terminal Repeat, GAG – Group Specific Antigen, IRES – Internal Ribosome Entry Site, GFP – Green Fluorescent Protein

Adapted and modified from Hewitt *et al* (unpublished)

Figure 2.2 – Vector maps for pCR®-Blunt II-TOPO® (top panel) and pRuf-iG2 (bottom panel).

Table 2.9 – Volume of reagents used for molecular cloning of Ph-like ALL fusions

Purpose	Materials	Volume/Amount	Total reaction volume (μL)
Restriction digest	Purified plasmid DNA	500 ng	10 μL
	10x CutSmart® Buffer	1 μL	
	Restriction enzyme	10 units per sample	
	NF-H_2O	Top up to 10 μL	
Klenow endfill	Purified Ph-like ALL insert DNA	19 μL	25 μL
	10x NEB Buffer 2	2.5 μL	
	10x dNTPs	2.5 μL	
	DNA Polymerase I, Large (Klenow) Fragment	1 μL	
Dephosphorylation with rSAP	Digested vector backbone (pRuf-iG2)	1 pmol	20 μL
	Shrimp alkaline phosphatase (rSAP)	2 μL	
	10x CutSmart® Buffer	2 μL	
	NF-H_2O	Top up to 20 μL	
T4 DNA ligation	T4 DNA ligase buffer (10x)	1 μL	10 μL
	T4 DNA ligase enzyme	1 μL	
	Insert DNA	5 μL	
	Vector DNA	1 μL	
	NF-H_2O	2 μL	

Table 2.10 – Incubation conditions for molecular cloning

Purpose	PCR Cycling Conditions
Restriction digestion + 'heat kill' deactivation	Lid: OFF Volume: 20 μL 1. 37°C for 1 hr 30 min 2. 65°C for 20 min 3. 4°C for ∞
Endfill of Ph-like ALL sticky-end insert with dNTP, via DNA Polymerase I, Large (Klenow) Fragment	Endfill conditions: Lid: OFF Volume: 25 μL 1. 25°C for 15 min 2. 4°C for ∞ Stop reaction (by adding EDTA to 10 mM): Lid: OFF Volume: 25 μL 1. 75°C for 20 min 2. 4°C for ∞
Dephosphorylation of recipient vector with rSAP	Lid: OFF Volume: 20 μL 1. 37°C for 30 min 2. 65°C for 20 min 3. 4°C for ∞
Ligation of insert and vector backbone	Lid: OFF Volume: 10 μL 1. 4°C for 5 hr 2. 16°C for 12 hr 3. 37°C for 30 min 4. 65°C for 20 min 5. 4°C for ∞

2.12.5. Generation of viral particles via transfection of HEK-293T cells

HEK-293T cells were seeded at a density of 1 x 10^6 into a T25 flask and allowed to rest overnight at 37°C. The following day, pRuf-iG2 vectors containing Ph-like ALL fusion genes were co-transfected along with its packaging vector pEQ-Eco (courtesy of Dr. Stephen Fitter and Professor Andrew Zannettino, The University of Adelaide), in the presence of Lipofectamine™ 2000 (Thermo Fisher Scientific, USA). This was performed by preparing two sterile round-bottom 5 mL tubes containing a transfection solution (500 μL serum-free DMEM media and 20 μL Lipofectamine™ 2000 transfection reagent) and plasmid-vector DNA (500 μL serum-free DMEM media with a combination of 5 μg plasmid DNA and packaging vectors).

The transfection solution was carefully added drop-wise into the tube containing plasmid DNA and packaging vector, allowing maximum incorporation of DNA particles into cationic liposome formulation. This final solution was incubated at RT for 30 min, prior to being added to HEK-293T cells in a drop-wise manner. HEK-293T cells were incubated in a humidified incubator at 37ºC (5% CO_2) overnight. The following day, the supernatant from transfected HEK-293T cells was collected using a 10 mL syringe (Terumo® Medical Corporation, USA) and filtered through a 0.45 μM sterile filter to obtain the viral supernatant.

2.12.6. Retroviral transduction of Ba/F3 parental wildtype pro-B cells

Viral supernatant was applied to Ba/F3 pro-B parental cells (5 x 10^4 cells per well, in a 6-well plate), in a biosafety class II cabinet. Polybrene® was added to a final concentration of 4 μg/mL, and plates were centrifuged with brake off for 30 min at 300 x g. Cells were incubated in a 37ºC humidified chamber (5% CO_2) with secondary containment, for 3 days to allow transduction to take place within dividing cells. After incubation, GFP positive (indicative of successful transduction) cells were collected using the BD FACSAria™ Fusion flow cytometer while GFP-negative cells were discarded.

2.12.7. Confirmation of incorporation of Ph-like ALL fusion constructs in Ba/F3 cells

Transduced Ba/F3 cells collected from FACS flow cytometry were incubated in media containing (+/-) IL-3 and viability assessed using Trypan blue exclusion following 3 days in culture. Cells surviving in the absence of IL-3 were deemed to have been transformed, as the expression of the Ph-like ALL fusion kinase provides signalling for IL-3 independent growth.

Expression of fusion genes was confirmed via genomic and complementary DNA (gDNA and cDNA, respectively) PCR using primers specific for the breakpoint and fusion construct (varies according to Ph-like ALL construct, see '**2.15.6** – Breakpoint sequencing of Ph-like ALL constructs'). The expression of fusion kinases was further verified using Western blot analysis (refer to '**2.10** – Protein Electrophoresis').

2.13. Analysis of TKI-sensitivity Prior to Generation of TKI-resistance

Prior to dose-escalations, TKI-sensitivity assays were performed on naïve Ba/F3 Ph-like ALL cells to investigate therapeutic responses at clinically-relevant concentrations. Cells were exposed to a panel of inhibitors (including Abl and Jak TKIs) at clinically-relevant concentrations (see individual results section for TKIs utilised). TKI-sensitivity was assessed via Annexin-V/7-AAD flow cytometry analysis (refer to '**2.8** – Annexin-V-PE/7-AAD Exclusion Assay'), phospho-flow of downstream kinase activity (see '**2.9** – Phosphoflow Assay') and western blotting of fusion kinases and downstream effector proteins (refer to '**2.10** – Protein Electrophoresis').

2.14. Generation of TKI-resistant Cells via Dose-escalation of TKI

TKI-resistant cells were generated by exposing cells to incrementally increasing concentrations of TKI over a significant period of time varying from 3 to 12 months, by adapting methods described by others, whereby cells were clonally selected for TKI-resistance[54,185,211-213]. In these studies, chronic myeloid leukaemia (CML) cell lines were exposed to an Abl-kinase inhibitor (i.e. imatinib, ponatinib, etc.), beginning from a concentration below its IC_{50} (i.e. IC_{50} for imatinib in K562 cells is 0.5 μM). Cells able to withstand the TKI concentration soon divide and outgrow others in culture. Viable cells were subsequently exposed to an increased concentration of TKI upon next passage. This method was repeated until cells achieve a clinically-relevant concentration of TKI resistance. This *in vitro* approach was used to recapitulate CML treatment, and thus biological changes observed *in vitro* can be indicative of a mode of TKI resistance in a clinical setting.

In T75 culture flasks, 5 x 10^5 / mL SUP-B15 cells were exposed to 1 nM dasatinib and ponatinib separately. In 12-well plates, 5 x 10^4 / mL of Ba/F3 Ph-like ALL cells were exposed to TKI (depending on sensitivity of fusion kinase, starting at 0.1 μM imatinib, 1 nM dasatinib, 1 nM ponatinib, 0.1 μM ruxolitinib, 0.1 μM BMS-911543). To account for any changes seen as a result of TKI reconstituted in DMSO, a parallel set of passage-matched control cells were simultaneously cultured (both naïve and DMSO) throughout the long-term dose-escalation process.

Cells were cultured in a humidified chamber at 37°C in the presence of 5% CO_2 and passaged every 3 days. The concentration of TKI was increased only when Trypan blue counts and microscopy analysis indicate more than 85% viable cells in culture. For SUP-B15 cells, at each point of dose-escalation, both TKI-resistant and sensitive control lines were stored at 1 x 10^7 (in cryoprotectant) and 5 x 10^6 in TRIzol® for RNA extraction. For Ba/F3 Ph-like ALL cells, as 12-well plates allow for culturing of multiple samples, positions of wells from each sub-culture were maintained throughout the entire dose-escalation process. This method enabled monitoring of TKI-resistant biological replicates.

2.15. Genomic Studies

2.15.1. RNA extraction of TRIzol® samples

For each sample, 5 x 10^6 cells were collected into a 2 mL microcentrifuge tube and cells were pelleted by centrifugation at 550 x *g* for 5 min. Media was discarded and cells re-suspended in 1 mL TRIzol® solution. Upon achieving a homogenous mixture, tubes were stored in -80^{o}C until required.

In a fume hood, 200 μL of chloroform was added and tubes were vigorously shaken. Samples were incubated at RT for 2-3 min, followed by centrifugation at 1,200 x *g* for 15 min at 4^{o}C. The aqueous upper phase was collected by pipette into a new pre-labelled 1.7 mL tube, avoiding any interphase or organic layers. After the addition of 500 μL of 100% analytical-grade isopropanol and 1 μg molecular-grade glycogen, tubes were vigorously shaken, followed by incubation at RT for 10 min.

Samples were then centrifuged at 1,200 x *g* for 10 min at 4^{o}C. The supernatant was discarded and the pellet washed in 1 mL 75% ethanol (diluted in reagent-quality Milli-Q® water). The samples were centrifuged for 5 min at 7,500 x *g* (4^{o}C) and the supernatant discarded. The pellet was briefly centrifuged and any excess ethanol removed using a micropipette, followed by brief air-drying. Thirty microliters of NF-H_2O were then added, and tubes incubated at 55^{o}C for 10 min to rehydrate the RNA. Samples were immediately placed on ice and RNA quantity and quality measured using the Nanodrop^{TM} 8000 spectrophotometer. Samples were then placed at -80^{o}C for long-term storage.

2.15.2. cDNA synthesis

Using the QuantiTect reverse transcription kit (Qiagen, Hilden, Germany), 1000 ng of RNA was synthesised into a final volume of 20 μL cDNA. In a single reaction, 2 μL of 7x gDNA Wipeout Buffer was added to each tube and samples incubated for 2 min at 42^{o}C to ensure gDNA elimination.

A volume of 6 μL mastermix comprising of 4 μL 5x Quantiscript buffer, 1 μL primer mix and 1 μL Quantiscript reverse transcriptase was added into each sample, according to the manufacturer's protocol. Using an Eppendorf Mastercycler®

thermal cycler, samples were incubated for 30 min at 42°C, then 3 min at 95°C. The resulting cDNA were stored at -20°C until required.

2.15.3. DNA extraction by phenol-chloroform

For each sample, 5 x 10^6 cells were collected into a 1.7 mL microcentrifuge tube and washed in 1x PBS buffer followed by centrifugation at 550 x *g* for 5 min. The supernatant was aspirated and cell pellets stored in -80°C as 'whole-cell pellet (WCP)'. For DNA extraction, WCPs were thawed on ice and washed in 1x PBS buffer at 550 x *g* for 5 min. Cells were then resuspended in 480 μL DNA lysis buffer, with 12.5 μl of 20% SDS and 10 μL Proteinase K (Roche Molecular Systems, Inc.) added into each tube. Samples were incubated at 37°C overnight.

The following day, 5 μL RNase A (Qiagen, Hilden, Germany) was added to each tube, inverted for approximately 50 times and incubated for 10 min at 37°C. Ten microlitres of 5 M NaCl and 1 μL glycogen carrier (Roche Molecular Systems, Inc.) were subsequently added to each tube. In a fume hood, 500 μL of buffer saturated phenol was added. Tubes were vigorously shaken, achieving a homogenous milky solution. Samples were then centrifuged at 16,000 x *g* for 5 min. The aqueous upper layer was carefully collected (without disturbing the interface between aqueous and organic layers) and dispensed into a new pre-labelled 1.7 mL tube.

A volume of 500 μL of Phenol:Chloroform:Isoamyl alcohol (PCI; 25:24:1, v/v) was added, and tubes vigorously shaken prior to centrifugation at 16,000 x *g* for 3 min. The aqueous upper layer was carefully collected and dispensed into a new 1.5 mL microcentrifuge tube. 1 mL of ice-cold 80% ethanol was added, precipitating the DNA. Tubes were centrifuged at 20,000 x *g* for 10 min, and the supernatant discarded. The DNA pellet was washed with 800 μL of 70% ethanol, followed by brief air-drying prior to resuspension of the pellet in 200 μL DNA hydration solution (Qiagen, Hilden, Germany).

2.15.4. Polymerase chain reaction (PCR) and Sanger sequencing

PCR master mixes were set-up in 0.2 μL tubes (Axygen®, Corning Inc., USA) on an Isofreeze® (Alpha laboratories, UK) tube cooler rack, in a clean PCR room and template added in a designated DNAse/RNAse free UV cabinet. A no template control (NTC) with NF-H_2O was included, to ensure primers do not amplify products in the mastermix. PCR cycling reactions were performed on the Bio-Rad® T1000™ thermal cycler, with amplicons resolved via electrophoresis on a 1% agarose gel for 30 min at 100V, alongside 1kb and 100bp molecular weight ladders (New England Biolabs® Inc., USA). Bands were visualised on the GelDoc™ XR+ (Bio-Rad®, CA, USA) gel documentation system, ensuring correct sizes and purity of samples.

PCR products were then purified using ExoSAP-IT™ express product clean-up reagent (Thermo Fisher Scientific, USA). In a pre-labelled 0.2 μL microcentrifuge tube, 5 μL of PCR product was added to a volume of 2 μL of ExoSAP-IT™. In a thermal cycler, samples were heated to 37°C for 15 min, followed by a 15 min incubation at 80°C. Samples were stored at 4°C for a maximum of 1 week, until required for sequencing.

Samples were submitted for Sanger sequencing at SA Pathology Flinders Sequencing Facility and/or Australian Genome Research Facility (AGRF). DNA chromatogram results were analysed using the DNA variant analysis software Mutation Surveyor® (SoftGenetics), as well as CLC sequence viewer 7.5 (CLC Bio, Qiagen, Hilden, Germany).

These methods apply to the upcoming three sections (**2.15.5**, **2.15.6** and **2.15.7**), which describes specific PCR protocols based on the polymerase system of choice (Expand™ Long Template, Phusion® High-fidelity and AmpliTaq Gold™). The various PCR systems utilised in this thesis were based on established protocols[64,73,211], for identifying and validating the various genomic alterations that were of interest.

2.15.5. Long PCR for kinase-domain sequencing

This PCR method was essential for the identification of kinase-domain mutations in the Ba/F3 Ph-like ALL cells. This was an adaptation of methods performed by others[185,211], where primers specific for a small section of the 5' gene was utilised in-combination to a primer flanking the 3' end. This was essential for successful amplification of the 3' kinase-encoding fusion partner gene, avoiding any amplification of its endogenous isoform. The specific primer sequences and reagents (**Table 2.12**) are listed below.

Primers utilised were as follows:

Table 2.11 – Primer sequences for the amplification of kinase domains within fusion genes in Ba/F3 Ph-like ALL cell lines

Fusion gene	Primer sequences (5' to 3')
RANBP2-ABL1	Forward primer (*RANBP2* exon 18): CCAGACTCAGTGCCTGATGG Reverse primer (LongR 0510): GAGGGAGCAATGGAGACACG
SSBP2-CSF1R	Forward primer (*SSBP2* exon 14): CCCATGGGTGGATTAGGAGGAATGG Reverse primer (IRES rv): ACACCGGCCTTATTCCAAG
PAX5-JAK2	Forward primer (M13F *PAX5* exon 5): GTAAAACGACGGCCAGTCTCGTCGTACTCCATCAG Reverse primer (M13R *JAK2* exon 25): CAGGAAACAGCTATGACCTCATCCAGCCATGTTATCCC

RANBP2 and *SSBP2* forward primer sequences were derived from Mullighan *et al*. (St. Jude's Children's Research Hospital Memphis, TN, USA)

Table 2.12 – Volume of components for 'Long PCR' master mix

Component	Final concentration	Volume for 1 sample (μL)
25 mM dNTP	0.75 mM	0.75
dH_2O		18.70
10 x Buffer 3	1.00 x	2.50
50 mM $MgCl_2$	3.50 mM	0.38
RANBP2-E18-H-FW (50 mM)	0.30 mM	0.15
LongR0510 (50 mM)	0.30 mM	0.15
Expand™ Enzyme Mix (0.75 μL per 50 μL rxn)	2.50 U	0.38
Final Volume		**23 μL** (plus 2 μL template cDNA)

PCR cycling conditions:

94°C for 2 min
94°C for 10 sec, 60°C for 30 sec, 68°C for 2 min: 10 cycles total
94°C for 10 sec, 60°C for 30 sec, 68°C for 2 min (increase by 20 sec for every cycle): 20 cycles total
68°C for 7 min
4°C for ∞

Following PCR reaction and confirmation of a single product size via DNA gel electrophoresis, Sanger sequencing was performed using primers specific for the kinase domain, depending on the Ph-like ALL fusion gene (**Table 2.15**). DNA chromatogram results were analysed using the DNA variant analysis software, Mutation Surveyor® (SoftGenetics), to identify the presence of any kinase-domain mutations.

Table 2.13 – Sequencing primers utilised for kinase domain mutation analysis in Ba/F3 Ph-like ALL cell lines

Fusion gene	Primer sequences (5' to 3')
RANBP2-ABL1	Forward primer (*ABL*kinaseF): CGCAACAAGCCCACTGTCT Reverse primer (NestR1010): CAAGGTACTCACAGCCCCACGGA
SSBP2-CSF1R	Forward primer (*CSF1R*-KD-F): GGGAGGCGTCGACTATAAGA Reverse primer (*CSF1R*-KD-R): TCGTCAACTCCTCAGCAGAA
PAX5-JAK2	Forward primer (M13F): GTAAAACGACGGCCAGT Reverse primer (M13R): CAGGAAACAGCTATGACC

2.15.6. Breakpoint sequencing of Ph-like ALL constructs

This section details a method of identification and confirmation of the presence of Ph-like ALL fusion genes, through the amplification of its genomic breakpoint region. PCR using primers specific for *RANBP2-ABL1* and *SSBP2-CSF1R* (**Table 2.14**) were performed using the Phusion® high-fidelity PCR system (**Table 2.15**). Sanger sequencing was further carried out to ensure amplified plasmid DNA contained the correct fusion.

Table 2.14 – Primer sequences for breakpoints of Ph-like ALL fusion genes

Fusion gene	Primer sequences (5' to 3')
RANBP2-ABL1	Forward primer: TGGTTCTTTGCGAAATGCAGATTCA Reverse primer: GCCACCGTCAGGCTGTATTTCTTCC
SSBP2-CSF1R	Forward primer: TCATGCCTAGTCCAGCAGATTCAACCA Reverse primer: TGGCTCATGATCTTCAGCTCGGACA

Primer sequences were derived from Mullighan *et al*. (St. Jude's Children's Research Hospital Memphis, TN, USA)[5].

Table 2.15 – Volume of reagents for 'Phusion PCR' master mix

Component	Final concentration	Volume for 1 sample (μL)
Water		13.00
5x HF buffer	1.00x	4.00
Primer F (5 μM)	0.20 μM	0.80
Primer R (5 μM)	0.20 μM	0.80
dNTP (10 mM)	200.00 μM	0.40
Phusion® High-fidelity DNA polymerase	1.00 unit / 50.00 μl PCR	0.20
cDNA (12.5 ng/μl)	10.00 ng	0.80
Reaction volume		20.00

PCR cycling conditions:

98°C for 1 min
98°C for 10 sec, 66°C for 15 sec, 72°C for 1 min: 33 cycles total
72°C for 10 min
4°C for ∞

2.15.7. Generic PCR with AmpliTaq Gold™ enzyme

This method was utilised to verify the presence of *RAS* mutations (detected by mRNA-seq) by employing gDNA as a template and using the primers listed in **Table 2.16**. The components of reagents are in **Table 2.17** and the reaction was performed as per manufacturer's protocol.

Table 2.16 – Primer sequences for confirmation of *RAS* mutations

***RAS* mutation**	**Primer sequences (5' to 3')**
***KRAS* c.34G>A (G12S)**	FW: GTAAAACGACGGCCAGTTTTTTCTTAAGCGTCGATGG RV: CAGGAAACAGCTATGACCGCACAGAGAGTGAACATCATGG
***NRAS* c.34G>A (G12S)**	FW: GTAAAACGACGGCCAGTAGCCTTCGGGGAGTAATAGG RV: CAGGAAACAGCTATGACCGGACAGGTTTTAGAAACTTCAGC

Primer sequences were derived from Roberts *et al*, 2014[73].

Table 2.17 – Volume of reagents for 'AmpliTaq Gold™ PCR' master mix

Reagent	Final Concentration	Volume for 1 sample (μL)
dNTP 10 mM	0.20 mM	0.50
$MgCl_2$ 25 mM	1.50 mM	1.50
10x buffer	-	2.50
Forward primer 5 μM	0.20 μM	1.00
Reverse primer 5 μM	0.20 μM	1.00
TaqGold	1.25 U	0.15
Sample cDNA (10 ng/μl)	variable	2.00
dH_2O to 25 μl	-	16.35

PCR cycling conditions:

95°C for 10 min
94°C for 30 sec, 59°C for 30 sec, 72°C for 30 sec: 40 cycles total
72°C for 10 min
4°C for ∞

Sanger sequencing was performed using the sequencing primers M13F (5' - GTAAAACGACGGCCAGT - 3') and M13R (5' - CAGGAAACAGCTATGACC - 3'), sequences already tagged onto the *RAS* PCR primers. Electropherogram results were analysed using the DNA variant analysis software Mutation Surveyor® (SoftGenetics).

2.15.8. Transcriptomic sequencing (mRNA-seq)

RNA samples were analysed for concentration, using the Qubit® RNA high-sensitivity assay kit (Thermo Fisher Scientific, USA) and comparing readouts against a standard curve provided by the manufacturer. As the RNA samples were highly concentrated according to the quantitation obtained using the Nanodrop, they were first diluted 1:30 in NF-H_2O followed by a further 1 in 200 dilution in the Qubit® working solution. Samples were briefly vortexed, incubated for 2 min at RT and analysed via the Qubit® 2.0 Fluorometer (Thermo Fisher Scientific, USA).

RNA was also measured for quality using the TapeStation 2200 system (Agilent Technologies, USA) kit, whereby 1 μL of RNA sample was added to 5 μL of sample buffer. An RNA ScreenTape ladder was included. Samples were vortexed for 1 min, denatured at 72°C for 3 min, pulse centrifuged and loaded onto an RNA ScreenTape for analysis on the TapeStation 2200 system (Agilent Technologies, USA). The RNA integrity number (RIN) algorithm, incorporating ratio of the 28s (large ribosomal subunit) and 18s (small ribosomal subunit) peaks were measured for each sample, with values greater than 8 indicating high-quality RNA.

The mRNA library was generated using the TruSeq Stranded mRNA Library Preparation Kit (Part #15031047, Illumina, USA) as per the manufacturer's protocol. Briefly, 3' polyadenylated (poly-A) containing mRNA were firstly purified using oligo-dT attached magnetic beads. This was followed by fragmentation in the presence of divalent cations, at 94°C for 8 min. Fragmentation allows for sizing of sequences to a desired length, preventing binding of randomly primed reverse-transcription at the 5' end that may otherwise introduce bias for downstream reads[214-216]. A cDNA synthesis step was then performed, followed by an end repair process, adenylation of 3' ends and ligation of indexed adapters. Samples were purified and further enriched via PCR to generate a final library.

Analysis of quantity and quality of the resultant library was conducted using the Qubit® dsDNA high-sensitivity assay kit (Thermo Fisher Scientific, USA), followed by the Agilent D1000 ScreenTape to assess library size (~260 base pairs) according to methods previously described (refer to paragraph 2 of this section). Following confirmation of library quality and quantity, cDNA libraries were pooled, diluted and loaded into the NextSeq 500 High Output V2 kit (150 cycles) (Illumina, #FC-404-2002). Samples were sequenced via the NextSeq 500 platform (Illumina, USA), with

paired-end reads (Read 1 at 101 cycles, index with 6 cycles and Read 2 at 51 cycles). Data generated was automatically uploaded onto the Illumina® BaseSpace Sequence Hub, prior to downloading onto the in-house SAHMRI high-performance-computing (HPC) platform for bioinformatics analyses.

2.15.9. Real-time Quantitative PCR (RQ-PCR)

RQ-PCR was conducted to validate gene expression results of mRNA-seq analysis, as well as investigation of *RANBP2-ABL1* fusion gene expression in the TKI-resistant lines. RQ-PCR was conducted using the RT^2 SYBR® Green RQ-PCR Mastermix kit (Qiagen, Hilden, Germany), with cDNA templates made prior (refer to section **2.15.2** for cDNA synthesis).

For validation of mRNA-seq data, three biological replicates of TKI-sensitive and TKI-resistant cells were analysed. RQ-PCR was performed in technical duplicate for two independent experimental repeats. Volumes of master mixes were adjusted accordingly, based on numbers of samples tested (**Table 2.18**). Primer sequences are detailed further in section **2.15.10**.

Table 2.18 – Volume of reagents for SYBR® Green RQ-PCR master mix

Reagents	**Volume per sample (μL)**
SYBR Green Buffer (2x)	5
Primer F/R (10 μM)	1
NF-H_2O	2
cDNA	2
Final Volume	10

PCR cycling conditions:

50°C for 2 min
95°C for 15 min
95°C for 15 sec, 60°C for 26 sec, 72°C for 10 sec: 40 cycles total
72°C for 30 sec
Melt curve gradient from 65°C to 95°C, in 0.5°C increments for 5 sec

RQ-PCR was performed on the Bio-Rad® CFX Connect™ real-time PCR detection system and data analysed via the Bio-Rad® CFX Manager™ software. To calculate the fold change of genes between sensitive and resistant samples, the comparative Ct ($2^{-\Delta\Delta Ct}$) method was applied[2,217].

2.15.10. Comprehensive RQ-PCR Primer List

Table 2.19 – Primers used for RQ-PCR of *RANBP2-ABL1* fusion gene in Ba/F3 cells

Primer Name	Sequence (5' -> 3')
KA_qPCR_*RANBP2*_e18_FW	GACCAGACTCAGTGCCTGATGGAT
KA_qPCR_*ABL1*_e2_RV	AGCGGCTTCACTCAGACCCTGAG

Table 2.20 – Primers used for validation of SUP-B15 Ph+ ALL mRNA-seq data (dasatinib-resistant line)

Gene symbol	Primer Name	Sequence (5' -> 3')
LGR5	*LGR5*_24475886c1_FW	CTCCCAGGTCTGGTGTGTTG
	*LGR5*_24475886c1_RV	GAGGTCTAGGTAGGAGGTGAAG
BACH2	*BACH2*_215276980c1_FW	AATACCAGCTTGCATGTACCAA
	*BACH2*_215276980c1_RV	TTATCTTCCCGGAATGTGCTTG
PDE1A	*PDE1A*_51102298c3_FW	GCATACAGGGACAACAAACAAC
	*PDE1A*_51102298c3_RV	TCTCAAGGACAGAGCGATCAT
EVL	*EVL*_50726984c1_FW	CTTCCGTGATGGTCTACGATG
	*EVL*_50726984c1_RV	TGCAACTTGACTCCAACGACT
ETS1	*ETS1*_219689117c1_FW	GATAGTTGTGATCGCCTCACC
	*ETS1*_219689117c1_RV	GTCCTCTGAGTCGAAGCTGTC
CD24	*CD24*_73623396c1_FW	CTCCTACCCACGCAGATTTATTC
	*CD24*_73623396c1_RV	AGAGTGAGACCACGAAGAGAC
DOCK8	*DOCK8*_302129690c1_FW	TTCACGCCAAAGGAATGTAGG
	*DOCK8*_302129690c1_RV	GTCCCTGACATGAGGGTCCA
SOCS7	*SOCS7*_313850979c3_FW	ACAGGTGAAACTGTGTCGCTT
	*SOCS7*_313850979c3_RV	TAGGCAGCGTCCCACTGATA
SLC25A46	*SLC25A46*_20270310c3_FW	TCTTTCCTTGATCTTCCCTACGG
	*SLC25A46*_20270310c3_RV	CAGCTAGGTGGCTATTGTAAGTC
PDGFA	*PDGFA*_197333758c1_FW	GCAAGACCAGGACGGTCATTT
	*PDGFA*_197333758c1_RV	GGCACTTGACACTGCTCGT
GBP5	*GBP5*_197333735c1_FW	CCATGTGCCTCATCGAGAACT
	*GBP5*_197333735c1_RV	ACAGGTTGCGTAATGGCAGAC
GAPDH	*GAPDH*_378404907c3_FW	CTGGGCTACACTGAGCACC
	*GAPDH*_378404907c3_RV	AAGTGGTCGTTGAGGGCAATG

Table 2.21 – Primers used for validation of SUP-B15 mRNA-seq via RQ-PCR (ponatinib-resistant line)

Gene symbol	Primer Name	Sequence (5' -> 3')
ARHGEF12	*ARHGEF12*_310832411c2_FW	GTCTTGTTCAGCGTTGCGTAA
	*ARHGEF12*_310832411c2_RV	GCATGGCTGCTCCATCTTCT
PLD4	*PLD4*_94681037c3_FW	GCTTGGCGCTGTCATCTATAA
	*PLD4*_94681037c3_RV	CCCCAGTACCCAGTAGGTCT
BEST3	*BEST3*_115527105c1_FW	AGGTAGCAGAGCAGCTTATCA
	*BEST3*_115527105c1_RV	TGCATTTCGTCCACAGCTAAAA
LILRB4	*LILRB4*_125987587c2_FW	CCCACAAGGTCCGTCTCAAC
	*LILRB4*_125987587c2_RV	CCCGATCAGTACCTCCCAGT
MME	*MME*_116256328c3_FW	TGGATCTTGTAAGCAGCCTCA
	*MME*_116256328c3_RV	GCACAACGTCTCCAAGTTGC
LILRA2	*LILRA2*_FW	ATCCCATCCATCACCTGGGA
	*LILRA2*_RV	GGTTTGCTGTAGGCTCCTGT
POU4F1	*POU4F1*_110347448c1_FW	GGGCAAGAGCCATCCTTTCAA
	*POU4F1*_110347448c1_RV	CTGTTCATCGTGTGGTACGTG
GAPDH	*GAPDH*_378404907c3_FW	CTGGGCTACACTGAGCACC
	*GAPDH*_378404907c3_RV	AAGTGGTCGTTGAGGGCAATG

Table 2.22 – Primers used for validation of Ba/F3 Ph-like ALL mRNA-seq data

Gene symbol	Primer Name	Sequence (5' -> 3')
Gli2	*Gli2*_124487480c3_FW	ACCCCTGATCCAGCCTTCA
	*Gli2*_124487480c3_RV	GTTGGCATCATTTAGACAGTTGC
Aldh1a1	*Aldh1a1*_118129922c1_FW	AACACAGGTTGGCAAGTTAATCA
	*Aldh1a1*_118129922c1_RV	TGCGACACAACATTGGCCTT
Fry	*Fry*_255069716c3_FW	ACACTGGCAATATGCACATTGT
	*Fry*_255069716c3_RV	TGATGCTTTGCACCACATAGG
Bcl11a	*Bcl11a*_339409204c1_FW	CAAACGGAAACAATGCAATGGC
	*Bcl11a*_339409204c1_RV	TTTTTCATCTCGATGGGAGAAGG
Lefty1	*Lefty1*_126012509c1_FW	CCAACCGCACTGCCCTTAT
	*Lefty1*_126012509c1_RV	CGCGAAACGAACCAACTTGT
Neo1	*Neo1*_112363081c1_FW	TTGCTCGGCATATTCTGAGCC
	*Neo1*_112363081c1_RV	TGGCGTCGATCATCTGATTCTAA
Rtp4	*Rtp4*_257196210c2_FW	GCCTCAGACCCGGAATACG
	*Rtp4*_257196210c2_RV	TGGCTCTATTTCACGTTGGGG
Rgs5	*Rgs5*_141801698c1_FW	GGGTTGCCTGTGAGAATTACA
	*Rgs5*_141801698c1_RV	TGAAGTGGTCAATGTTCACCTCT
Snai3	*Snai3*_7305643a1_FW	GGTCCCCAACTACGGGAAAC
	*Snai3*_7305643a1_RV	CTGTAGGGGGTCACTGGGATT
Casp12	*Casp12*_157951683c3_FW	AGACAGAGTTAATGCAGTTTGCT
	*Casp12*_157951683c3_RV	TTCACCCCACAGATTCCTTCC
Apol9b	*Apol9b*_30424585a1_FW	GGATACCTGTATAGCCTGGTGG
	*Apol9b*_30424585a1_RV	CAGTTCCCTCAGAGCTTTGTG
Rtp4	*Rtp4*_257196210c2_FW	GCCTCAGACCCGGAATACG
	*Rtp4*_257196210c2_RV	TGGCTCTATTTCACGTTGGGG

Mx2	*Mx2*_7549778c2_FW	AGAGGGAGAATGTCGCCTATT
	*Mx2*_7549778c2_RV	CGTCCACGGTACTGCTTTTCA
Oasl2	*Oasl2*_134053897c3_FW	TACCCACAGAGAGGGCAAAAG
	*Oasl2*_134053897c3_RV	GCATCGTAAGCTGGGAGGATA
Ly6a	*Ly6a*_31981636c1_FW	GAGGCAGCAGTTATTGTGGAT
	*Ly6a*_31981636c1_RV	CGTTGACCTTAGTACCCAGGA
Tgtp1	*Tgtp1*_31543861a2_FW	TGCACAGATGGGGATGAATTTC
	*Tgtp1*_31543861a2_RV	TCACTGTCGAGAGACTCCTGA
Csgalnact1	*Csgalnact1*_357933635c1_FW	GGGGTGGATTTCTCGGGTAGT
	*Csgalnact1*_357933635c1_RV	TGGTCGCCTTTTGGAGTGC
Tox2	*Tox2*_149408147c2_FW	AGTGCCTACGTGGGGATGA
	*Tox2*_149408147c2_RV	CATAGTCTTCGTTACTCTCGCC
F5	*F5*_111185910c2_FW	AGGGGCTTCTTACGCAGAC
	*F5*_111185910c2_RV	ACTGACGATCCATTCATAGGTGT
Bcl2a1a	*Bcl2a1a*_11024684a1_FW	GGCTGAGCACTACCTTCAGTA
	*Bcl2a1a*_11024684a1_RV	TGGCGGTATCTATGGATTCCAC
Ccl4	*Ccl4*_7305459a1_FW	TTCCTGCTGTTTCTCTTACACCT
	*Ccl4*_7305459a1_RV	CTGTCTGCCTCTTTTGGTCAG
Cyp4f40	*Cyp4f40*_157384933c1_FW	CCTCACCGTGGCTACTCTTTT
	*Cyp4f40*_157384933c1_RV	CCACAGAGACGTTGACACTTT
Fgf21	*Fgf21*_146134956c1_FW	GTGTCAAAGCCTCTAGGTTTCTT
	*Fgf21*_146134956c1_RV	GGTACACATTGTAACCGTCCTC
Zfhx3	*Zfhx3*_110225363c2_FW	TTCCCGAATACCTCAGCCCT
	*Zfhx3*_110225363c2_RV	GCTTTTGTGTCGCACGTCA
Cd80	*Cd80*_111038144c2_FW	TGCTGCTGATTCGTCTTTCAC
	*Cd80*_111038144c2_RV	GAGGAGAGTTGTAACGGCAAG
Mouse *β-actin*	Mouse_*β-actin*_FW	TTGCTGACAGGATGCAGAAG
	Mouse_*β-actin*_RV	AAGGGTGTAAAACGCAGCTC

2.16. Bioinformatics Analysis

2.16.1. Differential expression analysis of SUP-B15 Ph+ ALL lines

Differential expression analysis of SUP-B15 mRNA-seq data was courtesy of Dr. Chung Kok and Dr. Kelly Quek. Two biological replicates of each cell line were analysed. mRNA-seq data was aligned to the human genome using the Subread aligner (retrieved from Subread (http://subread.sourceforge.net)), and read summarisation performed with featureCounts[1,5].

Differential expression comparisons between non-resistant and TKI-resistant lines were conducted using the R package limma/voom, with multiple testing corrected via the Benjamini-Hochberg method[218-220]. Genes with a false discovery rate (FDR) of less than 0.05 and a fold-change greater than 2 were considered as significantly differentially-expressed.

2.16.2. Differential expression analysis of Ba/F3 Ph-like ALL lines

Differential expression analysis of mRNA-seq results for the Ba/F3 Ph-like ALL lines was courtesy of Dr. Jiyuan An and Dr. Max Moldovan. Three biological replicates of each cell line were acquired. mRNA-seq data was aligned to the mouse genome and reads quantified using the RSEM software[221]. Differential expression comparisons between non-resistant and TKI-resistant lines was performed using the Bioconductor package edgeR[219,222]. Genes with an FDR of less than 0.05 along with a fold-change greater than 2 were considered as significantly differentially-expressed.

2.16.3. Hierarchical clustering, heatmap and volcano plots via R studio

Hierarchical clustering (HC) dendrograms, heatmaps and volcano plots were generated using R Studio under the guidance of Dr. Chung Kok and Dr. Kelly Quek. HC dendrograms (also described as HC trees) were generated using unsupervised clustering of Fragments Per Kilobase of transcript per Million mapped reads (FPKM) values, enabling unbiased visualisation of Euclidean distances between individual

biological replicate samples. For graphical representations of differentially-expressed genes between biological replicate samples, heatmaps utilising significantly expressed genes (p<0.05) were generated. Volcano plots of differentially-expressed genes were generated by taking the average Log_2FC between biological replicates of sensitive and resistant lines (x-axis), and plotting this value with respect to FDRs obtained (y-axis). Genes of interests (GOIs) were annotated using the HUGO Gene Nomenclature Committee (HGNC) symbol.

2.16.4. Pathway analysis via InnateDB

Pathway analysis of differentially-expressed genes was performed under the guidance of A/Prof David Lynn. Ensembl gene symbols of significantly upregulated and downregulated genes ($Log_2FC > 1$, $p < 0.05$) in resistant cells compared to sensitive were uploaded onto the 'pathway analysis' tool in InnateDB[223,224]. A hypergeometric algorithm incorporating multiple testing corrected via the Benjamini Hochberg method was applied, identifying pathways that may be significantly altered in the TKI-resistance setting.

2.16.5. Network analysis via Cytoscape

Network analysis of differentially-expressed genes was performed under the guidance of A/Prof David Lynn, with figures generated courtesy of Dr. Sriganesh Srihari. Ensembl gene symbols of significantly upregulated and downregulated genes ($Log_2FC > 1$, $p< 0.05$) in resistant cells compared to sensitive were uploaded onto the 'network analysis' tool in InnateDB[28,29]. Data generated was visualised using Cytoscape 3.5.1 (The Cytoscape Consortium), with protein interactions further explored using the Contextual Hub Analysis Tool (CHAT)[225-227].

2.17. Statistical analysis

Figures were generated with GraphPad Prism 7 (GraphPad Software Inc., USA) and Microsoft Office Excel 2016 (Microsoft Corporation, USA) unless otherwise specified. Graphs represent the mean, with error bars indicating standard deviation (SD) or standard error of the mean (SEM). With sigmoidal dose-response curves in drug-treatment analyses, plots were generated using the variable slope model on

GraphPad Prism® software. Statistical analysis was performed using a 2-tailed Student's *t*-test and differences considered to be statistically significant when the probability value (*P*-value) was less than 0.05.

THIS PAGE INTENTIONALLY LEFT BLANK.

CHAPTER 3 –

TKI-RESISTANCE IN IMMORTALISED SUP-B15 Ph+ ALL CELLS IS MEDIATED BY A BCR-ABL INDEPENDENT MECHANISM

3.1. Introduction

Acute lymphoblastic leukaemia is an aggressive cancer of the blood and bone marrow, with alterations involving the Philadelphia-chromosome leukaemia known to present with a poorer prognosis[228]. In ALL, the major isoform of Bcr-Abl is the p190 kDa (rather than p210 as in CML). This smaller isoform, termed 'e1a2', is a product of the fusion of the minor region of *BCR* exon 1 (e1) to *ABL* exon 2 (a2), in contrast to Bcr-Abl p210, where an e14a2 fusion resulting from the translocation of the major *BCR* breakpoint to *ABL*, is present[229,230].

As Ph+ ALL often results in a poorer prognosis, intensive chemotherapy, followed by haematopoietic stem cell transplantation (HSCT) was the usual treatment approach prior to the TKI era[231,232]. HSCT, however, is dependent upon the availability of suitably matched donors[233] and is complicated by graft-versus-host disease (GVHD)[234].

The development of tyrosine kinase inhibitors (TKIs) such as imatinib enables the specific targeting of the Bcr-Abl oncoprotein[129], resulting in improvement of survival and treatment outcomes[189]. Specifically, administration of TKI as monotherapy in-combination with chemotherapy are reportedly effective in reducing leukaemic burden[230,235-237]. Despite the effectiveness of TKI use in Ph+ ALL, relapse as a result of TKI resistance remains a major clinical hurdle[238,239].

TKI-resistance can be attributed to the presence of point mutations within the Abl kinase domain[155,240], as well as independent mechanisms such as the upregulation of drug efflux transporters[241,242] or increased expression of the Raf/Mek/Erk (protein kinase C) pathway[243]. In a Ph+ ALL setting, resistance to the first generation TKI

imatinib has been extensively studied[152], however, there are fewer studies in the setting of second generation TKIs.

In this chapter, I hypothesise that TKI-resistance in Ph+ ALL is caused by the presence of Abl kinase domain mutations. Here, I aimed to model TKI-resistance using the immortalised Ph+ ALL cell line SUP-B15, derived from the bone marrow of an 8-year old patient diagnosed with Ph+ (*BCR-ABL1*+) B cell precursor ALL[244]. This chapter describes the development of characterisation of resistance to dasatinib and ponatinib (a second and third-generation Abl TKI respectively).

3.2. Approach

Immortalised SUP-B15 Ph+ ALL, cells at a concentration of 5 x 10^5/mL, were sub-cultured every three days, in increasing concentrations of dasatinib or ponatinib to a final concentration of 200 nM. Parallel naïve (TKI-sensitive) and 0.1% DMSO control (accounting for any changes as a drug diluent effect) were simultaneously passaged. In this chapter, cells resistant to the intermediate concentrations of 2, 5, 7, 20, 30 and 50 nM, alongside TKI-sensitive and the final concentration of 200 nM TKI-resistance, were utilised.

To monitor the onset of TKI-resistance, phosphorylated CrkL (an intermediate downstream effector of Bcr-Abl activity) was evaluated via Western blotting. Cells in dose-escalation concentrations of 2, 5, 7 and 20 nM dasatinib/ponatinib were analysed for p-CrkL IC_{50}. In 30 nM dasatinib/ponatinib resistant cells, TKI-sensitivity was evaluated using analyses of p-Bcr-Abl p190 and cleaved PARP protein in addition to p-CrkL expression, as well as Trypan blue exclusion to confirm cell viability. Cells resistant to 50 nM dasatinib/ponatinib were further analysed for phosphorylated Erk1/2 (p42/44 mitogen-activated protein kinase (MAPK)) expression, to elucidate any downstream activation of MAPK signalling associated with TKI-resistance.

Cells resistant to a concentration of 200 nM dasatinib/ponatinib (final concentration) *in vitro*, were analysed using p-CrkL IC_{50} and mRNA sequencing was also performed, as an approach to identifying the presence of any alternative signalling mechanisms. The mRNA-seq data was analysed using the Subread[1] aligner and featureCounts[5] algorithm, with normalisation and differential-expression analysis conducted using the limma/voom[218,219] package in R. Sequences from mRNA-seq

analysis were visualised using the Integrative Genomics Viewer (IGV)[245,246], with heatmap and volcano plots subsequently generated using RStudio[247].

To further investigate the presence of *RAS* oncogene mutations in TKI-resistant SUP-B15 cells, genomic DNA PCR using primers specific for *KRAS* and *NRAS*[73] was performed. Sanger sequencing data was analysed using the Mutation Surveyor Version 3.30 (SoftGenetics®, Pennsylvania USA)[248].

3.3. Results

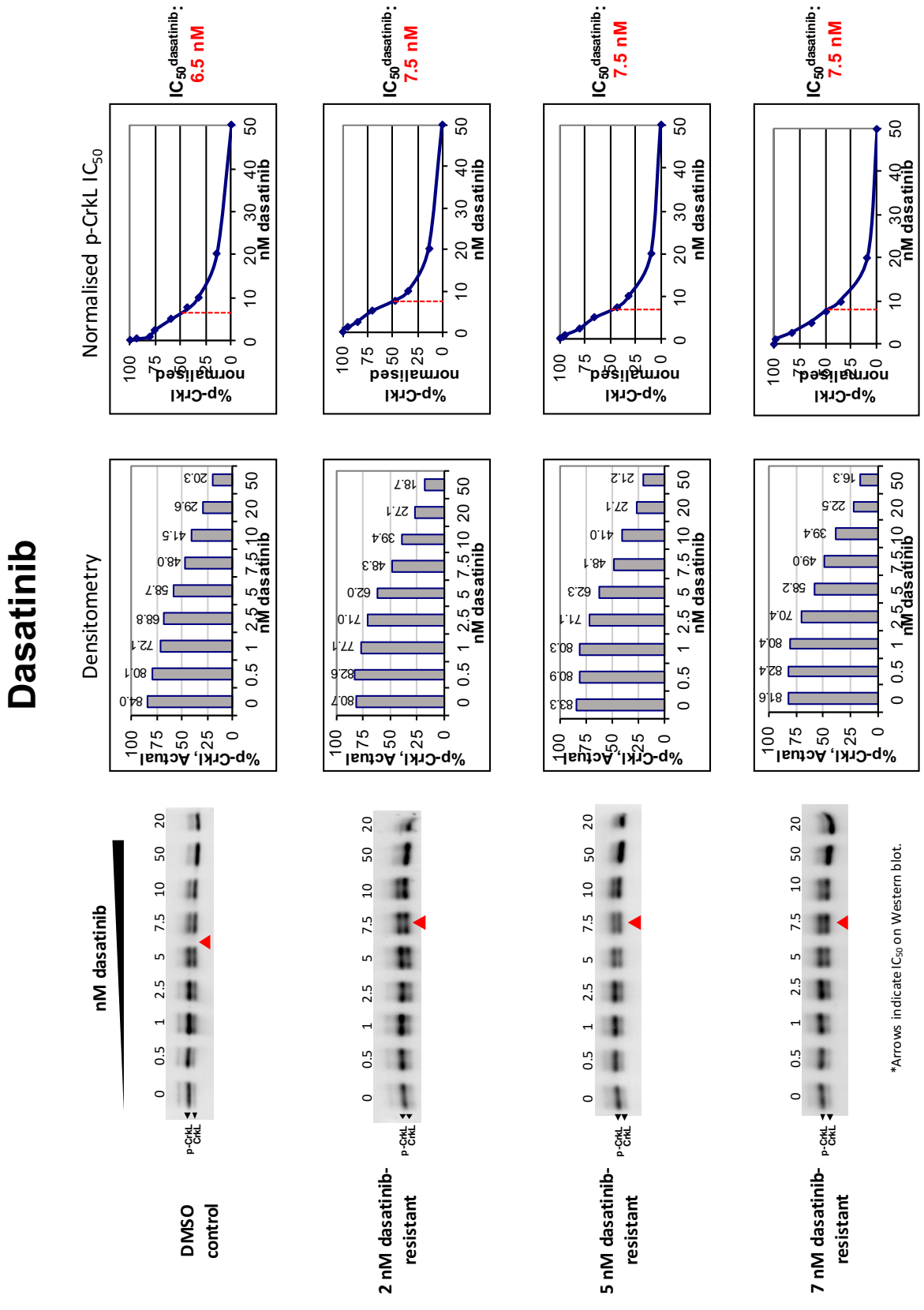
3.3.1. Investigation of p-CrkL activity in low-dose TKI-resistant SUP-B15 cell lines

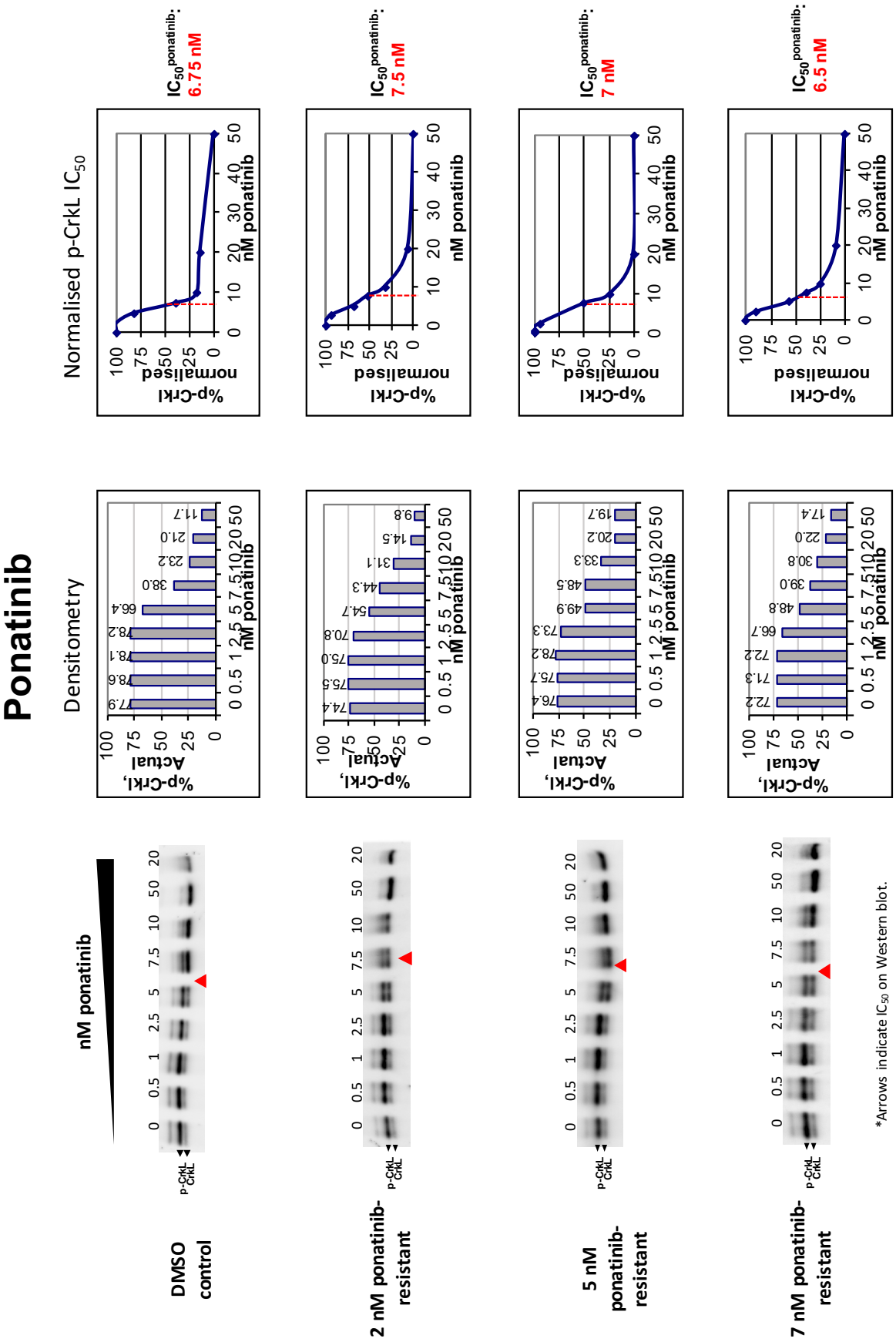
As SUP-B15 Ph+ ALL cells are sensitive to Abl TKIs under normal conditions, cells cultured in low-dose intermediate concentrations of dasatinib/ponatinib were monitored for phosphorylated CrkL activity. Evaluation of p-CrkL IC_{50} in SUP-B15 cells maintained in DMSO (control), 2 nM, 5 nM and 7 nM dasatinib/ponatinib indicated no marked differences in p-CrkL IC_{50} compared to TKI-sensitive controls (**Figure 3.1**). ($IC_{50}^{dasatinib}$ 6.5 nM (DMSO control), 7.5 nM (2 nM dasatinib-resistant), 7.5 nM (5 nM dasatinib-resistant) and 7.5 nM (7 nM dasatinib-resistant)) (**Figure 3.1A**). In ponatinib-treated cells, the $IC_{50}^{ponatinib}$ was 6.75 nM (DMSO control), 7.5 nM (2 nM ponatinib-resistant), 7 nM (5 nM ponatinib-resistant) and 6.5 nM (7 nM ponatinib-resistant) (**Figure 3.1B**).

Further investigation of SUP-B15 cells resistant to a concentration of 20 nM TKI revealed no differences in p-CrkL IC_{50} compared to control cell lines (**Figure 3.2**). ($IC_{50}^{dasatinib}$ of 5.9 nM in DMSO control cells, and, 4 nM in 20 nM dasatinib resistant cells) (**Figure 3.2A**). DMSO control and 20 nM ponatinib-resistant cells revealed an $IC_{50}^{ponatinib}$ of 5.25 and 2.5 nM respectively (**Figure 3.2B**).

Figure 3.1 – Dasatinib and ponatinib p-CrkL IC_{50} in control and low-dose TKI-resistant SUP-B15 cells.

Western immunoblotting of p-CrkL IC_{50} in TKI-sensitive and low-dose intermediate TKI-resistant (2, 5, and 7 nM dasatinib/ponatinib resistant) SUP-B15 cell lines. Cells were incubated in increasing concentrations of TKI (0, 0.5, 1, 2.5, 5, 7.5, 10, 20 and 50 nM) for 2 hrs at 37°C/5% CO_2, prior to lysis for protein electrophoreses and CrkL analysis. **A:** dasatinib IC_{50}; **B:** ponatinib IC_{50}. Western blots are indicated on the left-most column. Densitometry analysis was performed and the actual p-CrkL values are represented by bar graphs in the middle column. These values were later normalised to derive the p-CrkL IC_{50}, as represented by the red dotted line in the line graphs on the right-most column. Data shown is data of n=1 experiment.


A
Dasatinib
Densitometry
Normalised p-CrkL IC50
nM dasatinib
DMSO control
2 nM dasatinib-resistant
5 nM dasatinib-resistant
7 nM dasatinib-resistant
p-CrkL
CrkL
%p-CrkI, Actual
%p-CrkI normalised
nM dasatinib
IC50 dasatinib: 6.5 nM
IC50 dasatinib: 7.5 nM
IC50 dasatinib: 7.5 nM
IC50 dasatinib: 7.5 nM
*Arrows indicate IC50 on Western blot.


B
Ponatinib
Densitometry
Normalised p-CrkL IC50
nM ponatinib
0 0.5 1 2.5 5 7.5 10 20 50
p-CrkL
CrkL
DMSO control
2 nM ponatinib-resistant
5 nM ponatinib-resistant
7 nM ponatinib-resistant
%p-CrkL, Actual
%p-CrkL normalised
nM ponatinib
IC50ponatinib: 6.75 nM
IC50ponatinib: 7.5 nM
IC50ponatinib: 7 nM
IC50ponatinib: 6.5 nM
*Arrows indicate IC50 on Western blot.

THIS PAGE INTENTIONALLY LEFT BLANK.

Figure 3.2 – Dasatinib and ponatinib p-CrkL IC_{50} of 20 nM intermediate TKI-resistant cell lines suggest Bcr-Abl is not the driver of TKI-resistance

Western immunoblotting of p-CrkL indicates no marked increase in IC_{50} between TKI-sensitive and 20 nM dasatinib/ponatinib TKI-resistant cells. Cells were treated with TKI for 2 hrs at 37°C/5% CO_2, prior to preparation of cells for Western analysis as previously described. **A**: dasatinib treatment in DMSO control and 20 nM dasatinib-resistant cells. **B**: ponatinib treatment in DMSO control and 20 nM ponatinib-resistant cells. Red triangles on western blots indicate the approximate IC_{50} concentration, bar graphs comprise of the p-CrkL densitometry analyses while line graphs represent the normalised values for extrapolation of the IC_{50}, as indicated by the red dotted lines.

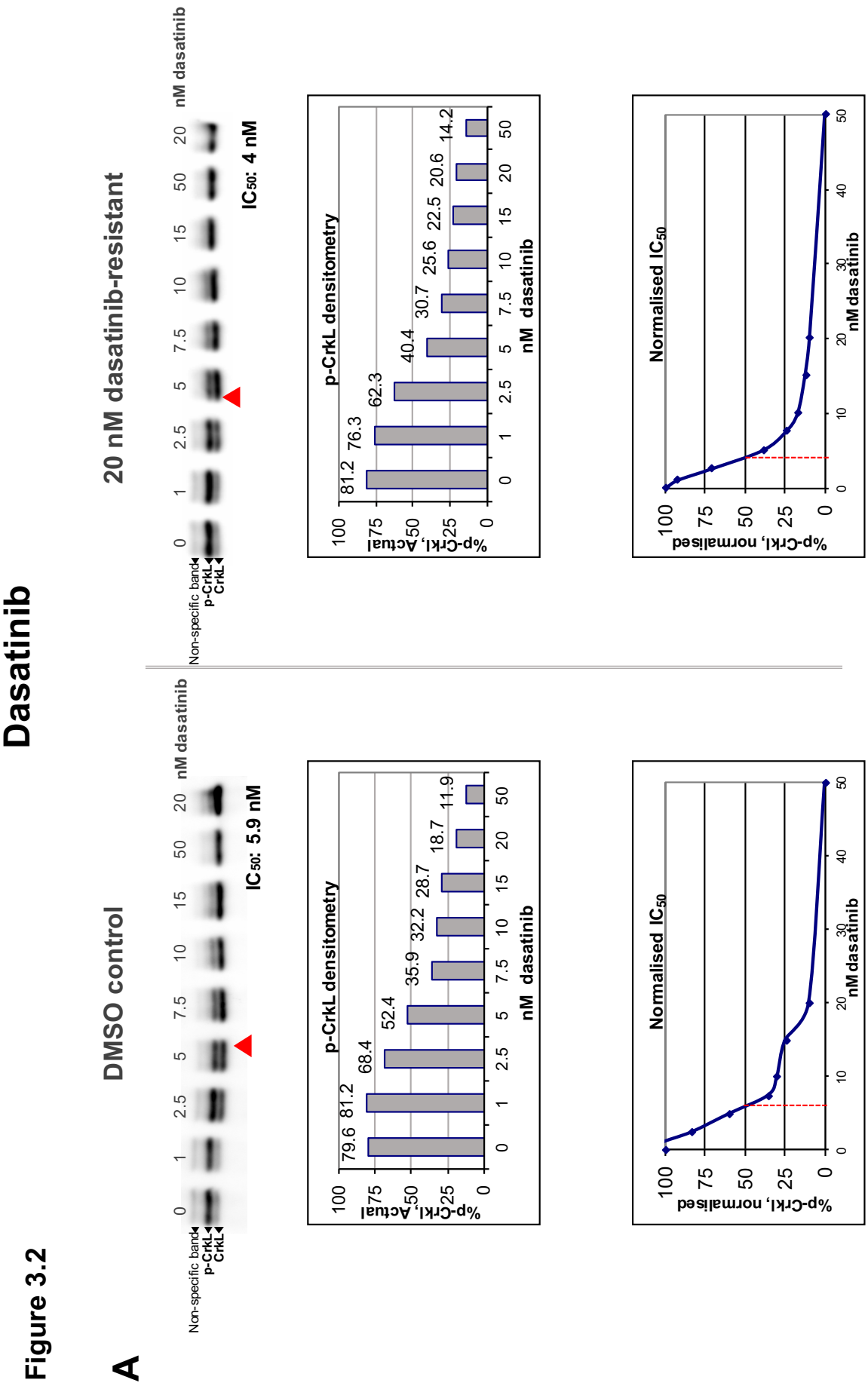
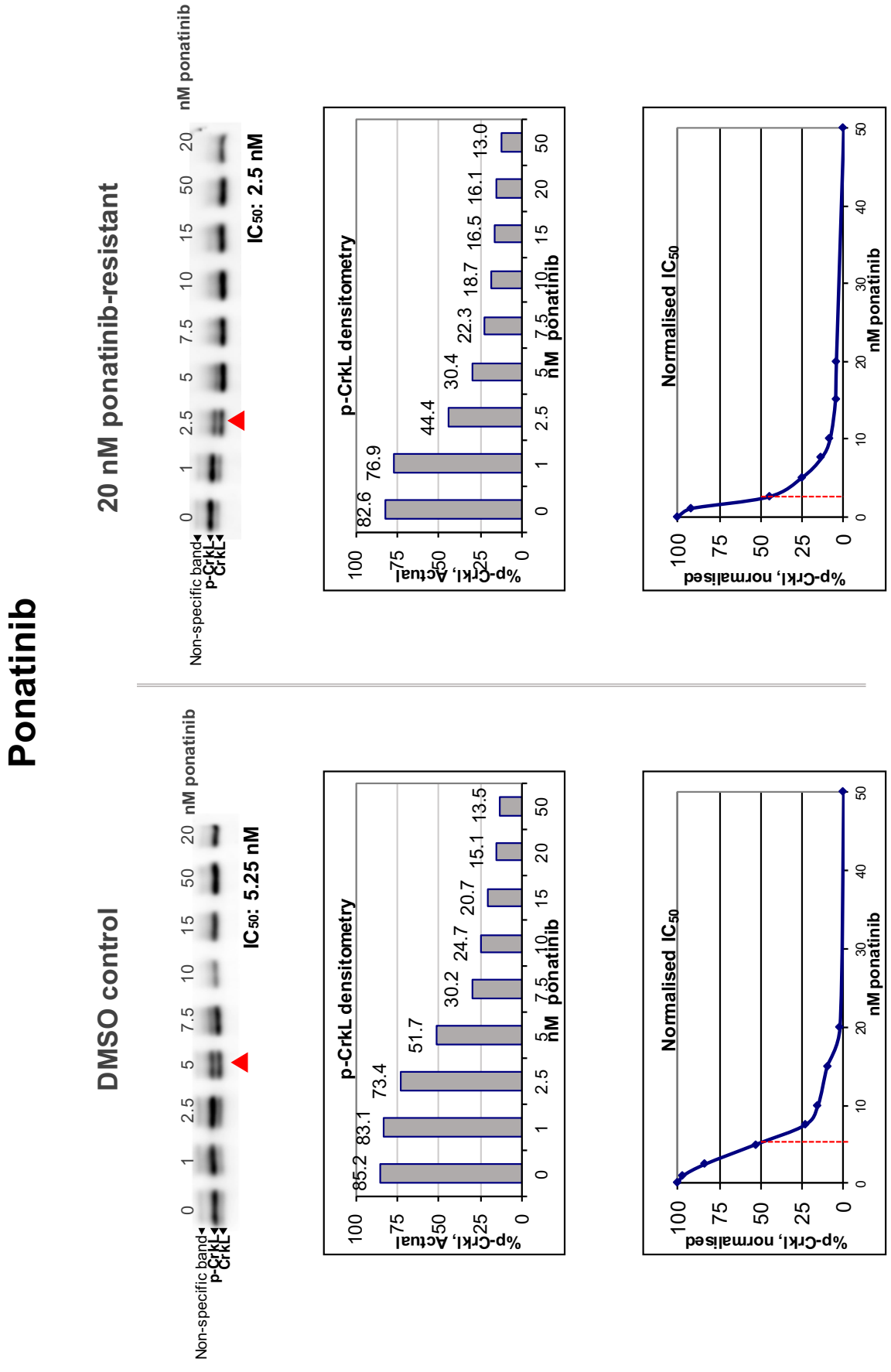

A
Dasatinib
DMSO control
20 nM dasatinib-resistant
Non-specific band
p-CrkL
CrkL
0 1 2.5 5 7.5 10 15 20 50 nM dasatinib
IC50: 5.9 nM
IC50: 4 nM
p-CrkL densitometry
%p-CrkL, Actual
nM dasatinib
79.6 81.2 68.4 52.4 35.9 32.2 28.7 18.7 11.9
81.2 76.3 62.3 40.4 30.7 25.6 22.5 20.6 14.2
Normalised IC50
%p-CrkL, normalised
nM dasatinib

Figure 3.2


B
Ponatinib
DMSO control
20 nM ponatinib-resistant
Non-specific band
p-CrkL
nM ponatinib
IC50: 5.25 nM
IC50: 2.5 nM
p-CrkL densitometry
%p-CrkL, Actual
nM ponatinib
85.2
83.1
73.4
51.7
30.2
24.7
20.7
15.1
13.5
82.6
76.9
44.4
30.4
22.3
18.7
16.5
16.1
13.0
Normalised IC50
%p-CrkL, normalised

3.3.2. SUP-B15 30 nM dasatinib/ponatinib-resistant SUP-B15 cells demonstrate no increase in p-Bcr-Abl or p-CrkL IC_{50}, despite abrogation of cleaved PARP cell death marker expression

Bcr-Abl and CrkL phosphorylation, as well as poly (ADP-ribose) polymerase (PARP) cleavage (a marker of cell death activity), were subsequently investigated in 30 nM TKI-resistant cell lines (**Figure 3.3** & **Figure 3.4**). In dasatinib treated cells, there was no difference in the IC_{50} based on p-Bcr-Abl and p-CrkL between DMSO control and 30 nM dasatinib-resistant cell lines (**Figure 3.3A**). The expression of p-Bcr-Abl in 0, 0.5, 5 and 50 nM TKI was 100%, 56.6%, 40.6% and 24.5% in DMSO control, and, 100%, 105.9%, 70.4% and 38.5% in 30 nM dasatinib-resistant cells. Analysis of the percentage of p-CrkL (by comparing p-CrkL vs CrkL bands which proportionately vary depending on treatment) also indicated a similar trend between TKI-sensitive and resistant cell lines (DMSO control: 100%, 91.6%, 52.4% and 40.8%; 30 nM dasatinib-resistant: 100%, 93.3%, 56.4% and 29.6% in 0, 0.5, 5 and 50 nM dasatinib).

Western blotting indicated an increased expression of cleaved PARP when DMSO control cells were treated with increasing concentrations (0, 0.5, 5 and 50 nM) of dasatinib (cleaved/full-length PARP ratio: 0.31, 0.47, 0.52 and 0.39) (**Figure 3.3B)**. A lack of cleaved PARP expression was observed in 30 nM dasatinib-resistant cells exposed to increasing concentrations of dasatinib (cleaved/full-length PARP ratio: 0.06, 0.07, 0.09 and 0.16 at 0, 0.5, 5 and 50 nM dasatinib). This result was supported by the levels of full-length uncleaved PARP (116 kDa), which was abundant in TKI-sensitive and resistant cell lines. Trypan blue exclusion analyses further supported this finding, where DMSO control cells remained sensitive to dasatinib, unlike 30 nM dasatinib-resistant cells (**Figure 3.3C**).

Western blotting analysis of p-Bcr-Abl and p-CrkL in 30 nM ponatinib-resistant SUP-B15 cells indicated no marked differences compared to DMSO control cells (**Figure 3.4A**). The expression of p-Bcr-Abl in cells treated with 0, 0.5, 5 and 50 nM ponatinib was 100%, 89.2%, 58.9% and 29.8% in DMSO control cells, and, 100%, 97.4%, 65.2% and 21.9% in 30 nM ponatinib-resistant cells. Analysis of p-CrkL percentages in cells exposed to 0, 0.5, 5 and 50 nM ponatinib indicated values of 100%, 97.6%, 72.3% and 37.0% in DMSO control cells, and, 100%, 94.4%, 85.7% and 47.0% in 30 nM ponatinib-resistant cells.

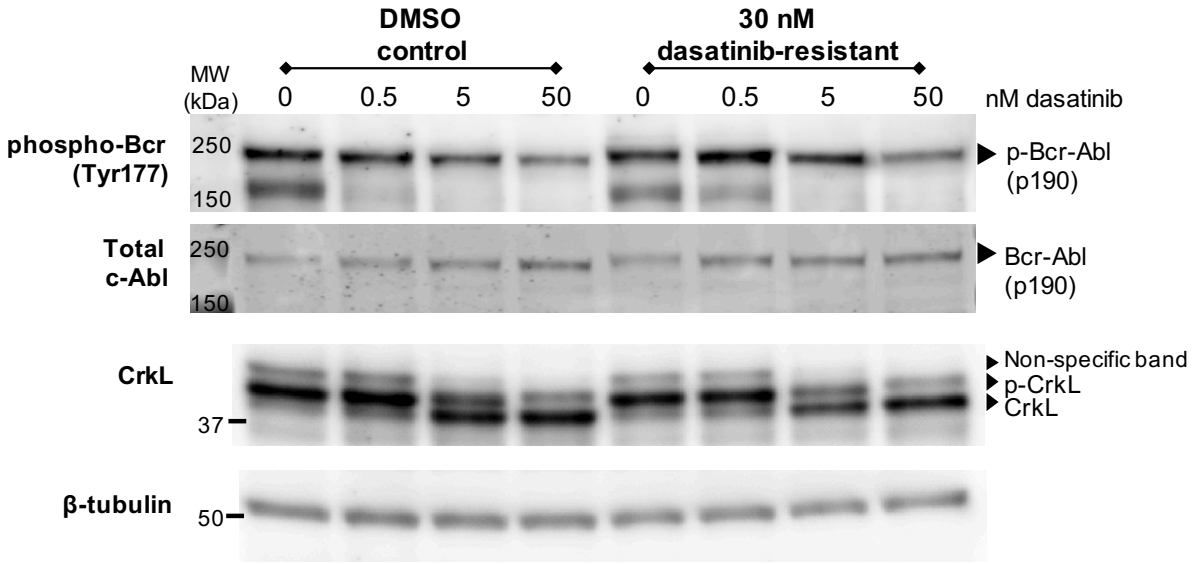
Analysis of cleaved PARP in cells treated with ponatinib revealed an increased expression in DMSO control cells, in contrast to 30 nM ponatinib-resistant cells. The ratio of cleaved PARP in DMSO control cells treated with 0, 0.5, 5 and 50 nM ponatinib was 0.91, 0.98, 0.17 and 0.70, while in 30 nM ponatinib-resistant cells, the cleaved PARP ratio was 0.05, 0.07, 0.09 and 0.13 (**Figure 3.4B**). Trypan blue exclusion analyses indicate stability of cell viability and proliferation in 30 nM ponatinib-resistant cells, despite increasing dose-exposure to ponatinib (**Figure 3.4C**).

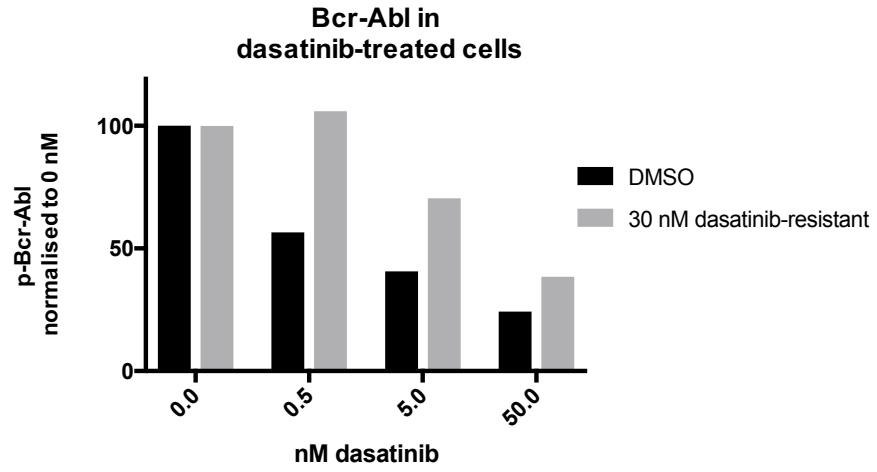
Figure 3.3 – 30 nM dasatinib-resistant cells do not demonstrate any increased Bcr-Abl activity, despite an abrogation of cell death

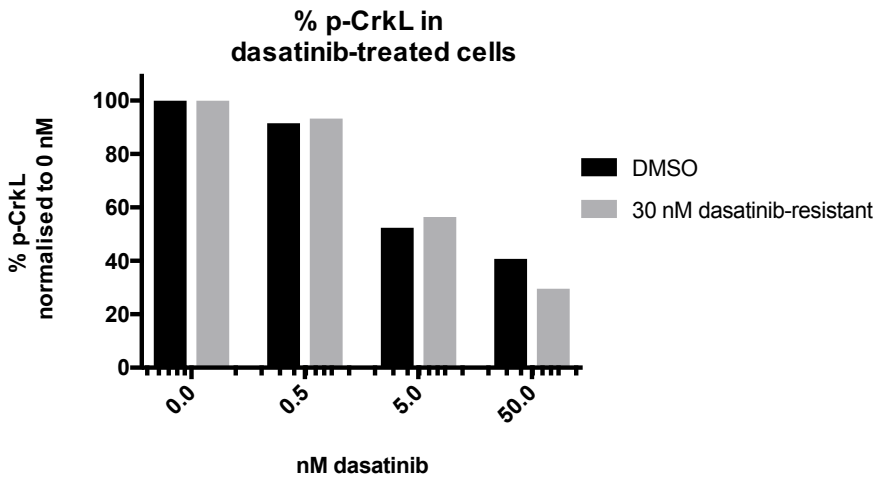
A: Western immunoblotting of p-Bcr-Abl and p-CrkL indicates no marked increase of IC_{50} between DMSO control and 30 nM dasatinib-resistant cells, where a decreasing trend was observed in both cell lines as confirmed by densitometry analysis. **B**: Cleaved PARP (a marker of cell death activity) and full-length PARP detected by Western blotting at 24 h treatment indicating increased cell death in DMSO control cells treated with increasing concentrations of dasatinib. No changes were observed in the 30 nM dasatinib-resistant cell line. **C**: Trypan blue exclusion analysis of dose-response over a 3-day (72 h) period verifying TKI-resistance in 30 nM dasatinib-resistant cells (stable % viability and increasing live cell density), in contrast to TKI-sensitive DMSO control cells (decreasing viability and density with increasing TKI concentration). Data is representative of n=1 experiment.

Figure 3.3

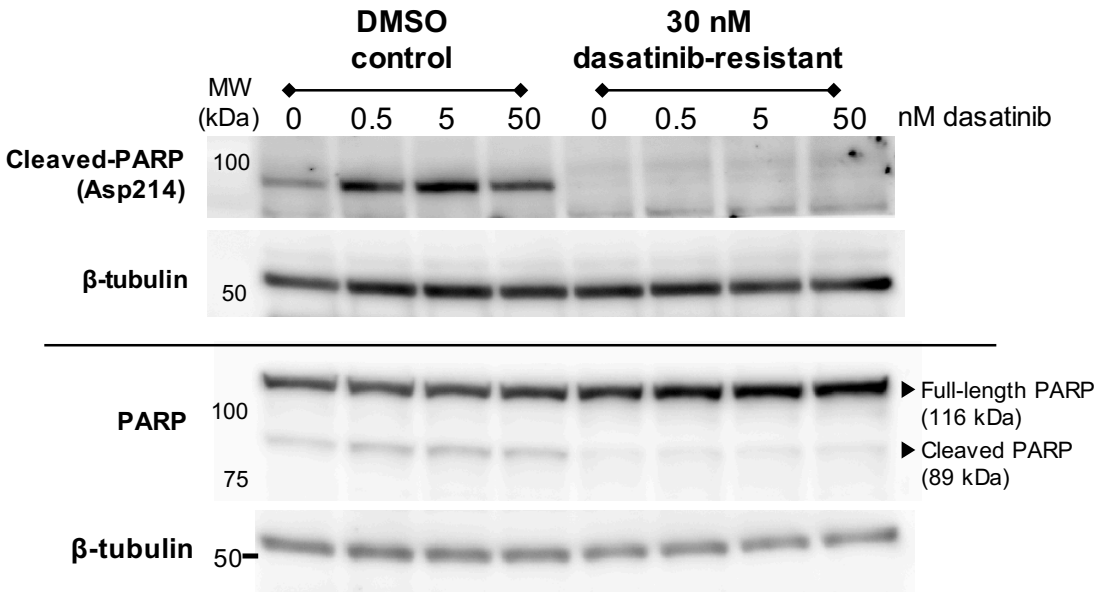
A

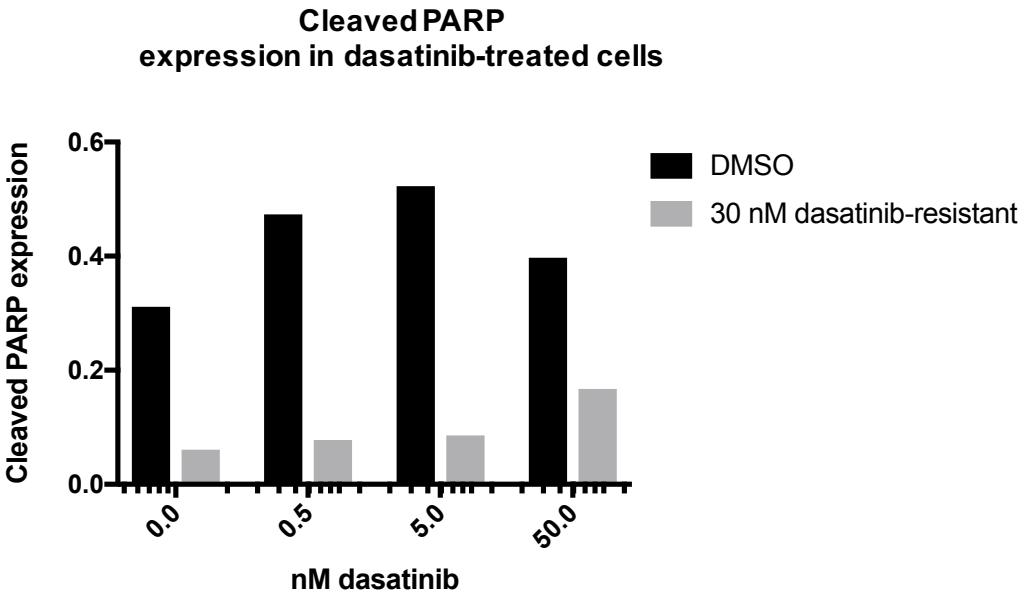

DMSO control
30 nM dasatinib-resistant
MW (kDa)
0
0.5
5
50
0
0.5
5
50
nM dasatinib
phospho-Bcr (Tyr177)
250
150
p-Bcr-Abl (p190)
Total c-Abl
250
150
Bcr-Abl (p190)
CrkL
37
Non-specific band
p-CrkL
CrkL
β-tubulin
50


Bcr-Abl in dasatinib-treated cells
p-Bcr-Abl normalised to 0 nM
100
50
0
DMSO
30 nM dasatinib-resistant
0.0
0.5
5.0
50.0
nM dasatinib

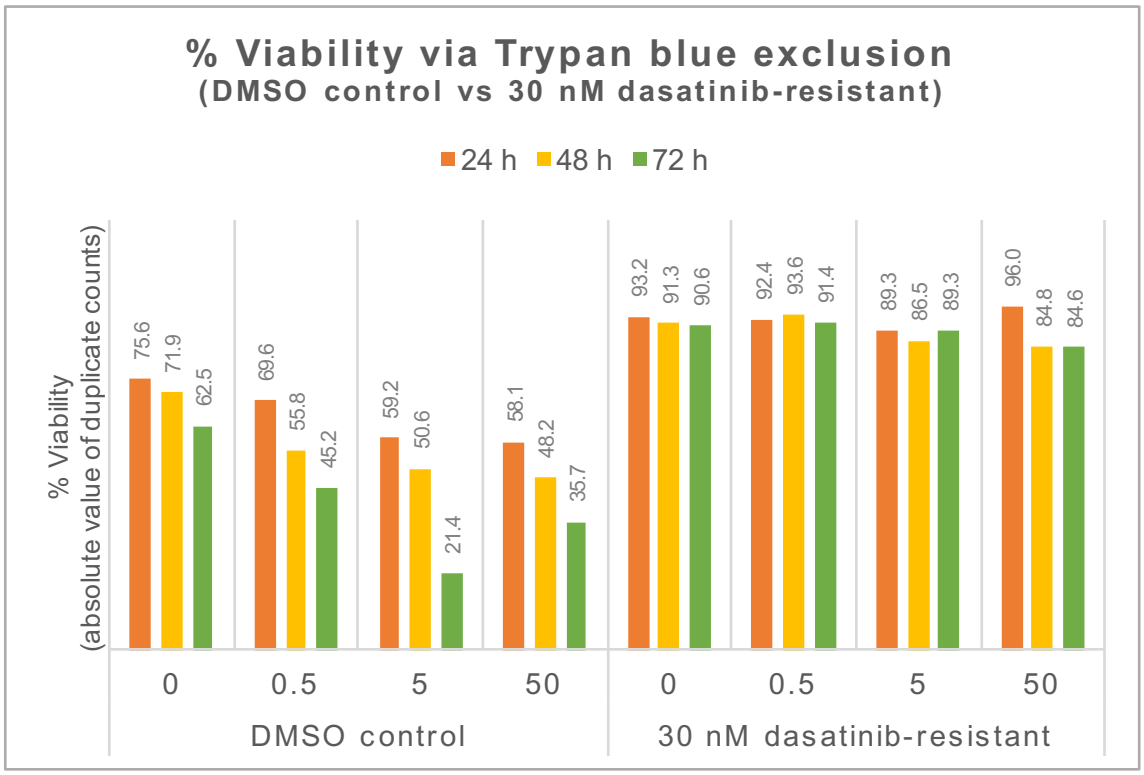

% p-CrkL in dasatinib-treated cells
% p-CrkL normalised to 0 nM
100
80
60
40
20
0
DMSO
30 nM dasatinib-resistant
0.0
0.5
5.0
50.0
nM dasatinib

B


DMSO control
30 nM dasatinib-resistant
MW (kDa)
0
0.5
5
50
0
0.5
5
50
nM dasatinib
Cleaved-PARP (Asp214)
100
β-tubulin
50
PARP
100
75
Full-length PARP (116 kDa)
Cleaved PARP (89 kDa)
β-tubulin
50


Cleaved PARP expression in dasatinib-treated cells
Cleaved PARP expression
0.6
0.4
0.2
0.0
DMSO
30 nM dasatinib-resistant
0.0
0.5
5.0
50.0
nM dasatinib

C


% Viability via Trypan blue exclusion
(DMSO control vs 30 nM dasatinib-resistant)
24 h
48 h
72 h
% Viability
(absolute value of duplicate counts)
75.6
71.9
62.5
69.6
55.8
45.2
59.2
50.6
21.4
58.1
48.2
35.7
93.2
91.3
90.6
92.4
93.6
91.4
89.3
86.5
89.3
96.0
84.8
84.6
0
0.5
5
50
0
0.5
5
50
DMSO control
30 nM dasatinib-resistant

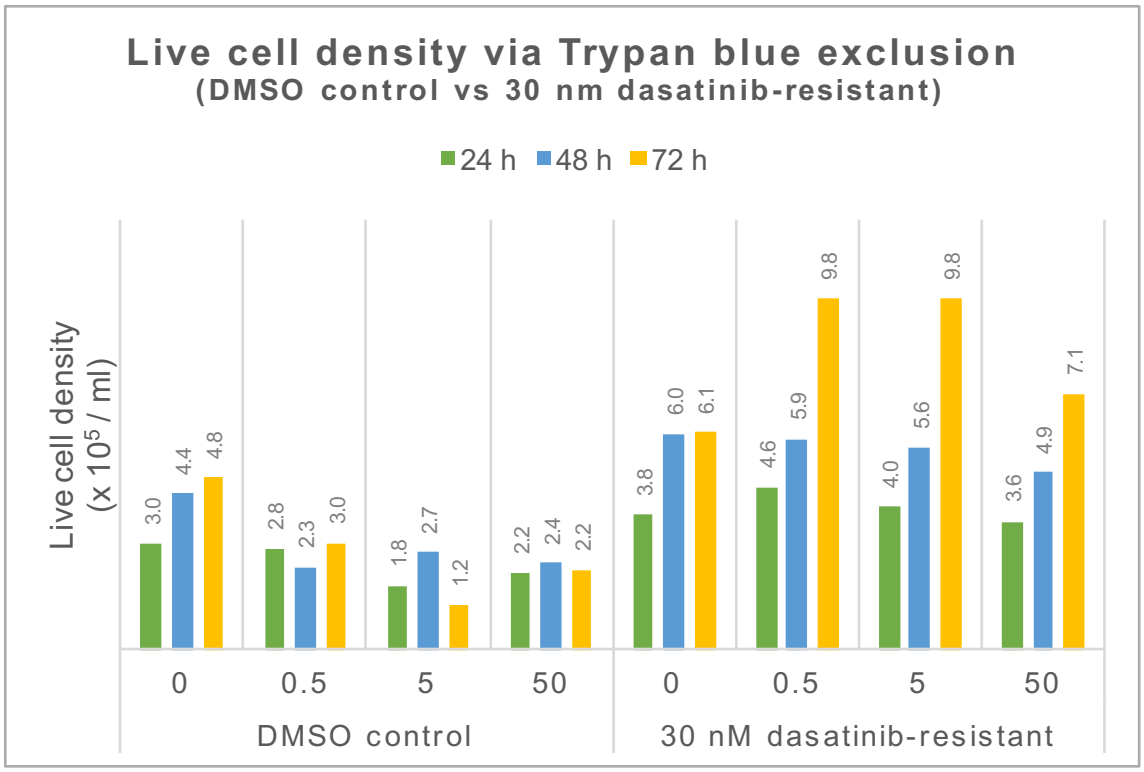
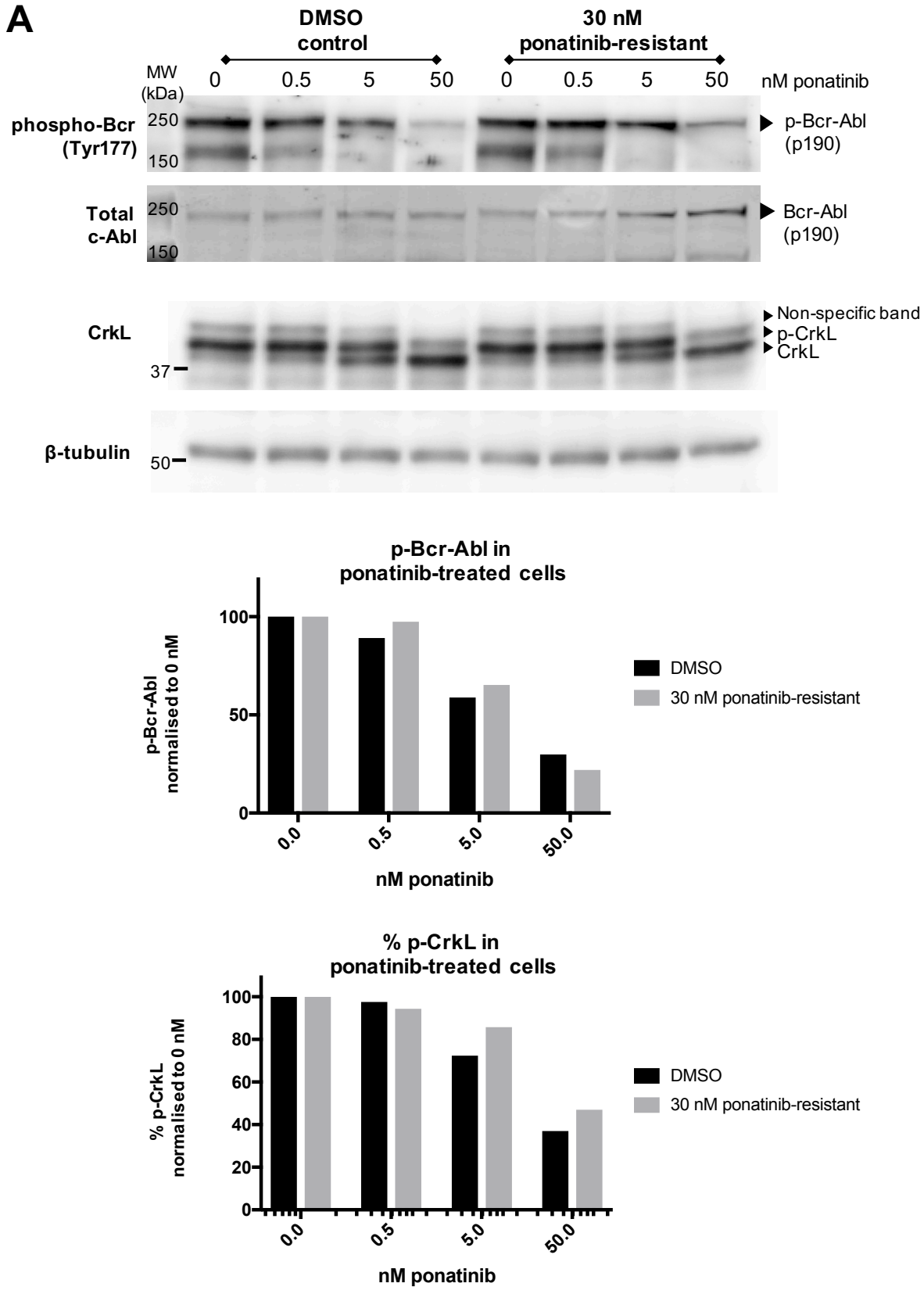

Live cell density via Trypan blue exclusion
(DMSO control vs 30 nm dasatinib-resistant)
24 h
48 h
72 h
Live cell density
(x 10^5 / ml)
3.0
4.4
4.8
2.8
2.3
3.0
1.8
2.7
1.2
2.2
2.4
2.2
3.8
6.0
6.1
4.6
5.9
9.8
4.0
5.6
9.8
3.6
4.9
7.1
0
0.5
5
50
0
0.5
5
50
DMSO control
30 nM dasatinib-resistant

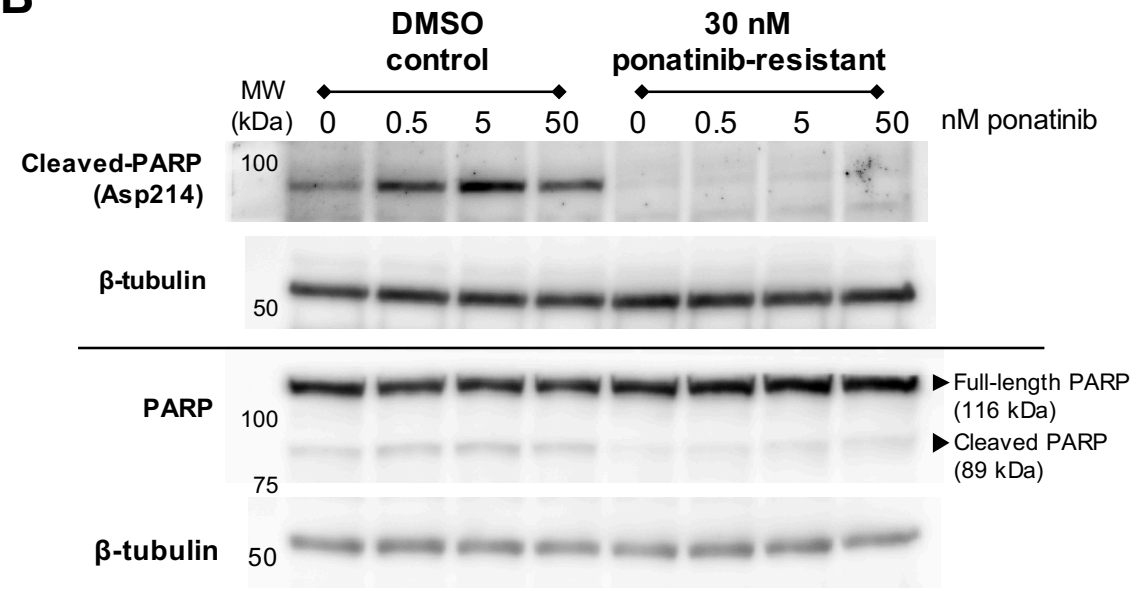
Figure 3.4 – 30 nM ponatinib-resistant cells indicate no increased Bcr-Abl activity, despite abrogation of cell death

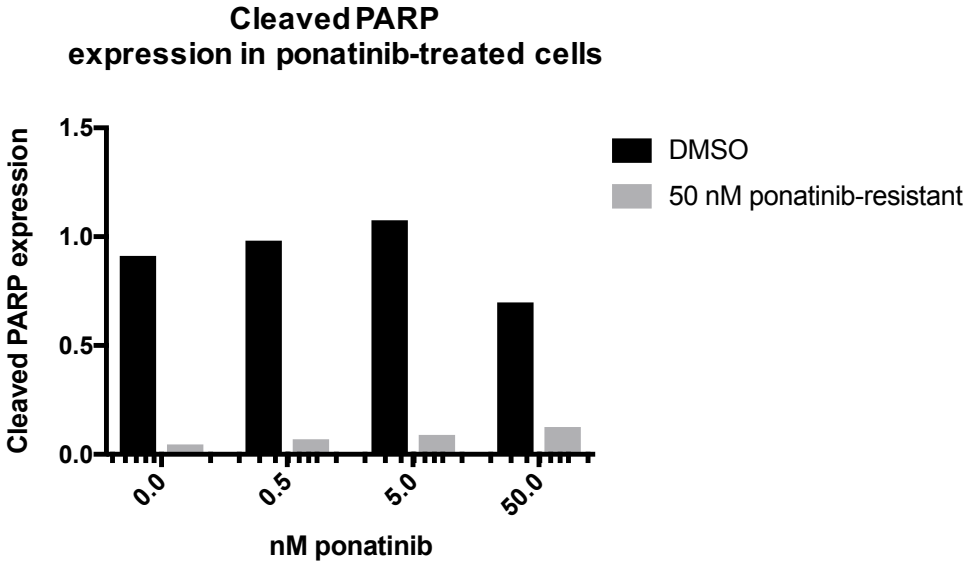
A: Western immunoblotting of p-Bcr-Abl and p-CrkL suggests no marked increase of IC_{50} between DMSO control and 30 nM ponatinib-resistant cells, where a decreasing trend was observed in both cell lines as confirmed by densitometry analysis. **B**: Cleaved PARP (a marker of cell death activity) and full-length PARP detected by western blotting at 24 h treatment indicate an increased cell death in DMSO control cells treated with increasing concentrations of ponatinib. No changes were observed in the 30 nM ponatinib-resistant cell line. **C**: Trypan blue exclusion analysis of dose-response over a 3-day (72 h) period confirms TKI-resistance in 30 nM dasatinib-resistant cells (stable % viability and increasing live cell density), in contrast to TKI-sensitive DMSO control cells (decreasing viability with increased TKI-exposure). Data is data of n=1 experiment.

Figure 3.4

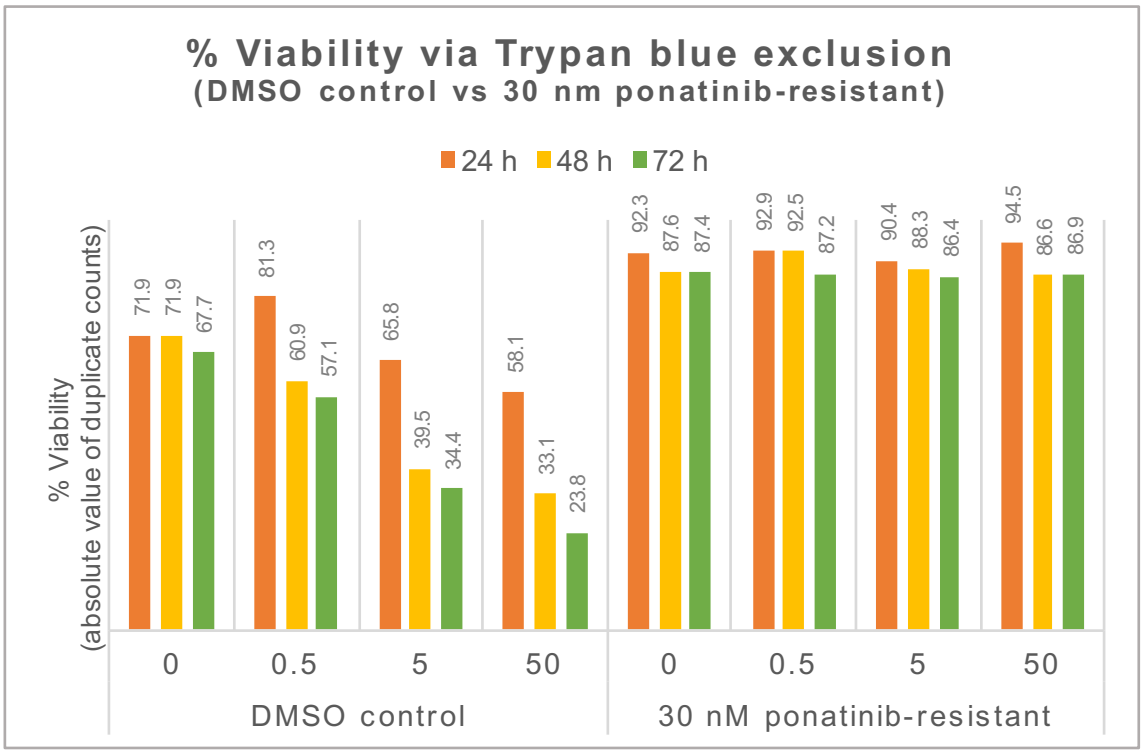

A
DMSO control
30 nM ponatinib-resistant
MW (kDa)
0
0.5
5
50
0
0.5
5
50
nM ponatinib
phospho-Bcr (Tyr177)
250
150
p-Bcr-Abl (p190)
Total c-Abl
250
150
Bcr-Abl (p190)
CrkL
37
Non-specific band
p-CrkL
CrkL
β-tubulin
50
p-Bcr-Abl in ponatinib-treated cells
p-Bcr-Abl normalised to 0 nM
100
50
0
0.0
0.5
5.0
50.0
nM ponatinib
DMSO
30 nM ponatinib-resistant
% p-CrkL in ponatinib-treated cells
% p-CrkL normalised to 0 nM
100
80
60
40
20
0
0.0
0.5
5.0
50.0
nM ponatinib
DMSO
30 nM ponatinib-resistant

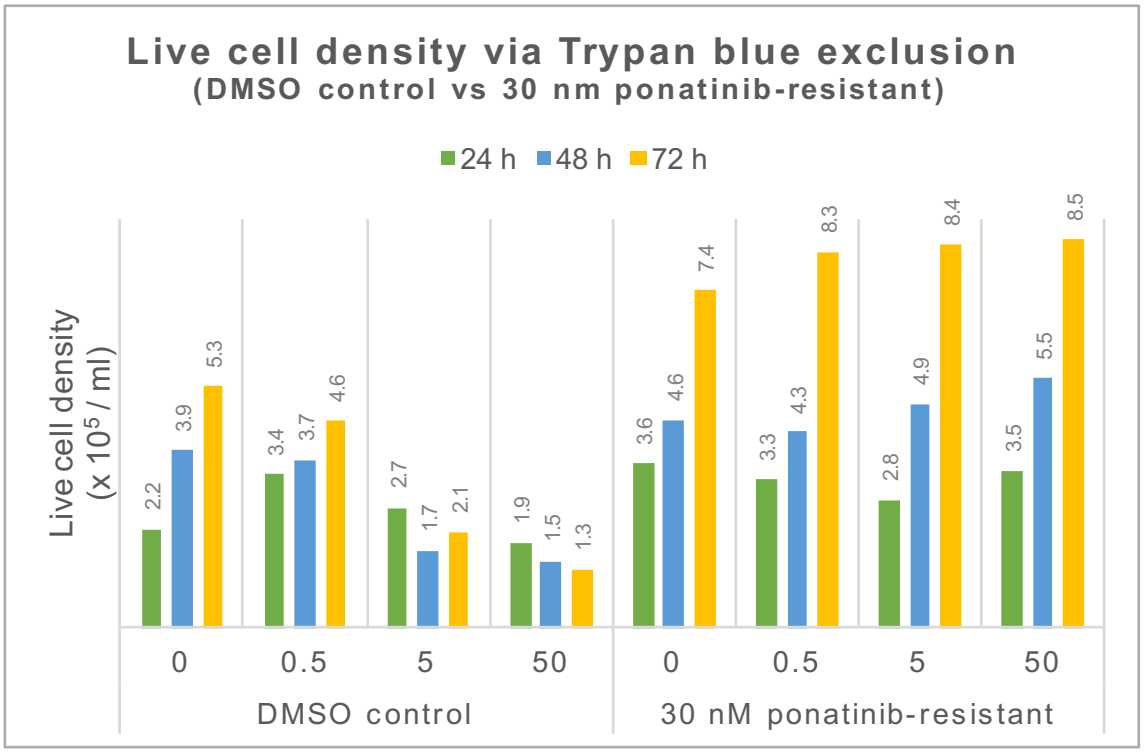
B


DMSO control
30 nM ponatinib-resistant
MW (kDa)
0
0.5
5
50
0
0.5
5
50
nM ponatinib
Cleaved-PARP (Asp214)
100
β-tubulin
50
PARP
100
75
β-tubulin
50
Full-length PARP (116 kDa)
Cleaved PARP (89 kDa)


Cleaved PARP expression in ponatinib-treated cells
Cleaved PARP expression
1.5
1.0
0.5
0.0
0.0
0.5
5.0
50.0
nM ponatinib
DMSO
50 nM ponatinib-resistant

C


% Viability via Trypan blue exclusion
(DMSO control vs 30 nm ponatinib-resistant)
24 h
48 h
72 h
% Viability
(absolute value of duplicate counts)
71.9
71.9
67.7
81.3
60.9
57.1
65.8
39.5
34.4
58.1
33.1
23.8
92.3
87.6
87.4
92.9
92.5
87.2
90.4
88.3
86.4
94.5
86.6
86.9
0
0.5
5
50
0
0.5
5
50
DMSO control
30 nM ponatinib-resistant


Live cell density via Trypan blue exclusion
(DMSO control vs 30 nm ponatinib-resistant)
24 h
48 h
72 h
Live cell density
(x 10⁵ / ml)
2.2
3.9
5.3
3.4
3.7
4.6
2.7
1.7
2.1
1.9
1.5
1.3
3.6
4.6
7.4
3.3
4.3
8.3
2.8
4.9
8.4
3.5
5.5
8.5
0
0.5
5
50
0
0.5
5
50
DMSO control
30 nM ponatinib-resistant

3.3.3. Analysis of Erk phosphorylation via western blotting indicates an increased phosphorylation in the 50 nM intermediate TKI-resistant cell lines

Analysis of phosphorylated Erk (p-Erk) in the 50 nM dasatinib-resistant SUP-B15 cell line indicated increased expression of p-Erk (ratio of phospho/total: 1.47) compared to that of DMSO control (ratio of phospho/total: 0.75) at 0 nM TKI (**Figure 3.5A**). When DMSO control cells were exposed to increasing concentrations of dasatinib, a decrease in p-Erk expression was observed (phospho/total ratio of 0.19, 0.16, 0.11 and 0.12 in 0.5, 5, 50 and 500 nM dasatinib respectively). In 50 nM dasatinib-resistant cells, a similar response of p-Erk to TKI was observed (phospho/total ratio of 0.79, 0.58, 0.44, 0.40 in 0.5, 5, 50 and 500 nM dasatinib respectively) (**Figure 3.5A**).

In 50 nM ponatinib-resistant cells, the expression of phospho-Erk was markedly increased compared to DMSO control cells (ratio of phospho/total at 0 nM ponatinib: 2.5 vs 0.18 respectively) when cells were untreated with ponatinib (**Figure 3.5B**; absolute ratio at 0 nM TKI). When DMSO control cells were exposed to increasing concentrations of ponatinib, a decrease in p-Erk phosphorylation was observed (phospho/total ratio of 0.12, 0.06, 0.03 and 0.01 at 0.5, 5, 50 and 500 nM ponatinib respectively). In 50 nM ponatinib-resistant cells, a similarly decreasing trend was observed (phospho/total p-Erk ratio of 1.40, 0.92, 0.86 and 0.92 at 0.5, 5, 50 and 500 nM ponatinib respectively).

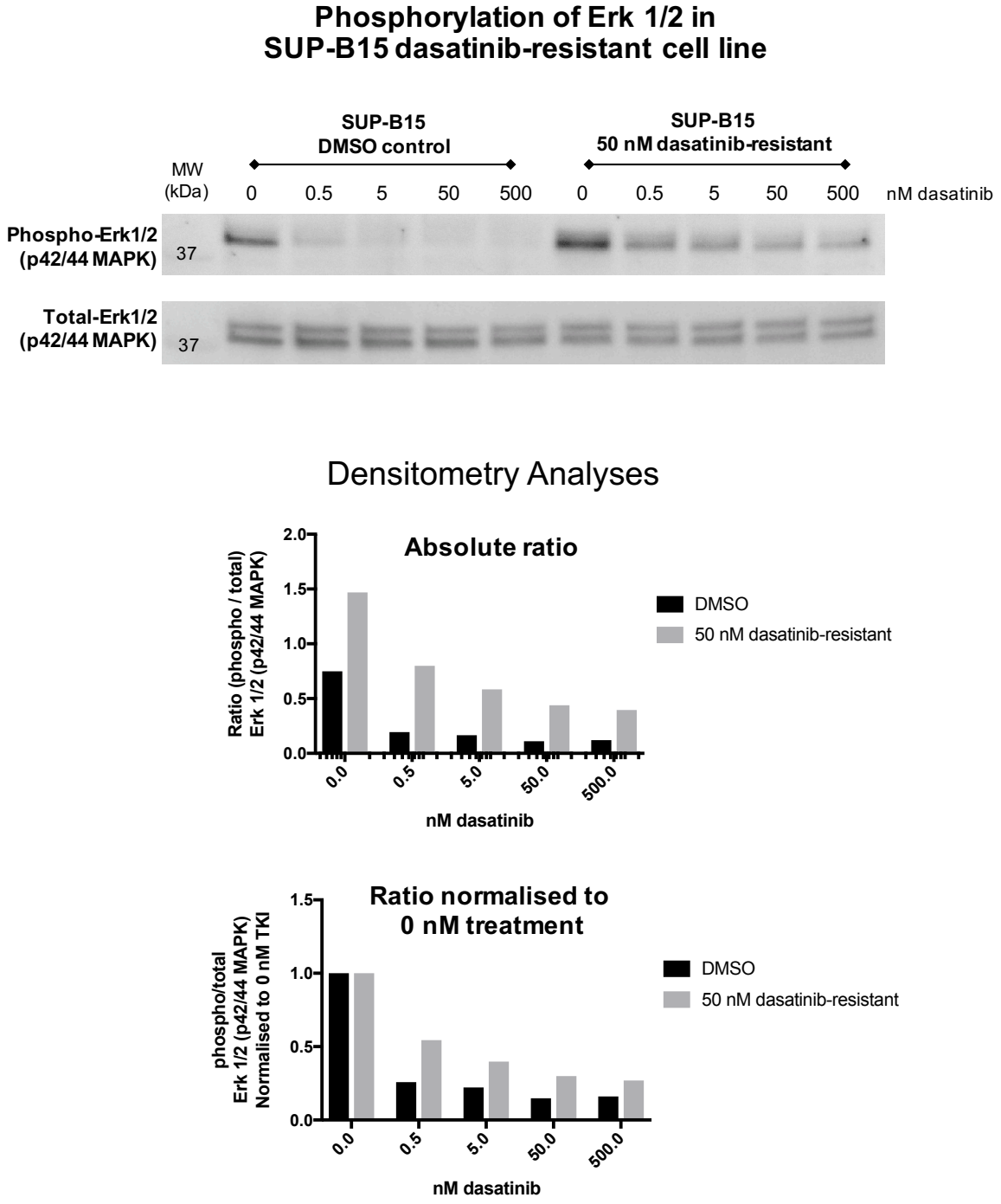
Importantly, an elevated expression of p-Erk remained in the dasatinib and ponatinib-resistant cell lines compared to DMSO control, despite exposure to 5, 50 and 500 nM dasatinib or ponatinib (**Figure 3.5A&B – lower panels**).

Figure 3.5 – TKI-resistant cells demonstrate increased p-Erk expression compared to DMSO control cells.

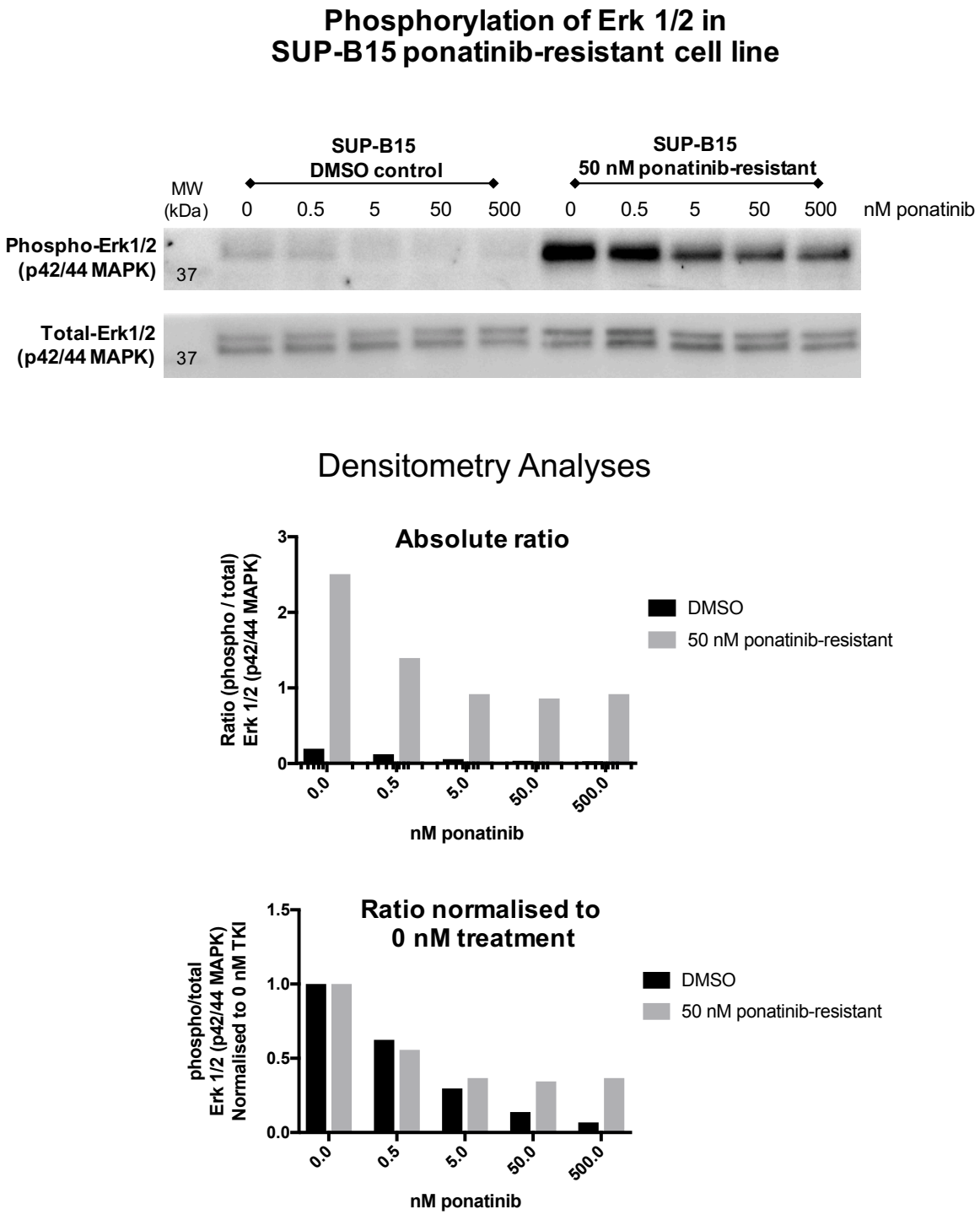
Western immunoblotting of TKI-sensitive and resistant cells exposed to increasing concentration of TKI for 24 hrs at 37°C/5% CO_2. PVDF membranes were incubated in antibodies specific for phosphorylated and total Erk 1/2 (p42/44 MAPK). The intensity the protein bands were measured, with the absolute and normalised (to 0 nM) ratios represented in graphs beneath western blots. **A**: Erk1/2 phosphorylation in DMSO control and 50 nM dasatinib-resistant cell lines treated with dasatinib. **B**: Erk1/2 phosphorylation in DMSO control and 50 nM ponatinib-resistant cell lines treated with ponatinib. Data is n=1 experiment.

Figure 3.5

A


Phosphorylation of Erk 1/2 in
SUP-B15 dasatinib-resistant cell line
SUP-B15
DMSO control
SUP-B15
50 nM dasatinib-resistant
MW
(kDa)
0
0.5
5
50
500
0
0.5
5
50
500
nM dasatinib
Phospho-Erk1/2
(p42/44 MAPK)
37
Total-Erk1/2
(p42/44 MAPK)
37
Densitometry Analyses
Absolute ratio
Ratio (phospho / total)
Erk 1/2 (p42/44 MAPK)
2.0
1.5
1.0
0.5
0.0
0.0
0.5
5.0
50.0
500.0
nM dasatinib
DMSO
50 nM dasatinib-resistant
Ratio normalised to
0 nM treatment
phospho/total
Erk 1/2 (p42/44 MAPK)
Normalised to 0 nM TKI
1.5
1.0
0.5
0.0
0.0
0.5
5.0
50.0
500.0
nM dasatinib
DMSO
50 nM dasatinib-resistant

B


Phosphorylation of Erk 1/2 in SUP-B15 ponatinib-resistant cell line
SUP-B15 DMSO control
SUP-B15 50 nM ponatinib-resistant
MW (kDa)
0 0.5 5 50 500 0 0.5 5 50 500 nM ponatinib
Phospho-Erk1/2 (p42/44 MAPK)
37
Total-Erk1/2 (p42/44 MAPK)
37
Densitometry Analyses
Absolute ratio
Ratio (phospho / total) Erk 1/2 (p42/44 MAPK)
DMSO
50 nM ponatinib-resistant
0.0 0.5 5.0 50.0 500.0
nM ponatinib
Ratio normalised to 0 nM treatment
phospho/total Erk 1/2 (p42/44 MAPK) Normalised to 0 nM TKI
DMSO
50 nM ponatinib-resistant
0.0 0.5 5.0 50.0 500.0
nM ponatinib

3.3.4. Highly-resistant SUP-B15 cell lines do not demonstrate increased p-CrkL IC_{50}

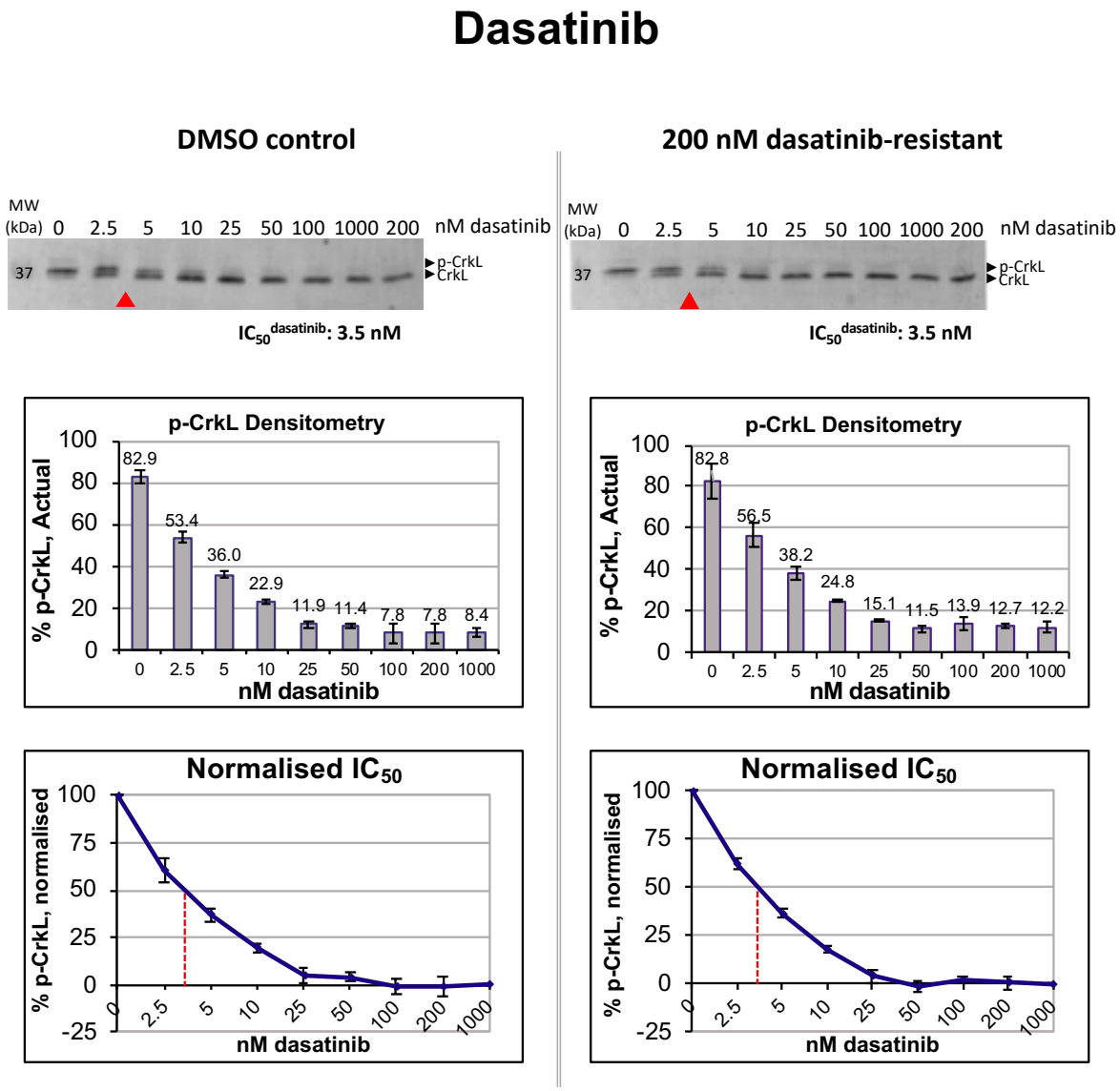
Cells resistant to 200 nM TKI (dasatinib or ponatinib) *in vitro*, cells were analysed for p-CrkL IC_{50} to confirm whether the *BCR-ABL1* independent activity noted in sections **3.3.1** and **3.3.2** remained. There were no differences between the p-CrkL IC_{50} of dasatinib in DMSO and 200 nM dasatinib-resistant cell lines ($IC_{50}^{dasatinib}$: 3.5 $\pm$ 0.2 nM in DMSO control and $IC_{50}^{dasatinib}$: 3.5 $\pm$ 0.1 nM in 200 nM dasatinib-resistant cells) (**Figure 3.6A**). In ponatinib-treated cells, a decrease in p-CrkL IC_{50} was observed in the 200 nM ponatinib-resistant cell line ($IC_{50}^{ponatinib}$: 1.6 $\pm$ 0.3 nM) compared to DMSO control cells ($IC_{50}^{ponatinib}$: 3.0 $\pm$ 0.1 nM) (**Figure 3.6B**). These observations were despite the ability of TKI-resistant cells to survive in 200 nM dasatinib/ponatinib (cell viability of >80% was routinely confirmed by Trypan blue analysis prior to CrkL assay).

Figure 3.6 – Highly-resistant SUP-B15 cell lines do not demonstrate an increased p-CrkL IC_{50} compared to DMSO control cells.

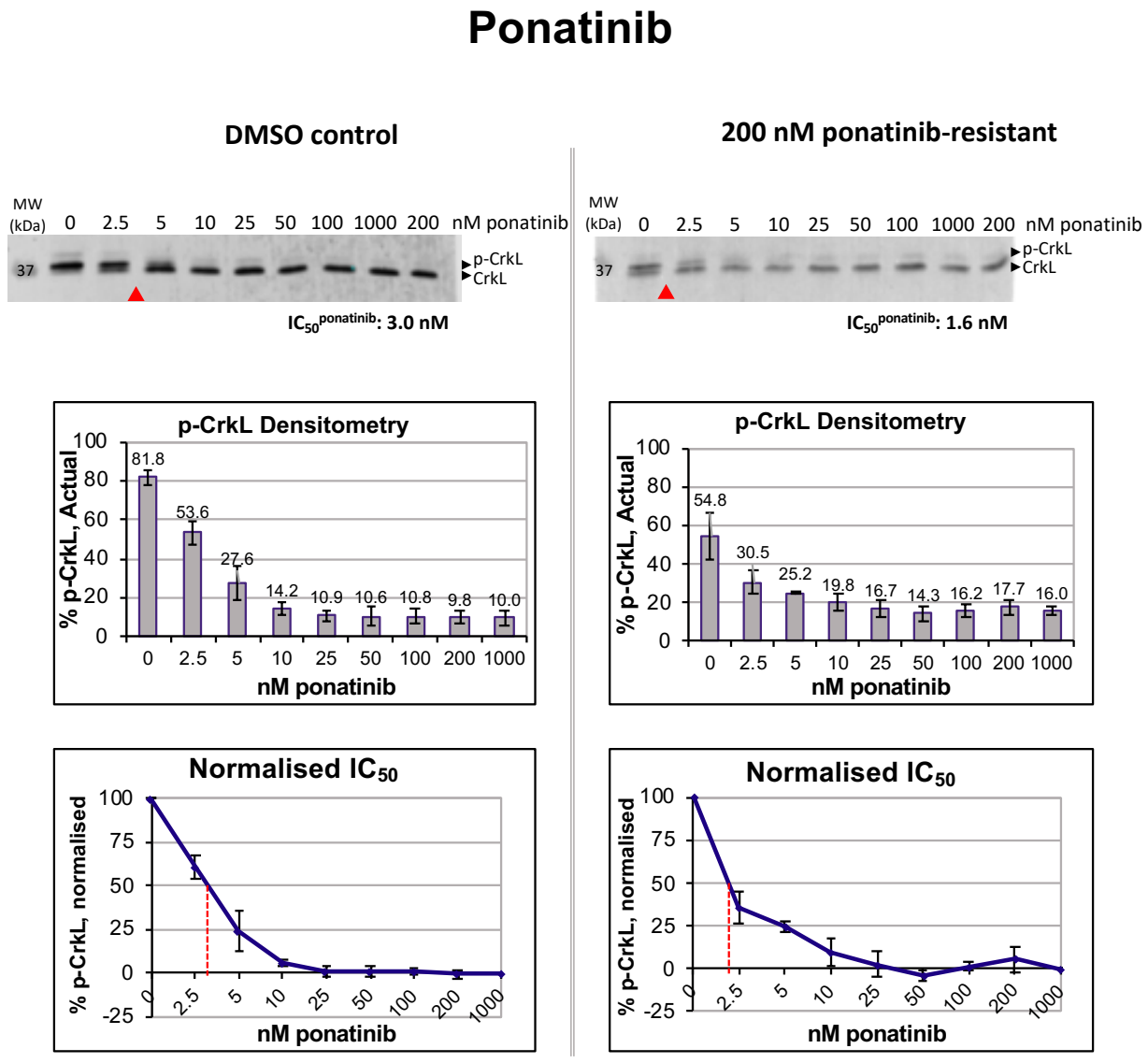
Western immunoblotting of p-CrkL IC_{50} in DMSO control and 200 nM dasatinib or 200 nM ponatinib resistant cell lines exposed to increasing concentrations of TKI. Cells were treated with 0, 2.5, 5, 10, 25, 50, 100, 200, 1000 nM dasatinib/ponatinib for 2 hrs at 37°C/5% CO_2, prior to preparation of lysates for p-CrkL assay as previously described. **A**: Dasatinib treatment in DMSO control and 200 nM dasatinib-resistant cells. **B**: Ponatinib treatment in DMSO control and 200 nM ponatinib-resistant cells. Western blots shown are representative of at least 3 independent experiments, with red triangles indicating the approximate IC_{50} concentrations. Bar graphs comprise of the absolute p-CrkL densitometry analyses, while line graphs represent the normalised values for extrapolation of the IC_{50}. Error bars denote ±SD of 3 independent experiments.

Figure 3.6

A


Dasatinib
DMSO control
200 nM dasatinib-resistant
MW (kDa) 0 2.5 5 10 25 50 100 1000 200 nM dasatinib
37
p-CrkL
CrkL
IC50 dasatinib: 3.5 nM
p-CrkL Densitometry
% p-CrkL, Actual
82.9
53.4
36.0
22.9
11.9
11.4
7.8
7.8
8.4
82.8
56.5
38.2
24.8
15.1
11.5
13.9
12.7
12.2
nM dasatinib
Normalised IC50
% p-CrkL, normalised

B


Ponatinib
DMSO control
200 nM ponatinib-resistant
MW (kDa) 0 2.5 5 10 25 50 100 1000 200 nM ponatinib
37
p-CrkL
CrkL
IC50ponatinib: 3.0 nM
IC50ponatinib: 1.6 nM
p-CrkL Densitometry
% p-CrkL, Actual
81.8
53.6
27.6
14.2
10.9
10.6
10.8
9.8
10.0
54.8
30.5
25.2
19.8
16.7
14.3
16.2
17.7
16.0
nM ponatinib
Normalised IC50
% p-CrkL, normalised

3.3.5. mRNA sequencing data suggests increased expression of *BCR-ABL1* independent signalling, in TKI-resistant SUP-B15 cell lines

To further explore canonical/noncanonical mechanisms of TKI-resistance, mRNA sequencing was performed using TKI-sensitive and 200 nM dasatinib/ponatinib-resistant SUP-B15 cells. A heatmap was generated to visualise hierarchical clustering of differentially expressed genes within samples (FDR < 0.05), which confirmed that TKI-sensitive and resistant SUP-B15 cell lines were transcriptomically different (**Figure 3.7**). Analysis of biological duplicate samples of naïve and DMSO control, as well as dasatinib and ponatinib resistant cell lines, indicated a close association between replicate samples, and a strong correlation between significantly upregulated and downregulated differentially-expressed genes in TKI-sensitive and resistant cell lines. In the heatmap, a difference between the expression of significantly upregulated and downregulated genes was observed in the 200 nM dasatinib-resistant SUP-B15 cell line compared to naïve and DMSO control. Interestingly, the heatmap also revealed a pattern of mostly upregulated genes, in ponatinib-resistant SUP-B15 cells.

A volcano plot was then generated to visualise the distribution of differentially-expressed genes in TKI-resistant cells, compared to DMSO control. In 200 nM dasatinib-resistant cells, results indicated the presence of 277 significantly differentially-expressed genes (false discovery rate (FDR) < 0.05), of which 103 were upregulated ($Log_2FC > 1$) and 174 were downregulated ($Log_2FC < 1$) (**Figure 3.8A**). Of these genes, 7 upregulated genes [phosphodiesterase 1A, calmodulin-dependent (*PDE1A*), Enah/Vasp-like (*EVL*), leucine-rich repeat containing G protein-coupled receptor 5 (*LGR5*), V-Ets avian erythroblastosis virus E26 oncogene homolog 1 (*ETS1*), cluster of differentiation 24 (isoform of small cell lung

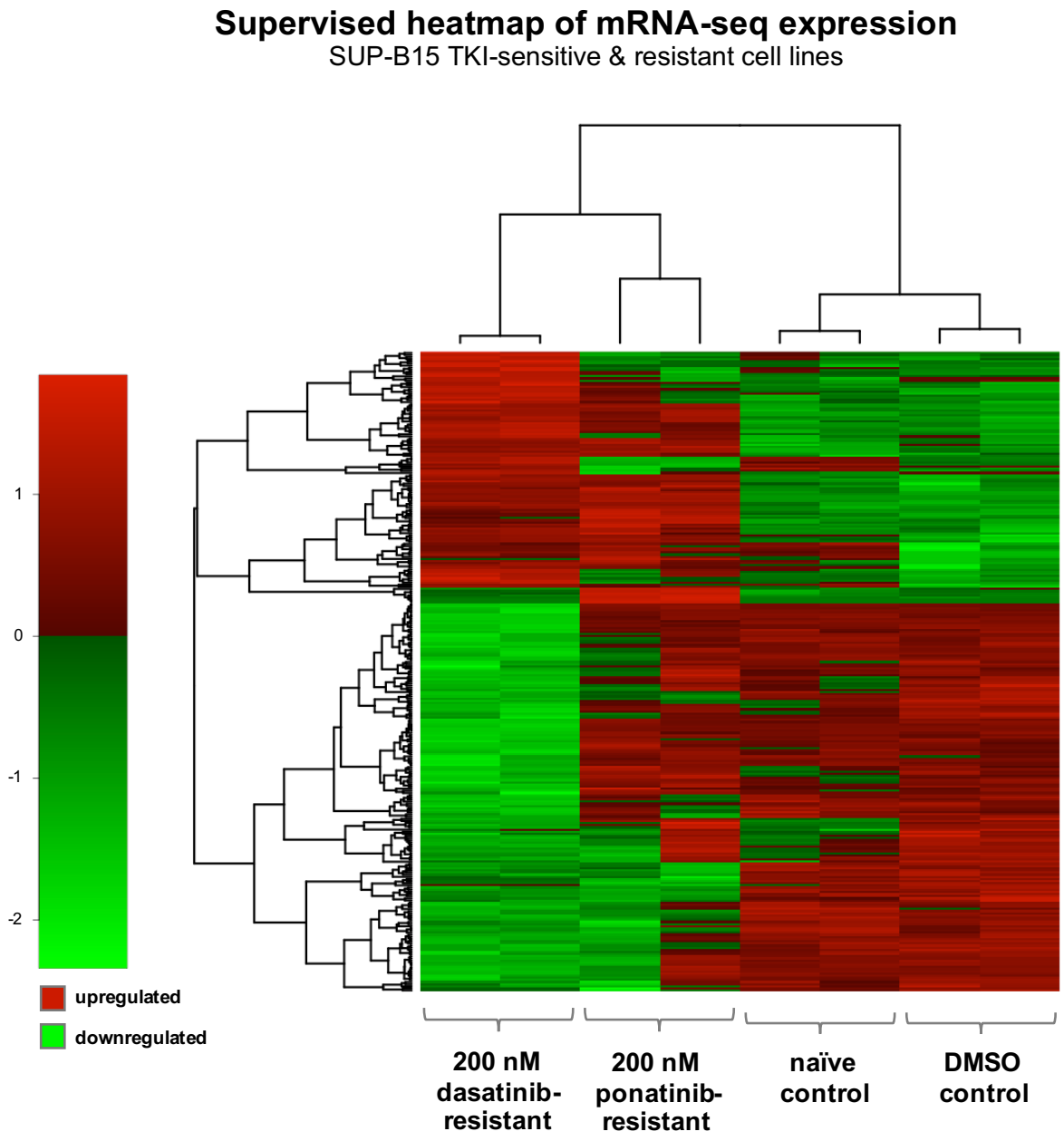
carcinoma cluster 4 antigen) (*CD24*), dedicator of cytokinesis 8 (*DOCK8*), BTB and CNC homology 1 basic leucine zipper transcription factor 2 (*BACH2*)] and 4 downregulated genes [platelet-derived growth factor alpha polypeptide (*PDGFA*), suppressor of cytokine signalling 7 (*SOCS7*), guanylate binding protein 5 (*GBP5*) and solute carrier family 25, member 46 (*SLC25A46*)] were selected for validation via RQ-PCR (**Figure 3.8B & C**). Results indicate a comparable association of upregulated and downregulated genes between the mRNA-seq and RQ-PCR datasets (for expression values and gene summary, refer to **Appendix 3.1**).

In ponatinib-resistant SUP-B15 cells, volcano plot analysis indicated the presence of seventeen significantly-expressed genes ($Log_2FC>1$; FDR < 0.05) which were mostly upregulated (**Figure 3.9A**), supporting results of the heatmap previously described. Of these genes, nine were selected for RQ-PCR validation [leukocyte immunoglobulin-like receptor, subfamily B member 4 (*LILRB4*), leukocyte immunoglobulin-like receptor subfamily A (with TM domain), member 2 (*LILRA2*), bestrophin 3 (*BEST3*), Rho guanine nucleotide exchange factor 12 (*ARHGEF12*), phospholipase d family, member 4 (*PLD4*), membrane metallo-endopeptidase (*MME*), *EVL*, *LGR5* and *BACH2*]. A downregulated gene with the smallest *P*-value [POU Class 4 Homeobox 1 (*POU4F1*); *P*=0.0589], was also included in the RQ-PCR validation assay to ensure the reliability of the mRNA-seq data. Results indicated a similar expression of differentially-expressed genes between the RNA sequencing (**Figure 3.9B**) and RQ-PCR (**Figure 3.9C**) validation data, where genes expected as upregulated were overexpressed in ponatinib-resistant cells, while *POU4F1* was downregulated in both mRNA-seq and RQ-PCR (for expression values and gene summary, refer to **Appendix 3.2**).

Figure 3.7 – mRNA-seq heatmap of SUP-B15 TKI-sensitive and 200 nM TKI-resistant cell lines

Duplicate samples of SUP-B15 TKI-sensitive (naïve and DMSO control), as well as TKI-resistant (dasatinib and ponatinib) cell lines, were analysed via RNA sequencing using the Illumina® NextSeq 500 platform. Results were interpreted using the methods of Liao *et al.* 2013[1] and 2014[5]. Heatmap represents supervised clustering of significantly differentially-expressed genes (FDR <0.05) using the Benjamini-Hochberg method[3,6]. Heatmap courtesy of Dr. Chung Kok, SAHMRI.

Figure 3.7


Supervised heatmap of mRNA-seq expression
SUP-B15 TKI-sensitive & resistant cell lines
1
0
-1
-2
upregulated
downregulated
200 nM dasatinib-resistant
200 nM ponatinib-resistant
naïve control
DMSO control

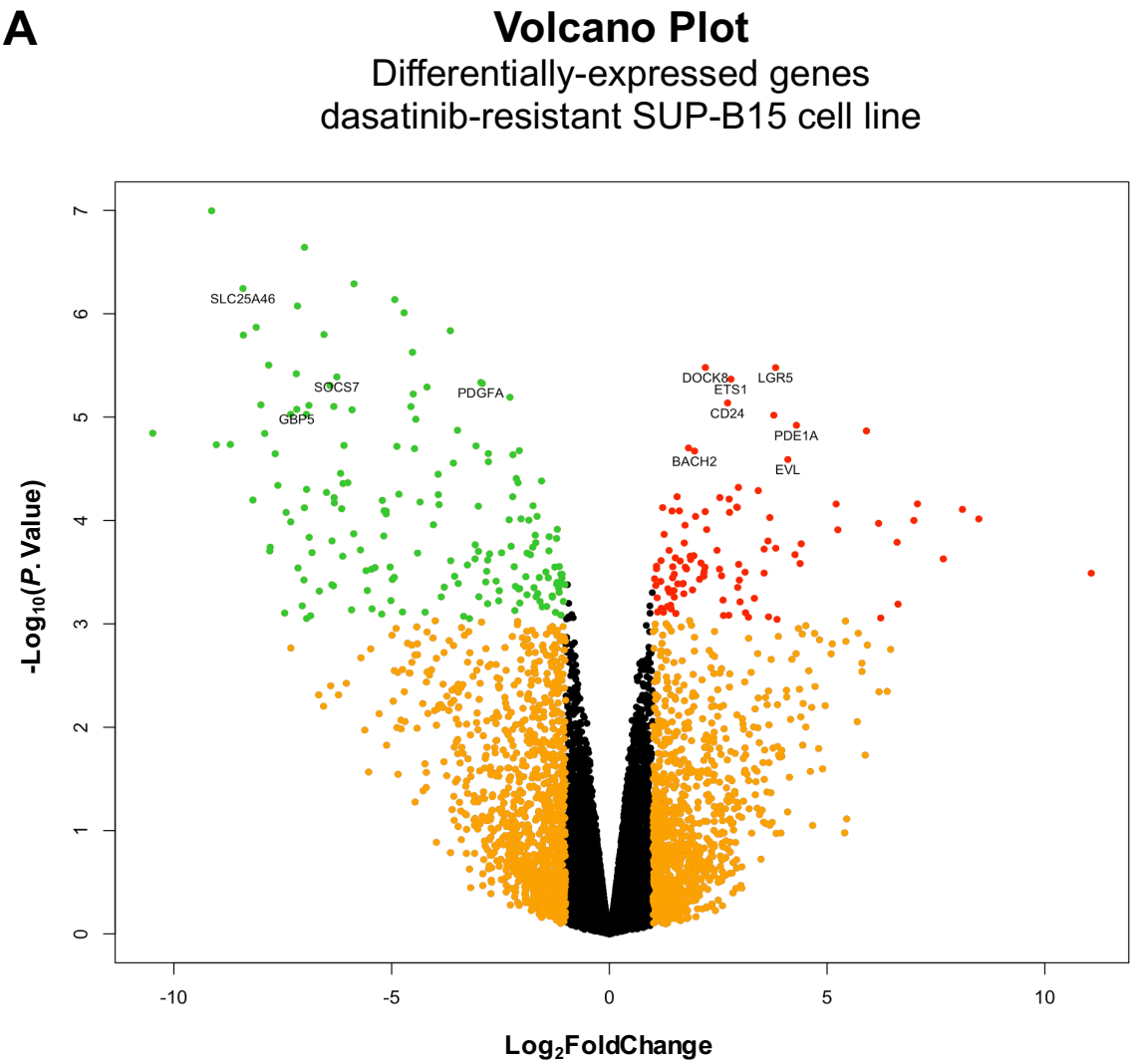
THIS PAGE INTENTIONALLY LEFT BLANK.

Figure 3.8 – Validation of mRNA-seq data in DMSO control and dasatinib-resistant SUP-B15 cell lines

A: Volcano plot of differentially-expressed genes in TKI-resistant cell line compared to DMSO control. **Orange**: Log_2FC <-1 & >1; **red**: Log_2FC > 1 and FDR < 0.05; **green**: Log_2FC < -1 and FDR < 0.05. Genes of interest for subsequent RQ-PCR validation are indicated by text on volcano plot with the descriptions noted in the legend beneath. **B**: Bar chart representing fold changes of significantly differentially-expressed genes in dasatinib-resistant SUP-B15 cells (for further details, refer to **Appendix 3.1**). **Red**: upregulated genes; **green**: downregulated genes. **C**: RQ-PCR validation of differentially-expressed genes in dasatinib-resistant SUP-B15 cells normalised to DMSO control (represented by the horizontal line at a threshold level of 1). Data was analysed via the comparative Ct method[2], using *GAPDH* as a loading control. n=3 biological replicates were utilised in this experiment.

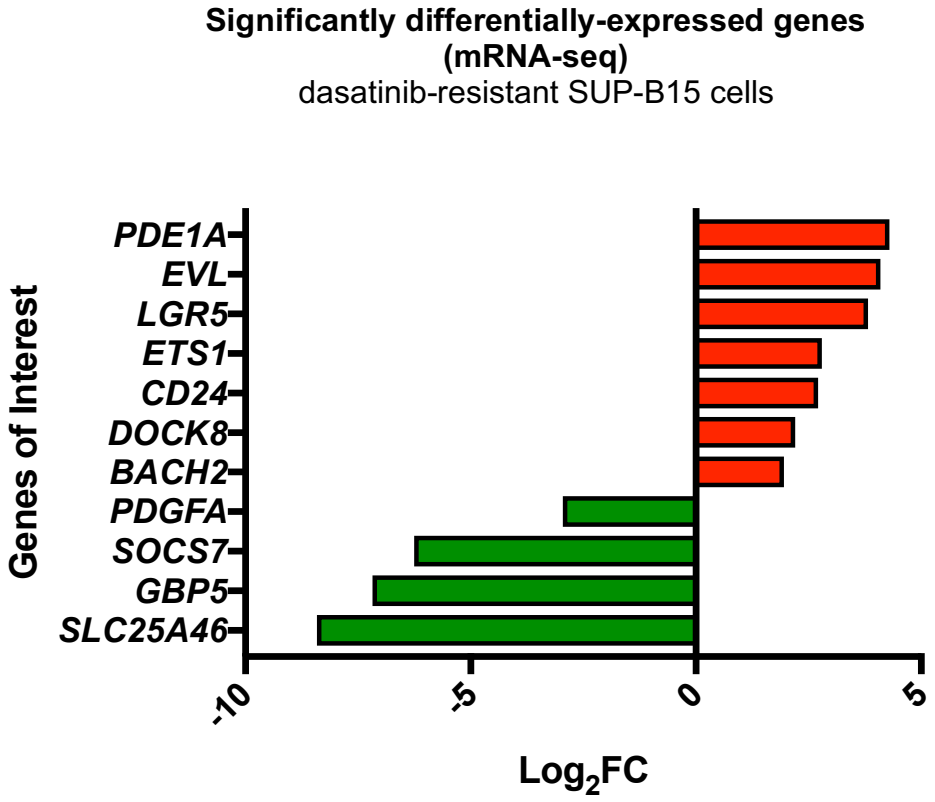
Figure 3.8

A

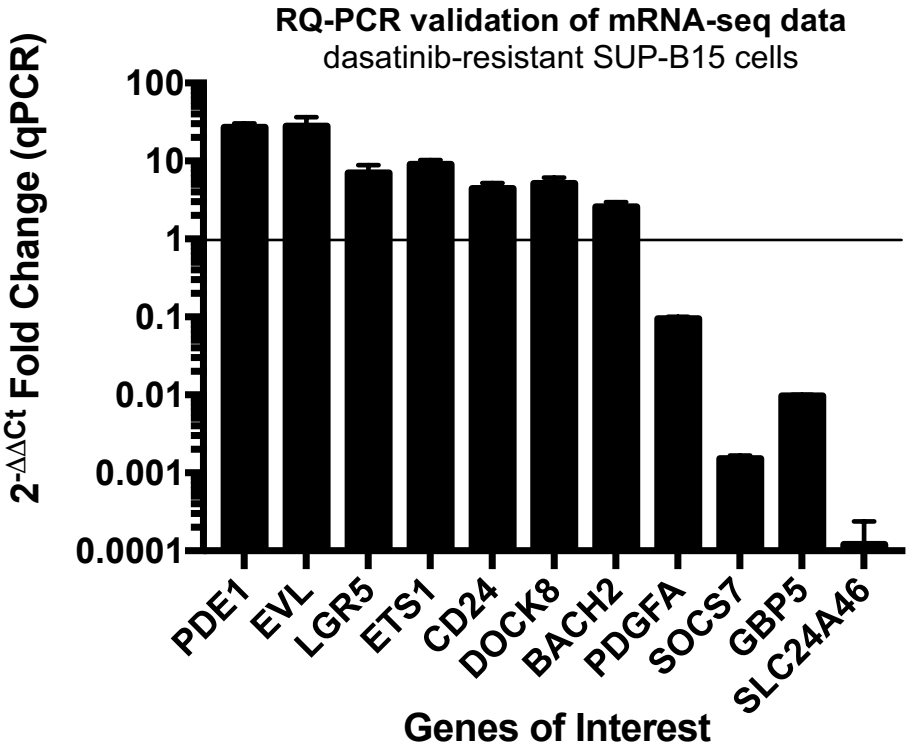


Legend:
BACH2 – BTB And CNC Homology 1, Basic Leucine Zipper Transcription Factor 2
CD24 – Cluster of Differentiation 24 (Isoform of Small Cell Lung Carcinoma Cluster 4 Antigen)
DOCK8 – Dedicator of Cytokinesis 8
ETS1 – V-Ets Avian Erythroblastosis Virus E26 Oncogene Homolog 1
EVL – Enah/Vasp-Like
GBP5 – Guanylate Binding Protein 5
LGR5 – Leucine-Rich Repeat Containing G Protein-Coupled Receptor 5
PDE1A – Phosphodiesterase 1A, Calmodulin-Dependent
PDFGA – Platelet-Derived Growth Factor Alpha Polypeptide
SLC25A46 – Solute Carrier Family 25, Member 46
SOCS7 – Suppressor of Cytokine Signalling 7

B


Significantly differentially-expressed genes
(mRNA-seq)
dasatinib-resistant SUP-B15 cells
PDE1A
EVL
LGR5
ETS1
CD24
DOCK8
BACH2
PDGFA
SOCS7
GBP5
SLC25A46
Genes of Interest
-10
-5
0
5
Log2FC

C

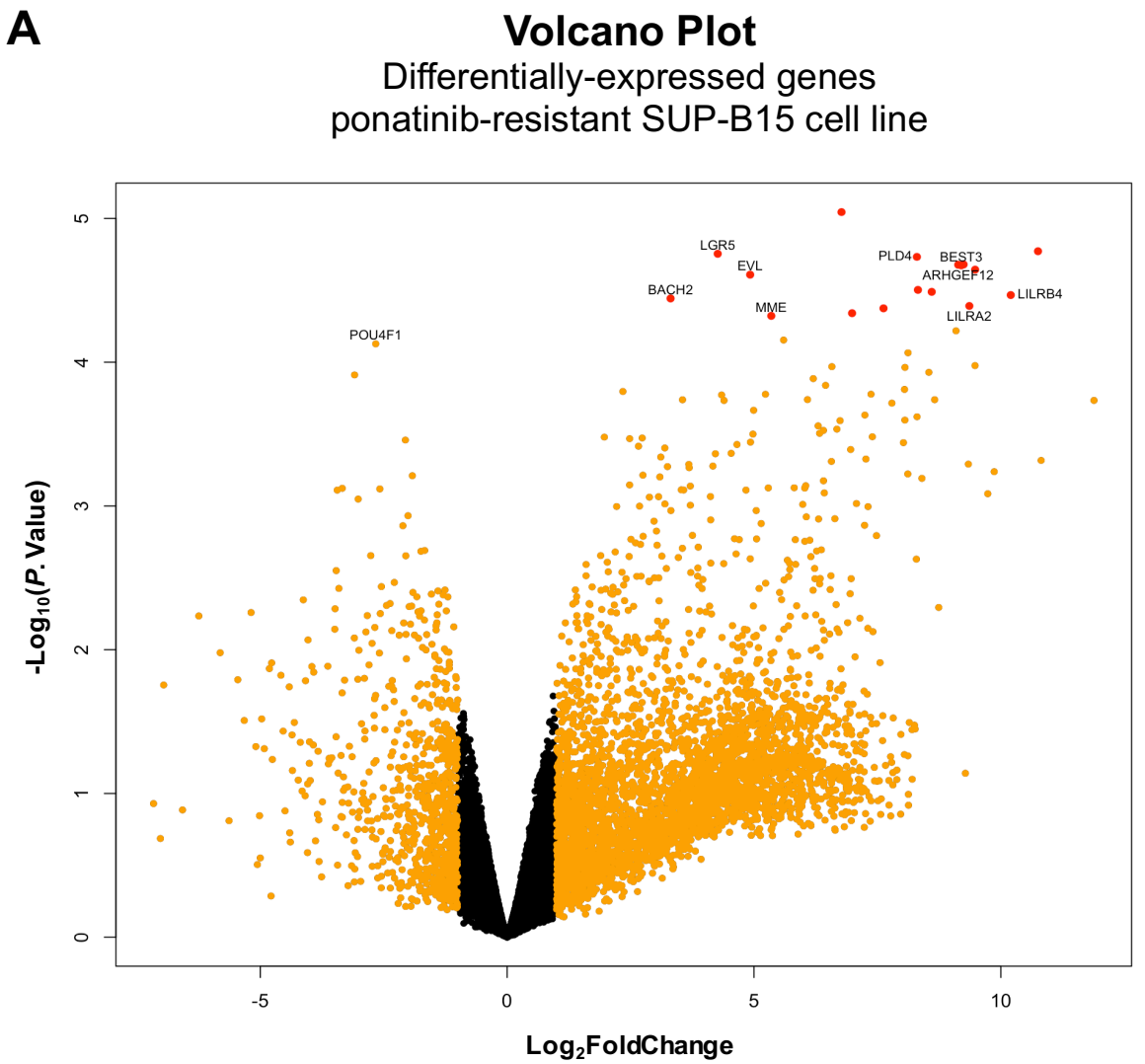

RQ-PCR validation of mRNA-seq data
dasatinib-resistant SUP-B15 cells
2-ΔΔCt Fold Change (qPCR)
100
10
1
0.1
0.01
0.001
0.0001
PDE1
EVL
LGR5
ETS1
CD24
DOCK8
BACH2
PDGFA
SOCS7
GBP5
SLC24A46
Genes of Interest

THIS PAGE INTENTIONALLY LEFT BLANK.

Figure 3.9 – Validation of mRNA-seq data in DMSO control and ponatinib-resistant SUP-B15 cell lines

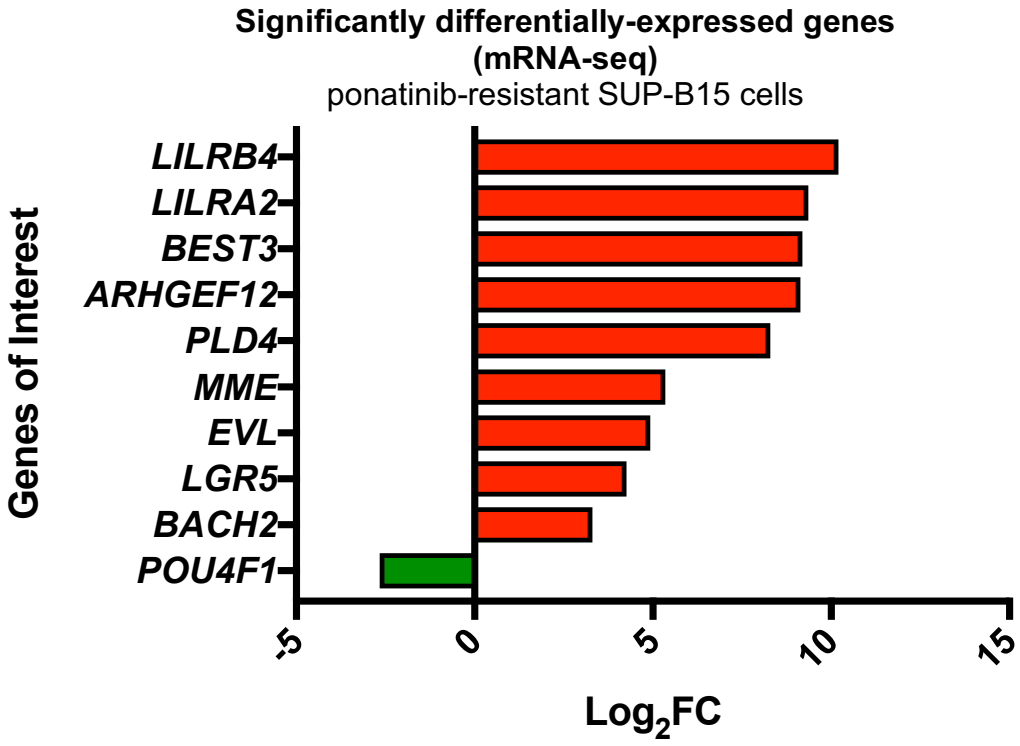
A: Volcano plot of differentially-expressed genes in TKI-resistant cell line compared to DMSO control. **Orange**: Log_2FC <-1 & >1; **red**: Log_2FC > 1 and FDR < 0.05. There were no significantly downregulated genes detectable. Genes of interest for subsequent RQ-PCR validation are indicated by text on volcano plot with the descriptions noted in the legend beneath. **B**: Bar chart representing fold changes of differentially expressed genes in ponatinib-resistant SUP-B15 cells (for further details, refer to **Appendix 3.2**). **Red**: upregulated genes; **green**: downregulated genes. **C**: RQ-PCR validation of differentially-expressed genes in ponatinib-resistant SUP-B15 cells normalised to DMSO control (represented by the horizontal line at a threshold level of 1). Data was analysed via the comparative Ct method as previously described, with n=3 biological replicates utilised in this experiment.

Figure 3.9

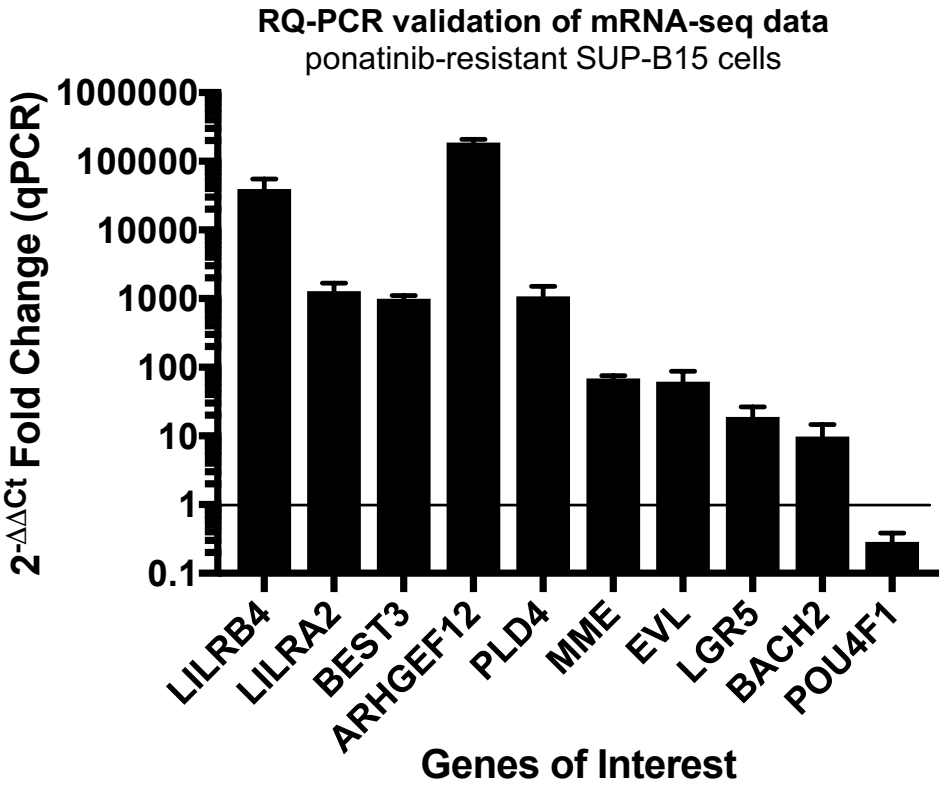


Legend:
ARHGEF12 – Rho Guanine Nucleotide Exchange Factor (GEF) 12
BACH2 – BTB And CNC Homology 1, Basic Leucine Zipper Transcription Factor 2
BEST3 – Bestrophin 3
EVL – Enah/Vasp-Like
LGR5 – Leucine-Rich Repeat Containing G Protein-Coupled Receptor 5
LILRA2 – Leukocyte Immunoglobulin-Like Receptor, Subfamily A (With TM Domain), Member 2
LILRB4 – Leukocyte Immunoglobulin-Like Receptor, Subfamily B (With TM and ITIM Domains), Member 4
MME – Membrane Metallo-Endopeptidase
PLD4 – Phospholipase D Family, Member 4
POU4F1 – POU Class 4 Homeobox 1

B


Significantly differentially-expressed genes
(mRNA-seq)
ponatinib-resistant SUP-B15 cells
Genes of Interest
LILRB4
LILRA2
BEST3
ARHGEF12
PLD4
MME
EVL
LGR5
BACH2
POU4F1
-5
0
5
10
15
Log2FC

C


RQ-PCR validation of mRNA-seq data
ponatinib-resistant SUP-B15 cells
2-ΔΔCt Fold Change (qPCR)
1000000
100000
10000
1000
100
10
1
0.1
LILRB4
LILRA2
BEST3
ARHGEF12
PLD4
MME
EVL
LGR5
BACH2
POU4F1
Genes of Interest

3.3.6. Identification of *RAS* mutations in the TKI-resistant SUP-B15 cell lines

In agreement with the findings of increased p-Erk expression in section **3.3.3**, genes associated with the MAPK/Erk pathway were further evaluated for the presence of any point mutations. The alignment of mRNA sequencing data using the Integrated Genomics Viewer (IGV, Broad Institute)[245,246] revealed an alteration in the *KRAS* gene on chromosome 12 of dasatinib-resistant SUP-B15 cells (**Figure 3.10**). Here, a mutation of guanine to adenine at coding position 34 resulting in a substitution of glycine to serine at the 12th residue of KRAS was identified. The mutation was confirmed by Sanger sequencing, where a mutation of *KRAS* G12S was detected at a rate of 37% in genomic DNA of dasatinib-resistant cells. No *KRAS* mutation was observed in DMSO control cells, as well as naïve control and ponatinib-resistant cells (**Appendix 3.3**).

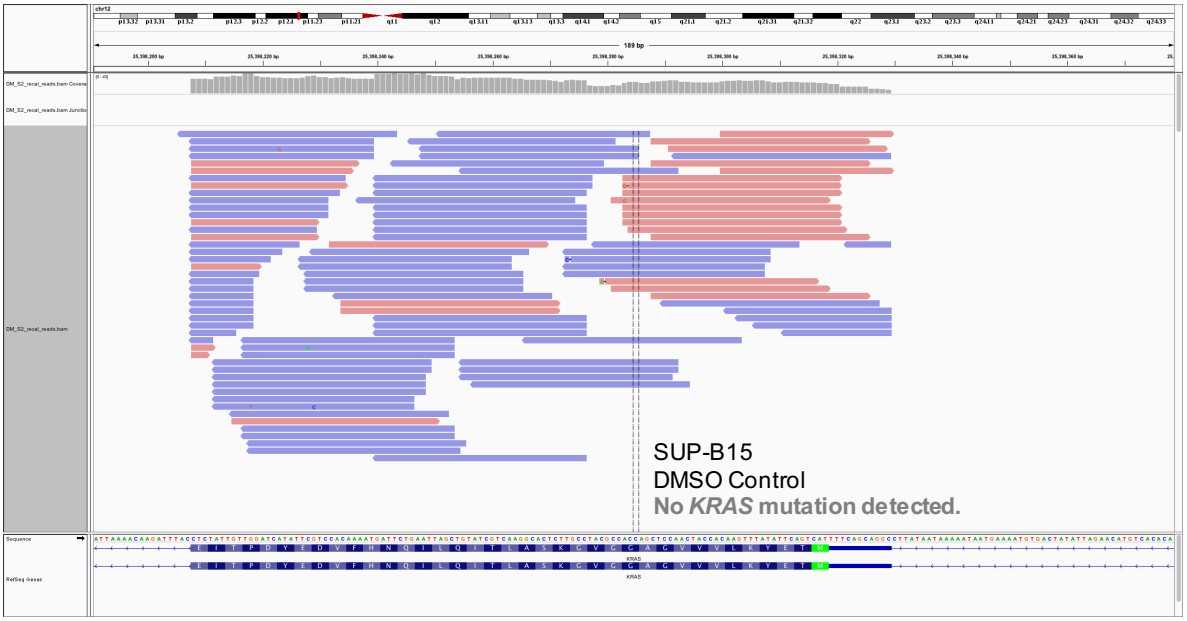
To further support this finding, an *NRAS* G12S mutation was identified on chromosome 1 of ponatinib-resistant SUP-B15 cells (**Figure 3.11**). Alignment results indicated the *NRAS* G12S mutation was unique in ponatinib-resistant cells and absent in SUP-B15 naïve, DMSO control and dasatinib-resistant cell lines (**Appendix 3.4**). Sanger sequencing further confirmed a 100% mutation rate of guanine to adenine, resulting in a substitution of glycine to serine at the 12th residue of NRAS.

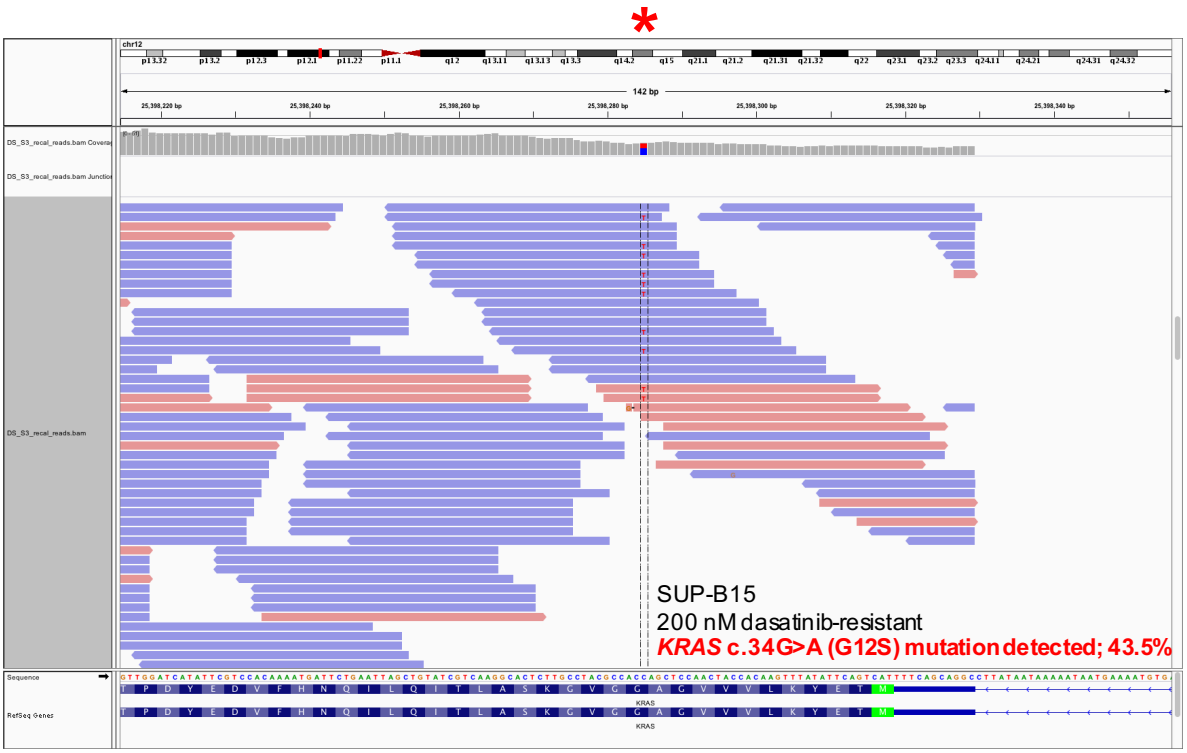
Figure 3.10 – Alignment of mRNA sequencing data reveals presence of a *KRAS*-G12S mutation in dasatinib-resistant SUP-B15 cells as confirmed by Sanger sequencing of genomic DNA

A: mRNA sequencing reads aligned on the integrated genomics viewer (IGV, Broad Institute) where a *KRAS* c.34G>A (G12S) mutation was identified on chromosome 12 of dasatinib-resistant cells (frequency of 43.5%) but absent in DMSO control. Red asterisk highlights the position of *KRAS*-G12S in dasatinib-resistant cells. Pink and blue horizontal bars represent the direction of sequencing reads (forward and reverse). **B**: Sanger sequencing of genomic DNA confirms the presence of the *KRAS*-G12S mutation at a rate of 37% in dasatinib-resistant cells, as marked by the red asterisk.

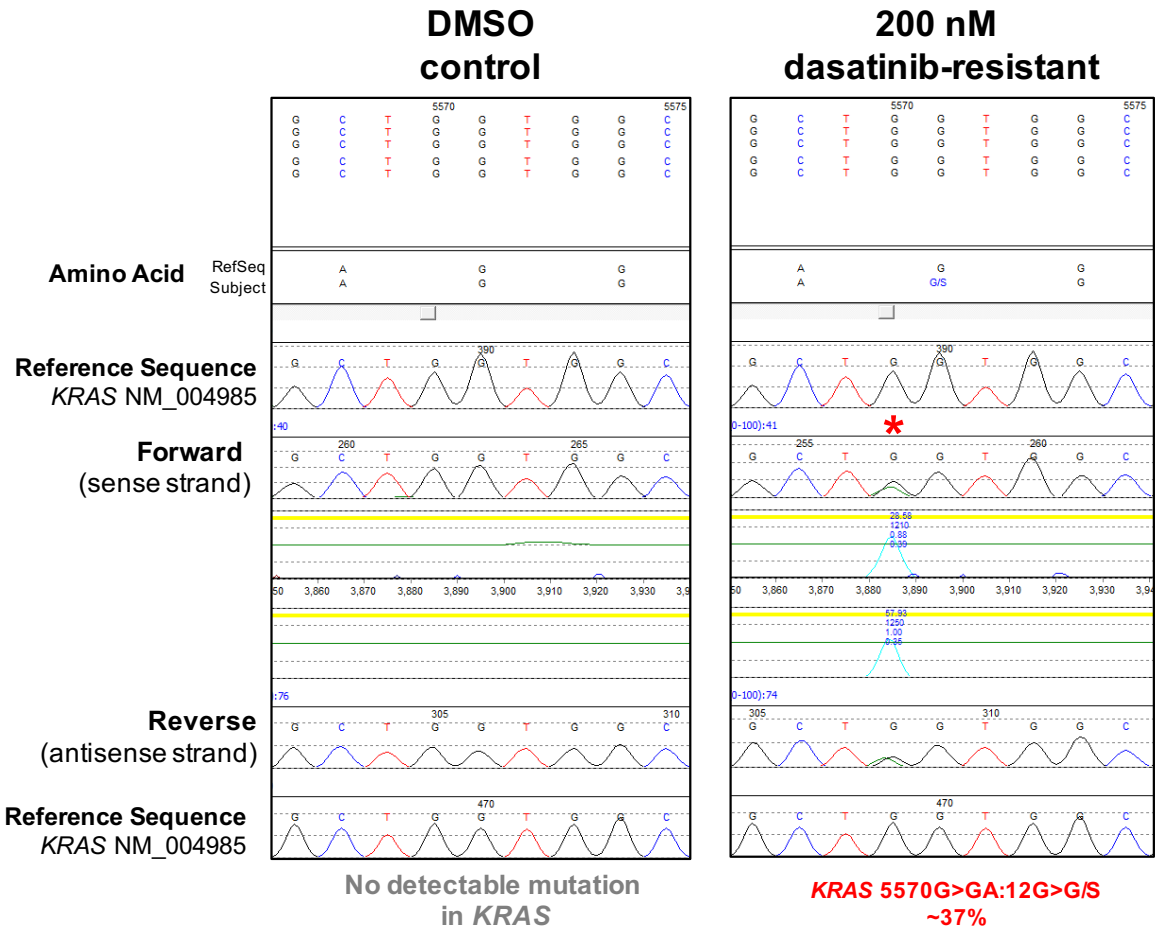
Figure 3.10

A **Identification of *KRAS* mutation in mRNAseq data of dasatinib-resistant SUP-B15 cells**





B ***KRAS* alignment**



THIS PAGE INTENTIONALLY LEFT BLANK.

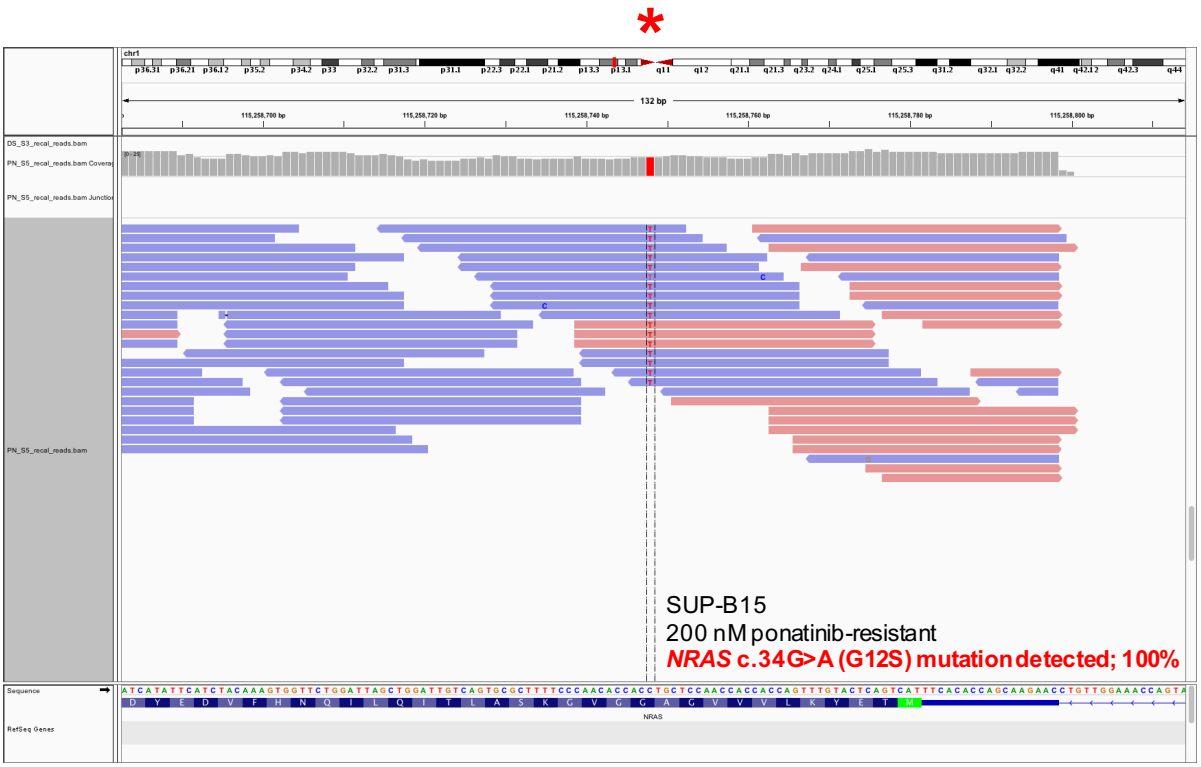
Figure 3.11 – Alignment of mRNA sequencing data revealed an *NRAS*-G12S mutation in ponatinib-resistant SUP-B15 cells as confirmed by Sanger sequencing of genomic DNA

A: mRNA sequencing reads aligned on the integrated genomics viewer (IGV, Broad Institute) where an *NRAS* c.34G>A (G12S) mutation was identified on chromosome 1 of ponatinib-resistant cells (frequency of 100%) but absent in DMSO control. Red asterisk highlights the position of *NRAS*-G12S in the ponatinib-resistant cell line. Pink and blue horizontal bars represent the direction of sequencing reads (forward and reverse). **B**: Sanger sequencing of genomic DNA confirms the presence of an *NRAS*-G12S mutation at a rate of 100% in ponatinib-resistant cells, as marked by the red asterisk.

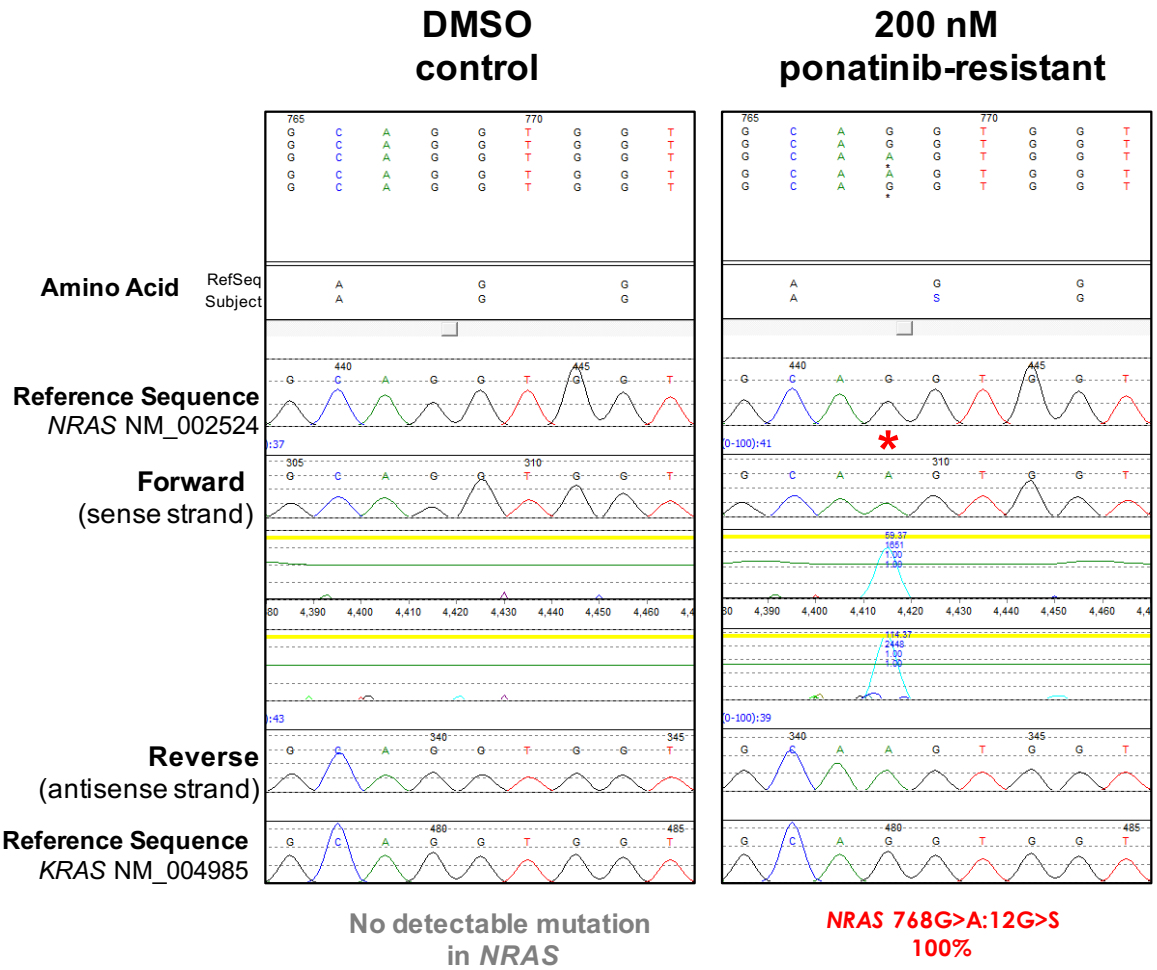
Figure 3.11

A **Identification of *NRAS* mutation in mRNAseq data of ponatinib-resistant SUP-B15 cells**





B ***NRAS* alignment**



3.4. Discussion

In this chapter, Ph+ ALL cells resistant to the Abl kinase inhibitors dasatinib and ponatinib were generated through the exposure of immortalised SUP-B15 cells to incrementally increasing concentrations of dasatinib and ponatinib. The final concentration of dasatinib and ponatinib deemed to be resistant for SUP-B15 was set to 200 nM, as this was above clinically-relevant trough levels of 50 nM dasatinib and 64 nM ponatinib in patients[167,249,250].

In an *in vitro* setting, a study performed by Janes *et al*. (2010) investigating the efficacy of Abl-kinase and mTOR inhibitors in Bcr-Abl-expressing cell lines, the 50% growth inhibition (GI_{50}) of dasatinib was found to be 42 nM (C.I. 32-58)[251]. These experiments were performed using (3-(4,5-dimethylthiazol-2-yl)-5-(3-carboxymethoxyphenyl)-2-(4-sulfophenyl)- 2H-tetrazolium) MTS assay, with cells exposed to TKI for 48 h before analysis[251,252]. Findings by Quentmeier *et al*. in 2011 suggested SUP-B15 cells were 'resistant' to imatinib-induced apoptosis (Annexin-V/7-AAD $IC_{50}^{imatinib}$: 2 µM; the cut-off for resistance in this article, however, was 0.05 to 0.2 µM imatinib) with the IC_{50} of dasatinib reported as 100 nM[253]. In a study performed by Xing *et al*. in 2012, the IC_{50} of dasatinib in SUP-B15 cells treated over a 72h time-point was noted as 21.99 $\pm$ 2.98 nM[152,254]. Studies using ponatinib in a SUP-B15 setting, however, has never been described in the literature.

In this chapter, p-CrkL IC_{50} was evaluated throughout the process of generating TKI-resistance, because any increase would indicate an involvement of Bcr-Abl kinase activity[211]. Overexpression of *BCR-ABL1*, or more importantly, the presence of kinase-domain mutations, can contribute to the development of TKI-resistance[238,255]. Along with CrkL, Bcr-Abl is known to phosphorylate other

downstream partners such as Stat5 and Erk, contributing towards the growth and proliferation of cells [55,256,257].

The lack of increase in p-CrkL IC_{50} (a direct downstream effector of Bcr-Abl activity) in dose-escalations of low TKI concentrations (2, 5 and 7 nM dasatinib/ponatinib) was not unexpected because these TKI concentrations were below the IC_{50}/GI_{50} as described in the literature. Therefore, no alterations in p-CrkL expression would be expected in these cell lines. Despite the establishment of TKI-resistant growth throughout the intermediate concentrations (20, 30, 50 nM dasatinib/ponatinib) and in the final concentration of 200 nM dasatinib/ponatinib, however, the sensitivity of p-CrkL to TKI was unchanged compared to DMSO control cells. This indicated an ability of TKI to inhibit CrkL phosphorylation despite cells maintaining viability, suggesting that a Bcr-Abl independent mechanism exists.

Bcr-Abl independent activation of cell survival potential has been associated with the acquisition of alternative mechanisms of resistance, involving other pathways. Studies have described the overexpression of multidrug-resistant / P-glycoprotein mediated drug efflux mechanism[258], as well as the activation of Lyn, resulting in the upregulation of B-cell lymphoma 2 (Bcl-2) – a pro-survival family member of the mitochondrial control of apoptosis as possible causes of Bcr-Abl independent mechanism of resistance[259].

The absence of a marked difference in p-Bcr-Abl and downstream p-CrkL, despite a pronounced difference in expression of cleaved PARP and stability in cell viability in TKI-resistant compared to TKI-sensitive cell lines, suggesting cells may have been clonally-selected for TKI-independent mechanisms of resistance. PARP, in its active full-length isoform, has been implicated in DNA-repair of breast and lung cancer[260-262]. The cleavage of PARP is associated with an induction of apoptosis,

normally executed by upstream active (cleaved) caspase-3 as part of programmed cell death signalling[263,264]. PARP cleavage has been described in imatinib/dasatinib TKI-induced cell death[263,265,266], therefore, its lack of expression in TKI-resistant SUP-B15 cells confirmed TKI-tolerance as expected. TKI-resistant SUP-B15 cell lines may have undergone clonal selection for cells with survival advantages, a characteristic well-described in various drug-resistant cancers, including relapsed childhood ALL[267,268], malignant T-cell ALL[269], and the progression of chronic lymphocytic leukaemia (CLL)[270].

It was therefore interesting to note the increase of Erk phosphorylation in the untreated (0 nM) samples of 50 nM dasatinib/ponatinib resistant, compared to TKI-sensitive SUP-B15 cells. Erk, also known as the mitogen-activated protein kinase (MAPK), is part of the Ras-Raf-Mek-Erk signalling cascade implicated as a downstream substrate of Bcr-Abl[55,271]. The identification of *RAS* mutations in dasatinib/ponatinib resistant SUP-B15 cells supported this evidence because *RAS* mutations are normally absent in TKI-sensitive SUP-B15 cells[253]. The *KRAS*-G12S (dasatinib-resistant SUP-B15) and *NRAS*-G12S (ponatinib-resistant SUP-B15) mutations may potentially be associated with TKI-resistance.

RAS mutations have been shown to be involved in ALL, where Perentesis and colleagues showed an incidence of 4.5% of ALL cases with *KRAS* and 9.3% with *NRAS* mutations affecting the 12/13th codon of each oncogene[272]. In a separate article, Irving *et al*. published findings where low-level *RAS* mutations were detected in patients, which later emerged at relapse, suggesting cells harbouring these survived initial therapy[111]. *RAS* mutations have also been implicated in other cancers, including colorectal[103], pancreatic[273] and lung[274]. Furthermore, evidence by Sunaga *et al*. indicated that a knockdown of oncogenic *KRAS* in non-small cell

lung cancer cells resulted in a suppression of tumour growth and re-sensitisation of cancer cells to therapy[100], suggesting *RAS* mutations can contribute to treatment resistance.

The notable differences in gene expression patterns between TKI-sensitive and resistant SUP-B15 cell lines also indicated how transcriptomically distinct these cell lines were. Treatment sensitive and resistant cells are known to be transcriptomically dissimilar, as described in other cancers such as pancreatic and breast [275,276]. Further mRNA sequencing revealed the association of genes involved in signal transduction (i.e. involvement of *PDE1A* in the cyclic AMP (cAMP) pathway[277]), G-protein coupled receptor (GPCR) (via *LGR5* and *SOCS7*)[278], and, Rho GTPase signalling (*DOCK8*)[279]. Specifically, *LGR5* have been implicated in stem cell development through the Wnt signalling pathway in intestine and skin[280]. *ETS1*, involved in Ras/Erk signalling[281], has also been associated with drug-resistant colorectal[282], prostate[283] and breast[284,285] cancers.

In mRNA-seq analysis of ponatinib-resistant SUP-B15 cells, the reduced distribution of significantly-expressed genes (specifically, the lack of significantly downregulated genes), was unexpected. This finding suggests the development of ponatinib-resistance requires an upregulation of a specific set of genes unique for an evasion of TKI therapy. A possible reason includes ponatinib being a highly potent Abl-kinase inhibitor[183,286,287]. Amongst the specific set of upregulated genes, *LILRB4* has been associated with the *ex vivo* expansion of haematopoietic cells[288]. Another gene, *ARHGEF12*, has been associated with Rho GTPase activity[289,290] which was noted as a myeloid/lymphoid fusion partner in MLL-rearranged acute leukaemia[291]. These genes are implicated in dysregulated *RAS* signalling, supporting the finding that *NRAS*-G12S is a driver of TKI-resistance. Furthermore, the upregulation of

BACH2 and *LGR5* in ponatinib-resistant SUP-B15 cells (similarly observed in dasatinib-resistance), suggests these genes complement towards the development of TKI-resistance. This is the first time that such findings are described in a Ph+ ALL setting.

Increased expression of *LGR5*, in-combination with *RAS* mutations, have been associated with oncogenic clonal expansion and survival of cells in intestinal cancer[292]. In addition, a study by Janes *et al*. demonstrated TKIs alone did not sufficiently suppress signalling of mechanistic target of rapamycin complex (mTORc) 1 and 2, leading to constant phosphorylation of downstream substrates such as ribosomal s6 kinase (S6K) and eukaryotic translation initiation factor 4E binding protein 1 (4E-BP1)[251].

As some of the genes implicated in TKI-resistant SUP-B15 cells converge along the cAMP signalling pathway, it may be possible for downstream mechanisms such as GPCR[293,294] and mTOR[295] to play a role in TKI-resistance. This was reflected in a study performed by Xing *et al.*, where imatinib-resistance in SUP-B15 cells was attributed to increased mTOR signalling[152]. Increased p-Erk expression was also noted in the study describing imatinib-resistant SUP-B15 cells, however, the mutation status of *RAS* was unknown[152]. In addition, a recent study has identified patterns of dysregulated GPCR signalling within distinct subgroups of AML patients[296] – a promising indication that GPCR signalling may be a relevant target in TKI-resistant SUP-B15 cells.

In summary, the findings of this chapter indicate that although *BCR-ABL1* may have been a driver of disease in immortalised naïve SUP-B15 cells, the mode of TKI-resistance is independent of the fusion gene (Figure 3.12). The low p-CrkL IC_{50} accompanied by an increased p-Erk expression, as well as the identification of *RAS*

mutations (*KRAS*-G12S in dasatinib-resistance; *NRAS*-G12S in ponatinib-resistance) suggest these genetic alterations as the main cause of dasatinib/ponatinib resistance (**Figure 3.12**). This data is further supported by mRNA-seq analysis, indicating significant expression (FDR < 0.05) of genes associated with signal transduction and stem-cell pathways. Taken together, dasatinib and ponatinib-resistance in SUP-B15 cells are not attributed to Bcr-Abl, but rather, possibly by a combination of noncanonical mechanisms driven by mutation of the *RAS* oncogene, which overrides TKI-sensitivity resulting in resistance and survival of cells in this highly-aggressive form of the disease. Potential future methods of overcoming resistance may include the use of therapies targeting these alternative pathways (i.e. MEK inhibitors[297,298], mTOR inhibitors[299,300], GPCR antagonists[301,302] or PDE inhibitors[303]), which may reverse resistance, eradicating leukaemia cells.

THIS PAGE INTENTIONALLY LEFT BLANK.

Figure 3.12

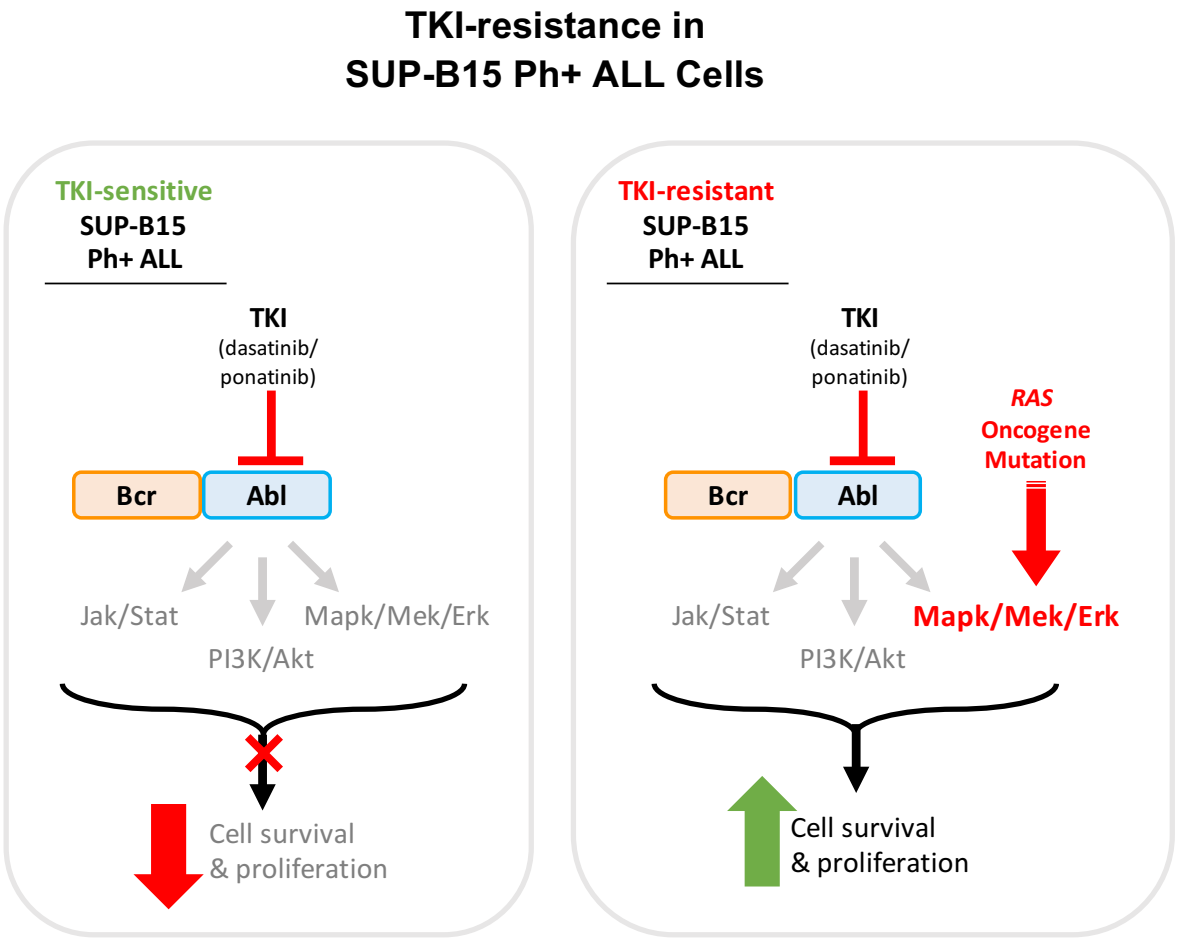


Figure 3.12 – Schematic representation of TKI-resistance in dasatinib and ponatinib-resistant SUP-B15 Ph+ ALL cells

Left: SUP-B15 cells (expressing the Bcr-Abl oncoprotein) are normally sensitive to TKIs such as dasatinib and ponatinib. Exposure of cells to these TKIs result in an inhibition of downstream kinase signalling such as the Jak/Stat, PI3k/Akt and Mapk/Mek/Erk. This, in turn, results in a reduction of cell survival and proliferation, eventually leading to the death of cancer cells. **Right:** In TKI-resistance, dasatinib and ponatinib were still able to inhibit Bcr-Abl activity, however, the presence of a *RAS* mutation (*KRAS*-G12S in dasatinib-resistant and *NRAS*-G12S in ponatinib-resistant) overrides this mechanism. The Bcr-Abl independent signalling allows for a downstream activation of cell survival and proliferation pathways including the expression of the Mapk/Mek/Erk signalling cascade.

Appendix 3.1 List of differentially-expressed genes in dasatinib-resistant SUP-B15 cells

Symbol	Description	Summary	RNAseq Data		qPCR Validation	
			Log_2 Fold Change (in decreasing order)	Adj.P.Val	$2^{-\Delta\Delta Ct}$ Mean	SD
PDE1A	Phosphodiesterase 1A, Calmodulin-Dependent	Cyclic nucleotide phosphodiesterases (*PDEs*) play a role in signal transduction by regulating intracellular cyclic nucleotide concentrations through hydrolysis of cAMP and/or cGMP to their respective nucleoside 5-prime monophosphates. Members of the *PDE1* family, such as *PDE1A*, are Ca(2+)/calmodulin (see CALM1; MIM 114180)-dependent *PDEs* (CaM-PDEs) that are activated by calmodulin in the presence of Ca(2+) (Michibata et al., 2001 [PubMed 11342109]; Fidock et al., 2002 [PubMed 11747989]).[supplied by OMIM, Oct 2009]	4.295781082	0.005271811	27.15619017	3.180953342
EVL	Enah/Vasp-Like	*EVL* (Enah/Vasp-Like) is a Protein Coding gene. Diseases associated with *EVL* include esophageal varix and hypersplenism. Among its related pathways are Class I MHC mediated antigen processing and presentation and L1CAM interactions. GO annotations related to this gene include actin binding and profilin binding. An important paralog of this gene is SPRED1.	4.098897844	0.007650064	27.98423855	8.578161925
LGR5	Leucine-Rich Repeat Containing G Protein-Coupled Receptor 5	*LGR5* (Leucine-Rich Repeat Containing G Protein-Coupled Receptor 5) is a Protein Coding gene. Among its related pathways are Wnt signaling pathway (KEGG). GO annotations related to this gene include G-protein coupled receptor activity and transmembrane signaling receptor activity. An important paralog of this gene is LGR6.	3.817155432	0.003493061	7.045767887	1.80677462
ETS1	V-Ets Avian Erythroblastosis Virus E26 Oncogene Homolog 1	This gene encodes a member of the *ETS* family of transcription factors, which are defined by the presence of a conserved *ETS* DNA-binding domain that recognizes the core consensus DNA sequence GGAA/T in target genes. These proteins function either as transcriptional activators or repressors of numerous genes, and are involved in stem cell development, cell senescence and death, and tumorigenesis. Alternatively spliced transcript variants encoding different isoforms have been described for this gene.[provided by RefSeq, Jul 2011]	2.792109078	0.003678814	9.119978419	1.189999936
CD24	Cluster of Differentiation 24 (Isoform of Small Cell Lung Carcinoma Cluster 4 Antigen)	This gene encodes a sialoglycoprotein that is expressed on mature granulocytes and B cells and modulates growth and differentiation signals to these cells. The precursor protein is cleaved to a short 32 amino acid mature peptide which is anchored via a glycosyl phosphatidylinositol (GPI) link to the cell surface. This gene was missing from previous genome assemblies, but is properly located on chromosome 6. Non-transcribed pseudogenes have been designated on chromosomes 1, 15, 20, and Y. Alternative splicing results in multiple transcript variants. [provided by RefSeq, Apr 2014]	2.715483648	0.004310112	4.42528689	0.795620019
DOCK8	Dedicator Of Cytokinesis 8	This gene encodes a member of the DOCK180 family of guanine nucleotide exchange factors. Guanine nucleotide exchange factors interact with Rho GTPases and are components of intracellular signaling networks. Mutations in this gene result in the autosomal recessive form of the hyper-IgE syndrome. Alternatively spliced transcript variants encoding different isoforms have been described.[provided by RefSeq, Jun 2010]	2.205728863	0.003493061	5.164895409	0.941586477
BACH2	BTB And CNC Homology 1, Basic Leucine Zipper Transcription Factor 2	*BACH2* (BTB And CNC Homology 1, Basic Leucine Zipper Transcription Factor 2) is a Protein Coding gene. Among its related pathways are Lymphocyte Signaling. GO annotations related to this gene include sequence-specific DNA binding transcription factor activity and sequence-specific DNA binding. An important paralog of this gene is NFE2.	1.956962085	0.006883713	2.579769772	0.382116269
PDGFA	Platelet-Derived Growth Factor Alpha Polypeptide	*PDGFA* (Platelet-Derived Growth Factor Alpha Polypeptide) is a Protein Coding gene. Diseases associated with PDGFA include tendinitis and denys-drash syndrome. Among its related pathways are PI3K-Akt signaling pathway and PI-3K cascade. GO annotations related to this gene include protein homodimerization activity and growth factor activity. An important paralog of this gene is *PDGFB*.	-2.95169435	0.003678814	0.095010644	0.005451639
SOCS7	Suppressor Of Cytokine Signaling 7	*SOCS7* (Suppressor Of Cytokine Signaling 7) is a Protein Coding gene. Among its related pathways are PI-3K cascade and Signaling by GPCR. GO annotations related to this gene includeSH3 domain binding. Regulates signaling cascades probably through protein ubiquitination and/or sequestration. Functions in insulin signaling and glucose homeostasis through IRS1 ubiquitination and subsequent proteasomal degradation. Inhibits also prolactin, growth hormone and leptin signaling by preventing STAT3 and STAT5 activation, sequestering them in the cytoplasm and reducing their binding to DNA. May be a substrate recognition component of a SCF-like E3 ubiquitin-protein ligase complex which mediates the ubiquitination and subsequent proteasomal degradation of target proteins (By similarity).	-6.257939595	0.003678814	0.001528611	0.000135255
GBP5	Guanylate Binding Protein 5	*GBP5* (Guanylate Binding Protein 5) is a Protein Coding gene. Diseases associated with GBP5 include chronic active epstein-barr virus infection. Among its related pathways are Interferon Signaling and Interferon Signaling. GO annotations related to this gene include identical protein binding and GTPase activity. An important paralog of this gene is GBP7.	-7.178378413	0.004328043	0.009665027	0.00039006
SLC25A46	Solute Carrier Family 25, Member 46	*SLC25A46* belongs to the SLC25 family of mitochondrial carrier proteins (Haitina et al., 2006 [PubMed 16949250]).[supplied by OMIM, Mar 2008]	-8.412808472	0.002210825	0.000120591	0.000118468

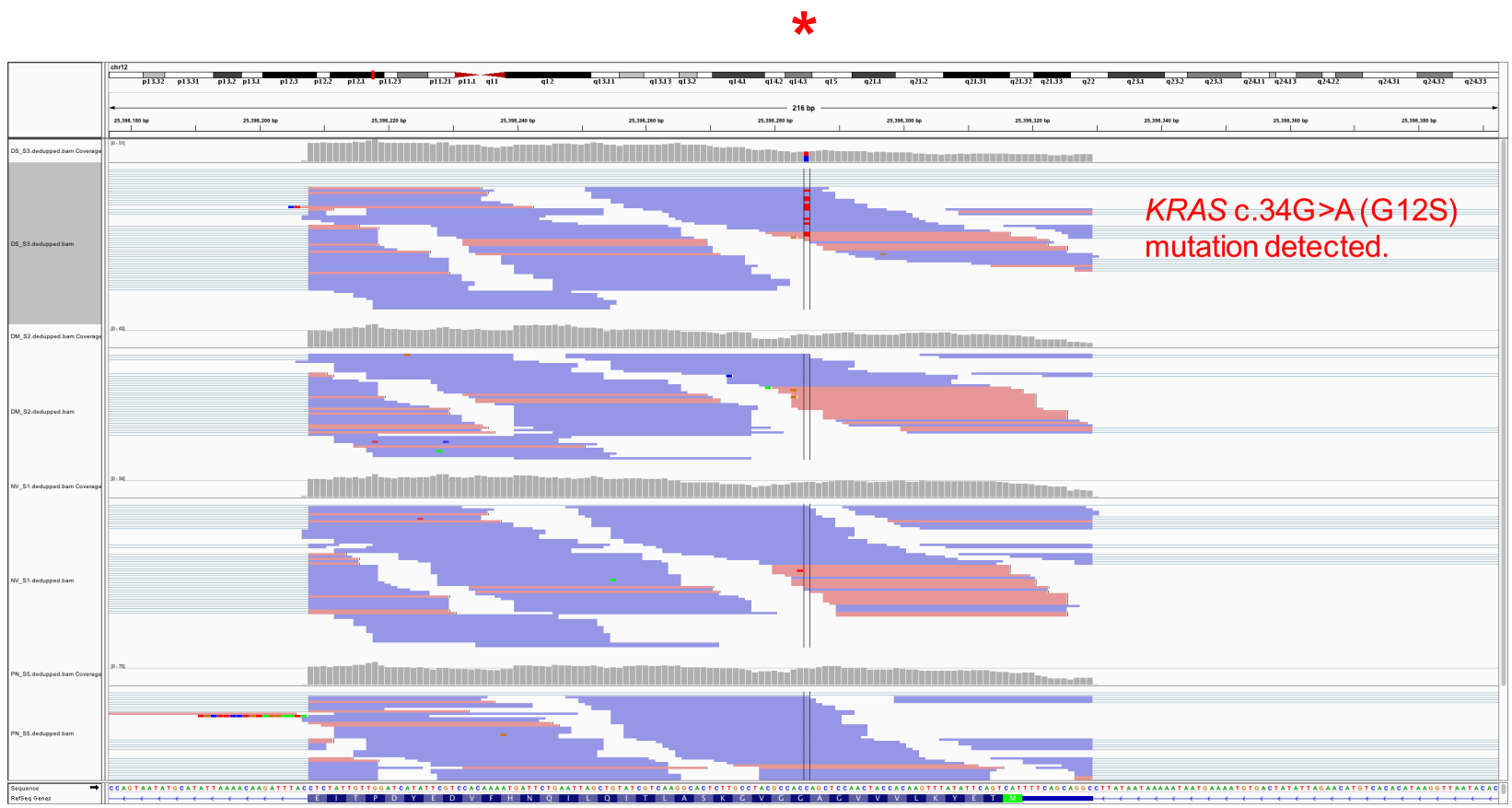
Appendix 3.2

List of differentially-expressed genes in ponatinib-resistant SUP-B15 cells

			RNAseq Data		qPCR Validation	
Symbol	Description	Summary	Log_2 Fold Change (in decreasing order)	Adj.P.Val	$2^{-\Delta\Delta Ct}$ Mean	SD
LILRB4	Leukocyte Immunoglobulin-Like Receptor, Subfamily B (With TM And ITIM Domains), Member 4	This gene is a member of the leukocyte immunoglobulin-like receptor (LIR) family, which is found in a gene cluster at chromosomal region 19q13.4. The encoded protein belongs to the subfamily B class of LIR receptors which contain two or four extracellular immunoglobulin domains, a transmembrane domain, and two to four cytoplasmic immunoreceptor tyrosine-based inhibitory motifs (ITIMs). The receptor is expressed on immune cells where it binds to MHC class I molecules on antigen-presenting cells and transduces a negative signal that inhibits stimulation of an immune response. The receptor can also function in antigen capture and presentation. It is thought to control inflammatory responses and cytotoxicity to help focus the immune response and limit autoreactivity. Multiple transcript variants encoding different isoforms have been found for this gene. [provided by RefSeq, Jul 2008]	10.20104366	0.043773608	39337.44235	16150.83226
LILRA2	Leukocyte Immunoglobulin-Like Receptor, Subfamily A (With TM Domain), Member 2	This gene encodes a member of a family of immunoreceptors that are expressed predominantly on monocytes and B cells, and at lower levels on dendritic cells and natural killer cells. The encoded protein is an activating receptor that inhibits dendritic cell differentiation and antigen presentation and suppresses innate immune response. Alternatively spliced transcript variants encoding different isoforms have been found. This gene is located in a cluster of related genes on chromosome 19 and there is a pseudogene for this gene on chromosome 3. [provided by RefSeq, Mar 2014]	9.36216578	0.0442599	1291.025322	391.7149201
BEST3	Bestrophin 3	*BEST3* (Bestrophin 3) is a Protein Coding gene. Diseases associated with *BEST3* include vitelliform macular dystrophy 2 and vitelliform macular dystrophy. Among its related pathways are Ion channel transport and Transport of glucose and other sugars, bile salts and organic acids, metal ions and amine compounds. GO annotations related to this gene include chloride channel activity. An important paralog of this gene is BEST2.	9.198431887	0.043253704	1002.662154	106.0541147
ARHGEF12	Rho Guanine Nucleotide Exchange Factor (GEF) 12	Rho GTPases play a fundamental role in numerous cellular processes that are initiated by extracellular stimuli working through G protein-coupled receptors. The encoded protein may form a complex with G proteins and stimulate Rho-dependent signals. This protein has been observed to form a myeloid/lymphoid fusion partner in acute myeloid leukemia. Three transcript variants encoding different isoforms have been found for this gene. [provided by RefSeq, Jul 2014]	9.137173986	0.043253704	187767.9812	22061.4995
PLD4	Phospholipase D Family, Member 4	*PLD4* (Phospholipase D Family, Member 4) is a Protein Coding gene. Among its related pathways are L1CAM interactions and Fcgamma receptor (FCGR) dependent phagocytosis. GO annotations related to this gene include phosphatidylinositol phospholipase C activity and N-acylphosphatidylethanolamine-specific phospholipase D activity. An important paralog of this gene is PLD5.	8.299801677	0.043253704	1074.741494	427.4901889
MME	Membrane Metallo-Endopeptidase	This gene encodes a common acute lymphocytic leukemia antigen that is an important cell surface marker in the diagnosis of human acute lymphocytic leukemia (ALL). This protein is present on leukemic cells of pre-B phenotype, which represent 85% of cases of ALL. This protein is not restricted to leukemic cells, however, and is found on a variety of normal tissues. It is a glycoprotein that is particularly abundant in kidney, where it is present on the brush border of proximal tubules and on glomerular epithelium. The protein is a neutral endopeptidase that cleaves peptides at the amino side of hydrophobic residues and inactivates several peptide hormones including glucagon, enkephalins, substance P, neurotensin, oxytocin, and bradykinin. This gene, which encodes a 100-kD type II transmembrane glycoprotein, exists in a single copy of greater than 45 kb. The 5' untranslated region of this gene is alternatively spliced, resulting in four separate mRNA transcripts. The coding region is not affected by alternative splicing. [provided by RefSeq, Jul 2008]	5.350272318	0.0442599	69.14376199	6.755586402
EVL	Enah/Vasp-Like	*EVL* (Enah/Vasp-Like) is a Protein Coding gene. Diseases associated with *EVL* include esophageal varix and hypersplenism. Among its related pathways are Class I MHC mediated antigen processing and presentation and L1CAM interactions. GO annotations related to this gene include actin binding and profilin binding. An important paralog of this gene is SPRED1.	4.92255178	0.043253704	61.49171241	25.90699111
LGR5	Leucine-Rich Repeat Containing G Protein-Coupled Receptor 5	*LGR5* (Leucine-Rich Repeat Containing G Protein-Coupled Receptor 5) is a Protein Coding gene. Among its related pathways are Wnt signaling pathway (KEGG). GO annotations related to this gene include G-protein coupled receptor activity and transmembrane signaling receptor activity. An important paralog of this gene is *LGR6*.	4.265370883	0.043253704	19.00035778	7.409702102
BACH2	BTB And CNC Homology 1, Basic Leucine Zipper Transcription Factor 2	*BACH2* (BTB And CNC Homology 1, Basic Leucine Zipper Transcription Factor 2) is a Protein Coding gene. Among its related pathways are Lymphocyte Signaling. GO annotations related to this gene include sequence-specific DNA binding transcription factor activity and sequence-specific DNA binding. An important paralog of this gene is NFE2.	3.310506042	0.043773608	9.806172524	4.983681755
POU4F1	POU Class 4 Homeobox 1	This gene encodes a member of the POU-IV class of neural transcription factors. This protein is expressed in a subset of retinal ganglion cells and may be involved in the developing sensory nervous system. This protein may also promote the growth of cervical tumors. A translocation of this gene is associated with some adult acute myeloid leukemias. [provided by RefSeq, Mar 2012] *POU4F1* (POU Class 4 Homeobox 1) is a Protein Coding gene. Among its related pathways are Integrin Pathway and Direct p53 effectors. GO annotations related to this gene include RNA polymerase II distal enhancer sequence-specific DNA binding transcription factor activity and RNA polymerase II distal enhancer sequence-specific DNA binding. An important paralog of this gene is POU6F1.	-2.66205612	0.058868817	0.288368293	0.09619136

Appendix 3.3

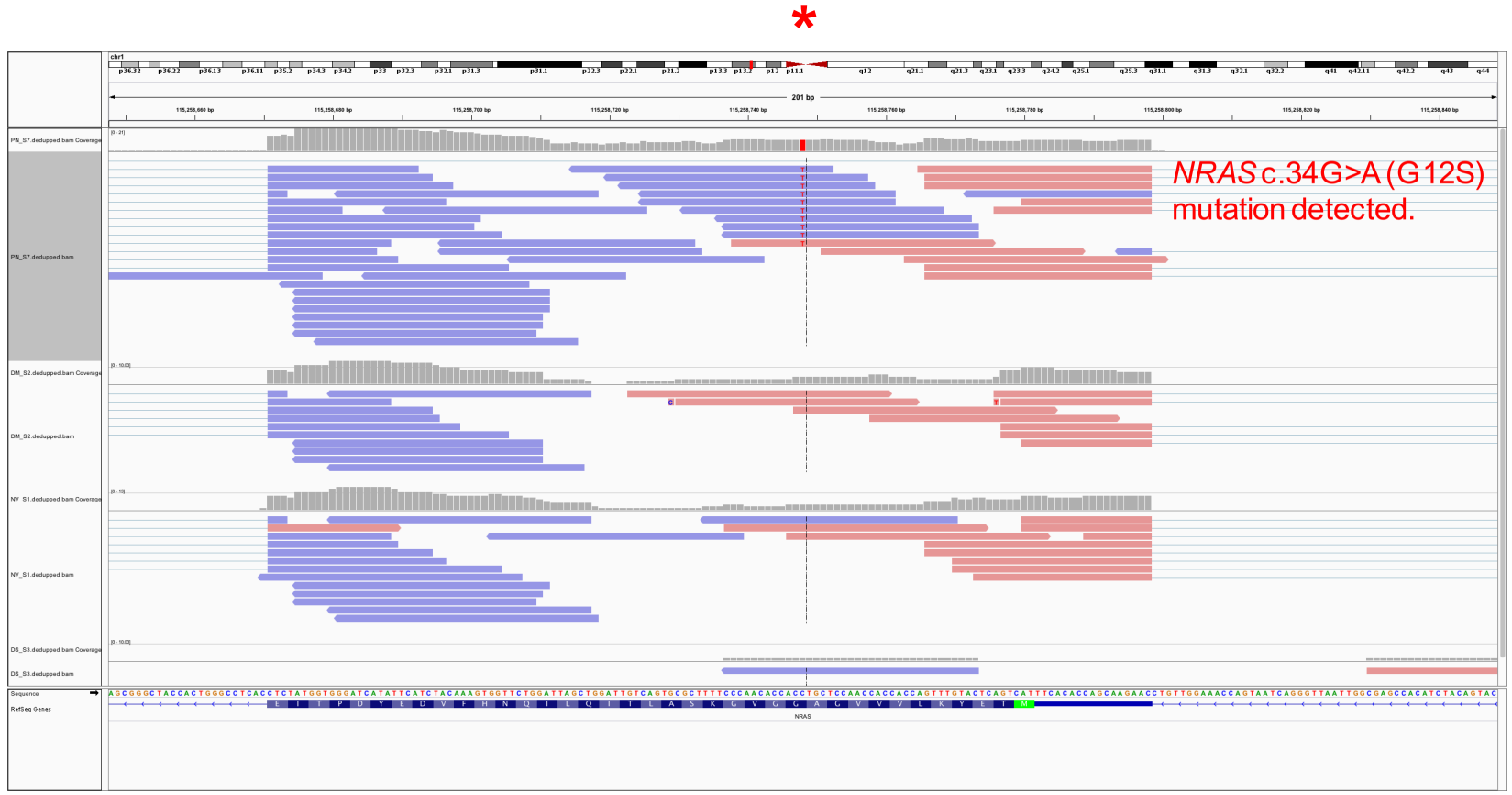
KRAS Alignment in SUP-B15 Cell Lines



Software: Integrated Genomics Viewer (IGV, Broad Institute)

Appendix 3.4

NRAS Alignment in SUP-B15 Cell Lines



Software: Integrated Genomics Viewer (IGV, Broad Institute)

THIS PAGE INTENTIONALLY LEFT BLANK.

CHAPTER 4 –

TKI-RESISTANCE IN *RANBP2-ABL1* CELL LINES IS MEDIATED BY CLINICALLY-RELEVANT POINT MUTATIONS AND NON-CANONICAL SIGNALLING

4.1. Introduction

The introduction of the TKI imatinib mesylate (STI571 / Glivec), a small molecule rationally-designed inhibitor to target the Bcr-Abl oncoprotein in Ph+ leukaemia, has revolutionised cancer therapy[304,305]. Bcr-Abl is constitutively activated in CML and Ph+ ALL and is encoded by *BCR-ABL1*, a product of the fusion between chromosomes 9 and 22 t(9;22)(q34;q11)[306]. Aberrant activation of the Abl kinase caused by this translocation leads to increased downstream phospho-signalling including phosphoinositide 3-kinase (PI3K) and mitogen-activated protein kinase (MAPK) pathways, resulting in upregulation of cell survival mechanisms[55,271,307,308]. In Ph+ ALL and blast-crisis CML, Bcr-Abl expression further leads to uncontrolled proliferation of blast cells that deregulate normal haematopoiesis, leading to infiltration of leukaemic cells into organs such as spleen and lymph nodes[309,310]. Progression of this disease can lead to mortality, however, the introduction of Abl-specific kinase inhibitors such as imatinib has greatly improved survival (>50% in Ph+ ALL[191,311]; >80% in CML[312-314]). In children and adolescents with Ph+ ALL, the 3-year event-free survival rate has increased from 35.4% to 80%[237,315] but relapse remains common.

Imatinib competitively binds the ATP binding pocket of Abl-kinase, interfering with normal phosphorylation and activation of downstream cell survival signalling proteins. This inhibits cell survival and proliferation, leading to apoptosis. The successful eradication of leukaemic cells, however, has been impeded by clinical relapse due to imatinib-resistance. The mechanisms vary between primary resistance (i.e. alterations in drug influx/efflux) and secondary resistance (including kinase-specific alterations such as *BCR-ABL1* amplification and kinase-domain mutations)[153]. To overcome imatinib-resistance, newer generation TKIs were since

developed (these include the second generation Abl TKIs nilotinib[316] and dasatinib[171], as well as the third generation Abl TKI ponatinib[317]), however, relapse remains a major clinical issue[318].

The identification and classification of Ph-like ALL as a subtype of leukaemia containing targetable kinase activating lesions has enabled anecdotal application of TKIs in this disease setting[64,90,91]. Despite this promising approach, TKI resistance as in CML and Ph+ ALL has been observed. In a recent report by Yeung *et al*., dasatinib in-combination with chemotherapy was administered to an 81-year old patient whose leukaemic cells harboured the *ETV6-ABL1* Ph-like ALL fusion. The patient subsequently relapsed and an *ABL1*-T315I kinase domain mutation was identified. TKI therapy was substituted to ponatinib (a third-generation TKI) and the treatment lasted for 4 weeks after which the patient was palliated[92].

At present, clinical trials are being initiated to investigate the potential translation of targeted therapy from a Ph+ setting into Ph-like ALL[147-149]. With the variety of kinase fusion-genes identified in Ph-like ALL[64], many are yet to be fully characterised. Most of these fusion genes are targetable using currently available TKIs[73,205,319], however, the development and mechanisms of TKI-resistance in Ph-like ALL is poorly understood.

Therefore, in this chapter, I have developed models of TKI-resistance in a Ph-like ALL setting using a known Abl kinase fusion (*RANBP2-ABL1*). This has been achieved by expressing this fusion gene in cell lines, followed by establishing TKI-resistance to imatinib, dasatinib and ponatinib independently. As TKI-resistance in a Ph+ setting has been very well-studied, modelling TKI-resistance in *RANBP2-ABL1* will inform whether similar mechanisms of resistance or if other canonical and/or non-canonical forms may arise.

4.2. Approach

To investigate the mechanisms of TKI-resistance associated with Abl-fusion kinase signalling, the Ph-like ALL fusion gene *RANBP2-ABL1* was selected. Patient-derived *RANBP2-ABL1* fusion gene[64] was subcloned from pCR®-Blunt II-TOPO® vector into a pRuf-iG2 retroviral backbone. The resulting retroviral construct was transduced into Ba/F3 pro-B cells, with the transformative ability of the fusion gene investigated by analysis of IL-3 independent survival and growth. To confirm that Ranbp2-Abl1 is targetable by clinically-available Abl inhibitors, drug sensitivity assays were conducted by exposing transformed Ba/F3 cells to a panel of Abl inhibitors (imatinib, dasatinib and ponatinib) and the Jak inhibitor ruxolitinib. Analysis of the effect of TKI treatment was performed using Annexin-V/7-AAD exclusion flow cytometry as well as phosphoflow analysis and western blotting of downstream Ranbp2-Abl1 kinase signalling including p-CrkL and p-Stat5.

Upon confirmation of TKI-sensitivity to TKIs, resistance was generated by exposing Ba/F3 cells expressing *RANBP2-ABL1* to incrementally increasing concentrations of imatinib, dasatinib and ponatinib (first, second and third-generation Abl-kinase inhibitors respectively) for 6-12 months using the well-plate subculturing method. Cells were considered TKI-resistant if they were tolerant to 10 μM imatinib, 200 nM dasatinib and 200 nM ponatinib in culture, exceeding clinically-relevant efficacy concentrations while mimicking peak plasma levels[181,250,320]. Following achievement of TKI-resistance, the ability of cells to survive in increased concentration of TKI was confirmed using drug-sensitivity assays as previously mentioned. In addition, Sanger sequencing was employed to further identify any alterations within the *RANBP2-ABL1* kinase domain. Where relevant, next-generation mRNA-seq was

performed to identify any canonical and/or non-canonical signalling mechanism involved.

4.3. Results

4.3.1. Ba/F3 cells transduced with *RANBP2-ABL1* Ph-like ALL fusion gene demonstrates kinase-independent survival capacity

Using molecular subcloning, the *RANBP2-ABL1* Ph-like ALL fusion gene was successfully isolated from the pCR®-Blunt II-TOPO® vector and ligated into the mammalian-expressing pRuf-iG2 retroviral vector (**Figure 4.1**). Restriction endonucleases utilised were specific for excision of the *RANBP2-ABL1* fusion gene (using NotI and SpeI) and linearisation of the pRuf-iG2 recipient vector (via SnaBI), for ultimate blunt-end cloning and transformation into DH5α competent cells. Three bacterial colonies (#3, 4 and 6) were found by PCR to contain *RANBP2-ABL1* (**Figure 4.2A**), confirming presence of the *RANBP2-ABL1* fusion gene (**Figure 4.2B**) in its correct orientation (**Figure 4.2C**) and size of 6 kb (**Figure 4.2D**), as determined by gel electrophoresis of PCR products.

Plasmids were then transfected into HEK-293T cells in the presence of the packaging vector pEQ-Eco, generating viral particles. Visualisation of GFP expression in HEK-293T cells at 24 h post-transfection via fluorescence microscopy revealed GFP positivity, confirming incorporation and expression of the pRuf-iG2 construct (**Figure 4.3A**). GFP positivity was quantified using flow cytometry (**Figure 4.3B**) with a transfection efficiency of 55.1% in cells transfected with pRuf-iG2 empty

vector, and 24.5% in cells transfected with pRuf-iG2 *RANBP2-ABL1* (**Figure 4.3B & C**).

Application of viral supernatant from HEK-293T transfected cells onto Ba/F3 parental wild-type cells resulted in successful transduction, which was confirmed by flow cytometry (**Figure 4.4B**, based on the strategy in **Figure 4.4A**). GFP analysis prior to FACS isolation indicated a presence of 34.0% and 27.0% of GFP+ cells in Ba/F3 cells transduced with the pRuf-iG2 empty vector control, and, pRuf-iG2 *RANBP2-ABL1* vector respectively (**Figure 4.4B**). These cells were collected and cultured at 37ºC/5% CO_2, followed by flow analysis 3 days later which confirmed 98.9% GFP+ in Ba/F3 pRuf-iG2 empty vector cells, and 98.9% GFP+ in Ba/F3 pRuf-iG2 *RANBP2-ABL1* cells (**Figure 4.4C**). Fluorescence microscopy of GFP positivity in transduced cells supported this data (**Figure 4.4D**).

Expression of *RANBP2-ABL1* was subsequently confirmed by PCR, utilising primers that specifically amplify the *RANBP2-ABL1* breakpoint region **(Figure 4.5A**)[64]. Western blotting confirmed the expression of this fusion protein in Ba/F3 *RANBP2-ABL1* cells (**Figure 4.5B**&**C**). The estimated molecular weight of Ranbp2-Abl1 fusion protein was ~220 kDa (translated from 5993 coding nucleotides), based on the sequence length of the fusion gene (~5993 bp).

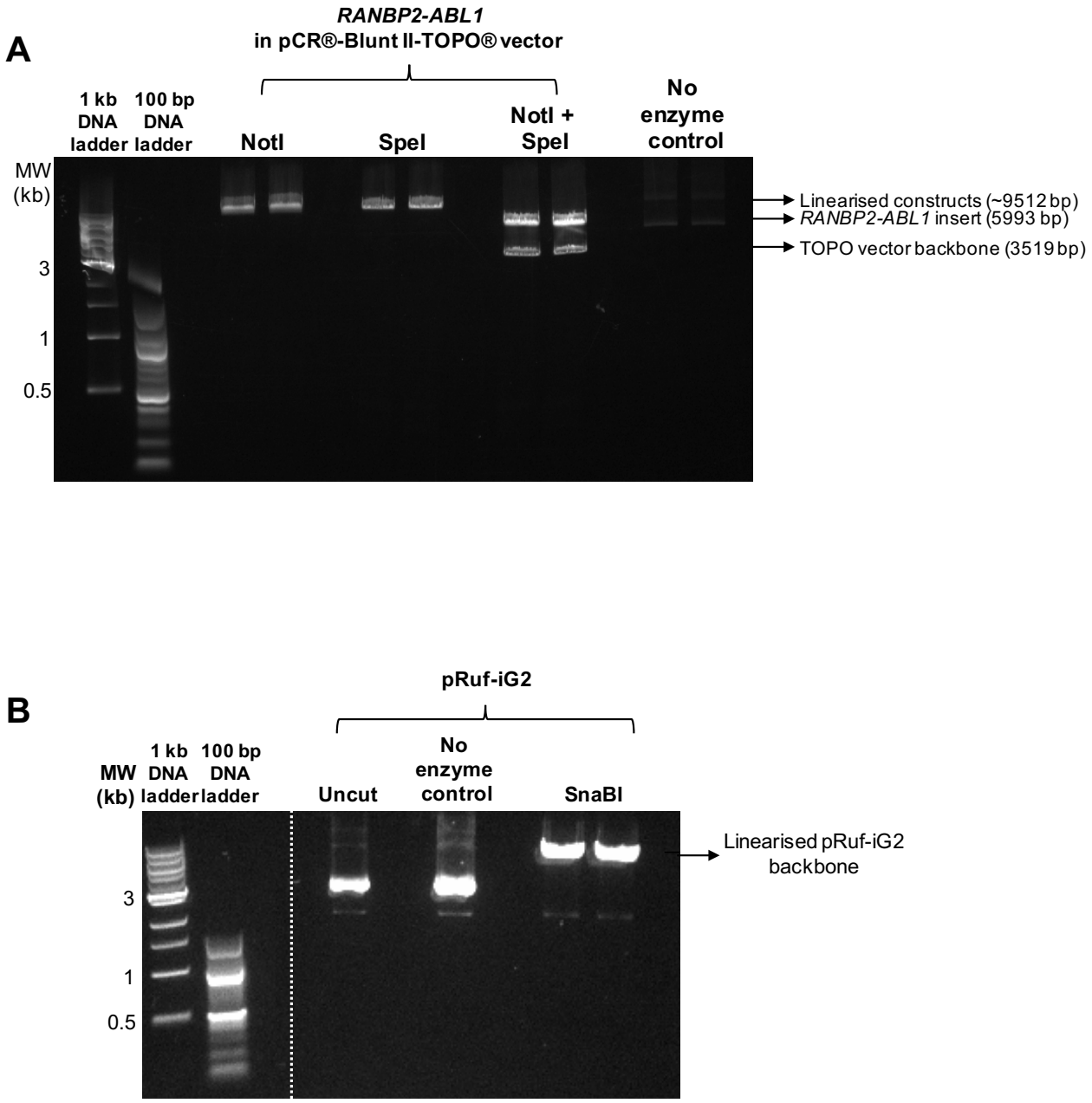
As Ba/F3 cells require the presence of IL-3 to survive in culture (in the absence of a transforming oncogene), the transforming ability of *RANBP2-ABL1* in the absence of cytokine was investigated. Ba/F3 parental wild-type cells were included as a non-transduced control, while Ba/F3 pRuf-iG2 empty vector cells represented controls that have undergone the transduction process. Results indicated that cells containing the *RANBP2-ABL1* fusion gene were viable ($P < 0.05$) in IL-3-free culture following 3-day incubation, maintaining an average viability of 91.8% (SD ±2.95),

compared to that of Ba/F3 parental wild-type control (28.4% ± 20.1) and pRuf-iG2 empty vector control (25.8% ± 18.6) (**Figure 4.6A**). Ba/F3 *RANBP2-ABL1* cells were also proliferating, resulting in a live cell density of 12.5 ± 0.68 x 10^5/ml on day 3 compared to control cells, which did not proliferate in the absence of IL-3 (live cell density: 0.77 ± 0.82 x 10^5/ml) (**Figure 4.6B**).

Figure 4.1 – Isolation of *RANBP2-ABL1* Ph-like ALL fusion gene from pCR®-Blunt II-TOPO® plasmids

DNA agarose gels of restriction digestion products. **A**: Single digests (NotI, SpeI) to ensure specificity of restriction endonuclease site, and, a double digest (NotI + SpeI) to isolate the *RANBP2-ABL1* Ph-like ALL fusion gene from the pCR®-Blunt II-TOPO® backbone. Products were divided into 2 lanes to prevent overloading of gel, allowing ease of cutting bands for molecular cloning purposes. **B**: Restriction digest and linearisation of the host retroviral vector pRuf-iG2, with SnaBI, an endonuclease that results in a blunt-ended product.

Figure 4.1

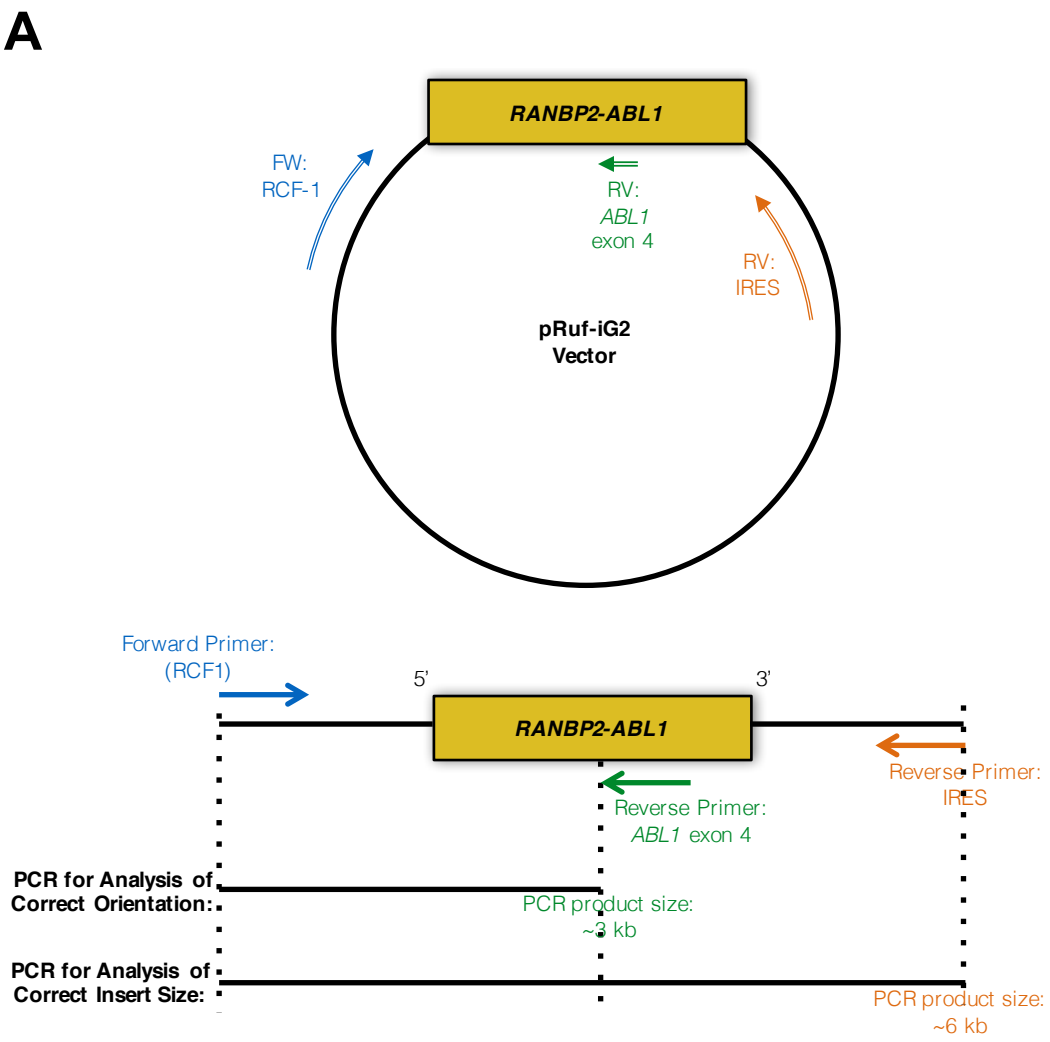

A
RANBP2-ABL1
in pCR®-Blunt II-TOPO® vector
1 kb DNA ladder
100 bp DNA ladder
NotI
SpeI
NotI + SpeI
No enzyme control
MW (kb)
3
1
0.5
Linearised constructs (~9512 bp)
RANBP2-ABL1 insert (5993 bp)
TOPO vector backbone (3519 bp)
B
pRuf-iG2
MW (kb)
1 kb DNA ladder
100 bp DNA ladder
Uncut
No enzyme control
SnaBI
3
1
0.5
Linearised pRuf-iG2 backbone

THIS PAGE INTENTIONALLY LEFT BLANK.

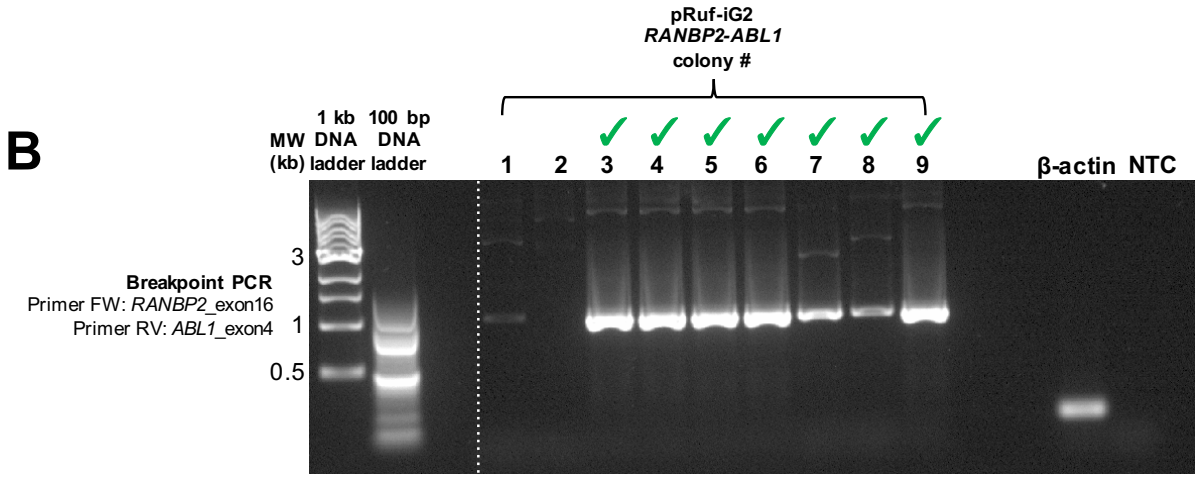
Figure 4.2 – PCR confirms presence of *RANBP2-ABL1* fusion gene in molecularly-cloned pRuf-iG2 retroviral vector

A: PCR strategy for confirmation of *RANBP2-ABL1* insert size and direction in the pRuf-iG2 retroviral vector. **B**: DNA agarose gel of PCR products amplifying the *RANBP2-ABL1* breakpoint, with green tick marks indicating bacterial colonies harbouring plasmids with the fusion gene. **C**: Directional PCR confirming colonies containing the correct orientation of *RANBP2-ABL1* (5' – 3'), as indicated by green tick marks. **D**: Analysis of full-length *RANBP2-ABL1* insert size in bacterial colonies, confirming # 3, 4 and 6, contains a correct insert size of ~6 kb.

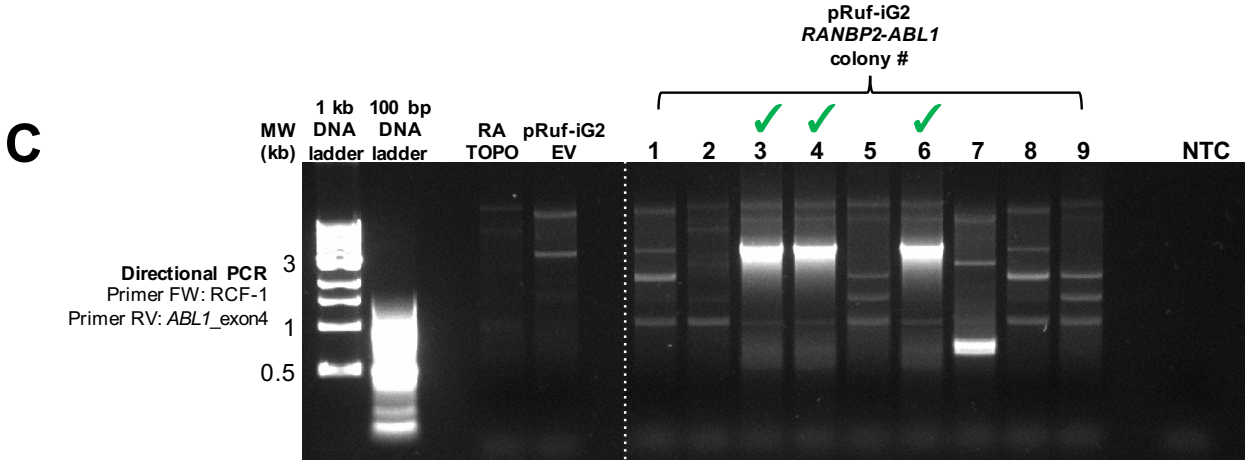
Figure 4.2


A
RANBP2-ABL1
FW:
RCF-1
RV:
ABL1
exon 4
RV:
IRES
pRuf-iG2
Vector
Forward Primer:
(RCF1)
5'
3'
RANBP2-ABL1
Reverse Primer:
IRES
Reverse Primer:
ABL1 exon 4
PCR for Analysis of
Correct Orientation:
PCR product size:
~3 kb
PCR for Analysis of
Correct Insert Size:
PCR product size:
~6 kb

B

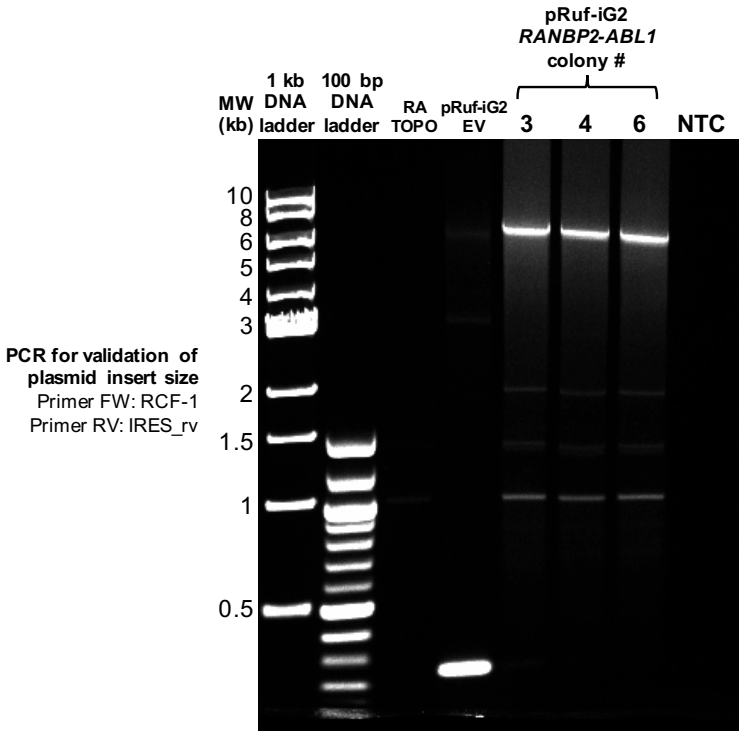


C



Expected PCR product size: ~3kb

D



Expected PCR product size: ~6kb

Legend:
EV: pRuf-iG2 empty vector
MW: molecular weight marker
RA: *RANBP2-ABL1*
TOPO: pCR®-Blunt II-TOPO® vector
NTC: no template control

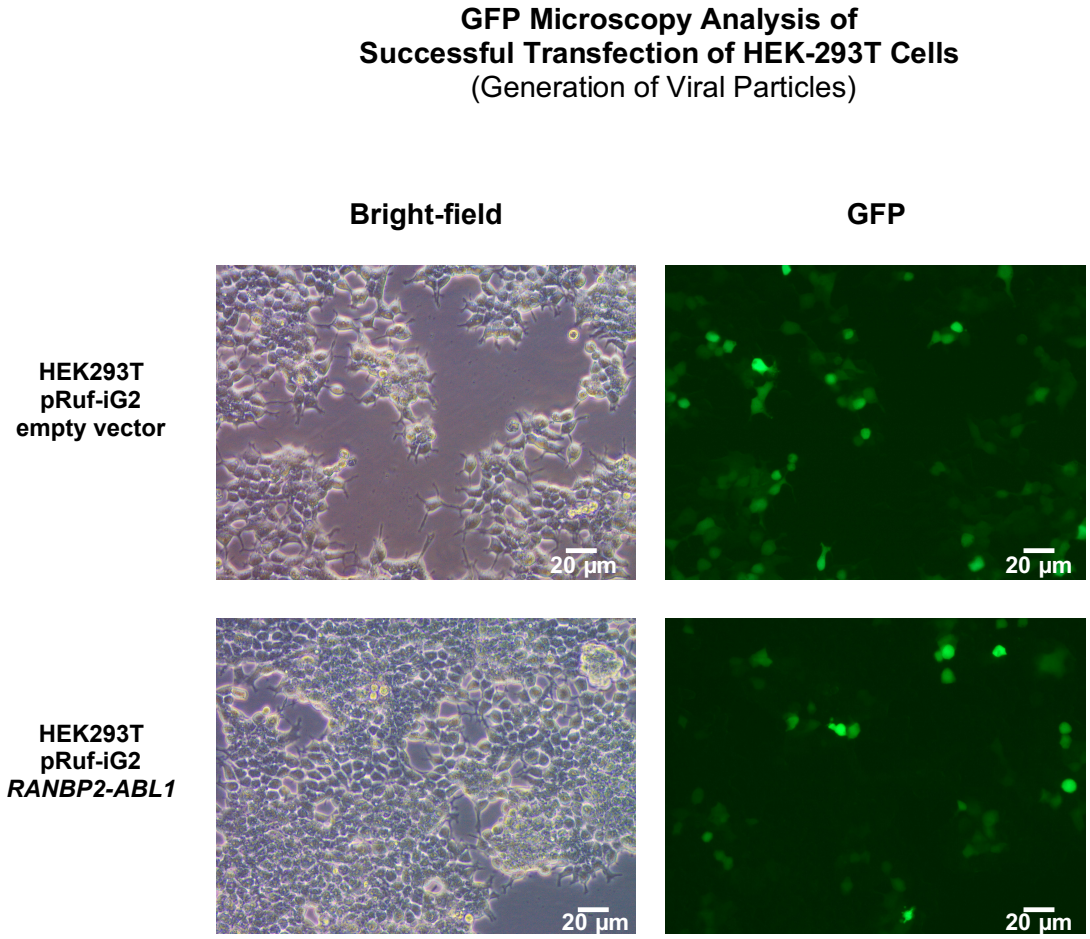
THIS PAGE INTENTIONALLY LEFT BLANK.

Figure 4.3 – GFP expression in HEK-293T cells retrovirally-transfected with pRuf-iG2 *RANBP2-ABL1* in parallel with the empty vector

A: Bright-field and GFP microscopy images of HEK-293T cells transfected with pRuf-iG2 empty vector control, and pRuf-iG2 *RANBP2-ABL1*. Images were obtained 24h post-transfection. Scale bar represents 20 μm. **B:** Flow cytometry gating strategy applied for analysis of GFP+ percentage in HEK-293T cells. This data is representative of cells transfected with the pRuf-iG2 empty vector. **C**: Left to right – percentage of GFP+ cells in untransfected HEK-293T, cells transfected with pRuf-iG2 empty vector and cells transfected with pRuf-iG2 *RANBP2-ABL1*.

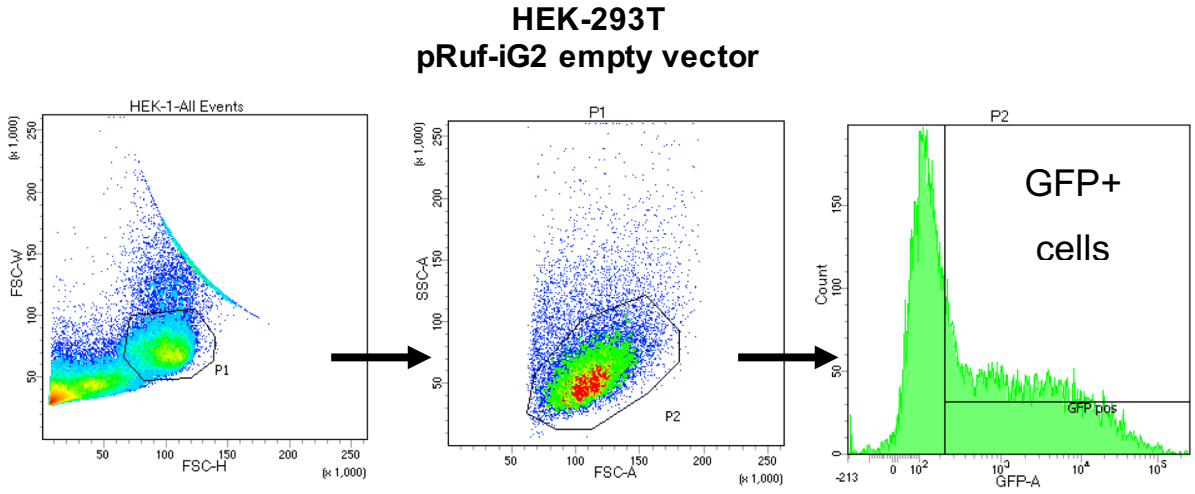
Figure 4.3

A


GFP Microscopy Analysis of
Successful Transfection of HEK-293T Cells
(Generation of Viral Particles)
Bright-field
GFP
HEK293T
pRuf-iG2
empty vector
HEK293T
pRuf-iG2
RANBP2-ABL1
20 µm
20 µm
20 µm
20 µm

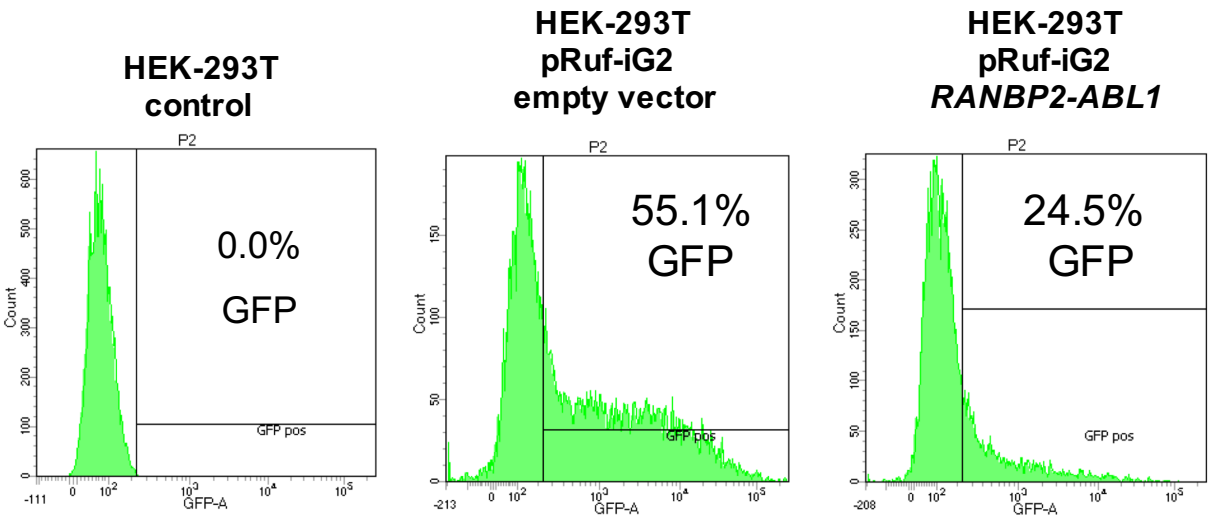
B

Flow cytometry analysis strategy



C

GFP expression in cells



THIS PAGE INTENTIONALLY LEFT BLANK.

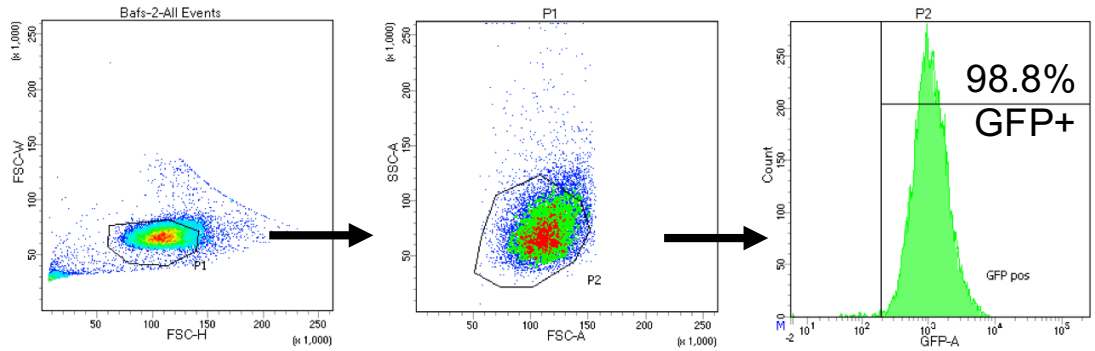
Figure 4.4 – Ba/F3 cells successfully transduced with pRuf-iG2 constructs express GFP positivity

Ba/F3 cells were analysed and sorted using the BD FACS Aria®, 3 days after application of viral particles. Expression of GFP indicates integration of retroviral constructs into the genome. **A**: Gating strategy utilised for FACS and analysis of GFP positive cells. Data is representative of Ba/F3 pRuf-iG2 *RANBP2-ABL1* cells. **B**: GFP analysis during FACS isolation of Ba/F3 cells at 3 days post-transduction. GFP positivity in Ba/F3 parental wild-type control (untransduced), pRuf-iG2 empty vector and pRuf-iG2 *RANBP2-ABL1* fusion gene are 0, 34.0 and 27.0% respectively. **C**: GFP analysis of Ba/F3 cells at 3 days post-sort, confirming stability of GFP expression. GFP positivity in Ba/F3 parental wild-type control (untransduced), pRuf-iG2 empty vector and pRuf-iG2 *RANBP2-ABL1* fusion gene are 0, 98.9 and 98.8% respectively. **D**: Bright-field and fluorescence microscopy of transduced Ba/F3 cells using the 40x objective. Top: pRuf-iG2 empty vector; bottom: pRuf-iG2 *RANBP2-ABL1*. Scale bar represents 10 μm.

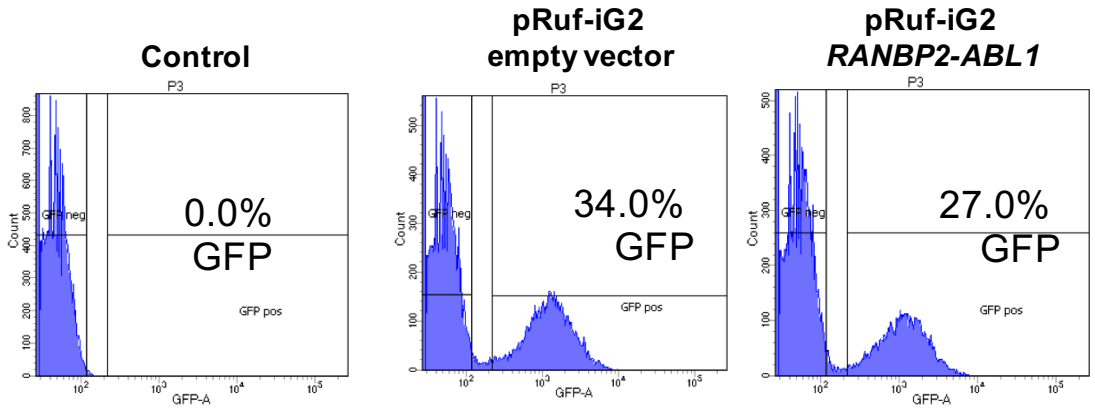
Figure 4.4

A **FACS gating strategy**

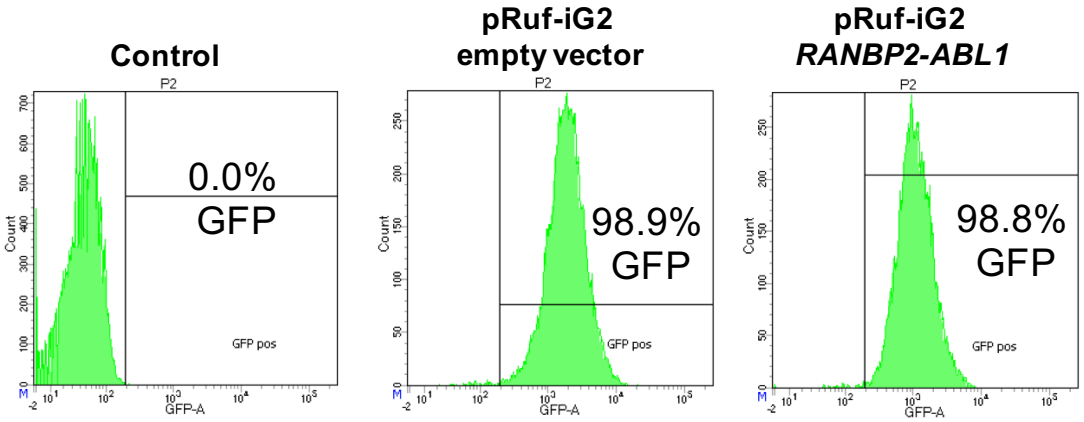
Ba/F3
pRuf-iG2_*RANBP2-ABL1*



B **GFP-expression, 3 days post-transduction**



C **GFP expression, 3 days post-sort**



D

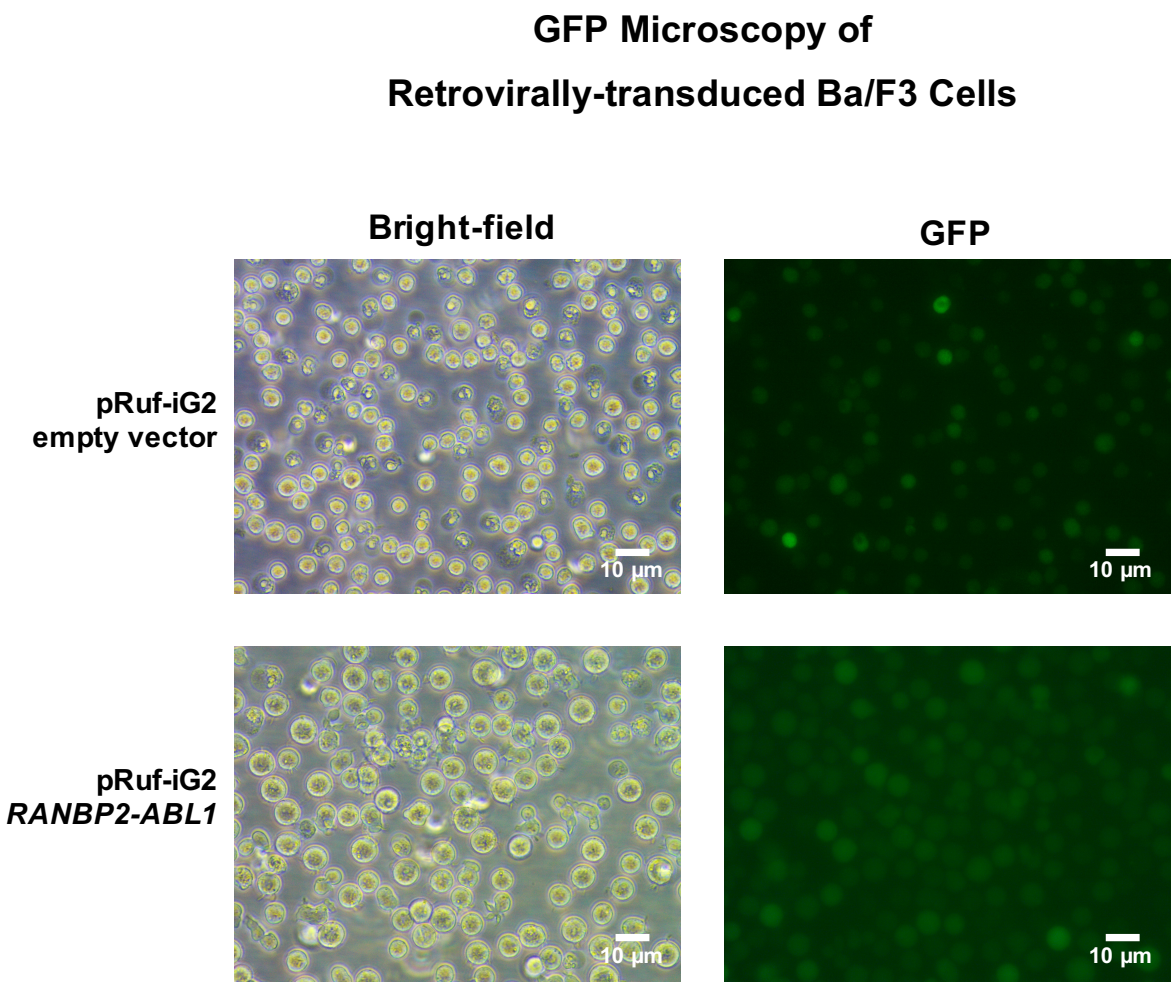
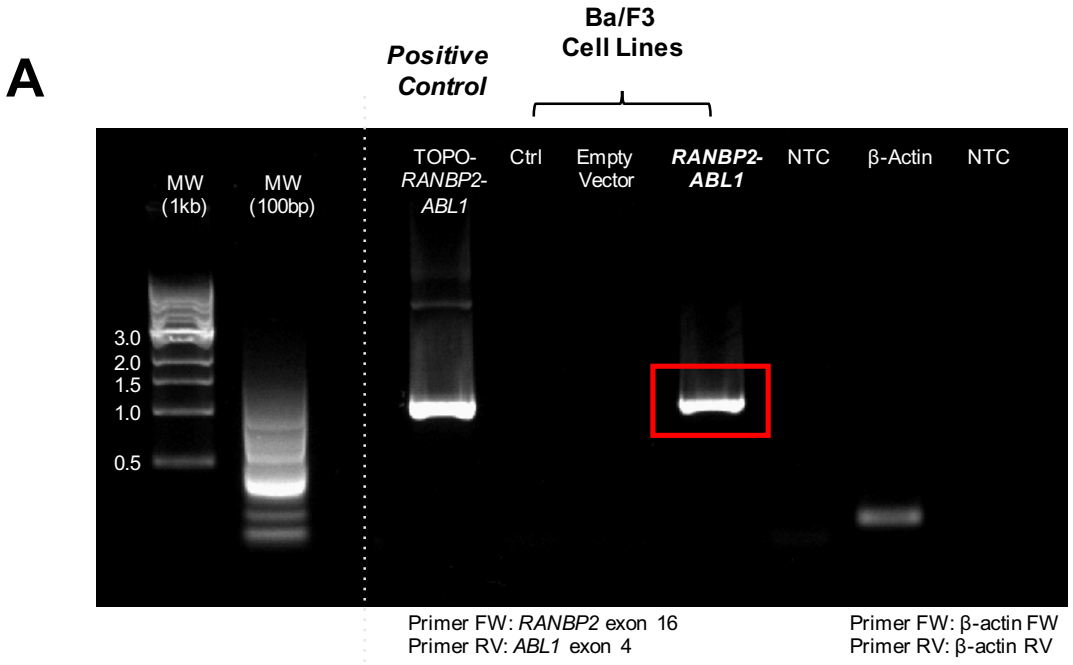
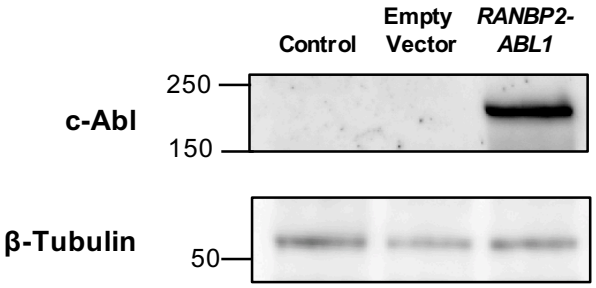

GFP Microscopy of
Retrovirally-transduced Ba/F3 Cells
Bright-field
GFP
pRuf-iG2
empty vector
pRuf-iG2
RANBP2-ABL1
10 µm
10 µm
10 µm
10 µm

Figure 4.5 – Ba/F3 cells transduced with pRuf-iG2 *RANBP2-ABL1* express the fusion gene and protein.

A: Gel electrophoresis of PCR products from pCR®-Blunt II-TOPO® plasmid, Ba/F3 parental control, Ba/F3 cells transduced with pRuf-iG2 empty vector and Ba/F3 cells transduced with pRuf-iG2 *RANBP2-ABL1*. Red rectangle highlights the presence of *RANBP2-ABL1* fusion gene in Ba/F3 pRuf-iG2 *RANBP2-ABL1* cells. MW: molecular weight marker. NTC: no template control. **B**: Western blotting for Ranbp2-Abl1 fusion protein in lysates from Ba/F3 parental control, Ba/F3 cells transduced with pRuf-iG2 empty vector, and, pRuf-iG2 *RANBP2-ABL1*. Blots were incubated in antibodies specific for c-Abl and β-tubulin. **C**: Densitometry analysis of Ranbp2-Abl1 fusion protein compared to β-tubulin loading control, across all samples. Asterisk confirms significant expression of Ranbp2-Abl1 protein ($P < 0.05$) in cells transduced with pRuf-iG2 *RANBP2-ABL1*.

Figure 4.5


A
Positive Control
Ba/F3 Cell Lines
MW (1kb)
MW (100bp)
TOPO-RANBP2-ABL1
Ctrl
Empty Vector
RANBP2-ABL1
NTC
β-Actin
NTC
3.0
2.0
1.5
1.0
0.5
Primer FW: RANBP2 exon 16
Primer RV: ABL1 exon 4
Primer FW: β-actin FW
Primer RV: β-actin RV


B
Control
Empty Vector
RANBP2-ABL1
c-Abl
250
150
β-Tubulin
50

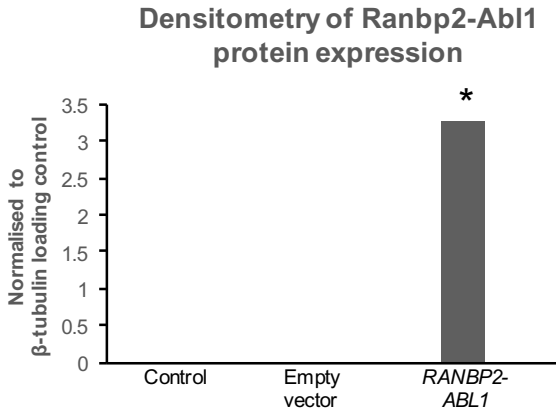
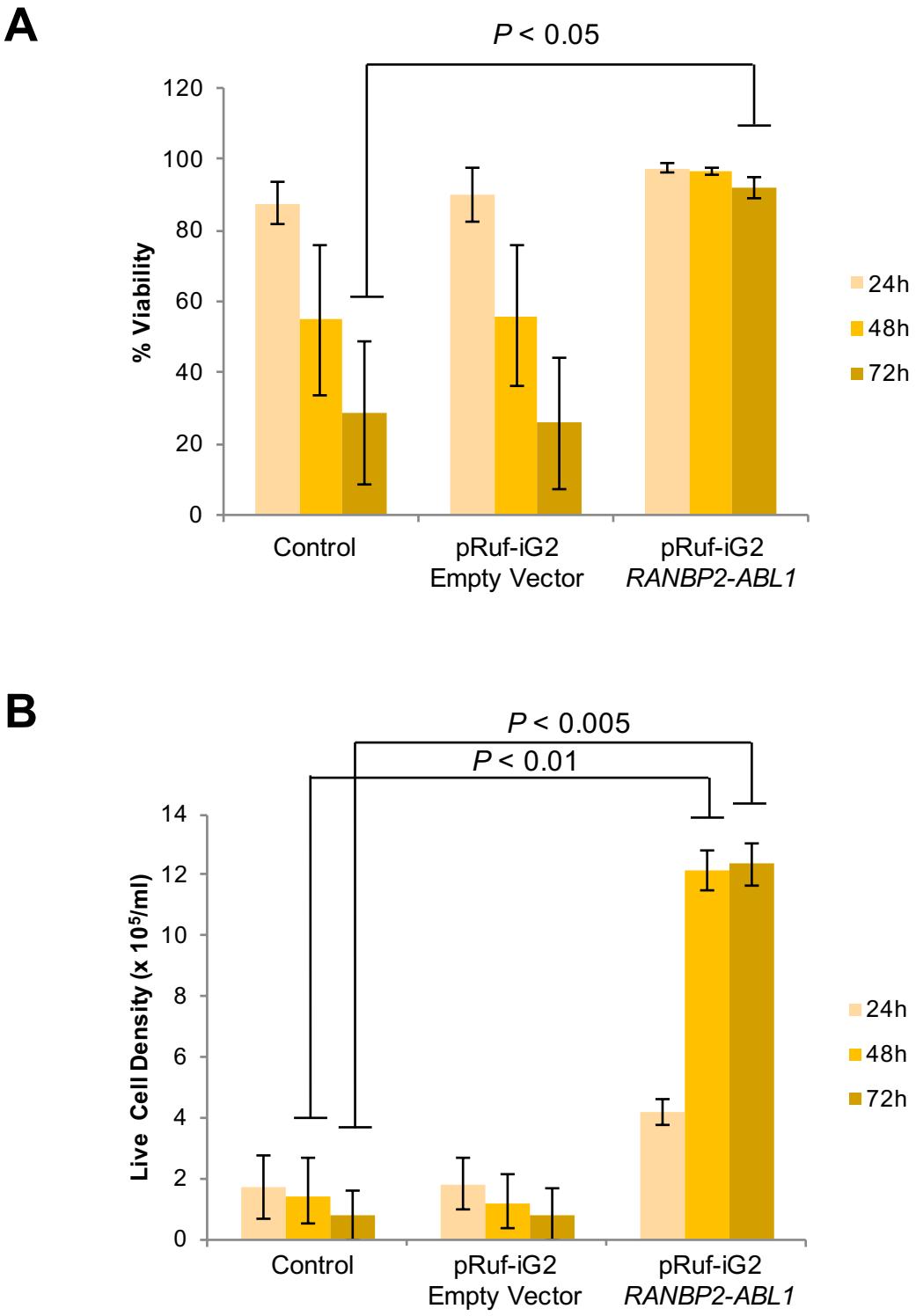

C
Densitometry of Ranbp2-Abl1 protein expression
Normalised to β-tubulin loading control
3.5
3
2.5
2
1.5
1
0.5
0
*
Control
Empty vector
RANBP2-ABL1

Figure 4.6 – Ba/F3 cells containing the *RANBP2-ABL1* Ph-like fusion gene demonstrate IL-3 independent growth.

Ba/F3 cells [control (untransduced Ba/F3 parental), pRuf-iG2 empty vector and pRuf-iG2 *RANBP2-ABL1*) were cultured in the absence of IL-3, at 37ºC/5% CO_2 for 3 days. Cell viability (**A**) and live cell density (**B**) determined via Trypan blue exclusion analysis reveal increased growth and proliferation of cells transduced with pRuf-iG2 *RANBP2-ABL1*. Columns represent mean of 3 independent experiments. Error bars denote standard deviation (SD), with statistical significance indicated by *P* values as determined using the Students' T-test.

Figure 4.6


A
P < 0.05
120
100
80
60
40
20
0
% Viability
24h
48h
72h
Control
pRuf-iG2 Empty Vector
pRuf-iG2 RANBP2-ABL1
B
P < 0.005
P < 0.01
14
12
10
8
6
4
2
0
Live Cell Density (x 10⁵/ml)
24h
48h
72h
Control
pRuf-iG2 Empty Vector
pRuf-iG2 RANBP2-ABL1

4.3.2. Ba/F3 *RANBP2-ABL1* cells are sensitive to clinically-available TKIs

To evaluate if Ba/F3 *RANBP2-ABL1* cells are sensitive to currently-available TKI, cells were exposed to 0 and 100 nM dasatinib, in parallel with the *BCR-ABL1*+ CML cell lines KU-812 and K562. Exposure of cells to TKI for 2 hours at 37ºC/5% CO_2 resulted in a decrease in phosphorylation of Ranbp2-Abl1 as demonstrated by western blotting (slight molecular weight difference between Ranbp2-Abl1 and Bcr-Abl1, due to differences in length of nucleotides), as well as phospho-Erk (p-Erk) and phospho-CrkL (p-CrkL) (**Figure 4.7**). For p-CrkL, a decrease in molecular weight from 39 to 38 kDa can be observed when Ba/F3 *RANBP2-ABL1* cells were treated with the Abl-specific TKI dasatinib (**Figure 4.7**). This was highly comparable to KU-812 (ratio phospho/total CrkL: 4.4 in 0 nM and 0.3 in 100 nM dasatinib), and K562 (ratio phospho/total CrkL: 2.6 in 0 nM and 0.5 in 100 nM dasatinib) which are known to be sensitive to dasatinib[250], hence utilised as positive controls.

Following confirmation of fusion kinase inhibition using dasatinib (**Figure 4.7**), Ba/F3 *RANBP2-ABL1* cells were exposed to a panel of TKIs including Abl and Jak kinase inhibitors (imatinib, dasatinib, ponatinib and ruxolitinib – **Figure 4.8**), and analysed via phosphoflow. Mean fluorescence intensity (MFI) of cells stained with p-CrkL and phospho-Stat5 (p-Stat5) antibodies indicate that in both lines, Abl-kinase specific inhibitors were able to reduce phosphorylation, suggesting a reduction of downstream signalling. The Jak1&2 kinase inhibitor ruxolitinib was however ineffective.

The ability of TKI to reduce downstream phospho-signalling (**Figure 4.8**) was subsequently validated by western blotting. In **Figure 4.9**, reduction in phosphorylation of Ranbp2-Abl1, Stat5 and Erk were observed in Ba/F3 *RANBP2-*

ABL1 cells treated with 5μM imatinib, 100 nM dasatinib and 100 nM ponatinib while no inhibition of phosphorylation was seen in cells treated with 1μM ruxolitinib. This confirmed that Ranbp2-Abl1 is targetable using currently-available TKIs specific for Abl-kinase.

In cell death analysis using Annexin-V/7-AAD exclusion, a significant decrease (P<0.0001) in cell viability following treatment with Abl-specific TKI was observed (**Figure 4.10**), supporting the data above. In Ba/F3 *RANBP2-ABL1* cells, imatinib resulted in a decrease in cell viability from 100% in 0 μM imatinib, to 34%, 29% and 1% in 1, 5 and 10 μM imatinib respectively. When cells were treated with dasatinib, the viability was 27%, 19% and 16% at 10, 50 and 100 nM dasatinib respectively. Treatment in ponatinib resulted in a viability of 31%, 24% and 15% in 10, 50 and 100 nM ponatinib respectively. Ruxolitinib did not result in any significant cell death (97%, 95%, and 91% at 1, 5 and 10 μM ruxolitinib).

Figure 4.7 – Ba/F3 pRuf-iG2 *RANBP2-ABL1* cells are sensitive to the second-generation TKI dasatinib

Ba/F3 cells expressing the *RANBP2-ABL1* fusion gene were exposed to 0 and 100 nM dasatinib for 2 h in IL-3 free media at 37ºC/5% CO_2. KU-812 and K562 CML cell lines were used as positive controls. **A**: Western blotting of protein lysates with antibodies specific for phosphorylated and total Abl, Erk and CrkL. Western blots were visualised using the Bio-Rad® ChemiDoc™ imager and analysed using the ImageLab™ software. Phospho/total-Ranbp2-Abl is of a different molecular weight compared to phospho/total Bcr-Abl, due to a difference in 5' fusion protein partner. Phospho/total-CrkL is of a slightly higher molecular weight in Ba/F3 *RANBP2-ABL1* cells compared to KU-812 or K562, due to endogenous differences between species (murine vs homo sapiens). **B**: Densitometry analysis of phosphorylated Abl fusion protein, Erk and CrkL analysed via ImageJ[4], with the ratio of phosphorylated/total protein graphed accordingly.

Figure 4.7

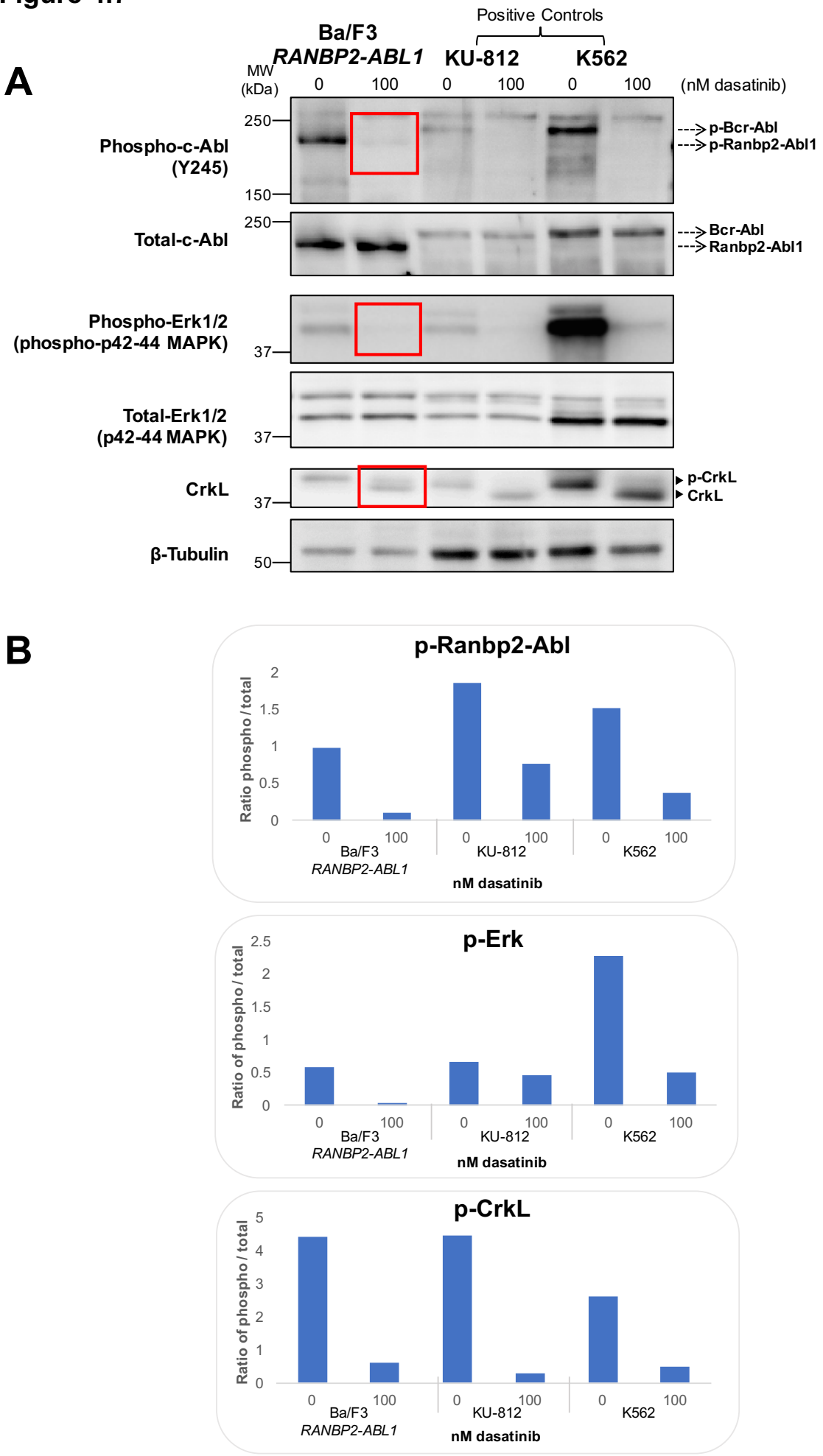
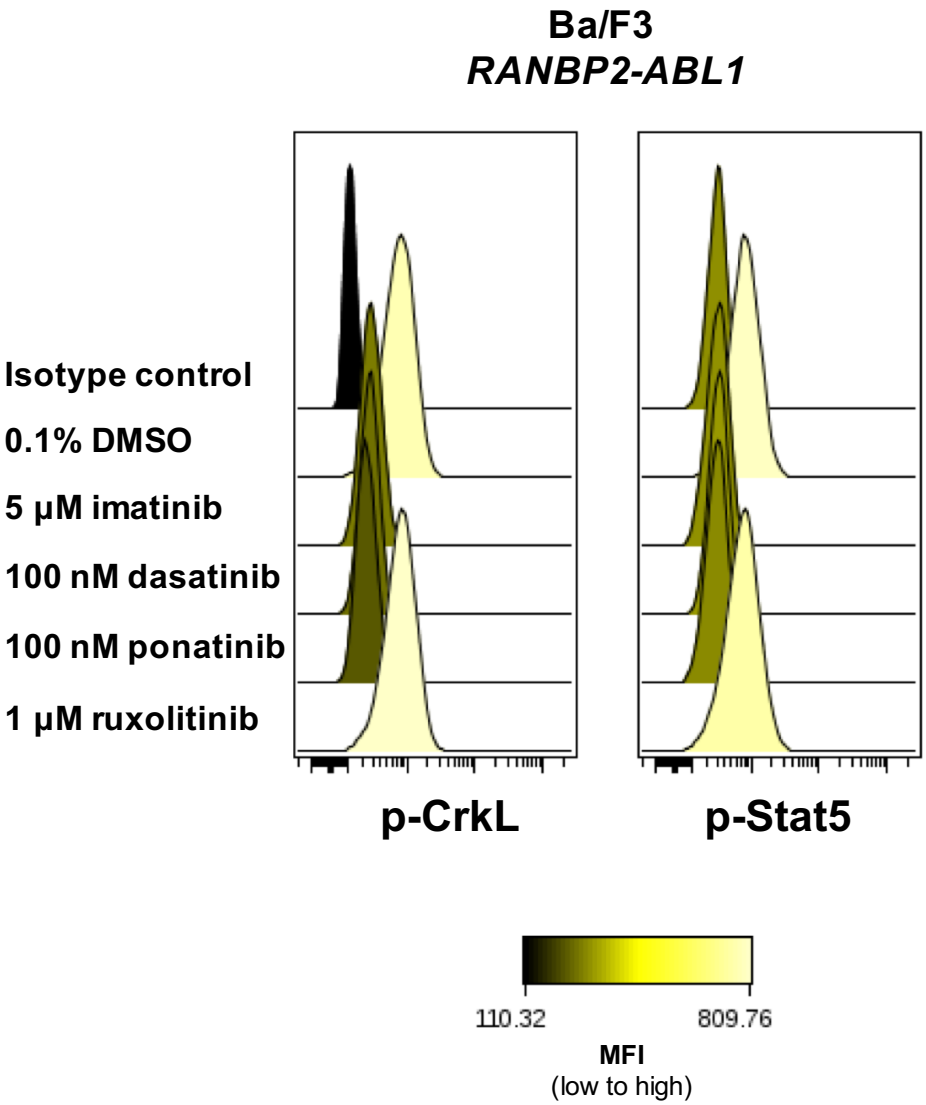

A
Ba/F3
RANBP2-ABL1
Positive Controls
KU-812
K562
MW (kDa)
0
100
0
100
0
100
(nM dasatinib)
250
150
Phospho-c-Abl (Y245)
---> p-Bcr-Abl
---> p-Ranbp2-Abl1
250
Total-c-Abl
---> Bcr-Abl
---> Ranbp2-Abl1
Phospho-Erk1/2 (phospho-p42-44 MAPK)
37
Total-Erk1/2 (p42-44 MAPK)
37
CrkL
37
p-CrkL
CrkL
β-Tubulin
50
B
p-Ranbp2-Abl
Ratio phospho / total
2
1.5
1
0.5
0
0
100
0
100
0
100
Ba/F3
RANBP2-ABL1
KU-812
K562
nM dasatinib
p-Erk
Ratio of phospho / total
2.5
2
1.5
1
0.5
0
0
100
0
100
0
100
Ba/F3
RANBP2-ABL1
KU-812
K562
nM dasatinib
p-CrkL
Ratio of phospho / total
5
4
3
2
1
0
0
100
0
100
0
100
Ba/F3
RANBP2-ABL1
KU-812
K562
nM dasatinib

Figure 4.8 – Ba/F3 *RANBP2-ABL1* cells are sensitive to Abl-kinase specific TKIs, as indicated by reduction in p-CrkL and p-Stat5 via phosphoflow

Ba/F3 *RANBP2-ABL1* cells were exposed to 0.1% DMSO (vehicle control), 5 μM imatinib, 100 nM dasatinib, 100 nM ponatinib and 1 μM ruxolitinib for 1 h in IL-3 free media at 37ºC/5% CO_2. Cells were prepared for phosphoflow and stained with antibodies specific for p-CrkL and p-Stat5. Isotype controls (IgG_{2a} for p-CrkL; IgG_1 for p-Stat5) were included and fluorescence intensity measured using the BD Fortessa™. Overlaid histograms were generated using Cytobank (Santa Clara, CA, USA), with rectangular gradient box indicating the minimum and maximum MFI (mean fluorescence intensity) of the experiment. Data are representative of 3 independent experiments.

Figure 4.8

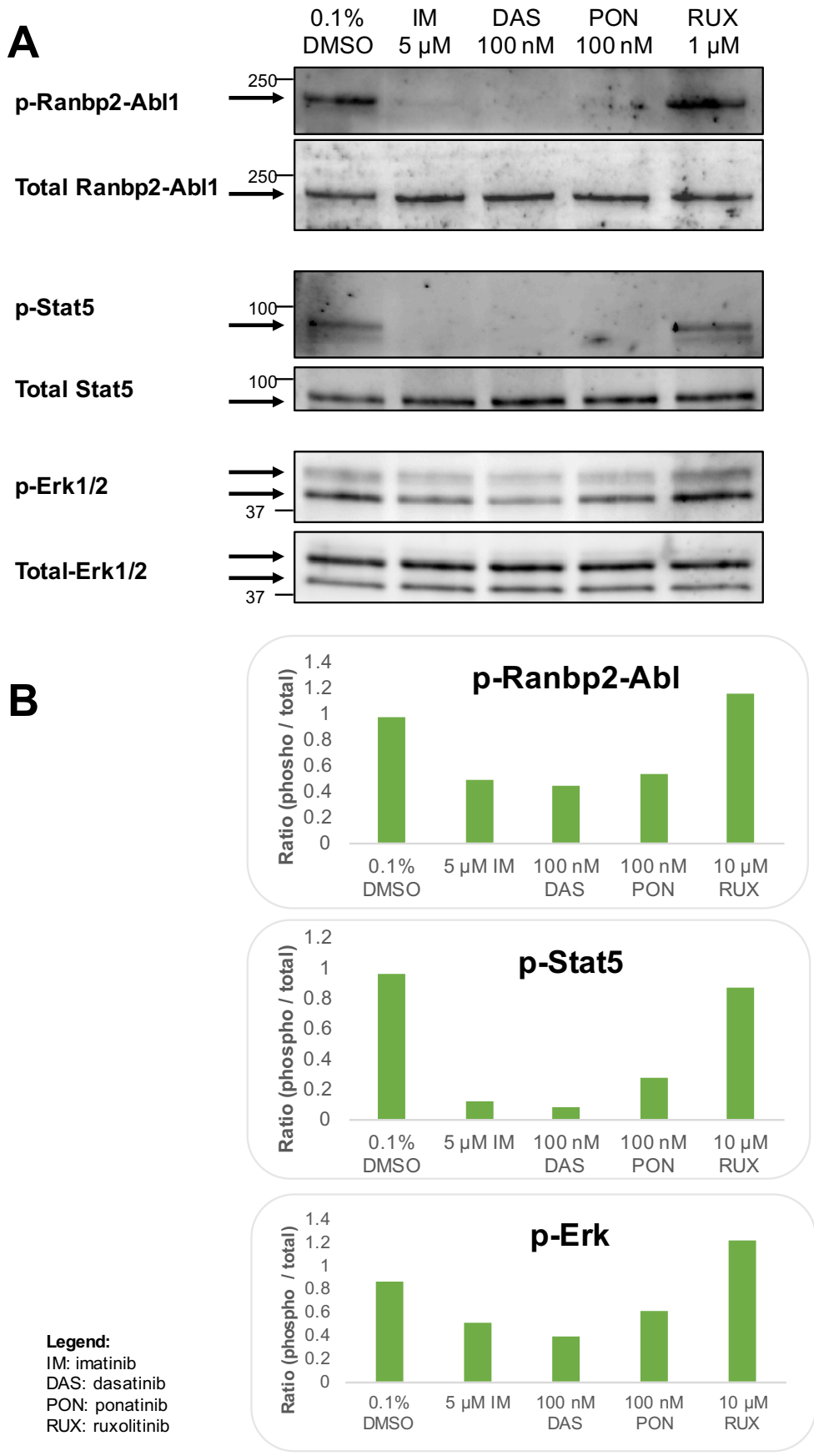


Treatment	MFI	
	p-CrkL	p-Stat5
Isotype control	110.32	307.44
0.1% DMSO	773.36	800.8
5 µM imatinib	280.84	310.24
100 nM dasatinib	264.88	320.88
100 nM ponatinib	231.28	300.72
1 µM ruxolitinib	809.76	754.32

Figure 4.9 – Ba/F3 *RANBP2-ABL1* cells exhibit decrease in downstream phospho-protein expression when treated with Abl-specific TKI by western blotting analysis

A: Ba/F3 *RANBP2-ABL1* cells were exposed to 0.1% DMSO, 5 μM imatinib, 100 nM dasatinib, 100 nM ponatinib and 1 μM ruxolitinib (JAK inhibitor) for 1 h in IL-3 free media at 37ºC/5% CO_2. Following incubation, cells were lysed for western blotting and membranes incubated with antibodies specific for phosphorylated/total Abl, Stat5 and Erk. Western blots were visualised using the Bio-Rad® ChemiDoc™ imager using the ImageLab™ software. **B**: Densitometry analysis of phosphorylated Ranbp2-Abl, Stat5 and Erk proteins graphed and normalised against their total isoforms. Data is n=1 experiment.

Figure 4.9



Legend:
IM: imatinib
DAS: dasatinib
PON: ponatinib
RUX: ruxolitinib

THIS PAGE INTENTIONALLY LEFT BLANK.

Figure 4.10

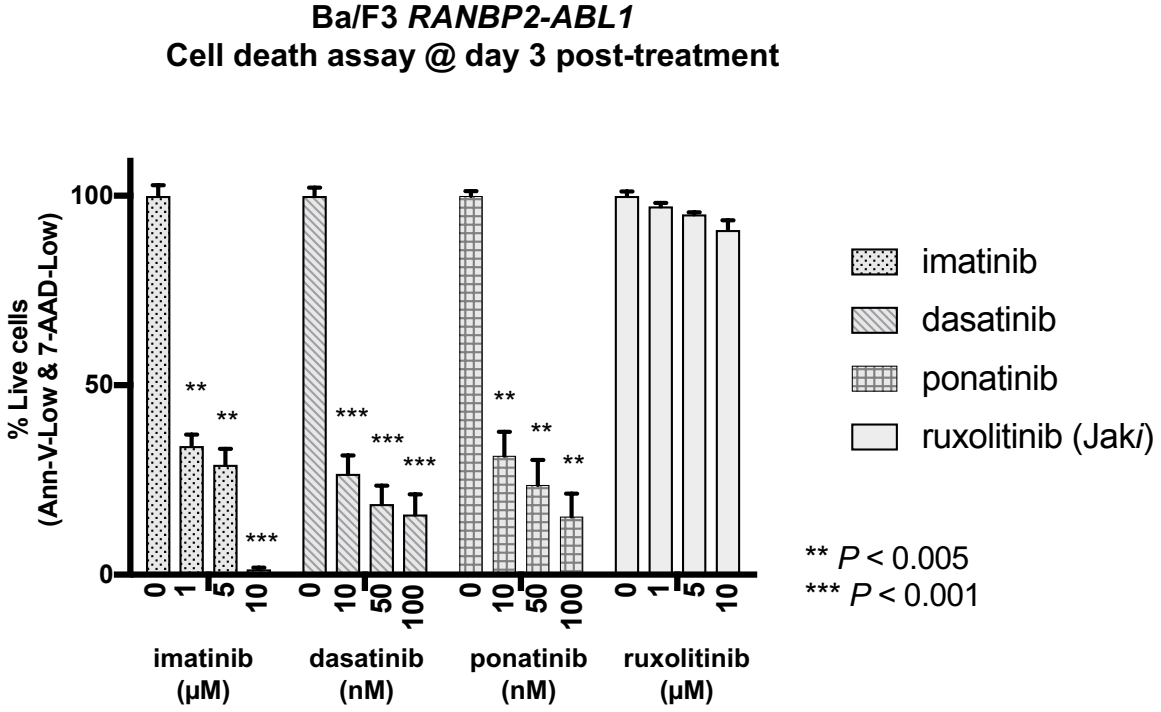


Figure 4.10 – Ba/F3 *RANBP2-ABL1* cells are sensitive to Abl-kinase targeted TKI

Cell viability analysis via Annexin-V/7-AAD flow cytometry exclusion in Ba/F3 *RANBP2-ABL1* cells, treated with a panel of TKIs (imatinib, dasatinib, ponatinib, and ruxolitinib). Cells were seeded in IL-3 free media and exposed to TKIs for 3 days prior to analysis. Columns represent the mean percentage of live cells. Error bars denote standard deviation (SD) of 3 independent experiments, with asterisks indicating $P < 0.05$.

4.3.3. Imatinib and dasatinib-resistant Ba/F3 *RANBP2-ABL1* cells are more tolerant to TKI compared to control lines

Ba/F3 *RANBP2-ABL1* cells were dose-escalated in imatinib and dasatinib, to model TKI-resistance as first-line therapy. Imatinib-resistant cells were cultured to a final concentration of 10 μM imatinib, with Annexin V/7-AAD cell death assay (**Figure 4.11A**) confirming significant resistance to imatinib compared to control ($LD_{50}^{imatinib}$: >10 μM and ~0.7 ± 0.1 μM respectively; P<0.05). Dasatinib-resistant cells were cultured to a final concentration of 200 nM dasatinib and cell death assay (**Figure 4.11B**) confirmed significant resistance to TKI ($LD_{50}^{dasatinib}$: >1000 nM in dasatinib-resistant and 3.1 ± 0.9 nM in control cells; P<0.05).

TKI-resistance was validated by western blotting of cell lysates from sensitive and resistant lines treated with TKI. In **Figure 4.12A**, phosphorylation of Ranbp2-Abl1 decreased when naïve control cells were exposed to an increasing concentration of TKI ($IC_{50}^{imatinib}$: 0.16μM), whereas in Ranbp2-Abl1 resistant cells p-Abl remained stable ($IC_{50}^{imatinib}$: >10 μM). Similarly, in the dasatinib-resistant samples in (**Figure 4.12B**) phosphorylation of Ranbp2-Abl1 decreased when DMSO control cells were exposed to an increasing concentration of TKI ($IC_{50}^{dasatinib}$: 2.5 nM), while in Ranbp2-Abl1 dasatinib-resistant cells, the levels of p-Abl remained stable ($IC_{50}^{dasatinib}$: >200 nM).

The expression of p-CrkL, a surrogate marker for Abl kinase activity, was further explored in the TKI-resistant lines. Imatinib-resistant cells (**Figure 4.13A**) were more resistant than naïve control ($IC_{50}^{imatinib}$: >100 μM and 7.5 μM respectively, supporting results of phosphorylated Ranbp2-Abl1 western blots mentioned above. Similarly, in dasatinib-resistant cells (**Figure 4.13B**), the pCrkL $IC_{50}^{dasatinib}$ was above 1000 nM compared to the DMSO control, which was 50 nM. Taken together, these data

indicate that TKI-resistance in imatinib-resistant and dasatinib-resistant lines may be attributed to a Ranbp2-Abl1 kinase-dependant mechanism of resistance.

Figure 4.11 – Confirmation of imatinib and dasatinib resistance in dose-escalated Ba/F3 *RANBP2-ABL1* cells via cell death assay

Flow cytometry analysis of cell viability via Annexin-V/7-AAD exclusion of Ba/F3 *RANBP2-ABL1* TKI-sensitive and TKI-resistant cells, exposed to TKIs for 3 days. To ensure the intracellular levels of TKI is consistent between sensitive and resistant lines, a drug-washout procedure was performed before experimental set-up by incubation of cells overnight in the absence of TKI at 37ºC/5% CO_2. Columns represent mean, while error bars represent the ± SD within 3 independent experiments. Dotted lines across the *y*-axis denote 50% of the TKI concentration required for lethal dose (LD_{50}), based on normalisation of data to controls at 0 nM TKI. TKI concentrations were based on snapshots of serially-diluted TKI. **A**: Ba/F3 *RANBP2-ABL1* TKI-sensitive (naïve) and TKI-resistant (imatinib-resistant) cells exposed to increasing concentrations of imatinib. **B**: Ba/F3 *RANBP2-ABL1* TKI-sensitive (DMSO) and TKI-resistant (dasatinib-resistant) cells exposed to increasing concentration of dasatinib. Asterisks denote statistical significance as calculated by the Student's *t*-test.

Figure 4.11

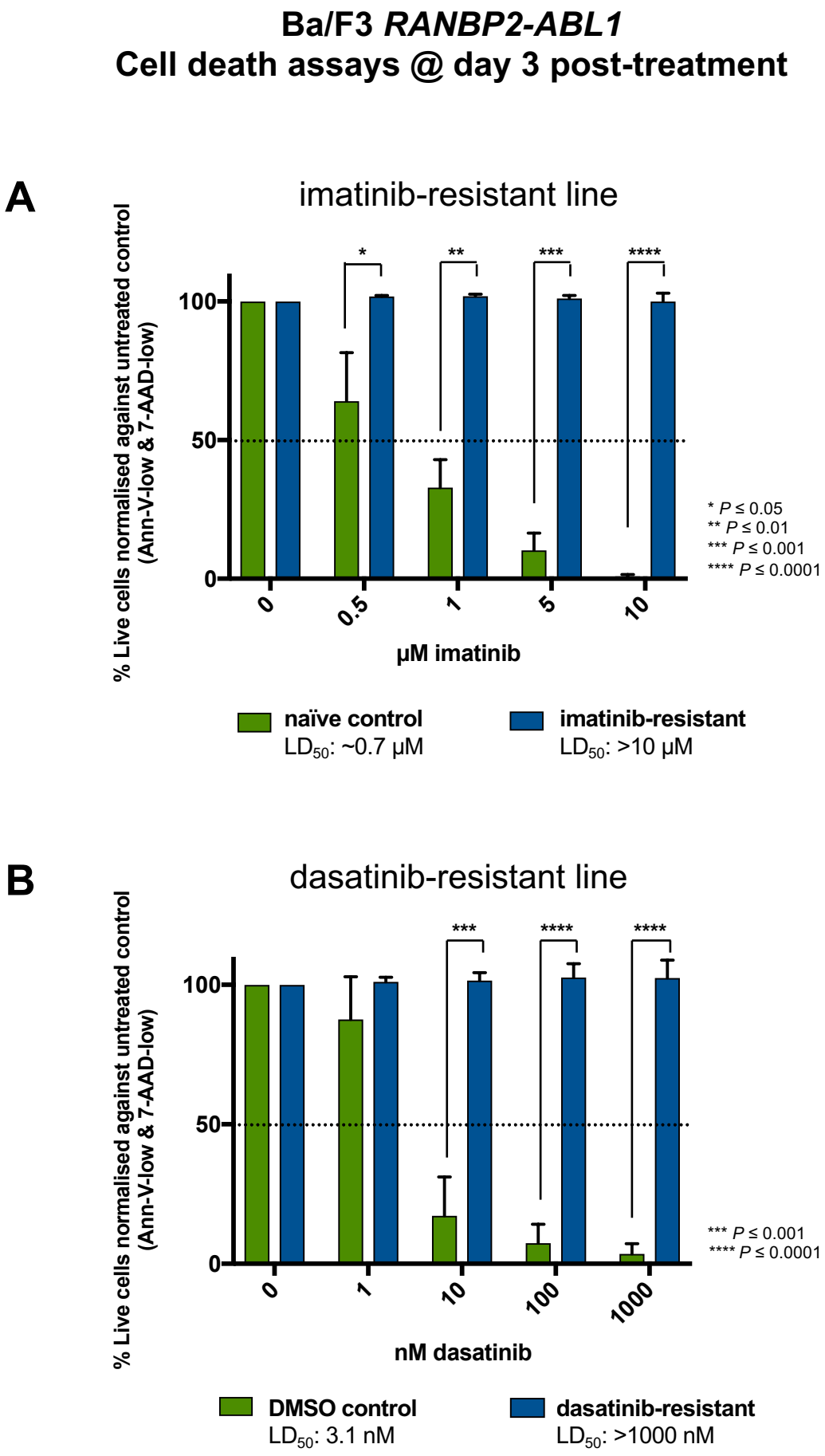

Ba/F3 RANBP2-ABL1
Cell death assays @ day 3 post-treatment
A
imatinib-resistant line
% Live cells normalised against untreated control (Ann-V-low & 7-AAD-low)
100
50
0
*
**
***
****
0
0.5
1
5
10
µM imatinib
* P ≤ 0.05
** P ≤ 0.01
*** P ≤ 0.001
**** P ≤ 0.0001
naïve control
LD50: ~0.7 µM
imatinib-resistant
LD50: >10 µM
B
dasatinib-resistant line
% Live cells normalised against untreated control (Ann-V-low & 7-AAD-low)
100
50
0
***
****
****
0
1
10
100
1000
nM dasatinib
*** P ≤ 0.001
**** P ≤ 0.0001
DMSO control
LD50: 3.1 nM
dasatinib-resistant
LD50: >1000 nM

Figure 4.12 – Imatinib and dasatinib-resistant Ba/F3 *RANBP2-ABL1* cells maintain p-Ranbp2-Abl1 in the presence of TKI

Western immunoblotting of Ba/F3 *RANBP2-ABL1* TKI-sensitive and TKI-resistant cells, treated with an increasing concentration of TKI for 1 h prior to collection of cells for protein analysis. To ensure comparable intracellular levels of TKI between resistant and sensitive cell lines, a drug washout procedure was performed as previously mentioned **A:** Ba/F3 *RANBP2-ABL1* TKI-sensitive (naïve, with water used as a vehicle for imatinib) and TKI-resistant (imatinib-resistant) cells. **B**: Ba/F3 *RANBP2-ABL1* TKI-sensitive (DMSO, a diluent for dasatinib) and TKI-resistant (dasatinib-resistant) cells. Western blots were probed with anti-phospho-Abl (Y245) and total-Abl antibodies. Phospho-Ranbp2-Abl1 bands were normalised against the total isoform, and densitometry graphed accordingly. Data indicates an experiment of n=1.

Figure 4.12

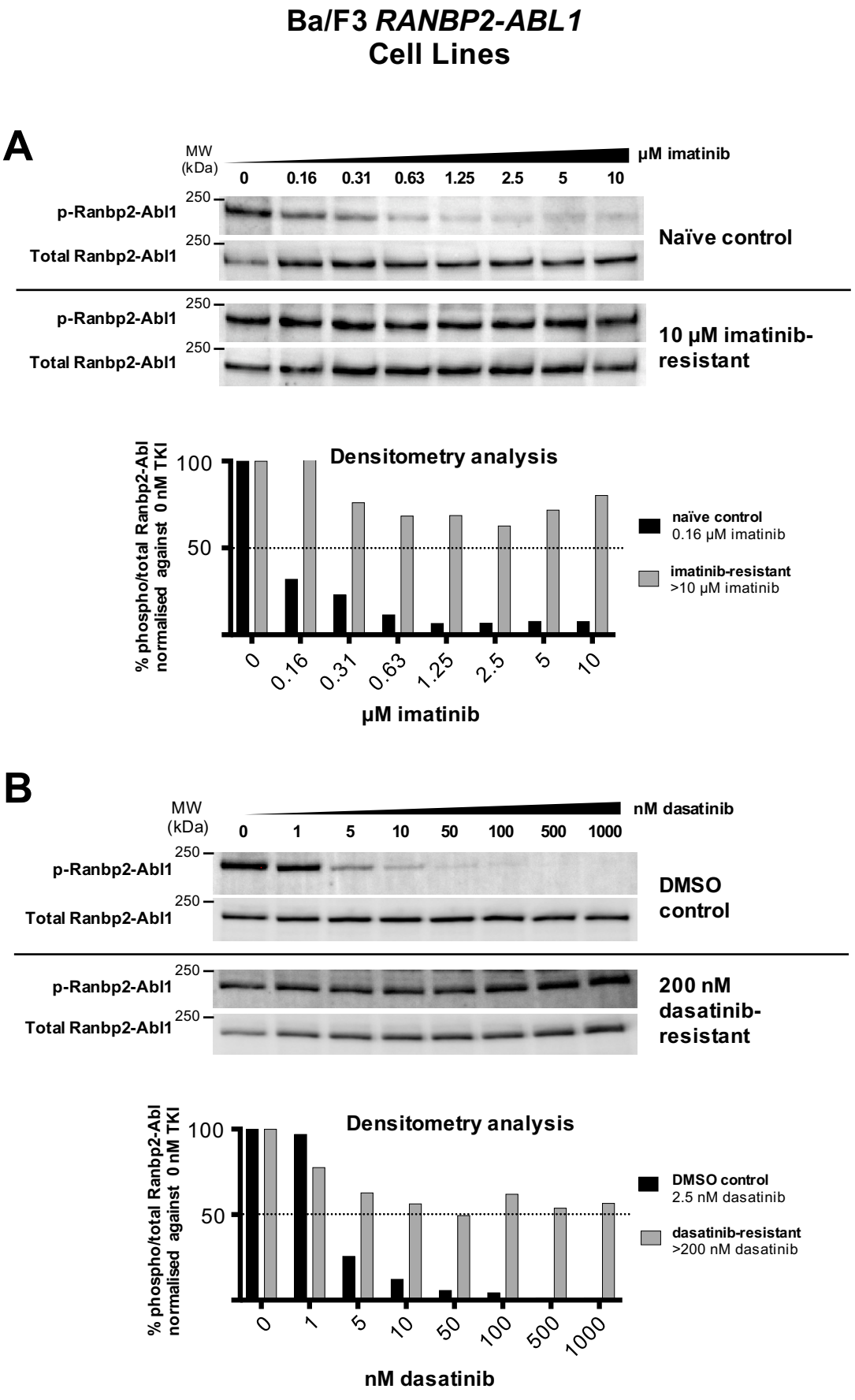
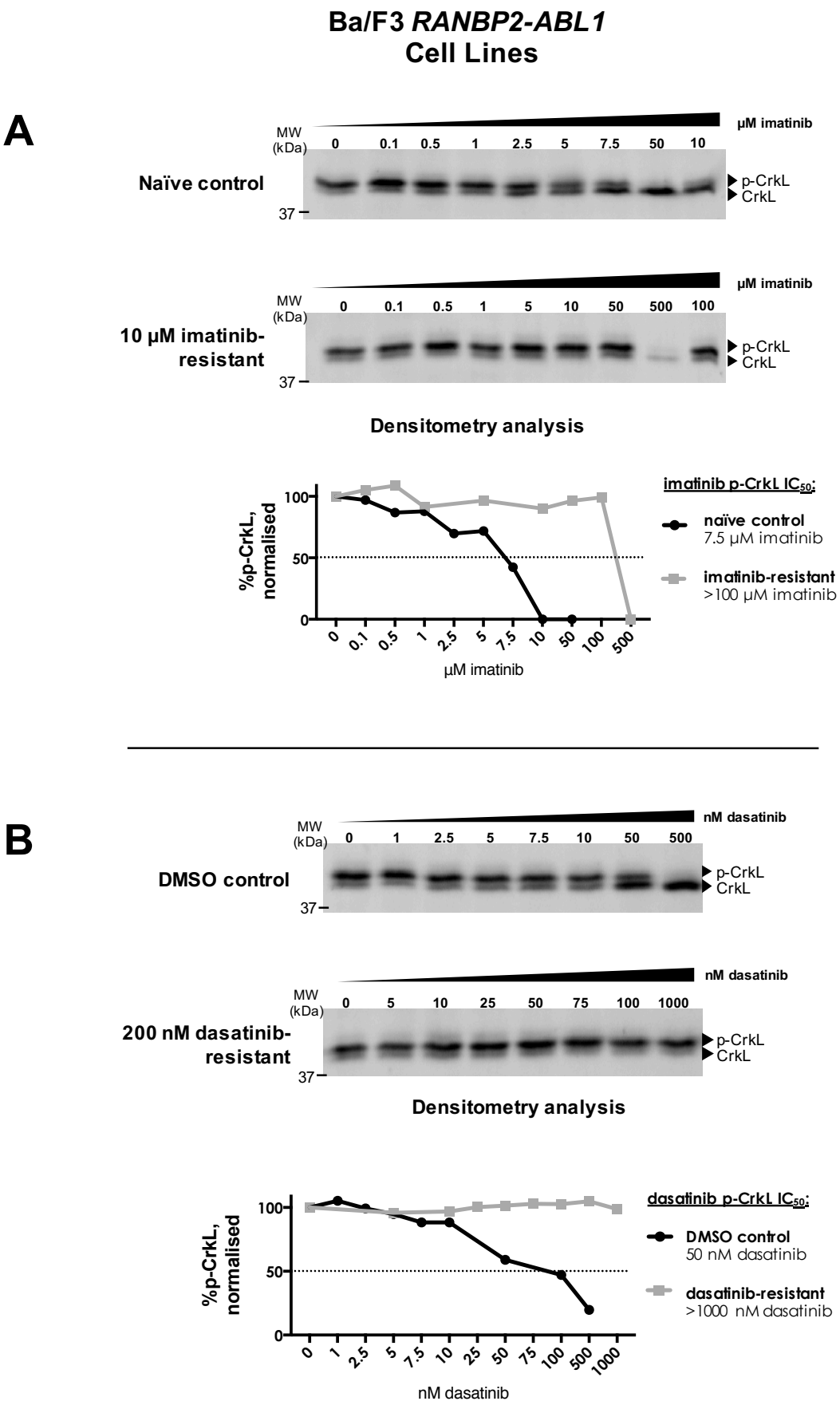

Ba/F3 RANBP2-ABL1
Cell Lines
A
MW (kDa)
0 0.16 0.31 0.63 1.25 2.5 5 10
µM imatinib
250
p-Ranbp2-Abl1
Total Ranbp2-Abl1
Naïve control
10 µM imatinib-resistant
Densitometry analysis
% phospho/total Ranbp2-Abl normalised against 0 nM TKI
100
50
naïve control
0.16 µM imatinib
imatinib-resistant
>10 µM imatinib
µM imatinib
B
MW (kDa)
0 1 5 10 50 100 500 1000
nM dasatinib
DMSO control
200 nM dasatinib-resistant
DMSO control
2.5 nM dasatinib
dasatinib-resistant
>200 nM dasatinib
nM dasatinib

Figure 4.13 – Imatinib and dasatinib-resistant Ba/F3 *RANBP2-ABL1* cells demonstrate increased phosphorylated CrkL (p-CrkL) IC_{50} compared to TKI-sensitive cells

Western immunoblotting of Ba/F3 *RANBP2-ABL1* TKI-sensitive and TKI-resistant cells, treated with an increasing concentration of TKI for 2 hr, prior to collection of cells for CrkL analysis. To ensure intracellular levels of TKI between resistant and sensitive cell lines were comparable, a drug washout procedure was performed as previously mentioned. **A:** Ba/F3 *RANBP2-ABL1* TKI-sensitive (naïve) compared to TKI-resistant (imatinib-resistant) cells. **B**: Ba/F3 *RANBP2-ABL1* TKI-sensitive (DMSO) compared to TKI-resistant (dasatinib-resistant) cells. Western blots were probed with anti-CrkL antibody and densitometry analysis performed by normalising intensity of p-CrkL against total CrkL bands. CrkL IC_{50} is defined by 50% CrkL inhibition in a particular TKI concentration. Data represents a minimum of n=1 experiment.

Figure 4.13


Ba/F3 RANBP2-ABL1 Cell Lines
A
MW (kDa)
μM imatinib
0 0.1 0.5 1 2.5 5 7.5 50 10
Naïve control
37
p-CrkL
CrkL
μM imatinib
0 0.1 0.5 1 5 10 50 500 100
10 μM imatinib-resistant
Densitometry analysis
%p-CrkL, normalised
imatinib p-CrkL IC50:
naïve control
7.5 μM imatinib
imatinib-resistant
>100 μM imatinib
μM imatinib
B
nM dasatinib
0 1 2.5 5 7.5 10 50 500
DMSO control
0 5 10 25 50 75 100 1000
200 nM dasatinib-resistant
dasatinib p-CrkL IC50:
DMSO control
50 nM dasatinib
dasatinib-resistant
>1000 nM dasatinib
nM dasatinib

THIS PAGE INTENTIONALLY LEFT BLANK.

4.3.4. Ba/F3 *RANBP2-ABL1* cells develop resistance to imatinib and dasatinib through the acquirement of the clinically-significant *ABL1*-T315I mutation (targetable by ponatinib)

As results in section **4.3.3** indicate stability of downstream kinase signalling in imatinib and dasatinib-resistant cells, this suggests that TKI-resistance may be attributed to a kinase-dependant factor. Sanger sequencing revealed an *ABL1*-T315I mutation in both TKI-resistant cell lines (60% and 100% in imatinib and dasatinib-resistant cell lines, respectively (**Figure 4.14**).

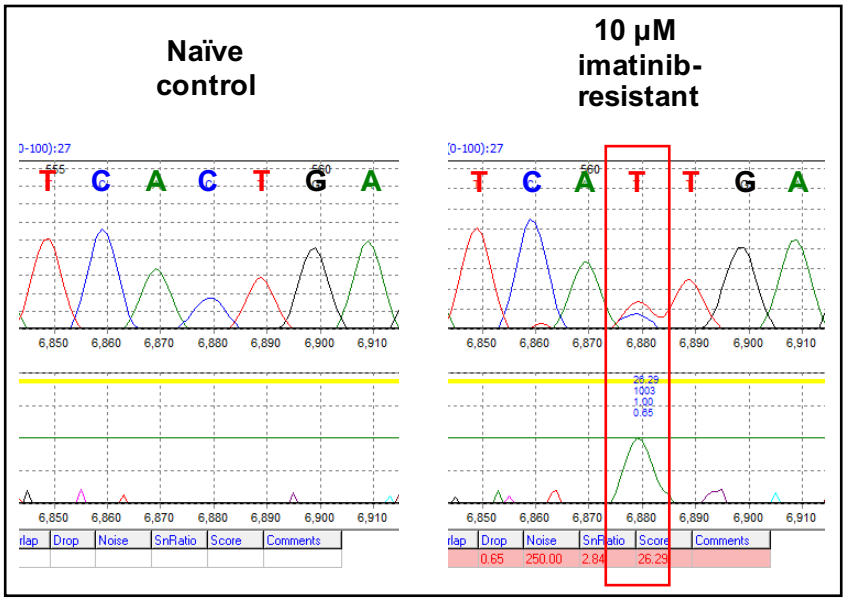
The *ABL1*-T315I mutation is known to be targetable by ponatinib, a third-generation TKI[183]. Using Annexin-V/7-AAD flow cytometry analysis, the LD_{50} of ponatinib in Ba/F3 *RANBP2-ABL1* imatinib-resistant cells was 22.6 $\pm$ 1.1 nM (1.6 $\pm$ 0.2 nM in naïve control) and 28.9 $\pm$ 1.7 nM in dasatinib-resistant cells (compared to 6.0 $\pm$ 0.5 nM in DMSO control) (**Figure 4.15**).

Figure 4.14 – Identification of the *ABL1*-T315I kinase-domain mutation as a cause of TKI-resistance

Sanger sequencing electropherograms of PCR products specific for the *ABL1* kinase-domain, in Ba/F3 *RANBP2-ABL1* TKI-resistant and TKI-sensitive lines. Red rectangle highlights the clinically-significant *ABL1*-T315I kinase-domain mutation in TKI-resistant cells, representative of 3 replicates. **A**: naïve (left) and imatinib-resistant (right) Ba/F3 *RANBP2-ABL1* cells. **B**: DMSO (left) and dasatinib-resistant (right) Ba/F3 *RANBP2-ABL1* cells. Sequences were analysed using the Mutation Surveyor® DNA analysis software. Data for resistant cells are representative of 3 sequencing reactions.

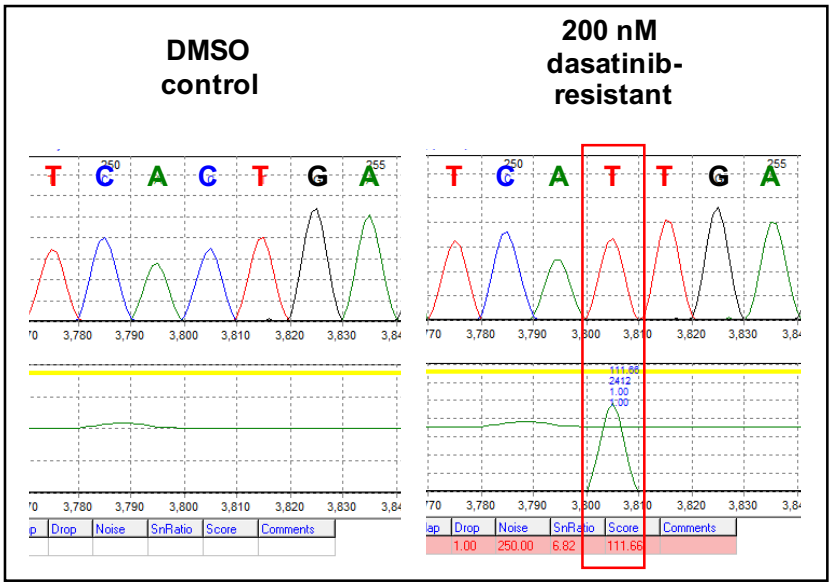
Figure 4.14

A



~60% *ABL1*-T315I (c.944C>T)

B

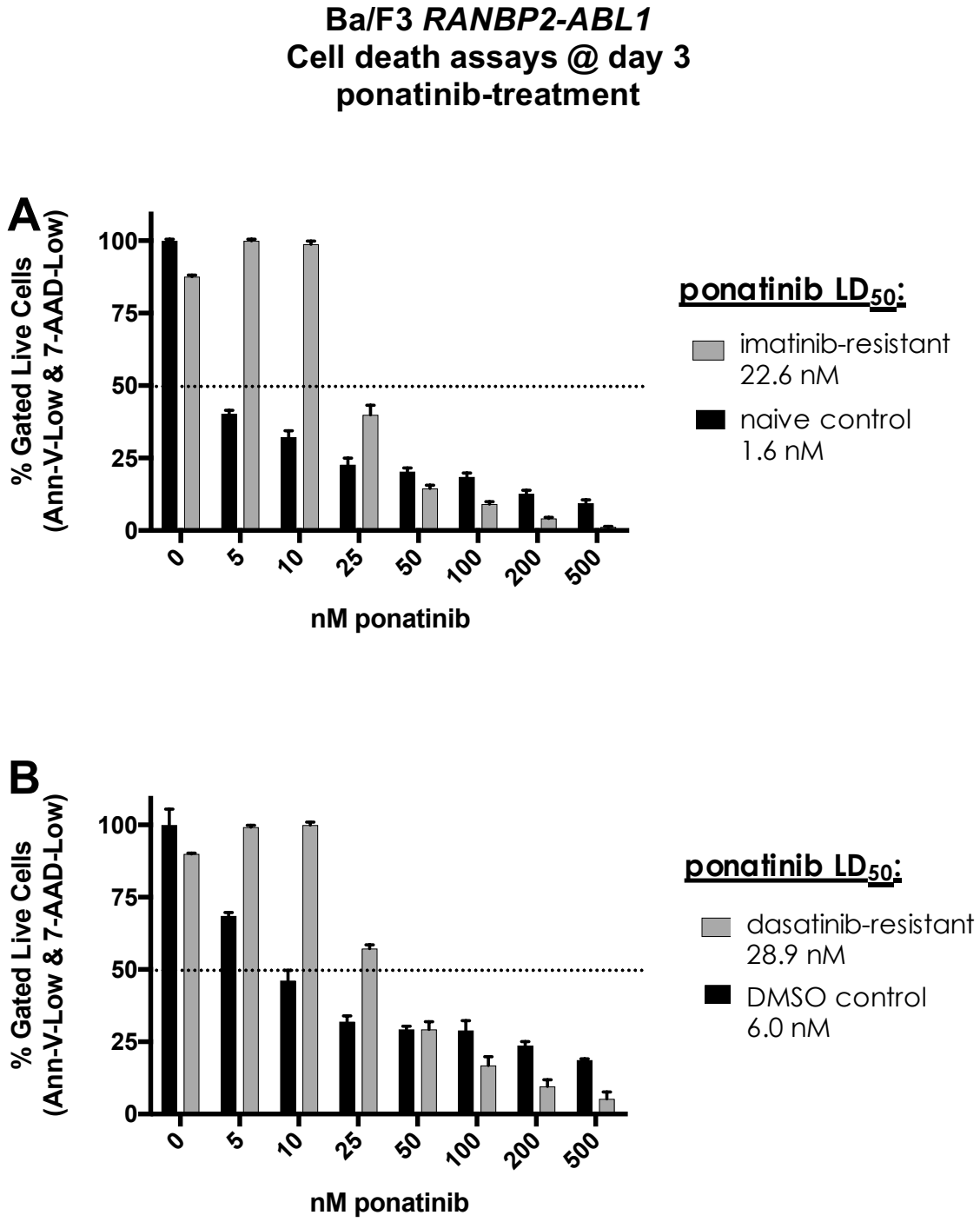


~100% *ABL1*-T315I (c.944C>T)

Figure 4.15 – Ba/F3 *RANBP2-ABL1* imatinib and dasatinib-resistant *ABL1*-T315I lines are sensitive to the third generation TKI ponatinib

Flow cytometry analysis of ponatinib sensitivity in Ba/F3 *RANBP2-ABL1* imatinib-resistant (**A**) and dasatinib-resistant (**B**) lines with their respective TKI-sensitive controls. An overnight washout procedure was performed prior to incubation of cells in TKI for 3 days in various concentrations of ponatinib at 37ºC/5% CO_2. Cells were stained with Annexin-V/7-AAD prior to flow cytometric analysis. Columns represent mean while error bars represent the ± SD of 3 technical replicates. Dotted line across the *y*-axis denotes 50% of the TKI concentration required for lethal dose (LD_{50}), with values calculated using GraphPad Prism.

Figure 4.15


Ba/F3 RANBP2-ABL1
Cell death assays @ day 3
ponatinib-treatment
A
% Gated Live Cells
(Ann-V-Low & 7-AAD-Low)
100
75
50
25
0
0
5
10
25
50
100
200
500
nM ponatinib
ponatinib LD50:
imatinib-resistant
22.6 nM
naive control
1.6 nM
B
% Gated Live Cells
(Ann-V-Low & 7-AAD-Low)
100
75
50
25
0
0
5
10
25
50
100
200
500
nM ponatinib
ponatinib LD50:
dasatinib-resistant
28.9 nM
DMSO control
6.0 nM

4.3.5. Secondary dose-escalation of Ba/F3 *RANBP2-ABL1* imatinib and dasatinib-resistant *ABL1*-T315I cells in ponatinib results in highly-resistant line

Following confirmation of ponatinib-sensitivity in Ba/F3 *RANBP2-ABL1* T315I lines (imatinib-resistant and dasatinib-resistant), these lines were further dose-escalated in ponatinib to investigate if further resistance mechanisms may arise, to counter the ponatinib treatment. This was to emulate what may occur when patients are exposed to third-generation inhibitors to overcome pre-existing mutations. The adjustment of cells to ponatinib required a significantly longer period of time (12 months compared to 6 in the establishment of imatinib-resistant and dasatinib-resistant lines) for the achievement of a final concentration of 100 nM ponatinib resistance, due to the potency of this TKI.

Ba/F3 imatinib and dasatinib-resistant *ABL1*-T315I cells were confirmed for ponatinib resistance using Annexin-V/7-AAD flow cytometry analysis. Dose-response curves revealed an increase in ponatinib LD_{50}, in secondary-escalated imatinib and dasatinib-resistant *ABL1*-T315I cells compared to their respective parental control lines (**Figure 4.16**). In imatinib-resistant cells, the ponatinib LD_{50} was >100 nM in the re-escalated imatinib-resistant *ABL1*-T315I / ponatinib-resistant cell line, compared to 14.7 $\pm$ 3.2 nM in imatinib-resistant *ABL1*-T315I and 3.0 $\pm$ 0.5 nM in naïve control (**Figure 4.16A**). In dasatinib-resistant cells, the ponatinib LD_{50} was >100 nM in re-escalated dasatinib-resistant *ABL1*-T315I / ponatinib-resistant cell line, compared to 24.6 $\pm$ 4.0 nM in dasatinib-resistant and 3.64 $\pm$ 0.66 nM in DMSO control (**Figure 4.16B**).

Following confirmation of ponatinib-resistance by cell death assay, western blotting of phosphorylated Ranbp2-Abl1 was performed (**Figure 4.17**). Exposure of cells to

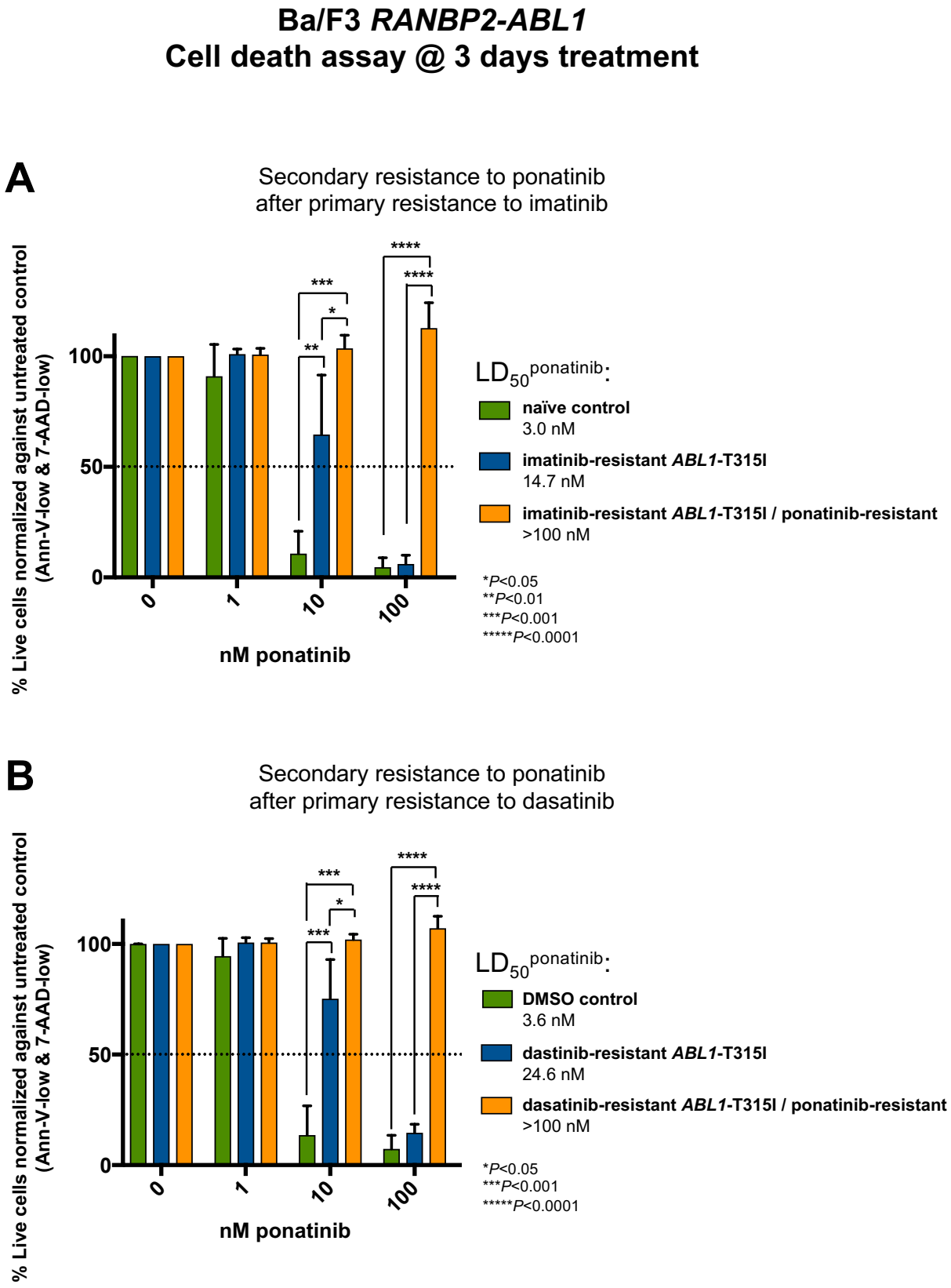
ponatinib concentrations similar to those utilised in the cell death assay (0, 1, 10, 100, 100 nM revealed an increased p-Ranbp2-Abl1 IC_{50} in the ponatinib-resistant *ABL1*-T315I lines compared to that of parental controls. In imatinib-resistant *ABL1*-T315I / ponatinib-resistant cells, the $IC_{50}^{ponatinib}$ of phosphorylated Ranbp2-Abl1 isoform was 235.5 nM, which was increased compared to imatinib-resistant *ABL1*-T315I (44.8 nM) and naïve control cells (11.3 nM) (**Figure 4.17A**). In dasatinib-resistant *ABL1*-T315I / ponatinib-resistant cells, the $IC_{50}^{ponatinib}$ value was 138.2 nM, compared to 11.3 nM in dasatinib-resistant *ABL1*-T315I and 8.7 nM in DMSO control cells (**Figure 4.17B**).

A p-CrkL assay indicated an $IC_{50}^{ponatinib}$ of 2.8 μM in imatinib-resistant *ABL1*-T315I / ponatinib-resistant cells, compared to 151.2 nM in imatinib-resistant *ABL1*-T315I and 16.0 nM in naïve control cells (**Figure 4.18A**). In dasatinib-resistant *ABL1*-T315I / ponatinib-resistant cells, the p-CrkL $IC_{50}^{ponatinib}$ was 1.4 μM, compared to 266.1 nM in dasatinib-resistant *ABL1*-T315I and 18.6 nM in DMSO control cells (**Figure 4.18B**).

Figure 4.16 – Re-escalation of imatinib-resistant Ba/F3 *RANBP2-ABL1* T315I cells in ponatinib confers greater resistance to ponatinib

Bar graphs representing % cell viability of Ba/F3 *RANBP2-ABL1* TKI-sensitive, *ABL1*-T315I and ponatinib-resistant lines, with the *x*-axis indicating TKI concentrations in a logarithmic scale. An overnight washout procedure before experimental set-up was performed as previously described. Cells were treated with ponatinib at 37ºC/5% CO_2 for 3 days. **A**: Secondary dose-escalated imatinib/ponatinib-resistant cells compared to respective parental cell lines (imatinib-resistant *ABL1*-T315I and naïve control). **B**: Secondary dose-escalated dasatinib/ponatinib-resistant cells compared to respective parental cell lines (dasatinib-resistant *ABL1*-T315I and DMSO control). Columns represent mean of 5 independent experiments, with error bars denoting ± SD. Horizontal dotted lines represent the LD_{50} of ponatinib treatment, while asterisks denote statistical significance calculated using the Student's *t*-test.

Figure 4.16


Ba/F3 RANBP2-ABL1
Cell death assay @ 3 days treatment
A
Secondary resistance to ponatinib
after primary resistance to imatinib
% Live cells normalized against untreated control
(Ann-V-low & 7-AAD-low)
100
50
0
0
1
10
100
nM ponatinib
LD50ponatinib:
naïve control
3.0 nM
imatinib-resistant ABL1-T315I
14.7 nM
imatinib-resistant ABL1-T315I / ponatinib-resistant
>100 nM
*P<0.05
**P<0.01
***P<0.001
*****P<0.0001
B
Secondary resistance to ponatinib
after primary resistance to dasatinib
% Live cells normalized against untreated control
(Ann-V-low & 7-AAD-low)
100
50
0
0
1
10
100
nM ponatinib
LD50ponatinib:
DMSO control
3.6 nM
dastinib-resistant ABL1-T315I
24.6 nM
dasatinib-resistant ABL1-T315I / ponatinib-resistant
>100 nM
*P<0.05
***P<0.001
*****P<0.0001

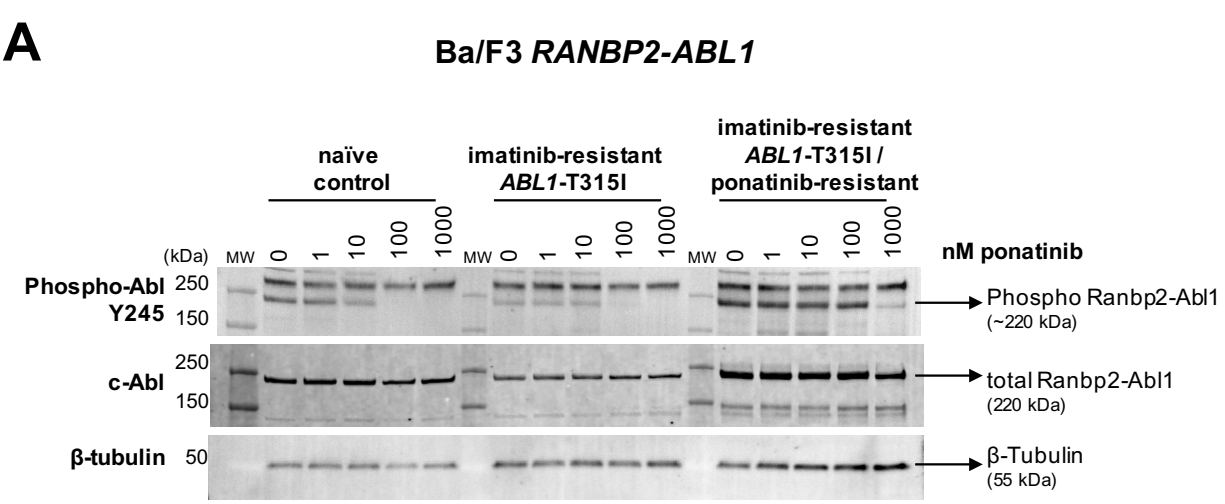
THIS PAGE INTENTIONALLY LEFT BLANK.

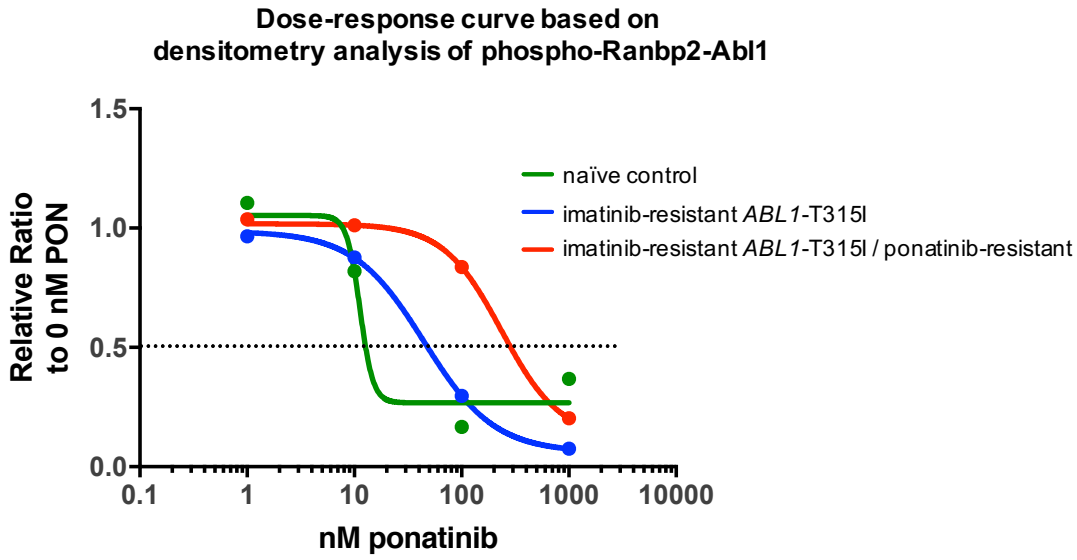
Figure 4.17 – Ponatinib-resistant *ABL1*-T315I cells demonstrate a higher phospho-Ranbp2-Abl1 IC_{50} compared to parental lines.

Ba/F3 TKI-sensitive, *ABL1*-T315I and ponatinib-resistant cells were exposed to tenfold increases in ponatinib concentration for 1 h at 37ºC/5% CO_2. Cells were collected, lysed and western blotting performed with membranes incubated in antibodies specific against phospho-Abl (Y245), c-Abl and β-tubulin as indicated. Densitometry analysis was performed using ImageStudio™, with normalised values of phosphorylated Ranbp2-Abl1 plotted on a logarithmic scale to reflect TKI concentrations used in this experiment. $IC_{50}^{ponatinib}$ values were calculated using GraphPad Prism ® as previously described. Data is representative of n=3 independent experiments. **A**: Ba/F3 *RANBP2-ABL1* naïve control, imatinib-resistant *ABL1*-T315I and imatinib-resistant *ABL1*-T315I / ponatinib-resistant cells. **B**: Ba/F3 *RANBP2-ABL1* DMSO control, dasatinib-resistant *ABL1*-T315I and dasatinib-resistant *ABL1*-T315I / ponatinib-resistant cells.

Figure 4.17

A

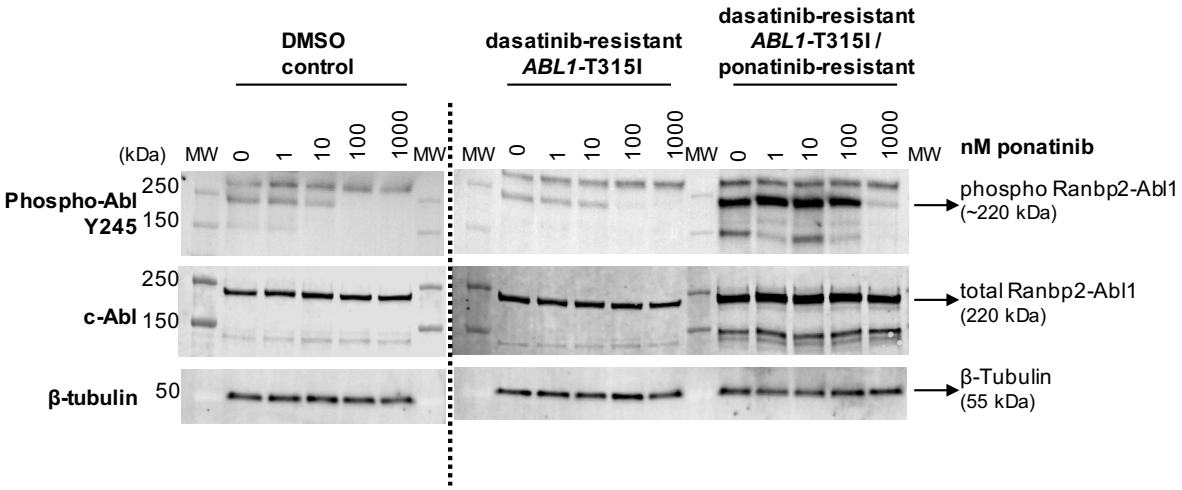




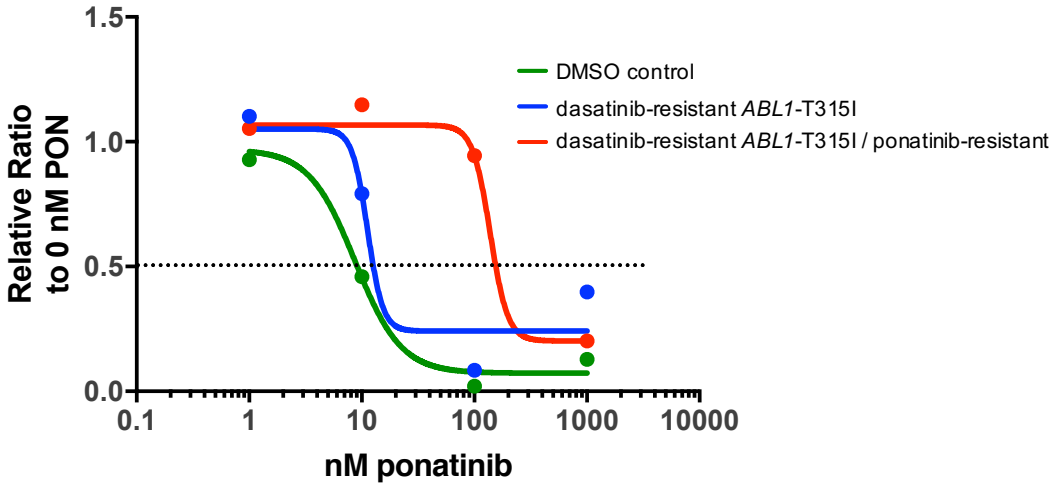
[Inhibitor] vs. response – Variable slope (four parameters)	naïve control	imatinib-resistant *ABL1*-T315I	imatinib-resistant *ABL1*-T315I / ponatinib-resistant
IC_{50} (nM ponatinib)	~ 11.3	44.8	235.5

B

Ba/F3 *RANBP2-ABL1*



Dose-response curve based on densitometry analysis of phospho-Ranbp2-Abl1



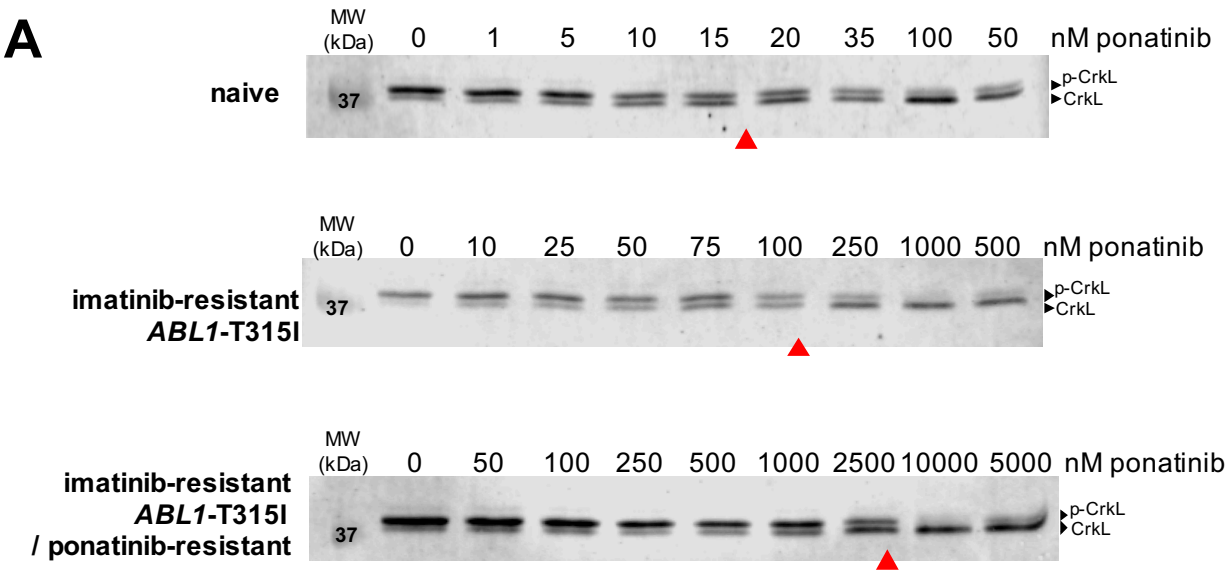
[Inhibitor] vs. response -- Variable slope (four parameters)	DMSO control	dasatinib-resistant *ABL1*-T315I	dasatinib-resistant *ABL1*-T315I / ponatinib-resisistant
IC_{50} (nM ponatinib)	8.7	~ 11.3	~ 138.2

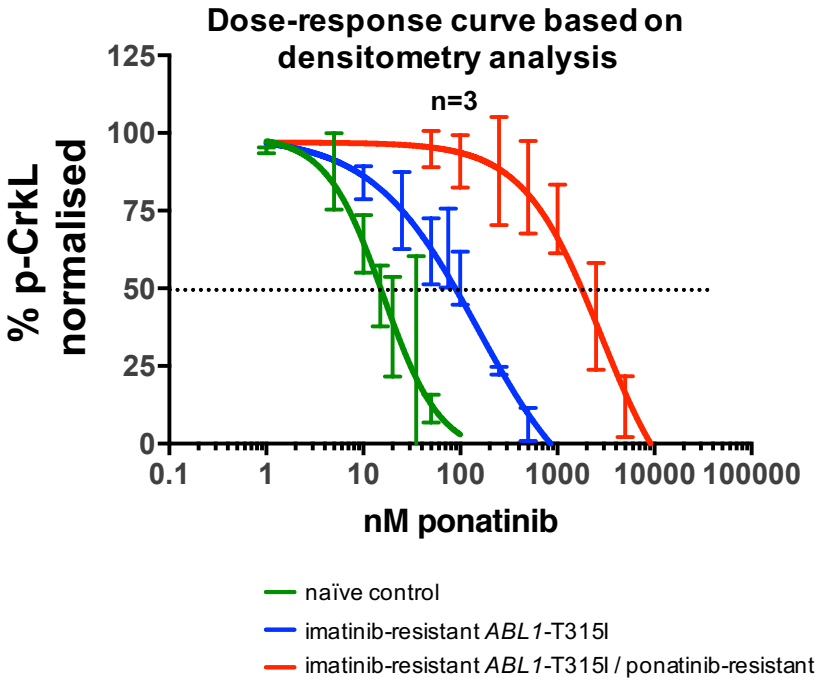
THIS PAGE INTENTIONALLY LEFT BLANK.

Figure 4.18 – Ponatinib-resistant *ABL1*-T315I cell lines demonstrate increased phosphorylated CrkL (p-CrkL) IC_{50} compared to parental lines.

Western immunoblotting of Ba/F3 *RANBP2-ABL1* TKI-sensitive, *ABL1*-T315I and ponatinib-resistant cells treated with an increasing concentration of ponatinib for 2 h prior to collection of cells for CrkL analysis. Prior to the experiment, a drug-washout procedure of TKI-resistant cells was performed by incubating cells overnight in the absence of TKI in culture. Western blots were probed with anti-CrkL antibody and densitometry analysis performed by normalising intensity of p-CrkL to total CrkL. Western blots shown are representative of each cell line and red triangles denote estimated positioning of 50% inhibition (IC_{50}) of p-CrkL. Sigmoidal plots were generated using GraphPad Prism, with dose-response curves representing the average of 3 independent experiments ± SD. IC_{50} values of collated data are reflected in tables beneath the plots. **A**: Ba/F3 *RANBP2-ABL1* naïve control, imatinib-resistant *ABL1*-T315I and imatinib-resistant *ABL1*-T315I/ponatinib-resistant cells. **B**: Ba/F3 *RANBP2-ABL1* DMSO control, dasatinib-resistant *ABL1*-T315I and dasatinib-resistant *ABL1*-T315I/ponatinib-resistant cells.

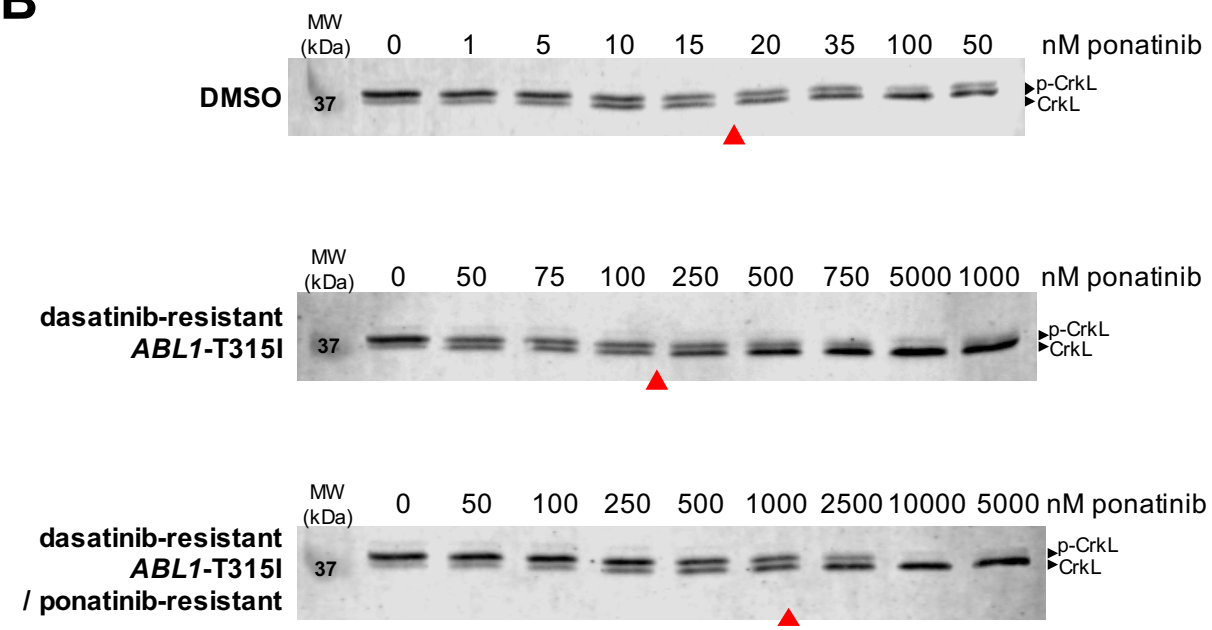
Figure 4.18

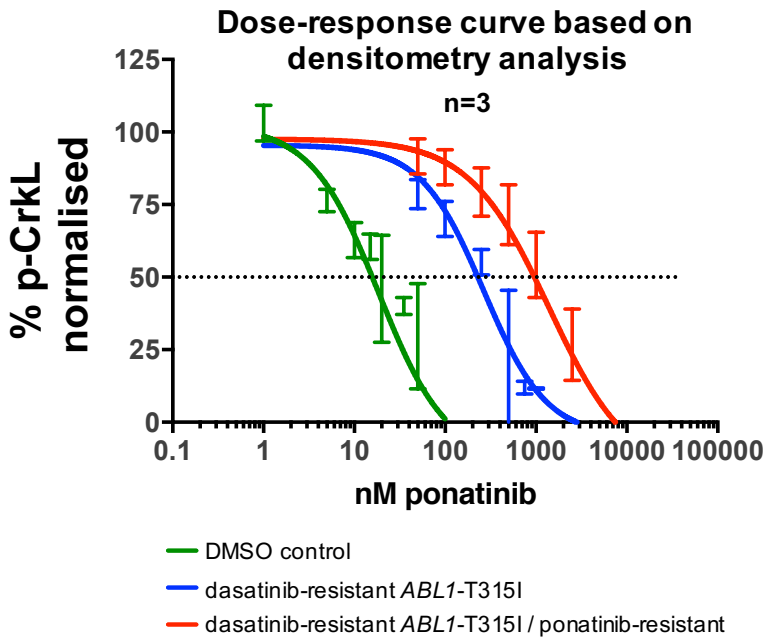




[Inhibitor] vs. response -- Variable slope (four parameters)	naïve control	imatinib-resistant *ABL1*-T315I	imatinib-resistant *ABL1*-T315I / ponatinib-resistant
IC_{50} (nM ponatinib)	16.0	151.2	2819.0

B





[Inhibitor] vs. response – Variable slope (four parameters)	DMSO control	dasatinib-resistant *ABL1*-T315I	dasatinib-resistant *ABL1*-T315I / ponatinib-resistant
IC_{50} (nM ponatinib)	18.6	266.1	1386.0

4.3.6. Secondary dose-escalation of Ba/F3 *RANBP2-ABL1* imatinib and dasatinib-resistant *ABL1*-T315I cells leads to the acquirement of compound mutations

Ba/F3 *RANBP2-ABL1 ABL1*-T315I ponatinib-resistant cells were subsequently analysed for the presence of point mutations in the *ABL1* kinase-domain, employing PCR and Sanger sequencing of the 3' fusion partner gene using primers designed to specifically span the breakpoint to prevent possible amplification of any endogenous *ABL1* genes. Analysis of these sequences using Mutation Surveyor® software revealed the presence of compound mutations that are known to be significant key contributors to ponatinib resistance[186].

In imatinib-resistant *ABL1*-T315I / ponatinib-resistant cells, the presence of a clinically significant *ABL1*-G250E/T315I compound mutation was detected (**Figure 4.19A**). *ABL1*-G250E (c.749G>A) was detected at a value of 93% in this line. The mutation was not present in parental control cells (imatinib-resistant *ABL1*-T315I and naïve). The *ABL1*-T315I mutation remains evident in both imatinib-resistant lines (imatinib-resistant *ABL1*-T315I and imatinib-resistant *ABL1*-T315I / ponatinib-resistant) at values of 94% and 100% respectively.

In dasatinib-resistant *ABL1*-T315I / ponatinib-resistant lines, a previously unreported *ABL1*-L302H/T315I compound mutation was found (**Figure 4.19B**). *ABL1*-L302H (c.905T>A) was detected at a rate of 98% in dasatinib-resistant *ABL1*-T315I / ponatinib-resistant cells, which was absent in the parental controls (dasatinib-resistant *ABL1*-T315I and naïve). The *ABL1*-T315I mutation remains evident in both imatinib-resistant lines (dasatinib-resistant *ABL1*-T315I and dasatinib-resistant *ABL1*-T315I / ponatinib-resistant), at 100%.

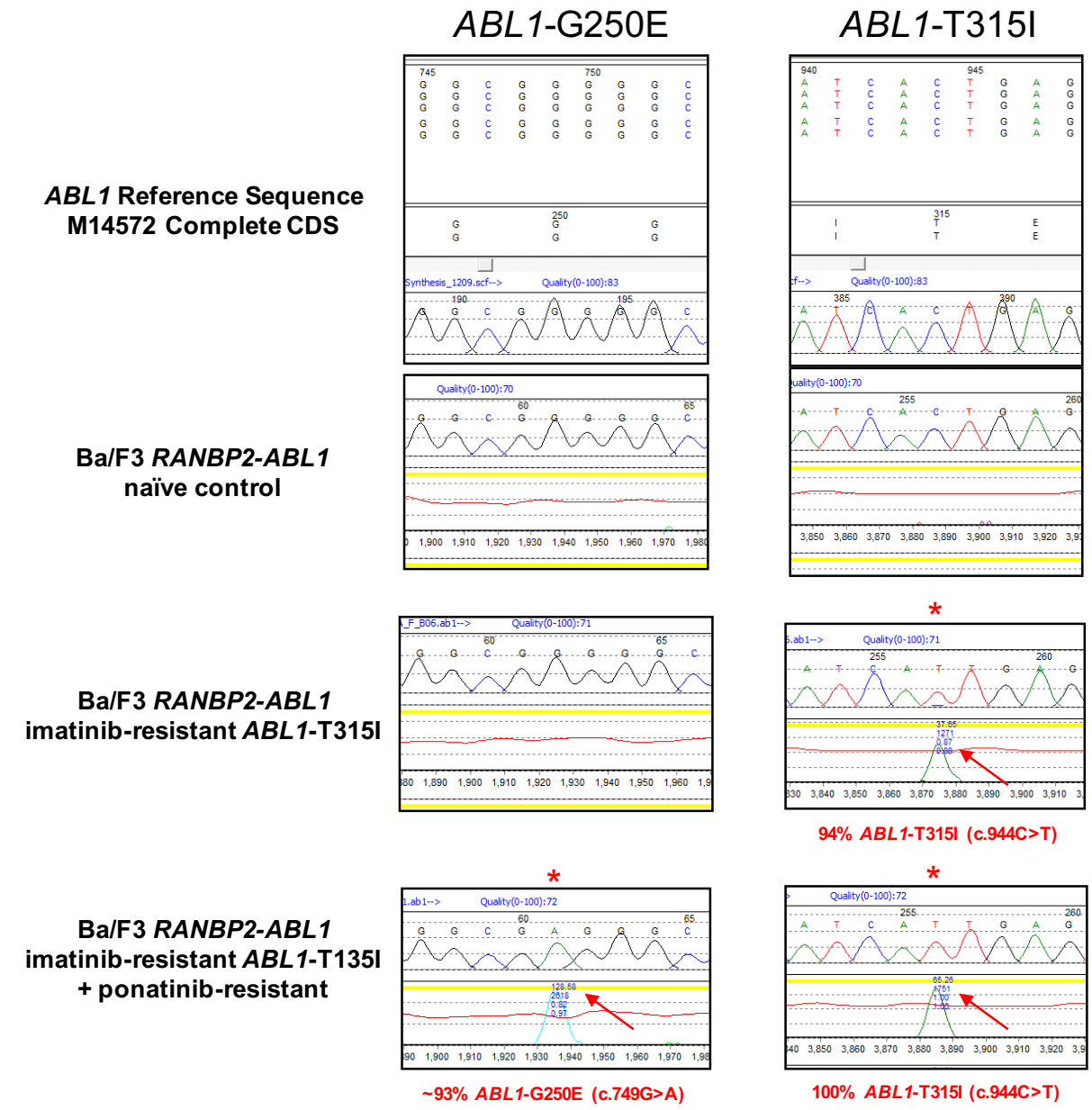
Figure 4.19 – Ponatinib-resistant *ABL1*-T315I Ba/F3 *RANBP2-ABL1* cells found to harbour compound mutations

Sanger sequencing of PCR products specific for the *ABL1* kinase-domain, in Ba/F3 *RANBP2-ABL1* TKI-resistant and TKI-sensitive lines. Red asterisks highlight the clinically-significant *ABL1*-T315I kinase-domain mutation in TKI-resistant cells. The *ABL1* reference sequence was included as a comparison. **A**: Ba/F3 *RANBP2-ABL1* naïve control, imatinib-resistant *ABL1*-T315I and imatinib-resistant *ABL1*-T315I / ponatinib-resistant cells. Detection of the *ABL1*-G250E (left) and *ABL1*-T315I (right) mutations. **B**: Ba/F3 *RANBP2-ABL1* DMSO control, dasatinib-resistant *ABL1*-T315I and dasatinib-resistant *ABL1*-T315I / ponatinib-resistant cells. Detection of the *ABL1*-L302H (left) and *ABL1*-T315I (right) mutations. Sequence analysis was performed on the Mutation Surveyor® DNA analysis software.

Figure 4.19

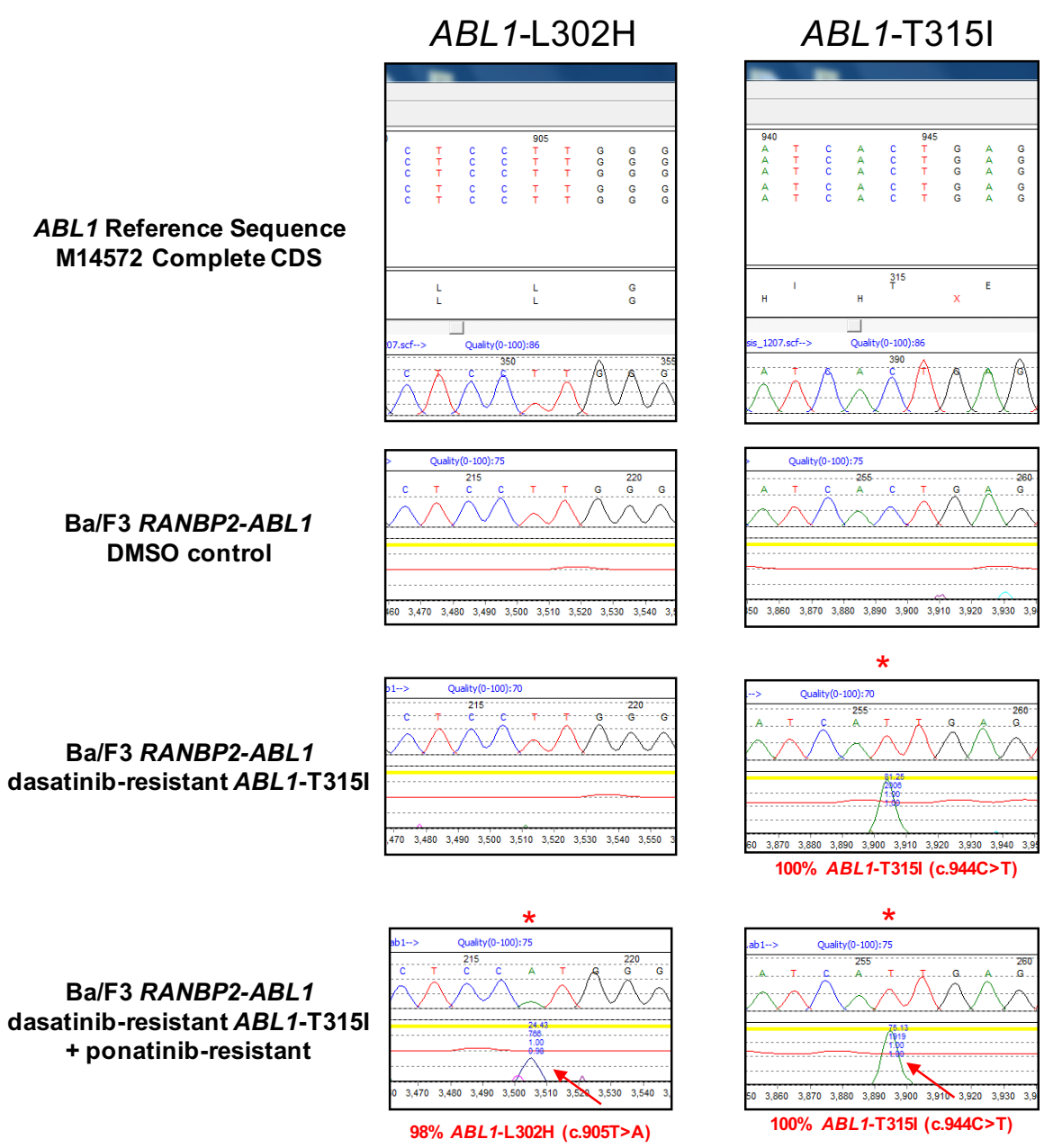
A

Kinase-domain mutation sequencing for secondary resistance in imatinib-resistant *ABL1*-T315I cells



B

Kinase-domain mutation sequencing for secondary resistance in dasatinib-resistant *ABL1*-T315I cells



4.3.7. Ba/F3 *RANBP2-ABL1* cells dose-escalated to ponatinib as first-line therapy are cross-resistant to first and second generation Abl TKIs

The TKI-sensitive Ba/F3 *RANBP2-ABL1* cells generated in section **4.3.1** (and TKI-sensitivity explored in **4.3.2**), were utilised for generation of ponatinib-resistance as first-line therapy. As ponatinib is a highly-potent third-generation Abl kinase inhibitor, a significant amount of time was required for the adjustment of Ba/F3 *RANBP2-ABL1* cells to ponatinib (~ 16 months).

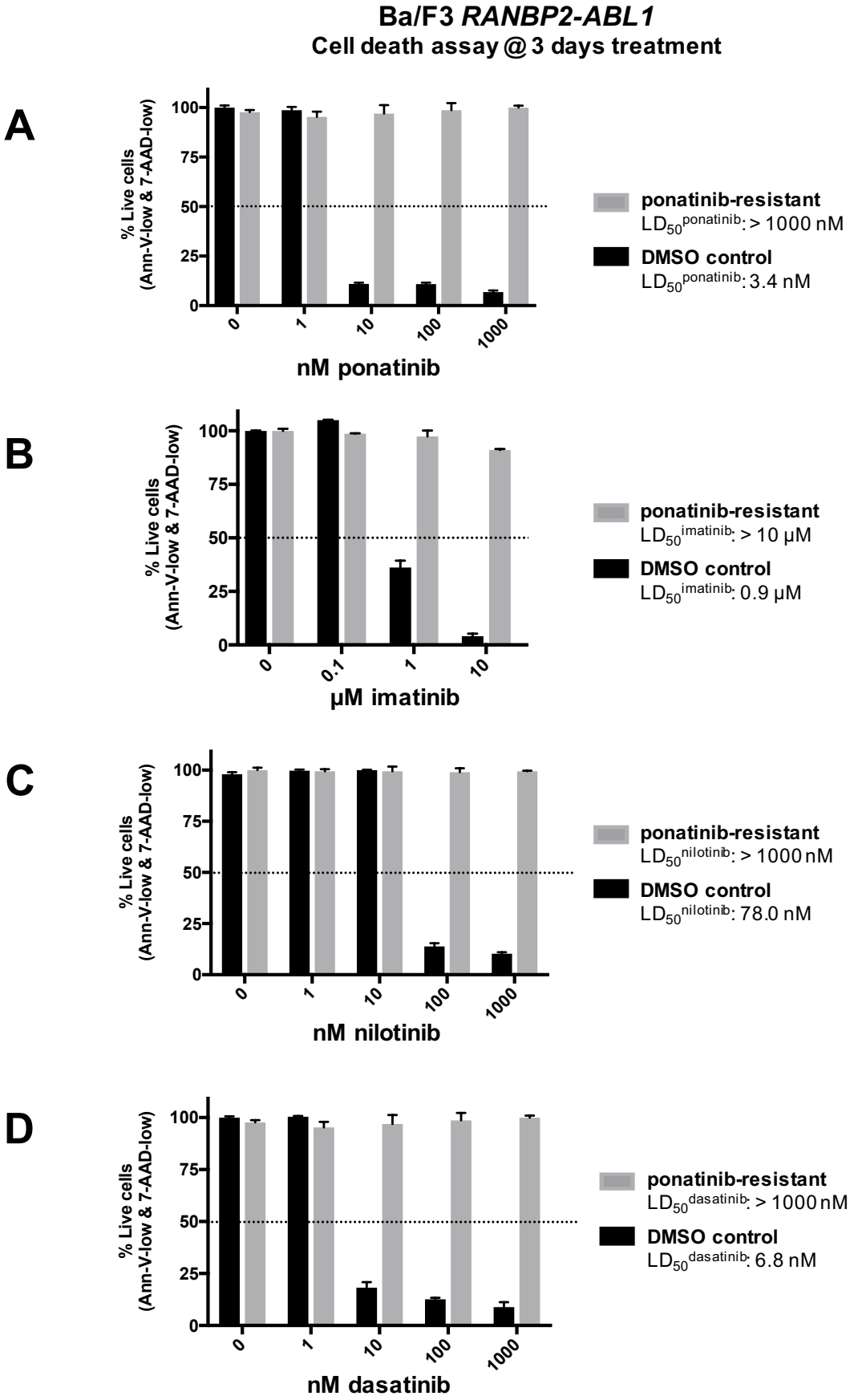
Ba/F3 *RANBP2-ABL1* cells escalated to a final concentration of 200 nM ponatinib in culture were tested for TKI sensitivity via Annexin-v/7-AAD exclusion assay (**Figure 4.20**). Results confirmed ponatinib-resistance, along with cross-resistance to other TKIs ($LD_{50}^{imatinib}$ > 10 μM, $LD_{50}^{nilotinib}$ > 1000 nM and $LD_{50}^{dasatinib}$ > 1000 nM). This was in contrast to TKI-sensitive Ba/F3 *RANBP2-ABL1* DMSO control cells that were sensitive to imatinib, nilotinib and dasatinib at LD_{50} concentrations of 0.9 μM, 78.0 nM and 6.8 nM respectively.

THIS PAGE INTENTIONALLY LEFT BLANK.

Figure 4.20 – Ba/F3 *RANBP2-ABL1* cells resistant to ponatinib as first-line therapy exhibits cross-resistance to first and second generation Abl TKIs.

Previously naïve Ba/F3 *RANBP2-ABL1* cells were dose-escalated to a final concentration of 200 nM ponatinib. TKI-resistant cells were collected and confirmed for TKI-resistance via Annexin-V/7-AAD exclusion flow cytometry analysis. A DMSO control line was included. Cells were exposed to increasing concentrations of ponatinib (**A**), imatinib, (**B**), nilotinib (**C**) and dasatinib (**D**) for 3 days at 37ºC/5% CO_2. The absence of cells at 100 μM imatinib was due to death by off-target effects. Data represents mean ± SD of 3 replicates. Dotted line across the *y*-axis denotes 50% of the TKI concentration required for lethal dose (LD_{50}). LD_{50} values indicated were calculated using GraphPad Prism® as previously described.

Figure 4.20


Ba/F3 RANBP2-ABL1
Cell death assay @ 3 days treatment
A
% Live cells (Ann-V-low & 7-AAD-low)
100
75
50
25
0
0
1
10
100
1000
nM ponatinib
ponatinib-resistant
LD50ponatinib: > 1000 nM
DMSO control
LD50ponatinib: 3.4 nM
B
% Live cells (Ann-V-low & 7-AAD-low)
0
0.1
1
10
µM imatinib
ponatinib-resistant
LD50imatinib: > 10 µM
DMSO control
LD50imatinib: 0.9 µM
C
% Live cells (Ann-V-low & 7-AAD-low)
nM nilotinib
ponatinib-resistant
LD50nilotinib: > 1000 nM
DMSO control
LD50nilotinib: 78.0 nM
D
% Live cells (Ann-V-low & 7-AAD-low)
nM dasatinib
ponatinib-resistant
LD50dasatinib: > 1000 nM
DMSO control
LD50dasatinib: 6.8 nM

THIS PAGE INTENTIONALLY LEFT BLANK.

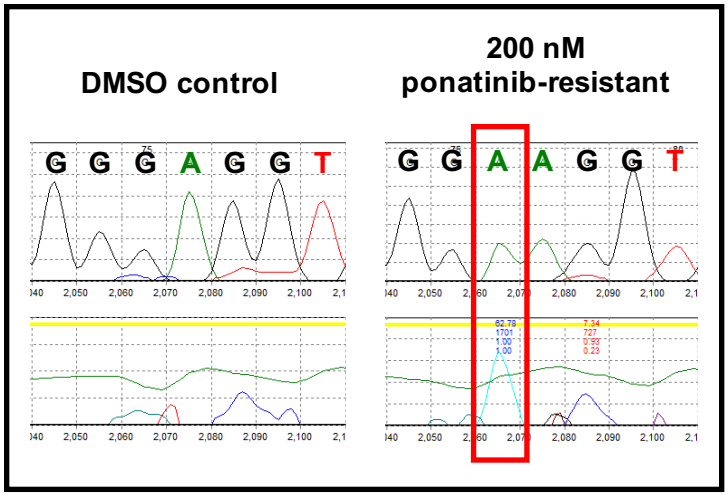
4.3.8. Clinically-relevant *ABL1*-E255K mutation identified in ponatinib-resistant Ba/F3 *RANBP2-ABL1* cells, but no corresponding fusion protein

Following confirmation of cross-resistance in Ba/F3 *RANBP2-ABL1* cells dose-escalated to ponatinib as primary therapy, PCR followed by Sanger sequencing of the *ABL1* kinase-domain was employed according to methods as previously described. Analysis of sequencing data uncovered a clinically-significant *ABL1*-E255K (c.763G>A) mutation in the *RANBP2-ABL1* kinase domain, at a mutation rate of 100% (**Figure 4.21A**).

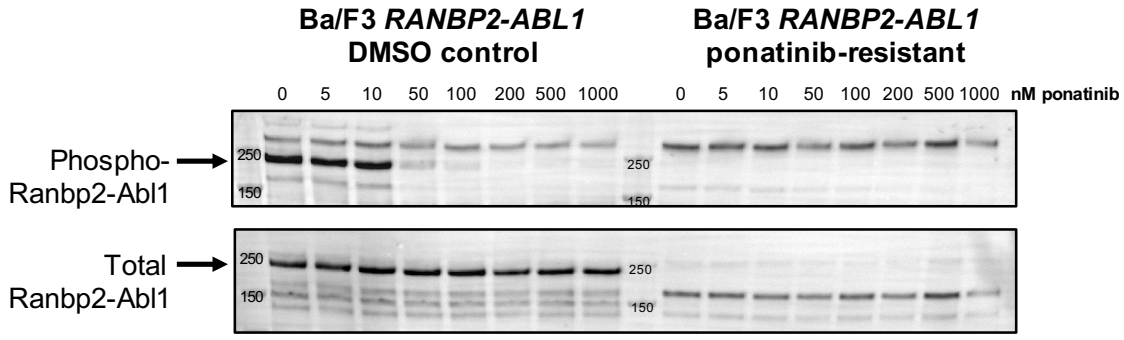
When Ranbp2-Abl1 kinase activity was further explored by Western blotting, data analysis revealed a decrease in the expression of p-Ranbp2-Abl1 in TKI-sensitive cells, however, no band of the expected molecular weight (~220 kDa) was detectable in the ponatinib-resistant samples (**Figure 4.21B**). This was consistently observed using different primary antibodies (p-c-Abl Y245 and c-Abl). Further analysis of Ba/F3 *RANBP2-ABL1* protein lysates in the presence of negative and positive control cell lines (Ba/F3 parental and empty vector control; Ba/F3 *RANBP2-ABL1* naïve and DMSO control) confirmed that no bands of the expected size (~220 kDa) were evident in the Ba/F3 *RANBP2-ABL1* ponatinib-resistant cells (**Figure 4.21C**). No evidence of the expected band was detected in intermediate concentrations that were tested simultaneously.

Figure 4.21

A



B



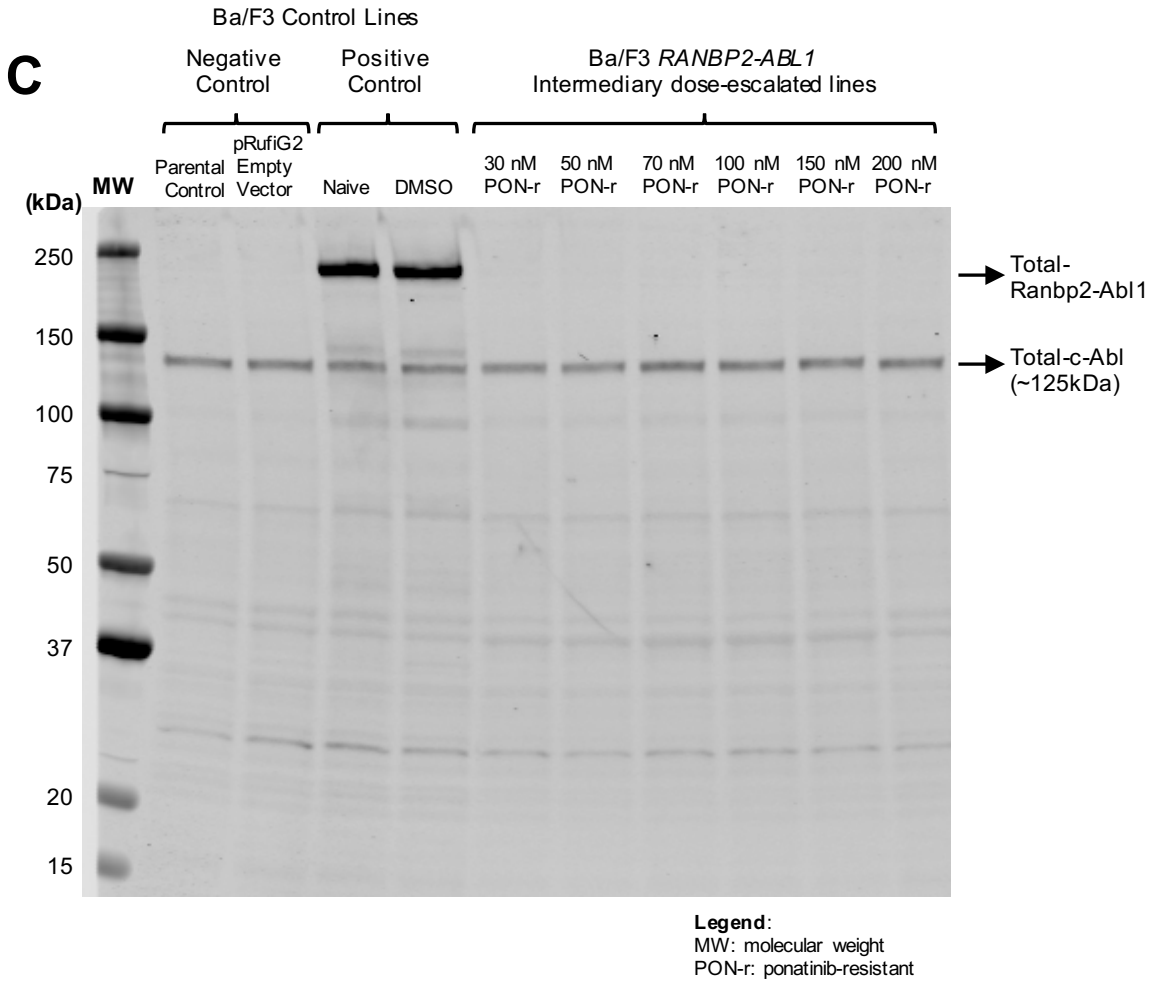


Figure 4.21 – Ba/F3 *RANBP2-ABL1* cells dose-escalated in ponatinib (as first-line treatment) exhibit an *ABL1*-E255K mutation, however, the fusion protein was undetectable via western blotting

A: Sanger sequencing of ponatinib-resistant Ba/F3 *RANBP2-ABL1* cells reveals a clinically-significant *ABL1*-E255K (c.763G>A) mutation, as highlighted by the red rectangle. Data is representative of n=3 sequencing reactions. **B**: Western-blotting of ponatinib-sensitivity assay indicates the absence of Ranbp2-Abl1 fusion protein (~220 kDa) in the ponatinib-resistant Ba/F3 *RANBP2-ABL1* cells. **C**: Further western blotting analysis comparing total c-Abl in Ba/F3 parental control, empty vector, *RANBP2-ABL1* TKI-sensitive and ponatinib-resistant lines (with intermediate concentrations), also demonstrated no detectable protein.

4.3.9. RQ-PCR confirms mRNA expression of Ba/F3 *RANBP2-ABL1* fusion gene, despite lack of detectable fusion protein

To confirm if the *RANBP2-ABL1* fusion gene was expressed in ponatinib-resistant Ba/F3, RQ-PCR was performed using primers specific for the fusion breakpoint. Results indicated mRNA expression of the gene in all Ba/F3 *RANBP2-ABL1* cell lines, while controls were negative as expected (**Figure 4.22**).

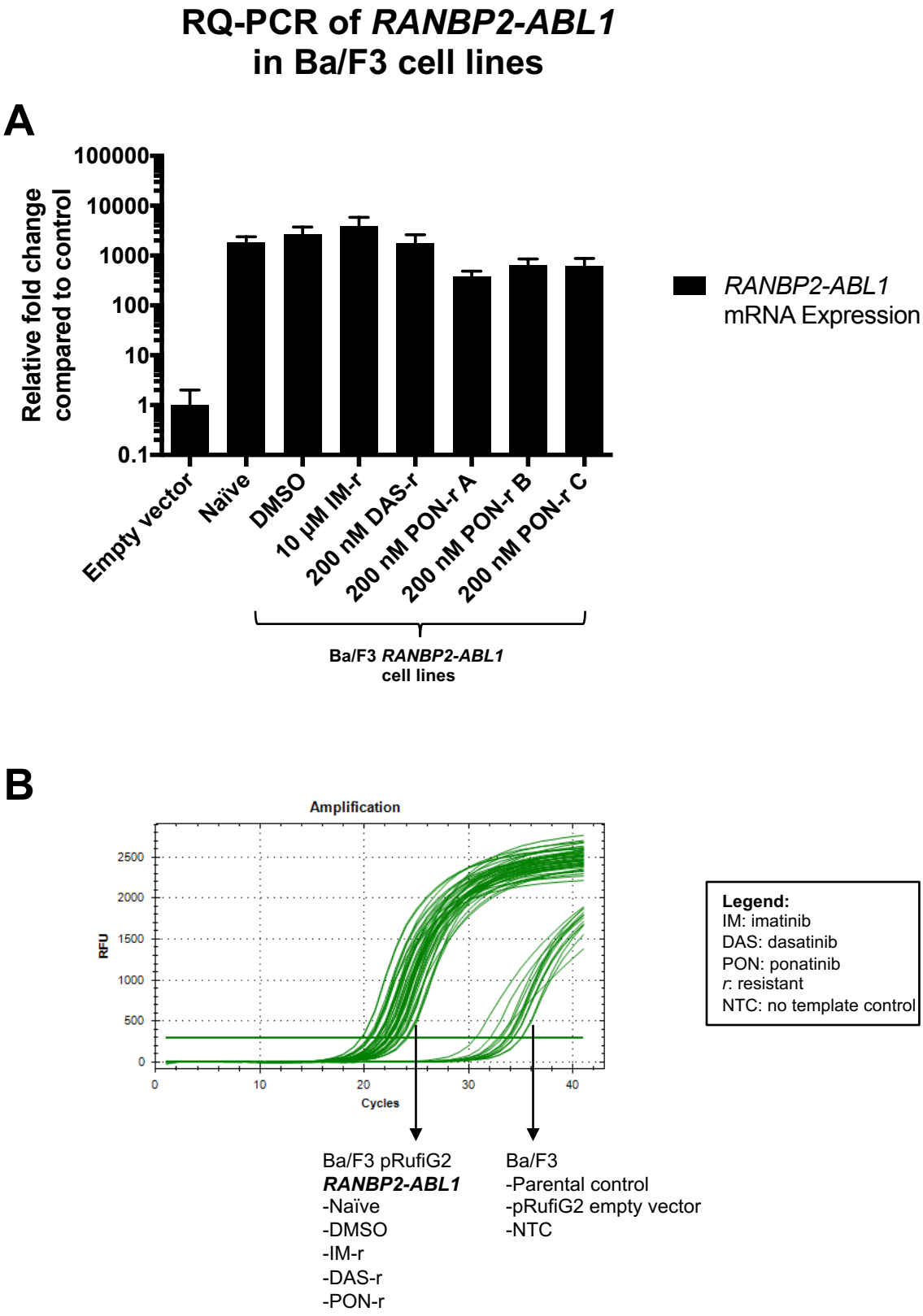
When comparing the expression of *RANBP2-ABL1* mRNA in TKI-resistant versus sensitive lines, imatinib-resistant cells had twice the expression (3.9×10^3) while no marked difference was observed in dasatinib-resistant cells (1.7×10^3), compared to naïve and DMSO control (1.8×10^3 and 2.7×10^3 respectively) (**Figure 4.22A**). The expression of *RANBP2-ABL1* was reduced in ponatinib-resistant cells, which was consistent across biological replicates (A: 0.4×10^3, B: 0.6×10^3, and C: 0.6 x 10). Amplification curves further confirm the expression of *RANBP2-ABL1* in Ba/F3 *RANBP2-ABL1* cells (TKI-sensitive and resistant), and, absent in Ba/F3 parental wildtype and empty vector control lines (**Figure 4.22B**).

THIS PAGE INTENTIONALLY LEFT BLANK.

Figure 4.22 – RQ-PCR confirms expression of *RANBP2-ABL1* fusion gene

A: Fold-change of *RANBP2-ABL1* expression in Ba/F3 TKI-sensitive and resistant lines, with biological replicate wells of the ponatinib-resistant line included (as indicated by the letters A, B and C). The *y*-axis denotes the relative fold change of *RANBP2-ABL1* mRNA expression compared to the empty vector control, as calculated by the comparative CT method. Columns represent mean while error bars denote ±SD of 3 biological replicate samples. **B**: A RQ-PCR amplification curves indicating expression of the *RANBP2-ABL1* fusion gene across all Ba/F3 *RANBP2-ABL1* lines (TKI-sensitive and resistant), in comparison to Ba/F3 parental control and pRuf-iG2 empty vector lines.

Figure 4.22


RQ-PCR of RANBP2-ABL1 in Ba/F3 cell lines
A
Relative fold change compared to control
100000
10000
1000
100
10
1
0.1
Empty vector
Naïve
DMSO
10 µM IM-r
200 nM DAS-r
200 nM PON-r A
200 nM PON-r B
200 nM PON-r C
Ba/F3 RANBP2-ABL1 cell lines
RANBP2-ABL1 mRNA Expression
B
Amplification
RFU
2500
2000
1500
1000
500
0
0
10
20
30
40
Cycles
Legend:
IM: imatinib
DAS: dasatinib
PON: ponatinib
r: resistant
NTC: no template control
Ba/F3 pRufiG2 RANBP2-ABL1
-Naïve
-DMSO
-IM-r
-DAS-r
-PON-r
Ba/F3
-Parental control
-pRufiG2 empty vector
-NTC

4.3.10. Identification of a C-terminal deletion in ponatinib-resistant Ba/F3 *RANBP2-ABL1* cells

Further investigation into a possible cause for the absence of Ranbp2-Abl1 in ponatinib-resistant cells, despite expression of *RANBP2-ABL1* mRNA and detection of an *ABL1*-E255K kinase-domain mutation, was performed. Using primers specific for the fusion breakpoint (*RANBP2*_exon18) and its 3' retroviral region (pRuf-iG2 Seq RV), the Abl kinase was amplified. Gel electrophoresis of PCR products indicated a decrease in the size of PCR product in Ba/F3 *RANBP2-ABL1* ponatinib-resistant cells, from 6 kb to 3 kb (**Figure 4.23A**). Analysis of Sanger sequencing results further confirmed a loss of approximately 1.5 kb in the C-terminus of ponatinib-resistant *RANBP2-ABL1*, compared to DMSO control (**Figure 4.23B**).

Following the validation of a C-terminal deletion within *RANBP2-ABL1* in the ponatinib-resistant cells, western blotting of Abl kinase activity was performed via a p-CrkL IC_{50} assay in control and resistant lines. When cells were treated with 0, 5, 10, 25, 50, 75, 100, and 1000 nM ponatinib, no significant difference in ponatinib IC_{50} was observed between DMSO control ($IC_{50}^{ponatinib}$: 25 nM) and ponatinib-resistant ($IC_{50}^{ponatinib}$: 25 nM) cells (**Figure 4.24**). Notably, in ponatinib-resistant cells, the ratio between p-CrkL and CrkL was 50% in TKI-free media, differing greatly compared to parental DMSO cells.

Figure 4.23 – Ba/F3 *RANBP2-ABL1* ponatinib-resistant cells comprise of a C-terminal deletion in its Ph-like ALL fusion gene

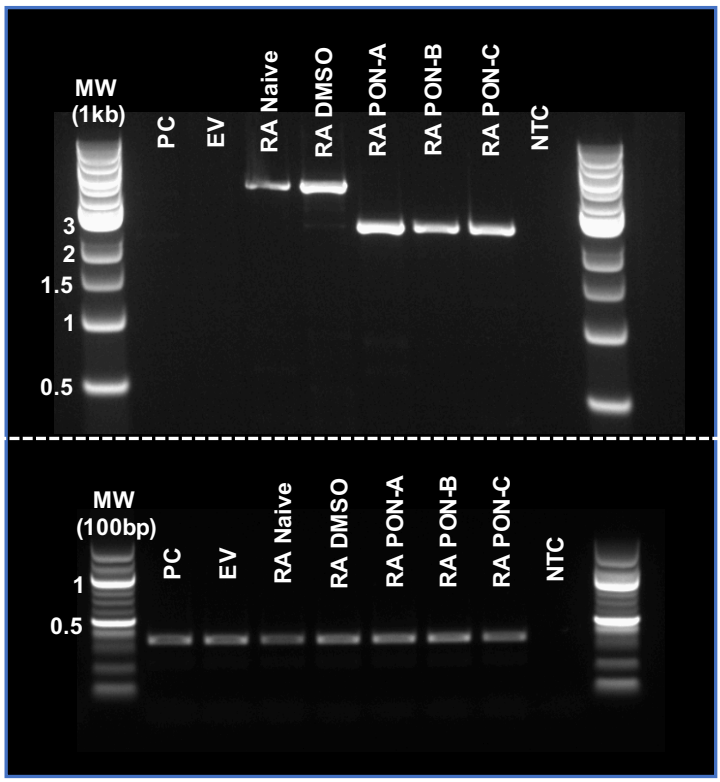
A: Gel electrophoresis of PCR products – top: *RANBP2-ABL1* fusion gene, with a forward primer specific for the *RANBP2* breakpoint region and a reverse primer specific for the '3 end of the retroviral cloning site; bottom: β–actin loading control. Note the smaller band size in biological replicate samples (A, B & C) of ponatinib-resistant Ba/F3 *RANBP2-ABL1* cells. **B**: Sanger sequencing electropherograms indicating the absence of sequence in the C-terminal region of the *RANBP2-ABL1* fusion gene in the ponatinib-resistant cell line (highlighted with red asterisks).

Figure 4.23

A

For 3' partner gene:
Primer FW: *RANBP2*_exon18
Primer RV: IRES rv

For loading control:
Primer FW: Mouse *β-actin*
Primer RV: Mouse *β-actin*



Legend:
EV: empty vector
FW: forward
MW: molecular weight marker
NTC: no template control
PC: parental control
PON: ponatinib (resistant)
RA: *RANBP2-ABL1*
RV: reverse

B

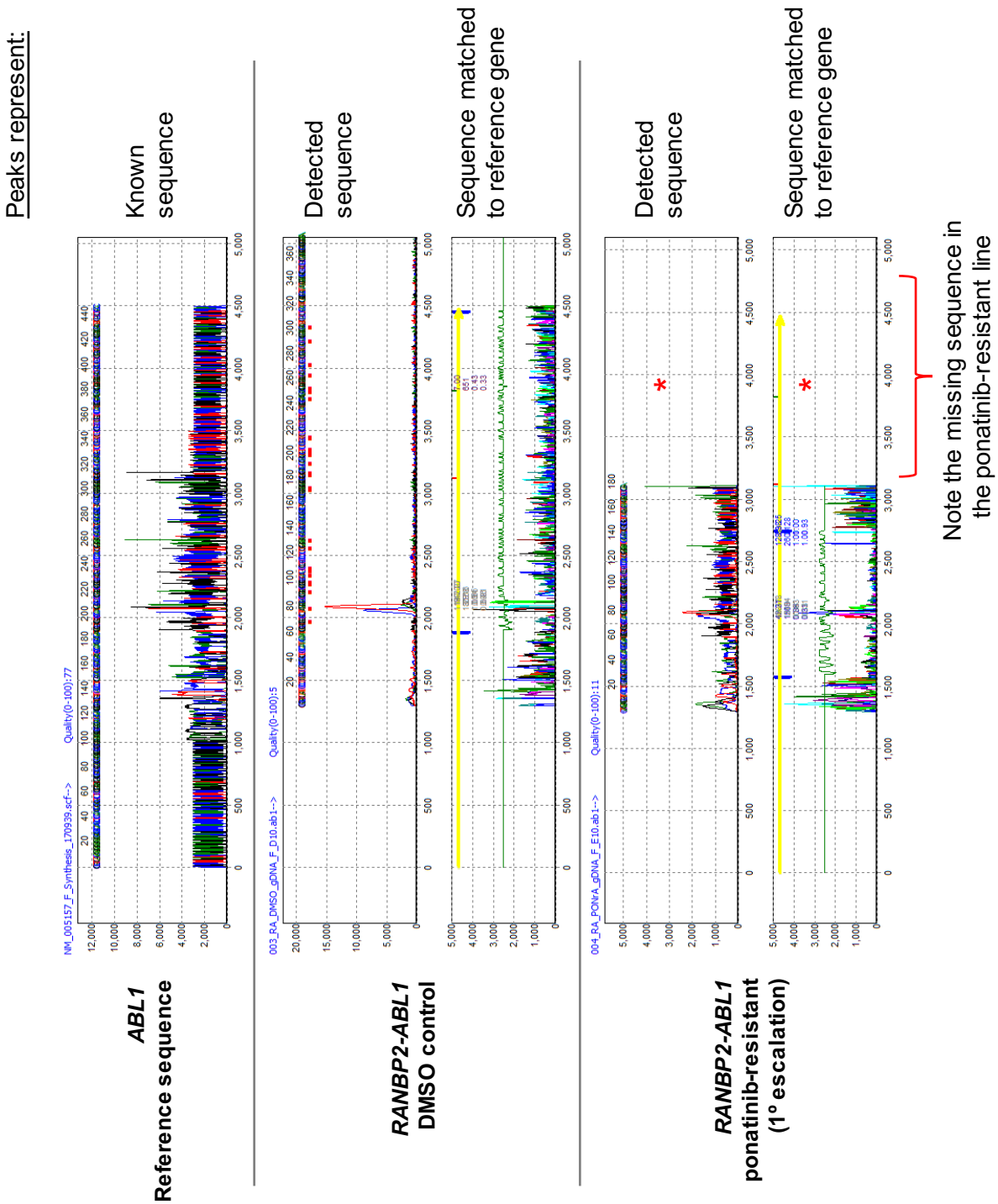
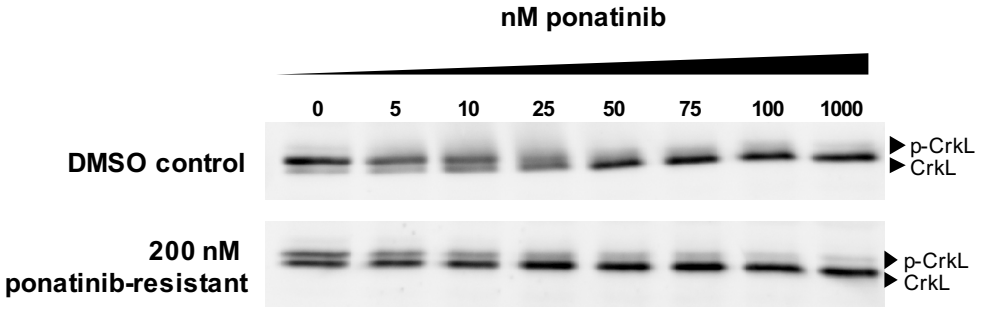

Peaks represent:
Known sequence
Detected sequence
Sequence matched to reference gene
ABL1
Reference sequence
RANBP2-ABL1
DMSO control
RANBP2-ABL1
ponatinib-resistant
(1º escalation)
Note the missing sequence in the ponatinib-resistant line

Figure 4.24 – Ba/F3 *RANBP2-ABL1* ponatinib-resistant cells demonstrate no marked increase in p-CrkL IC_{50} compared to TKI-sensitive line

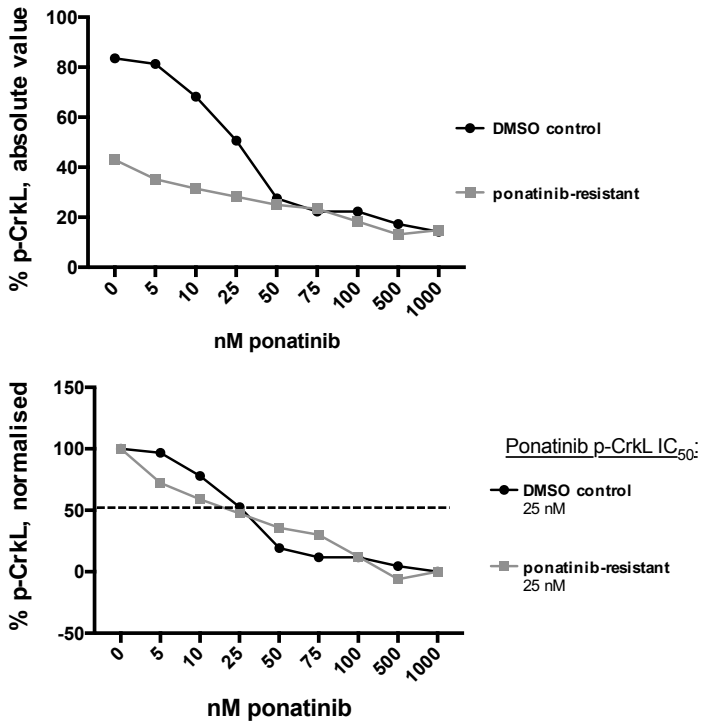
A: Western blotting of Ba/F3 *RANBP2-ABL1* DMSO control and ponatinib-resistant cells treated with increasing concentrations of ponatinib. Data is a minimum of n=1 experimental repeats. **B**: Densitometry analysis of p-CrkL expression in ponatinib-sensitive and resistant lines. Top panel: absolute p-CrkL densitometry; bottom panel: relative densitometry comparing against 0 nM ponatinib exposure as a control, with dotted line representing the IC_{50}. It is interesting to note that despite similar ponatinib p-CrkL IC_{50} concentrations in these cell lines, the ratio of p-CrkL to CrkL in ponatinib-resistant cells was 1:1 at 0 nM ponatinib, suggesting no upregulation of CrkL phosphorylation in TKI-resistant cells and an Abl-independent mechanism exists.

Figure 4.24

A



B



4.3.11. Identification of non-canonical signalling pathways in ponatinib-resistant Ba/F3 *RANBP2-ABL1* cells

To further explore alternative signalling pathways in the ponatinib-resistant Ba/F3 *RANBP2-ABL1* cells, mRNA sequencing was performed on three biological replicates with TKI-sensitive cells used as a control. As expected, hierarchical clustering indicated a close association between the 3 biological replicate samples (**Figure 4.25A**). Furthermore, a heatmap of supervised clustering data indicated a strong correlation of highly upregulated and downregulated genes within biological replicates (**Figure 4.25B**). The top five most interesting significantly upregulated and downregulated differentially-expressed genes (upregulated: *Rtp4*, *Apol9b*, *Oasl1*, *Tgtp1*, *Mx2*; downregulated: *Cd80*, *Tox2, Zfhx3*, *Fgf21* and *Cyp4f40*) (**Figure 4.26A**) were selected for validation via RQ-PCR (**Figure 4.26B**). In the upregulated gene dataset, the log_2 fold change (log_2FC) values were 14.14 (*Rtp4*), 10.29 (*Apol9b*), 9.58 (*Oasl2*), 9.44 (*Tgtp1*) and 9.31 (*Mx2*) respectively in resistant cells compared to control. In the downregulated gene dataset, the log_2FC values were -4.57 (*Cd80*), -5.21 (*Tox2*), -5.32 (*Zfhx3*), -5.37 (*Fgf21*) and -6.96 (*Cyp4f40*) respectively (**Figure 4.26A** and **Appendix 2.1**).

Validation of mRNA-seq data via RQ-PCR confirmed these results, where comparative Ct calculations indicate fold changes of 1100.78 (*Rtp4*), 1.63 (*Apol9b*), 42.10 (*Oasl2*), 79.66 (*Tgtp1*) and 359.67 (*Mx2*) in genes that were upregulated in ponatinib-resistant Ba/F3 *RANBP2-ABL1* cells compared to DMSO control. In genes that were downregulated, comparative Ct analysis yielded fold changes of 0.54 (*Cd80*), 0.47 (*Tox2*), 0.57 (*Zfhx3*), 0.01 (*Fgf21*) and 0.56 (*Cyp4f40*) respectively (**Figure 4.26B** and **Appendix 2.1**).

Further pathway analysis of differentially-expression genes via InnateDB[223] led to the identification of alternative signalling pathways potentially involved in ponatinib-resistance. In **Figure 4.27A**, pathway analysis conducted using genes that were significantly upregulated ($P < 0.05$) with a cut-off value of 2 ($Log_2FC > 1$) revealed an enrichment of pathways associated with immune, cytokine and metabolic signalling (**Appendix 4.2A**). When cross-examined with raw differential-expression (DE) data, results indicate a correlation between significant pathways and significantly-expressed genes. For example, 2'-5'-oligoadenylate synthetase-like-1 (*Oasl1*) which was common across the immunity and cytokine signalling pathways, was upregulated at a log_2FC of 5.85 compared to TKI-sensitive DMSO control cells.

When pathway analysis was performed using a cohort of genes that were significantly downregulated ($P < 0.05$) with a cut-off value of -2 ($Log_2FC < 1$), an enrichment of pathways associated with vitamin D metabolism, transportation of small molecules and cytokine receptor interactions was observed (**Figure 4.27B** and **Appendix 4.2B**). Further cross-referencing with the DE dataset indicated genes such as cubilin (*Cubn*) and ATP-binding cassette sub-family A (ABC1) member 4 (*Abca4*) were under-expressed at a log_2FC of -2.40 and -5.31 respectively in ponatinib-resistant cells compared to DMSO control.

Figure 4.25 – Clustering of mRNA-seq data confirms difference in gene expression between Ba/F3 *RANBP2-ABL1* DMSO control and ponatinib-resistant cell lines

A: Hierarchical clustering of Ba/F3 *RANBP2-ABL1* DMSO control and ponatinib-resistant cell lines, confirming similarity of biological replicates. **B**: Heatmap of supervised clustering indicate a distinct signature in differentially-expressed genes between TKI-sensitive and ponatinib-resistant cell lines, where there are more upregulated genes in ponatinib-resistant cells, compared to DMSO control cells.

Figure 4.25

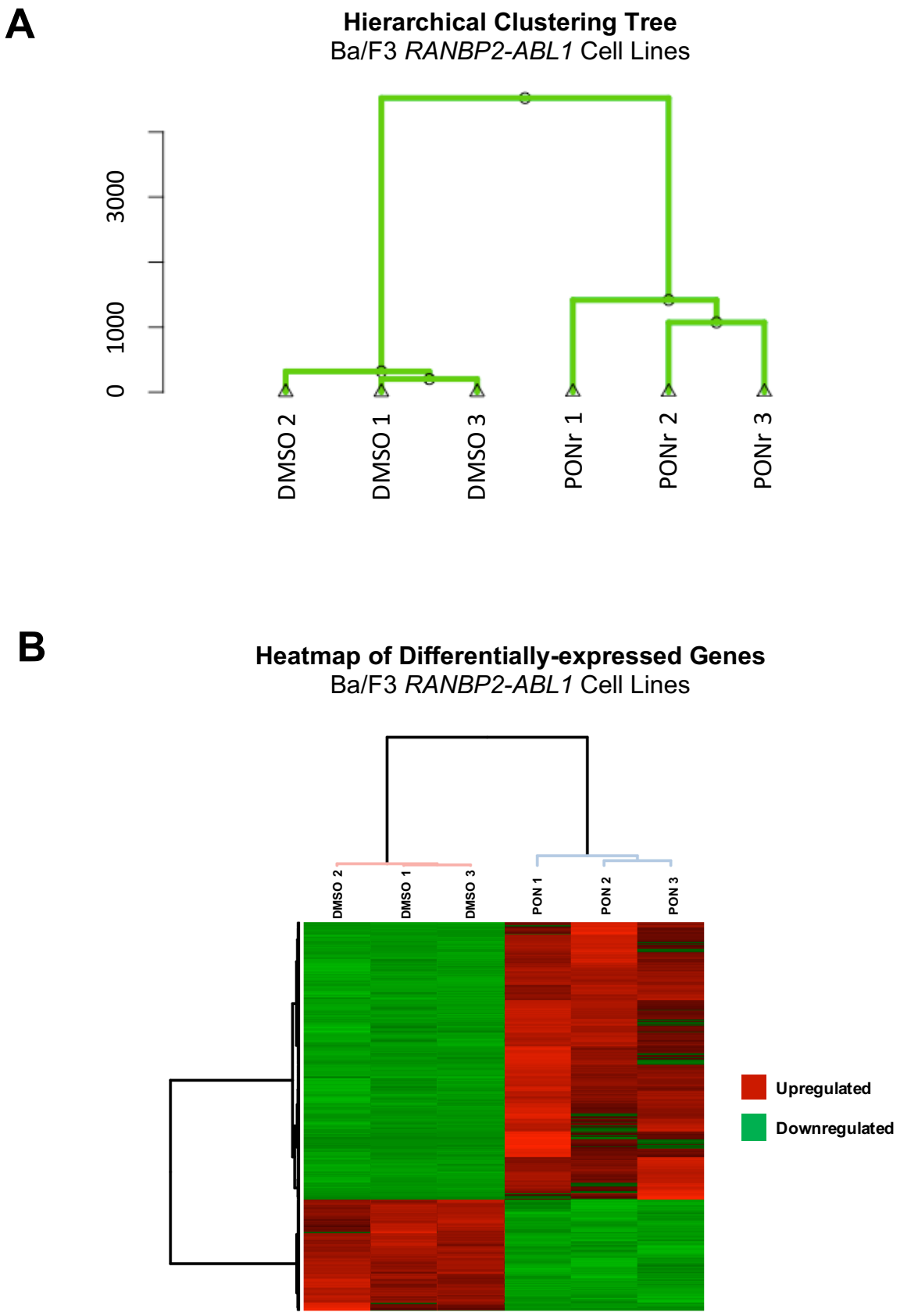
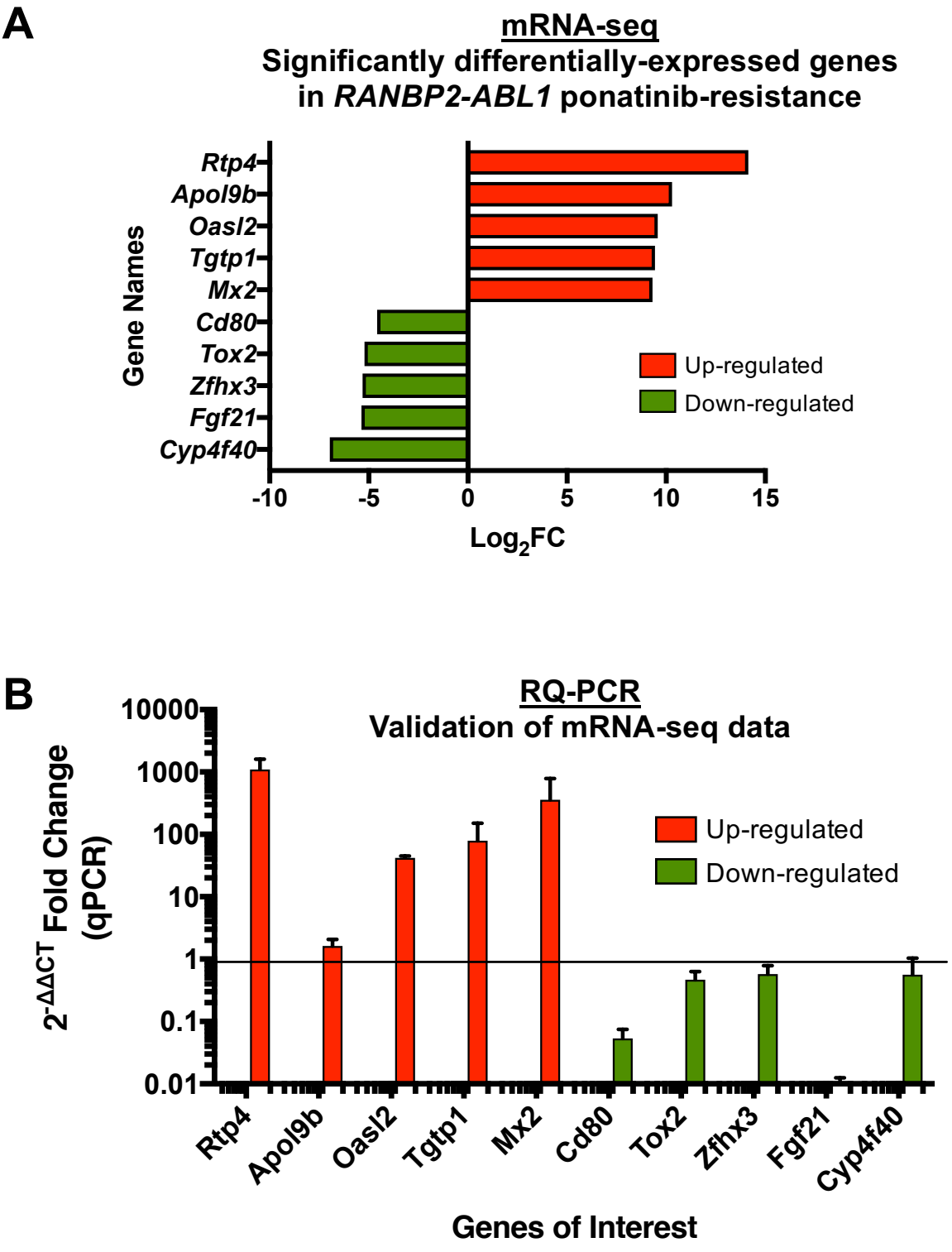

A
Hierarchical Clustering Tree
Ba/F3 RANBP2-ABL1 Cell Lines
0
1000
3000
DMSO 2
DMSO 1
DMSO 3
PONr 1
PONr 2
PONr 3
B
Heatmap of Differentially-expressed Genes
Ba/F3 RANBP2-ABL1 Cell Lines
DMSO 2
DMSO 1
DMSO 3
PON 1
PON 2
PON 3
Upregulated
Downregulated

Figure 4.26 – Validation of mRNA-seq differentially-expressed genes in ponatinib-resistant compared to DMSO control Ba/F3 *RANBP2-ABL1* cells, via RQ-PCR

A: Bar chart representing significantly differentially-expressed genes in Ba/F3 *RANBP2-ABL1* ponatinib-resistant cells. The top 5 upregulated and downregulated genes are represented. **B**: RQ-PCR validation of up and downregulated genes in ponatinib-resistant line, using the comparative Ct method incorporating the DMSO control cell. Columns represent mean while error bars are the standard deviation of 3 biological replicates, performed across 2 independent experiments. The line on the *y*-axis denotes a threshold level of 1. For further details regarding genes of interest for validation of mRNA-seq analysis, refer to **Appendix 2.1**.

Figure 4.26

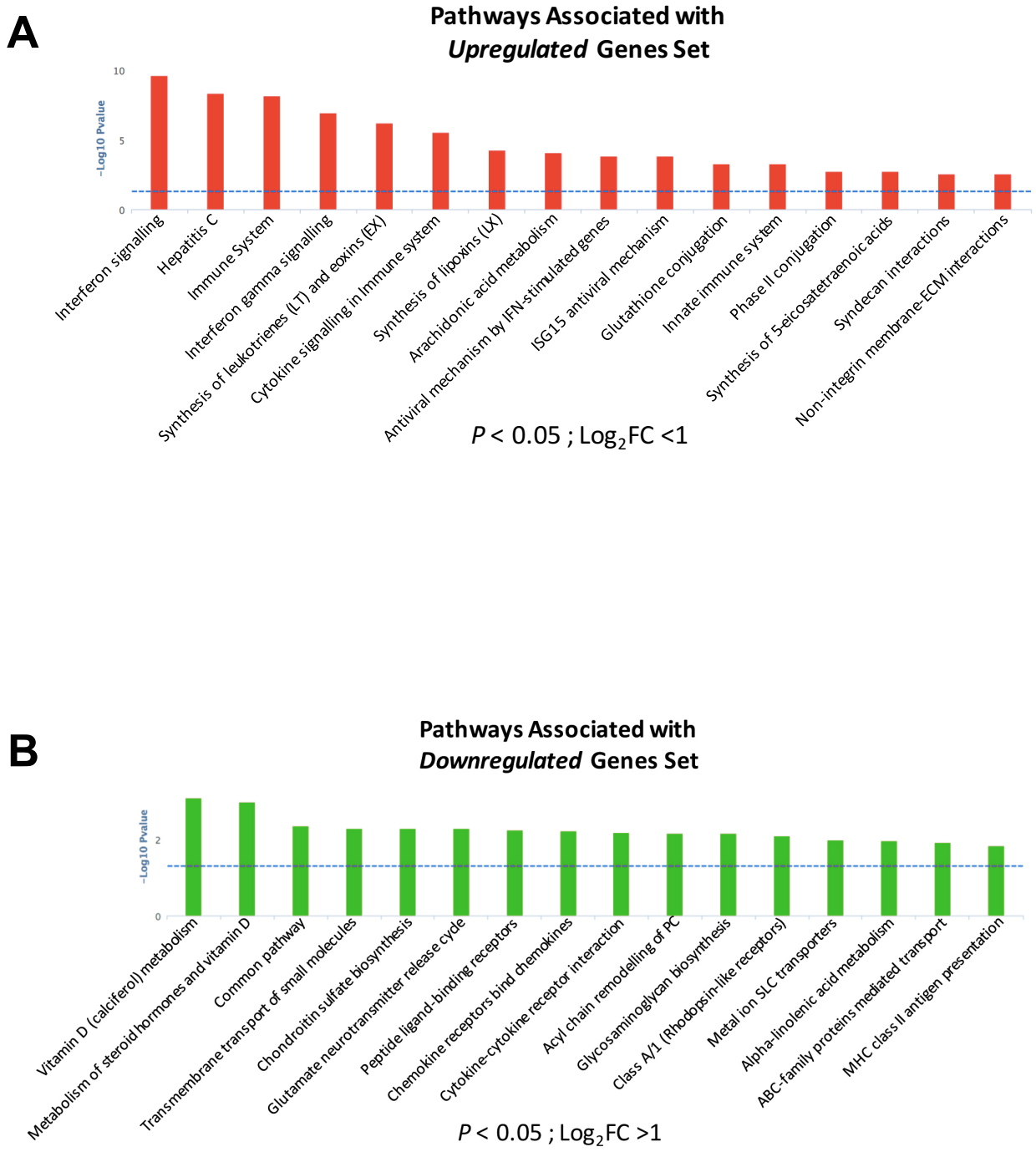


Abbreviations (in alphabetical order):
Apol9b: Apolipoprotein L 9b; *Cd80*: Cluster of differentiation 80; *Cyp4f40*: Cytochrome P450, *Fgf21*: Fibroblast growth factor 21; family 4, subfamily f, polypeptide 40; *Mx2*: MX dynamin like GTPase 2; *Oasl2*: 2'-5'-Oligoadenylate synthetase like; *Rtp4*: Receptor transporter protein 4; *Tgtp1*: T-cell-specific guanine nucleotide triphosphate-binding protein 1; *Tox2*: TOX high mobility group box family member 2; *Zhfx3*: Zinc finger homeobox 3

Figure 4.27 – Pathway enrichment analysis of mRNA-seq data uncovers association of non-canonical pathways in TKI-resistance

Genes significantly differentially-expressed were uploaded onto InnateDB, a gene ontology pathway analysis tool that enables the investigation of pathways significantly enriched. **A** and **B** are plots generated using significantly upregulated and downregulated genes respectively, with their DE inputs indicated in texts underneath graphs. The *y*-axis denotes $-\log_{10}$ of the *P*-value, with dashed blue lines representing a threshold level of significance of $\alpha<0.05$. Values were corrected for multiple testing using the Benjamini-Hochberg method[3]. For further info regarding genes associated with pathways, refer to **Appendix 4.2**.

Figure 4.27


A
Pathways Associated with
Upregulated Genes Set
-Log10 Pvalue
10
5
0
Interferon signalling
Hepatitis C
Immune System
Interferon gamma signalling
Synthesis of leukotrienes (LT) and eoxins (EX)
Cytokine signalling in Immune system
Synthesis of lipoxins (LX)
Arachidonic acid metabolism
Antiviral mechanism by IFN-stimulated genes
ISG15 antiviral mechanism
Glutathione conjugation
Innate immune system
Phase II conjugation
Synthesis of 5-eicosatetraenoic acids
Syndecan interactions
Non-integrin membrane-ECM interactions
P < 0.05 ; Log2FC <1
B
Pathways Associated with
Downregulated Genes Set
-Log10 Pvalue
2
0
Vitamin D (calciferol) metabolism
Metabolism of steroid hormones and vitamin D
Common pathway
Transmembrane transport of small molecules
Chondroitin sulfate biosynthesis
Glutamate neurotransmitter release cycle
Peptide ligand-binding receptors
Chemokine receptors bind chemokines
Cytokine-cytokine receptor interaction
Acyl chain remodelling of PC
Glycosaminoglycan biosynthesis
Class A/1 (Rhodopsin-like receptors)
Metal ion SLC transporters
Alpha-linolenic acid metabolism
ABC-family proteins mediated transport
MHC class II antigen presentation
P < 0.05 ; Log2FC >1

4.4. Discussion

4.4.1. Modelling of *RANBP2-ABL1* Ph-like ALL

Ph-like ALL fusion genes obtained from patient bone marrow samples have enabled modelling of this leukaemic subtype[64,86]. Transduction of *RANBP2-ABL1* resulted in cytokine-independent growth, altering downstream cell survival and proliferative signalling involving Abl-kinase and its downstream partners such as Stat5. This was supported by previous disease modelling in CML where Ba/F3 cells transduced with the *BCR-ABL1* oncogene exhibit cytokine-independent survival capacity[321].

As *RANBP2-ABL1* comprises of a 3' partner that can be targeted using currently available Abl-kinase inhibitors such as imatinib and dasatinib[73,207,315], analysis of dasatinib-sensitivity in Ba/F3 *RANBP2-ABL1* cells indicated similar responses to known sensitive controls KU-812 and K562. Further exploration indicated a reduction in p-Stat5, p-Erk and p-CrkL (known targets of downstream Abl kinase signalling[256,322,323]) and decrease in cell viability when Ba/F3 *RANBP2-ABL1* were treated with the Abl-kinase inhibitors imatinib, dasatinib and ponatinib, but not the Jak inhibitor ruxolitinib.

These data confirmed the specificity of targeting *RANBP2-ABL1* using currently-available Abl kinase inhibitors, which was similar to known responses in CML and Ph+ ALL[129,172]. Ba/F3 *RANBP2-ABL1* cells were subsequently utilised as a model for studies of TKI-resistance in Ph-like ALL.

4.4.2. T315I as a mechanism of imatinib and dasatinib resistance in *RANBP2-ABL1* Ph-like ALL

As Ba/F3 *RANBP2-ABL1* cells can be targeted using currently-available TKIs, and as demonstrated in CML and Ph+ ALL, the development of TKI-resistance is a possibility[92,155,240]. Modelling of imatinib and dasatinib-resistant *RANBP2-ABL1* cells demonstrated a stable expression of Ranbp2-Abl1 kinase signalling, suggesting a possible lack of binding of imatinib and dasatinib to the Ranbp2-Abl1 fusion kinase.

A clinically-significant *ABL1*-T315I mutation (also known as the 'gatekeeper' mutation[174]), was identified in imatinib and dasatinib-resistant Ba/F3 *RANBP2-ABL1* cells. *ABL1*-T315I is highly resistant to most Abl kinase inhibitors, due to the mutation causing a steric hindrance in drug-binding[175,178]. Interestingly, the higher expression of *ABL1*-T315I in dasatinib-resistant cells (100%), compared to imatinib-resistant (60%), suggests that the type of TKI utilised may influence the outcome/likelihood of developing such a mutation. A recent study demonstrated this phenomenon in CML, where the occurrence of *ABL1*-T315I was found to be more common in patients administered dasatinib compared to imatinib as first-line therapy[324]. In a study performed by Soverini *et al*. in 2007, mutations at the 315/317 residue of Abl was also frequently reported (20 out of 45 patients after administration of dasatinib for 12 months) in patients who were treated with dasatinib, to overcome prior imatinib intolerance[325]. As dasatinib was designed to target imatinib-resistant Abl kinase-domain mutations, hypothetically, the acquirement of dasatinib-resistance would require selection for mutants that are highly-resistant, such as the *ABL1*-T315I[172].

The gatekeeper *ABL1*-T315I mutation can, however, be overcome by the third-generation TKI ponatinib. Ponatinib targets the *ABL1*-T315I mutation by negating

the bulky isoleucine residue in Abl, where first and second generation TKIs usually bind[183]. Imatinib and dasatinib-resistant *ABL1*-T315I cells treated with ponatinib demonstrated similar responses to TKI-sensitive controls, comparable to the efficacy observed in preclinical studies, where trough blood concentrations of 40 nM were effective in overcoming kinase-domain mutations in Ph+ leukaemia[181].

4.4.3. Compound mutations as a mechanism of TKI-resistance in cells exposed to ponatinib as secondary therapy

Since ponatinib is currently in use as a secondary therapy in CML and Ph+ ALL[326], imatinib and dasatinib *ABL1*-T315I resistant cell lines were exposed in ponatinib to investigate further resistance mechanisms that may arise. Stable downstream signalling indicated the presence of a possible on-target mechanism of ponatinib resistance, as downstream p-Ranbp2-Abl1 and p-CrkL IC_{50} were increased.

Sanger sequencing revealed the increase in IC_{50} was a result of a compound mutation, *ABL1*-G250E/T315I, that has been observed in Ph+ leukaemia as a possible mechanism of ponatinib resistance[186,327]. Compound mutations result in an alteration of the drug-binding pocket, decreasing TKI sensitivity in cells[328]. In these cells, the increase in p-Ranbp2-Abl1 and p-CrkL IC_{50} confirmed a stable expression of the mutated kinase.

Singularly, the *ABL1*-G250E mutation is located on the ATP-binding loop (P-loop) of the Abl-kinase, a highly-conserved region that interacts with phosphate groups of ATP[159,172,329]. Mutations within the P-loop of the Abl kinase domain are associated with poorer prognosis, resulting in higher rates of mortality (92% of patients with P-loop mutations, compared to 21% of patients with mutations outside the P-loop of *BCR-ABL1* in CML)[330]. Therefore, when simultaneously expressed with the

'gatekeeper' *ABL1*-T315I mutation, the *ABL1*-G250E/T315I compound mutation confers a greater resistance to ponatinib[327].

In dasatinib-resistant *ABL1*-T315I / ponatinib-resistant cells, a previously unreported *ABL1*-L302H/T315I compound mutation was found. Little is known about the *ABL1*-L302H mutation situated adjacent to the SH3 contact region of the Abl kinase[184]. Further alignment of translated *ABL1*-L302H protein sequences using Clustal Omega[331,332] revealed that the *ABL1*-L302H/T315I compound mutation is located in a highly conserved region (this mutation was absent across various species including *Mus musculus*, *Bos taurus* and *Gallus gallus*). The *ABL1*-L302H/T315I mutation was therefore unique to Ba/F3 *RANBP2-ABL1* dasatinib-resistant *ABL1*-T315I/ponatinib-resistant cells and previous studies have demonstrated that a substitution of an amino acid residue within a protein can result in further alteration of its structure and function[333,334]. Histidine is bulkier than leucine (155.2 vs 131.2 g/mol, respectively) and further comparisons between their molecular structures indicate the presence of a non-polar side-chain in leucine (compared to a positively-charged side-chain in histidine), which may provide steric hindrance in ponatinib binding.

Taken together, the development of ponatinib resistance may have been attributed to a clonal selection of cells possessing compound mutations within the *ABL1* kinase domain[327]. This is interesting because sequential Abl TKI therapy has been documented to select for compound drug-resistant Abl kinase-domain mutations that have altered oncogenic potency[335]. In a study by Shah and colleagues, CML patients demonstrating relapse after sequential treatment with Abl-kinase inhibitors (imatinib/nilotinib/dasatinib) were found to harbour compound mutations including the *ABL1*-E255V/V299L, *ABL1*-Y253H/T315I and *ABL1*-M244V/T315I/L364I, which

resulted in oncogenicity when modelled in transformation assays[335].Therefore, using imatinib or dasatinib as first-line TKI therapy, followed by ponatinib, may result in a selection of Abl-kinase domain compound mutations in Ph-like ALL.

4.4.4. Ponatinib as first-line therapy results in genetic aberrations and activation of alternative signalling pathways

To elucidate the mechanisms of resistance that may arise if ponatinib was used as first-line therapy, dose-escalation of TKI-sensitive Ba/F3 *RANBP2-ABL1* cells in ponatinib was performed. These cells demonstrated cross-resistance to other Abl kinase inhibitors (imatinib, nilotinib and dasatinib), suggesting the presence of a kinase-domain mutation[336]. A clinically-relevant *ABL1*-E255K mutation (also shown to be less sensitive to ponatinib in previous studies[328,337]) was identified in ponatinib-resistant Ba/F3 *RANBP2-ABL1* cells.

Interestingly, when TKI-sensitivity of p-Ranbp2-Abl1 was investigated, Western blotting revealed an absence of a detectable band. As *RANBP2-ABL1* mRNA was still expressed in cells, a disruption between the translation of nucleotides to post-translational modification of Ranbp2-Abl1 in ponatinib-resistant cells possibly exists.

A significant deletion in the C-terminus of ponatinib-resistant Ba/F3 *RANBP2-ABL1* cells was found, which may have been a consequence of genetic instability due to long-term ponatinib exposure. Genetic instability resulting in deletions have been documented in therapy-resistant cancer[338] and in the context of ponatinib-resistant Ba/F3 *RANBP2-ABL1* cells, selection of cells harbouring this mutation may have been advantageous for ponatinib-resistant growth.

The effects of a c-terminus deletion in a Ph-like ALL setting is unknown, however, such deletion has been reported in other studies. In *Escherichia coli* (*E. coli*), a C-

terminal deletion in MarR, a multiple antibiotic resistance protein, resulted in an increased efflux of fluoroquinolones (FQ) and ciprofloxacin antibiotics in resistant cells[339,340]. A C-terminal deletion in the breast cancer 1 (*BRCA1*) gene was found to confer cells to platinum and poly(ADP-ribose) polymerase (PARP) inhibitor therapy resistance, by stabilisation of heat shock protein 90 and tumour protein p53[341]. Of importance, in the Abl kinase, the C-terminal region harbours the F-actin domain, which appears to be essential for cell survival and proliferation[342]. Deletion in the C-terminus of Abl has also been postulated to result in reversal of apoptotic suppression of CML cells[343,344], despite conflicting reports[345]. Interestingly, this deletion also conferred a proliferative advantage in CML progenitor cells[343].

Further experiments to elucidate downstream p-Ranbp2-Abl1 in ponatinib-resistant Ba/F3 *RANBP2-ABL1* cells were performed, using p-CrkL analysis. A finding of no significant difference in p-CrkL $IC_{50}^{ponatinib}$ between Ba/F3 *RANBP2-ABL1* DMSO control and ponatinib-resistant cells suggests that an alternative mechanism of resistance may potentially exist[257].

Further investigation using mRNA-seq confirmed a strong correlation of hierarchical clustering between biological replicate samples of Ba/F3 *RANBP2-ABL1* DMSO control and ponatinib-resistant cells, indicating that first-line therapy ponatinib-resistant *RANBP2-ABL1* is genetically distinct from TKI-sensitive control cells. Such distinct differences in genetic pattern between sensitive and resistant lines have been well-described in other settings, including MAPKi-resistant melanoma[346] and chemotherapy (cisplatin/paclitaxel/doxorubicin) resistant ovarian cancer[347]. Further validation of significantly differentially-expressed upregulated and downregulated genes (P<0.05) via RQ-PCR confirmed that the differential expression pipeline utilised was reliable and the data valid for subsequent pathway analysis[348-350].

This includes the upregulation of genes such as *Rtp4* and *Mx2*, which are known to be associated with G protein-coupled receptor[351] and GTPase activity[352,353], respectively. Interestingly, the significant upregulation of *Apol9b*, *Oasl2* and *Tgtp1* – genes associated with antiviral and resistance signalling[354-356] – suggest perhaps an upregulation of a common mechanism between immune-related pathways and cell survival signalling exists. In fact, these genes converge along the interferon (IFN) signalling pathway, which has been associated with the modulation of downstream cell survival mechanisms such as Jak/Stat and MAPK[357-359].

Genes indicated to have downregulated mRNA-seq expression as validated by RQ-PCR includes *Cd80* (also known as B7-1), described as a negative regulator of B-cell proliferation and IgG release in B cell lymphoma[360]. Inhibition of CD80 by anti-CD80 antibody results in the proliferation of T cells when co-cultured with macrophages obtained from pseudo-pregnant mice, in a study performed by Maj *et al*.[361]. Another significantly downregulated gene validated in the mRNA-seq pipeline was *Tox2*, a chromatin-binding protein shown to be methylated and significantly reduced in breast and lung cancer ($p<0.05$), with the administration of decitabine (5-Aza-2-deoxycytidine – a DNA demethylation and epigenetic modifier) shown to reactivate expression of *Tox2*[362].

In addition to *Cd80* and *Tox2*, the genes *Zfhx3*, *Fgf21and Cyp4f40* were also significantly downregulated in ponatinib-resistant cells. *Zfhx3* has been known to transactivate p21 (a potent cell cycle cyclin-dependent kinase inhibitor)[363], and cells with high p21 expression harbour a G_0/quiescent state, according to Spencer *et al*.[364]. Deletions of *Zfhx3* in-combination with phosphatase and tensin homolog (PTEN) have been implicated in the tumorigenesis of prostate cancer[365], while an

impairment of FGF21 signalling (a regulator of glucose metabolism) has been associated with an 'insulin-resistant-like' state in obese mice[366,367].

Little is known about *Cyp4f40*, however in gene ontogeny analysis of murine liver samples, this gene was recently described to be a part of the cytochrome P450 4 (Cyp4) family and potentially involved in the metabolism of xenobiotics and fatty acids[368-370]. Certain anticancer drugs require metabolic activation (i.e. multi-phosphorylative events in the conversion of cytarabine / AraC to its active form AraC-triphosphate in AML therapy) and decrease in drug activation may lead to drug resistance[371,372]. In the context of ponatinib-resistance, decreased expression of *Cyp4f40* has never been described in the literature. Taken together, these downregulated genes may be a consequence of alternative mechanisms associated with genetic instability, leading to ponatinib-resistance in Ba/F3 *RANBP2-ABL1* cells.

Pathway analysis indicated a significant association of pathways related to immune, cytokine and metabolic signalling in the upregulated gene set in the ponatinib-resistant *RANBP2-ABL1* cells, suggesting that these may contribute to TKI-resistance. Cytokines have been shown to be involved in glucocorticoid-resistance (through impairment of glucocorticoid receptor function, by chronic exposure to inflammatory cytokines[373]), implicating signal transduction proteins such as NF-κB, MAPK, Jak and Stat[374]. This finding was interesting because the transcription factor NF-κB has been shown to be fundamentally upregulated in ALL[375], while activation of the cell survival and proliferative signalling pathways MAPK and Jak/Stat have been implicated in leukaemogenesis[376-379]. Upregulation of genes involved in lipid metabolism (arachidonic acid) pathway was another key finding through pathway

analysis, as increased lipid synthesis is known to be key for cells maintaining cancer drug resistance[380,381].

Interestingly, in an analysis of pathways associated with significantly downregulated genes, vitamin D was implicated, through downregulation of *Cubn*, a cotransporter in vitamin metabolism[382,383]. In a recent study, lack of *CUBN* expression in renal cell carcinoma has been associated with poorer outcome[384]. Depletion of vitamin D signalling has also been associated with an increased risk of prostate cancer[385] as vitamin D suppresses the expression of proteins, such as Myc, an important transcription factor for cell survival[386]. Therefore, a decrease in the vitamin D pathway of ponatinib-resistant cells may imply an upregulation in cell survival signalling such as Myc.

A correlation between pathways associated with a decrease of genes related to drug transporters was also uncovered in ponatinib-resistant Ba/F3 *RANBP2-ABL1* cells. This was in contrast to reports of the overexpression of drug efflux transporter ABCB1 in CML, described to be significantly increased prior to the onset of TKI-resistant mutations[387]. In other forms of leukaemia, however, the association between drug transporter protein and treatment resistance may vary, depending on leukaemic subtype and chemotherapeutic regimen applied (i.e. impaired ABCG2 function in vincristine-resistant chronic lymphocytic leukaemia)[388]. The decrease in *ABCB1* transcript levels has also been described in colorectal cancer[389,390], while in prostate cancer, down-regulation of ABC transporter genes were associated with promoter hypermethylation, preventing efflux of intratumoural androgens essential for cancer cell survival[391].

In summary, results in this chapter have confirmed successful modelling and targeting of cells harbouring the *RANBP2-ABL1* fusion using currently-available

TKIs, and that TKI resistance will likely emerge as a clinical concern with TKI therapy (**Figure 4.28**). This chapter has also explored possible mechanisms of resistance, such as the development of an *ABL1*-T315I kinase-domain mutation following imatinib and dasatinib therapy. Although *ABL1*-T315I in this disease setting can be targeted by ponatinib, further compound mutations arose in response, including the clinically-significant *ABL1*-G250E/T315I (cells dose-escalated from imatinib-resistance) and a previously unreported *ABL1*-L302H/T315I (cells dose-escalated from dasatinib-resistance). Importantly, the application of ponatinib as first-line therapy resulted in the acquisition of a clinically-significant *ABL1*-E255K mutation. Ponatinib-resistance as frontline therapy, however, resulted in multiple other alterations, including the loss of Ranbp2-Abl1 function due to the acquirement of a subsequent c-terminal deletion and involvement of alternative signalling mechanisms. Such mechanisms include an upregulation of immune-mediated cell survival signalling pathways and dysregulation of noncanonical metabolic signalling cascades, contributing towards TKI-resistance. As current TKI-therapy in Ph-like ALL seems to be a suitable treatment approach, it is imperative that we understand the possible long-term consequence of such treatment so future resistance can be averted.

THIS PAGE INTENTIONALLY LEFT BLANK.

Figure 4.28

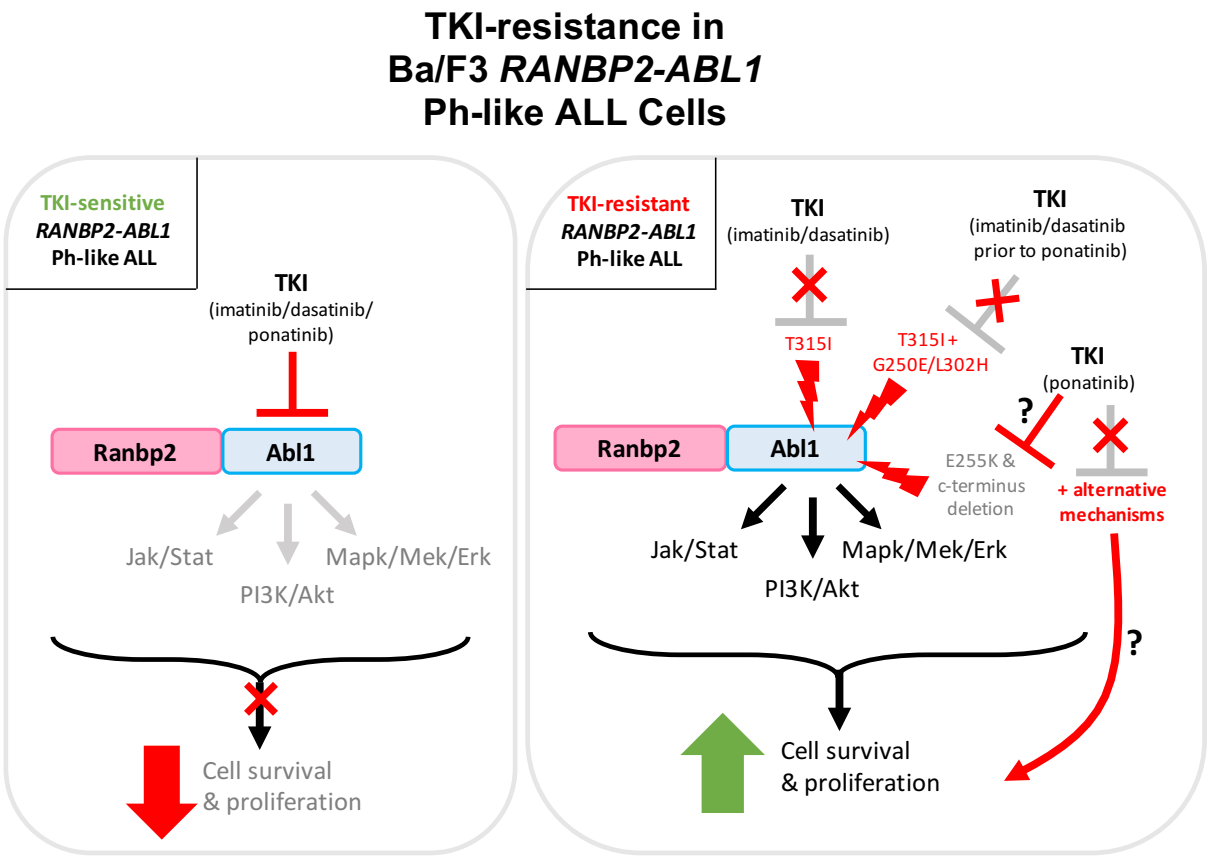


Figure 4.28 – Schematic representations of TKI-resistance in Ba/F3 *RANBP2-ABL1* Ph-like ALL cells

Left: Ba/F3 *RANBP2-ABL1* cells are sensitive to Abl-kinase specific TKIs (i.e. imatinib, dasatinib and ponatinib), where exposure to these TKIs results in an inhibition of downstream Abl-kinase related cell survival and proliferation pathways as previously described. **Right:** In TKI-resistance, the acquisition of point mutations (as represented by the red lightning bolts) varies according to the treatment strategy. In Ba/F3 *RANBP2-ABL1* cells, imatinib/dasatinib use as first-line therapy resulted in the development of an *ABL*-T315I mutation, with secondary dose-escalation in ponatinib leading to the development of a compound mutation (acquisition of an *ABL1*-G250E or novel *ABL1*-L302H in-addition to the pre-existing *ABL1*-T315I mutation). When ponatinib was utilised as first-line therapy, cells developed an *ABL1*-E255K point mutation and c-terminus deletion which may still be amenable to TKI, however, the presence of alternative signalling mechanisms may have possibly overridden this sensitivity, leading to the downstream activation of cell survival and proliferative signals.

THIS PAGE INTENTIONALLY LEFT BLANK.

Appendix 4.1 – mRNA-seq and RQ-PCR readouts of Ba/F3 *RANBP2-ABL1* ponatinib-resistant cells

				mRNAseq Data		RT-qPCR Validation	
Ensembl Gene ID	Symbol	Description	Summary	Log_2 Fold Change (in decreasing order)	Adj.P.Val	$2^{-\Delta\Delta Ct}$ Mean	± SD
ENSMUSG00000033355	***Rtp4***	Receptor Transporter Protein 4	*RTP4* (Receptor Transporter Protein 4) is a Protein Coding gene. Among its related pathways are Signaling by GPCR and Olfactory Signaling Pathway. An important paralog of this gene is *RTP3*. [Source: GeneCards.org] Probable chaperone protein which facilitates trafficking and functional cell surface expression of some G-protein coupled receptors (GPCRs). Promotes functional expression of the bitter taste receptor TAS2R16 (PubMed:16720576). Also promotes functional expression of the opioid receptor heterodimer OPRD1-OPRM1 (By similarity). [Source:UniProtKB/Swiss-Prot]	14.14124399	0.002611938	1100.778662	500.6877346
ENSMUSG00000068246	***Apol9b***	Apolipoprotein L 9b	*Apol9b* transcribes into ApoL9b, an antiviral protein induced by interferon, whose lack of expression in primary neurons likely contributes to the high sensitivity of these cells to viral infection. [Source: Kreit et al., J. Virol. 2014, via NCBI GenBank]	10.29558484	0.001101963	1.625849216	0.438704805
ENSMUSG00000029561	***Oasl2***	2'-5' Oligoadenylate Synthetase-Like 2	Interferon-induced, dsRNA-activated antiviral enzyme which plays a critical role in cellular innate antiviral response. Synthesizes oligomers of 2'-5'-oligoadenylates (2-5A) from ATP which then bind to the inactive monomeric form of ribonuclease L (RNase L) leading to its dimerization and subsequent activation. Activation of RNase L leads to degradation of cellular as well as viral RNA, resulting in the inhibition of protein synthesis, thus terminating viral replication. Can mediate the antiviral effect via the classical RNase L-dependent pathway or an alternative antiviral pathway independent of RNase L. [Source: UniProtKB]	9.581053084	6.76E-06	42.09562093	2.769267617
ENSMUSG00000078922	***Tgtp1***	T-cell-specific Guanine Nucleotide Triphosphate-Binding Protein 1	Involved in innate cell-autonomous resistance to intracellular pathogens, such as Toxoplasma gondii. During avirulent type II T. gondii infection, recruited to the parasitophorous vacuole (PV) membrane, leading to PV vesiculation and rupture, and subsequent digestion of the parasite within the cytosol (PubMed:19265156, PubMed:24563254). Not recruited to virulent type I T. gondii PV membrane (PubMed:19265156). May confer an antiviral state for vesicular stomatitis virus (PubMed:9725230). [Source: UniProtKB]	9.440190958	0.001582979	79.6591828	71.58954785
ENSMUSG00000023341	***Mx2***	Myxovirus Dynamin Like GTPase 2	The protein encoded by this gene has a nuclear and a cytoplasmic form and is a member of both the dynamin family and the family of large GTPases. The nuclear form is localized in a granular pattern in the heterochromatin region beneath the nuclear envelope. A nuclear localization signal (NLS) is present at the amino terminal end of the nuclear form but is lacking in the cytoplasmic form due to use of an alternate translation start codon. This protein is upregulated by interferon-alpha but does not contain the antiviral activity of a similar myxovirus resistance protein 1. [provided by RefSeq, Jul 2008]	9.311119012	0.00331994	359.6727268	426.2085245
ENSMUSG00000075122	***Cd80***	Cluster of Differentiation 80	The protein encoded by this gene is a membrane receptor that is activated by the binding of CD28 or CTLA-4. The activated protein induces T-cell proliferation and cytokine production. This protein can act as a receptor for adenovirus subgroup B and may play a role in lupus neuropathy. [provided by RefSeq, Aug 2011]	-4.570263817	0.000377895	0.053576139	0.020976075
ENSMUSG00000074607	***Tox2***	TOX High Mobility Group Box Family Member 2	*TOX2* (TOX High Mobility Group Box Family Member 2) is a Protein Coding gene. GO annotations related to this gene include chromatin binding and RNA polymerase II transcription factor binding. An important paralog of this gene is *TOX*. [Source: GeneCards.org]	-5.210184633	0.013321983	0.466583315	0.167317092
ENSMUSG00000038872	***Zfhx3***	Zinc Finger Homeobox 3	This gene encodes a transcription factor with multiple homeodomains and zinc finger motifs, and regulates myogenic and neuronal differentiation. The encoded protein suppresses expression of the alpha-fetoprotein gene by binding to an AT-rich enhancer motif. The protein has also been shown to negatively regulate c-Myb, and transactivate the cell cycle inhibitor cyclin-dependent kinase inhibitor 1A (also known as p21CIP1). This gene is reported to function as a tumor suppressor in several cancers, and sequence variants of this gene are also associated with atrial fibrillation. Multiple transcript variants expressed from alternate promoters and encoding different isoforms have been found for this gene. [provided by RefSeq, Sep 2009]	-5.317844695	0.003191297	0.574130691	0.209721819
ENSMUSG00000030827	***Fgf21***	Fibroblast Growth Factor 21	This gene encodes a member of the fibroblast growth factor (FGF) family. FGF family members possess broad mitogenic and cell survival activities and are involved in a variety of biological processes. This protein is a secreted endocrine factor that functions as a major metabolic regulator. The encoded protein stimulates the uptake of glucose in adipose tissue. [provided by RefSeq, Mar 2016]	-5.373194579	9.66E-05	0.01102354	0.001476664
ENSMUSG00000090700	***Cyp4f40***	Cytochrome P450, Family 4, Subfamily F, Polypeptide 40	Cyp4f40 has been shown to enable monooxygenase activity, fatty acid binding, iron (heme/metal) ion binding and oxidoreductase activity (via acting on paired donors, with incorporation or reduction of molecular oxygen - NAD(P)H as one donor and the incorporation of one atom of oxygen). Cyp4f40 has also been suggested to be involved in fatty acid metabolism, menaquinone, phylloquinone and vitamin K catabolisms, as well as oxidation-reduction processes intracellularly. [Source: EMBL-EBI GO annotations]	-6.960164577	0.004830614	0.560122924	0.471716791

Appendix 4.2A – Upregulated gene set in Ba/F3 *RANBP2-ABL1* ponatinib-resistant line

Pathway Name	Pathway ID	Source Name	Organism	Pathway uploaded gene count	Genes in InnateDB for this entity	Pathway p-value	Adj. pathway p-value	Gene Symbols
Interferon Signaling	18616	REACTOME	10090	12	72	2.50E-10	7.28E-08	*Gbp2; Ifit1; Irf7; Irf9; Isg15; Oas1a; Oas2; Oas3; Oasl1; Sp100; Ube2l6; Usp18;*
Hepatitis C	10396	KEGG	10090	14	135	4.84E-09	7.05E-07	*Ddx58; Eif2ak2; Gm14446; Ifit1; Irf7; Irf9; Ldlr; Oas1a; Oas1b; Oas1g; Oas2; Oas3; Stat1; Stat2;*
Immune System	17702	REACTOME	10090	35	884	6.99E-09	6.78E-07	*C8g; Cd247; Cd3g; Cfb; Ddx58; Dnm1; Dtx3l; Fbxo27; Fcer1a; Gbp2; Ifit1; Irf7; Irf9; Isg15; Kif5a; Lat2; Map3k8; Nlrp3; Oas1a; Oas2; Oas3; Oasl1; P2rx7; Psmb9; Psme2b-ps; Rap1gap2; Siglec5; Sp100; Tapbp; Tlr12; Trex1; Txk; Ube2l6; Usp18; Zbp1;*
Interferon gamma signaling	18614	REACTOME	10090	8	43	1.13E-07	8.24E-06	*Gbp2; Irf7; Irf9; Oas1a; Oas2; Oas3; Oasl1; Sp100;*
Synthesis of Leukotrienes (LT) and Eoxins (EX)	19815	REACTOME	10090	5	13	5.84E-07	3.40E-05	*Alox15; Alox5; Alox5ap; Cyp4f18; Ptgr1;*
Cytokine Signaling in Immune system	17370	REACTOME	10090	13	194	2.92E-06	1.42E-04	*Gbp2; Ifit1; Irf7; Irf9; Isg15; Map3k8; Oas1a; Oas2; Oas3; Oasl1; Sp100; Ube2l6; Usp18;*
Synthesis of Lipoxins (LX)	18447	REACTOME	10090	3	6	5.20E-05	0.002161851	*Alox5; Alox5ap; Ptgr1;*
Arachidonic acid metabolism	19749	REACTOME	10090	6	53	8.95E-05	0.003256818	*Alox15; Alox5; Alox5ap; Cyp4f18; Ephx2; Ptgr1;*
Antiviral mechanism by IFN-stimulated genes	17667	REACTOME	10090	4	20	1.49E-04	0.004342894	*Ifit1; Isg15; Ube2l6; Usp18;*
ISG15 antiviral mechanism	17669	REACTOME	10090	4	20	1.49E-04	0.004342894	*Ifit1; Isg15; Ube2l6; Usp18;*
Glutathione conjugation	18170	REACTOME	10090	4	27	5.01E-04	0.013257335	*Gsta3; Gstm1; Gstt1; Mgst3;*
Innate Immune System	16733	REACTOME	10090	16	450	5.16E-04	0.012508442	*C8g; Cd247; Cd3g; Cfb; Ddx58; Dnm1; Fcer1a; Irf7; Lat2; Nlrp3; P2rx7; Siglec5; Tlr12; Trex1; Txk; Zbp1;*
Phase II conjugation	17330	REACTOME	10090	5	63	0.001825447	0.040861925	*Gsta3; Gstm1; Gstt1; Mgst3; Papss2;*
Synthesis of 5-eicosatetraenoic acids	19138	REACTOME	10090	2	5	0.001892844	0.03934412	*Alox5; Alox5ap;*
Syndecan interactions	16738	REACTOME	10090	3	21	0.002965754	0.05753563	*Cask; Col5a1; Itgb3;*
Non-integrin membrane-ECM interactions	19127	REACTOME	10090	4	43	0.002965813	0.053940724	*Agrn; Cask; Col5a1; Itgb3;*

Appendix 4.2B – Downregulated gene set in Ba/F3 *RANBP2-ABL1* ponatinib-resistant line

Pathway Name	Pathway ID	Source Name	Organism	Pathway uploaded gene count	Genes in InnateDB for this entity	Pathway p-value	Adj. pathway p-value	Gene Symbols
Vitamin D (calciferol) metabolism	17442	REACTOME	10090	2	7	8.22E-04	0.104357142	*Cubn; Lgmn;*
Metabolism of steroid hormones and vitamin D	19620	REACTOME	10090	3	32	0.001068592	0.06785558	*Cubn; Hsd3b4; Lgmn;*
Common Pathway	19351	REACTOME	10090	2	16	0.004525678	0.191587049	*F5; Pros1;*
Transmembrane transport of small molecules	18857	REACTOME	10090	9	518	0.005088885	0.161572109	*Abca4; Abcb1b; Ano10; Casq1; Cp; Lcn2; Slc11a1; Slc1a1; Slc29a1;*
Chondroitin sulfate biosynthesis	19160	REACTOME	10090	2	17	0.005108199	0.10812355	*Chst15; Csgalnact1;*
Glutamate Neurotransmitter Release Cycle	19545	REACTOME	10090	2	17	0.005108199	0.10812355	*Bzrap1; Slc1a1;*
Peptide ligand-binding receptors	18683	REACTOME	10090	5	181	0.005747442	0.104275015	*Ccl3; Ccl4; Ccr7; Mc5r; Oprl1;*
Chemokine receptors bind chemokines	19018	REACTOME	10090	3	58	0.005914232	0.093888427	*Ccl3; Ccl4; Ccr7;*
Cytokine-cytokine receptor interaction	604	KEGG	10090	6	264	0.006425773	0.090674795	*Ccl3; Ccl4; Ccr7; Il12rb2; Il21r; Lta;*
Acyl chain remodelling of PC	16891	REACTOME	10090	2	20	0.007049636	0.081391247	*Pla2g4f; Plb1;*
Glycosaminoglycan biosynthesis	706	KEGG	10090	2	20	0.007049636	0.081391247	*Chst15; Csgalnact1;*
Class A/1 (Rhodopsin-like receptors)	17050	REACTOME	10090	6	277	0.008070018	0.085407693	*Ccl3; Ccl4; Ccr7; Gpr55; Mc5r; Oprl1;*
Metal ion SLC transporters	19686	REACTOME	10090	2	24	0.010075007	0.098425069	*Cp; Slc11a1;*
alpha-Linolenic acid metabolism	742	KEGG	10090	2	25	0.010906623	0.098938653	*Pla2g4f; Plb1;*
ABC-family proteins mediated transport	19283	REACTOME	10090	2	26	0.011767548	0.099631908	*Abca4; Abcb1b;*
MHC class II antigen presentation	18215	REACTOME	10090	3	80	0.014272626	0.113288969	*Cd74; Dync2li1; Lgmn;*

THIS PAGE INTENTIONALLY LEFT BLANK.

CHAPTER 5 –

TKI-RESISTANCE IN A *SSBP2-CSF1R* CELL LINE IS ATTRIBUTABLE TO AN ACCUMULATION OF GENETIC ALTERATIONS

5.1. Introduction

The identification of genomic alterations in Ph-like ALL has enabled the anecdotal application of targeted TKI therapies, alongside administration of existing chemotherapeutic approaches in anecdotal cases[90,91]. As previously described in **Chapter 4**, Abl-kinase inhibitors are known to be effective in treating Ph+ ALL and Ph-like ALL cells in patients harbouring Abl-class fusion genes[14,64,86]. Despite the effectiveness of such therapies, TKI-resistance remains a leading cause of clinical relapse[92,128,155]. Abl-kinase inhibitors are known to target not only Abl, but also other kinases with similar homology such as PDGFR[392-394], c-kit[395] and c-fms (also known as macrophage colony-stimulating factor receptor – M-CSFR/CSF1R)[396,397].

SSBP2-CSF1R is a recurring fusion gene identified in a subset of high-risk B-ALL patients in various age groups[69,73,398]. *SSBP2* encodes the single-strand DNA binding protein 2, a tumour suppressor that regulates the growth and differentiation of myeloid cells. An absence of Ssbp2 protein expression has been implicated in AML, where an inducible re-expression was found to result in cellular differentiation[399]. *CSF1R* encodes the macrophage colony stimulating factor 1 receptor (also known as c-fms), which is activated upon binding to its ligand CSF1/M-CSF and IL-34, essential in the developmental lineage of mononuclear phagocytes[400-402].

The Abl kinase imatinib was first described to be effective against CSF1R (c-fms) at therapeutically effective concentrations, by Dewar *et al*. in 2005[396]. The Abl-kinase inhibitors known to target CSF1R include imatinib and dasatinib[403-405], and studies have demonstrated the efficacy of these inhibitors in alterations such as *MEF2D-CSF1R*[406], *RBM6-CSF1R*[407] and *SSBP2-CSF1R*[73].

In recent studies, murine Ba/F3 pro-B and Arf-/- pre-B cells transduced with *SSBP2-CSF1R* (5q14.1; 5q32) in-combination with IK6 (a dominant negative isoform of Ikaros commonly found in Ph-like ALL) resulted in a transformation of cells through cytokine-independent growth (IL-3-independent in Ba/F3 and IL-7-independent in Arf-/-)[12,20,205]. In-addition to an induction of leukaemogenesis *in vitro* and *in vivo*, the Ssbp2-Csf1r fusion kinase was also identified to be sensitive to the Abl-kinase inhibitor dasatinib, resulting in a reduction in spleen size of mice engrafted with patient-derived xenografts (dasatinib-treated: 156.2 ± 12.2 mg; vehicle: 430.0 ± 40.2 mg –daily oral administration of 20 mg/kg dasatinib)[205].

However, despite such promising outcomes, imatinib-resistance has been documented in FDC-P1 mouse bone marrow cells harbouring the *CSF1R*-D802V point mutation[408,409]. In these experiments, cells harbouring this point mutation were highly resistant to imatinib ($IC_{50}^{imatinib}$: >10 μM) compared to cells harbouring wildtype *CSF1R* ($IC_{50}^{imatinib}$: ~0.5 μM). Therefore, in this chapter, the *SSBP2-CSF1R* Ph-like ALL fusion was modelled in Ba/F3 pro-B cells to further elucidate whether TKI resistance is likely, and associated with any genetic alterations within *SSBP2-CSF1R*.

5.2. Approach

A Ba/F3 cell line expressing the *SSBP2-CSF1R* fusion gene was generated according to methods as described in **Chapter 4** (sub-cloning of the fusion gene into the pRuf-iG2 retroviral vector, followed by transfection and transduction into Ba/F3 parental cells). Expression of *SSBP2-CSF1R* was confirmed by DNA and protein analysis. Annexin-V/7-AAD flow cytometry and phosphoflow analysis were utilised to verify TKI-sensitivity.

TKI-resistance was generated by exposure of cells to incrementally increasing concentrations[211] of imatinib and dasatinib (first and second-generation Abl-kinase inhibitors, respectively) to a final concentration of 10 μM imatinib or 200 nM dasatinib in culture. TKI-tolerance was confirmed using drug-sensitivity assays as previously mentioned (Annexin-V/7-AAD and western blotting of phospho-proteins). In addition, Sanger sequencing was employed to further identify any alterations within the *SSBP2-CSF1R* kinase domain.

5.3. Results

5.3.1. Ba/F3 cells transduced with *SSBP2-CSF1R* demonstrate kinase-independent survival capacity

Successful isolation of the *SSBP2-CSF1R* Ph-like ALL fusion gene from the pCR®-Blunt II-TOPO® vector (**Figure 5.1A**) and excision of the recipient pRuf-iG2 retroviral construct (**Figure 5.1B**) allowed for subsequent ligation and generation of pRuf-iG2 *SSBP2-CSF1R* constructs. Following molecular cloning, transformation of DH5α competent cells indicated that five bacterial colonies (#2, 5, 10, 13 and 14) were found to contain *SSBP2-CSF1R* in its correct orientation and size (**Figure 5.2)**.

The generation of viral particles via transfection of HEK-293T cells confirmed cells were successfully producing GFP positivity, via microscopy (**Figure 5.3A**) and flow cytometry (**Figure 5.3B & C**), with a transfection efficiency of 92.1% in cells transfected with pRuf-iG2 empty vector and 77.3% in cells transfected with pRuf-iG2 *SSBP2-CSF1R*. Produced viral particles placed onto Ba/F3 parental wild-type cells resulted in successful transduction (**Figure 5.4**). FACS sorting of GFP+ Ba/F3 cells (**Figure 5.4B**, based on the strategy indicated in **Figure 5.4A**) confirmed a GFP expression of 14.4% in Ba/F3 cells transduced with pRuf-iG2 empty vector control, and 29.0% in cells transduced with pRuf-iG2 *SSBP2-CSF1R*. Importantly, collection and culturing (37ºC/5% CO_2) of GFP+ cells confirmed a retention of GFP expression and incorporation of constructs into the genome (**Figure 5.4C**), where Ba/F3 pRuf-iG2 empty vector cells were 94.4% GFP+ and Ba/F3 pRuf-iG2 *SSBP2-CSF1R* cells 97.7% GFP+ as confirmed by flow cytometric analysis. This data was further supported by fluorescence microscopy, where GFP positivity was observed in transduced cells (**Figure 5.4D**).

Using primers specific for the breakpoint region[64] in a cDNA PCR reaction, DNA gel electrophoresis of PCR products indicated a presence of the *SSBP2-CSF1R* fusion in cells transduced with pRuf-iG2 *SSBP2-CSF1R* (**Figure 5.5A**). This band was at a similar size as the positive control (TOPO-*SSBP2-CSF1R*), and Ba/F3 parental and pRuf-iG2 vector control cells did not contain *SSBP2-CSF1R*. Western blotting confirmed expression of Ssbp2-Csf1r in the transduced Ba/F3 *SSBP2-CSF1R* cells. The estimated molecular weight of the Ssbp2-Csf1r fusion protein is ~91 kDa (**Figure 5.5B**).

In **Figure 5.6**, Ba/F3 parental (non-transduced control), pRuf-iG2 empty vector control (cells that have undergone the transduction process) and pRuf-iG2 *SSBP2-CSF1R* cells were cultured in the absence of cytokine (IL-3) over 3 days. Results indicated that cells containing *SSBP2-CSF1R* remained viable in IL-3-free culture following 3-day incubation, maintaining an average viability of 92.2% (SD $\pm$ 3.2%), compared to that of Ba/F3 parental wild-type control (27.4% $\pm$ 10.4%; $P<0.05$), and pRuf-iG2 empty vector control (31.7% $\pm$ 18.0%) (**Figure 5.6A**). Ba/F3 *SSBP2-CSF1R* cells were also proliferating, resulting in a live cell density of 14.9 $\pm$ 1.6 x 10^5/ml on day 3 (72h) compared to control cells, that did not proliferate in the absence of IL-3 (parental control: 0.7 $\pm$ 0.5 x 10^5/ml, $P<0.005$; empty vector cells: 0.7 $\pm$ 0.5 x 10^5/ml, $P<0.005$) (**Figure 5.6B**).

Figure 5.1

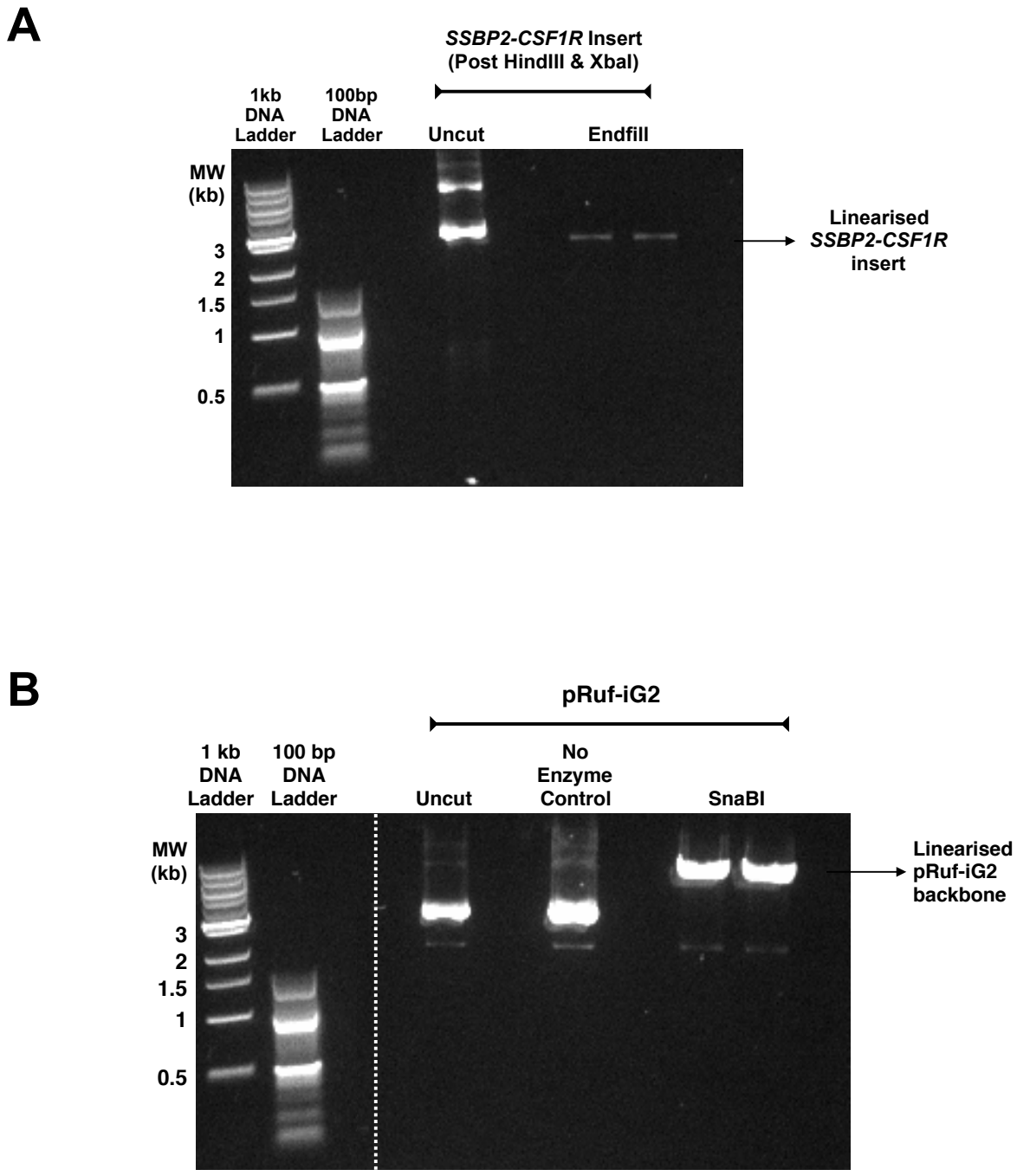


Figure 5.1 – Isolation of *SSBP2-CSF1R* fusion gene from pCR®-Blunt II-TOPO® plasmids

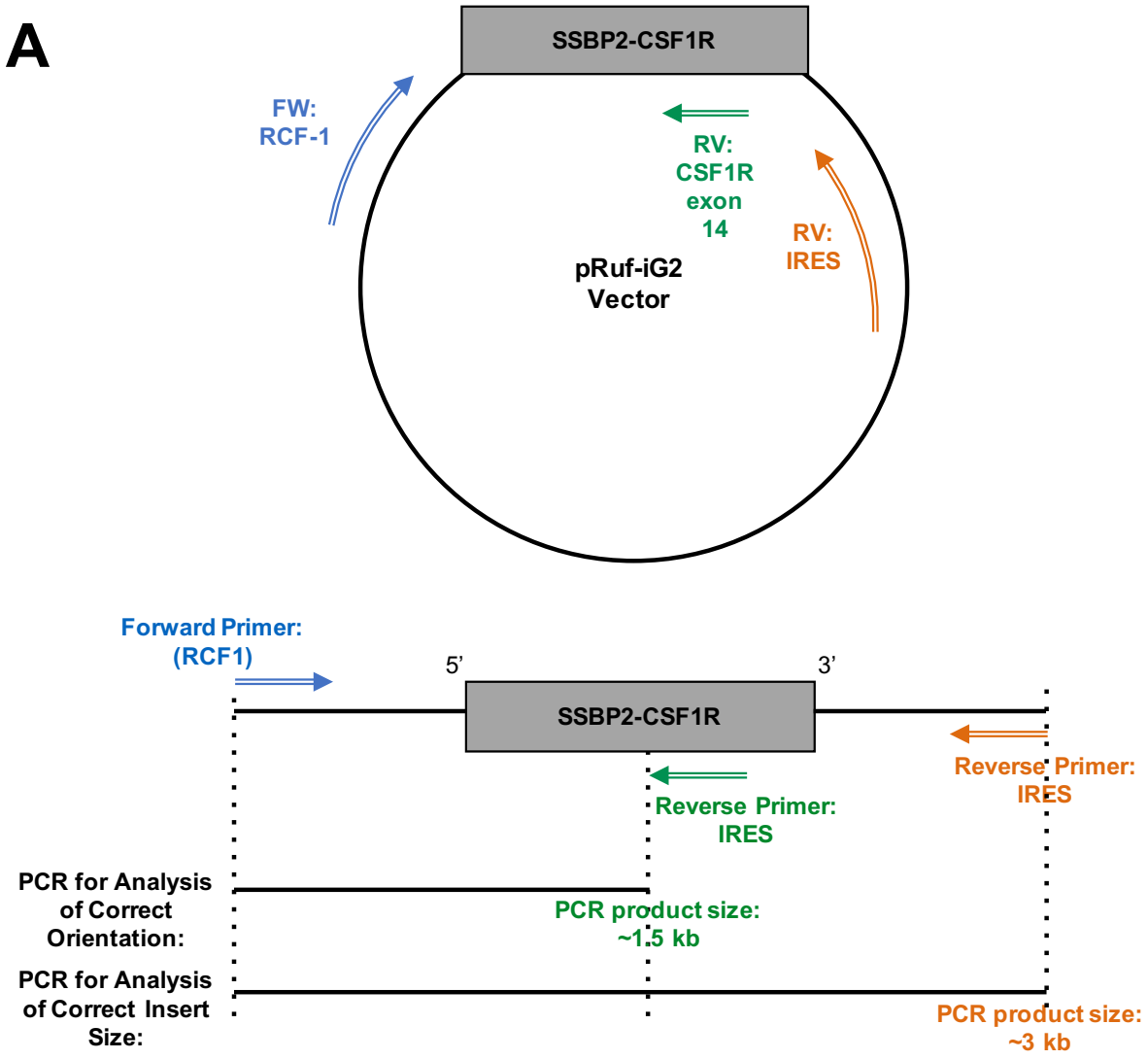
DNA agarose gels of restriction digestion products. **A**: pCR®-Blunt II-TOPO® *SSBP2-CSF1R* double-digested with HindIII and XbaI, with the arrow indicating the linearised insert in the 'endfill' lanes. **B**: Restriction digest and linearisation of the host retroviral vector pRuf-iG2 using SnaBI, an endonuclease resulting in a blunt-ended product.

THIS PAGE INTENTIONALLY LEFT BLANK.

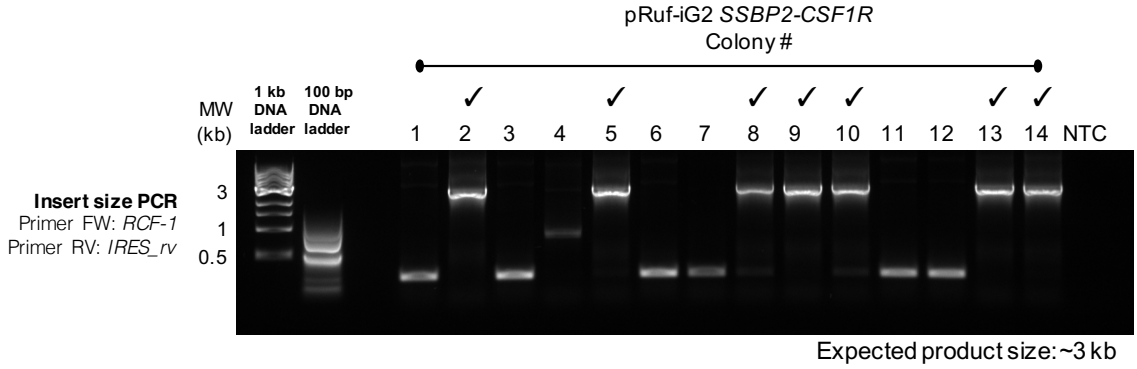
Figure 5.2 – Confirmation of molecularly-cloned *SSBP2-CSF1R* Ph-like ALL fusion gene in pRuf-iG2 retroviral vector

A: PCR strategy for confirmation of *SSBP2-CSF1R* insert size and direction in the pRuf-iG2 retroviral vector, using primers as indicated. **B**: Confirmation of transformed DH5α colonies containing the correct insert size of *SSBP2-CSF1R* in the pRuf-iG2 vector, using primers specific for the cloning region. Tick marks indicate plasmids containing inserts with an expected size of 3 kb. **C:** Confirmation of colonies expressing *SSBP2-CSF1R* in the correct orientation/direction (5' – 3'). Tick marks indicate plasmids containing inserts with the correct orientation (1.5 kb from 5' start site to *CSF1R* breakpoint region). MW: molecular weight; NTC: no template control

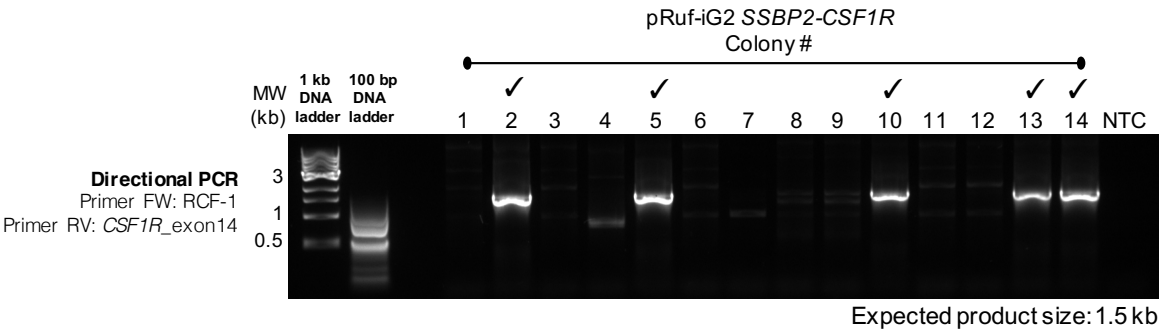
Figure 5.2


A
SSBP2-CSF1R
FW:
RCF-1
RV:
CSF1R
exon
14
RV:
IRES
pRuf-iG2
Vector
Forward Primer:
(RCF1)
5'
3'
SSBP2-CSF1R
Reverse Primer:
IRES
Reverse Primer:
IRES
PCR for Analysis
of Correct
Orientation:
PCR product size:
~1.5 kb
PCR for Analysis
of Correct Insert
Size:
PCR product size:
~3 kb

B Confirmation of Insert Size



C Confirmation of *SSBP2-CSF1R* Orientation

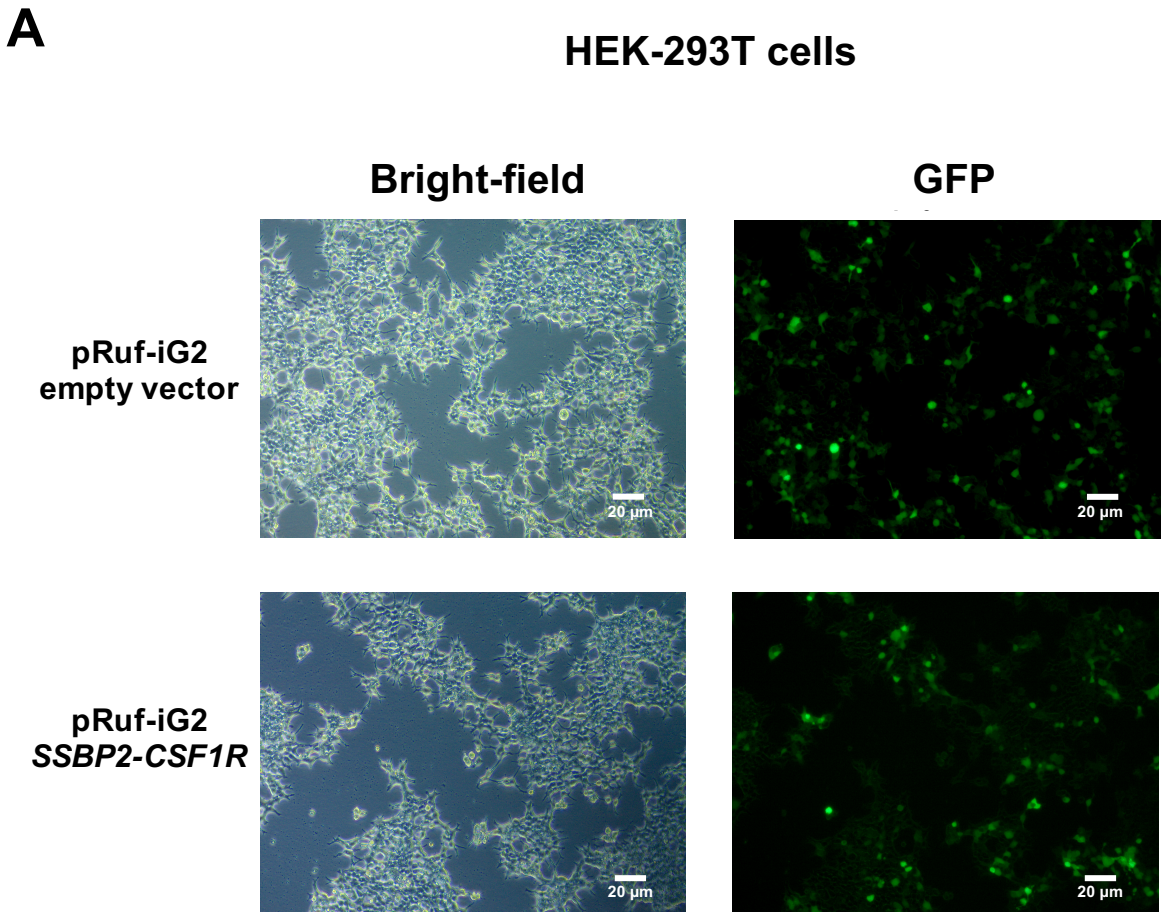


THIS PAGE INTENTIONALLY LEFT BLANK.

Figure 5.3 – GFP expression in HEK-293T cells transfected with pRuf-iG2 constructs

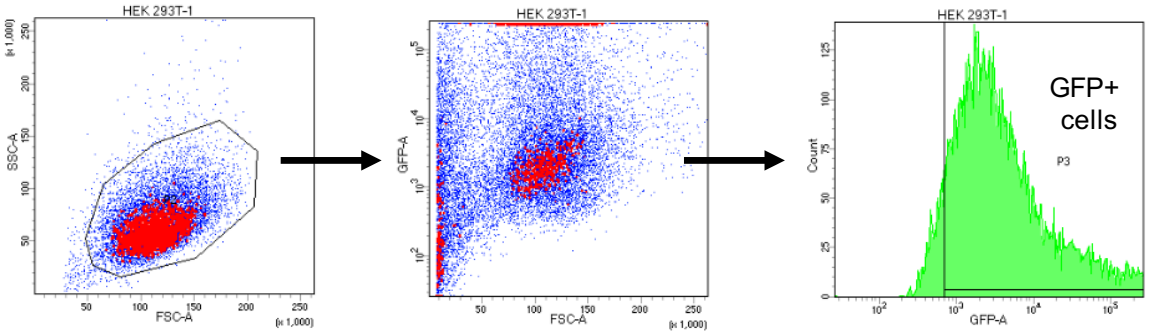
A: Bright-field and GFP microscopy images of HEK-293T cells transfected with pRuf-iG2 empty vector control and pRuf-iG2 *SSBP2-CSF1R*. Images were obtained 24h post-transfection. Scale bar represents 20 μm. **B:** Flow cytometry gating strategy utilised to analyse percentage of GFP+ in HEK-293T cells, quantifying transfection efficiency. This data is representative of cells transfected with the pRuf-iG2 empty vector. **C**: Left to right – Percentage of GFP+ cells in untransfected HEK-293T, cells transfected with pRuf-iG2 empty vector and cells transfected with pRuf-iG2 *SSBP2-CSF1R*.

Figure 5.3


A
HEK-293T cells
Bright-field
GFP
pRuf-iG2
empty vector
pRuf-iG2
SSBP2-CSF1R
20 µm
20 µm
20 µm
20 µm

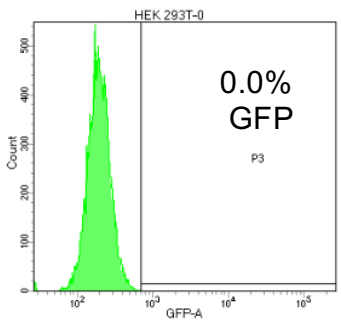
B FACS gating strategy

HEK-293T
pRuf-iG2 empty vector

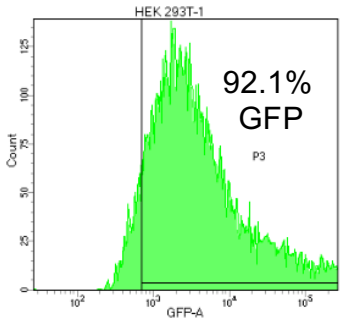


C GFP expression in cells

HEK-293T



HEK-293T
pRuf-iG2
empty vector



HEK-293T
pRuf-iG2
SSBP2-CSF1R

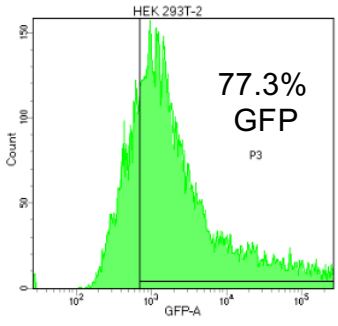


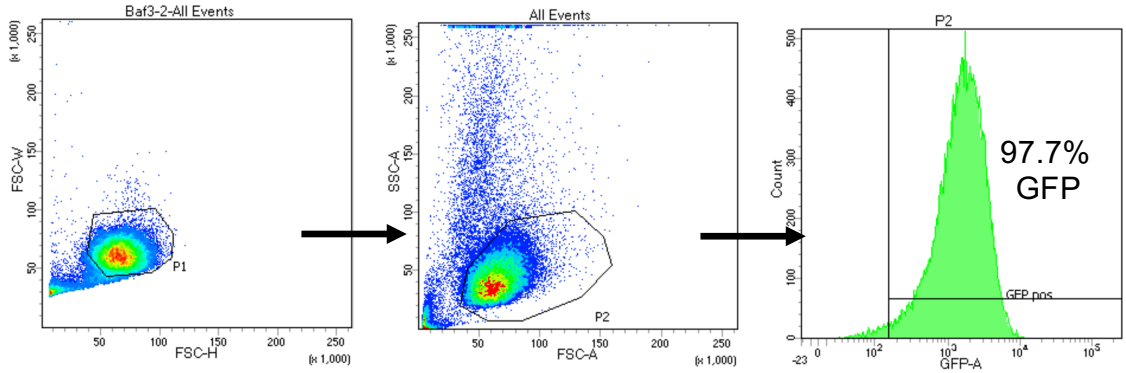
Figure 5.4 – GFP positivity of Ba/F3 cells successfully transduced with pRuf-iG2 *SSBP2-CSF1R*

Ba/F3 cells were analysed and sorted using the BD FACS Aria®, 3 days post-transduction. Expression of GFP indicates the integration of retroviral constructs into the genome. **A**: Gating strategy for sorting of GFP+ cells, indicating forward and side scatter plots with polygon gates drawn around the population of interest, and histogram quantifying the percentage of GFP positive cells. Data shown is for Ba/F3 pRuf-iG2 *SSBP2-CSF1R* cells. **B**: Flow cytometric analysis of Ba/F3 cells at 3 days post-transduction (blue peaks). **C**: Flow cytometric analysis of Ba/F3 cells at 3 days post-sort (green peaks), to confirm the stability of GFP expression. **D**: Bright-field and GFP microscopy images of transduced Ba/F3 cells 3 days post-sort, using a 40x objective. Scale bar represents 10 μm.

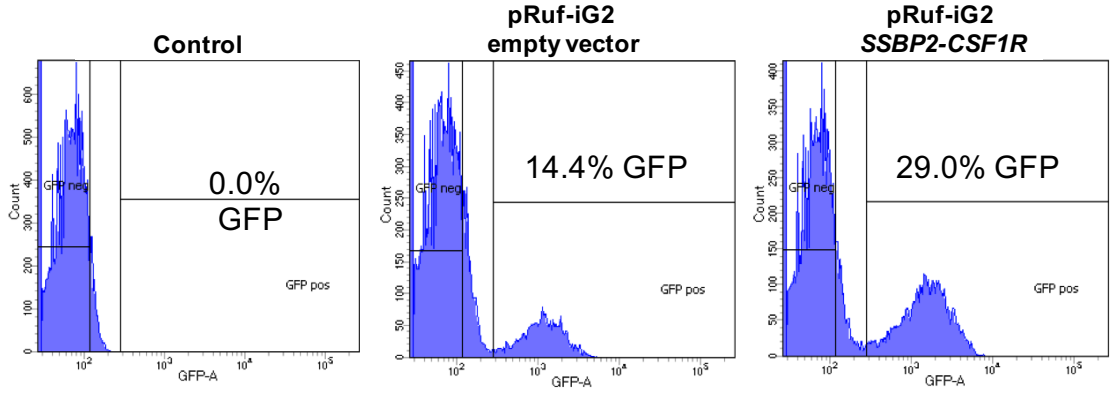
Figure 5.4

A **FACS gating strategy**

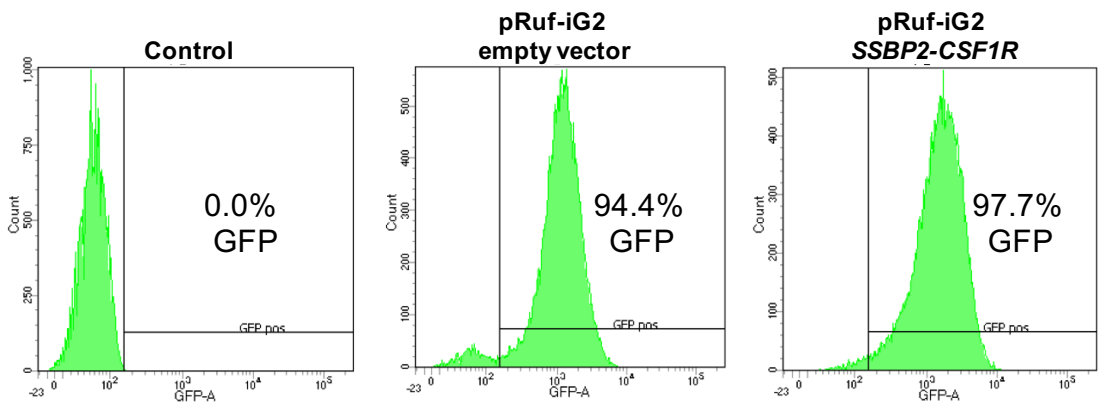
Ba/F3
pRuf-iG2_*SSBP2-CSF1R*



B **GFP expression, 3 days post-transduction**



C **GFP expression, 3 days post-sort**



THIS PAGE INTENTIONALLY LEFT BLANK.

D

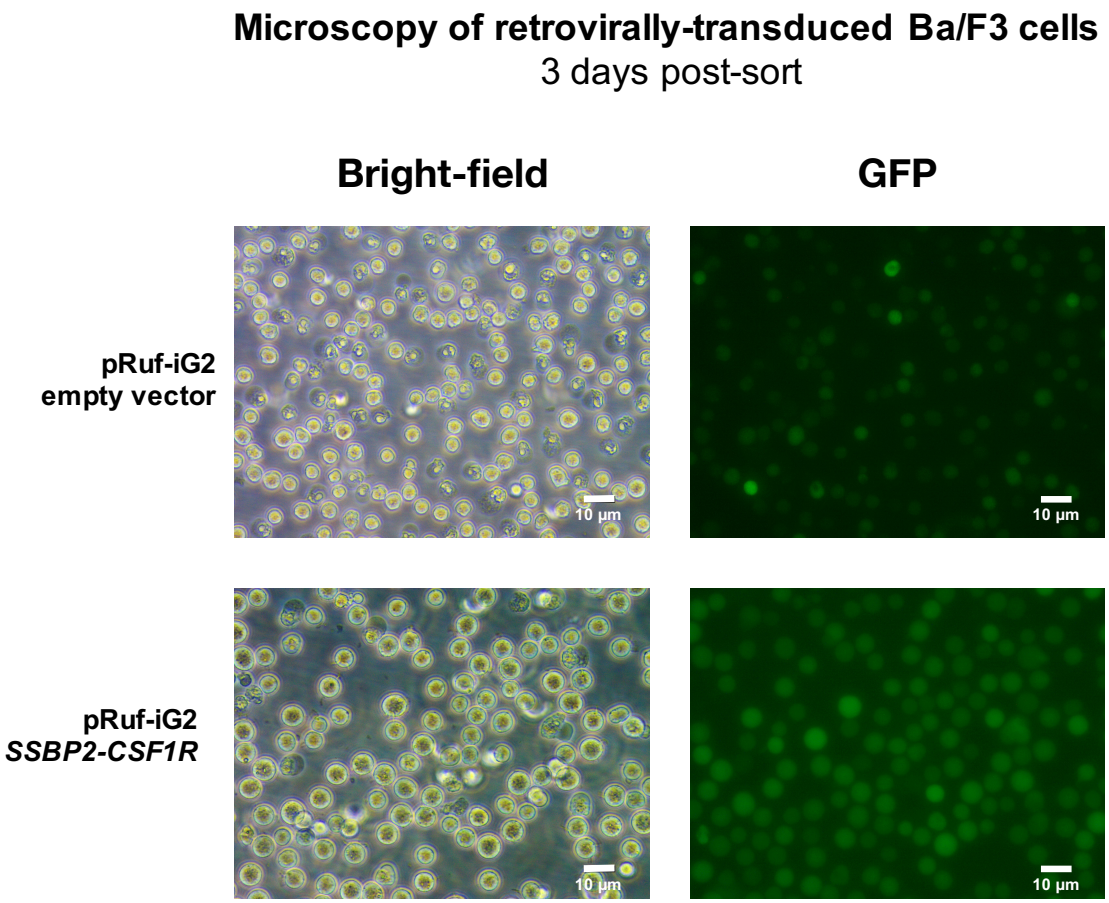
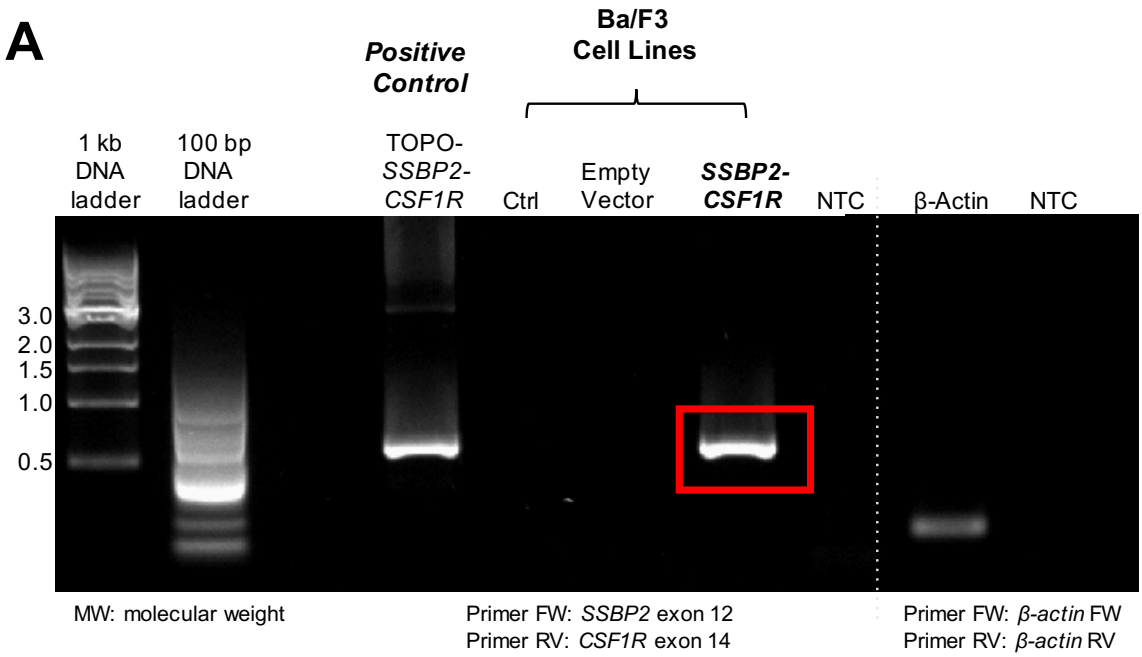

Microscopy of retrovirally-transduced Ba/F3 cells
3 days post-sort
Bright-field
GFP
pRuf-iG2
empty vector
pRuf-iG2
SSBP2-CSF1R
10 µm
10 µm
10 µm
10 µm

Figure 5.5 – Ba/F3 cells transduced with pRuf-iG2 *SSBP2-CSF1R* expresses both the fusion gene and the protein.

A: Gel electrophoresis of PCR products from pCR®-Blunt II-TOPO® plasmid, Ba/F3 parental control, Ba/F3 cells transduced with pRuf-iG2 empty vector and Ba/F3 cells transduced with pRuf-iG2 *SSBP2-CSF1R*, using primers specific for the fusion kinase. Red rectangle highlights the presence of the *SSBP2-CSF1R* fusion gene in Ba/F3 pRuf-iG2 *SSBP2-CSF1R* cells. MW: molecular weight marker. NTC: no template control. **B**: Western blot detection of the Ssbp2-Csf1r fusion protein (~91 kDa) in cell lysates from Ba/F3 cells transduced with *SSBP2-CSF1R*. PVDF membranes were incubated in antibodies specific for M-CSFR (CSF1R) and β-tubulin. Densitometry analysis of Ssbp2-Csf1r fusion protein compared to β-tubulin loading control across all samples is represented graphically underneath. A marked expression of the Ssbp2-Csf1r protein can be seen in cells transduced with pRuf-iG2 *SSBP2-CSF1R*.

Figure 5.5


A
Positive Control
Ba/F3 Cell Lines
1 kb DNA ladder
100 bp DNA ladder
TOPO-SSBP2-CSF1R
Ctrl
Empty Vector
SSBP2-CSF1R
NTC
β-Actin
NTC
3.0
2.0
1.5
1.0
0.5
MW: molecular weight
Primer FW: SSBP2 exon 12
Primer RV: CSF1R exon 14
Primer FW: β-actin FW
Primer RV: β-actin RV

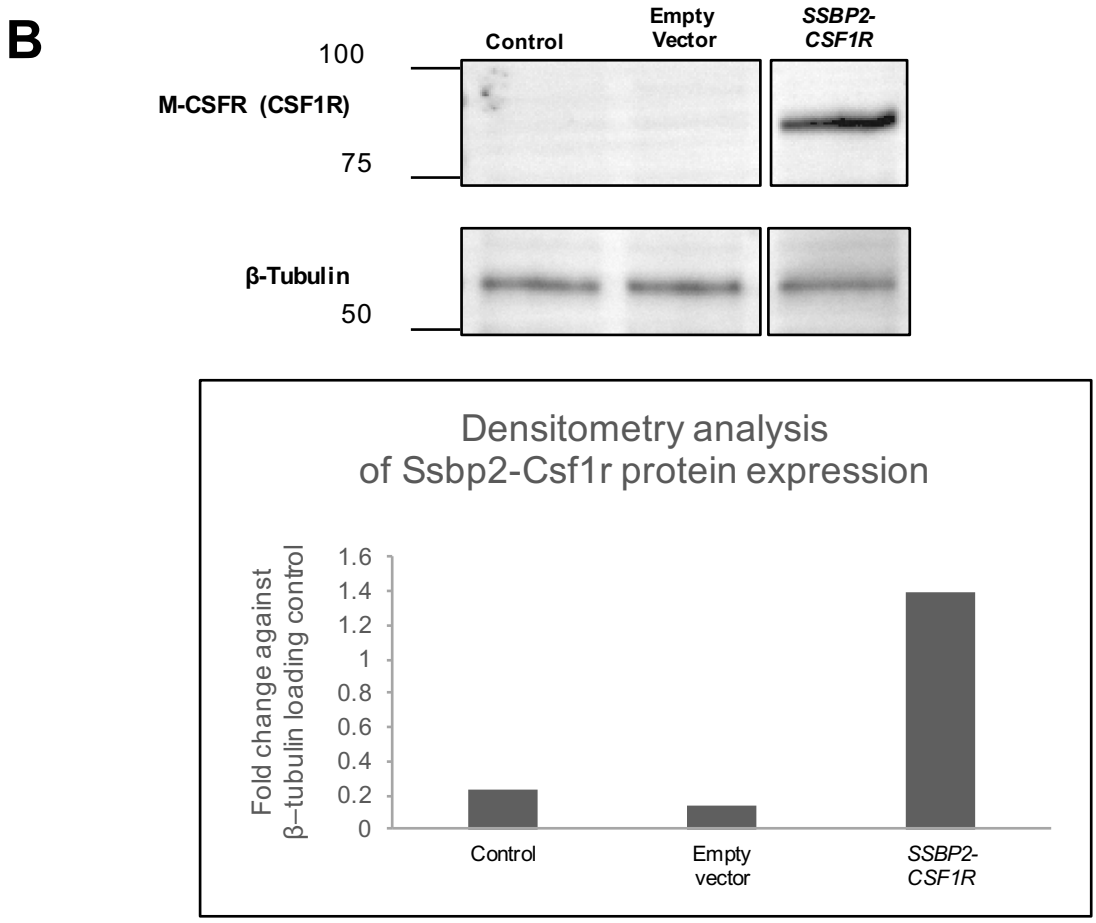
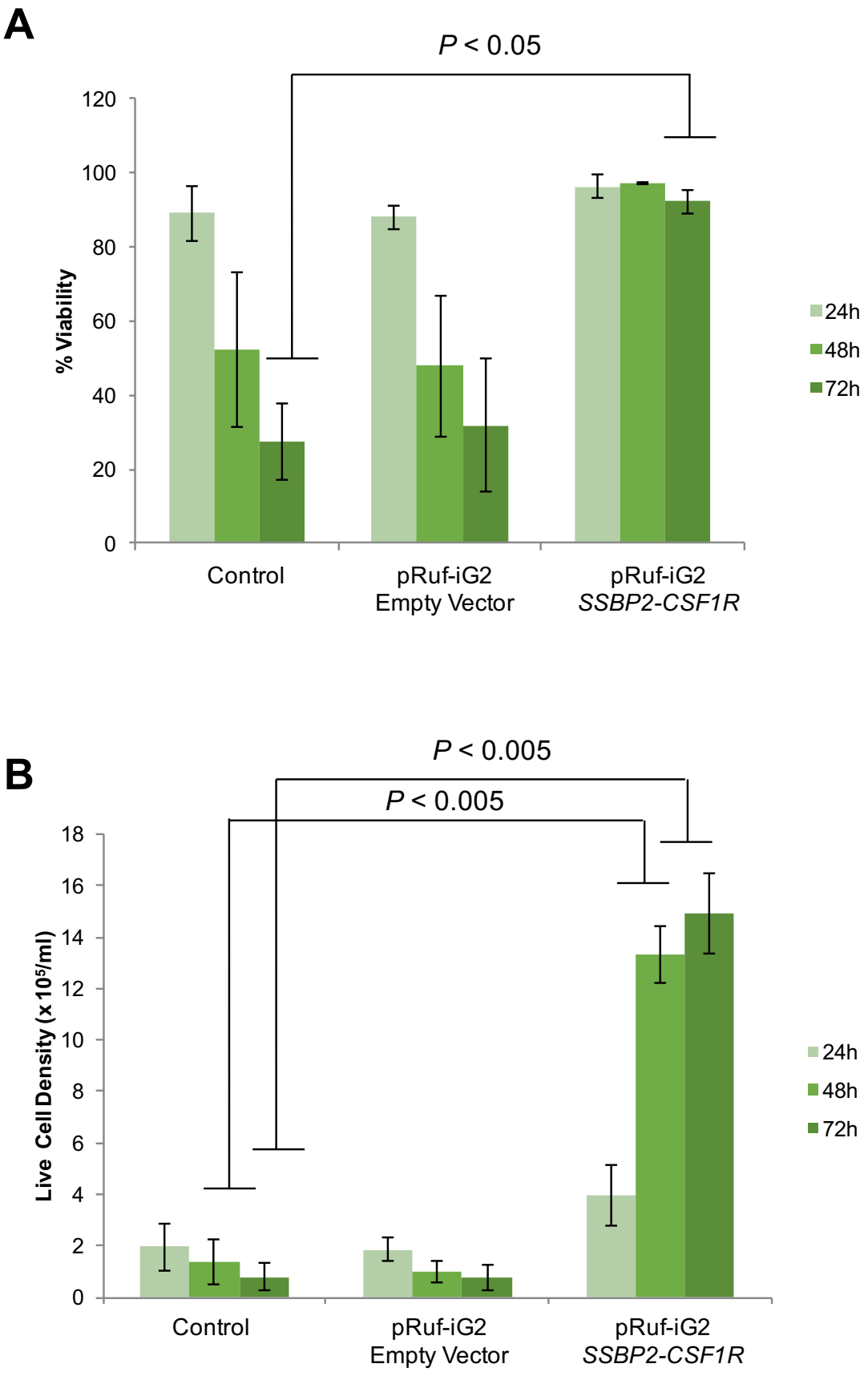

B
Control
Empty Vector
SSBP2-CSF1R
100
M-CSFR (CSF1R)
75
β-Tubulin
50
Densitometry analysis
of Ssbp2-Csf1r protein expression
Fold change against β–tubulin loading control
1.6
1.4
1.2
1
0.8
0.6
0.4
0.2
0
Control
Empty vector
SSBP2-CSF1R

Figure 5.6 – Ba/F3 cells containing the *SSBP2-CSF1R* fusion gene demonstrate IL-3 independent survival and proliferation.

Ba/F3 cells [control (untransduced Ba/F3 parental); pRuf-iG2 empty vector, and, pRuf-iG2 *SSBP2-CSF1R*] were cultured in the absence of IL-3 at 37ºC/5%CO_2 for 3 days. Cell viability (**A**) and live cell density (**B**) were determined via Trypan blue exclusion analysis. Columns represent mean of 3 independent experiments. Error bars denote standard deviation (SD), with statistical significance indicated by *P* values as determined using the Students' T-test.

Figure 5.6


A
P < 0.05
120
100
80
60
40
20
0
% Viability
Control
pRuf-iG2 Empty Vector
pRuf-iG2 SSBP2-CSF1R
24h
48h
72h
B
P < 0.005
P < 0.005
18
16
14
12
10
8
6
4
2
0
Live Cell Density (x 10⁵/ml)
Control
pRuf-iG2 Empty Vector
pRuf-iG2 SSBP2-CSF1R
24h
48h
72h

5.3.2. Ba/F3 *SSBP2-CSF1R* cells are sensitive to clinically-available TKIs

To evaluate the sensitivity of Ba/F3 *SSBP2-CSF1R* cells are sensitive to currently-available TKIs, cells were exposed to a panel of Abl and Jak kinase inhibitors (imatinib, dasatinib, ponatinib and ruxolitinib – **Figure 5.7**). Ba/F3 *SSBP2-CSF1R* cells were sensitive to imatinib ($LD_{50}^{imatinib}$: 1.3 ± 0.1 μM) and dasatinib ($LD_{50}^{dasatinib}$: 6.8 ± 0.6 nM). Interestingly, higher concentrations of ponatinib and ruxolitinib were required to induce cell death ($LD_{50}^{ponatinib}$: 39.7 ± 3.5 nM; $LD_{50}^{ruxolitinib}$: ~9.7 ± 16.7 μM), based on a nonlinear regression curve analysis on GraphPad Prism.

Investigation of phospho-CrkL and phospho-Stat5 indicated a reduction in mean fluorescence intensity (MFI) of these target proteins in Ba/F3 *SSBP2-CSF1R* cells treated with imatinib, dasatinib and ponatinib. Ruxolitinib did not decrease the expression of p-CrkL, however, reduced p-Stat5 expression was noted in these cells (**Figure 5.8**).

CSF1R phosphorylative activity was further measured by western blotting (**Figure 5.9**). A decrease in p-M-CSFR (CSF1R) protein expression was observed when Ba/F3 *SSBP2-CSF1R* cells were exposed to 5 μM imatinib and 100 nM dasatinib (**Figure 5.9A**). No decrease was observed when cells were treated with 100 nM ponatinib, a third-generation Abl-kinase inhibitor. A similar result was observed when cells were treated with 1 μM ruxolitinib (Jak inhibitor), which was confirmed by densitometry analysis (**Figure 5.9B**).

Figure 5.7

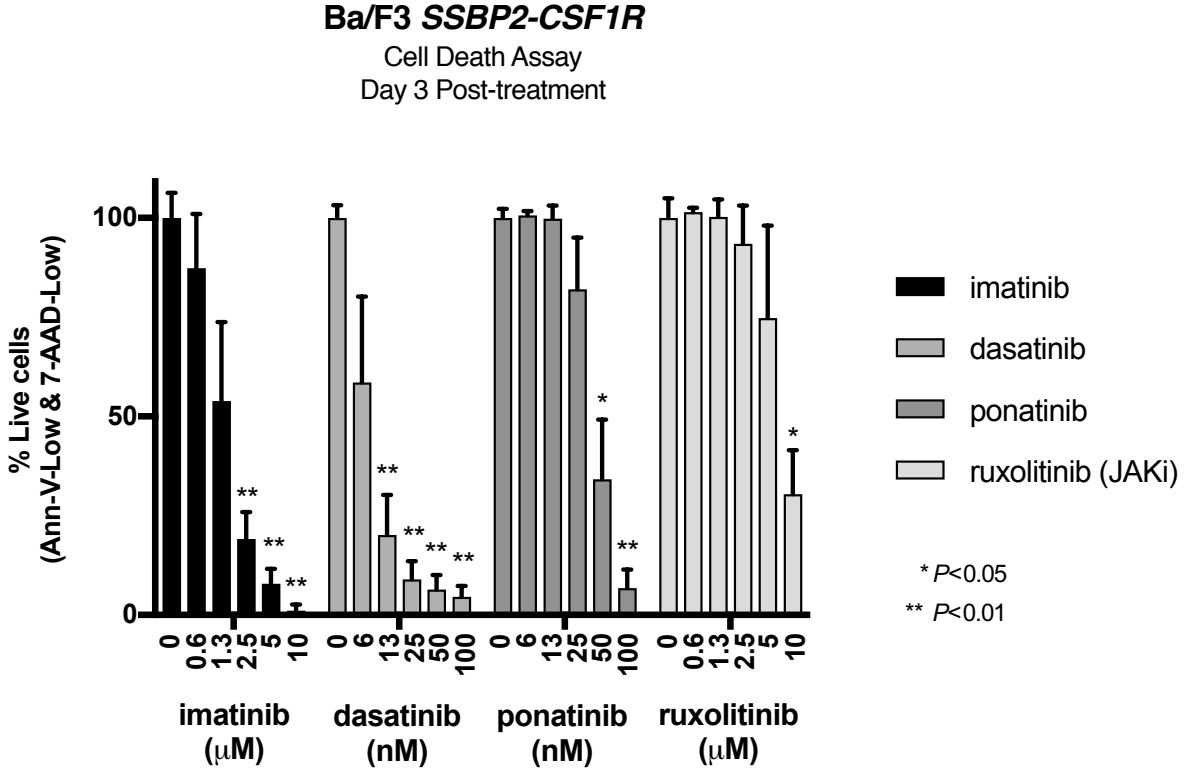


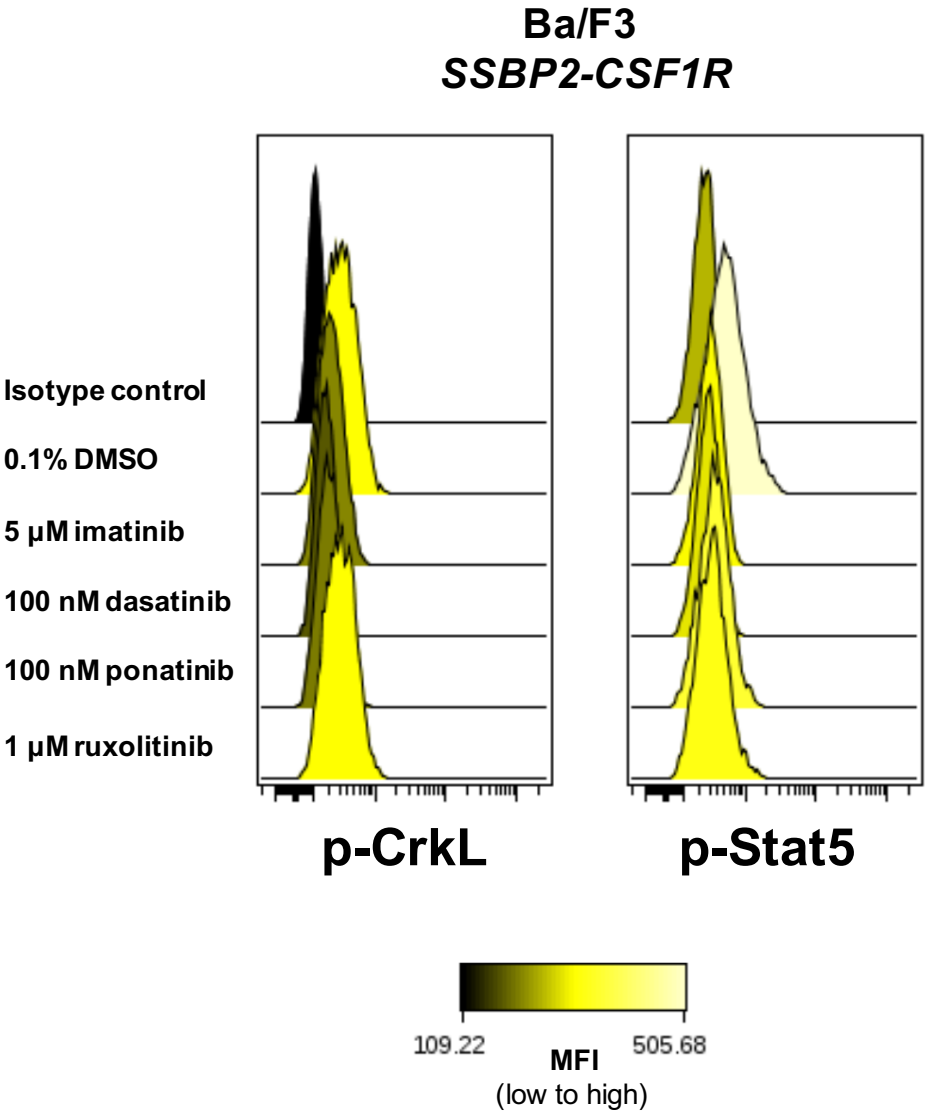
Figure 5.7 – Clinically-available tyrosine kinase inhibitors induce cell death in Ba/F3 *SSBP2-CSF1R* cells

Cell viability analysis via Annexin-V/7-AAD flow cytometry exclusion in Ba/F3 *SSBP2-CSF1R* cells, treated with a panel of TKIs (imatinib, dasatinib, ponatinib, and ruxolitinib). Cells were seeded in IL-3 free media and exposed to TKIs for 3 days prior to analysis. Columns represent the mean percentage of live cells. Error bars denote ± SD of 3 independent experiments. **P*<0.05, ***P*<0.01. Subsequent LD_{50} concentrations derived from this curve was generated via the nonlinear regression (inhibitor response) curve fit method on GraphPad Prism®.

Figure 5.8 – Phosphoflow analysis of TKI-treatment in Ba/F3 *SSBP2-CSF1R* cells reveals sensitivity to Abl-kinase inhibitors.

Histogram plots representing p-CrkL and p-Stat5 expression in Ba/F3 *SSBP2-CSF1R* cells, as analysed via phosphoflow. Cells were treated with 0.1% DMSO (vehicle control), 5 μM imatinib, 100 nM dasatinib, 100 nM ponatinib and 1 μM ruxolitinib for 1 h in IL-3 free media at 37ºC/5%CO_2. Isotype controls (IgG_{2a} for p-CrkL; IgG_1 for p-Stat5) were included and fluorescence intensity measured using the BD Fortessa™. Overlaid histograms were generated using Cytobank (Santa Clara, CA, USA), with rectangular gradient box indicating the minimum and maximum MFI (mean fluorescence intensity) of the experiment, with values indicated in the table beneath. Data are representative of 3 independent experiments.

Figure 5.8



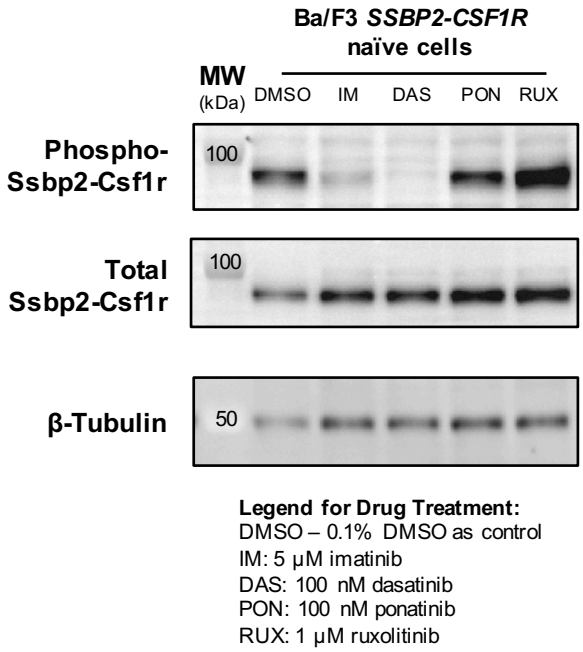
Treatment	MFI	
	p-CrkL	p-Stat5
Isotype Control	109.22	250.26
0.1% DMSO	308.74	505.68
5 µM imatinib	214.14	305.3
100 nM dasatinib	177.16	287.24
100 nM ponatinib	205.54	356.9
1 µM ruxolitinib	307.88	326.8

Figure 5.9 – Western immunoblotting of TKI-sensitivity in Ba/F3 *SSBP2-CSF1R* cells

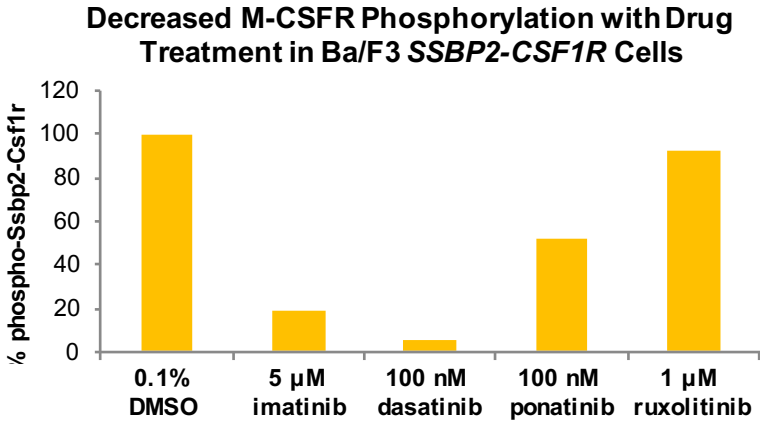
A: Phosphorylated Ssbp2-Csf1r, total Ssbp2-Csf1r and β-tubulin analysis of TKI-sensitivity in Ba/F3 *SSBP2-CSF1R* cells. Cells were treated in 0.1% DMSO (vehicle control), 5 μM imatinib, 100 nM dasatinib, 100 nM ponatinib, 1 μM ruxolitinib (Jak inhibitor as a negative control) for 1 h in IL-3 free media at 37ºC/5%CO_2. Western blots were visualised using the Bio-Rad® ChemiDoc™ imager using the ImageLab™ software. Blots shown are n=1 experiment. **B**: Bar chart representing densitometry analysis of phosphorylated Ssbp2-Csf1r in the drug treatment dataset, normalised against the total isoform with band intensities derived using ImageJ[4].

Figure 5.9

A


Ba/F3 SSBP2-CSF1R naïve cells
MW (kDa)
DMSO
IM
DAS
PON
RUX
Phospho-Ssbp2-Csf1r
Total Ssbp2-Csf1r
β-Tubulin
100
100
50
Legend for Drug Treatment:
DMSO – 0.1% DMSO as control
IM: 5 µM imatinib
DAS: 100 nM dasatinib
PON: 100 nM ponatinib
RUX: 1 µM ruxolitinib

B


Decreased M-CSFR Phosphorylation with Drug Treatment in Ba/F3 SSBP2-CSF1R Cells
% phospho-Ssbp2-Csf1r
120
100
80
60
40
20
0
0.1% DMSO
5 µM imatinib
100 nM dasatinib
100 nM ponatinib
1 µM ruxolitinib

5.3.3. Generation of imatinib-resistance in Ba/F3 *SSBP2-CSF1R* cells results in an acquired novel point mutation

Ba/F3 *SSBP2-CSF1R* cells were dose-escalated in imatinib, to generate imatinib-resistance in *SSBP2-CSF1R* cells, and assess the modes of resistance. Cells were exposed to increasing doses of imatinib to a final concentration of 10 μM. Imatinib-resistant Ba/F3 *SSBP2-CSF1R* cells were resistant to higher concentrations of imatinib compared to control samples, as confirmed by viability analysis using Annexin-V/7-AAD exclusion (**Figure 5.10**) where the LD_{50} for imatinib in naïve control and imatinib-resistant cells were 2.7±0.3 μM and >10 μM respectively.

Imatinib-resistant cells exhibited a sub-optimal viability when exposed to lower concentrations of imatinib (~50% viable with TKI withdrawn). Despite this phenomenon, further western immunoblotting analysis of p-Ssbp2-Csf1r protein indicated an ability of imatinib-resistant cells to tolerate an increased concentration of TKI (IC_{50}: > 25 μM imatinib) compared to control (IC_{50}: 1 μM) (**Figure 5.11**). When the Ssbp2-Csf1r levels in imatinib-resistant cells were explored, a decreased expression was noted in resistant compared to control cells, despite the increased p-Ssbp2-Csf1r imatinib IC_{50}.

Kinase-domain mutation analysis via Sanger sequencing was then performed. Results indicate the presence of a *CSF1R*-L785M (c.2566C>A) mutation (**Figure 5.12**). When *CSF1R*-L785M was further aligned onto Clustal W (a protein alignment software)[331,410], analysis of the alignment results revealed *CSF1R*-L785M being in a highly-conserved region and unmutated across various species (i.e. Homo sapiens, Mus musculus, etc.) (**Figure 5.13**).

THIS PAGE INTENTIONALLY LEFT BLANK.

Figure 5.10 – Investigation of TKI resistance in Ba/F3 *SSBP2-CSF1R* cells via Annexin-V/7-AAD cell death analysis

Bar graph depicts flow cytometry analysis of Ba/F3 *SSBP2-CSF1R* naïve (imatinib-sensitive) and imatinib-resistant cells treated in increasing concentrations of imatinib. An overnight drug-washout procedure was performed prior to incubation of cells in imatinib for 3 days at 37ºC/5%CO_2. Cells were harvested and prepared for Annexin-V/7-AAD flow cytometry acquisition & analysis as previously described. Columns represent mean of 4 independent experiments, with error bars indicating ± SD as analysed on GraphPad Prism®. Asterisks are indicative of statistical significance, calculated using the Student's *t*-test method.

Figure 5.10

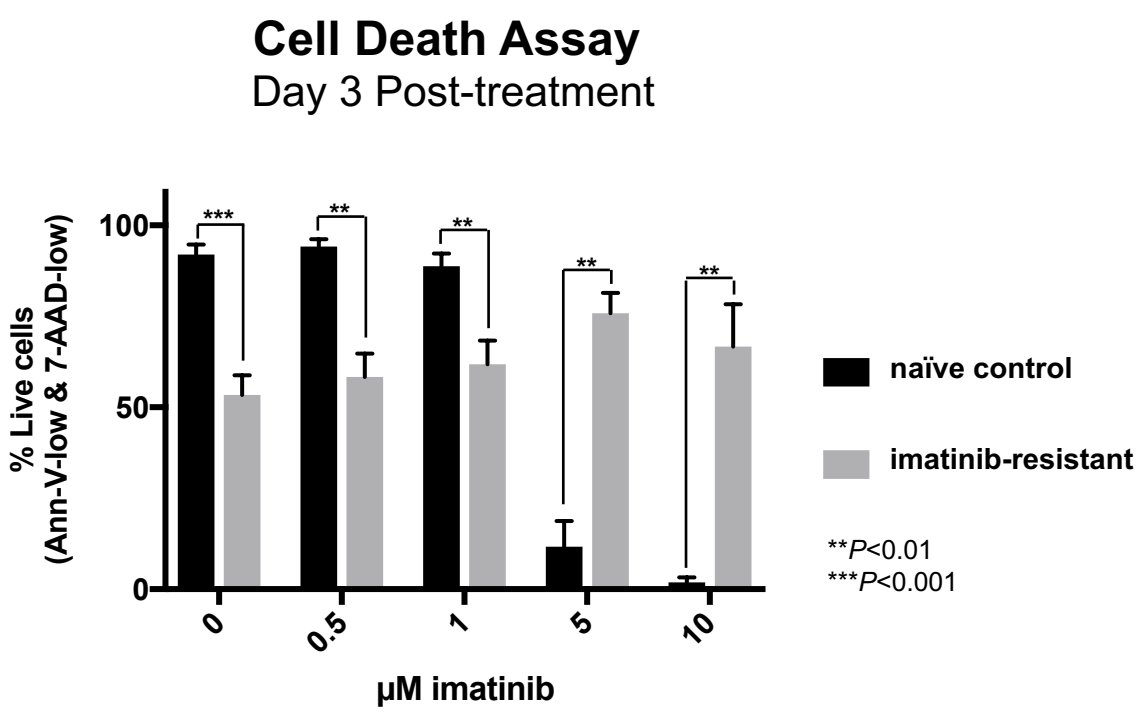

Cell Death Assay
Day 3 Post-treatment
% Live cells
(Ann-V-low & 7-AAD-low)
100
50
0
***
**
**
**
**
0
0.5
1
5
10
µM imatinib
naïve control
imatinib-resistant
**P<0.01
***P<0.001

Figure 5.11 – Investigation of TKI resistance in Ba/F3 *SSBP2-CSF1R* cells via p-Ssbp2-Csf1r western blotting analysis

Western blotting and densitometry analyses of Ba/F3 *SSBP2-CSF1R* naïve and imatinib-resistant cells treated with increasing concentrations of imatinib. An overnight drug-washout procedure was performed prior to TKI treatment for 1 hour at 37ºC/5%CO_2. Cells were collected and prepared for western blotting analysis as previously described, with PVDF membranes incubated in antibodies specific for phosphorylated M-CSFR (Tyr723), total M-CSFR and β-tubulin. **A:** Western blot detection of phospho/total Ssbp2-Csf1r and β-tubulin in cells treated with 0, 0.5, 1, 5, 10, 25 μM imatinib. **B:** Densitometry analysis of phosphorylated/total Ssbp2-Csf1r (incorporating the β-tubulin loading control). **C:** Normalised graph of p-Ssbp2-Csf1r against 0 nM TKI, for purpose of IC_{50} analysis. Band intensities were measured using the Bio-Rad® Image Lab (version 5.0) software, while plots were generated and analysed using GraphPad Prism®. Data shown is representative of 3 independent experimental repeats. MW: molecular weight

Figure 5.11

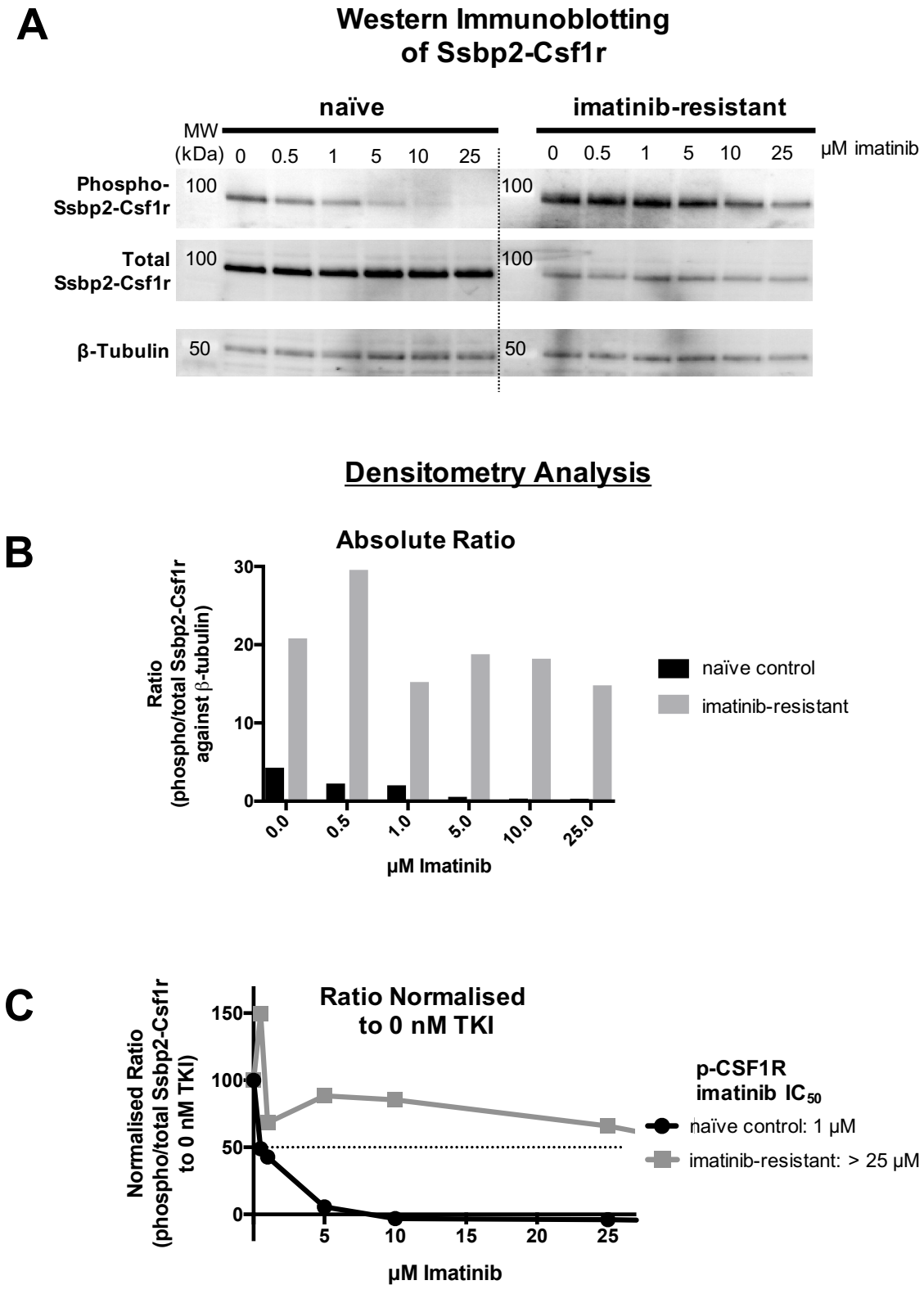
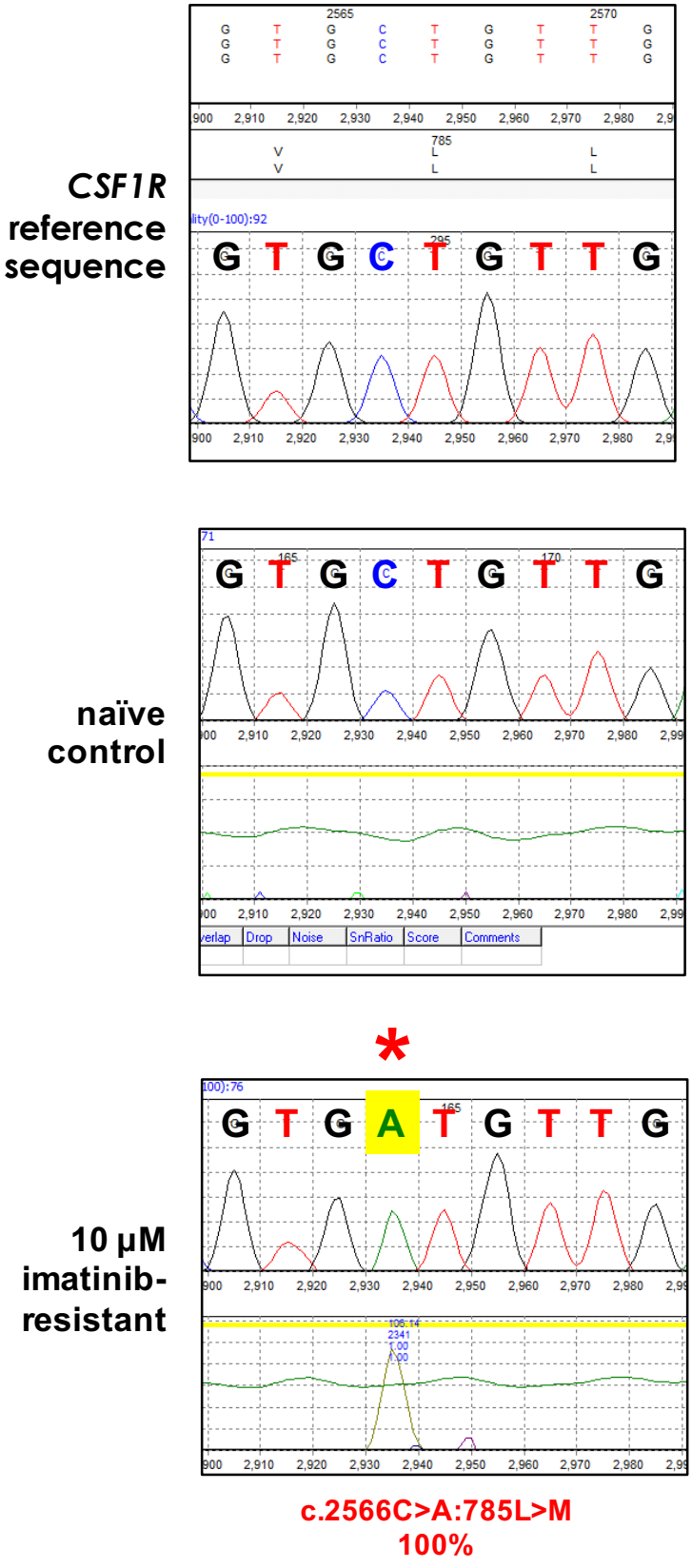

A
Western Immunoblotting of Ssbp2-Csf1r
naïve
imatinib-resistant
MW (kDa)
0 0.5 1 5 10 25
0 0.5 1 5 10 25
µM imatinib
Phospho-Ssbp2-Csf1r
Total Ssbp2-Csf1r
β-Tubulin
100
100
100
100
50
50
Densitometry Analysis
B
Absolute Ratio
Ratio (phospho/total Ssbp2-Csf1r against β-tubulin)
30
20
10
0
0.0
0.5
1.0
5.0
10.0
25.0
µM Imatinib
naïve control
imatinib-resistant
C
Ratio Normalised to 0 nM TKI
Normalised Ratio (phospho/total Ssbp2-Csf1r to 0 nM TKI)
150
100
50
0
5
10
15
20
25
µM Imatinib
p-CSF1R imatinib IC50
naïve control: 1 µM
imatinib-resistant: > 25 µM

Figure 5.12 – Identification of the *CSF1R*-L785M kinase-domain mutation as probable cause of imatinib-resistance

Sanger sequencing results of Ba/F3 *SSBP2-CSF1R* TKI-resistant and naïve (TKI-sensitive) lines, compared to a *CSF1R* reference sequence (NM 001288705.1). Red asterisk highlights the identification of a *CSF1R*-L785M kinase-domain mutation in imatinib-resistant cells. Sequences were analysed using the Mutation Surveyor® DNA analysis software. Data are representative of 3 biological replicates.

Figure 5.12


CSF1R reference sequence
naïve control
10 µM imatinib-resistant
*
c.2566C>A:785L>M
100%

THIS PAGE INTENTIONALLY LEFT BLANK.

Figure 5.13

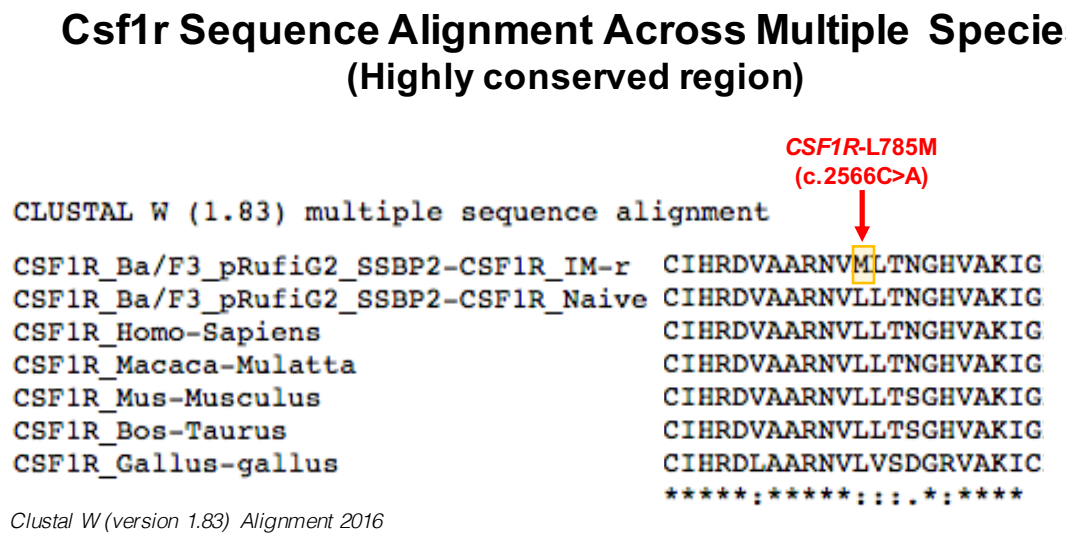


Figure 5.13 – *CSF1R*-L785M is a novel kinase-domain mutation

Protein sequence alignment of *CSF1R*-L785M in Ba/F3 *SSBP2-CSF1R* imatinib-resistant line (highlighted in red) in comparison to sequences from across various species, using the Clustal W platform (EMBL-EBI, Cambridge UK)[331,410].

THIS PAGE INTENTIONALLY LEFT BLANK.

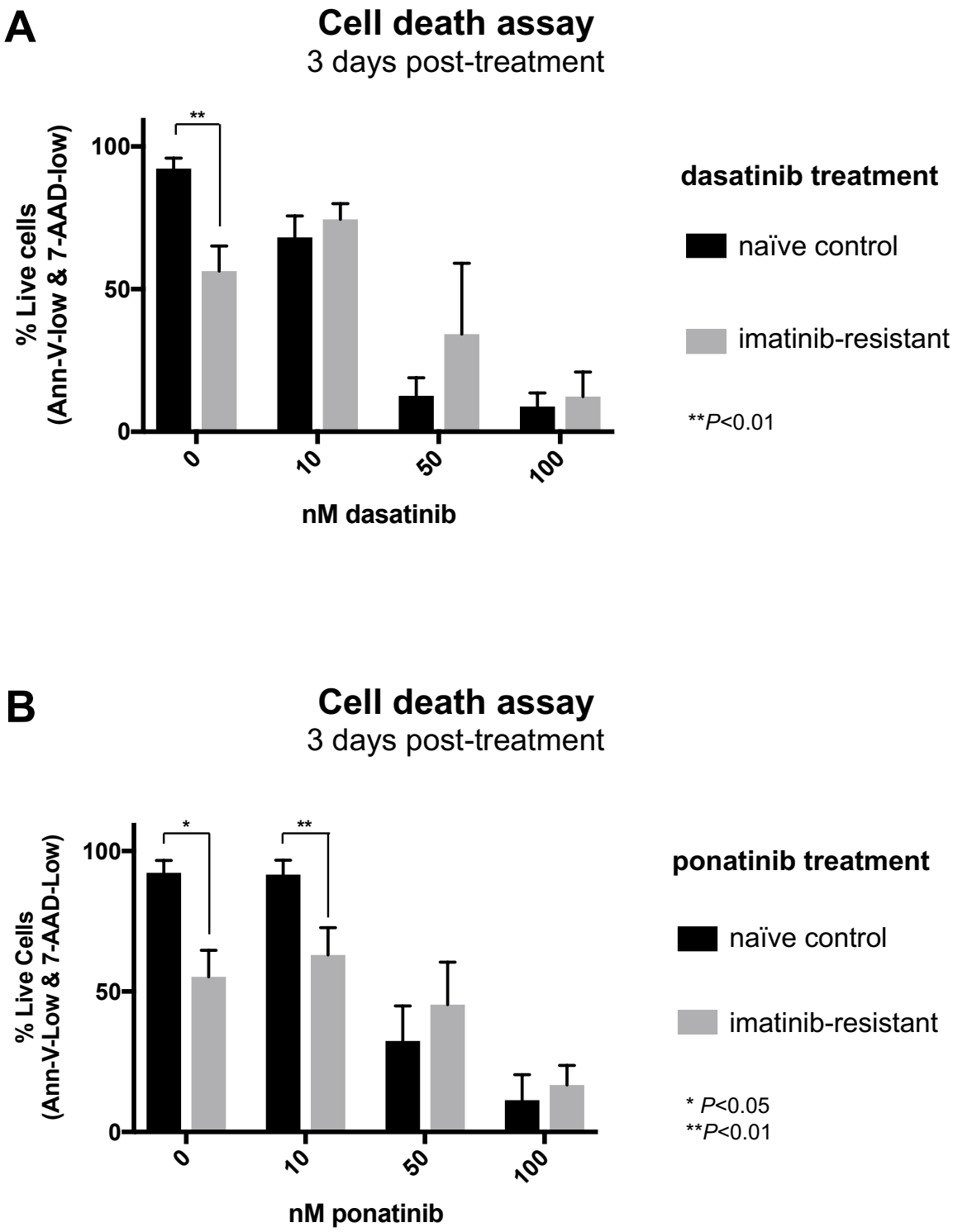
5.3.4. Imatinib-resistant Ba/F3 *SSBP2-CSF1R* L785M cells were sensitive to other TKIs

Investigation of drug sensitivity of imatinib-resistant *SSBP2-CSF1R* cells to second and third-generation Abl-kinase inhibitors was performed (**Figure 5.14**). When naïve and imatinib-resistant Ba/F3 *SSBP2-CSF1R* cells were exposed to dasatinib, the LD_{50} values were 14.9 and 48.1 nM dasatinib respectively (**Figure 5.14A**). When cells were treated with ponatinib, a similar drug-response was observed where the IC_{50} of ponatinib was 38.6 nM in naïve control cells, and, 55.6 nM in imatinib-resistant cells (**Figure 5.14B**). The percentage viability of imatinib-resistant Ba/F3 *SSBP2-CSF1R* cells was decreased over 3 days in the absence of TKI. The observation of drug dependency will be discussed later in this chapter, to elucidate the possible reasons for this finding.

Figure 5.14 – Imatinib-resistant Ba/F3 *SSBP2-CSF1R* cells are similarly sensitive to second and third generation Abl-kinase inhibitors as naïve control cells

Flow cytometry analysis of dasatinib (**A**) and ponatinib (**B**) sensitivity in Ba/F3 *SSBP2-CSF1R* naïve and imatinib-resistant cells via Annexin-V/7-AAD exclusion. An overnight washout procedure was performed prior to incubation of cells in TKI for 3 days at 37ºC / 5% CO_2, followed by flow cytometry acquisition & analysis. Columns represent mean while error bars are standard deviation of 3 independent experiments, analysed using GraphPad Prism®. Asterisks depict statistical significance based on the Student's *t*-test method.

Figure 5.14


A
Cell death assay
3 days post-treatment
% Live cells
(Ann-V-low & 7-AAD-low)
100
50
0
**
0
10
50
100
nM dasatinib
dasatinib treatment
naïve control
imatinib-resistant
**P<0.01
B
Cell death assay
3 days post-treatment
% Live Cells
(Ann-V-Low & 7-AAD-Low)
100
50
0
*
**
0
10
50
100
nM ponatinib
ponatinib treatment
naïve control
imatinib-resistant
* P<0.05
**P<0.01

5.3.5. Generation of dasatinib-resistance in Ba/F3 *SSBP2-CSF1R* cells results in the accumulation of multiple genetic alterations

Ba/F3 *SSBP2-CSF1R* TKI-sensitive cells were dose-escalated in dasatinib to a final resistance concentration of 200 nM, to study the effects of dasatinib-resistance. Uniquely what is observed in the resistant cells is a loss of viability in the absence of drug over 3 days. This indicates a dependence on TKI for the resistant mechanism. This was observed in dasatinib-resistant cells exposed to a panel of Abl TKIs including imatinib and ponatinib (**Figure 5.15**).

Dasatinib-resistant Ba/F3 *SSBP2-CSF1R* cells were more resistant to high concentrations of dasatinib, compared to control samples (viability at 0, 5, 10, 50 and 100 nM dasatinib: DMSO: 91±4%, 89±5%, 66±19%, 16±12% and 12±9%; dasatinib-resistant: 8±5%, 24±6%, 46±17%, 72±12% and 66±15% respectively) (**Figure 5.15A**). When cells were treated with 0, 0.5, 1, 5 and 10 μM imatinib, the respective viabilities were 90±5%, 93±4%, 89±6%, 17±12% and 2±1% in DMSO control and, 11±8%, 34±14%, 47±18%, 63±14% and 7±7% in dasatinib-resistant cells (**Figure 5.15B**). Ponatinib treatment (0, 10, 50, 100) resulted in a viability of 90±6%, 91±5%, 39±9% and 14±8% in DMSO control cells, while in dasatinib-resistant cells the viability observed was 8±5%, 51±21%, 13±9% and 3±2% respectively (**Figure 5.15C**).

Next, DNA PCR followed by Sanger sequencing was employed to identify the presence of any kinase-domain mutations that may have arisen during dasatinib resistance development. Gel electrophoresis of DNA PCR products expanding the *CSF1R* kinase domain of *SSBP2-CSF1R* revealed a truncation in the dasatinib-resistant line compared to control and imatinib-resistant (**Figure 5.16**). Further DNA

analysis revealed a deletion spanning over the breakpoint, in both *SSBP2* and *CSF1R* (**Figure 5.17** and **Appendix 5.1**) in dasatinib-resistant samples, where 118 nucleotides were deleted in the former and 89 in the latter. In total, this resulted in a truncation of 207 nucleotides (0.2 kb), comparable to that observed in the DNA gel (**Figure 5.16**). When Sanger sequencing data of the protein kinase domain were analysed, results revealed a point mutation in *CSF1R*-A652V (c.2168C>T), at a rate of 100% (**Figure 5.18**). Further alignment of *CSF1R*-A652V on the Clustal Omega platform (EMBL-EBI, Cambridge UK)[332] revealed that the *CSF1R*-A652V point mutation was located in a highly conserved region and the mutation absent across various species (i.e. Homo sapiens, Mus musculus, etc.) (**Figure 5.19**).

In keeping with the observation above, western blot revealed a reduction in the molecular weight of SSBP2-CSF1R (**Figure 5.20A**). Densitometry analysis data revealed an approximately 15-fold increase of p-Stat5-Csf1r protein expression in dasatinib-resistant cells compared to DMSO control in the absence of TKI (**Figure 5.20B**). When the p-Ssbp2-Csf1r response to dasatinib was normalised against the untreated (0 nM TKI) concentration, there was no difference between DMSO control and dasatinib-resistant cells ($IC_{50}^{dasatinib}$: 5 and 10 nM respectively) (**Figure 5.20C**).

Figure 5.15 – Dasatinib-resistant Ba/F3 *SSBP2-CSF1R* cells are tolerant of dasatinib and imatinib but not ponatinib

Flow cytometry analysis of dasatinib (**A**), imatinib (**B**) and ponatinib (**C**) treatment in Ba/F3 *SSBP2-CSF1R* DMSO control and dasatinib-resistant cells, indicating percentage cell viability with increasing concentration of TKI. An overnight washout procedure was performed prior to incubation of cells in TKI for 3 days at 37ºC/5%CO_2, followed by Annexin-V/7-AAD flow cytometry acquisition & analysis. Columns represent mean of 3 independent experimental repeats while error bars denote the standard deviation, as analysed using GraphPad Prism®. Asterisks depict statistical significance according to the Student's *t*-test method.

Figure 5.15

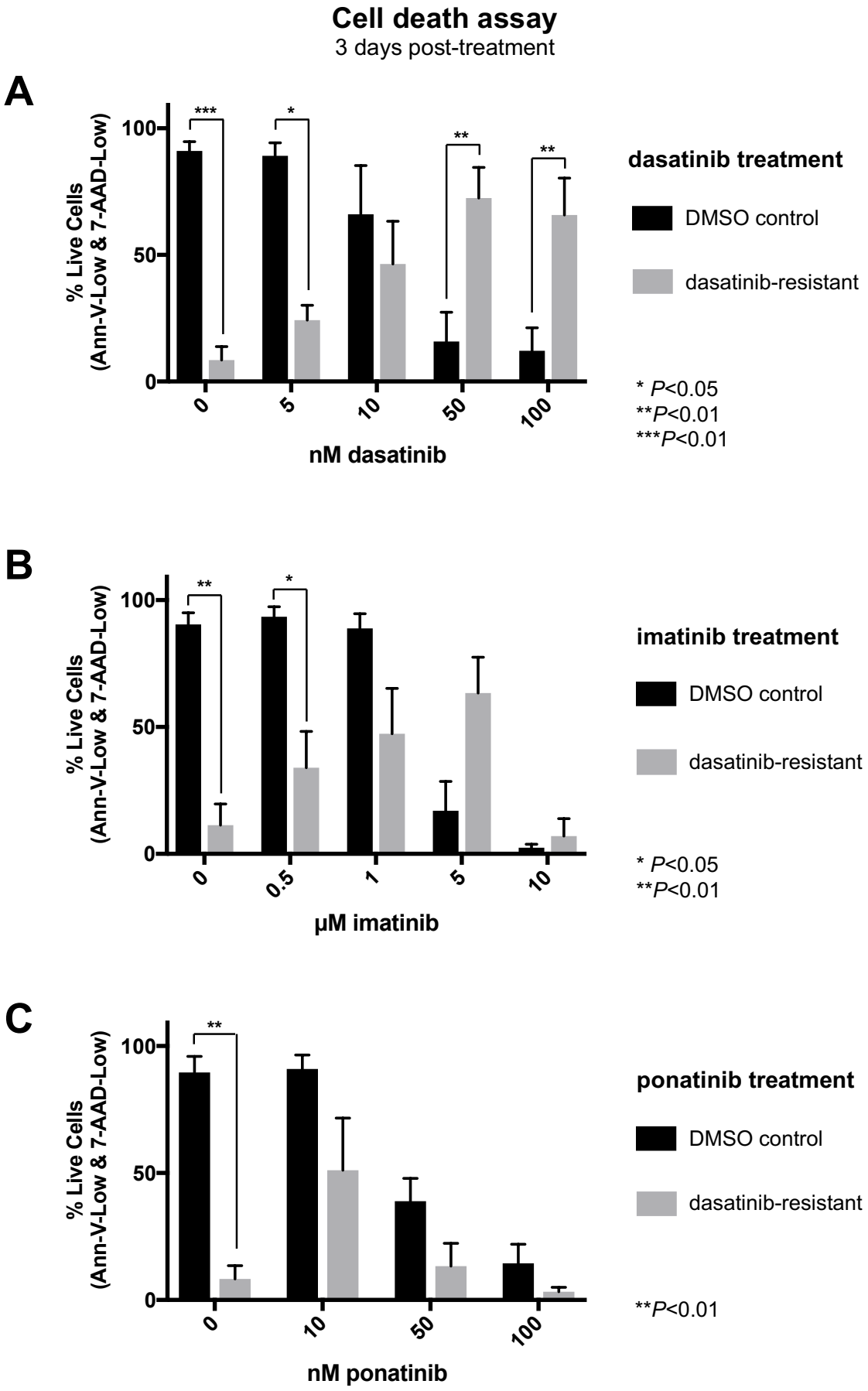
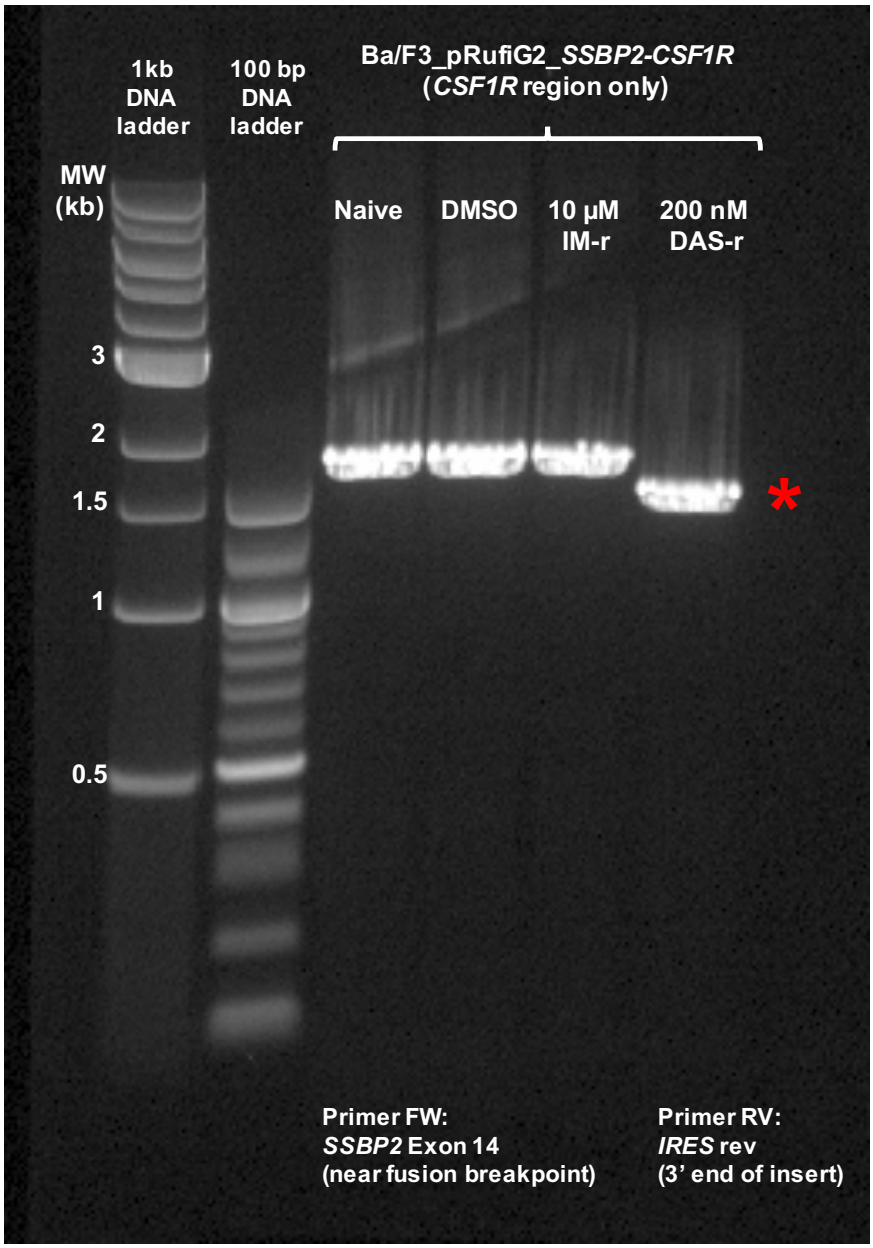

Cell death assay
3 days post-treatment
A
% Live Cells (Ann-V-Low & 7-AAD-Low)
100
50
0
***
*
**
**
0
5
10
50
100
nM dasatinib
dasatinib treatment
DMSO control
dasatinib-resistant
* P<0.05
**P<0.01
***P<0.01
B
% Live Cells (Ann-V-Low & 7-AAD-Low)
100
50
0
**
*
0
0.5
1
5
10
µM imatinib
imatinib treatment
DMSO control
dasatinib-resistant
* P<0.05
**P<0.01
C
% Live Cells (Ann-V-Low & 7-AAD-Low)
100
50
0
**
0
10
50
100
nM ponatinib
ponatinib treatment
DMSO control
dasatinib-resistant
**P<0.01

Figure 5.16 – Dasatinib-resistant Ba/F3 *SSBP2-CSF1R* cells exhibit a truncation in the *CSF1R* 3' partner gene

DNA agarose gel electrophoresis of PCR products from amplification of the *CSF1R* 3' partner gene in Ba/F3 *SSBP2-CSF1R* cell lines, spanning over the *SSBP2-CSF1R* breakpoint. Samples analysed include the TKI-sensitive control lines (naïve and DMSO), as well as TKI-resistant (imatinib and dasatinib-resistant) lines. Note the smaller band size in the dasatinib-resistant line, highlighted by the red asterisk. Gel image is n=1 experiment

Figure 5.16



Legend:
MW: molecular weight marker
IM-r: imatinib-resistant
DAS-r: dasatinib-resistant

Figure 5.17 – Identification of genetic deletion spanning the *SSBP2-CSF1R* breakpoint region in dasatinib-resistant cells

Schematic diagram of a deletion spanning over the breakpoint region, in dasatinib-resistant *SSBP2-CSF1R* cells. Blue and green rounded rectangles represent the native *SSBP2-CSF1R* fusion gene, while red rectangle signifies the deleted region in dasatinib-resistant cells. DNA sequence alignment revealed a deletion of sequences within exon 15 and 16 in *SSBP2* and a portion of exon 12 in *CSF1R*. For further information regarding the exact truncated DNA sequences, please see **Appendix 5.1**.

Figure 5.17

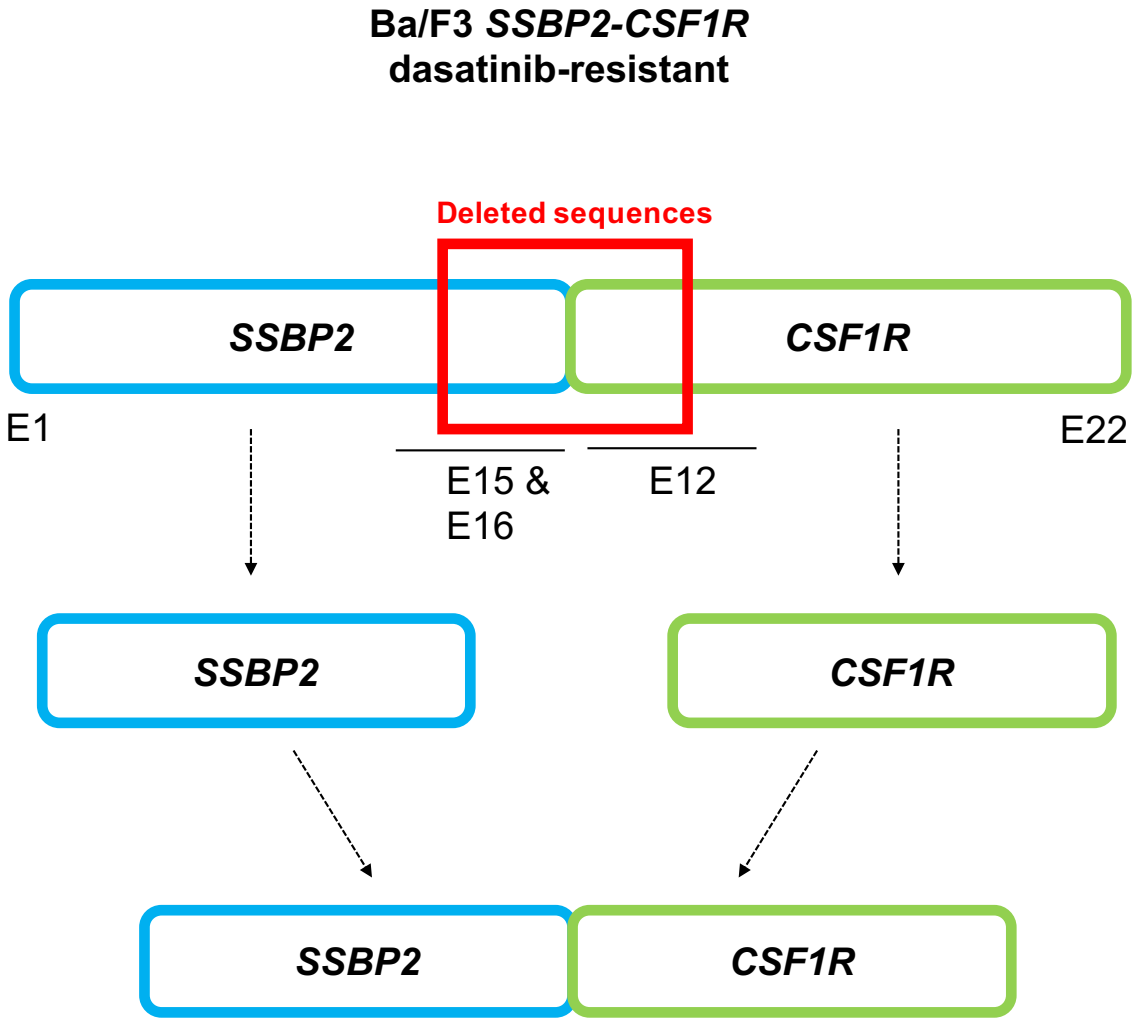
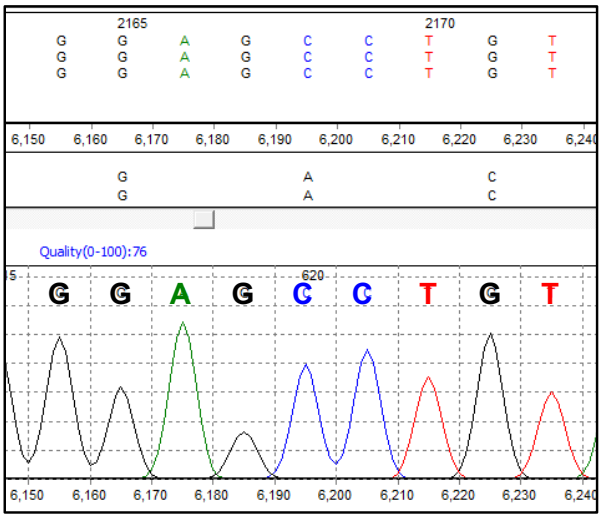

Ba/F3 SSBP2-CSF1R
dasatinib-resistant
Deleted sequences
SSBP2
CSF1R
E1
E22
E15 &
E16
E12
SSBP2
CSF1R
SSBP2
CSF1R

Figure 5.18 – Identification of a *CSF1R*-A652V mutation in dasatinib-resistant Ba/F3 *SSBP2-CSF1R* cells

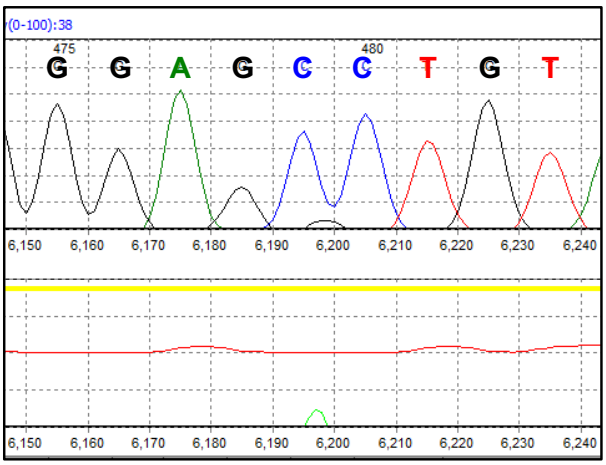
Sanger sequencing results of Ba/F3 *SSBP2-CSF1R* TKI-resistant and TKI-sensitive lines, compared to a *CSF1R* reference sequence (NM 001288705.1). Red asterisk highlights a point mutation from cytosine to thymine at coding nucleotide position 2168, resulting in a substitution of alanine to valine at the 652nd residue. Sequences were analysed using the Mutation Surveyor® DNA analysis software, as previously described. Data is n=1 biological replicate sample.

Figure 5.18

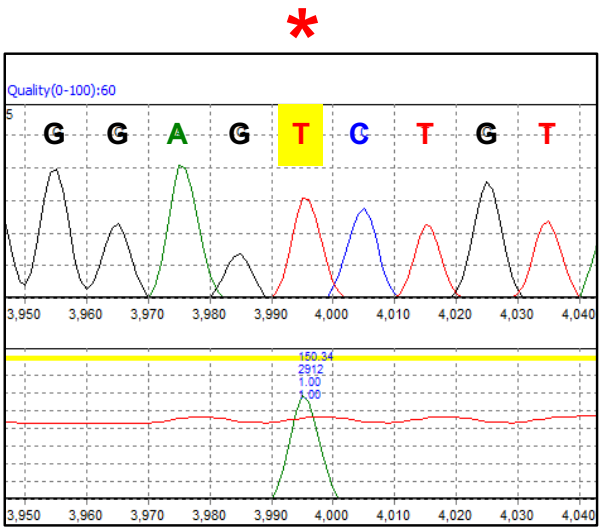
***CSF1R* reference sequence**



DMSO control



200 nM dasatinib-resistant



c.2168C>T:652A>V; 100%

THIS PAGE INTENTIONALLY LEFT BLANK.

Figure 5.19

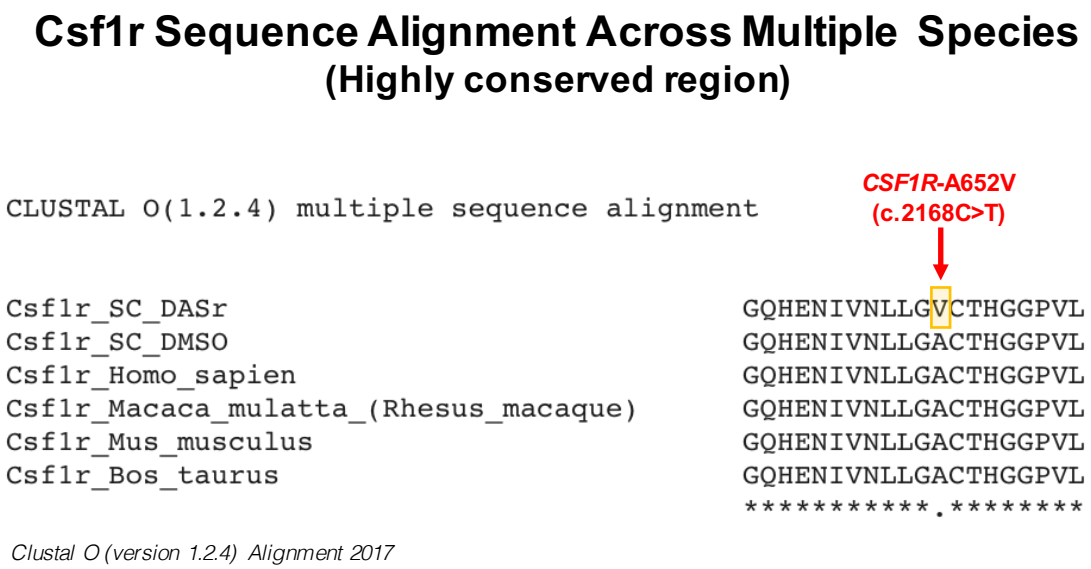


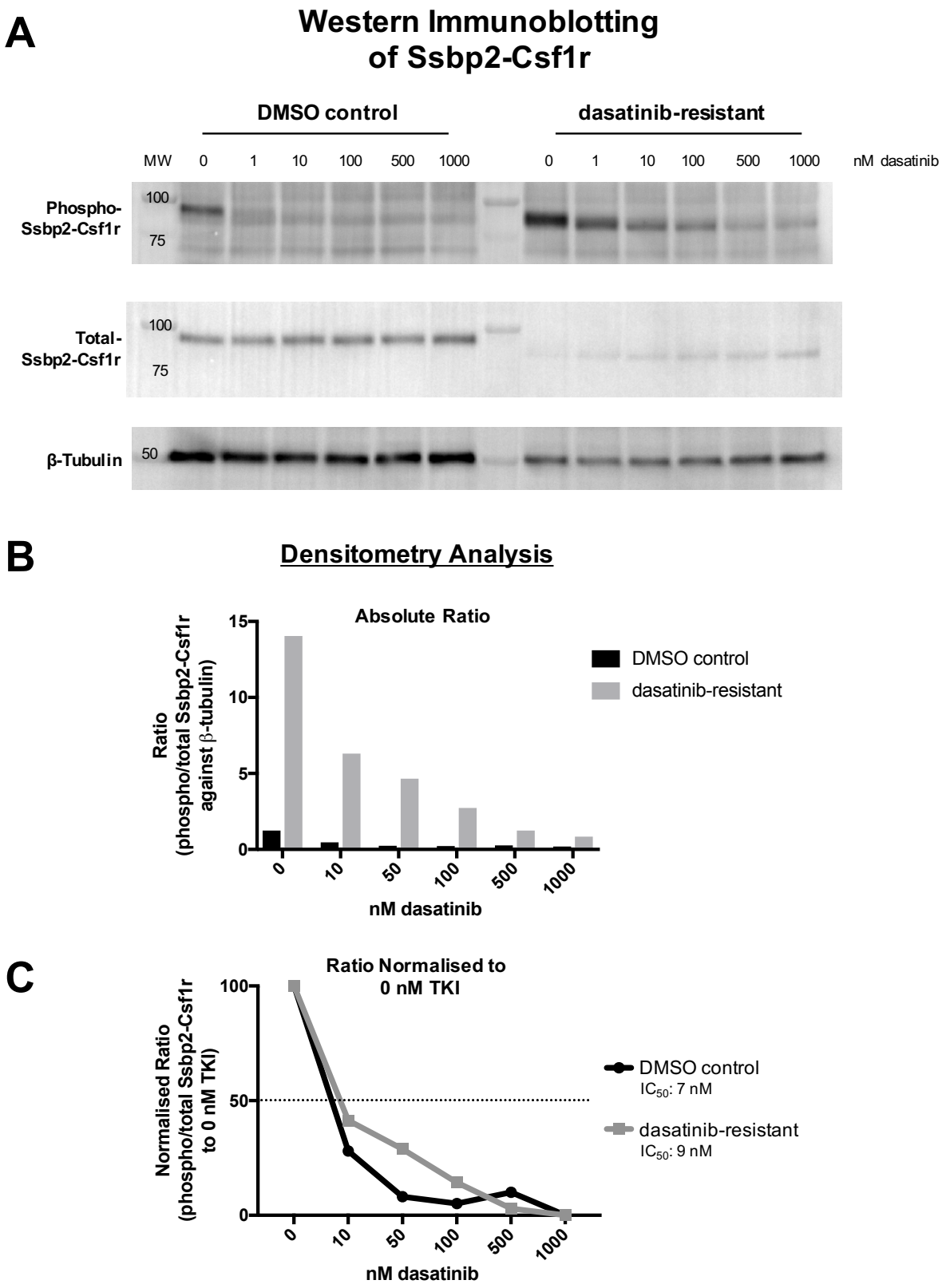
Figure 5.19 – *CSF1R*-A652V identified in dasatinib-resistant Ba/F3 *SSBP2-CSF1R* cells is a novel kinase-domain mutation

A: Protein sequence alignment of *CSF1R*-A652V in Ba/F3 *SSBP2-CSF1R* dasatinib-resistant line (highlighted in yellow) in comparison to sequences from across various species, using the Clustal Omega platform (EMBL-EBI, Cambridge UK)[332].

Figure 5.20 – Investigation of p-Ssbp2-Csf1r in dasatinib-resistant Ba/F3 *SSBP2-CSF1R* cells reveal a truncation in protein band size and unchanged p-Csf1r dasatinib IC_{50}.

A: Western immunoblotting of Ba/F3 *SSBP2-CSF1R* DMSO control and dasatinib-resistant cells exposed to dasatinib at the concentrations indicated, for 1 hour at 37ºC / 5% CO_2. Following incubation, cells were prepared for western blotting analysis and detected for phospho/total Ssbp2-Csf1r and β-tubulin. The left panel comprises of DMSO control cells, while the right panel is dasatinib-resistant. In dasatinib-resistant cells, a decrease in the molecular weight of Ssbp2-Csf1r was observed. **B**: Densitometry analysis of p-Ssbp2-Csf1r bands normalised against the total isoform as previously described. Values plotted are the absolute values. **C**: Normalised graph of p-Ssbp2-Csf1r in concentrations indicated, relative to 0 nM dasatinib exposure. IC_{50} values were analysed using GraphPad Prism® as previously described. Data shown is representative of 3 experimental repeats. MW: molecular weight

Figure 5.20


A
Western Immunoblotting of Ssbp2-Csf1r
DMSO control
dasatinib-resistant
MW 0 1 10 100 500 1000 0 1 10 100 500 1000 nM dasatinib
Phospho-Ssbp2-Csf1r
100
75
Total-Ssbp2-Csf1r
100
75
β-Tubulin
50
B
Densitometry Analysis
Absolute Ratio
Ratio (phospho/total Ssbp2-Csf1r against β-tubulin)
15
10
5
0
DMSO control
dasatinib-resistant
0 10 50 100 500 1000
nM dasatinib
C
Ratio Normalised to 0 nM TKI
Normalised Ratio (phospho/total Ssbp2-Csf1r to 0 nM TKI)
100
50
0
DMSO control
IC50: 7 nM
dasatinib-resistant
IC50: 9 nM
0 10 50 100 500 1000
nM dasatinib

5.4. Discussion

In this chapter, the *SSBP2-CSF1R* Ph-like ALL was successfully modelled in Ba/F3 pro-B cells, where transformative potential (through IL-3 independent growth) suggested that the expression of this fusion gene can contribute to leukaemogenesis[73,89]. Cells harbouring the Ssbp2-Csf1r fusion were sensitive to imatinib and dasatinib, indicating a potential for the use of these clinically available TKIs in patients harbouring the *SSBP2-CSF1R* fusion[69,86]. Ba/F3 *SSBP2-CSF1R* cells also exhibited sensitivity to high concentrations of ponatinib and ruxolitinib which, however, aren't clinically relevant. The structural differences between ponatinib and imatinib/dasatinib may result in differences in binding affinity of TKI into the Csf1r catalytic pocket, affecting sensitivity[411].

As Ba/F3 Ssbp2-Csf1r cells were sensitive to imatinib, it was critical to model treatment-resistance in this setting. Imatinib-resistant Ba/F3 *SSBP2-CSF1R* cells appeared to phosphorylate Ssbp2-Csf1r at a higher rate compared to control. This suggests that the increased p-Ssbp2-Csf1r may be due to an alteration in intracellular dynamics, such as an increase in downstream pathways (i.e. Grb2-Sos-MAPK/Erk and PI3K/Akt pathway), resulting in the transcription of cell survival and proliferative signalling[412-414]. The process of generating TKI-resistant cells by dose-escalation may have resulted in the selection of cells expressing an abundance of p-Ssbp2-Csf1r, to overcome TKI sensitivity. This mechanism has been observed in other cancers such as CML (*BCR-ABL1* overexpression contributing to TKI resistance)[415,416] and lung cancer (*MET* amplification resulting in increased ErbB3-PI3K signalling and gefitinib resistance)[417].

Further investigation of *CSF1R*-L785M using the Catalogue of Somatic Mutations in Cancer (COSMIC) database revealed this was a previously unreported kinase-

domain mutation, hence a novel discovery[418]. Since this alteration was in a highly conserved region, a substitution of the amino acid leucine (131.17 g/mol) to methionine (149.21 g/mol) would result in the presence of a bulkier side-chain. This bulkier residue may negate critical drug-binding (**Figure 5.21**), affecting downstream TKI sensitivity which is well-known in CML and solid tumours[333,419,420]. In the Csf1r setting, the *CSF1R*-D802V point mutation has been documented to be imatinib-insensitive[409].

THIS PAGE INTENTIONALLY LEFT BLANK.

Figure 5.21

A

B

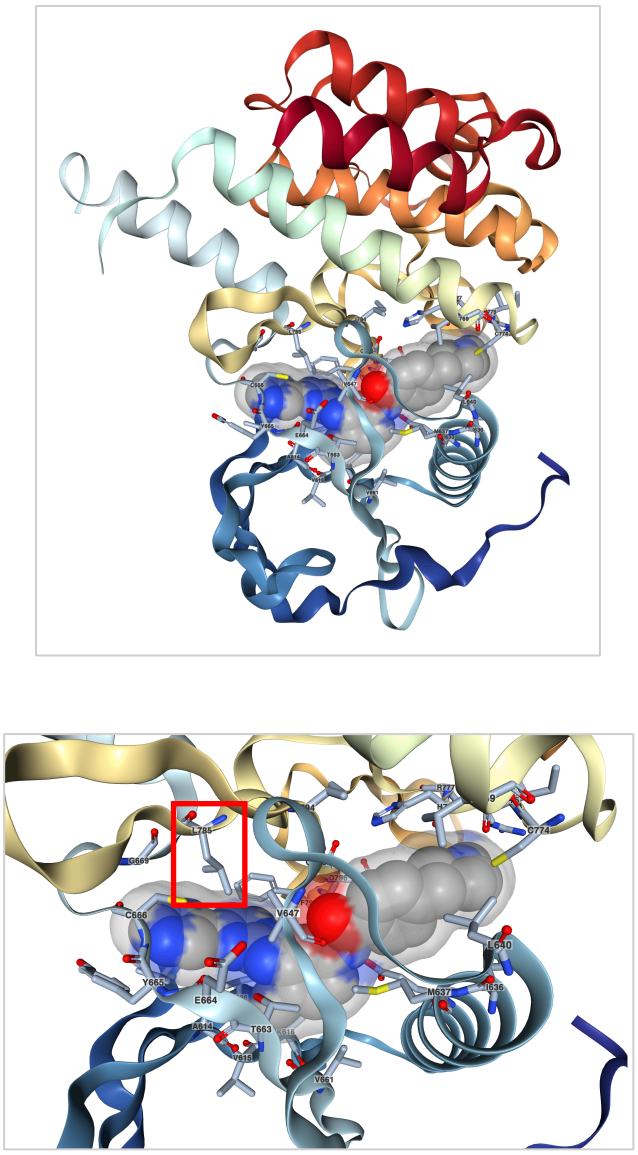


Figure 5.21 – Visualisation of the L785 residue in imatinib-bound Csf1r

A: Crystal structure of Csf1r (rainbow quaternary structure) bound to imatinib (grey spacefill structure) within the Csf1r kinase domain. **B:** Increased magnification of van der Waals interaction between Csf1r and imatinib, indicating the involvement of L785 (as highlighted by the red rectangle) in critical drug-binding. Structures were obtained from RCSB PDB[421] (ID: 4R7I; 10.2210/pdb4r7i/pdb)[422].

Interestingly, imatinib-resistant cells were sensitive to dasatinib and ponatinib, albeit at slightly higher concentrations compared to non-resistant cells. As was the observation of a decrease in cell viability when TKI was withdrawn in resistant cells, similar to the phenomenon observed in earlier experiments with imatinib. Such decrease in cell viability in the absence of TKI suggests a possible 'addiction' of cells to drug[423,424]. This phenomenon has been observed in other settings, where melanoma and lung cancer cells were found to be 'addicted' to BRAF and MEK inhibitors[425]. In this study, melanoma cells demonstrated a remarkable decrease in cell viability when cancer treatment was withdrawn, due to a phenotypic switch involving a dependency on Erk2, transcription factor JunB and the Fos-related antigen 1 (FRA1) signalling mechanisms[425]. Therefore, it is possible that imatinib-resistant cells were dependent on inhibition of downstream Csf1r-dependent signalling pathways, allowing for stabilisation of an alternative secondary survival mechanism. Furthermore, Csf1r has also been indirectly implicated in the stabilisation and nuclear translocation of β-catenin, a transcriptional co-activator of the Wnt/β-catenin signalling pathway through crosstalk with Src[426-428].

In dasatinib-resistant Ba/F3 *SSBP2-CSF1R* cells, a similar phenomenon of TKI 'addiction' was also observed, suggesting possible dependency of TKI-resistant cells on the activation of alternative pathways [425]. Dasatinib-resistant Csf1r cells also harboured a previously unreported *CSF1R*-A652V kinase domain mutation (based on data mining on the COSMIC database[418]), resulting in possible alteration of the kinase-domain[429,430]. In the *CSF1R*-A652V mutation, alanine (89.09 g/mol) is substituted to valine (117.15 g/mol) in a highly conserved region, and the presence of a bulkier valine side-chain accompanied with an increase in molecular mass may affect potential drug-binding, contributing towards TKI-resistance. This was because

a study demonstrated an adjacent mutation, *CSF1R*-T663I, conferring resistance to dasatinib. *CSF1R*-T663I was described to be functionally identical to the *ABL1*-T315I kinase-domain mutation [431].

The identification of a truncation over the *SSBP2-CSF1R* breakpoint in dasatinib-resistance was unexpected, indicating that the genetic alterations acquired in the process of development of TKI-resistance in cells may depend on the inhibitor. Dasatinib is structurally different to imatinib[432,433], binding to a different catalytic conformation (active vs inactive) in an Abl kinase setting[172,432]. The deletion spanning the breakpoint included a small region of both Ssbp2 and Csf1r, suggesting protein structure and downstream function may also be affected.

Taken together, this chapter has demonstrated that *SSBP2-CSF1R* Ph-like ALL cells can develop TKI-resistance, through an accumulation of multiple genetic alterations (**Figure 5.22**). These alterations are unique depending on TKI (imatinib or dasatinib), as these TKIs are structurally different, potentially binding to the kinase domain of Ssbp2-Csf1r in slightly different conformations. TKI-resistant Ba/F3 *SSBP2-CSF1R* cells were also surprisingly 'addicted' to their TKI, indicating a switch in a phenotype advantageous for TKI resistance may have occurred.

It is important to note that in a Csf1r setting, the presence of genetic alterations may, therefore, contribute to TKI-resistance through various methods; 1) negation of optimal drug-binding through an alteration within the drug-binding domain[409]; 2) increased phosphorylation of Csf1r[434,435] (which may be the scenario for imatinib-resistant Ba/F3 *SSBP2-CSF1R* cells), or, 3) loss of protein function[429,436], allowing for cells to adapt to a phenotypic switch / dependence on an alternative signalling mechanism of survival. The 'addiction' of TKI-resistant Ba/F3 *SSBP2-CSF1R* cells to certain concentrations of TKI suggests that an inhibition of fusion-derived Csf1r,

to a limited extent, is also required for the stable maintenance of cellular survival and proliferative mechanisms.

As the application of TKI-therapy in Ph-like ALL is an emerging field[205,398,437], the discoveries described in this chapter will inform future mechanisms that may arise in the event of treatment resistance. This may include the potential use of combination therapies involving inhibitors that are structurally different (i.e. the VEGFR inhibitor ABT-869 (Linifanib))[438], or inhibitors that target an alternative pathway (i.e. Hsp-90 inhibitor AUY922)[238,439,440]. These findings hope to thus provide an avenue for future studies into overcoming TKI-resistance in *SSBP2-CSF1R* Ph-like ALL.

Figure 5.22

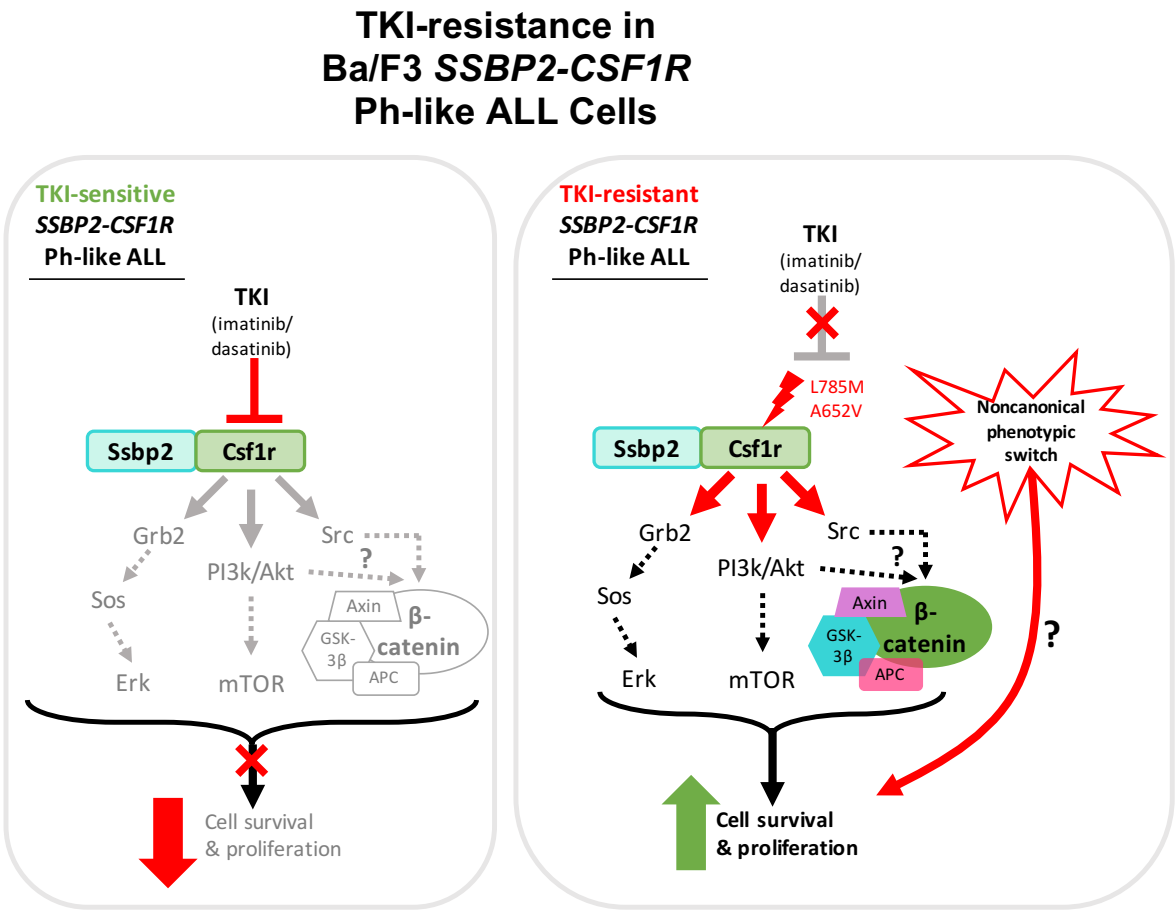


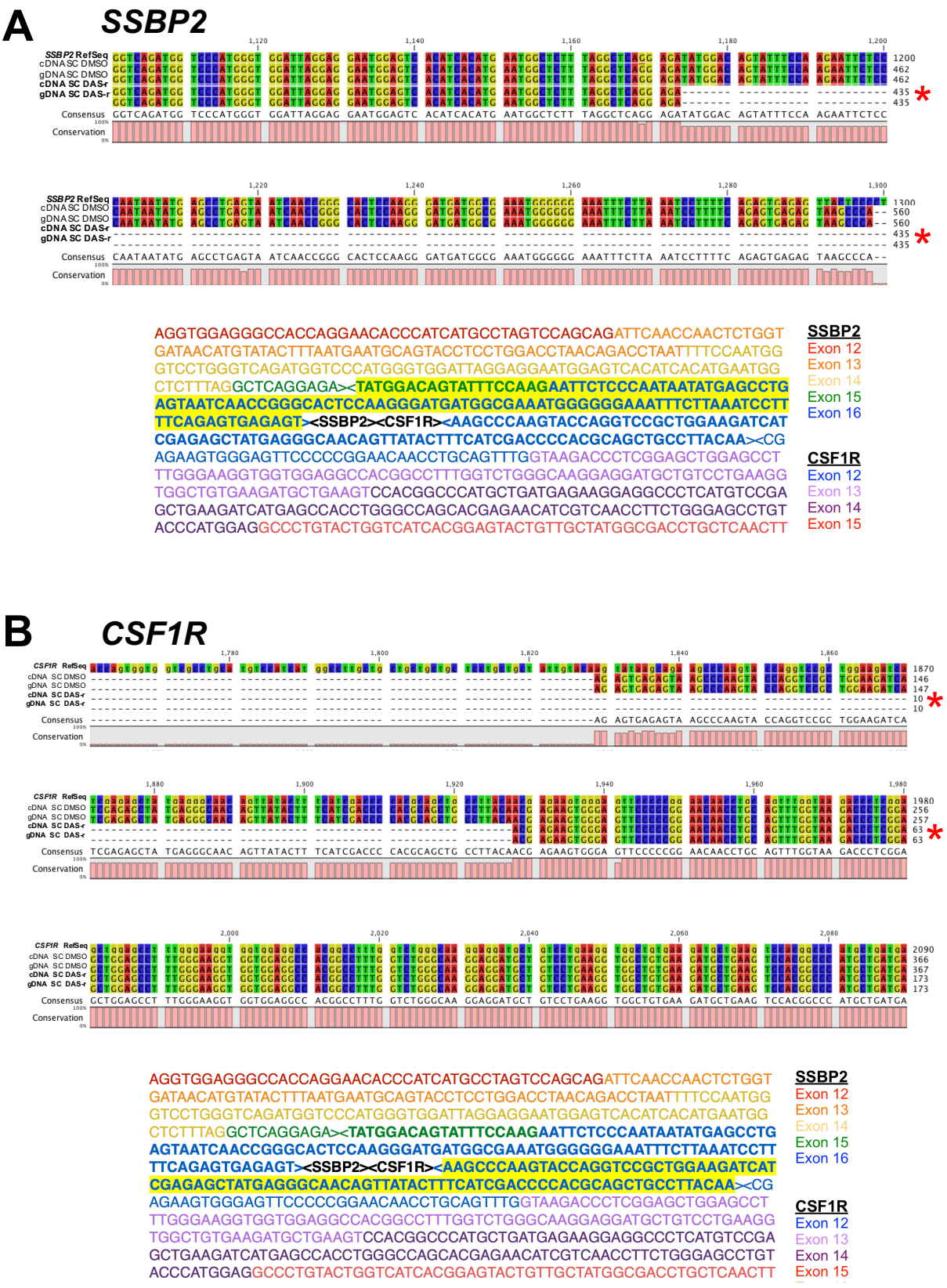
Figure 5.22 – Schematic diagram of TKI-resistance in Ba/F3 *SSBP2-CSF1R* Ph-like ALL cells

Left: Ba/F3 *SSBP2-CSF1R* cells are sensitive to the Abl-kinase TKIs imatinib and dasatinib, with exposure resulting in an inhibition of downstream signalling cascades (i.e. Grb2, PI3K/Akt, Src and possibly the β-catenin pathway) leading to an ultimate decrease in cell survival and proliferation. **Right:** In a TKI-resistant setting, Ba/F3 *SSBP2-CSF1R* cells were found to express the novel point mutations (imatinib-resistant: *CSF1R*-L785M; dasatinib-resistant: *CSF1R*-A652V), which may contribute towards a decreased TKI-sensitivity. As TKI-resistant Ba/F3 *SSBP2-CSF1R* cells were also dependent on the presence of TKI for cell survival and proliferation, a noncanonical phenotypic switch may have occurred, facilitating this process.

Appendix 5.1

Alignment of DNA sequences via CLC Sequence Viewer 7 (Qiagen, Hilden Germany), indicating a deletion spanning over the *SSBP2-CSF1R* breakpoint in dasatinib-resistant cells. *SSBP2* (NM 001256736.1) and *CSF1R* (NM 001288705.1) reference sequences were included, along with DMSO control and Ba/F3 *SSBP2-CSF1R* samples. Red asterisks highlight the deleted region in dasatinib-resistant samples, as reflected by the sequence maps beneath (yellow highlights).

Appendix 5.1



DNA alignment performed via CLC Sequence Viewer 7 (Qiagen, Hilden Germany)

THIS PAGE INTENTIONALLY LEFT BLANK.

CHAPTER 6 –

MECHANISMS OF TKI-RESISTANCE IN BA/F3 CELLS HARBOURING THE *PAX5-JAK2* Ph-LIKE ALL FUSION

6.1. Introduction

The discovery of *JAK* fusions in Ph-like ALL (i.e. *EBF1-JAK2*, *BCR-JAK2* and *PAX5-JAK2*) has enabled studies into the efficacy of utilising Jak inhibitors as a potential form of targeted therapy[64,73,204]. Such therapy includes the use of ruxolitinib, an FDA-approved Jak1/2 inhibitor currently used in the treatment of myeloproliferative neoplasms (MPNs) including myelofibrosis[132] and polycythaemia vera[441]. Ruxolitinib is a 'type I' Jak inhibitor, binding to the catalytic ATP-binding site in the active conformation of the Jak kinase domain[442,443]. Other 'type I' Jak inhibitors include BMS-911543 (targeting Jak1/2/3 and Tyk2 in MPN)[444,445] and fedratinib (also known as SAR302503, a Jak2 / Flt 3 inhibitor in phase II trials in myelofibrosis). Fedratinib appeared to be promising in clinical trials, however, reports of Wernicke's encephalopathy resulted in a discontinuation of use[446-449]. More recently, momelotinib (CYT-387 – a Jak1/2, Tyk2 and Alk2 inhibitor)[450,451] has been clinically investigated in phase I/II trials as a treatment for myelofibrosis, polycythaemia vera and essential thrombocythemia[452-454].

The Jak family of intracellular non-receptor tyrosine kinases (Jak1, Jak2, Jak3 and Tyk2) each function as a mediator between cytokines and growth factor receptor signalling (i.e. interferon, TSLP and IL-7Rα) and the activation of downstream signal transduction of STAT transcription factor family of proteins[455-458]. Endogenously, Jak2 is tagged onto its receptor and upon ligand binding, a conformational dimerisation of the receptor occurs, resulting in activation of the tyrosine kinase domain[459,460]. Structurally, Jak2 comprises of 7 subunits, resulting in the formation of the 4.1 ezrin, radixin and moesin (FERM), SH2-like, JH2 (pseudokinase) and JH1 (kinase) domains[461,462]. The pseudokinase domain, a fundamental autoinhibitory domain essential for prevention of pathogenesis of Jak2, is aberrantly activated by

the *JAK2*-V617F mutation in MPNs[463-465]. Jak kinase inhibitors have been used clinically to overcome the *JAK2*-V617F mutation[466,467]. Targeting the kinase domain of Jak2, however, has its caveats as recent studies have demonstrated the occurrence of point mutations such as *JAK2*-G935R, *JAK2*-R938L and *JAK2*-Y931C, resulting in drug resistance to ATP-competitive Jak inhibitors[200,468,469].

As Jak inhibitors, such as ruxolitinib, present an attractive therapeutic option in the treatment of Jak fusions in Ph-like ALL, it is key to investigate the mechanisms that lead to treatment resistance. To date, however, Jak kinase inhibitor resistance in a Ph-like ALL setting has not been fully explored. In this chapter, the mechanisms of TKI-resistance in Ba/F3 cells harbouring the *PAX5-JAK2* Ph-like ALL fusion gene were investigated through the establishment of ruxolitinib and BMS-911543 resistance. *PAX5* is essential for the function and maintenance of B-cell identity, and alterations/mutations/deletions in the gene are associated with inhibition of B-cell maturation resulting in leukaemogenesis[22,25-27]. The 3-prime kinase partner of *PAX5-JAK2* comprises a sole JH2 kinase domain, hyperactivated due to a lack of autoinhibitory mechanisms. Therefore, studying this model will allow for identification of resistance mechanisms unique to the catalytic kinase domain of Jak2. As clinical trials of ruxolitinib in ALL are currently underway[470,471], the outcome of studies in this chapter will inform future therapeutic considerations in targeting *PAX5-JAK2* (and potentially other Jak fusions) in Ph-like ALL.

6.2. Approach

Retrovirally-transduced Ba/F3 MSCV *PAX5-JAK2* cells were confirmed for TKI-sensitivity by exposure to a panel of Abl-kinase inhibitors (imatinib, nilotinib, dasatinib and ponatinib), Jak-kinase inhibitors (ruxolitinib and BMS-911543) as well as the Flt3 inhibitor quizartinib. Cell death was evaluated by Annexin-V/7-AAD exclusion analysis.

TKI-resistance was generated by exposing cells to incrementally increasing concentrations of ruxolitinib and BMS-911543, to a final concentration of 10 μM *in vitro*. In a parallel culture, TKI-sensitive control cells were passaged in 0.1% DMSO (vehicle for ruxolitinib and BMS-911543) to account for any changes that may occur as a result of long-term DMSO exposure. TKI-resistance was confirmed via cell death assay analysis, as well as western blotting of Stat5 phosphorylation (a downstream marker of Jak2 kinase activity). Sanger sequencing was further employed to identify any mutations within the *JAK2* kinase-domain, and an MTS assay was performed to determine the proliferation capacity of ruxolitinib-resistant cells compared to DMSO control.

mRNA sequencing was subsequently performed using samples of three biological replicate passages of ruxolitinib-resistant and DMSO control cells, with reads aligned to the mouse genome and differential-expression analysis validated by RQ-PCR. Hierarchical clustering tree, heatmap and volcano plots were generated using RStudio[247]. Further data interrogation was performed using significantly upregulated and downregulated differentially-expressed genes (Log_2FC >1, P<0.05), via the pathway analysis tool on InnateDB[223]. A network analysis using the top 50 upregulated/downregulated genes was generated via NetworkAnalyst[472]. To identify nodes that were contextually-relevant, a separate network analysis utilising

differentially-expressed genes that were significantly upregulated and downregulated (Log_2FC >1, P<0.05) was performed using the Contextual Hub Analysis Tool (CHAT)[227] application via the Cytoscape[225] network visualisation software.

6.3. Results

6.3.1. Ba/F3 *PAX5-JAK2* Ph-like ALL cells are sensitive to Jak-specific TKIs

To investigate TKI-sensitivity in Ba/F3 cells harbouring the *PAX5-JAK2* fusion gene, cells were exposed to increasing concentrations of Jak-specific inhibitors (i.e. ruxolitinib and BMS-911543) as well as inhibitors designed for other kinases (i.e. the Abl-kinase inhibitors imatinib, nilotinib, dasatinib, ponatinib, and, the Flt3 inhibitor quizartinib) for 3 days prior to viability analysis via Annexin-V/7-AAD flow cytometry. In cells treated with imatinib (0, 1.25, 2.5, 5 and 10 μM), nilotinib (0, 12.5, 25, 50, 100 nM), dasatinib (0, 12.5, 25, 50, 100 nM) and ponatinib (0, 12.5, 25, 50, 100 nM), no decrease in cell viability was observed (**Figure 6.1**). A significant decrease in cell viability was observed, however, when cells were exposed to ruxolitinib (0, 1.25, 2.5, 5 and 10 μM – 100%, 51±10%, 6±7%, 3±4% and 2±4% viable respectively; $P < 0.05$) and BMS-911543 (0, 1.25, 2.5, 5 and 10 μM – 100%, 82±8%, 48±11%, 5±7% and 1±1% viable respectively; $P < 0.05$). No decrease in viability was observed in cells treated with the Flt3 inhibitor quizartinib. When western immunoblotting of Pax5-Jak2 protein phosphorylation status was performed, no differences were observed in the presence of TKIs (**Appendix 6.1A**).

Figure 6.1

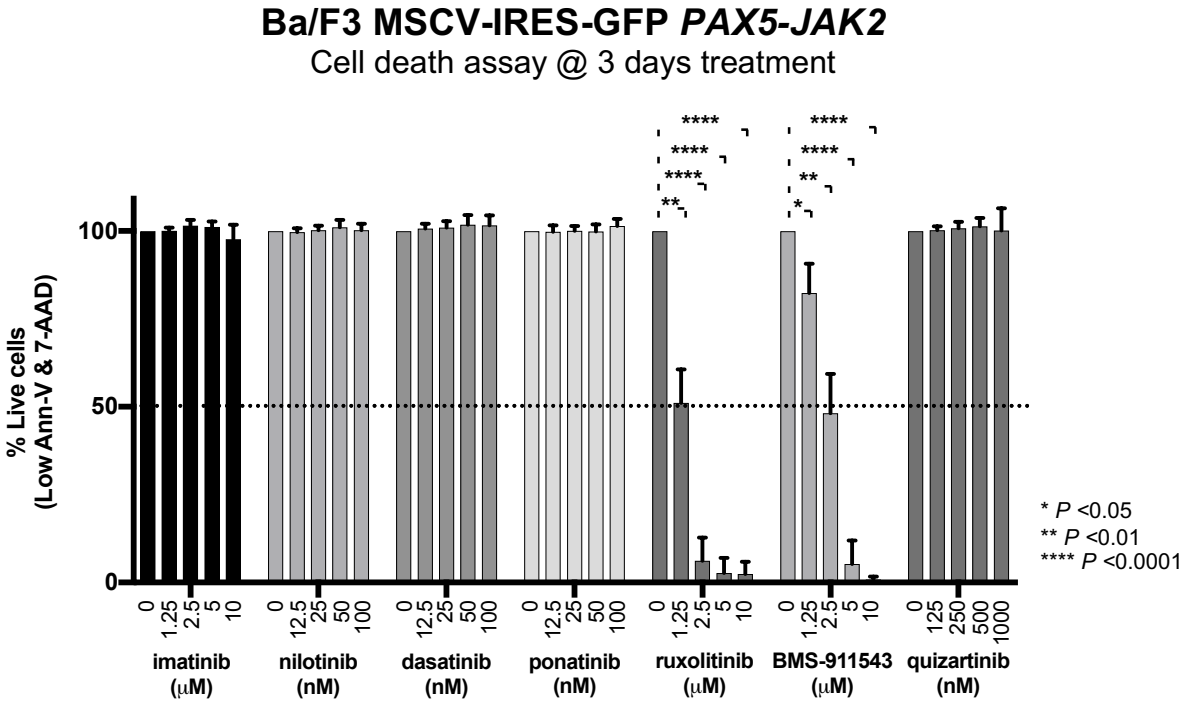


Figure 6.1 – Ba/F3 *PAX5-JAK2* cells are sensitive to the Jak-specific inhibitors ruxolitinib and BMS-911543

Annexin-V/7-AAD exclusion flow cytometry of TKI-sensitivity in BaF3 *PAX5-JAK2* cell line, with the graph indicating the percentage of cell viability (*y*-axis) and TKI concentrations (*x*-axis). Cells were treated with a panel of TKIs including Abl kinase inhibitors (imatinib, nilotinib, dasatinib and ponatinib), Jak kinase inhibitors (ruxolitinib, BMS-911543) and a Flt3 inhibitor (quizartinib) for 3 days at 37ºC / 5% CO_2. Columns represent mean of 4 independent experiments, while error bars denote the standard deviation. Dotted line depicts the half maximal lethal dose concentration (LD_{50}) of inhibitors in Ba/F3 *PAX5-JAK2* cells. Asterisks indicate statistical significance based on the Student's *t*-test method.

6.3.2. TKI-resistant Ba/F3 *PAX5-JAK2* cell lines are cross-resistant to ruxolitinib and BMS-911543 (Jak2*i*) compared to DMSO control cells

Following confirmation of TKI-sensitivity of Ba/F3 *PAX5-JAK2* cells to Jak inhibitors, cells were exposed to incrementally increasing doses of TKI, to a final concentration of 10 μM ruxolitinib and BMS-911543. TKI-resistance was confirmed by analysis of cell viability using Annexin-V/7-AAD flow cytometry, as well as western blotting of downstream phosphorylated Stat5.

Using Annexin-V/7-AAD, an increased ruxolitinib LD_{50} was observed in ruxolitinib-resistant Ba/F3 *PAX5-JAK2* cells ($LD_{50}^{ruxolitinib}$: >10 μM) compared to DMSO control ($LD_{50}^{ruxolitinib}$: 2.5 μM) (**Figure 6.2A**). The percentage viability of cells was significantly different in cells exposed to 2.5 μM ruxolitinib (DMSO – 60% ± 1%; ruxolitinib-resistant – 97% ± 5%, P<0.01; BMS911654-resistant – 111% ± 10%, P<0.05), 5 μM ruxolitinib (DMSO – 5% ± 4%; ruxolitinib-resistant – 94% ± 6%, P<0.01; BMS911654-resistant – 108% ± 8%, P<0.001) and 10 μM ruxolitinib (DMSO – 3% ± 2%; ruxolitinib-resistant – 88% ± 3%, P<0.001; BMS911654-resistant – 36% ± 6%, P<0.01).

BMS911543-resistant cells also demonstrated cross-resistance to ruxolitinib ($LD_{50}^{ruxolitinib}$: 7.5 μM). A similar cell death assay was performed in the presence of 0, 1, 2.5, 5, 10 and 50 μM BMS-911543, where flow cytometry analysis revealed an $LD_{50}^{BMS\text{-}911543}$ of 2 μM in DMSO control cells, >50 μM in ruxolitinib-resistant cells and 30 μM in BMS911543-resistant cells (**Figure 6.2B**). The cell viability was significantly different in cells exposed to 5 μM BMS911654 (DMSO – 6% ± 5%; ruxolitinib-resistant – 97% ± 12%, P<0.01; BMS911654-resistant – 116% ± 15%,

P<0.05) and 10 μM BMS911654 (DMSO – 0.2% ± 0.1%; ruxolitinib-resistant – 97% ± 14%, *P*<0.01; BMS911654-resistant – 124% ± 14%, *P*<0.001).

Further analysis of phosphorylated Stat5 expression by Western blot in TKI-sensitive and resistant Ba/F3 *PAX5-JAK2* cells revealed an increased IC_{50} in ruxolitinib and BMS-911543 resistant cells compared to DMSO control (**Figure 6.3**). Exposure of cells to an increasing concentration of ruxolitinib (0, 0.1, 0.5, 1, 5 and 10 μM – 1 hr treatment) indicated an $IC_{50}^{ruxolitinib}$ of 0.09 μM in DMSO control cells, 1.3 μM in ruxolitinib-resistant and 0.5 μM in BMS911543-resistant cells (**Figure 6.3A**). In the analysis of p-Stat5 expression in cells treated with an increasing concentration of BMS-911543 (0, 0.1, 0.5, 1, 5 and 10 μM), the $IC_{50}^{BMS-911543}$ of p-Stat5 was 0.1 μM in DMSO control cells, 4.5 μM in ruxolitinib-resistant and 0.8 μM in BMS911543-resistant cell lines (**Figure 6.3B**). Western immunoblotting of phosphorylated Pax5-Jak2 protein isoform did not indicate any differences, despite downstream inhibition of p-Stat5 (**Appendix 6.1B**).

Figure 6.2 – Annexin-V/7-AAD cell death exclusion assay confirms Jak*i*-resistance in Ba/F3 *PAX5-JAK2* ruxolitinib and BMS-911543 resistant cell lines

Ba/F3 *PAX5-JAK2* DMSO control, ruxolitinib and BMS-911543 resistant cells were exposed to 0, 0.1, 0.5, 1, 5 and 10 μM ruxolitinib (**A**) or 0, 1, 2.5, 5, 10 and 50 μM BMS-911543 (**B**) for 3 days at 37 ºC, prior to harvesting of cells for Annexin-V/7-AAD analysis via flow cytometry. Columns represent mean of 3 independent experiments while error bars denote ± SD. Asterisks depict significant *P* values, as analysed via the multiple comparisons method on GraphPad® Prism. The dotted line represents the LD_{50} concentration of Jak-inhibitor treatment in TKI-sensitive and resistant Ba/F3 *PAX5-JAK2* cell lines normalised against the untreated controls.

Figure 6.2

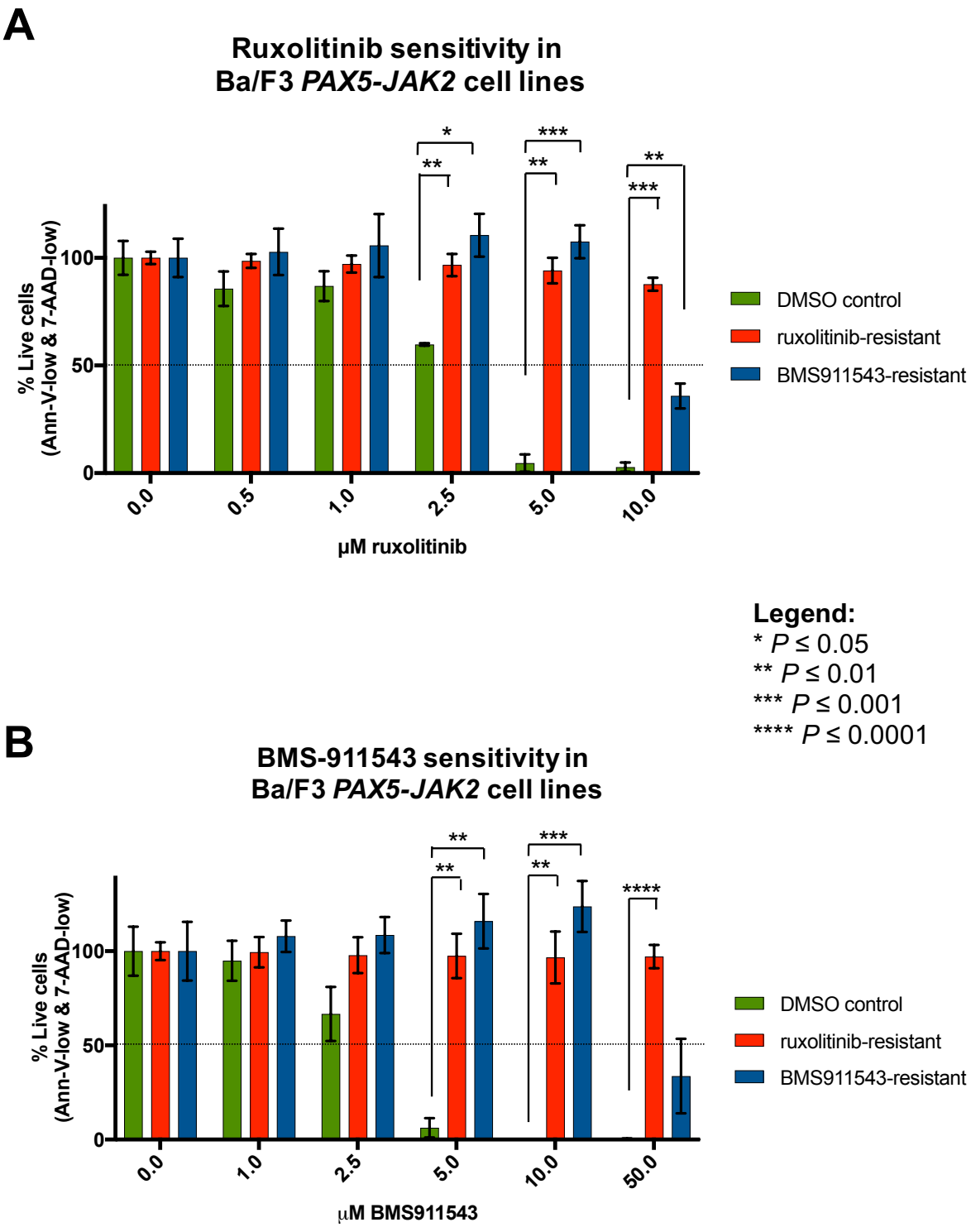
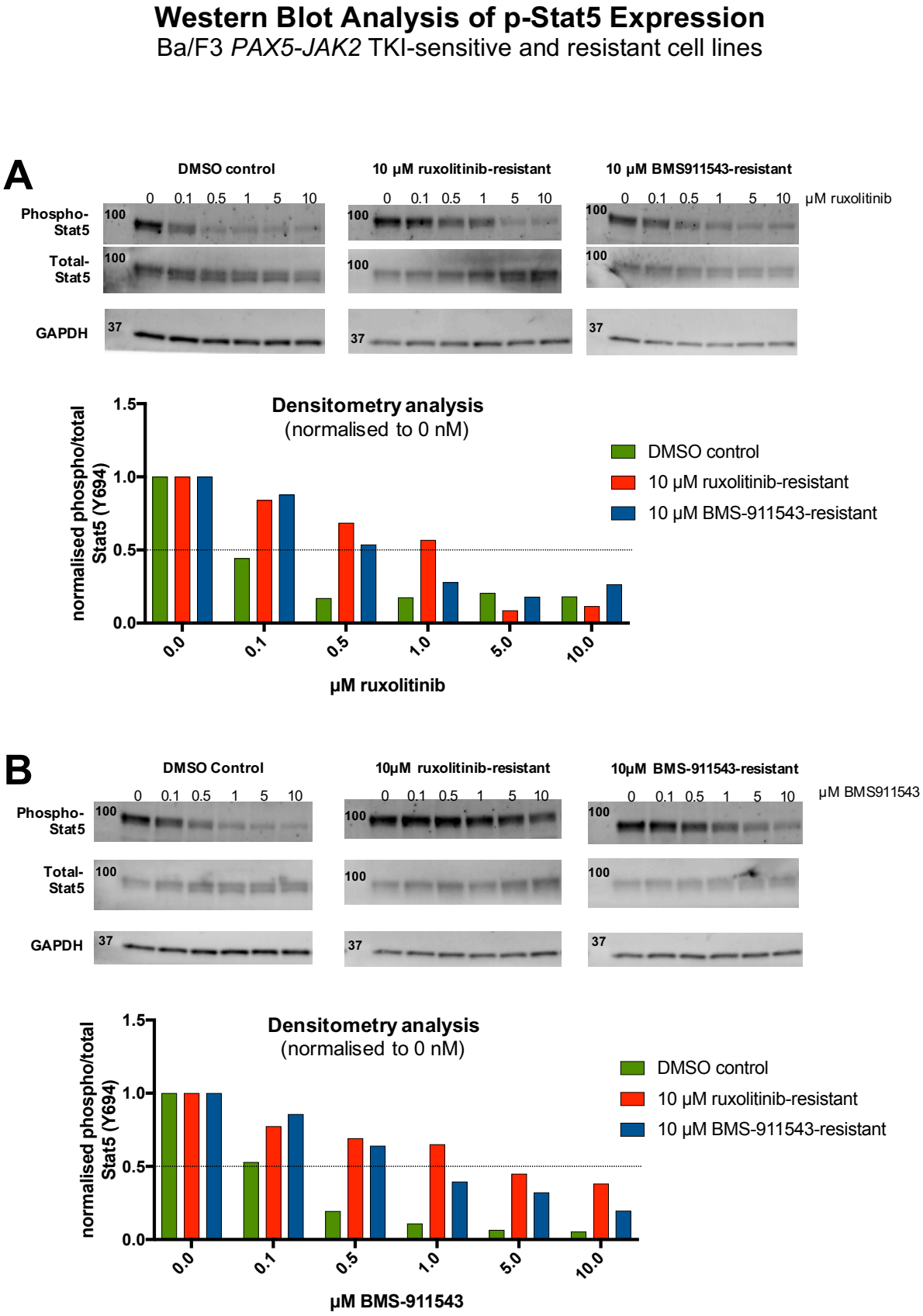

A
Ruxolitinib sensitivity in
Ba/F3 PAX5-JAK2 cell lines
% Live cells
(Ann-V-low & 7-AAD-low)
100
50
0
0.0
0.5
1.0
2.5
5.0
10.0
µM ruxolitinib
*
**
***
DMSO control
ruxolitinib-resistant
BMS911543-resistant
Legend:
* P ≤ 0.05
** P ≤ 0.01
*** P ≤ 0.001
**** P ≤ 0.0001
B
BMS-911543 sensitivity in
Ba/F3 PAX5-JAK2 cell lines
% Live cells
(Ann-V-low & 7-AAD-low)
100
50
0
0.0
1.0
2.5
5.0
10.0
50.0
µM BMS911543
****
DMSO control
ruxolitinib-resistant
BMS911543-resistant

Figure 6.3 – Western blotting of p-Stat5 (direct downstream partner of Jak2 activity) indicates an increased pStat5 IC_{50} in ruxolitinib and BMS-911543 resistant Ba/F3 *PAX5-JAK2* cell lines, compared to DMSO control

Ba/F3 *PAX5-JAK2* DMSO control, ruxolitinib and BMS-911543 resistant cells were exposed to 0, 0.1, 0.5, 1, 5 and 10 μM ruxolitinib (**A**) or BMS-911543 (**B**) for 1 hour at 37ºC / 5% CO_2, prior to collection of cells for western blot analysis. Membranes were incubated with antibodies specific for phosphorylated Stat5 (Y694), total Stat5 and GAPDH (as a loading control). The intensity of protein bands was measured using the ImageLab™ software and densitometry graphs plotted via GraphPad® Prism™ as previously described. Plots beneath indicate normalised values relative to 0 nM treatment, with dotted lines representing the p-Stat5 IC_{50}. Blots shown are representative of n=3 independent experiments.

Figure 6.3


Western Blot Analysis of p-Stat5 Expression
Ba/F3 PAX5-JAK2 TKI-sensitive and resistant cell lines
A
DMSO control
10 µM ruxolitinib-resistant
10 µM BMS911543-resistant
0 0.1 0.5 1 5 10
µM ruxolitinib
Phospho-Stat5
Total-Stat5
GAPDH
100
37
Densitometry analysis
(normalised to 0 nM)
normalised phospho/total Stat5 (Y694)
1.5
1.0
0.5
0.0
0.0 0.1 0.5 1.0 5.0 10.0
µM ruxolitinib
DMSO control
10 µM ruxolitinib-resistant
10 µM BMS-911543-resistant
B
DMSO Control
10µM ruxolitinib-resistant
10µM BMS-911543-resistant
µM BMS911543
Densitometry analysis
(normalised to 0 nM)
µM BMS-911543

THIS PAGE INTENTIONALLY LEFT BLANK.

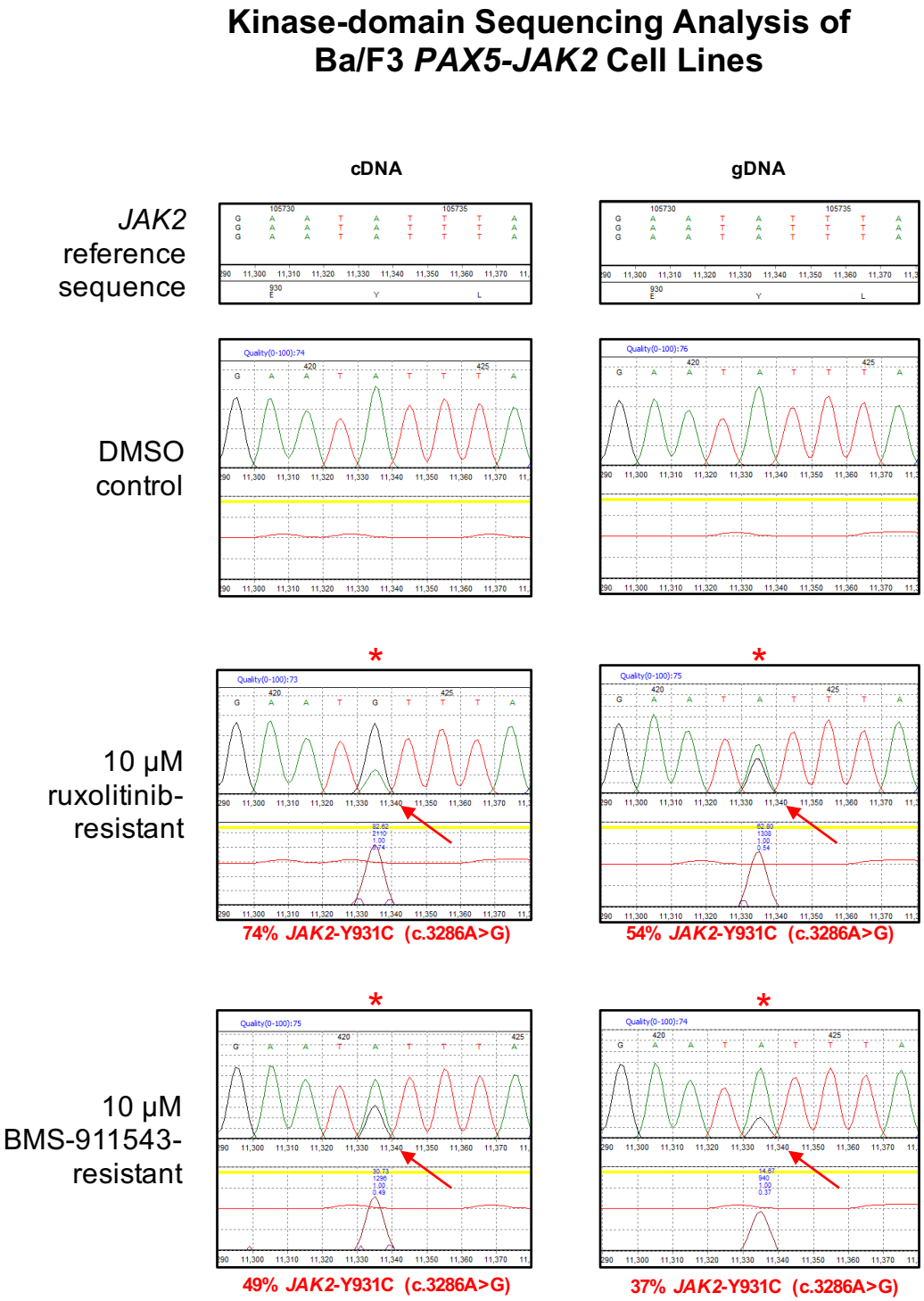
6.3.3. Identification of a *JAK2*-Y931C kinase-domain mutation in TKI-resistant Ba/F3 *PAX5-JAK2* cell lines

To determine whether TKI-resistance in Ba/F3 *PAX5-JAK2* ruxolitinib and BMS-911543 resistant cell lines were attributed to genetic alterations within the protein kinase domain, molecular amplification of the kinase domain, followed by Sanger sequencing, was performed. Mutation analysis of DNA electropherograms revealed an alteration of the nucleotide adenine to guanine, resulting in a substitution of the amino acid tyrosine to cysteine at position 931 of the Jak2 kinase domain (**Figure 6.4**). DNA templates utilised for kinase domain mutation analysis include both complementary and genomic DNA (cDNA and gDNA respectively), resulting in a finding of 74% (cDNA) and 54% (gDNA) *JAK2*-Y931C mutational burden in the 10 μM ruxolitinib-resistant cell line, as well as 49% (cDNA) and 37% (gDNA) *JAK2*-Y931C in the 10 μM BMS911543-resistant cell line.

Figure 6.4 – Sanger sequencing uncovers a *JAK2*-Y931C kinase-domain mutation in ruxolitinib and BMS-911543 resistant Ba/F3 *PAX5-JAK2* cell lines

DNA electropherograms of Sanger sequencing analysis specific for the 3' kinase-fusion partner in Ba/F3 *PAX5-JAK2* DMSO control, ruxolitinib-resistant and BMS-911543-resistant cell lines. Data derived from PCR products obtained using cDNA and gDNA are represented in the left and right columns, respectively. Mutation analysis was performed using the Mutation Surveyor® DNA analysis software, with a reference sequence included (indicated in the top panel). Red asterisks indicate the presence of a *JAK2*-Y931C (c.3286A>G) kinase domain mutation (as highlighted by the red arrows), and frequency noted beneath samples.

Figure 6.4


Kinase-domain Sequencing Analysis of
Ba/F3 PAX5-JAK2 Cell Lines
cDNA
gDNA
JAK2 reference sequence
DMSO control
10 µM ruxolitinib-resistant
10 µM BMS-911543-resistant
*
74% JAK2-Y931C (c.3286A>G)
54% JAK2-Y931C (c.3286A>G)
49% JAK2-Y931C (c.3286A>G)
37% JAK2-Y931C (c.3286A>G)

6.3.4. Ruxolitinib-resistant Ba/F3 *PAX5-JAK2* Y931C cells demonstrate a higher proliferation rate compared to DMSO control cells

Following the identification of a *JAK2*-Y931C kinase domain mutation in Ba/F3 *PAX5-JAK2* cells resistant to a final concentration of 10 μM ruxolitinib, the proliferative capacity of ruxolitinib-resistant compared to DMSO control cells was assessed over a period of 3 days. Exposure of cells to increasing concentrations of ruxolitinib (0, 0.1, 0.5, 1, 2.5, 5, 10, 25 and 50 μM) resulted in a decreased cell proliferation in DMSO control cells (EC_{50}: <2.5 μM) compared to ruxolitinib-resistant cells (EC_{50}: >10 μM) (**Figure 6.5**).

An increase in the absorbance reading (indicating increased cell density) was observed over the 3-day period, where DMSO control cells proliferated at a rate of 2.7 times between 24 h to 48 h (OD_{490nm} of 0.35 vs 0.95 respectively), and a rate of 1.8 between the 48 h and 72 h time-points in the absence (0 nM) of TKI (OD_{490nm} of 0.95 vs 1.66 respectively). In ruxolitinib-resistant cells, a proliferation rate of 2.9 (OD_{490nm} 0.29 and 0.83 from 24 to 48h respectively) and 2.1 (OD_{490nm} 0.83 and 1.75 from 48 to 72 h) was observed at 0 nM TKI (**Figure 6.5A**). A decrease in cell proliferation of DMSO control cells was observed when cells were exposed to ruxolitinib concentrations higher than 0.1 μM, while in ruxolitinib-resistant cells, a marked decrease in proliferation was observed in concentrations above 10 μM ruxolitinib (**Figure 6.5A**).

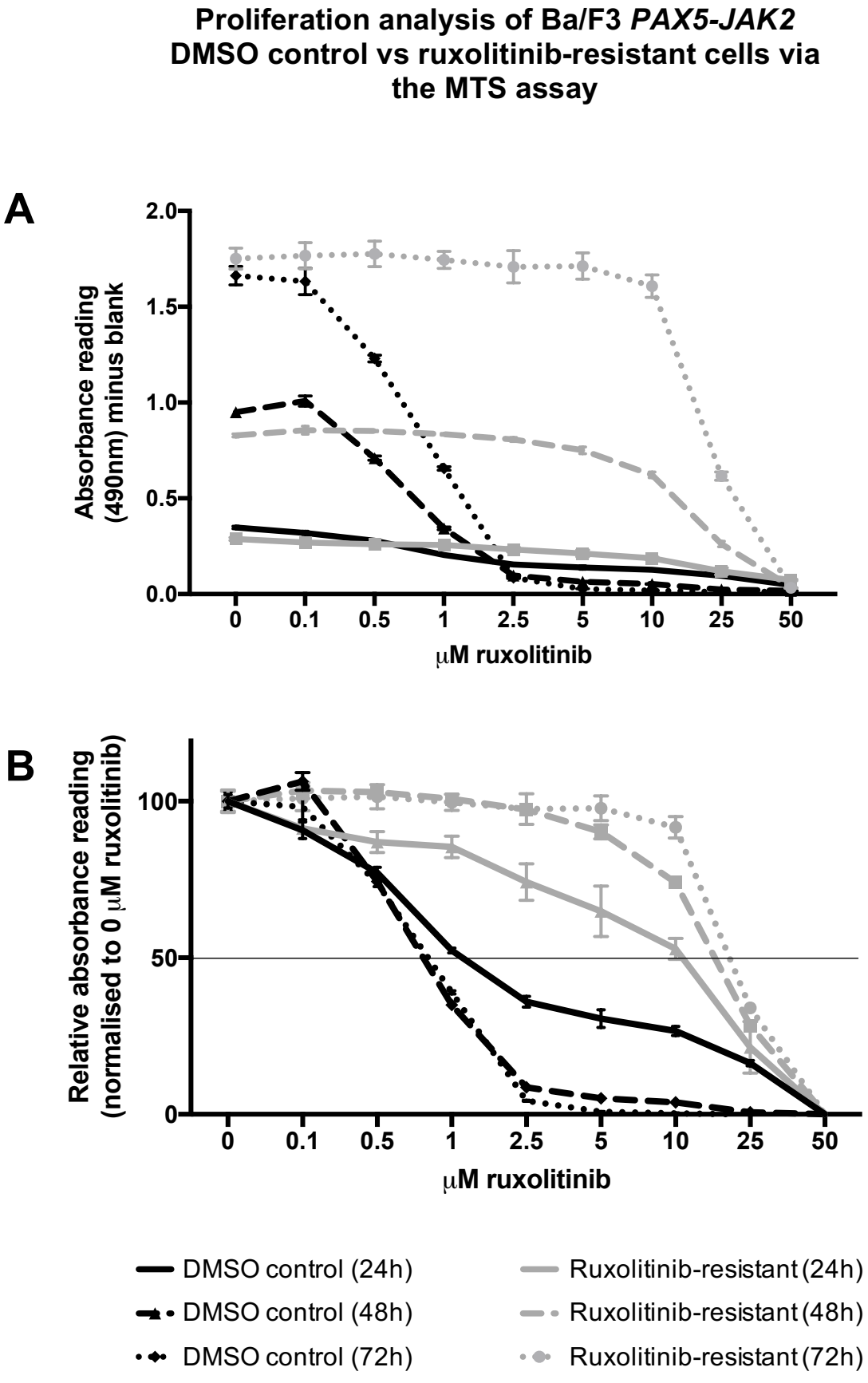
Further normalisation of cell proliferation assay data confirmed increased 50% effective concentration (EC_{50}) of ruxolitinib in resistant cells, compared to control (**Figure 6.5B**). In DMSO control cells, a decrease in EC_{50} was observed as the time-points increased, indicating TKI-sensitivity. In ruxolitinib-resistant cells, the EC_{50} of ruxolitinib increased as cells were incubated for 24, 48 and 72 h. The increased IC_{50}

confirmed ruxolitinib tolerance and a proliferative advantage in the TKI-resistant cells (**Figure 6.5B**).

Figure 6.5 – Ba/F3 *PAX5-JAK2* ruxolitinib-resistant cells demonstrate a higher proliferation rate compared to DMSO control cell line

Ba/F3 *PAX5-JAK2* DMSO control (represented by black lines) and ruxolitinib-resistant cells (represented by grey lines) were treated in increasing concentrations of ruxolitinib (0, 0.1, 0.5, 1, 2.5, 5, 10, 25, 50 μM) in 37ºC / 5% CO_2. Cells were seeded at 5 x 10^4 / mL and proliferation measured via the MTS assay (absorbance reading of 490 nm) at 24, 48 and 72 h as indicated in the legend. Results were analysed and plotted using GraphPad® Prism™, with the absolute reading presented in the upper panel (**A**) and relative reading (normalised to 0 nM ruxolitinib) presented in the lower panel (**B**). Line across the *y*-axis denotes the TKI concentration required for 50% of growth inhibition, based on normalisation of data to controls at 0 nM TKI. Error bars indicate ± SD of technical triplicates.

Figure 6.5


Proliferation analysis of Ba/F3 PAX5-JAK2 DMSO control vs ruxolitinib-resistant cells via the MTS assay
A
Absorbance reading (490nm) minus blank
2.0
1.5
1.0
0.5
0.0
0
0.1
0.5
1
2.5
5
10
25
50
μM ruxolitinib
B
Relative absorbance reading (normalised to 0 μM ruxolitinib)
100
50
0
0
0.1
0.5
1
2.5
5
10
25
50
μM ruxolitinib
DMSO control (24h)
DMSO control (48h)
DMSO control (72h)
Ruxolitinib-resistant (24h)
Ruxolitinib-resistant (48h)
Ruxolitinib-resistant (72h)

..

6.3.5. mRNA sequencing identifies non-canonical signalling pathways associated with ruxolitinib-resistance in Ba/F3 *PAX5-JAK2* cell line

To further elucidate if ruxolitinib-resistance in Ba/F3 *PAX5-JAK2* cells have alternative signalling mechanisms that may contribute to TKI-resistance, mRNA sequencing was performed. Supervised hierarchical clustering confirmed a close association between 3 biological replicate samples from 3 different passages of each cell line (DMSO control and ruxolitinib-resistant) (**Figure 6.6A**). Further heatmap analysis confirmed a unique pattern between significantly differentially-expressed genes (P<0.05), whereby genes that were upregulated in DMSO control samples were downregulated in ruxolitinib-resistant samples and vice versa (**Figure 6.6B**).

Subsequent volcano plot results indicated a number of significantly differentially-expressed genes in ruxolitinib-resistant Ba/F3 *PAX5-JAK2* cells (**Figure 6.7A**). There were 238 significantly upregulated genes ($Log_2FC > 1$; P<0.05) and 219 significantly downregulated genes ($Log_2FC < -1$; P<0.05) in ruxolitinib-resistant cells compared to DMSO control. Of these genes, 10 genes were selected for validation using RQ-PCR. Five genes were upregulated (FRY microtubule binding protein (*Fry*), Aldehyde dehydrogenase family 1, subfamily A1 (*Aldh1a1*), GLI-Kruppel family member GLI2 (*Gli2*), left-right determination factor 1 (*Lefty1*) and B cell CLL / lymphoma 11A zinc finger protein (*Bcl11a*). The remaining 5 downregulated genes validated were Snail family transcriptional repressor 3 (*Snai3*), regulator of G-protein signalling 5 (*Rgs5*), caspase 12 (*Casp12*), receptor transporter protein 4 (*Rtp4*) and Neogenin 1 (*Neo1*) (**Figure 6.7**and **Appendix 6.2**). Results of differentially-expressed gene analysis between control and resistant cell lines correlated with RQ-PCR validation results, where genes expected to be upregulated indicated a comparative fold change of more than 1 ($\Delta\Delta C_T$ fold changes – *Fry*:1.97 $\pm$ 0.67;

Aldh1a1: 5347.65 ± 2054.15; *Gli2*: 23.83 ± 15.82; *Lefty1*: 21.50 ± 3.33 and *Bcl11a*: 1.16 ± 0.72) (**Figure 6.7B&C** and **Appendix 6.2**). Genes that were downregulated were similarly decreased in validation analysis ($\Delta\Delta C_T$ fold changes –*Snai3*: 0.22 ± 0.03; *Rgs5*: 0.04 ± 0.01; *Casp12*: 0.08 ± 0.02; *Rtp4*: 0.01 ± 0.01 and *Neo1*: 0.57 ± 0.09) (**Figure 6.7B**&**C** and **Appendix 6.2**).

A pathway enrichment analysis was subsequently performed using significantly differentially-expressed downregulated ($Log_2FC < -1$; $P<0.05$) and upregulated ($Log_2FC > 1$; $P<0.05$) gene sets, via InnateDB (**Figure 6.8**). A hypergeometric distribution test for pathways enriched using the downregulated genes indicated a significant enrichment ($P<0.05$) of pathways associated with interferon and immune signalling (*B2m*, *Gbp2* as well as the *Oas* and *Socs* families of genes) (**Figure 6.8A** & **Appendix 6.3A**). Interestingly, pathways associated with metabolism such as glycolysis and gluconeogenesis (*Aldoa*, *Eno1*, *Gm5506*, *Pgam* and *Pgk1*), as well as Jak-STAT signalling (*Irf9*, *Socs1*, *Socs3* and *Stat1*) and cellular differentiation (*Junb*, *Map2k1* and *Relb*) were identified (**Figure 6.8A** & **Appendix 6.3A**).

Pathway enrichment analysis using significantly upregulated genes revealed an association with ethanol oxidation (*Aldh1a1* and *Aldh1a7*), caspase-mediated cleavage of cytoskeletal proteins (*Casp6* and *Mapt*), G alpha (12/13) signalling events (*Arhgef18*, *Arghef3* and *Itsn1*), and transportation of molecules (*Rhag*, *Slc14a1*, *Slc22a3* and *Slc44a4*) (**Figure 6.8B** & **Appendix 6.3B**). There was, however, a lack of statistical significance when upregulated genes were utilised as the smallest *P* value resulting from the pathway analysis was more than 0.05 (pancreatic secretion pathway – $P = 0.16$) (**Figure 6.8B** & **Appendix 6.3B**).

To investigate how differentially-regulated genes might interact with each other, network analysis via NetworkAnalyst[472] using the top 50 most upregulated and

downregulated genes was performed (**Figure 6.9**). Specifically, a network of these genes using publicly available protein-protein interaction (PPI) maps from the IMEx dataset was constructed. Analysis of the network highlighted several hubs associated with Jak-STAT signalling (2 degrees of interaction between *Socs3* and *Irf1*, which were also major hubs), along with the interaction between downregulated genes *Lefty1* and *Gli2* (**Figure 6.9** and **Appendix 6.4**). These hubs also showed high betweenness, that is, these formed bottlenecks in the network thereby reiterating their topological centrality in the network (**Figure 6.9** and **Appendix 6.4**). Of note, bottlenecks incorporating the downregulated genes include *Irf1* (41 and 4869.7), *Socs3* (29 and 4449.13) and *Nos1* (11 and 1619.94) (degree and betweenness score respectively). Bottlenecks involving genes that were upregulated include *Gli2* (13 and 1401.87), *Gab1* (11 and 1714.5), Lefty1 (8 and 1274.93) and Gbp2 (7 and 1255.58) (degree and betweenness score respectively) (**Figure 6.9** and **Appendix 6.4**).

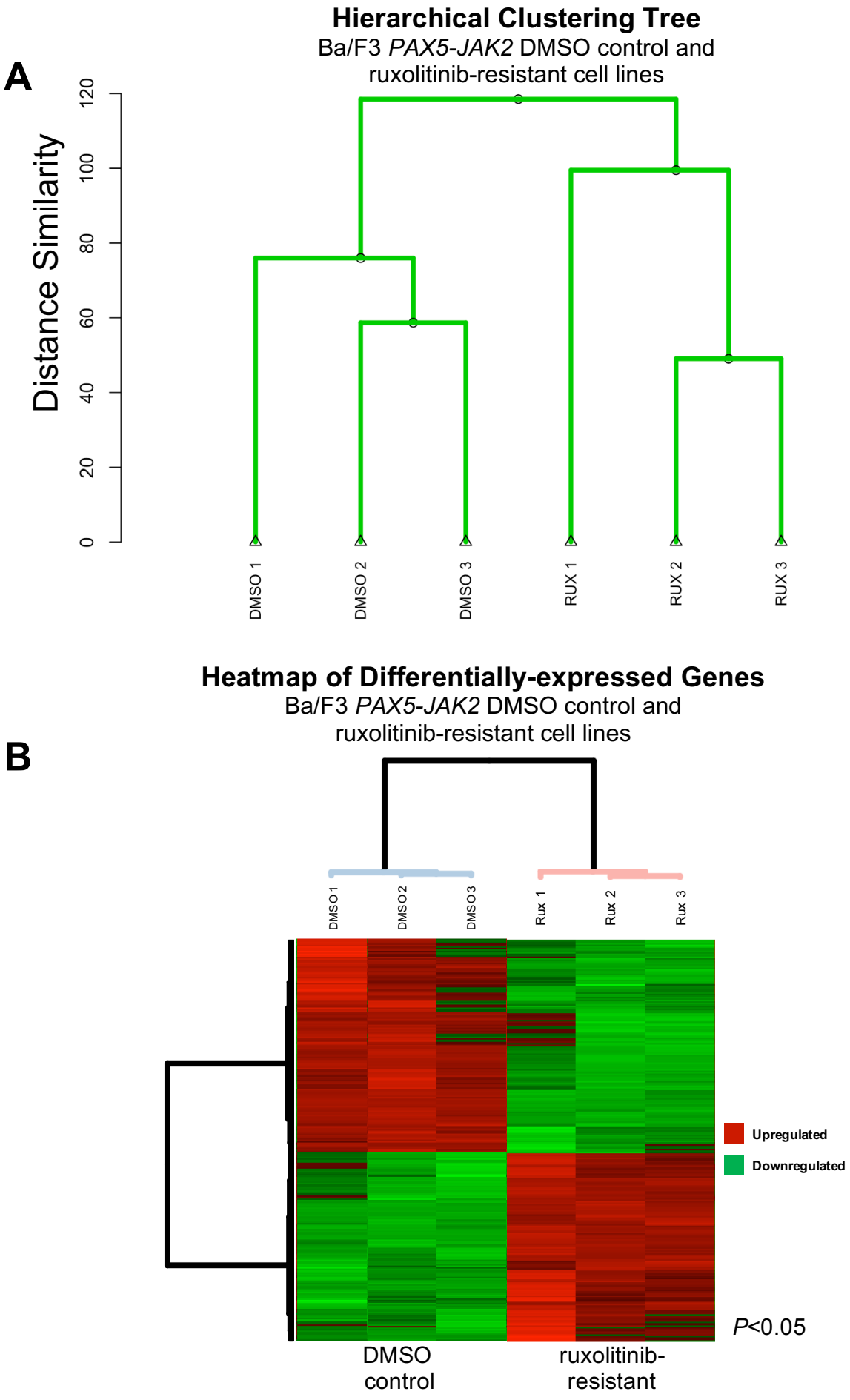
To further investigate contextually-relevant hubs between the IMEx PPI network and differentially-expressed genes, application of the CHAT analysis tool revealed hubs that were associated with signal transducer and activator of transcription (STAT), and interferon regulatory factors (IRFs). Precisely, a close association was observed between IRF1, STAT2 and C-X-C motif chemokine ligand 10 (CXCL10). Interestingly, an association between NF-κB subunit 65 (RELA), STAT6 and guanylate binding protein 1 (GBP1) was also identified. Other significant hubs in the CHAT analysis include C-C motif ligand 19 (CCL19), interferon alpha 1 (IFNA1), Enah/VASP-like protein (EVL), interferon induced transmembrane protein 1 (IFITM1), interferon alpha-inducible protein 6 (IFI6), STAT3 and STAT6 (**Figure 6.10**).

THIS PAGE INTENTIONALLY LEFT BLANK.

Figure 6.6 – Hierarchical clustering and heatmap of mRNA-seq data confirms close association and significantly differentially-expressed genes between biological replicates of Ba/F3 *PAX5-JAK2* TKI-sensitive and resistant cell lines

A: Hierarchical clustering tree of Ba/F3 *PAX5-JAK2* TKI-sensitive (DMSO control) and TKI-resistant (ruxolitinib-resistant) samples, with 3 biological replicates utilised for mRNA-seq analysis. **B:** Heatmap of differentially-expressed genes in Ba/F3 *PAX-JAK2* DMSO control and ruxolitinib-resistant cell lines, with supervised clustering performed using an input of $P<0.05$. Heatmap was generated using the 'Heatplus' Bioconductor package on RStudio®[247,473].

Figure 6.6


A
Hierarchical Clustering Tree
Ba/F3 PAX5-JAK2 DMSO control and
ruxolitinib-resistant cell lines
Distance Similarity
0
20
40
60
80
100
120
DMSO 1
DMSO 2
DMSO 3
RUX 1
RUX 2
RUX 3
B
Heatmap of Differentially-expressed Genes
Ba/F3 PAX5-JAK2 DMSO control and
ruxolitinib-resistant cell lines
DMSO 1
DMSO 2
DMSO 3
Rux 1
Rux 2
Rux 3
Upregulated
Downregulated
P<0.05
DMSO
control
ruxolitinib-
resistant

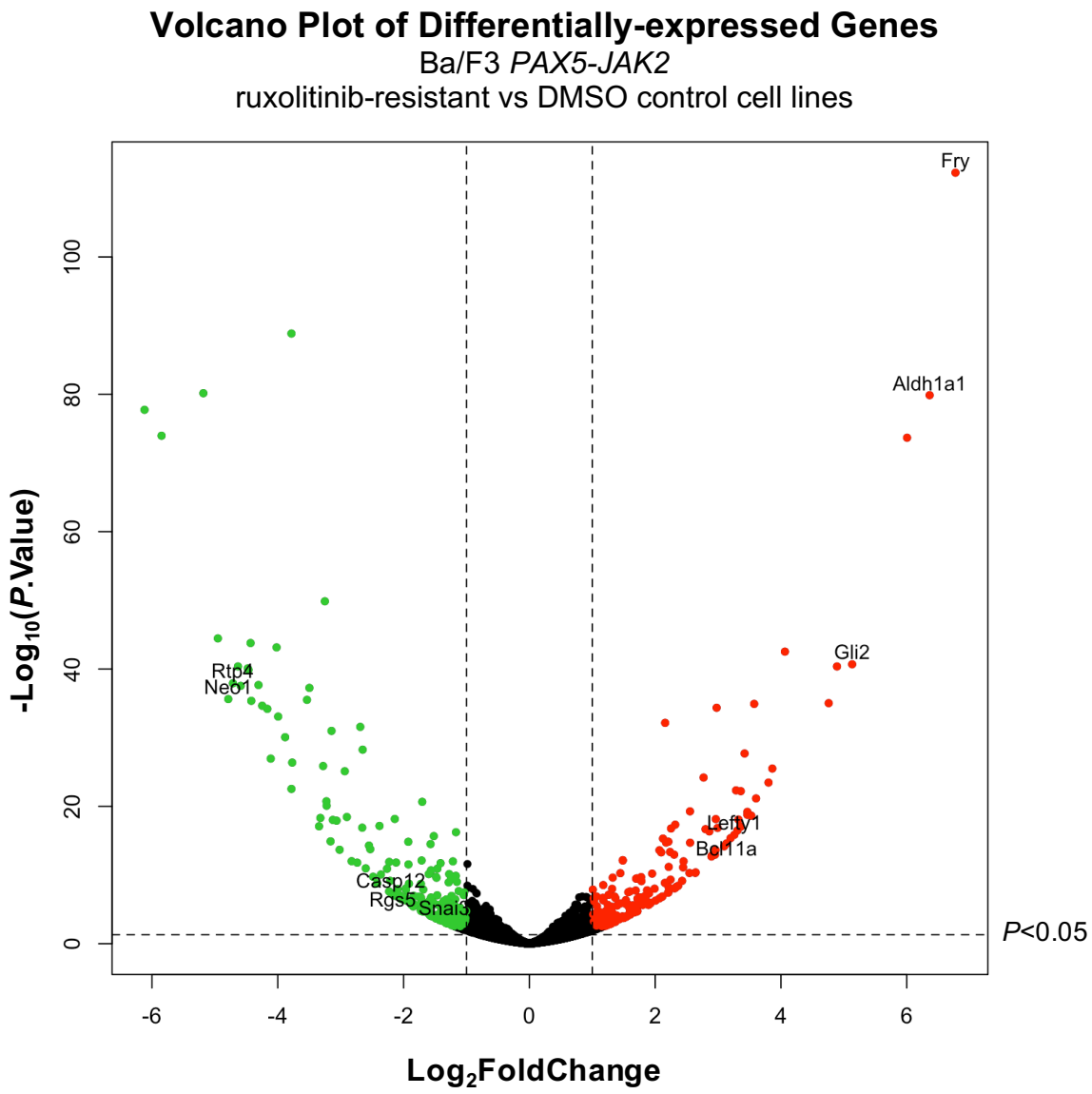
THIS PAGE INTENTIONALLY LEFT BLANK.

Figure 6.7 – Volcano plot of differentially-expressed genes and validation of mRNA-seq data via RQ-PCR in Ba/F3 *PAX5-JAK2* ruxolitinib-resistant and DMSO control cells

A: Volcano plot of differentially-expressed genes, with significantly upregulated (**red** – $P<0.05$; $Log_2FC>1$) and downregulated (**green** – $P<0.05$; $Log_2FC<1$) in ruxolitinib-resistant Ba/F3 *PAX5-JAK2* cells depicted accordingly. The genes of interest identified for purposes of RQ-PCR validation of mRNA-seq data are highlighted. **B:** mRNA-seq differential expression values of genes that were further validated by RQ-PCR. **C:** RQ-PCR validation of genes of interest identified in mRNA-seq. Data were analysed using the $2^{-\Delta\Delta CT}$ (comparative CT) method, with dotted lines representing a threshold mean value of 1 in DMSO control cells. Columns represent the mean while error bars depict the standard deviation of 3 biological replicates within 2 independent experiments. For values and gene summary, refer to **Appendix 6.2**.

Figure 6.7

A



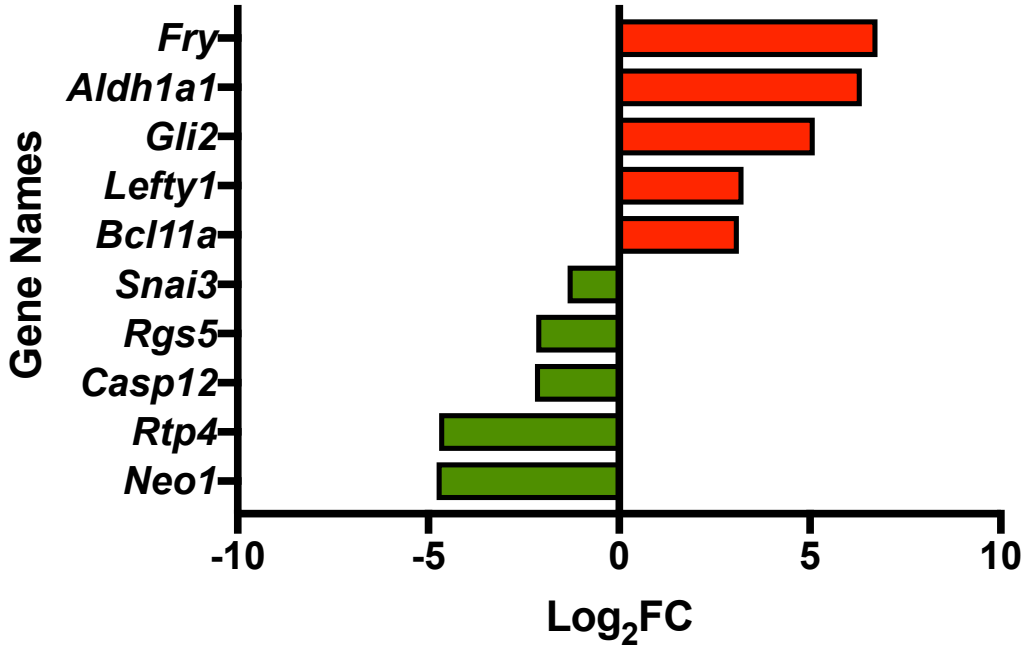
Legend:

Gli2 – GLI-Kruppel family member GLI2
Aldh1a1 – Aldehyde dehydrogenase family 1, subfamily A1
Fry – FRY microtubule binding protein
Bcl11a – B cell CLL/lymphoma 11A (zinc finger protein)
Lefty1 – Left-right determination factor 1
Casp12 – Caspase 12
Snai3 – Snail family transcriptional repressor 3
Rgs5 – Regulator of G-protein signaling 5
Rtp4 – Receptor transporter protein 4
Neo1 – Neogenin 1

B

mRNA-seq Expression

Significantly differentially-expressed genes
in Ba/F3 *PAX5-JAK2* ruxolitinib-resistant cell lines



C

RQ-PCR Validation of mRNA-seq Expression

Ba/F3 *PAX5-JAK2* ruxolitinib-resistant cell line

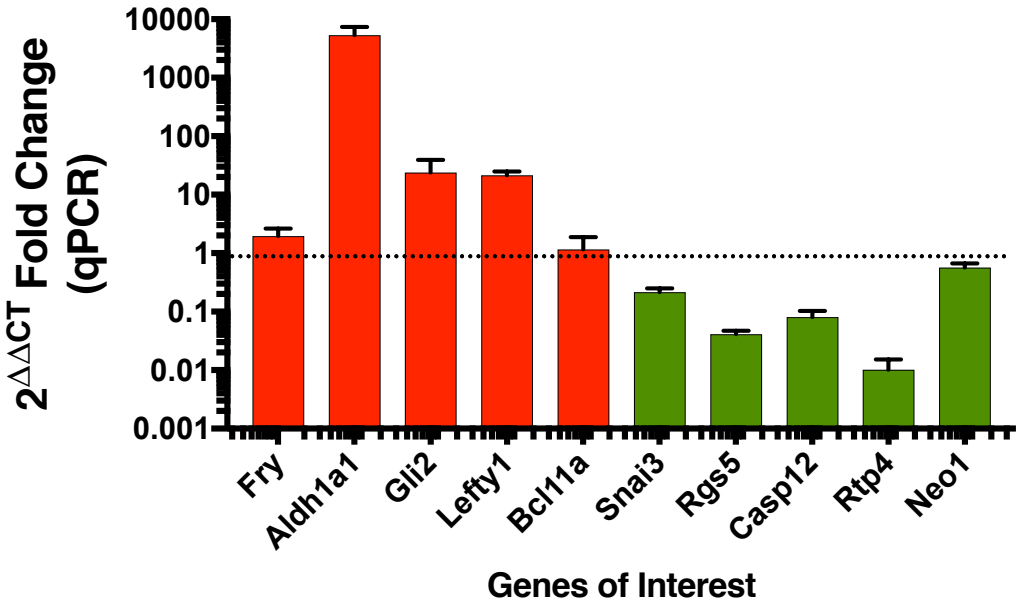


Figure 6.8 – Pathway enrichment analysis of differentially-expressed genes identifies noncanonical signalling pathways in ruxolitinib-resistance

Significantly differentially-expressed genes (downregulated and upregulated cohorts, $P<0.05$) at a cut-off Log_2FoldChange value of 1 were analysed via the integrated pathway enrichment analysis platform on InnateDB[223]. DE genes were analysed via the hypergeometric algorithm and corrected for multiple testing via the Benjamini-Hochberg method of analysis[3,220]. Texts beneath plots represent pathways identified based on the KEGG/REACTOME database, with dotted blue lines denoting a threshold of $\alpha<0.05$. **A**: downregulated gene set; **B**: upregulated gene set. For further details regarding pathway enrichment readouts, refer to **Appendix 6.3A** (downregulated cohort) and **Appendix 6.3B** (upregulated cohort).

Figure 6.8

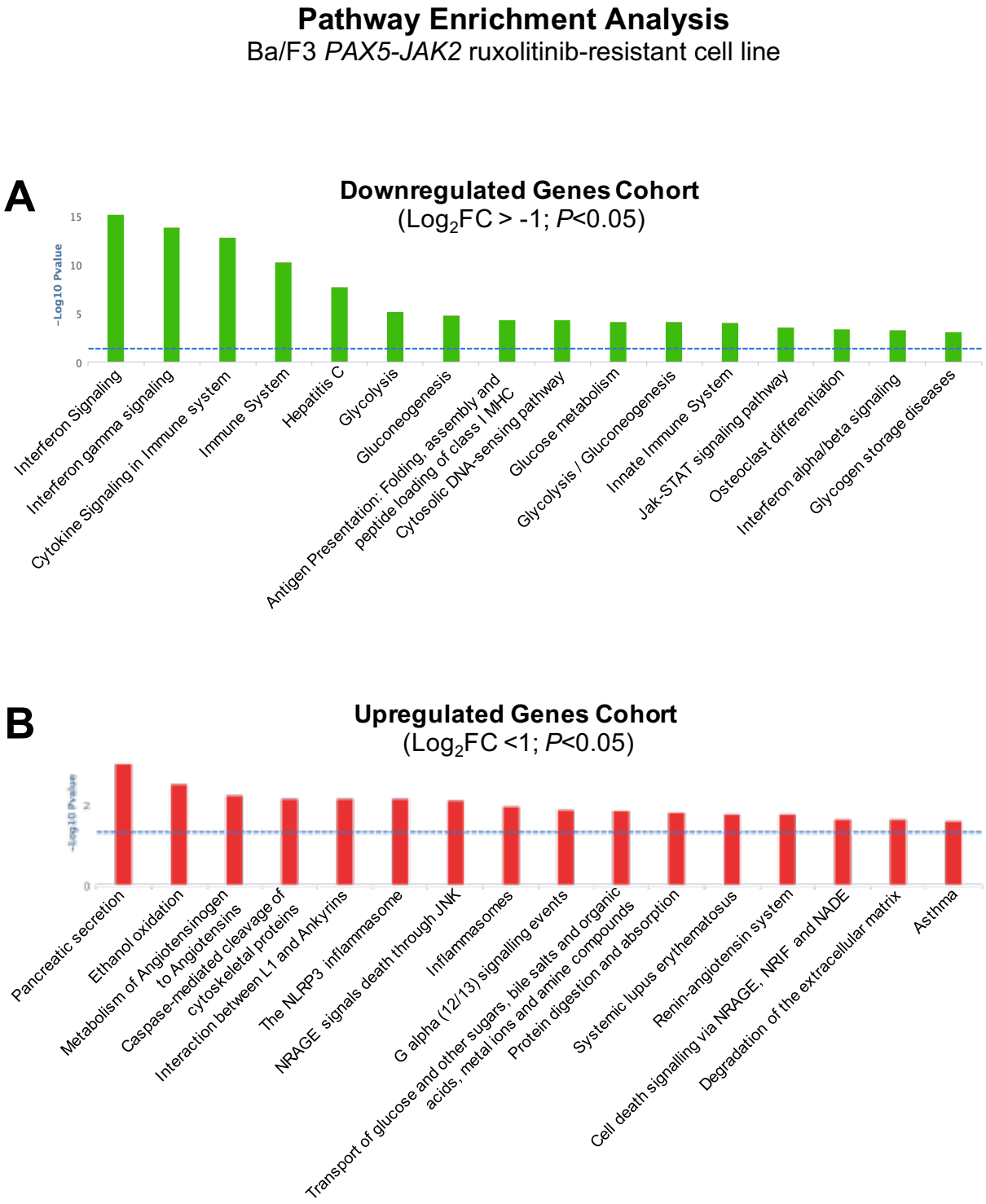

Pathway Enrichment Analysis
Ba/F3 PAX5-JAK2 ruxolitinib-resistant cell line
A
Downregulated Genes Cohort
(Log2FC > -1; P<0.05)
-Log10 Pvalue
15
10
5
0
Interferon Signaling
Interferon gamma signaling
Cytokine Signaling in Immune system
Immune System
Hepatitis C
Glycolysis
Gluconeogenesis
Antigen Presentation: Folding, assembly and peptide loading of class I MHC
Cytosolic DNA-sensing pathway
Glucose metabolism
Glycolysis / Gluconeogenesis
Innate Immune System
Jak-STAT signaling pathway
Osteoclast differentiation
Interferon alpha/beta signaling
Glycogen storage diseases
B
Upregulated Genes Cohort
(Log2FC <1; P<0.05)
Pancreatic secretion
Ethanol oxidation
Metabolism of Angiotensinogen to Angiotensins
Caspase-mediated cleavage of cytoskeletal proteins
Interaction between L1 and Ankyrins
The NLRP3 inflammasome
NRAGE signals death through JNK
Inflammasomes
G alpha (12/13) signalling events
Transport of glucose and other sugars, bile salts and organic acids, metal ions and amine compounds
Protein digestion and absorption
Systemic lupus erythematosus
Renin-angiotensin system
Cell death signalling via NRAGE, NRIF and NADE
Degradation of the extracellular matrix
Asthma

Figure 6.9 – Network analysis of ruxolitinib-resistant *PAX5-JAK2* cells reveals a close association between Jak/Stat and cancer signalling gene sets in ruxolitinib-resistant *PAX5-JAK2* cells

A network meta-analysis of the most relevant protein-protein interactions (PPIs) involved in ruxolitinib-resistance in Ba/F3 *PAX5-JAK2* cells, as analysed via NetworkAnalyst[472]. The top 50 upregulated and downregulated differentially-expressed genes (P<0.05) were utilised as the input data, with reference to the International Molecular Exchange Consortium (IMEx)[474] interactome database applied in the analysis. Circular attributes represent PPI 'nodes' (**red**: upregulated; **green**: downregulated) while lines denote 'edges' (known interactions between proteins). Nodes with the highest degree of interactions with neighbouring nodes are referred to as 'hubs', while nodes with a high degree of *betweenness centrality* (highest number of shortest paths passing through a node) are defined as 'bottlenecks'[475,476]. For detailed values, refer to **Appendix 6.4**.

Figure 6.9

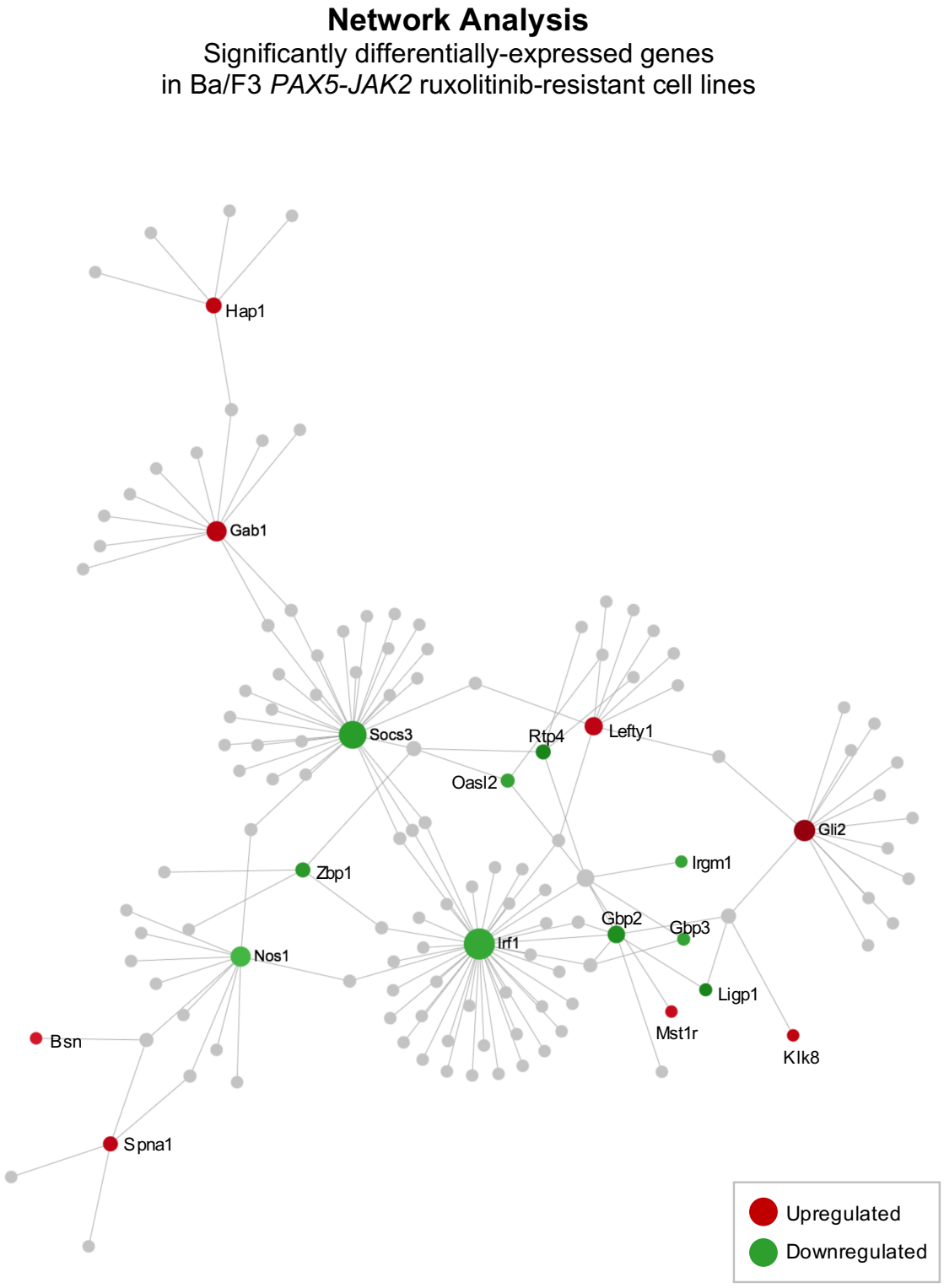
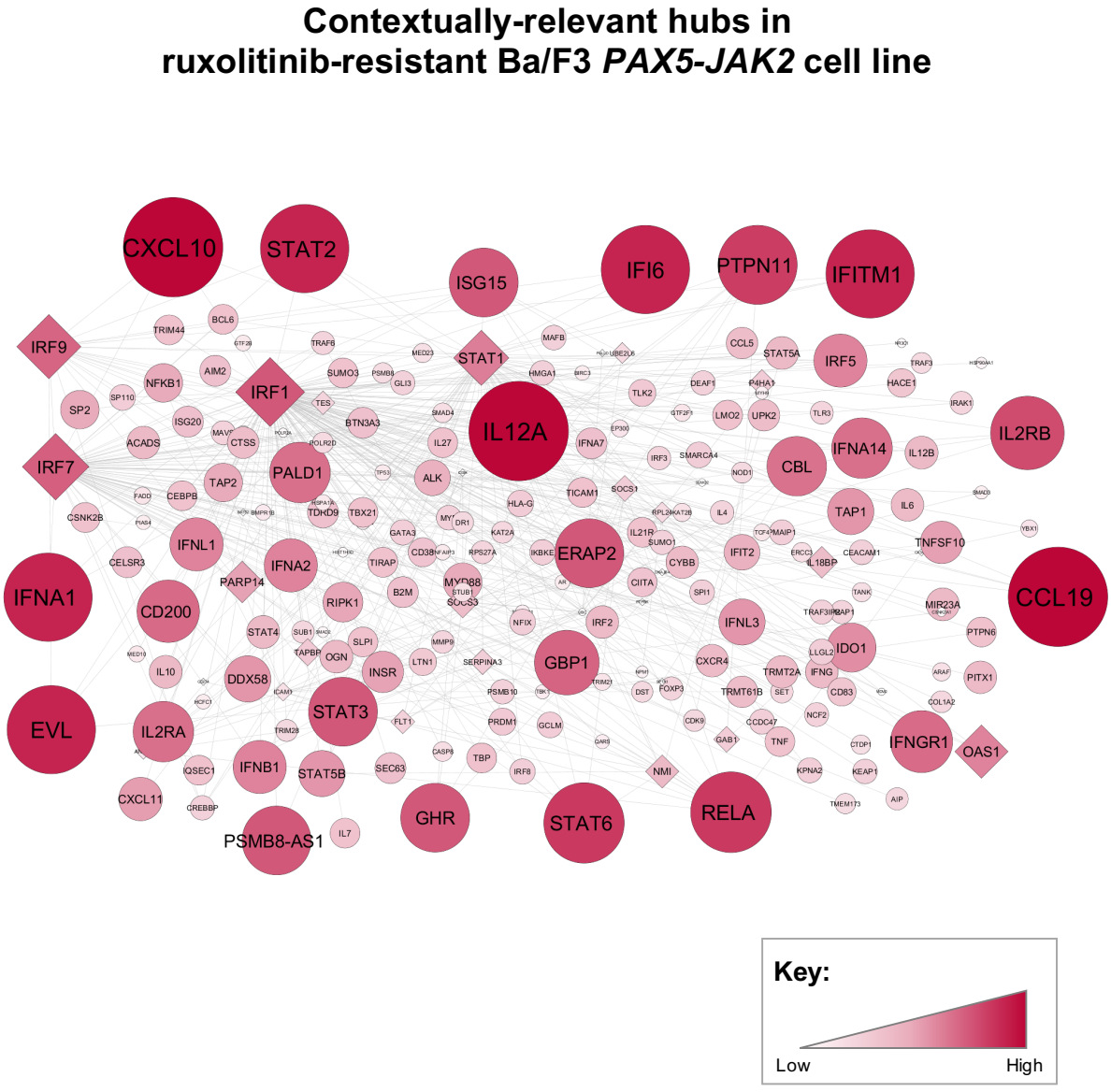

Network Analysis
Significantly differentially-expressed genes
in Ba/F3 PAX5-JAK2 ruxolitinib-resistant cell lines
Hap1
Gab1
Socs3
Rtp4
Lefty1
Oasl2
Gli2
Zbp1
Irgm1
Gbp2
Gbp3
Irf1
Nos1
Ligp1
Mst1r
Klk8
Bsn
Spna1
Upregulated
Downregulated

Figure 6.10 – Network analysis of contextually-relevant hubs associated with TKI-resistance in Ba/F3 *PAX5-JAK2* ruxolitinib-resistant cell line

Differentially-expressed genes (Log_2FC >1<; P<0.05) were analysed using the contextual hub analysis tool (CHAT) application[227] as visualised in the Cytoscape software[225], highlighting proteins that are contextually-relevant in a ruxolitinib-resistant *PAX5-JAK2* setting. Diamonds represent nodes derived from the differentially-expressed gene list, while circles represent nodes derived by PPI association identified in the IMEx database. Sizes of nodes are associated with colour contrast, with larger nodes (more intense red) indicating hubs that are more contextually-relevant. Figure courtesy of Dr. Sriganesh Srihari, EMBL, SAHMRI.

Figure 6.10


Contextually-relevant hubs in
ruxolitinib-resistant Ba/F3 PAX5-JAK2 cell line
CXCL10
STAT2
ISG15
IFI6
PTPN11
IFITM1
IRF9
IRF1
IL12A
IRF7
PALD1
IFNL1
IFNA2
IFNA1
CD200
PARP14
RIPK1
STAT4
DDX58
INSR
STAT3
EVL
IL2RA
IFNB1
STAT5B
CXCL11
PSMB8-AS1
GHR
STAT6
RELA
NMI
IFNGR1
OAS1
CCL19
IL2RB
IFNA14
CBL
TAP1
TNFSF10
ERAP2
IFNL3
IDO1
GBP1
IRF5
STAT1
IRF2
Key:
Low
High

6.4. Discussion

In this chapter, TKI-resistance in the setting of *PAX5-JAK2* Ph-like ALL was investigated. The *PAX5-JAK2* Ph-like ALL fusion gene transforms Ba/F3 and Arf-/- cells, resulting in cytokine (IL-3) independent growth[73,477]. Using transformed Ba/F3 cells expressing *PAX5-JAK2*, TKI-sensitivity of cells to Jak-specific TKIs (rather than Abl or Flt3 inhibitors) confirmed potential use of these TKIs for therapy[73]. Importantly, the use of Jak-specific inhibitors is currently the subject of clinical trials, where a phase II trial of ruxolitinib in combination with chemotherapy in childhood ALL (younger than 21 years old)[470], as well as the investigation of ruxolitinib/dasatinib in-combination with chemotherapy in Ph-like ALL patients (10 years or older)[471] are currently ongoing.

Treatment-resistance remains an urgent clinical issue leading to relapse[478-480] and a phase I/II study evaluating the efficacy of combination therapy using ruxolitinib/nilotinib in a TKI-resistant setting is currently underway (in a Ph+ ALL setting, however)[481]. As Pax5-Jak2 is targetable using Jak-specific inhibitors (ruxolitinib and BMS-911543), it was, therefore, important to identify relevant mechanisms that may arise in the event of TKI-resistance.

The identification of cross-resistance between ruxolitinib and BMS-91154 resistant Ba/F3 *PAX5-JAK2* cells suggests the presence of a common resistance mechanism associated with Jak kinase signalling. Therefore, Stat5 phosphorylation – a direct downstream partner of Jak2[482-484] – was investigated. Western blotting of p-Stat5, rather than p-Jak2, was implemented because preliminary studies did not show any differences in protein expression when an antibody specific for the Jak2 Y1007/1008 phosphorylation site was utilised (**Appendix 6.1A**; despite TKI-sensitivity as observed in **Figure 6.1**). In fact, previous studies had indicated a stabilisation of p-

Jak2 (Y1007/1008) expression when type I Jak inhibitors (such as ruxolitinib and BMS-911543, that bind to the active conformation of phosphorylated Jak2) were utilised, despite inhibition of downstream p-Stat5 signalling[442,485].

In the Jak2 Western blots, an absence in the reduction of phosphorylated Pax5-Jak2 expression despite the use of Jak2 TKIs may be because endogenously, Jak2 is activated via heterodimerisation of its ligand (i.e. erythropoietin receptor[486,487], granulocyte-macrophage cell stimulating factor / GM-CSF[488] and growth hormone receptor[457]). Andraos *et al*. suggested that for a type I Jak inhibitor-induced increase in phosphorylation of the Jak2 activation loop to occur, an intact conformation of the FERM, JH2 (pseudokinase) and JH1 (kinase) domains are necessary[485]. In Pax5-Jak2, only the kinase domain is present[64]. Therefore, a constant phosphorylation at tyrosine residue 1007/1008 despite the absence of the other domains, was interesting to note. An explanation may be the replacement of these domains with Pax5 (in the 5' / N-terminus region), allowing for a constant Jak2 phosphorylation due to a lack of autoinhibition[489].

The increased p-Stat5 IC_{50} accompanied with increased LD_{50} in ruxolitinib and BMS-911543 resistant Ba/F3 *PAX5-JAK2* cell lines suggests a common mechanism associated with Jak2 inhibitor binding exists. This was because genomic alterations within the Jak2 kinase domain have been described to contribute to resistance against Jak inhibitors[200,468,469]. The identification of a *JAK2*-Y931C kinase domain mutation present in both ruxolitinib and BMS-911543 resistant Ba/F3 *PAX5-JAK2* cell lines suggests a contribution of this mutation to TKI cross-resistance in a *PAX5-JAK2* setting. This kinase domain mutation is located within the adenine-binding side chain of the hinge region (a highly conserved domain) which interacts directly with ATP-competitive inhibitors, affecting potential TKI sensitivity[201,490]. The *JAK2*-Y931C mutation has also been well-described in previous studies to be highly-

resistant to ATP-competitive (type I) inhibitors, including Jak inhibitor 1, CMP6 (pyridone 6) and tofacitinib in myeloproliferative neoplasms (MPNs)[201,202,469,491].

The increased proliferation rate of ruxolitinib-resistant *PAX5-JAK2* cells with the *JAK*-Y931C mutation demonstrates a highly-resistant cell line. Such proliferative advantage in a TKI-resistant setting has been observed in CML (*ABL1*-T315I)[492], non-small cell lung cancer (*EGFR*-T790M)[493] and AML (*FLT3*-ITD-N676K)[420], where cells harbouring kinase-domain mutations demonstrate an increased proliferation rate compared to control. Whether such proliferative advantage is due to decreased TKI sensitivity (as a direct consequence of the kinase-domain mutation), or due to an activation of alternative signalling mechanisms, is unknown. This concept, in-combination with the observation of p-Stat5 expression in ruxolitinib/BMS911543-resistant Ba/F3 *PAX5-JAK2* cells, suggests a noncanonical mechanism of TKI-resistance exists.

TKI-resistance may be attributable to the expression of many other factors. As the expression of p-Stat5 in TKI-resistant cells appears to have a dose-response effect (despite an increased IC_{50} compared to DMSO control cells), mRNA sequencing was employed. Upregulated differentially-expressed genes in Ba/F3 *PAX5-JAK2* ruxolitinib-resistant cells included *Fry*, *Aldh1a1*, *Gli2*, *Lefty1* and *Bcl11a*. *Fry*, a microtubule binding protein originally characterised in *Drosophila*, has been implicated in the morphogenesis of sensory bristles[494]. Its human homolog, *AF4P12*, has been described as a novel fusion partner in mixed lineage leukaemia (MLL) leading to recruitment of transcriptional machinery mechanisms and overexpression of *HOXA* and *FLT3*[495].

Aldh1a1 has been implicated as a marker of bone marrow haematopoietic stem cells[496] and mediator of solid tumour metastasis[497,498]. *Gli2* has been associated

with cancer metastasis through its association with transforming growth factor beta (TGFβ) and hedgehog signalling pathways[499-501], while *Lefty1* is associated with Kruppel-like factor 4 (*Klf4*), a gene involved in breast cancer tumour suppression and oncogenesis[502]. *Klf4* activates the *Lefty1* promoter binding sites for *Sox2* and *Oct3/4* in embryonic stem cells, supporting leukaemia inhibitory factor independent self-renewal[503]. The overexpression of *Bcl11a* has been associated with triple-negative breast cancer[504] and lymphoid malignancies[505]. Taken together, the upregulated genes suggest that ruxolitinib-resistance in Ba/F3 *PAX5-JAK2* cells may be associated with pluripotent cell renewal and metastasis.

In the downregulated gene set *(Snai3*, *Rgs5, Casp12*, *Rtp4*, *Neo1)*, *Snai3* (part of the Snail family of zinc-finger transcription factors) has been associated with decreased cell proliferation[506-508] (hence an inversed expression in ruxolitinib-resistant Ba/F3 *PAX5-JAK2* cells). *Rgs5* is known to inhibit G-protein coupled receptor signalling[509], with decreased *Rgs5* expression associated with an increase in cancer vasculature invasion and metastasis of the lymph node in NSCLC[510]. Overexpression of *Rgs5* has been observed to increase the response of radiotherapy in human lung cancer cells[511].

The downregulation of *Casp12* has been implicated in colitis inflammation-associated colorectal cancer tumorigenesis[512,513], while *Rtp4*, a chaperone protein that escorts G-protein coupled receptors to the cell membrane[514], has interestingly been associated with poorer outcome in human epithelial growth factor receptor ($HER2^+$) breast cancer[279]. Decreased expression of *Neo1*, a gene encoding neogenin (part of the immunoglobulin superfamily), has also been implicated in colorectal adenocarcinoma[515,516], suggesting that ruxolitinib-resistance in *PAX5-*

JAK2 Ph-like ALL associates with a variety of dysregulated immune-related signalling mechanisms.

Data interrogation utilising pathway and network analysis resulted in very few pathways that were significantly enriched (α<0.05) utilising a dataset of genes upregulated in ruxolitinib-resistant Ba/F3 *PAX5-JAK2* cells. This included the identification of *Aldh1a1*, which was associated with the pancreatic secretion and ethanol oxidation pathways in the pathway enrichment analysis. As described above, *Aldh1a1*, a marker of haematopoietic stem cells and involved in metastasis of solid tumours, may potentially be a cause of TKI-resistance. Previous studies have highlighted an overexpression of *ALDH1A1* in lung adenocarcinoma[517], drug resistance in colorectal cancer stem cells[518] and breast cancer[519]. Aldh1a1 has been shown to facilitate various catabolic processes in cells, including the conversion of vitamin A to retinoic acid and ethanol to amine in other studies[518,520]. Therefore, an increased expression of Aldh1a1 in ruxolitinib-resistance may hypothetically result in increased ruxolitinib metabolism, leading to an increased detoxification/deactivation of the drug, reducing TKI sensitivity.

It was interesting to note how genes that were downregulated resulted in findings of more significantly enriched pathways associated with metabolism (glycolysis/gluconeogenesis), as well as decreased immune cell signalling. This was because cancer cells are classically known to be metabolically active as a result of the 'Warburg' effect, where glucose is converted into lactate during aerobic glycolysis[521-523]. This suggests that ruxolitinib-resistant cells have low levels of aerobic glycolysis, possibly maintaining a more 'stem-cell-like' state, where anaerobic glycolysis is more pronounced[524]. Potentially, a decreased glycolytic cellular metabolism, accompanied by an increase in enzymes that detoxify

ruxolitinib, contributes to TKI-resistance in Ba/F3 *PAX5-JAK2* ruxolitinib-resistant cells.

The findings of decreased immune signalling correlated with network analysis of the top 50 upregulated and downregulated genes, where an enrichment of hubs associated with downregulated interferon signalling (such as *Irf1*, *Socs3* and *Oasl2*) was identified (**Figure 6.9** & **Appendix 6.4**). Importantly, network analysis allowed for the identification of bottlenecks (identified by increased degree and betweenness centrality of PPIs), highlighting hubs that were significant in ruxolitinib-resistant Ba/F3 *PAX5-JAK2* cells. This included *Irf1*, which has been shown to exhibit tumour suppression activity through the induction of caspase-activated apoptosis[525,526]. Therefore, suppression of *Irf1* in ruxolitinib-resistant Ba/F3 *PAX5-JAK2* cells may enable the maintenance of cancer cell survival, despite the presence of ruxolitinib.

The identification of *Socs3* (suppressor of cytokine signalling 3 – a downregulated gene in the ruxolitinib-resistant cell line) as a bottleneck suggests that this gene is significantly involved in TKI-resistance. The Socs family of proteins function as a negative regulator of Jak/Stat signalling[527,528] and epigenetic silencing of *SOCS3* has been associated with hepatocellular carcinoma[529] and a more aggressive disease phenotype in prostate cancer[530]. In a study performed recently by Shang *et al*., decreased *SOCS3* and increased *STAT3* expression were also found in tumour tissues of ovarian cancer patients[531], further supporting the data observed in ruxolitinib-resistant Ba/F3 *PAX5-JAK2* cells, suggesting decreased negative-regulation of the Jak/Stat signalling pathway exists.

Interestingly, *Nos1* and *Gab1* (respectively downregulated and upregulated in ruxolitinib-resistance) were also implicated as bottlenecks in the network analysis (**Figure 6.9** & **Appendix 6.4**). *Nos1* encodes the enzyme nitric oxide synthase 1,

involved in the catalysis of nitric oxide from nicotinamide adenine dinucleotide phosphate (NADPH), L-arginine and O_2[532,533]. In a review by Choudhari *et al*., the role of nitric oxide is diverse in cancer (pro-tumorigenic and tumouricidal, depending on cancer subtype)[534] and loss of *NOS1* expression has been associated with renal cell carcinoma[535]. Increased *Gab1* (Grb2 associated-binding protein 1) has been shown to mediate tumour progression in colorectal cancer[536], with Meng and colleagues suggesting an association of *Gab1* with the activation of Mapk/Erk signalling[537]. This was interesting because Mapk/Erk signalling is involved in cell survival and proliferation, and its constitutive activation has been associated with many cancers including breast[538], pancreas[539], AML[540] and ALL[541].

To further elucidate the contextual significance of differentially-expressed genes, interrogation of mRNA-seq data using the CHAT application developed by Muetze and colleagues[227] was applied. In comparison to a typical network analysis which identifies network topology (hubs, nodes and edges) based upon phenotypic importance[542,543], the CHAT analysis incorporates biological relevance by taking the values of differentially-expressed genes into account, identifying contextually-relevant hubs associated with a pre-constructed IMEx PPI network[227]. CHAT analysis of ruxolitinib-resistance in Ba/F3 *PAX5-JAK2* cells revealed proteins, mostly transcription factors associated with immune signalling mechanisms (i.e. STATs and IRFs), as contextually-relevant, indicating that the signalling governing TKI-resistance possibly converges on these transcription factors (**Figure 6.10**).

RELA, a proto-oncogene subunit as part of the NF-κB transcription factor, is known to be involved in the insulin-like growth factor 1 (IGF1) receptor and Akt signal transduction signaling[544] suggesting that ruxolitinib-resistance implicates a possible dysregulation in NF-κB signalling. *EVL*, which was previously found to be

upregulated in 'Chapter 3 – TKI-resistance in SUP-B15 Ph+ ALL cells' in this thesis, has been implicated in colorectal cancer where silencing of its microRNA hsa-miR-342 was observed[545]. CXCL10 (also known as IFN-γ-inducible protein 10), a member of the chemokine family which binds to the G-coupled protein receptor CXCR3[546,547], has been implicated in colorectal carcinoma[548], malignant melanoma[549] and the pathogenesis of acute graft versus host disease[550,551].

IL12A, which encodes for the interleukin 12 subunit alpha, is essential for the induction of IFN-γ signalling – a cytokine known to be involved in immune surveillance and cancer cell proapoptosis[552-554]. The IFN-γ signalling pathway, however, is a double-edged sword exhibiting protumourigenic properties as studies have shown that IFN-γ enhances the expression of MHC class I molecules, allowing cancer cells to evade detection and lysis by cytotoxic killer T cells[555,556]. Taken together, these contextually-relevant nodes suggest that ruxolitinib-resistance in a *PAX5-JAK2* Ph-like ALL setting involves major cross-talk between various immune regulatory signalling pathways, and this is the first time such findings have been described in a TKI-resistant leukaemic setting.

In summary, this chapter has shown that despite initial TKI sensitivity to Jak-kinase inhibitors in Ba/F3 cells expressing the *PAX5-JAK2* Ph-like ALL fusion gene, TKI-resistance may be inevitable (**Figure 6.11**). The identification of a *JAK2*-Y931C kinase domain mutation, known to be resistant to ATP-competitive inhibitors in a myeloproliferative neoplastic setting, is novel in ruxolitinib and BMS-911543 resistant *PAX5-JAK2* Ph-like ALL. The presence of *JAK2*-Y931C in both TKI-resistant *PAX5-JAK2* cell lines suggests a likelihood of this mutation occurring in the clinical setting. The dose-response of p-Stat5 in highly-resistant cells indicates, however, that a non-canonical mechanism of resistance exists, enabling survival of

cells despite high concentrations of TKI. Importantly, the application of advanced high-throughput sequencing technology and multiple data interrogation pipelines (pathway, network and CHAT analyses) has enabled the identification of these noncanonical mechanisms. These include decreased immune regulatory and cell metabolism signalling, increased drug metabolism and possible cross-talk between various immune-regulatory mechanisms (interferon signalling pathways) and decreased cellular metabolic activity (glycolysis & gluconeogenesis). Such parallel mechanisms are important for the survival of highly-resistant cells, and findings within this chapter provide a platform towards a future determination of the exact driver/passenger mechanisms[557,558] associated with Jak-inhibitor resistance in *PAX5-JAK2* Ph-like ALL. The findings within this chapter also illustrate how TKI-resistance can be a highly complex process, involving more than just a point mutation. Rather, a dynamic association between various alternative mechanisms are necessary for a truly highly-resistant phenotype and clinically, this study informs what may occur in the event of TKI-resistance in a *PAX5-JAK2* (or potentially other Jak2 fusions treated with 'type I' Jak-specific inhibitors), in a Ph-like ALL setting.

Figure 6.11

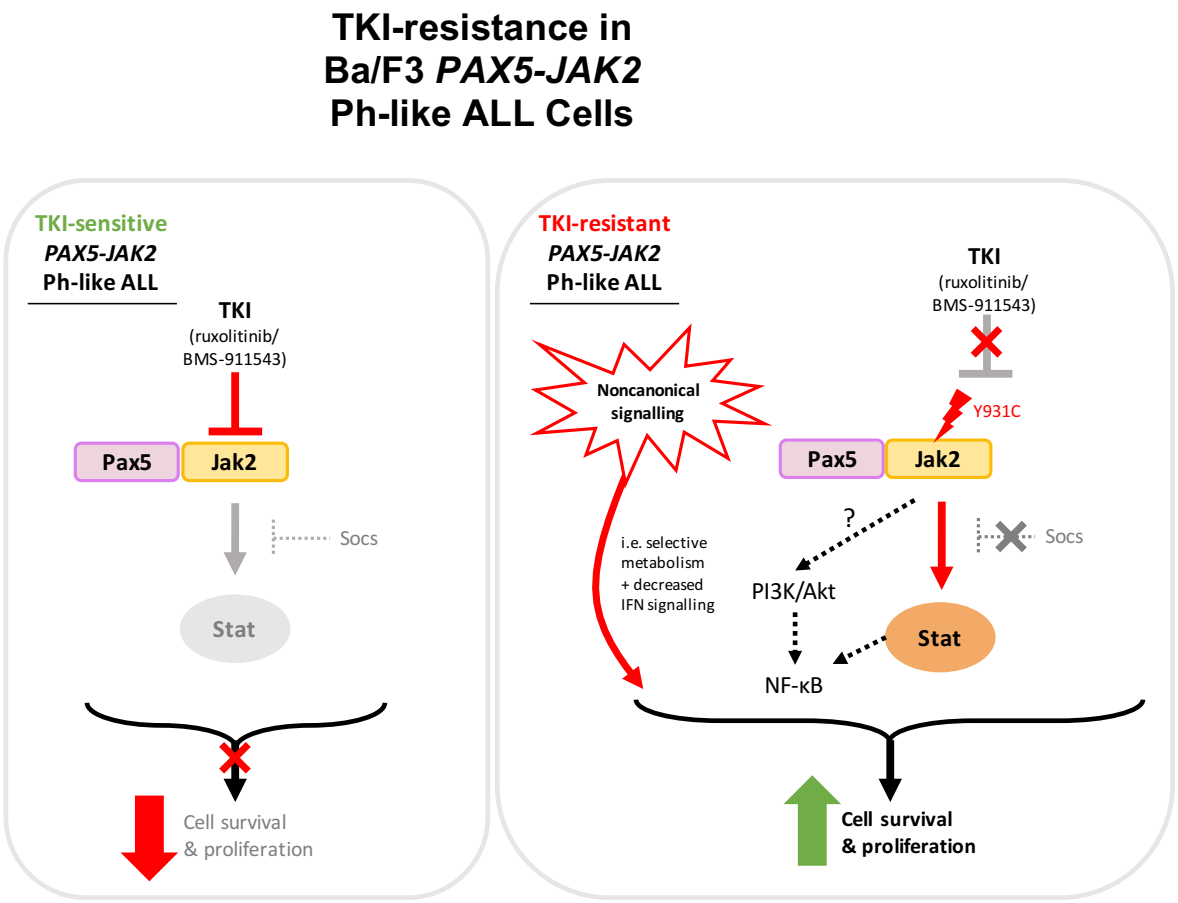


Figure 6.11 – Schematic representation of TKI-resistance in Ba/F3 *PAX5-JAK2* Ph-like ALL cells

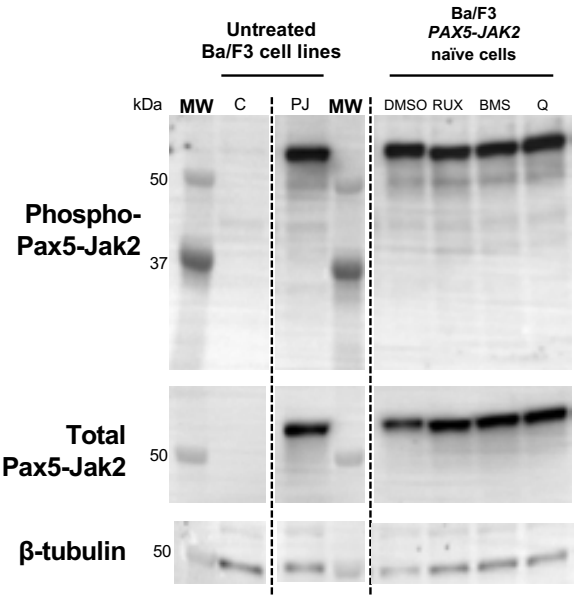
Left: The exposure of Ba/F3 *PAX5-JAK2* cells to Jak TKIs such as ruxolitinib and BMS-911543 results in an inhibition of downstream signalling (i.e. Stat, Mapk/Erk and possibly PI3K/Akt), leading to an abrogation of cell survival and proliferation. **Right:** In TKI-resistant Ba/F3 *PAX5-JAK2* cells, the presence of a *JAK2*-Y931C kinase domain mutation prevents TKI-binding, allowing for the persistence of downstream signalling cascades such as Stat families (i.e. Stat5). mRNA-seq analysis has also revealed canonical (Socs, a negative inhibitor of Jak2) and various noncanonical signalling pathways (i.e. dysregulated metabolism, interferon and NF-κB responses) contributing towards TKI-resistance in *PAX5-JAK2* Ph-like ALL.

Appendix 6.1- Western blotting of p-Jak2 (Y1007/1008) in Ba/F3 *PAX5-JAK2* cell lines

A: Phosphorylated/total Jak2 and β-tubulin analysis of TKI treatment in Ba/F3 *PAX5-JAK2* cell lines. Cells were incubated in TKI as indicated, for 1 hr at 37ºC / 5% CO_2 prior to collection of cells for western blot analysis. **B:** p-Jak2 (Y1007/1008) expression in DMSO control and BMS-911543-resistant Ba/F3 *PAX5-JAK2* cell lines treated in increasing concentrations of BMS-911543 for an hour. The intensity of protein bands was measured using the ImageLab™ software and densitometry graphs plotted via GraphPad® Prism™ as previously described. Blots shown are representative of n=3 independent experiments.

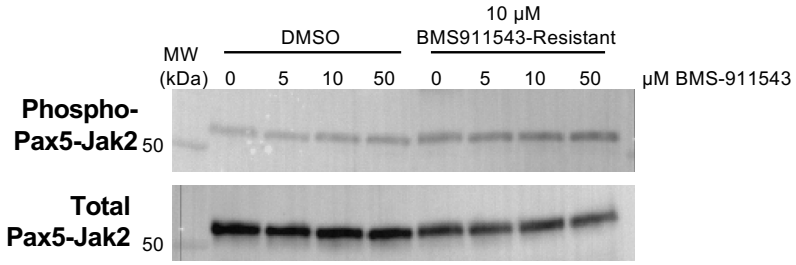
Appendix 6.1

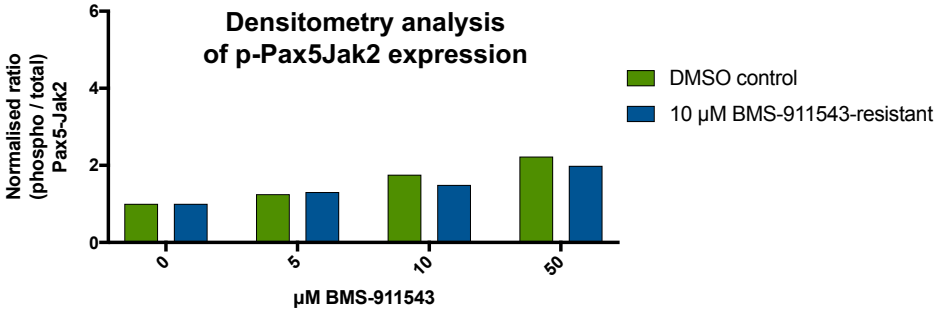
A

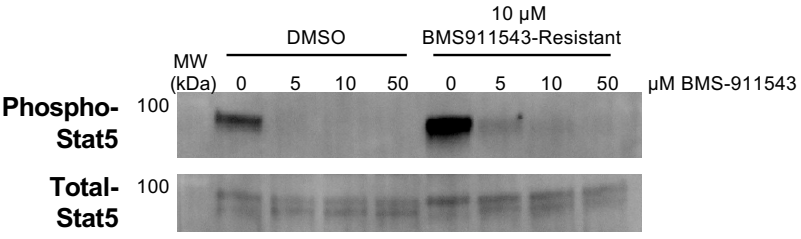


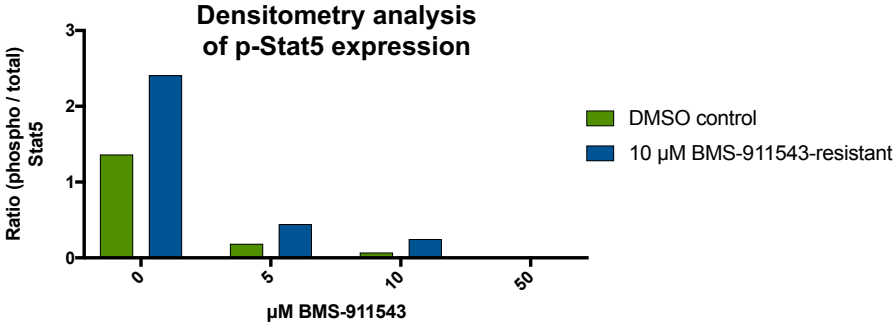
Legend:
C: Ba/F3 parental control
PJ: Ba/F3 *PAX5-JAK2* naïve control
DMSO: 0.1% DMSO vehicle control
RUX: 1 μM ruxolitinib
BMS: 1 μM BMS-911543
Q: 10 nM quizartinib

B









THIS PAGE INTENTIONALLY LEFT BLANK.

Appendix 6.2

mRNA-seq and RQ-PCR readouts of Ba/F3 *PAX5-JAK2* ruxolitinib-resistant cells compared to DMSO control

Symbol	Description	Summary	RNAseq Expression		qPCR Validation	
			Log_2 Fold Change (in decreasing order)	Adj.P.Val	$2^{-\Delta\Delta Ct}$ Mean	± SD
Fry	*FRY* microtubule binding protein	Plays a crucial role in the structural integrity of mitotic centrosomes and in the maintenance of spindle bipolarity by promoting PLK1 activity at the spindle poles in early mitosis. May function as a scaffold promoting the interaction between AURKA and PLK1, thereby enhancing AURKA-mediated PLK1 phosphorylation. [Source: UniProtKB/Swiss-Prot]	6.774484911	6.84E-109	1.965502326	0.674394312
Aldh1a1	Aldehyde dehydrogenase family 1, subfamily A1	The protein encoded by this gene belongs to the aldehyde dehydrogenase family. Aldehyde dehydrogenase is the next enzyme after alcohol dehydrogenase in the major pathway of alcohol metabolism. There are two major aldehyde dehydrogenase isozymes in the liver, cytosolic and mitochondrial, which are encoded by distinct genes, and can be distinguished by their electrophoretic mobility, kinetic properties, and subcellular localization. This gene encodes the cytosolic isozyme. Studies in mice show that through its role in retinol metabolism, this gene may also be involved in the regulation of the metabolic responses to high-fat diet. [provided by RefSeq, Mar 2011]	6.364057032	1.35E-80	5347.644177	2054.145919
Gli2	*GLI*-Kruppel family member *GLI2*	This gene encodes a protein which belongs to the C2H2-type zinc finger protein subclass of the *Gli* family. Members of this subclass are characterized as transcription factors which bind DNA through zinc finger motifs. These motifs contain conserved H-C links. Gli family zinc finger proteins are mediators of Sonic hedgehog (Shh) signaling and they are implicated as potent oncogenes in the embryonal carcinoma cell. The protein encoded by this gene localizes to the cytoplasm and activates patched Drosophila homolog (PTCH) gene expression. It is also thought to play a role during embryogenesis. The encoded protein is associated with several phenotypes- Greig cephalopolysyndactyly syndrome, Pallister-Hall syndrome, preaxial polydactyly type IV, postaxial polydactyly types A1 and B. [provided by RefSeq, Jul 2008]	5.132073282	2.06E-41	23.82928083	15.81615558
Lefty1	Left-right determination factor 1	This gene encodes a secreted ligand of the TGF-beta (transforming growth factor-beta) superfamily of proteins. Ligands of this family bind various TGF-beta receptors leading to recruitment and activation of SMAD family transcription factors that regulate gene expression. The encoded preproprotein is proteolytically processed to generate the mature protein, which plays a role in left-right asymmetry determination of organ systems during development. This gene is closely linked to both a related family member and a related pseudogene. [provided by RefSeq, Aug 2016]	3.259361881	1.39E-16	21.50257383	3.334872468
Bcl11a	B cell CLL/lymphoma 11A (zinc finger protein)	This gene encodes a C2H2 type zinc-finger protein by its similarity to the mouse Bcl11a/Evi9 protein. The corresponding mouse gene is a common site of retroviral integration in myeloid leukemia, and may function as a leukemia disease gene, in part, through its interaction with BCL6. During hematopoietic cell differentiation, this gene is down-regulated. It is possibly involved in lymphoma pathogenesis since translocations associated with B-cell malignancies also deregulates its expression. Multiple transcript variants encoding several different isoforms have been found for this gene. [provided by RefSeq, Jul 2008]	3.136399531	2.47E-15	1.161778931	0.721164885
Snai3	Snail family transcriptional repressor 3	*SNAI3* is a member of the *SNAIL* gene family, named for the Drosophila snail gene, which plays roles in mesodermal formation during embryogenesis (Katoh and Katoh, 2003 [PubMed 12579345]).[supplied by OMIM, Apr 2009]	-1.353735732	0.000383149	0.216868732	0.032632061
Rgs5	Regulator of G-protein signaling 5	This gene encodes a member of the regulators of G protein signaling (RGS) family. The RGS proteins are signal transduction molecules which are involved in the regulation of heterotrimeric G proteins by acting as GTPase activators. This gene is a hypoxia-inducible factor-1 dependent, hypoxia-induced gene which is involved in the induction of endothelial apoptosis. This gene is also one of three genes on chromosome 1q contributing to elevated blood pressure. Alternatively spliced transcript variants have been identified. [provided by RefSeq, Dec 2011]	-2.17267966	5.94E-08	0.04137159	0.005680232
Casp12	Caspase 12	Caspases are cysteine proteases that cleave C-terminal aspartic acid residues on their substrate molecules. This gene is most highly related to members of the ICE subfamily of caspases that process inflammatory cytokines. In rodents, the homolog of this gene mediates apoptosis in response to endoplasmic reticulum stress. However, in humans this gene contains a polymorphism for the presence or absence of a premature stop codon. The majority of human individuals have the premature stop codon and produce a truncated non-functional protein. The read-through codon occurs primarily in individuals of African descent and carriers have endotoxin hypo-responsiveness and an increased susceptibility to severe sepsis. Several alternatively spliced transcript variants have been noted for this gene. [provided by RefSeq, Feb 2011]	-2.201818557	4.08E-08	0.081127434	0.021868641
Rtp4	Receptor transporter protein 4	RTP4 (Receptor Transporter Protein 4) is a Protein Coding gene. Among its related pathways are Signaling by GPCR and Olfactory Signaling Pathway. An important paralog of this gene is *RTP3*. [Source: GeneCards.org] Probable chaperone protein which facilitates trafficking and functional cell surface expression of some G-protein coupled receptors (GPCRs). Promotes functional expression of the bitter taste receptor TAS2R16 (PubMed:16720576). Also promotes functional expression of the opioid receptor heterodimer OPRD1-OPRM1 (By similarity). [Source:UniProtKB/Swiss-Prot]	-4.713664316	1.20E-38	0.010224097	0.004983114
Neo1	Neogenin 1	This gene encodes a cell surface protein that is a member of the immunoglobulin superfamily. The encoded protein consists of four N-terminal immunoglobulin-like domains, six fibronectin type III domains, a transmembrane domain and a C-terminal internal domain that shares homology with the tumor suppressor candidate gene DCC. This protein may be involved in cell growth and differentiation and in cell-cell adhesion. Defects in this gene are associated with cell proliferation in certain cancers. Alternate splicing results in multiple transcript variants. [provided by RefSeq, Feb 2010]	-4.787348387	2.41E-36	0.572667117	0.092472011

Appendix 6.3A

Pathways enriched with downregulated genes in Ba/F3 *PAX5-JAK2* ruxolitinib-resistant cells

Pathway Name	Pathway Id	Source Name	Organism	Pathway uploaded gene count	Genes in InnateDB for this entity	Pathway p-value	Pathway p-value (corrected)	Gene Symbols
Interferon Signaling	18616	REACTOME	10090	15	72	7.24E-16	1.97E-13	*B2m; Gbp2; H2-T23; Icam1; Ifit1; Irf1; Irf7; Irf9; Isg15; Oas2; Oas3; Oasl1; Socs1; Socs3; Ube2l6;*
Interferon gamma signaling	18614	REACTOME	10090	12	43	1.46E-14	1.99E-12	*B2m; Gbp2; H2-T23; Icam1; Irf1; Irf7; Irf9; Oas2; Oas3; Oasl1; Socs1; Socs3;*
Cytokine Signaling in Immune system	17370	REACTOME	10090	19	194	1.49E-13	1.35E-11	*B2m; Casp1; Cish; Gbp2; H2-T23; Icam1; Ifit1; Il6; Irf1; Irf7; Irf9; Isg15; Map2k1; Oas2; Oas3; Oasl1; Socs1; Socs3; Ube2l6;*
Immune System	17702	REACTOME	10090	33	884	5.81E-11	3.95E-09	*B2m; C2; Casp1; Cd274; Cd81; Cdkn1a; Cish; Ddx58; Dtx3l; Dusp6; Erap1; Gbp2; H2-T23; Icam1; Ifit1; Il6; Irf1; Irf7; Irf9; Isg15; Map2k1; Nlrc5; Oas2; Oas3; Oasl1; Psmb9; Socs1; Socs3; Tapbp; Tmem173; Ube2l6; Unc93b1; Zbp1;*
Hepatitis C	10396	KEGG	10090	12	135	1.96E-08	1.07E-06	*Cd81; Cdkn1a; Ddx58; Ifit1; Irf1; Irf7; Irf9; Oas1g; Oas2; Oas3; Socs3; Stat1;*
Glycolysis	17429	REACTOME	10090	5	25	5.96E-06	2.70E-04	*Aldoa; Eno1; Gm5506; Pgam1; Pgk1;*
Gluconeogenesis	18823	REACTOME	10090	5	30	1.53E-05	5.96E-04	*Aldoa; Eno1; Gm5506; Pgam1; Pgk1;*
Cytosolic DNA-sensing pathway	8116	KEGG	10090	6	61	4.70E-05	0.001420281	*Casp1; Ddx58; Il6; Irf7; Tmem173; Zbp1;*
Antigen Presentation: Folding, assembly and peptide loading of class I MHC	19905	REACTOME	10090	4	19	4.40E-05	0.001495387	*B2m; Erap1; H2-T23; Tapbp;*
Glycolysis / Gluconeogenesis	680	KEGG	10090	6	66	7.36E-05	0.001820721	*Aldoa; Eno1; Gm5506; Pgam1; Pgk1; Pgm2;*
Glucose metabolism	17651	REACTOME	10090	6	65	6.75E-05	0.001836597	*Aldoa; Eno1; Gm5506; Pgam1; Pgk1; Pgm2;*
Innate Immune System	16733	REACTOME	10090	15	450	8.76E-05	0.001986645	*B2m; C2; Casp1; Cdkn1a; Ddx58; Dusp6; Il6; Irf1; Irf7; Map2k1; Nlrc5; Socs1; Tmem173; Unc93b1; Zbp1;*
Jak-STAT signaling pathway	651	KEGG	10090	8	154	2.49E-04	0.005216096	*Cish; Il6; Irf9; Mpl; Osm; Socs1; Socs3; Stat1;*
Osteoclast differentiation	10372	KEGG	10090	7	126	4.11E-04	0.00798896	*Irf9; Junb; Map2k1; Relb; Socs1; Socs3; Stat1;*
Interferon alpha/beta signaling	19567	REACTOME	10090	3	15	5.08E-04	0.009208077	*Irf9; Socs1; Socs3;*
Glycogen storage diseases	18944	REACTOME	10090	9	228	7.74E-04	0.011688754	*Aldoa; Cspg4; Eno1; Gm5506; Pgam1; Pgk1; Pgm2; Slc2a1; St3gal6;*

Appendix 6.3B

Pathways enriched with upregulated genes in Ba/F3 *PAX5-JAK2* ruxolitinib-resistant cells

Pathway Name	Pathway Id	Source Name	Organism	Pathway uploaded gene count	Genes in InnateDB for this entity	Pathway p-value	Pathway p-value (corrected)	Gene Symbols
Pancreatic secretion	10399	KEGG	10090	6	105	9.30E-04	0.166528571	*Adcy6; Atp1b2; Cela3b; Clca1; Cpa3; Slc26a3;*
Ethanol oxidation	17277	REACTOME	10090	2	8	0.003107732	0.278141984	*Aldh1a1; Aldh1a7;*
Metabolism of Angiotensinogen to Angiotensins	18691	REACTOME	10090	2	11	0.005976785	0.356614867	*Cpa3; Ctsg;*
Caspase-mediated cleavage of cytoskeletal proteins	18244	REACTOME	10090	2	12	0.007121866	0.212468996	*Casp6; Mapt;*
Interaction between L1 and Ankyrins	18376	REACTOME	10090	2	12	0.007121866	0.212468996	*Ank1; Spna1;*
The NLRP3 inflammasome	18131	REACTOME	10090	2	12	0.007121866	0.212468996	*P2rx7; Pstpip1;*
NRAGE signals death through JNK	17436	REACTOME	10090	3	38	0.007867175	0.201174904	*Arhgef18; Arhgef3; Itsn1;*
Inflammasomes	18382	REACTOME	10090	2	15	0.01109402	0.248228695	*P2rx7; Pstpip1;*
G alpha (12/13) signalling events	18452	REACTOME	10090	3	46	0.013305318	0.264627998	*Arhgef18; Arhgef3; Itsn1;*
Transport of glucose and other sugars, bile salts and organic acids, metal ions and amine compounds	16992	REACTOME	10090	4	86	0.013894605	0.248713437	*Rhag; Slc14a1; Slc22a3; Slc44a4;*
Protein digestion and absorption	10377	KEGG	10090	4	89	0.015590884	0.253706204	*Atp1b2; Cela3b; Col4a2; Cpa3;*
Systemic lupus erythematosus	2813	KEGG	10090	5	139	0.017193623	0.256471539	*Cd80; Ctsg; Hist1h2be; Hist1h2br; Hist1h4i;*
Renin-angiotensin system	660	KEGG	10090	2	19	0.017568354	0.241902721	*Cpa3; Ctsg;*
Cell death signalling via NRAGE, NRIF and NADE	18269	REACTOME	10090	3	56	0.022492439	0.287581903	*Arhgef18; Arhgef3; Itsn1;*
Degradation of the extracellular matrix	19757	REACTOME	10090	4	100	0.022901834	0.273295223	*Adam8; Col4a2; Ctsg; Mmp9;*
Asthma	2791	KEGG	10090	2	23	0.025277364	0.266155771	*Epx; Prg2;*

THIS PAGE INTENTIONALLY LEFT BLANK.

Appendix 6.4

Statistical Data of Nodes Explored via NetworkAnalyst

Id	Label	Degree	Betweenness
P15314	Irf1	41	4869.7
O35718	Socs3	29	4449.13
Q0VGT2	Gli2	13	1401.87
Q9QYY0	Gab1	11	1714.5
Q9Z0J4	Nos1	11	1619.94
Q64280	Lefty1	8	1274.93
Q9Z0E6	Gbp2	7	1255.58
P23611	Irf8	7	688
O35668	Hap1	5	514
P0CG50	Ubc	4	964.87
Q9WVH4	Foxo3	4	520.27
Q9ER80	Rtp4	4	306.89
Q9QY24	Zbp1	4	278.49
P08032	Spna1	4	260
P35438	Grin1	3	319
Q9Z2F2	Oasl2	3	177.89
P25799	Nfkb1	3	54.67
Q05769	Ptgs2	2	934.85
Q8BUN5	Smad3	2	867.76
P47941	Crkl	2	862.5
P35235	Ptpn11	2	862.5
Q01147	Creb1	2	710.09
P15209	Ntrk2	2	630
P20263	Pou5f1	2	597.2
P42227	Stat3	2	596.39
P52633	Stat6	2	596.39
P42230	Stat5a	2	596.39
P08775	Polr2a	2	388.97
Q9WUN2	Tbk1	2	205.34
P63101	Ywhaz	2	189
Q61107	Gbp3	2	2.87

THIS PAGE INTENTIONALLY LEFT BLANK.

CHAPTER 7 –

FINAL DISCUSSION

7.1. Introduction

The advancement of next-generation sequencing (NGS) technologies such as mRNA sequencing, whole genomic sequencing (WGS) and whole exome sequencing (WES) has enabled the identification of an array of genomic lesions associated with high-risk childhood ALL[47,65,559]. This has facilitated studies into a subtype termed Ph-like/*BCR-ABL1*-like ALL[19,58], where cytokine and kinase-activating genomic lesions were discovered (i.e. *CRLF2* rearrangements accompanied with concomitant *JAK* mutations, and, fusion genes involving Jak/Stat and Abl kinase signalling)[64,73]. Importantly, these alterations are sensitive to currently-available TKIs[64,73,204,205,319] and anecdotal applications of TKIs in the clinic (i.e. use of dasatinib in patients with the *EBF1-PDGFRβ* fusion gene)[90,91] appears promising for a potential eradication of leukaemic cells.

Despite this promising approach, studies of TKI-use in other cancers (i.e. CML[180,560,561], Ph+ ALL[562,563], AML[420], NSCLC[564,565], etc.) have described TKI-resistance as a major cause of clinical relapse. TKI-resistance can occur as a result of primary or secondary factors[153,154,566], as well as mechanisms that are dependent or independent to the initial causative lesion[307,567,568]. As Ph-like ALL is an emerging field, the mechanism of TKI-resistance in this setting is largely unknown. To date, the only case of clinical relapse due to TKI-resistance in a Ph-like ALL setting was documented by Yeung *et al*., where a B-ALL patient identified with the *ETV6-ABL1* fusion was administered dasatinib, whom later developed an *ABL1*-T315I kinase domain mutation and subsequently relapsed[92].

Very few *in vitro* studies of TKI-resistance in a Ph-like setting exist. In a sole recent report by Tran *et al*., TKI-resistant Ph-like ALL was modelled via an *in vitro* saturation mutagenesis screening of *EBF1-PDGFRβ*, enabling direct manipulation of genes and subsequent generation of random mutants[569]. Constructs of *EBF1-PDGFRβ* harbouring kinase domain mutations were transduced into Ba/F3 cells, with TKI-resistance determined by the ability of cells to form colonies in clonogenic assays in the presence of TKIs. The authors identified colonies containing the *PDGFRβ*-N666S and *PDGFRβ*-T681I mutations as most commonly resistant to imatinib and dasatinib[569]. Although this method enabled the generation of a large variety of mutants, this did not represent a clinical setting where mutations occur

stochastically, as a result of selection pressure through long-term TKI exposure[327,570,571]. Therefore, this thesis aimed to address this concern by culturing cells in incrementally increasing concentrations of TKI, allowing for the evolution and selection of cells harbouring TKI-resistance.

Ph+ and Ph-like ALL are highly-aggressive subsets and with relapse a likely issue, investigation into the underlying causes of potential TKI-resistance is urgent. Furthermore, clinical trials of TKI use in Ph-like ALL are currently underway[470,572,573], presenting an urgent need to elucidate this. The findings in this thesis will therefore address the various genetic and genomic alterations that may arise, depending on the fusion kinase present and TKI therapy applied.

7.2. Major Findings

7.2.1. TKI-resistance in Ph+ ALL is attributable to *RAS* mutations

In order to model TKI-resistance in high-risk ALL, experiments were first performed using SUP-B15s, a Ph+ ALL cell line. The generation of dasatinib and ponatinib-resistant SUP-B15 cells to clinically relevant concentrations has never been reported. Studies to date have only documented resistance of SUP-B15 cells to imatinib (a first-generation Abl TKI)[152], or, CML cells to dasatinib/ponatinib[185,211]. It was therefore imperative to investigate the mechanisms of resistance that may arise, if Ph+ ALL were exposed to second generation TKIs as alternative therapy.

Throughout the course of the dose-escalation process, downstream p-Bcr-Abl and CrkL assays repeatedly indicated a lack of IC_{50} changes in resistant cell lines compared to control. This was surprising because clinically, TKI-resistance has been associated with the development of point mutations within the Abl kinase domain[156,239,574], which should lead to a subsequent increase in p-Bcr-Abl and p-CrkL IC_{50}. The lack of increased IC_{50} in dasatinib/ponatinib resistant cells suggested that the TKI was still able to target Bcr-Abl, despite survival of cells in high concentrations of the drugs. This observation led to the hypothesis that despite the downstream inhibition of Bcr-Abl, a Bcr-Abl independent mechanism for growth and survival exists, allowing TKI-resistant SUP-B15 cells to thrive *in vitro*.

The use of mRNA sequencing enabled the identification of *RAS* mutations, where the *KRAS*-G12S and *NRAS*-G12S mutations were identified in dasatinib and ponatinib-resistant SUP-B15 cells, respectively. *RAS* mutations have been implicated in many cancers, including solid tumours (i.e. colorectal cancer[575,576], lung cancer[577,578] and melanoma[579]) as well as in haematological malignancies (i.e. multiple myeloma[580], AML[581] and childhood ALL[272,582]). In TKI-resistance, the *NRAS*-G12D and *NRAS*-Q61K mutations are involved in Flt3-inhibitor resistant AML[583]. In a Ph+ ALL setting, a previous study investigating imatinib-resistant SUP-B15 cells also suggested an upregulation of the Erk and Akt/mTOR signalling pathways, despite the absence of Abl kinase-domain mutations[152]. The study, however, did not utilise any NGS – a technique that may have revealed other genomic lesions possibly involved in their observed imatinib-resistance. In a separate study performed by Suzuki *et al*. using Ph+ ALL patient-derived cells, the involvement of a Mapk/Erk-dependent pathway was similarly implicated in imatinib-resistance[584].

7.2.2. TKI-resistance in Ph-like ALL varies according to the fusion gene present and the applied TKI

7.2.2.1. TKI-resistance in *RANBP2-ABL1* Ph-like ALL mimics the pattern of resistance observed in CML and Ph+ ALL

The mechanisms of TKI resistance associated with Abl kinase have been widely studied in CML and Ph+ ALL, where relapse cases from the use of Glivec (imatinib) and other Abl-kinase inhibitors are observed clinically[158,238,585]. As Abl TKIs are applicable in targeting Abl kinase fusions in Ph-like ALL, any alterations identified in TKI-resistant *RANBP2-ABL1* may potentially be clinically-relevant. The identification of the clinically-significant *ABL1*-T315I point mutation in imatinib and dasatinib-resistant *RANBP2-ABL1* cell lines demonstrated that prolonged TKI therapy in cells harbouring this fusion can result in a selection for cells harbouring the 'gatekeeper' mutation[174,574,586]. The *ABL1*-T315I mutation has been well-described to be resistant to first and second-generation TKIs[166,587], and an identification of this clinically-significant point mutation in both imatinib and dasatinib-resistant *RANBP2-ABL1* cells suggested a likelihood for cells to clonally select for this mutation, which

supports a similar clinical finding recently described by Yeung and colleagues (*ABL1*-T315I in dasatinib-resistant *ETV6-ABL1*)[92].

Despite being cross-resistant to first and second-generation Abl TKIs, the *ABL1*-T315I kinase domain mutation is targetable using the third-generation TKI ponatinib[286,317]. Resistance to ponatinib use, however, has been associated with the development of compound mutations[186,327]. In Ba/F3 *RANBP2-ABL1* cells, this was strongly evidenced by the acquisition of an *ABL1*-T315I/G250E mutation in imatinib-resistant cells and a previously unreported *ABL1*-L302H/T315I mutation in dasatinib-resistant cells that were dose-escalated in ponatinib as secondary therapy. Compound mutations as causes of ponatinib-resistance remains a highly debatable field, however, as a recent study has suggested that compound mutations were non-drivers of ponatinib-resistance in chronic phase CML[588]. In the aforementioned study[588], the use of NGS enabled the identification of multiple polyclonal and compound mutations within *ABL1*, some of these undetectable via Sanger sequencing and absent at the end of the study period. As most patients remained on therapy, limited post-treatment samples were available[588] and therefore a larger sample size may be required for a more comprehensive analysis.

When ponatinib was utilised as first-line treatment in Ba/F3 *RANBP2-ABL1* cells, a *BCR-ABL1* independent mechanism of resistance was acquired. Despite cells expressing the *ABL1*-E255K mutation, this mutation has been described to be less sensitive to ponatinib, in-comparison to other *ABL* kinase domain mutations[589,590]. Strategically, *RANBP2-ABL1* cells may have developed the *ABL1*-E255K mutation as a preliminary method of evading lower concentrations of ponatinib in culture, prior to adaptation to a potent 200 nM final concentration of ponatinib. Hence, an alternative mechanism of signalling was potentially required. The exact role of the c-terminus deletion in ponatinib-resistant *RANBP2-ABL1* is unknown and may either be causative or an artefact of ponatinib-resistance – further modelling will help to determine its exact function. Previous studies have documented the Abl c-terminus region as an F-actin binding domain essential for apoptotic suppression in Ara-C resistance, although deletion of this region also conferred a proliferative advantage in progenitor FDCP-mix multipotent cells that were transduced with *BCR-ABL1*[343]. In breast cancer, deletion of the c-terminus in *BRCA2* has been implicated in therapeutic resistance against the PARP inhibitor KU0058948[338].

More importantly, mRNA sequencing pathway analysis revealed the involvement of alternative mechanisms associated with ponatinib-resistance. This included an enrichment of downregulated vitamin D signalling – an increase of which is rather known to be associated with a reduction of cancer risk[591-593]. An enrichment of upregulated genes associated with immune signalling (i.e. *Oas* and *Irf* families) was also identified in ponatinib-resistant *RANBP2-ABL1* cells, indicating a possible contribution of the interferon pathway in ponatinib-resistance. Interferon signalling has been associated with downstream activation of Stat1[594], while Stat1 signalling has been described in the resistance of myeloma[595], ovarian carcinoma[596] and melanoma[597] cells to various anticancer therapies. The *Oas* family is associated with the ribonuclease L pathway, an enzyme involved in the degradation of viral and cellular RNA in innate immunity[598-600]. In pancreatic adenocarcinoma cells, constitutive expression of Oas signalling was implicated in increased resistance to an oncolytic agent comprising of recombinant vesicular stomatitis virus (VSV), targeting interferon signalling in cells[601,602]. In other studies, polymorphisms in *OAS* were also implicated in increased risk of prostate cancer (*OAS1*-rs2660)[603] and chronic lymphocytic leukaemia (*OAS3*-rs10735079)[604].

Taken together, the findings in **Chapter 4** describe how despite the targetability of *RANBP2-ABL1* using currently-available TKIs, resistance can occur through varying mechanisms according to the applied TKI. Point mutations such as *ABL1*-T315I may arise, and despite the use of ponatinib to overcome resistance, compound mutations such as the previously unreported *ABL1*-L302H/T315I may occur. Importantly, the use of ponatinib as a first-line treatment resulted in the acquisition of various genetic alterations. Despite the presence of the clinically-relevant ponatinib resistant *ABL1*-E255K mutation, the development of a c-terminus deletion, accompanied by dysregulation of various noncanonical signalling mechanisms, illustrates the complexity of TKI-resistance in this setting.

7.2.2.2. TKI-resistance in *SSBP2-CSF1R* is attributable to multiple genetic alterations, including the identification of novel kinase-domain mutations

In **Chapter 5**, the mode of TKI-resistance in an *SSBP2-CSF1R* Ph-like setting was investigated. Csf1r, also known as M-Csfr or c-fms, is sensitive to imatinib and dasatinib according to previous studies[73,396,431]. In imatinib-resistant Ba/F3 *SSBP2-CSF1R* cells, a novel *CSF1R*-L785M kinase-domain mutation was identified by mutation analysis. A separate mutation, the *CSF1R*-D802V, was previously reported to be resistant to imatinib[409]. The substitution of leucine to methionine resulted in the presence of a bulkier residue, which potentially negates critical drug binding. *CSF1R*-L785M, however, was also targetable using the 2nd and 3rd generation TKIs dasatinib and ponatinib, suggesting that these newer generation TKIs may be utilised to overcome imatinib-resistance in an *SSBP2-CSF1R* Ph-Like ALL setting.

In dasatinib-resistant *SSBP2-CSF1R* cells, a previously unreported *CSF1R*-A652V kinase domain mutation was identified. A study performed by Brownlow and colleagues indicated that FD-CP1 haematopoietic cells harbouring the nearby *CSF1R*-T663I mutation was resistant to dasatinib, phenocopying characteristics of the *ABL1*-T315I gatekeeper mutation[431]. Further molecular modelling in their study confirmed that dasatinib interacts with residues adjacent to the hinge region within the ATP binding pocket of Csf1r (similar to dasatinib-binding in the Abl kinase)[172], therefore any substitution within this vicinity may potentially negate drug-binding[605]. *CSF1R*-A652V results in a substitution from alanine to valine, which comprises of a bulkier side-chain. Therefore, the identification of this point mutation in *SSBP2-CSF1R* is highly clinically-relevant and future studies into overcoming this mutation are warranted.

Interestingly, dasatinib-resistant Ba/F3 *SSBP2-CSF1R* cells also harboured an additional deletion spanning the fusion breakpoint region. At present, no such breakpoint deletion has been reported in Ph-like ALL. In a Ph+ leukaemia setting, however, breakpoint deletions have been well-characterised and deletions within the fusion gene are noted to result in a more aggressive cancer phenotype[606,607]. In fact, in dasatinib-resistant Ba/F3 *SSBP2-CSF1R* cells, Western blotting indicated increased p-Ssbp2-Csf1r compared to DMSO control, suggesting increased autophosphorylation as an added consequence of TKI-resistance[608-610].

At present, downstream signalling of Csf1r includes the Grb2-Sos-Erk[611-613] and PI3K/Akt/mTOR signalling pathways[614-616], contributing towards an activation of cell survival and proliferation signalling cascades. Csf1r also interacts with Src, which is known to be potentially associated with the β-catenin pathway[617,618], with Wnt/β-catenin indicated as essential for the development of AML leukaemic stem cells[619]. Therefore, in TKI-resistant *SSBP2-CSF1R* cells, the acquisition of the *CSF1R*-L785M and *CSF1R*-A652V kinase domain mutations may potentially allow for downstream activation of these associated pathways, leading to cell survival. The dependency on TKI for the survival of TKI-resistant *SSBP2-CSF1R* cells also suggests transcriptional reprogramming may have occurred, a phenomenon similarly observed in other drug-resistant cancers (i.e. BRAF/MEK inhibitor-resistant melanoma and lung cancers)[424,425,620,621].

The adaptation of *SSBP2-CSF1R* cells to TKIs possibly encompasses epigenetic changes that modulate coactivators and corepressors of transcription factors associated with cell proliferation and survival[424,620,621]. Subsequent withdrawal of TKI in *SSBP2-CSF1R* imatinib/dasatinib resistant cells may then lead to a signalling flux, altering intracellular haematopoiesis. This can potentially result in the dysregulation of cellular survival signalling cascades and the induction of cell death. If validated in a Ph-like setting, this theory provides a potential avenue for the application of future therapies that can override treatment-resistance.

7.2.2.3. TKI-resistance in *PAX5-JAK2* Ph-like ALL is attributable to the acquisition of clinically-relevant point mutations and possibly the presence of noncanonical signalling mechanisms

Modelling of *PAX5-JAK2* in **Chapter 6** has enabled the investigation of the modes of TKI-resistance that may arise in a Jak fusion setting. Despite modelling of ruxolitinib and BMS-911543 resistance in separate cultures, TKI-resistant *PAX5-JAK2* cells were highly cross-resistant to both inhibitors. This finding indicated that the mode of resistance was perhaps due to the presence of a common mechanism within the drug-binding domain of Jak2, that is normally inhibited by ruxolitinib and BMS-911543[141]. The identification of a *JAK2*-Y931C kinase-domain mutation in both TKI-resistant cell lines confirmed this assumption, as previous studies have

demonstrated *JAK2*-Y931C to be resistant to ATP-competitive type I Jak inhibitors[202,469]. Homologous to the *JAK1*-F958C mutation, which also confers resistance to ATP-competitive Jak TKIs[202], *JAK2*-Y931C is situated within the catalytic ATP-binding domain of Jak2[491]. As noted by Fridman and Sarlis, however, the *JAK2*-Y931C mutation has yet to be described in a clinical setting[622]. Studies of *JAK2*-Y931C have thus far developed the mutation via random site-directed mutagenesis[201,202,491]. As the *JAK2*-Y931C in Ba/F3 *PAX5-JAK2* cells was observed in two separate long-term cultures (ruxolitinib and BMS-911543), this suggested that the *JAK2*-Y931C mutation is highly clinically-relevant, comparable to other studies that have identified the same mutation using independent methodologies. Most recently, we have observed a relapse sample with the *JAK2*-Y931C (Dr. Sue Heatley, personal communication) – further studies into whether these cells are resistant to ATP-competitive Jak inhibitors will help to confirm these findings.

Due to the potential clinical relevance of the *JAK2*-Y931C mutation, mRNA sequencing was subsequently performed on ruxolitinib-resistant and DMSO control Ba/F3 *PAX5-JAK2* cells. Bioinformatics analyses revealed an association between decreased glycolysis/gluconeogenesis and immune-regulated signalling, as well as a potential increase in drug metabolism pathways – both of which are likely unrelated to Jak/Stat signalling. Glycolysis and gluconeogenesis are key metabolic pathways commonly active in cancer cells, due to characteristics of the 'Warburg effect' important for energy in cancer cells[623-625]. The decreased expression of these pathways in ruxolitinib-resistant *PAX5-JAK2* cells compared to DMSO control was therefore intriguing, as these were in contrast to previous reports where increased glycolysis was observed at diagnosis and relapsed AML and ALL[626-628]. Interestingly, studies have also suggested an increased targetability of metabolically-active leukaemic cells to therapy[626], although this varies according to the cell type[629]. In pancreatic cancer, a recent study demonstrated that glycolytic metabolism was, in fact, decreased in oncogene-ablated (resistant) cells due to a dependency on mitochondrial respiration. The authors also noted that most of these cells appeared to be a tumour-initiating / cancer stem cell phenotype[630]. Therefore, in the context of ruxolitinib-resistant *PAX5-JAK2*, it is reasonable to consider whether cells may have adapted a more 'primitive' state, to evade drug therapy.

The decreased genomic expression of immune-signalling pathways such as *Socs* (a negative regulator of Jak)[527] and *Irf* (associated with growth arrest[631] and

proapoptotic Puma signalling[632]) further indicated mechanisms which were previously unreported, in ruxolitinib-resistant *PAX5-JAK2* Ph-like ALL. These mechanisms support ruxolitinib-resistance by enabling a stable expression of Jak2, maintaining cell growth and proliferation despite a presence of TKI.

The upregulation of drug metabolism signalling (i.e. *Aldh1a1*) also suggested a possible alteration of mechanisms controlling intracellular TKI bioavailability, which may reduce overall TKI concentrations in resistant cells[633,634]. Importantly, the use of computational network biology revealed genomic 'bottlenecks' (i.e. *Irf1*, *Socs3*, *Gli2* & *Gab1*) that serve as attractive future targets for the reversal of TKI-resistance, with contextual hub analysis cementing the implication of pathways such as NF-κB (via *Rela*) in ruxolitinib-resistance.

NF-κB is commonly associated with the well-studied PI3K/Akt signalling pathway, implicated in the metastasis of solid tumours (i.e. lung[635], gastric[636] and oesophageal cancers[637]). The expression of NF-κB can also be influenced by other factors, including the overexpression of ZNF300 (which enhances growth and metastasis)[638], Stat3 (cross-talk in the pathogenesis of cancer)[639], and Erk 1/2 (leading to increased Mcl-1 and Bcl-2, in rituximab-resistant lymphoma)[640]. Many studies in other haematological malignancies (i.e. multiple myeloma[641], MDS and AML[642], as well as T-cell leukaemia and lymphoma[643]) have since proposed NF-κB as an attractive therapeutic target, therefore, its role in ruxolitinib-resistant *PAX5-JAK2* Ph-like ALL may be clinically relevant.

There are therefore considerations to be made when administering Jak inhibitors in Ph-like ALL therapy, as this study has revealed that TKI-resistance is a complex issue, involving more than just the *JAK2*-Y931C mutation in ruxolitinib-resistance. The application of future therapies that may either bind to Jak in an alternative fashion (i.e. type II Jak inhibitors such as CHZ868[644]), or target alternative pathways (i.e. HSP90 inhibitors[201]) may potentially avert resistance, improving treatment outcomes.

7.3. Overall Summary & Future Directions

Modelling of TKI-resistance in Ph+ and Ph-like ALL has enabled the identification of previously unreported point mutations (*ABL1*-L302H/T315I, *CSF1R*-A652V and *CSF1R*-L785M), as well as clinically-relevant mutations analogous to those previously described in the literature (*ABL1*-T315I, *ABL1*-E255K and *ABL1*-G250E/T315I in CML[186,328,588]; *JAK2*-Y931C in MPN[469]). These molecular alterations implicate pathways such as PI3K/Akt/mTOR[645,646], Jak/Stat[647,648], Ras/Raf/Mek/Erk[649,650] and β-catenin signalling[651-654], known to cross-talk[655-659] and associated with cell survival, proliferation and inhibition of apoptosis (**Figure 7.1**).

In-addition, the use of high throughput NGS (mRNA-seq) and bioinformatics analyses has enabled the identification of multiple alternative mechanisms (i.e. *RAS* mutations, dysregulation of GPCR, immune-regulatory and metabolic signalling pathways) that are critical in TKI-resistance. These mechanisms further imply how TKI-resistance is a highly complex issue, involving molecular dysregulation other than genetic alterations.

Whether the mechanisms identified are drivers of TKI-resistance is currently unknown. Potential methods of resolving this include the use of *in silico* knockout of 'hubs of interest' (i.e. genomic bottlenecks) in the mRNA-seq data, to identify specific driver mechanisms. The use of genome editing systems[660] as a follow-up (i.e. RNAi[661-663], transcription activator-like effector nuclease (TALEN)[664,665], or, clustered regularly interspaced short palindromic repeats – associated system (CRISPR/Cas)[666-668] can then potentially confirm whether a knock-in/knock-out reverts TKI-resistant cells into a non-resistant mode. Reversal of resistance will allow for application/repurposing of currently-available therapies, to ultimately eliminate leukaemic cells. Evaluating the metabolomic status of TKI-resistant cells would also be valuable, as the mRNA-seq expression data appeared promising and dysregulated metabolism is well-known in cancer[669-671].

Of note, TKI-resistance in Ph-like ALL (Chapters 4, 5 and 6) was modelled in a murine cell line (Ba/F3 pro-B cells). While modelling of Ph-like ALL in a human cell line would be more clinically-appropriate, Ba/F3 pro-B cells have been widely utilised in studies investigating gene transformation potential due to its dependency

on IL-3[64,425,672,673]. Furthermore, the immortalisation of cells from relapsed primary samples remains a relatively challenging approach to date[674-676].

Modelling of TKI-resistance in Ba/F3 cells also provides a platform for future murine *in vivo* xenograft studies, reducing inter-species issues such as the need for humanising of the immune system as observed in patient-derived xenograft (PDX) models[677,678]. As such, it is imperative that contemporary models of specific Ph-like ALL fusions and their relapsed counterparts be currently-available, for identification and discovery of better treatment strategies. As the TKI-resistant Ba/F3 cell lines described in this thesis were generated using fusion genes derived from primary patient samples, any alterations perturbing critical drug-binding would most likely be representative of a clinical setting. This was noted through the development of the clinically-relevant *ABL1*-T315I mutation (Chapter 4), which served as a 'proof of concept' for the genetic alterations identified in the subsequent chapters.

Future work investigating the evolution of events leading to specific TKI-resistant genomic alterations is therefore also of high importance, best elucidated through the characterisation of cells at various points of dose-escalation[211,242]. It is important to note that because TKI-resistance was generated through an *in vitro* concept, this experimental method may have resulted in a selection for survival of the 'fittest' clones, which may differ from the achievement of a potentially diverse mechanism of resistance otherwise observed in an *in vivo* model. Hence, future studies investigating PDX models comprising of relapsed primary Ph-like ALL samples, or generation of TKI-resistant PDX models, would therefore be ideal. Such studies will also allow for the investigation of whether a 'stem-cell-like' phenotype exists in TKI-resistant Ph+ and Ph-like ALL, as studies have described the importance of stem cells in cancer drug evasion and malignancy[518,679,680].

With genomic sequencing and precision medicine becoming increasingly common clinical practice, the findings presented in this thesis greatly highlights the possible scenarios that may arise in the event of treatment relapse[681-684]. The genetic alterations described in this thesis will serve as a potential guide for future monitoring of a patients' genomic profile, from initial TKI exposure through the course of treatment. Early detection of genetic alterations associated with TKI-resistance is key, for administration of alternative treatment strategies that may overcome and prevent downstream complications associated with relapse.

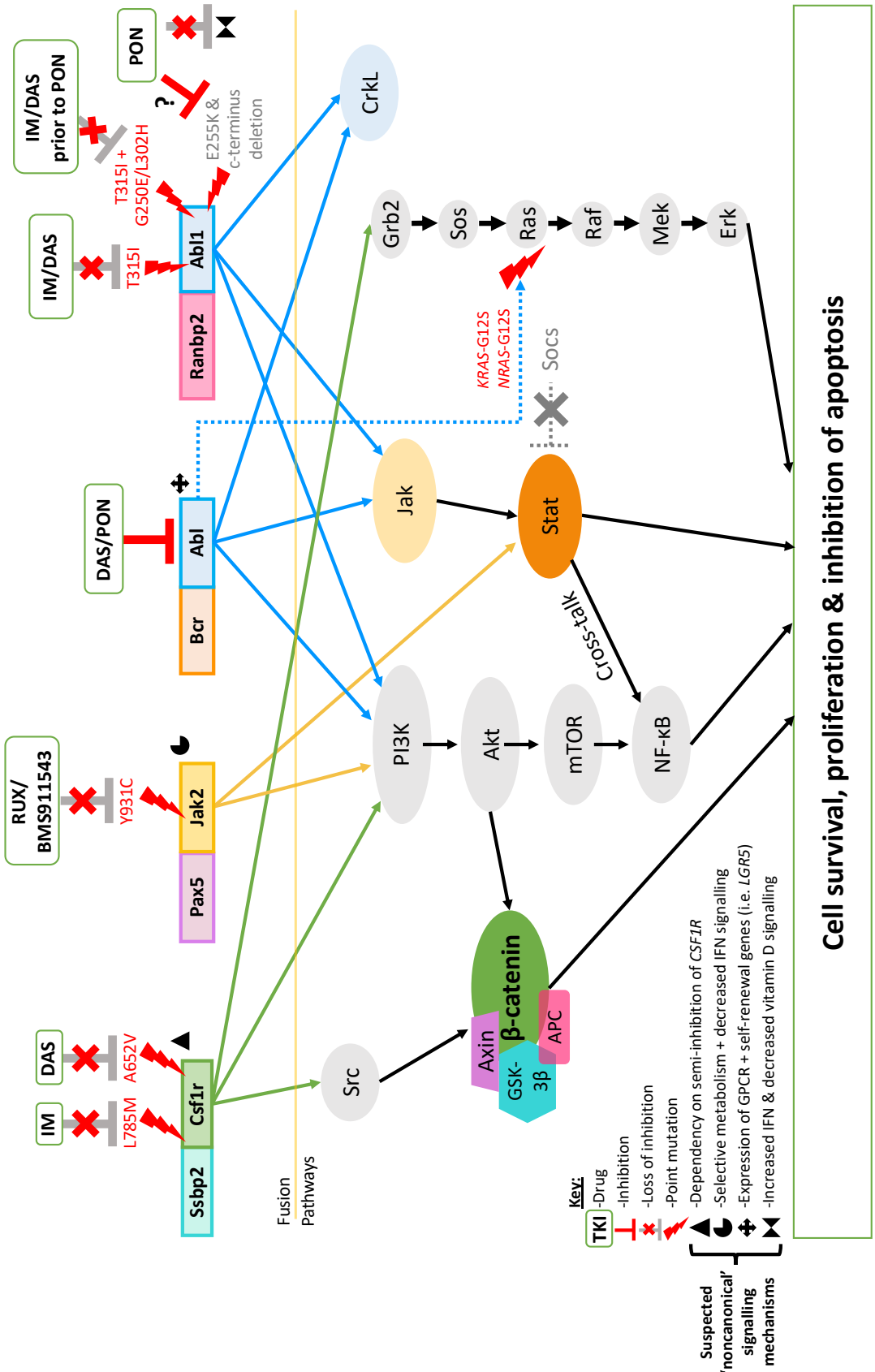
Such future treatment strategy may include the potential use of inhibitors that co-target alternative pathways (i.e. BH3-mimetics or mTOR/PI3K inhibitors)[685-688]. Thus, performing of a high-throughput drug screening with the TKI-resistant models generated in this thesis will hopefully enable identification of future combinatorial therapies, for potential translation into *in vivo* PDX models and overcoming of TKI-resistance. In addition, further studies into the status of cell surface marker expression in TKI-resistant Ph+ and Ph-like ALL may also pave the way for future application of CAR-T cells, an emerging method of targeting relapsed ALL[228,689-691]. Serving as a vital platform to inform future clinical decision-making, the novel findings described in this thesis will hopefully bring us a step closer towards eradicating treatment-resistant leukaemia, in the search for a potential cure and ultimate improvement of patient outcome.

Figure 7.1 – Schematic summary of TKI-resistance in SUP-B15 Ph+ ALL and Ba/F3 Ph-like ALL cell lines identified in this study

Despite the targetability of activated fusion kinases in Ph-like ALL (Ssbp2-Csf1r, Pax5-Jak2 and Ranbp2-Abl1) and Ph+ ALL (Bcr-Abl), clinically relevant TKI-resistance is likely to arise. Mutations (as depicted by red text) within the kinase domain and other signalling pathways not directly associated with the fusion (i.e. Ras) can reduce TKI-sensitivity, affecting downstream signalling (arrows colour-coded according to fusion). Most importantly, these kinases converge along similar pathways, resulting in the subsequent increase in cell survival signalling. The symbols represent possible alternative pathways that may contribute towards TKI-resistance, which is thus a complex issue. IM: imatinib, DAS: dasatinib, PON: ponatinib, RUX: ruxolitinib

Figure 7.1

Summary of TKI-resistance in *in vitro* modelling of Ph+ and Ph-like ALL



THIS PAGE INTENTIONALLY LEFT BLANK.

REFERENCES

1. Liao Y, Smyth GK, Shi W. The Subread aligner: fast, accurate and scalable read mapping by seed-and-vote. *Nucleic Acids Res* 2013; **41**(10)**:** e108.

2. Schmittgen TD, Livak KJ. Analyzing real-time PCR data by the comparative CT method. *Nature Protocols* 2008; **3**(6)**:** 1101-1108.

3. Benjamini Y, Drai D, Elmer G, Kafkafi N, Golani I. Controlling the false discovery rate in behavior genetics research. *Behav Brain Res* 2001; **125**(1-2)**:** 279-284.

4. Schneider CA, Rasband WS, Eliceiri KW. NIH Image to ImageJ: 25 years of image analysis. *Nat Methods* 2012; **9**(7)**:** 671-675.

5. Liao Y, Smyth GK, Shi W. featureCounts: an efficient general purpose program for assigning sequence reads to genomic features. *Bioinformatics* 2014; **30**(7)**:** 923-930.

6. Kolb H-J. Graft-versus-leukemia effects of transplantation and donor lymphocytes. *Blood* 2008; **112:** 4371-4383.

7. Hunger SP, Mullighan CG. Acute Lymphoblastic Leukemia in Children. *N Engl J Med* 2015; **373**(16)**:** 1541-1552.

8. Harrison CJ, Foroni L. Cytogenetics and molecular genetics of acute lymphoblastic leukemia. *Rev Clin Exp Hematol* 2002; **6**(2)**:** 91-113; discussion 200-112.

9. Mrozek K, Harper DP, Aplan PD. Cytogenetics and molecular genetics of acute lymphoblastic leukemia. *Hematol Oncol Clin North Am* 2009; **23**(5)**:** 991-1010, v.

10. Pui CH, Robison LL, Look AT. Acute lymphoblastic leukaemia. *Lancet* 2008; **371**(9617)**:** 1030-1043.

11. AIHW. Australian Institute of Health and Welfare 2017, Cancer in Australia 2017. *Cancer series no101 Cat no CAN 100 Canberra: AIHW* 2017.

12. Barrington-Trimis JL, Cockburn M, Metayer C, Gauderman WJ, Wiemels J, McKean-Cowdin R. Rising rates of acute lymphoblastic leukemia in Hispanic children: trends in incidence from 1992 to 2011. *Blood* 2015; **125**(19)**:** 3033-3034.

13. Pui CH, Relling MV, Downing JR. Acute lymphoblastic leukemia. *N Engl J Med* 2004; **350**(15)**:** 1535-1548.

14. Bernt KM, Hunger SP. Current concepts in pediatric Philadelphia chromosome-positive acute lymphoblastic leukemia. *Front Oncol* 2014; **4**(March)**:** 54.

15. Tallen G, Ratei R, Mann G, Kaspers G, Niggli F, Karachunsky A*, et al.* Long-term outcome in children with relapsed acute lymphoblastic leukemia after time-point and site-of-relapse stratification and intensified short-course multidrug chemotherapy: results of trial ALL-REZ BFM 90. *J Clin Oncol* 2010; **28**(14)**:** 2339-2347.

16. Hunger SP, Loh ML, Whitlock JA, Winick NJ, Carroll WL, Devidas M*, et al.* Children's Oncology Group's 2013 Blueprint for Research: Acute Lymphoblastic Leukemia. *Pediatric blood & cancer* 2013; **60**(6)**:** 957-963.

17. Pieters R, Schrappe M, De Lorenzo P, Hann I, De Rossi G, Felice M*, et al.* A treatment protocol for infants younger than 1 year with acute lymphoblastic leukaemia (Interfant-99): an observational study and a multicentre randomised trial. *Lancet* 2007; **370**(9583)**:** 240-250.

18. Mullighan CG, Goorha S, Radtke I, Miller CB, Coustan-Smith E, Dalton JD*, et al.* Genome-wide analysis of genetic alterations in acute lymphoblastic leukaemia. *Nature* 2007; **446**(7137)**:** 758-764.

19. Mullighan CG, Su X, Zhang J, Radtke I, Phillips LA, Miller CB*, et al.* Deletion of IKZF1 and prognosis in acute lymphoblastic leukemia. *N Engl J Med* 2009; **360**(5)**:** 470-480.

20. Mullighan CG, Miller CB, Radtke I, Phillips LA, Dalton J, Ma J*, et al.* BCR-ABL1 lymphoblastic leukaemia is characterized by the deletion of Ikaros. *Nature* 2008; **453**(7191)**:** 110-+.

21. Shah S, Schrader KA, Waanders E, Timms AE, Vijai J, Miething C*, et al.* A recurrent germline PAX5 mutation confers susceptibility to pre-B cell acute lymphoblastic leukemia. *Nat Genet* 2013; **45**(10)**:** 1226-1231.

22. Liu GJ, Cimmino L, Jude JG, Hu Y, Witkowski MT, McKenzie MD*, et al.* Pax5 loss imposes a reversible differentiation block in B-progenitor acute lymphoblastic leukemia. *Genes Dev* 2014; **28**(12)**:** 1337-1350.

23. Cobaleda C, Schebesta A, Delogu A, Busslinger M. Pax5: the guardian of B cell identity and function. *Nat Immunol* 2007; **8**(5)**:** 463-470.

24. Nutt SL, Kee BL. The transcriptional regulation of B cell lineage commitment. *Immunity* 2007; **26**(6)**:** 715-725.

25. Revilla IDR, Bilic I, Vilagos B, Tagoh H, Ebert A, Tamir IM*, et al.* The B-cell identity factor Pax5 regulates distinct transcriptional programmes in early and late B lymphopoiesis. *EMBO J* 2012; **31**(14)**:** 3130-3146.

26. Familiades J, Bousquet M, Lafage-Pochitaloff M, Bene MC, Beldjord K, De Vos J*, et al.* PAX5 mutations occur frequently in adult B-cell progenitor acute lymphoblastic leukemia and PAX5 haploinsufficiency is associated with BCR-ABL1 and TCF3-PBX1 fusion genes: a GRAALL study. *Leukemia* 2009; **23**(11)**:** 1989-1998.

27. Iacobucci I, Lonetti A, Paoloni F, Papayannidis C, Ferrari A, Storlazzi CT*, et al.* The PAX5 gene is frequently rearranged in BCR-ABL1-positive acute lymphoblastic leukemia but is not associated with outcome. A report on behalf of the GIMEMA Acute Leukemia Working Party. *Haematologica* 2010; **95**(10)**:** 1683-1690.

28. Medina KL, Pongubala JM, Reddy KL, Lancki DW, Dekoter R, Kieslinger M*, et al.* Assembling a gene regulatory network for specification of the B cell fate. *Dev Cell* 2004; **7**(4)**:** 607-617.

29. Hagman J. Chapter 3 - Transcriptional Regulation of Early B Cell Development A2 - Alt, Frederick W. In: Honjo T, Radbruch A, Reth M (eds). *Molecular Biology of B Cells (Second Edition)*. Academic Press: London, 2015, pp 35-53.

30. Decker T, Pasca di Magliano M, McManus S, Sun Q, Bonifer C, Tagoh H*, et al.* Stepwise activation of enhancer and promoter regions of the B cell commitment gene Pax5 in early lymphopoiesis. *Immunity* 2009; **30**(4)**:** 508-520.

31. Heltemes-Harris LM, Willette MJ, Ramsey LB, Qiu YH, Neeley ES, Zhang N*, et al.* Ebf1 or Pax5 haploinsufficiency synergizes with STAT5 activation to initiate acute lymphoblastic leukemia. *J Exp Med* 2011; **208**(6)**:** 1135-1149.

32. Somasundaram R, Prasad MA, Ungerback J, Sigvardsson M. Transcription factor networks in B-cell differentiation link development to acute lymphoid leukemia. *Blood* 2015; **126**(2)**:** 144-152.

33. Yoshida T, Ng SY, Zuniga-Pflucker JC, Georgopoulos K. Early hematopoietic lineage restrictions directed by Ikaros. *Nat Immunol* 2006; **7**(4)**:** 382-391.

34. Busslinger M. Transcriptional control of early B cell development. *Annu Rev Immunol* 2004; **22:** 55-79.

35. Heizmann B, Kastner P, Chan S. Ikaros is absolutely required for pre-B cell differentiation by attenuating IL-7 signals. *J Exp Med* 2013; **210**(13)**:** 2823-2832.

36. Reynaud D, Demarco IA, Reddy KL, Schjerven H, Bertolino E, Chen Z*, et al.* Regulation of B cell fate commitment and immunoglobulin heavy-chain gene rearrangements by Ikaros. *Nat Immunol* 2008; **9**(8)**:** 927-936.

37. Pui CH, Carroll WL, Meshinchi S, Arceci RJ. Biology, risk stratification, and therapy of pediatric acute leukemias: an update. *J Clin Oncol* 2011; **29**(5)**:** 551-565.

38. Mullighan CG. Genomic profiling of B-progenitor acute lymphoblastic leukemia. *Best Pract Res Clin Haematol* 2011; **24**(4)**:** 489-503.

39. Iacobucci I, Mullighan CG. Genetic Basis of Acute Lymphoblastic Leukemia. *J Clin Oncol* 2017; **35**(9)**:** 975-983.

40. Zhang J, McCastlain K, Yoshihara H, Xu B, Chang Y, Churchman ML*, et al.* Deregulation of DUX4 and ERG in acute lymphoblastic leukemia. *Nat Genet* 2016; **48**(12)**:** 1481-1489.

41. Garcia DR, Arancibia AM, Ribeiro RC, Land MG, Silva ML. Intrachromosomal amplification of chromosome 21 (iAMP21) detected by ETV6/RUNX1 FISH screening in childhood acute lymphoblastic leukemia: a case report. *Rev Bras Hematol Hemoter* 2013; **35**(5)**:** 369-371.

42. Harrison CJ. Blood Spotlight on iAMP21 acute lymphoblastic leukemia (ALL), a high-risk pediatric disease. *Blood* 2015; **125**(9)**:** 1383-1386.

43. Gocho Y, Kiyokawa N, Ichikawa H, Nakabayashi K, Osumi T, Ishibashi T*, et al.* A novel recurrent EP300-ZNF384 gene fusion in B-cell precursor acute lymphoblastic leukemia. *Leukemia* 2015; **29**(12)**:** 2445-2448.

44. Dou H, Chen X, Huang Y, Su Y, Lu L, Yu J*, et al.* Prognostic significance of P2RY8-CRLF2 and CRLF2 overexpression may vary across risk subgroups of childhood B-cell acute lymphoblastic leukemia. *Genes Chromosomes Cancer* 2017; **56**(2)**:** 135-146.

45. Palmi C, Vendramini E, Silvestri D, Longinotti G, Frison D, Cario G*, et al.* Poor prognosis for P2RY8-CRLF2 fusion but not for CRLF2 over-expression in children with intermediate risk B-cell precursor acute lymphoblastic leukemia. *Leukemia* 2012; **26**(10)**:** 2245-2253.

46. Yoda A, Yoda Y, Chiaretti S, Bar-Natan M, Mani K, Rodig SJ*, et al.* Functional screening identifies CRLF2 in precursor B-cell acute lymphoblastic leukemia. *Proc Natl Acad Sci U S A* 2010; **107**(1)**:** 252-257.

47. Mullighan CG. The molecular genetic makeup of acute lymphoblastic leukemia. *Hematology Am Soc Hematol Educ Program* 2012; **2012:** 389-396.

48. Jain N, Roberts KG, Jabbour E, Patel K, Eterovic AK, Chen K*, et al.* Ph-like acute lymphoblastic leukemia: a high-risk subtype in adults. *Blood* 2017; **129**(5)**:** 572-581.

49. Deininger MW, Goldman JM, Melo JV. The molecular biology of chronic myeloid leukemia. *Blood* 2000; **96**(10)**:** 3343-3356.

50. Grebien F, Hantschel O, Wojcik J, Kaupe I, Kovacic B, Wyrzucki AM*, et al.* Targeting the SH2-kinase interface in Bcr-Abl inhibits leukemogenesis. *Cell* 2011; **147**(2)**:** 306-319.

51. Ren R. Mechanisms of BCR-ABL in the pathogenesis of chronic myelogenous leukaemia. *Nat Rev Cancer* 2005; **5**(3)**:** 172-183.

52. Goldman JM, Melo JV. BCR-ABL in chronic myelogenous leukemia--how does it work? *Acta Haematol* 2008; **119**(4)**:** 212-217.

53. Fabbro D. BCR-ABL signaling: A new STATus in CML. *Nat Chem Biol* 2012; **8**(3)**:** 228-229.

54. Mahon FX, Deininger MW, Schultheis B, Chabrol J, Reiffers J, Goldman JM*, et al.* Selection and characterization of BCR-ABL positive cell lines with differential sensitivity to the tyrosine kinase inhibitor STI571: diverse mechanisms of resistance. *Blood* 2000; **96**(3)**:** 1070-1079.

55. Steelman LS, Pohnert SC, Shelton JG, Franklin RA, Bertrand FE, McCubrey JA. JAK/STAT, Raf/MEK/ERK, PI3K/Akt and BCR-ABL in cell cycle progression and leukemogenesis. *Leukemia* 2004; **18**(2)**:** 189-218.

56. Melo JV, Deininger MW. Biology of chronic myelogenous leukemia--signaling pathways of initiation and transformation. *Hematol Oncol Clin North Am* 2004; **18**(3)**:** 545-568, vii-viii.

57. van der Veer A, Waanders E, Pieters R, Willemse ME, Van Reijmersdal SV, Russell LJ*, et al.* Independent prognostic value of BCR-ABL1-like signature and IKZF1 deletion, but not high CRLF2 expression, in children with B-cell precursor ALL. *Blood* 2013; **122**(15)**:** 2622-2629.

58. Den Boer ML, van Slegtenhorst M, De Menezes RX, Cheok MH, Buijs-Gladdines JG, Peters ST*, et al.* A subtype of childhood acute lymphoblastic leukaemia with poor treatment outcome: a genome-wide classification study. *Lancet Oncol* 2009; **10**(2)**:** 125-134.

59. Vitanza NA, Zaky W, Blum R, Meyer JA, Wang J, Bhatla T*, et al.* Ikaros deletions in BCR-ABL-negative childhood acute lymphoblastic leukemia are associated with a distinct gene expression signature but do not result in intrinsic chemoresistance. *Pediatr Blood Cancer* 2014; **61**(10)**:** 1779-1785.

60. Roberts KG. The biology of Philadelphia chromosome-like ALL. *Best Practice & Research Clinical Haematology* 2017.

61. Izraeli S. Beyond Philadelphia: 'Ph-like' B cell precursor acute lymphoblastic leukemias - diagnostic challenges and therapeutic promises. *Curr Opin Hematol* 2014; **21**(4)**:** 289-296.

62. Pui CH, Roberts KG, Yang JJ, Mullighan CG. Philadelphia Chromosome-like Acute Lymphoblastic Leukemia. *Clin Lymphoma Myeloma Leuk* 2017; **17**(8)**:** 464-470.

63. Boer JM, Marchante JR, Evans WE, Horstmann MA, Escherich G, Pieters R*, et al.* BCR-ABL1-like cases in pediatric acute lymphoblastic leukemia: a comparison between DCOG/Erasmus MC and COG/St. Jude signatures. *Haematologica* 2015; **100**(9)**:** e354-357.

64. Roberts KG, Morin RD, Zhang J, Hirst M, Zhao Y, Su X*, et al.* Genetic alterations activating kinase and cytokine receptor signaling in high-risk acute lymphoblastic leukemia. *Cancer Cell* 2012; **22**(2)**:** 153-166.

65. Loh ML, Zhang J, Harvey RC, Roberts K, Payne-Turner D, Kang H*, et al.* Tyrosine kinome sequencing of pediatric acute lymphoblastic leukemia: a report from the Children's Oncology Group TARGET Project. *Blood* 2013; **121**(3)**:** 485-488.

66. Reshmi SC, Harvey RC, Roberts KG, Stonerock E, Smith A, Jenkins H*, et al.* Targetable kinase gene fusions in high-risk B-ALL: a study from the Children's Oncology Group. *Blood* 2017; **129**(25)**:** 3352-3361.

67. Roberts KG, Gu Z, Payne-Turner D, McCastlain K, Harvey RC, Chen IM*, et al.* High Frequency and Poor Outcome of Philadelphia Chromosome-Like Acute Lymphoblastic Leukemia in Adults. *J Clin Oncol* 2017; **35**(4)**:** 394-401.

68. Kang H, Roberts KG, Chen I-ML, Atlas SR, Bedrick EJ, Gastier-Foster JM*, et al.* Development and Validation Of a Highly Sensitive and Specific Gene Expression Classifier To Prospectively Screen and Identify B-Precursor Acute Lymphoblastic Leukemia (ALL) Patients With a Philadelphia Chromosome-Like (“Ph-like” or “BCR-ABL1-Like”) Signature For Therapeutic Targeting and Clinical Intervention. *Blood* 2013; **122:** 826-826.

69. Boer JM, Steeghs EM, Marchante JR, Boeree A, Beaudoin JJ, Beverloo HB*, et al.* Tyrosine kinase fusion genes in pediatric BCR-ABL1-like acute lymphoblastic leukemia. *Oncotarget* 2017; **8**(3)**:** 4618-4628.

70. Boer JM, Koenders JE, van der Holt B, Exalto C, Sanders MA, Cornelissen JJ*, et al.* Expression profiling of adult acute lymphoblastic leukemia identifies a BCR-ABL1-like subgroup characterized by high non-response and relapse rates. *Haematologica* 2015; **100**(7)**:** e261-264.

71. Tasian SK, Loh ML, Hunger SP. Philadelphia chromosome-like acute lymphoblastic leukemia. *Blood* 2017; **130**(19)**:** 2064-2072.

72. Herold T, Schneider S, Metzeler KH, Neumann M, Hartmann L, Roberts KG*, et al.* Adults with Philadelphia chromosome-like acute lymphoblastic leukemia frequently have IGH-CRLF2 and JAK2 mutations, persistence of minimal residual disease and poor prognosis. *Haematologica* 2017; **102**(1)**:** 130-138.

73. Roberts KG, Li Y, Payne-Turner D, Harvey RC, Yang YL, Pei D*, et al.* Targetable kinase-activating lesions in Ph-like acute lymphoblastic leukemia. *N Engl J Med* 2014; **371**(11)**:** 1005-1015.

74. Harvey RC, Mullighan CG, Wang X, Dobbin KK, Davidson GS, Bedrick EJ*, et al.* Identification of novel cluster groups in pediatric high-risk B-precursor acute lymphoblastic leukemia with gene expression profiling: correlation with genome-wide DNA copy number alterations, clinical characteristics, and outcome. *Blood* 2010; **116**(23)**:** 4874-4884.

75. Tibshirani R, Hastie T, Narasimhan B, Chu G. Diagnosis of multiple cancer types by shrunken centroids of gene expression. *Proc Natl Acad Sci U S A* 2002; **99**(10)**:** 6567-6572.

76. Chen IM, Harvey RC, Mullighan CG, Gastier-Foster J, Wharton W, Kang H*, et al.* Outcome modeling with CRLF2, IKZF1, JAK, and minimal residual disease in pediatric acute lymphoblastic leukemia: a Children's Oncology Group study. *Blood* 2012; **119**(15)**:** 3512-3522.

77. Iacobucci I, Li Y, Roberts KG, Dobson SM, Kim JC, Payne-Turner D*, et al.* Truncating Erythropoietin Receptor Rearrangements in Acute Lymphoblastic Leukemia. *Cancer Cell* 2016; **29**(2)**:** 186-200.

78. Zhang W, Wang J, Wang Q, Chen G, Zhang J, Chen T*, et al.* Identification of a novel type I cytokine receptor CRL2 preferentially expressed by human dendritic cells and activated monocytes. *Biochem Biophys Res Commun* 2001; **281**(4)**:** 878-883.

79. Shochat C, Tal N, Bandapalli OR, Palmi C, Ganmore I, te Kronnie G*, et al.* Gain-of-function mutations in interleukin-7 receptor-alpha (IL7R) in childhood acute lymphoblastic leukemias. *J Exp Med* 2011; **208**(5)**:** 901-908.

80. van Bodegom D, Zhong J, Kopp N, Dutta C, Kim MS, Bird L*, et al.* Differences in signaling through the B-cell leukemia oncoprotein CRLF2 in response to TSLP and through mutant JAK2. *Blood* 2012; **120**(14)**:** 2853-2863.

81. Russell LJ, Capasso M, Vater I, Akasaka T, Bernard OA, Calasanz MJ*, et al.* Deregulated expression of cytokine receptor gene, CRLF2, is involved in lymphoid transformation in B-cell precursor acute lymphoblastic leukemia. *Blood* 2009; **114**(13)**:** 2688-2698.

82. Harvey RC, Mullighan CG, Chen IM, Wharton W, Mikhail FM, Carroll AJ*, et al.* Rearrangement of CRLF2 is associated with mutation of JAK kinases, alteration of IKZF1, Hispanic/Latino ethnicity, and a poor outcome in pediatric B-progenitor acute lymphoblastic leukemia. *Blood* 2010; **115**(26)**:** 5312-5321.

83. Tasian SK, Doral MY, Borowitz MJ, Wood BL, Chen IM, Harvey RC*, et al.* Aberrant STAT5 and PI3K/mTOR pathway signaling occurs in human CRLF2-rearranged B-precursor acute lymphoblastic leukemia. *Blood* 2012; **120**(4)**:** 833-842.

84. Cario G, Zimmermann M, Romey R, Gesk S, Vater I, Harbott J*, et al.* Presence of the P2RY8-CRLF2 rearrangement is associated with a poor prognosis in non-high-risk precursor B-cell acute lymphoblastic leukemia in children treated according to the ALL-BFM 2000 protocol. *Blood* 2010; **115**(26)**:** 5393-5397.

85. Mullighan CG, Collins-Underwood JR, Phillips LA, Loudin MG, Liu W, Zhang J*, et al.* Rearrangement of CRLF2 in B-progenitor- and Down syndrome-associated acute lymphoblastic leukemia. *Nat Genet* 2009; **41**(11)**:** 1243-1246.

86. Roberts KG, Pei D, Campana D, Payne-Turner D, Li Y, Cheng C*, et al.* Outcomes of children with BCR-ABL1-like acute lymphoblastic leukemia treated with risk-directed therapy based on the levels of minimal residual disease. *J Clin Oncol* 2014; **32**(27)**:** 3012-3020.

87. Kobayashi K, Mitsui K, Ichikawa H, Nakabayashi K, Matsuoka M, Kojima Y*, et al.* ATF7IP as a novel PDGFRB fusion partner in acute lymphoblastic leukaemia in children. *Br J Haematol* 2014; **165**(6)**:** 836-841.

88. Zhou MH, Gao L, Jing Y, Xu YY, Ding Y, Wang N*, et al.* Detection of ETV6 gene rearrangements in adult acute lymphoblastic leukemia. *Ann Hematol* 2012; **91**(8)**:** 1235-1243.

89. Li Y, Payne-Turner D, Harvey RC, Cheng J, Zhang J, Song G*, et al.* Genomic Characterization and Experimental Modeling Of BCR-ABL1-Like Acute Lymphoblastic Leukemia. *American Society of Hematology* 2013; **122**(21).

90. Weston BW, Hayden MA, Roberts KG, Bowyer S, Hsu J, Fedoriw G*, et al.* Tyrosine kinase inhibitor therapy induces remission in a patient with refractory EBF1-PDGFRB-positive acute lymphoblastic leukemia. *J Clin Oncol* 2013; **31**(25)**:** e413-416.

91. Lengline E, Beldjord K, Dombret H, Soulier J, Boissel N, Clappier E. Successful tyrosine kinase inhibitor therapy in a refractory B-cell precursor acute lymphoblastic leukemia with EBF1-PDGFRB fusion. *Haematologica* 2013; **98**(11)**:** e146-148.

92. Yeung DT, Moulton DJ, Heatley SL, Nievergall E, Dang P, Braley J*, et al.* Relapse of BCR-ABL1-like ALL mediated by the ABL1 kinase domain mutation T315I following initial response to dasatinib treatment. *Leukemia* 2015; **29**(1)**:** 230-232.

93. Kralik JM, Kranewitter W, Boesmueller H, Marschon R, Tschurtschenthaler G, Rumpold H*, et al.* Characterization of a newly identified ETV6-NTRK3 fusion transcript in acute myeloid leukemia. *Diagn Pathol* 2011; **6:** 19.

94. Leeman-Neill RJ, Kelly LM, Liu P, Brenner AV, Little MP, Bogdanova TI*, et al.* ETV6-NTRK3 is a common chromosomal rearrangement in radiation-associated thyroid cancer. *Cancer* 2014; **120**(6)**:** 799-807.

95. Li Z, Tognon CE, Godinho FJ, Yasaitis L, Hock H, Herschkowitz JI*, et al.* ETV6-NTRK3 fusion oncogene initiates breast cancer from committed mammary progenitors via activation of AP1 complex. *Cancer Cell* 2007; **12**(6)**:** 542-558.

96. Tognon C, Knezevich SR, Huntsman D, Roskelley CD, Melnyk N, Mathers JA*, et al.* Expression of the *ETV6-NTRK3* gene fusion as a primary event in human secretory breast carcinoma. *Cancer Cell* 2002; **2**(5)**:** 367-376.

97. Del Castillo M, Chibon F, Arnould L, Croce S, Ribeiro A, Perot G*, et al.* Secretory Breast Carcinoma: A Histopathologic and Genomic Spectrum Characterized by a Joint Specific ETV6-NTRK3 Gene Fusion. *Am J Surg Pathol* 2015; **39**(11)**:** 1458-1467.

98. Zebisch A, Czernilofsky AP, Keri G, Smigelskaite J, Sill H, Troppmair J. Signaling through RAS-RAF-MEK-ERK: from basics to bedside. *Current medicinal chemistry* 2007; **14**(5)**:** 601--623.

99. Miranda C, Nucifora M, Molinari F, Conca E, Anania MC, Bordoni A*, et al.* KRAS and BRAF mutations predict primary resistance to imatinib in gastrointestinal stromal tumors. *Clin Cancer Res* 2012; **18**(6)**:** 1769-1776.

100. Sunaga N, Shames DS, Girard L, Peyton M, Larsen JE, Imai H*, et al.* Knockdown of oncogenic KRAS in non-small cell lung cancers suppresses tumor growth and sensitizes tumor cells to targeted therapy. *Mol Cancer Ther* 2011; **10**(2)**:** 336-346.

101. Kwong LN, Costello JC, Liu H, Jiang S, Helms TL, Langsdorf AE*, et al.* Oncogenic NRAS signaling differentially regulates survival and proliferation in melanoma. *Nat Med* 2012; **18**(10)**:** 1503-1510.

102. Drosten M, Dhawahir A, Sum EY, Urosevic J, Lechuga CG, Esteban LM*, et al.* Genetic analysis of Ras signalling pathways in cell proliferation, migration and survival. *EMBO J* 2010; **29**(6)**:** 1091-1104.

103. Zenonos K, Kyprianou K. RAS signaling pathways, mutations and their role in colorectal cancer. *World J Gastrointest Oncol* 2013; **5**(5)**:** 97-101.

104. Brems H, Beert E, de Ravel T, Legius E. Mechanisms in the pathogenesis of malignant tumours in neurofibromatosis type 1. *Lancet Oncol* 2009; **10**(5)**:** 508-515.

105. Madanikia SA, Bergner A, Ye X, Blakeley JO. Increased risk of breast cancer in women with NF1. *Am J Med Genet A* 2012; **158A**(12)**:** 3056-3060.

106. Nissan MH, Pratilas CA, Jones AM, Ramirez R, Won H, Liu C*, et al.* Loss of NF1 in cutaneous melanoma is associated with RAS activation and MEK dependence. *Cancer Res* 2014; **74**(8)**:** 2340-2350.

107. Chan G, Kalaitzidis D, Usenko T, Kutok JL, Yang W, Mohi MG*, et al.* Leukemogenic Ptpn11 causes fatal myeloproliferative disorder via cell-autonomous effects on multiple stages of hematopoiesis. *Blood* 2009; **113**(18)**:** 4414-4424.

108. Tartaglia M, Niemeyer CM, Fragale A, Song X, Buechner J, Jung A*, et al.* Somatic mutations in PTPN11 in juvenile myelomonocytic leukemia, myelodysplastic syndromes and acute myeloid leukemia. *Nat Genet* 2003; **34**(2)**:** 148-150.

109. Yamamoto T, Isomura M, Xu Y, Liang J, Yagasaki H, Kamachi Y*, et al.* PTPN11, RAS and FLT3 mutations in childhood acute lymphoblastic leukemia. *Leuk Res* 2006; **30**(9)**:** 1085-1089.

110. Borthakur G, Popplewell L, Boyiadzis M, Foran JM, Platzbecker U, Vey N*, et al.* Phase I/II Trial of the MEK1/2 Inhibitor Trametinib (GSK1120212) in Relapsed/Refractory Myeloid Malignancies: Evidence of Activity in Patients with RAS Mutation-Positive Disease. *Blood* 2012; **120:** 677-677.

111. Irving J, Matheson E, Minto L, Blair H, Case M, Halsey C*, et al.* Ras pathway mutations are prevalent in relapsed childhood acute lymphoblastic leukemia and confer sensitivity to MEK inhibition. *Blood* 2014; **124**(23)**:** 3420-3430.

112. Gokbuget N, Hoelzer D. Treatment of adult acute lymphoblastic leukemia. *Semin Hematol* 2009; **46**(1)**:** 64-75.

113. Inaba H, Greaves M, Mullighan CG. Acute lymphoblastic leukaemia. *Lancet* 2013; **381**(9881)**:** 1943-1955.

114. Stanulla M, Schrappe M. Treatment of childhood acute lymphoblastic leukemia. *Semin Hematol* 2009; **46**(1)**:** 52-63.

115. Visentin M, Zhao R, Goldman ID. The antifolates. *Hematol Oncol Clin North Am* 2012; **26**(3)**:** 629-648, ix.

116. Pui CH, Evans WE. Treatment of acute lymphoblastic leukemia. *N Engl J Med* 2006; **354**(2)**:** 166-178.

117. Fotoohi AK, Albertioni F. Mechanisms of antifolate resistance and methotrexate efficacy in leukemia cells. *Leuk Lymphoma* 2008; **49**(3)**:** 410-426.

118. Pui C-H, Howard SC. Current management and challenges of malignant disease in the CNS in paediatric leukaemia. *The Lancet Oncology* 2008; **9**(3)**:** 257-268.

119. Narta UK, Kanwar SS, Azmi W. Pharmacological and clinical evaluation of L-asparaginase in the treatment of leukemia. *Crit Rev Oncol Hematol* 2007; **61**(3)**:** 208-221.

120. Redaelli A, Laskin BL, Stephens JM, Botteman MF, Pashos CL. A systematic literature review of the clinical and epidemiological burden of acute lymphoblastic leukaemia (ALL). *Eur J Cancer Care (Engl)* 2005; **14**(1)**:** 53-62.

121. Brignardello E, Felicetti F, Castiglione A, Chiabotto P, Corrias A, Fagioli F*, et al.* Endocrine health conditions in adult survivors of childhood cancer: the need for specialized adult-focused follow-up clinics. *Eur J Endocrinol* 2013; **168**(3)**:** 465-472.

122. Steffens M, Beauloye V, Brichard B, Robert A, Alexopoulou O, Vermylen C*, et al.* Endocrine and metabolic disorders in young adult survivors of childhood acute lymphoblastic leukaemia (ALL) or non-Hodgkin lymphoma (NHL). *Clin Endocrinol (Oxf)* 2008; **69**(5)**:** 819-827.

123. Deininger M, Buchdunger E, Druker BJ. The development of imatinib as a therapeutic agent for chronic myeloid leukemia. *Blood* 2005; **105**(7)**:** 2640-2653.

124. O'Hare T, Corbin AS, Druker BJ. Targeted CML therapy: controlling drug resistance, seeking cure. *Curr Opin Genet Dev* 2006; **16**(1)**:** 92-99.

125. Hari SB, Merritt EA, Maly DJ. Sequence determinants of a specific inactive protein kinase conformation. *Chem Biol* 2013; **20**(6)**:** 806-815.

126. Quintas-Cardama A, Kantarjian H, Cortes J. Imatinib and beyond--exploring the full potential of targeted therapy for CML. *Nat Rev Clin Oncol* 2009; **6**(9)**:** 535-543.

127. Drake JM, Lee JK, Witte ON. Clinical targeting of mutated and wild-type protein tyrosine kinases in cancer. *Mol Cell Biol* 2014; **34**(10)**:** 1722-1732.

128. Leoni V, Biondi A. Tyrosine kinase inhibitors in BCR-ABL positive acute lymphoblastic leukemia. *Haematologica* 2015; **100**(3)**:** 295-299.

129. Piccaluga PP, Paolini S, Martinelli G. Tyrosine kinase inhibitors for the treatment of Philadelphia chromosome-positive adult acute lymphoblastic leukemia. *Cancer* 2007; **110**(6)**:** 1178-1186.

130. Law V, Knox C, Djoumbou Y, Jewison T, Guo AC, Liu Y*, et al.* DrugBank 4.0: shedding new light on drug metabolism. *Nucleic Acids Res* 2014; **42**(Database issue)**:** D1091-1097.

131. Azvolinsky A, Jacobson A. Current and Future Options for Targeting Activated Kinases in Acute and Chronic Leukemias. In: Oncologist T, editor. Conference Perspectives: Highlights from 2013 ASCO Annual Meeting; 2013.

132. Mascarenhas J, Hoffman R. Ruxolitinib: the first FDA approved therapy for the treatment of myelofibrosis. *Clin Cancer Res* 2012; **18**(11)**:** 3008-3014.

133. Harrison C, Vannucchi AM. Ruxolitinib: a potent and selective Janus kinase 1 and 2 inhibitor in patients with myelofibrosis. An update for clinicians. *Ther Adv Hematol* 2012; **3**(6)**:** 341-354.

134. Wang Y, Xia J, Wu X, Hu Y. A Patient With BCR-ABL and JAK2 V617F Double-Positive Myeloproliferative Neoplasm With Overlapping Clinical Phenotypes. *Am J Med Sci* 2015; **350**(1)**:** 68-69.

135. Mamorska-Dyga A, Wu J, Khattar P, Ronny FM, Islam H, Seiter K*, et al.* Acute promyelocytic leukemia co-existing with JAK2 V617F positive myeloproliferative neoplasm: a case report. *Stem Cell Investig* 2016; **3:** 8.

136. Malysz J, Crisan D. Correlation of JAK2 V617F mutant allele quantitation with clinical presentation and type of chronic myeloproliferative neoplasm. *Ann Clin Lab Sci* 2009; **39**(4)**:** 345-350.

137. McLornan D, Percy M, McMullin MF. JAK2 V617F: a single mutation in the myeloproliferative group of disorders. *Ulster Med J* 2006; **75**(2)**:** 112-119.

138. Vaddi K, Sarlis NJ, Gupta V. Ruxolitinib, an oral JAK1 and JAK2 inhibitor, in myelofibrosis. *Expert Opin Pharmacother* 2012; **13**(16)**:** 2397-2407.

139. Mesa RA. Ruxolitinib, a selective JAK1 and JAK2 inhibitor for the treatment of myeloproliferative neoplasms and psoriasis. *IDrugs* 2010; **13**(6)**:** 394-403.

140. Luque Paz D, Ianotto JC, Chauveau A, Guibourg B, Lecucq L, Lippert E*, et al.* Expansion of a BCR-ABL clone in a JAK2 V617F myeloproliferative neoplasm treated by ruxolitinib. *Ann Hematol* 2016; **95**(2)**:** 349-350.

141. Furumoto Y, Gadina M. The arrival of JAK inhibitors: advancing the treatment of immune and hematologic disorders. *BioDrugs* 2013; **27**(5)**:** 431-438.

142. Naqvi K, Verstovsek S, Kantarjian H, Ravandi F. A potential role of ruxolitinib in leukemia. *Expert Opin Investig Drugs* 2011; **20**(8)**:** 1159-1166.

143. Maude SL, Dolai S, Delgado-Martin C, Vincent T, Robbins A, Selvanathan A*, et al.* Efficacy of JAK/STAT pathway inhibition in murine xenograft models of early T-cell precursor (ETP) acute lymphoblastic leukemia. *Blood* 2015; **125**(11)**:** 1759-1767.

144. Duan Y, Chen L, Chen Y, Fan XG. c-Src binds to the cancer drug Ruxolitinib with an active conformation. *PLoS One* 2014; **9**(9)**:** e106225.

145. Degryse S, Cools J. JAK kinase inhibitors for the treatment of acute lymphoblastic leukemia. *J Hematol Oncol* 2015; **8:** 91.

146. COG. A Phase 2 Study of Ruxolitinib With Chemotherapy in Children With Acute Lymphoblastic Leukemia. https://ClinicalTrials.gov/show/NCT02723994; 2017.

147. NCI. Blinatumomab and Combination Chemotherapy or Dasatinib, Prednisone, and Blinatumomab in Treating Older Patients With Acute Lymphoblastic Leukemia. https://ClinicalTrials.gov/show/NCT02143414; 2014.

148. MDACC. Ruxolitinib or Dasatinib With Chemotherapy in Patients With Philadelphia Chromosome (Ph)-Like Acute Lymphoblastic Leukemia (ALL). https://ClinicalTrials.gov/show/NCT02420717; 2015.

149. NCI. Combination Chemotherapy in Treating Young Patients With Newly Diagnosed High-Risk B Acute Lymphoblastic Leukemia and Ph-Like TKI Sensitive Mutations. https://ClinicalTrials.gov/show/NCT02883049; 2016.

150. Kobayashi K, Miyagawa N, Mitsui K, Matsuoka M, Kojima Y, Takahashi H*, et al.* TKI dasatinib monotherapy for a patient with Ph-like ALL bearing ATF7IP/PDGFRB translocation. *Pediatr Blood Cancer* 2015; **62**(6)**:** 1058-1060.

151. Hunger SP. Tyrosine kinase inhibitor use in pediatric Philadelphia chromosome-positive acute lymphoblastic anemia. *Hematology Am Soc Hematol Educ Program* 2011; **2011:** 361-365.

152. Xing H, Yang X, Liu T, Lin J, Chen X, Gong Y. The study of resistant mechanisms and reversal in an imatinib resistant Ph+ acute lymphoblastic leukemia cell line. *Leuk Res* 2012; **36**(4)**:** 509-513.

153. Quintas-Cardama A, Kantarjian HM, Cortes JE. Mechanisms of primary and secondary resistance to imatinib in chronic myeloid leukemia. *Cancer Control* 2009; **16**(2)**:** 122-131.

154. Zhang WW, Cortes JE, Yao H, Zhang L, Reddy NG, Jabbour E*, et al.* Predictors of primary imatinib resistance in chronic myelogenous leukemia are distinct from those in secondary imatinib resistance. *J Clin Oncol* 2009; **27**(22)**:** 3642-3649.

155. Soverini S, De Benedittis C, Papayannidis C, Paolini S, Venturi C, Iacobucci I*, et al.* Drug resistance and BCR-ABL kinase domain mutations in Philadelphia chromosome-positive acute lymphoblastic leukemia from the imatinib to the second-generation tyrosine kinase inhibitor era: The main changes are in the type of mutations, but not in the frequency of mutation involvement. *Cancer* 2014; **120**(7)**:** 1002-1009.

156. Jones D, Thomas D, Yin CC, O'Brien S, Cortes JE, Jabbour E*, et al.* Kinase domain point mutations in Philadelphia chromosome-positive acute lymphoblastic leukemia emerge after therapy with BCR-ABL kinase inhibitors. *Cancer* 2008; **113**(5)**:** 985-994.

157. Bhamidipati PK, Kantarjian H, Cortes J, Cornelison AM, Jabbour E. Management of imatinib-resistant patients with chronic myeloid leukemia. *Ther Adv Hematol* 2013; **4**(2)**:** 103-117.

158. Bixby D, Talpaz M. Mechanisms of resistance to tyrosine kinase inhibitors in chronic myeloid leukemia and recent therapeutic strategies to overcome resistance. *Hematology Am Soc Hematol Educ Program* 2009**:** 461-476.

159. Cang S, Liu D. P-loop mutations and novel therapeutic approaches for imatinib failures in chronic myeloid leukemia. *J Hematol Oncol* 2008; **1:** 15.

160. Baran Y, Ural AU, Gunduz U. Mechanisms of cellular resistance to imatinib in human chronic myeloid leukemia cells. *Hematology* 2007; **12**(6)**:** 497-503.

161. Milojkovic D, Apperley J. Mechanisms of Resistance to Imatinib and Second-Generation Tyrosine Inhibitors in Chronic Myeloid Leukemia. *Clin Cancer Res* 2009; **15**(24)**:** 7519-7527.

162. Thomas J, Wang L, Clark RE, Pirmohamed M. Active transport of imatinib into and out of cells: implications for drug resistance. *Blood* 2004; **104**(12)**:** 3739-3745.

163. White DL, Radich J, Soverini S, Saunders VA, Frede AK, Dang P*, et al.* Chronic phase chronic myeloid leukemia patients with low OCT-1 activity randomized to high-dose imatinib achieve better responses and have lower failure rates than those randomized to standard-dose imatinib. *Haematologica* 2012; **97**(6)**:** 907-914.

164. Bitencourt R, Zalcberg I, Louro ID. Imatinib resistance: a review of alternative inhibitors in chronic myeloid leukemia. *Rev Bras Hematol Hemoter* 2011; **33**(6)**:** 470-475.

165. Soverini S, Vitale A, Poerio A, Gnani A, Colarossi S, Iacobucci I*, et al.* Philadelphia-positive acute lymphoblastic leukemia patients already harbor BCR-ABL kinase domain mutations at low levels at the time of diagnosis. *Haematologica* 2011; **96**(4)**:** 552-557.

166. Weisberg E, Manley PW, Cowan-Jacob SW, Hochhaus A, Griffin JD. Second generation inhibitors of BCR-ABL for the treatment of imatinib-resistant chronic myeloid leukaemia. *Nat Rev Cancer* 2007; **7**(5)**:** 345-356.

167. O'Hare T, Walters DK, Stoffregen EP, Jia T, Manley PW, Mestan J*, et al.* In vitro activity of Bcr-Abl inhibitors AMN107 and BMS-354825 against clinically relevant imatinib-resistant Abl kinase domain mutants. *Cancer Res* 2005; **65**(11)**:** 4500-4505.

168. Aleksandrov A, Simonson T. A molecular mechanics model for imatinib and imatinib:kinase binding. *J Comput Chem* 2010; **31**(7)**:** 1550-1560.

169. Weisberg E, Manley PW, Breitenstein W, Bruggen J, Cowan-Jacob SW, Ray A*, et al.* Characterization of AMN107, a selective inhibitor of native and mutant Bcr-Abl. *Cancer Cell* 2005; **7**(2)**:** 129-141.

170. Hughes T, Saglio G, Branford S, Soverini S, Kim DW, Muller MC*, et al.* Impact of baseline BCR-ABL mutations on response to nilotinib in patients with chronic myeloid leukemia in chronic phase. *J Clin Oncol* 2009; **27**(25)**:** 4204-4210.

171. Das J, Chen P, Norris D, Padmanabha R, Lin J, Moquin RV*, et al.* 2-aminothiazole as a novel kinase inhibitor template. Structure-activity relationship studies toward the discovery of N-(2-chloro-6-methylphenyl)-2-[[6-[4-(2-hydroxyethyl)-1-piperazinyl)]-2-methyl-4-pyrimidinyl]amino)]-1,3-thiazole-5-carboxamide (dasatinib, BMS-354825) as a potent pan-Src kinase inhibitor. *J Med Chem* 2006; **49**(23)**:** 6819-6832.

172. Tokarski JS, Newitt JA, Chang CY, Cheng JD, Wittekind M, Kiefer SE*, et al.* The structure of Dasatinib (BMS-354825) bound to activated ABL kinase domain elucidates its inhibitory activity against imatinib-resistant ABL mutants. *Cancer Res* 2006; **66**(11)**:** 5790-5797.

173. Laurini E, Posocco P, Fermeglia M, Gibbons DL, Quintas-Cardama A, Pricl S. Through the open door: Preferential binding of dasatinib to the active form of BCR-ABL unveiled by in silico experiments. *Mol Oncol* 2013; **7**(5)**:** 968-975.

174. Gibbons DL, Pricl S, Kantarjian H, Cortes J, Quintas-Cardama A. The rise and fall of gatekeeper mutations? The BCR-ABL1 T315I paradigm. *Cancer* 2012; **118**(2)**:** 293-299.

175. Jabbour E, Kantarjian H, Jones D, Breeden M, Garcia-Manero G, O'Brien S*, et al.* Characteristics and outcomes of patients with chronic myeloid leukemia and T315I mutation following failure of imatinib mesylate therapy. *Blood* 2008; **112**(1)**:** 53-55.

176. Soverini S, Colarossi S, Gnani A, Rosti G, Castagnetti F, Poerio A*, et al.* Contribution of ABL kinase domain mutations to imatinib resistance in different subsets of Philadelphia-positive patients: by the GIMEMA Working Party on Chronic Myeloid Leukemia. *Clin Cancer Res* 2006; **12**(24)**:** 7374-7379.

177. Modugno M, Casale E, Soncini C, Rosettani P, Colombo R, Lupi R*, et al.* Crystal structure of the T315I Abl mutant in complex with the aurora kinases inhibitor PHA-739358. *Cancer Res* 2007; **67**(17)**:** 7987-7990.

178. Pricl S, Fermeglia M, Ferrone M, Tamborini E. T315I-mutated Bcr-Abl in chronic myeloid leukemia and imatinib: insights from a computational study. *Mol Cancer Ther* 2005; **4**(8)**:** 1167-1174.

179. Chan WW, Wise SC, Kaufman MD, Ahn YM, Ensinger CL, Haack T*, et al.* Conformational control inhibition of the BCR-ABL1 tyrosine kinase, including the gatekeeper T315I mutant, by the switch-control inhibitor DCC-2036. *Cancer Cell* 2011; **19**(4)**:** 556-568.

180. Jabbour E, Kantarjian H. Chronic myeloid leukemia: 2014 update on diagnosis, monitoring, and management. *Am J Hematol* 2014; **89**(5)**:** 547-556.

181. Cortes JE, Kantarjian H, Shah NP, Bixby D, Mauro MJ, Flinn I*, et al.* Ponatinib in refractory Philadelphia chromosome-positive leukemias. *N Engl J Med* 2012; **367**(22)**:** 2075-2088.

182. Sanford DS, Kantarjian H, O'Brien S, Jabbour E, Cortes J, Ravandi F. The role of ponatinib in Philadelphia chromosome-positive acute lymphoblastic leukemia. *Expert Rev Anticancer Ther* 2015; **15**(4)**:** 365-373.

183. Zhou T, Commodore L, Huang WS, Wang Y, Thomas M, Keats J*, et al.* Structural mechanism of the Pan-BCR-ABL inhibitor ponatinib (AP24534): lessons for overcoming kinase inhibitor resistance. *Chem Biol Drug Des* 2011; **77**(1)**:** 1-11.

184. Soverini S, Hochhaus A, Nicolini FE, Gruber F, Lange T, Saglio G*, et al.* BCR-ABL kinase domain mutation analysis in chronic myeloid leukemia patients treated with tyrosine kinase inhibitors: recommendations from an expert panel on behalf of European LeukemiaNet. *Blood* 2011; **118**(5)**:** 1208-1215.

185. Lu L, Saunders VA, Leclercq TM, Hughes TP, White DL. Ponatinib is not transported by ABCB1, ABCG2 or OCT-1 in CML cells. *Leukemia* 2015; **29**(8)**:** 1792-1794.

186. Zabriskie MS, Eide CA, Tantravahi SK, Vellore NA, Estrada J, Nicolini FE*, et al.* BCR-ABL1 compound mutations combining key kinase domain positions confer clinical resistance to ponatinib in Ph chromosome-positive leukemia. *Cancer Cell* 2014; **26**(3)**:** 428-442.

187. Volpe G, Panuzzo C, Ulisciani S, Cilloni D. Imatinib resistance in CML. *Cancer Lett* 2009; **274**(1)**:** 1-9.

188. Hochhaus A. Chronic myelogenous leukemia (CML): resistance to tyrosine kinase inhibitors. *Ann Oncol* 2006; **17 Suppl 10**(Supplement 10)**:** x274-279.

189. Gruber F, Mustjoki S, Porkka K. Impact of tyrosine kinase inhibitors on patient outcomes in Philadelphia chromosome-positive acute lymphoblastic leukaemia. *Br J Haematol* 2009; **145**(5)**:** 581-597.

190. Thomas DA, Faderl S, Cortes J, O'Brien S, Giles FJ, Kornblau SM*, et al.* Treatment of Philadelphia chromosome-positive acute lymphocytic leukemia with hyper-CVAD and imatinib mesylate. *Blood* 2004; **103**(12)**:** 4396-4407.

191. Thomas DA, Kantarjian HM, Cortes JE, Ravandi F, Faderl S, Jones D*, et al.* Outcome after frontline therapy with the hyper-CVAD and imatinib mesylate regimen for adults with de novo or minimally treated Philadelphia (Ph) positive acute lymphoblastic leukemia (ALL). *Journal of Clinical Oncology (ASCO Annual Meeting Proceedings)* 2008; **26**(7019).

192. Yanada M, Takeuchi J, Sugiura I, Akiyama H, Usui N, Yagasaki F*, et al.* High complete remission rate and promising outcome by combination of imatinib and chemotherapy for newly diagnosed BCR-ABL-positive acute lymphoblastic leukemia: a phase II study by the Japan Adult Leukemia Study Group. *J Clin Oncol* 2006; **24**(3)**:** 460-466.

193. Yanada M, Takeuchi J, Sugiura I, Akiyama H, Usui N, Yagasaki F*, et al.* Karyotype at diagnosis is the major prognostic factor predicting relapse-free survival for patients with Philadelphia chromosome-positive acute lymphoblastic leukemia treated with imatinib-combined chemotherapy. *Haematologica* 2008; **93**(2)**:** 287-290.

194. Foa R, Vitale A, Guarini A, De Propris A, Elia R, Cimino G*, et al.* Dasatinib monotherapy effective and feasible as first-line treatment of adult Philadelphia-chromosome positive acute lymphoblastic leukemia: final results of the GIMEMA LAL1205 study. *Blood* 2008; **112:** 119a.

195. Ravandi F, O'Brien S, Thomas D, Faderl S, Jones D, Garris R*, et al.* First report of phase 2 study of dasatinib with hyper-CVAD for the frontline treatment of patients with Philadelphia chromosome-positive (Ph+) acute lymphoblastic leukemia. *Blood* 2010; **116**(12)**:** 2070-2077.

196. Talpaz M, Shah NP, Kantarjian H, Donato N, Nicoll J, Paquette R*, et al.* Dasatinib in imatinib-resistant Philadelphia chromosome-positive leukemias. *N Engl J Med* 2006; **354**(24)**:** 2531-2541.

197. Ottmann O, Dombret H, Martinelli G, Simonsson B, Guilhot F, Larson RA*, et al.* Dasatinib induces rapid hematologic and cytogenetic responses in adult patients with Philadelphia chromosome positive acute lymphoblastic leukemia with resistance or intolerance to imatinib: interim results of a phase 2 study. *Blood* 2007; **110**(7)**:** 2309-2315.

198. Porkka K, Koskenvesa P, Lundan T, Rimpilainen J, Mustjoki S, Smykla R*, et al.* Dasatinib crosses the blood-brain barrier and is an efficient therapy for central nervous system Philadelphia chromosome-positive leukemia. *Blood* 2008; **112**(4)**:** 1005-1012.

199. Giles FJ, Kantarjian HM, le Coutre PD, Baccarani M, Mahon FX, Blakesley RE*, et al.* Nilotinib is effective in imatinib-resistant or -intolerant patients with chronic myeloid leukemia in blastic phase. *Leukemia* 2012; **26**(5)**:** 959-962.

200. Deshpande A, Reddy MM, Schade GO, Ray A, Chowdary TK, Griffin JD*, et al.* Kinase domain mutations confer resistance to novel inhibitors targeting JAK2V617F in myeloproliferative neoplasms. *Leukemia* 2012; **26**(4)**:** 708-715.

201. Weigert O, Lane AA, Bird L, Kopp N, Chapuy B, van Bodegom D*, et al.* Genetic resistance to JAK2 enzymatic inhibitors is overcome by HSP90 inhibition. *J Exp Med* 2012; **209**(2)**:** 259-273.

202. Hornakova T, Springuel L, Devreux J, Dusa A, Constantinescu SN, Knoops L*, et al.* Oncogenic JAK1 and JAK2-activating mutations resistant to ATP-competitive inhibitors. *Haematologica* 2011; **96**(6)**:** 845-853.

203. Koppikar P, Bhagwat N, Kilpivaara O, Manshouri T, Adli M, Hricik T*, et al.* Heterodimeric JAK-STAT activation as a mechanism of persistence to JAK2 inhibitor therapy. *Nature* 2012; **489**(7414)**:** 155-159.

204. Maude SL, Tasian SK, Vincent T, Hall JW, Sheen C, Roberts KG*, et al.* Targeting JAK1/2 and mTOR in murine xenograft models of Ph-like acute lymphoblastic leukemia. *Blood* 2012; **120**(17)**:** 3510-3518.

205. Roberts KG, Yang Y-L, Payne-Turner D, Lin W, Files JK, Dickerson K*, et al.* Oncogenic role and therapeutic targeting of ABL-class and JAK-STAT activating kinase alterations in Ph-like ALL. *Blood Advances* 2017; **1**(20)**:** 1657-1671.

206. Schafranek L, Nievergall E, Powell JA, Hiwase DK, Leclercq T, Hughes TP*, et al.* Sustained inhibition of STAT5, but not JAK2, is essential for TKI-induced cell death in chronic myeloid leukemia. *Leukemia* 2015; **29**(1)**:** 76-85.

207. White D, Saunders V, Lyons AB, Branford S, Grigg A, To LB*, et al.* In vitro sensitivity to imatinib-induced inhibition of ABL kinase activity is predictive of molecular response in patients with de novo CML. *Blood* 2005; **106**(7)**:** 2520-2526.

208. Noll JE, Hewett DR, Williams SA, Vandyke K, Kok C, To LB*, et al.* SAMSN1 is a tumor suppressor gene in multiple myeloma. *Neoplasia* 2014; **16**(7)**:** 572-585.

209. Fitter S, Gronthos S, Ooi SS, Zannettino AC. The Mesenchymal Precursor Cell Marker Antibody STRO-1 Binds to Cell Surface Heat Shock Cognate 70. *Stem Cells* 2017; **35**(4)**:** 940-951.

210. Feliciello I, Chinali G. A modified alkaline lysis method for the preparation of highly purified plasmid DNA from Escherichia coli. *Anal Biochem* 1993; **212**(2)**:** 394-401.

211. Tang C, Schafranek L, Watkins DB, Parker WT, Moore S, Prime JA*, et al.* Tyrosine kinase inhibitor resistance in chronic myeloid leukemia cell lines: investigating resistance pathways. *Leuk Lymphoma* 2011; **52**(11)**:** 2139-2147.

212. Coutre PI, Tassi E, Varella-Garcia M, Barni R, Mologni L, Cabrita G*, et al.* Induction of resistance to the Abelson inhibitor STI571 in human leukemic cells through gene amplification. *Blood* 2000; **95**(5)**:** 1758-1766.

213. Gromicho M, Rueff J, Rodrigues AS. Dynamics of Expression of Drug Transporters: Methods for Appraisal. *Methods Mol Biol* 2016; **1395:** 75-85.

214. Head SR, Komori HK, LaMere SA, Whisenant T, Van Nieuwerburgh F, Salomon DR*, et al.* Library construction for next-generation sequencing: overviews and challenges. *Biotechniques* 2014; **56**(2)**:** 61-64, 66, 68, passim.

215. van Dijk EL, Jaszczyszyn Y, Thermes C. Library preparation methods for next-generation sequencing: tone down the bias. *Exp Cell Res* 2014; **322**(1)**:** 12-20.

216. Roberts A, Trapnell C, Donaghey J, Rinn JL, Pachter L. Improving RNA-Seq expression estimates by correcting for fragment bias. *Genome Biol* 2011; **12**(3)**:** R22.

217. Ginzinger DG. Gene quantification using real-time quantitative PCR. *Experimental Hematology* 2002; **30**(6)**:** 503-512.

218. Law CW, Chen Y, Shi W, Smyth GK. voom: Precision weights unlock linear model analysis tools for RNA-seq read counts. *Genome Biol* 2014; **15**(2)**:** R29.

219. Law CW, Alhamdoosh M, Su S, Smyth GK, Ritchie ME. RNA-seq analysis is easy as 1-2-3 with limma, Glimma and edgeR. *F1000Research* 2016; **5:** 1408.

220. Thissen D, Steinberg L, Kuang D. Quick and Easy Implementation of the Benjamini-Hochberg Procedure for Controlling the False Positive Rate in Multiple Comparisons. *Journal of Educational and Behavioral Statistics* 2002; **27**(1)**:** 77-83.

221. Li B, Dewey CN. RSEM: accurate transcript quantification from RNA-Seq data with or without a reference genome. *BMC Bioinformatics* 2011; **12**(1)**:** 323.

222. Robinson MD, McCarthy DJ, Smyth GK. edgeR: a Bioconductor package for differential expression analysis of digital gene expression data. *Bioinformatics* 2010; **26**(1)**:** 139-140.

223. Breuer K, Foroushani AK, Laird MR, Chen C, Sribnaia A, Lo R*, et al.* InnateDB: systems biology of innate immunity and beyond--recent updates and continuing curation. *Nucleic Acids Res* 2013; **41**(Database issue)**:** D1228-1233.

224. Lynn DJ, Chan C, Naseer M, Yau M, Lo R, Sribnaia A*, et al.* Curating the innate immunity interactome. *BMC Syst Biol* 2010; **4**(1)**:** 117.

225. Shannon P, Markiel A, Ozier O, Baliga NS, Wang JT, Ramage D*, et al.* Cytoscape: a software environment for integrated models of biomolecular interaction networks. *Genome Res* 2003; **13**(11)**:** 2498-2504.

226. Cline MS, Smoot M, Cerami E, Kuchinsky A, Landys N, Workman C*, et al.* Integration of biological networks and gene expression data using Cytoscape. *Nat Protoc* 2007; **2**(10)**:** 2366-2382.

227. Muetze T, Goenawan IH, Wiencko HL, Bernal-Llinares M, Bryan K, Lynn DJ. Contextual Hub Analysis Tool (CHAT): A Cytoscape app for identifying contextually relevant hubs in biological networks. *F1000Res* 2016; **5:** 1745.

228. Terwilliger T, Abdul-Hay M. Acute lymphoblastic leukemia: a comprehensive review and 2017 update. *Blood Cancer J* 2017; **7**(6)**:** e577.

229. Chasseriau J, Rivet J, Bilan F, Chomel JC, Guilhot F, Bourmeyster N*, et al.* Characterization of the different BCR-ABL transcripts with a single multiplex RT-PCR. *J Mol Diagn* 2004; **6**(4)**:** 343-347.

230. Ribera JM, Oriol A, Gonzalez M, Vidriales B, Brunet S, Esteve J*, et al.* Concurrent intensive chemotherapy and imatinib before and after stem cell transplantation in newly diagnosed Philadelphia chromosome-positive acute lymphoblastic leukemia. Final results of the CSTIBES02 trial. *Haematologica* 2010; **95**(1)**:** 87-95.

231. Fielding AK, Rowe JM, Richards SM, Buck G, Moorman AV, Durrant IJ*, et al.* Prospective outcome data on 267 unselected adult patients with Philadelphia chromosome–positive acute lymphoblastic leukemia confirms superiority of allogeneic transplantation over chemotherapy in the pre-imatinib era: results from the International ALL Trial MRC UKALLXII/ECOG2993. *Blood* 2009; **113:** 4489-4496.

232. Bassan R, Hoelzer D. Modern Therapy of Acute Lymphoblastic Leukemia. *Journal of Clinical Oncology* 2011; **29**(5)**:** 532-543.

233. Goldstone AH, Richards SM, Lazarus HM, Tallman MS, Buck G, Fielding AK*, et al.* In adults with standard-risk acute lymphoblastic leukemia, the greatest benefit is achieved from a matched sibling allogeneic transplantation in first complete remission, and an autologous transplantation is less effective than conventional consolidation/maintenance chemotherapy in all patients: final results of the International ALL Trial (MRC UKALL XII/ECOG E2993). *Blood* 2008; **111**(4)**:** 1827-1833.

234. Mohty B, Mohty M. Long-term complications and side effects after allogeneic hematopoietic stem cell transplantation: an update. *Blood Cancer Journal* 2011; **1**(4)**:** e16.

235. Foa R, Vitale A, Vignetti M, Meloni G, Guarini A, De Propris MS*, et al.* Dasatinib as first-line treatment for adult patients with Philadelphia chromosome-positive acute lymphoblastic leukemia. *Blood* 2011; **118**(25)**:** 6521-6528.

236. Wassmann B, Pfeifer H, Scheuring UJ, Binckebanck A, Gokbuget N, Atta J*, et al.* Early prediction of response in patients with relapsed or refractory Philadelphia chromosome-positive acute lymphoblastic leukemia (Ph+ALL) treated with imatinib. *Blood* 2004; **103**(4)**:** 1495-1498.

237. Schultz KR, Bowman WP, Aledo A, Slayton WB, Sather H, Devidas M*, et al.* Improved early event-free survival with imatinib in Philadelphia chromosome-positive acute lymphoblastic leukemia: a children's oncology group study. *J Clin Oncol* 2009; **27**(31)**:** 5175-5181.

238. Focosi D, Simionato F, Carbone C, Tortora G, Melisi D. Resistance to Tyrosine Kinase Inhibitors. 2016.

239. Chang BH, Willis SG, Stork L, Hunger SP, Carroll WL, Camitta BM*, et al.* Imatinib resistant BCR-ABL1 mutations at relapse in children with Ph+ALL: a Children's Oncology Group (COG) study. *British Journal of Haematology* 2012; **157**(4)**:** 507-510.

240. Aoe M, Shimada A, Muraoka M, Washio K, Nakamura Y, Takahashi T*, et al.* ABL kinase mutation and relapse in 4 pediatric Philadelphia chromosome-positive acute lymphoblastic leukemia cases. *Int J Hematol* 2014; **99**(5)**:** 609-615.

241. Burger H, van Tol H, Boersma AW, Brok M, Wiemer EA, Stoter G*, et al.* Imatinib mesylate (STI571) is a substrate for the breast cancer resistance protein (BCRP)/ABCG2 drug pump. *Blood* 2004; **104**(9)**:** 2940-2942.

242. Eadie LN, Hughes TP, White DL. ABCB1 Overexpression Is a Key Initiator of Resistance to Tyrosine Kinase Inhibitors in CML Cell Lines. *PLoS One* 2016; **11**(8)**:** e0161470.

243. Ma L, Shan Y, Bai R, Xue L, Eide CA, Ou J*, et al.* A therapeutically targetable mechanism of BCR-ABL-independent imatinib resistance in chronic myeloid leukemia. *Sci Transl Med* 2014; **6**(252)**:** 252ra121.

244. Waanders E, Scheijen B, van der Meer LT, van Reijmersdal SV, van Emst L, Kroeze Y*, et al.* The Origin and Nature of Tightly Clustered BTG1 Deletions in Precursor B-Cell Acute Lymphoblastic Leukemia Support a Model of Multiclonal Evolution. *PLOS Genetics* 2012; **8**(2)**:** e1002533.

245. Thorvaldsdottir H, Robinson JT, Mesirov JP. Integrative Genomics Viewer (IGV): high-performance genomics data visualization and exploration. *Brief Bioinform* 2013; **14**(2)**:** 178-192.

246. Robinson JT, Thorvaldsdottir H, Winckler W, Guttman M, Lander ES, Getz G*, et al.* Integrative genomics viewer. *Nat Biotechnol* 2011; **29**(1)**:** 24-26.

247. RStudio-Team. RStudio: Integrated Development for R. 1.0.143 ed. RStudio, Inc., Boston, MA; 2016.

248. Minton JA, Flanagan SE, Ellard S. Mutation surveyor: software for DNA sequence analysis. *Methods Mol Biol* 2011; **688:** 143-153.

249. O'Hare T, Shakespeare WC, Zhu X, Eide CA, Rivera VM, Wang F*, et al.* AP24534, a pan-BCR-ABL inhibitor for chronic myeloid leukemia, potently inhibits the T315I mutant and overcomes mutation-based resistance. *Cancer Cell* 2009; **16**(5)**:** 401-412.

250. Shah NP, Kasap C, Weier C, Balbas M, Nicoll JM, Bleickardt E*, et al.* Transient potent BCR-ABL inhibition is sufficient to commit chronic myeloid leukemia cells irreversibly to apoptosis. *Cancer Cell* 2008; **14**(6)**:** 485-493.

251. Janes MR, Limon JJ, So L, Chen J, Lim RJ, Chavez MA*, et al.* Effective and selective targeting of leukemia cells using a TORC1/2 kinase inhibitor. *Nat Med* 2010; **16**(2)**:** 205-213.

252. O'Toole SA, Sheppard BL, McGuinness EP, Gleeson NC, Yoneda M, Bonnar J. The MTS assay as an indicator of chemosensitivity/resistance in malignant gynaecological tumours. *Cancer Detect Prev* 2003; **27**(1)**:** 47-54.

253. Quentmeier H, Eberth S, Romani J, Zaborski M, Drexler HG. BCR-ABL1-independent PI3Kinase activation causing imatinib-resistance. *J Hematol Oncol* 2011; **4:** 6.

254. van Meerloo J, Kaspers GJ, Cloos J. Cell sensitivity assays: the MTT assay. *Methods Mol Biol* 2011; **731:** 237-245.

255. Patel AB, O'Hare T, Deininger MW. Mechanisms of Resistance to ABL Kinase Inhibition in Chronic Myeloid Leukemia and the Development of Next Generation ABL Kinase Inhibitors. *Hematol Oncol Clin North Am* 2017; **31**(4)**:** 589-612.

256. Mizuchi D, Kurosu T, Kida A, Jin ZH, Jin A, Arai A*, et al.* BCR/ABL activates Rap1 and B-Raf to stimulate the MEK/Erk signaling pathway in hematopoietic cells. *Biochem Biophys Res Commun* 2005; **326**(3)**:** 645-651.

257. Jilani I, Kantarjian H, Gorre M, Cortes J, Ottmann O, Bhalla K*, et al.* Phosphorylation levels of BCR-ABL, CrkL, AKT and STAT5 in imatinib-resistant chronic myeloid leukemia cells implicate alternative pathway usage as a survival strategy. *Leuk Res* 2008; **32**(4)**:** 643-649.

258. Illmer T, Schaich M, Platzbecker U, Freiberg-Richter J, Oelschlagel U, von Bonin M*, et al.* P-glycoprotein-mediated drug efflux is a resistance mechanism of chronic myelogenous leukemia cells to treatment with imatinib mesylate. *Leukemia* 2004; **18**(3)**:** 401-408.

259. Dai Y, Rahmani M, Corey SJ, Dent P, Grant S. A Bcr/Abl-independent, Lyn-dependent Form of Imatinib Mesylate (STI-571) Resistance Is Associated with Altered Expression of Bcl-2. *Journal of Biological Chemistry* 2004; **279**(33)**:** 34227-34239.

260. Geng L, Huehls AM, Wagner JM, Huntoon CJ, Karnitz LM. Checkpoint signaling, base excision repair, and PARP promote survival of colon cancer cells treated with 5-fluorodeoxyuridine but not 5-fluorouracil. *PLoS One* 2011; **6**(12)**:** e28862.

261. Cardnell RJ, Feng Y, Diao L, Fan YH, Masrorpour F, Wang J*, et al.* Proteomic markers of DNA repair and PI3K pathway activation predict response to the PARP inhibitor BMN 673 in small cell lung cancer. *Clin Cancer Res* 2013; **19**(22)**:** 6322-6328.

262. Jacot W, Thezenas S, Senal R, Viglianti C, Laberenne AC, Lopez-Crapez E*, et al.* BRCA1 promoter hypermethylation, 53BP1 protein expression and PARP-1 activity as biomarkers of DNA repair deficit in breast cancer. *BMC Cancer* 2013; **13:** 523.

263. Moehring A, Wohlbold L, Aulitzky WE, van der Kuip H. Role of poly(ADP-ribose) polymerase activity in imatinib mesylate-induced cell death. *Cell Death Differ* 2005; **12**(6)**:** 627-636.

264. Bharti AC, Takada Y, Aggarwal BB. PARP cleavage and caspase activity to assess chemosensitivity. *Methods Mol Med* 2005; **111:** 69-78.

265. Song L, Morris M, Bagui T, Lee FY, Jove R, Haura EB. Dasatinib (BMS-354825) selectively induces apoptosis in lung cancer cells dependent on epidermal growth factor receptor signaling for survival. *Cancer Res* 2006; **66**(11)**:** 5542-5548.

266. Pichot CS, Hartig SM, Xia L, Arvanitis C, Monisvais D, Lee FY*, et al.* Dasatinib synergizes with doxorubicin to block growth, migration, and invasion of breast cancer cells. *Br J Cancer* 2009; **101**(1)**:** 38-47.

267. Choi S, Henderson MJ, Kwan E, Beesley AH, Sutton R, Bahar AY*, et al.* Relapse in children with acute lymphoblastic leukemia involving selection of a preexisting drug-resistant subclone. *Blood* 2007; **110**(2)**:** 632-639.

268. Mullighan CG, Phillips LA, Su X, Ma J, Miller CB, Shurtleff SA*, et al.* Genomic Analysis of the Clonal Origins of Relapsed Acute Lymphoblastic Leukemia. *Science* 2008; **322:** 1377-1380.

269. Clappier E, Gerby B, Sigaux F, Delord M, Touzri F, Hernandez L*, et al.* Clonal selection in xenografted human T cell acute lymphoblastic leukemia recapitulates gain of malignancy at relapse. *The Journal of Experimental Medicine* 2011; **208:** 653-661.

270. Schuh A, Becq J, Humphray S, Alexa A, Burns A, Clifford R*, et al.* Monitoring chronic lymphocytic leukemia progression by whole genome sequencing reveals heterogeneous clonal evolution patterns. *Blood* 2012; **120:** 4191-4196.

271. Goss VL, Lee KA, Moritz A, Nardone J, Spek EJ, MacNeill J*, et al.* A common phosphotyrosine signature for the Bcr-Abl kinase. *Blood* 2006; **107**(12)**:** 4888-4897.

272. Perentesis JP, Bhatia S, Boyle E, Shao Y, Shu XO, Steinbuch M*, et al.* RAS oncogene mutations and outcome of therapy for childhood acute lymphoblastic leukemia. *Leukemia* 2004; **18**(4)**:** 685-692.

273. Li D, Xie K, Wolff R, Abbruzzese JL. Pancreatic cancer. *Lancet* 2004; **363**(9414)**:** 1049-1057.

274. Mascaux C, Iannino N, Martin B, Paesmans M, Berghmans T, Dusart M*, et al.* The role of RAS oncogene in survival of patients with lung cancer: a systematic review of the literature with meta-analysis. *Br J Cancer* 2005; **92**(1)**:** 131-139.

275. Mira A, Isella C, Renzulli T, Cantarella D, Martelli ML, Medico E. The GAB2 signaling scaffold promotes anchorage independence and drives a transcriptional response associated with metastatic progression of breast cancer. *Oncogene* 2009; **28**(50)**:** 4444-4455.

276. Xu J, Wang T, Cao Z, Huang H, Li J, Liu W*, et al.* MiR-497 downregulation contributes to the malignancy of pancreatic cancer and associates with a poor prognosis. *Oncotarget* 2014; **5**(16)**:** 6983-6993.

277. Sato Y, Hashiguchi Y, Nishida M. Evolution of multiple phosphodiesterase isoforms in stickleback involved in cAMP signal transduction pathway. *BMC Syst Biol* 2009; **3:** 23.

278. Kumar KK, Burgess AW, Gulbis JM. Structure and function of LGR5: an enigmatic G-protein coupled receptor marking stem cells. *Protein Sci* 2014; **23**(5)**:** 551-565.

279. Laurin M, Huber J, Pelletier A, Houalla T, Park M, Fukui Y*, et al.* Rac-specific guanine nucleotide exchange factor DOCK1 is a critical regulator of HER2-mediated breast cancer metastasis. *Proc Natl Acad Sci U S A* 2013; **110**(18)**:** 7434-7439.

280. Haegebarth A, Clevers H. Wnt signaling, lgr5, and stem cells in the intestine and skin. *Am J Pathol* 2009; **174**(3)**:** 715-721.

281. Plotnik JP, Budka JA, Ferris MW, Hollenhorst PC. ETS1 is a genome-wide effector of RAS/ERK signaling in epithelial cells. *Nucleic Acids Res* 2014; **42**(19)**:** 11928-11940.

282. Wai PY, Mi Z, Gao C, Guo H, Marroquin C, Kuo PC. Ets-1 and runx2 regulate transcription of a metastatic gene, osteopontin, in murine colorectal cancer cells. *J Biol Chem* 2006; **281**(28)**:** 18973-18982.

283. Kosaka T, Miyajima A, Shirotake S, Kikuchi E, Hasegawa M, Mikami S*, et al.* Ets-1 and hypoxia inducible factor-1α inhibition by angiotensin II type-1 receptor blockade in hormone-refractory prostate cancer. *The Prostate* 2010; **70**(2)**:** 162-169.

284. Kars MD, Iseri OD, Gunduz U. Drug resistant breast cancer cells overexpress ETS1 gene. *Biomed Pharmacother* 2010; **64**(7)**:** 458-462.

285. Li W, Zang W, Liu P, Wang Y, Du Y, Chen X*, et al.* MicroRNA-124 inhibits cellular proliferation and invasion by targeting Ets-1 in breast cancer. *Tumor Biology* 2014; **35**(11)**:** 10897-10904.

286. Frankfurt O, Licht JD. Ponatinib--a step forward in overcoming resistance in chronic myeloid leukemia. *Clin Cancer Res* 2013; **19**(21)**:** 5828-5834.

287. Cortes JE, Kim DW, Pinilla-Ibarz J, le Coutre P, Paquette R, Chuah C*, et al.* A phase 2 trial of ponatinib in Philadelphia chromosome-positive leukemias. *N Engl J Med* 2013; **369**(19)**:** 1783-1796.

288. Kang X, Kim J, Deng M, John S, Chen H, Wu G*, et al.* Inhibitory leukocyte immunoglobulin-like receptors: Immune checkpoint proteins and tumor sustaining factors. *Cell Cycle* 2016; **15**(1)**:** 25-40.

289. Fukuhara S, Chikumi H, Gutkind JS. Leukemia-associated Rho guanine nucleotide exchange factor (LARG) links heterotrimeric G proteins of the G(12) family to Rho. *FEBS Lett* 2000; **485**(2-3)**:** 183-188.

290. Hodges A, Sharrocks K, Edelmann M, Baban D, Moris A, Schwartz O*, et al.* Activation of the lectin DC-SIGN induces an immature dendritic cell phenotype triggering Rho-GTPase activity required for HIV-1 replication. *Nat Immunol* 2007; **8**(6)**:** 569-577.

291. Meyer C, Kowarz E, Hofmann J, Renneville A, Zuna J, Trka J*, et al.* New insights to the MLL recombinome of acute leukemias. *Leukemia* 2009; **23**(8)**:** 1490-1499.

292. Snippert HJ, Schepers AG, van Es JH, Simons BD, Clevers H. Biased competition between Lgr5 intestinal stem cells driven by oncogenic mutation induces clonal expansion. *EMBO Rep* 2014; **15**(1)**:** 62-69.

293. Vilardaga J-P, Jean-Alphonse FG, Gardella TJ. Endosomal generation of cAMP in GPCR signaling. *Nature Chemical Biology* 2014; **10:** 700.

294. Vadas O, Dbouk HA, Shymanets A, Perisic O, Burke JE, Abi Saab WF*, et al.* Molecular determinants of PI3Kγ-mediated activation downstream of G-protein–coupled receptors (GPCRs). *Proceedings of the National Academy of Sciences* 2013; **110**(47)**:** 18862-18867.

295. Blancquaert S, Wang L, Paternot S, Coulonval K, Dumont JE, Harris TE*, et al.* cAMP-Dependent Activation of Mammalian Target of Rapamycin (mTOR) in Thyroid Cells. Implication in Mitogenesis and Activation of CDK4. *Molecular Endocrinology* 2010; **24**(7)**:** 1453-1468.

296. Maiga A, Lemieux S, Pabst C, Lavallée VP, Bouvier M, Sauvageau G*, et al.* Transcriptome analysis of G protein-coupled receptors in distinct genetic subgroups of acute myeloid leukemia: identification of potential disease-specific targets. *Blood Cancer Journal* 2016; **6:** e431.

297. Chappell WH, Steelman LS, Long JM, Kempf RC, Abrams SL, Franklin RA*, et al.* Ras/Raf/MEK/ERK and PI3K/PTEN/Akt/mTOR inhibitors: rationale and importance to inhibiting these pathways in human health. *Oncotarget* 2011; **2**(3)**:** 135-164.

298. Jain N, Curran E, Iyengar NM, Diaz-Flores E, Kunnavakkam R, Popplewell L*, et al.* Phase II study of the oral MEK inhibitor selumetinib in advanced acute myelogenous leukemia: a University of Chicago phase II consortium trial. *Clinical Cancer Research* 2014; **20**(2)**:** 490-498.

299. Serra V, Markman B, Scaltriti M, Eichhorn PJA, Valero V, Guzman M*, et al.* NVP-BEZ235, a Dual PI3K/mTOR Inhibitor, Prevents PI3K Signaling and Inhibits the Growth of Cancer Cells with Activating PI3K Mutations. *Cancer Research* 2008; **68:** 8022-8030.

300. Witzig TE, Reeder CB, LaPlant BR, Gupta M, Johnston PB, Micallef IN*, et al.* A phase II trial of the oral mTOR inhibitor everolimus in relapsed aggressive lymphoma. *Leukemia* 2010; **25:** 341.

301. Innamorati G, Valenti MT, Giovinazzo F, Dalle Carbonare L, Parenti M, Bassi C. Molecular Approaches To Target GPCRs in Cancer Therapy. *Pharmaceuticals* 2011; **4**(4)**:** 567.

302. Ayoub MA, Damian M, Gespach C, Ferrandis E, Lavergne O, De Wever O*, et al.* Inhibition of Heterotrimeric G Protein Signaling by a Small Molecule Acting on Gα Subunit. *The Journal of Biological Chemistry* 2009; **284**(42)**:** 29136-29145.

303. Sengupta R, Sun T, Warrington NM, Rubin JB. Treating brain tumors with PDE4 inhibitors. *Trends in Pharmacological Sciences* 2011; **32**(6)**:** 337-344.

304. Druker BJ. Imatinib as a paradigm of targeted therapies. *Adv Cancer Res* 2004; **91:** 1-30.

305. Gambacorti-Passerini C. Part I: Milestones in personalised medicine--imatinib. *Lancet Oncol* 2008; **9**(6)**:** 600.

306. Baccarani M, Dreyling M, Group EGW. Chronic myeloid leukaemia: ESMO Clinical Practice Guidelines for diagnosis, treatment and follow-up. *Annals of Oncology* 2010; **21**(suppl_5)**:** v165-v167.

307. Nestal de Moraes G, Souza PS, Costas FC, Vasconcelos FC, Reis FR, Maia RC. The Interface between BCR-ABL-Dependent and -Independent Resistance Signaling Pathways in Chronic Myeloid Leukemia. *Leuk Res Treatment* 2012; **2012:** 671702.

308. Cilloni D, Saglio G. Molecular pathways: BCR-ABL. *Clin Cancer Res* 2012; **18**(4)**:** 930-937.

309. Hutter JJ. Childhood leukemia. *Pediatrics in Review* 2010; **31**(6)**:** 234.

310. Haferlach T, Bacher U, Kern W, Schnittger S, Haferlach C. The diagnosis of BCR/ABL-negative chronic myeloproliferative diseases (CMPD): a comprehensive approach based on morphology, cytogenetics, and molecular markers. *Annals of Hematology* 2008; **87**(1)**:** 1-10.

311. de Labarthe A, Rousselot P, Huguet-Rigal F, Delabesse E, Witz F, Maury S*, et al.* Imatinib combined with induction or consolidation chemotherapy in patients with de novo Philadelphia chromosome–positive acute lymphoblastic leukemia: results of the GRAAPH-2003 study. *Blood* 2007; **109:** 1408-1413.

312. Kantarjian H, O'Brien S, Jabbour E, Garcia-Manero G, Quintas-Cardama A, Shan J*, et al.* Improved survival in chronic myeloid leukemia since the introduction of imatinib therapy: a single-institution historical experience. *Blood* 2012; **119:** 1981-1987.

313. Deininger M, O'Brien SG, Guilhot F, Goldman JM, Hochhaus A, Hughes TP*, et al.* International Randomized Study of Interferon Vs STI571 (IRIS) 8-Year Follow up: Sustained Survival and Low Risk for Progression or Events in Patients with Newly Diagnosed Chronic Myeloid Leukemia in Chronic Phase (CML-CP) Treated with Imatinib. *Blood* 2009; **114:** 1126-1126.

314. Roy L, Guilhot J, Krahnke T, Guerci-Bresler A, Druker BJ, Larson RA*, et al.* Survival advantage from imatinib compared with the combination interferon-alpha plus cytarabine in chronic-phase chronic myelogenous leukemia: historical comparison between two phase 3 trials. *Blood* 2006; **108**(5)**:** 1478-1484.

315. Schultz KR, Carroll A, Heerema NA, Bowman WP, Aledo A, Slayton WB*, et al.* Long-term follow-up of imatinib in pediatric Philadelphia chromosome-positive acute lymphoblastic leukemia: Children's Oncology Group study AALL0031. *Leukemia* 2014; **28**(7)**:** 1467-1471.

316. Weisberg E, Manley P, Mestan J, Cowan-Jacob S, Ray A, Griffin JD. AMN107 (nilotinib): a novel and selective inhibitor of BCR-ABL. *Br J Cancer* 2006; **94**(12)**:** 1765-1769.

317. Shah NP. Ponatinib: targeting the T315I mutation in chronic myelogenous leukemia. *Clin Adv Hematol Oncol* 2011; **9**(12)**:** 925-926.

318. Soverini S, Gnani A, Colarossi S, Castagnetti F, Abruzzese E, Paolini S*, et al.* Philadelphia-positive patients who already harbor imatinib-resistant Bcr-Abl kinase domain mutations have a higher likelihood of developing additional mutations associated with resistance to second- or third-line tyrosine kinase inhibitors. *Blood* 2009; **114**(10)**:** 2168-2171.

319. Tasian SK, Teachey DT, Li Y, Shen F, Harvey RC, Chen I-M*, et al.* Potent efficacy of combined PI3K/mTOR and JAK or ABL inhibition in murine xenograft models of Ph-like acute lymphoblastic leukemia. *Blood* 2017; **129:** 177-187.

320. Peng B, Lloyd P, Schran H. Clinical pharmacokinetics of imatinib. *Clinical pharmacokinetics* 2005; **44**(9)**:** 879-894.

321. Shah NP, Nicoll JM, Nagar B, Gorre ME, Paquette RL, Kuriyan J*, et al.* Multiple BCR-ABL kinase domain mutations confer polyclonal resistance to the tyrosine kinase inhibitor imatinib (STI571) in chronic phase and blast crisis chronic myeloid leukemia. *Cancer Cell* 2002; **2**(2)**:** 117-125.

322. Birge RB, Kalodimos C, Inagaki F, Tanaka S. Crk and CrkL adaptor proteins: networks for physiological and pathological signaling. *Cell Commun Signal* 2009; **7:** 13.

323. Hoelbl A, Schuster C, Kovacic B, Zhu B, Wickre M, Hoelzl MA*, et al.* Stat5 is indispensable for the maintenance of bcr/abl-positive leukaemia. *EMBO Mol Med* 2010; **2**(3)**:** 98-110.

324. Hughes TP, Saglio G, Quintas-Cardama A, Mauro MJ, Kim DW, Lipton JH*, et al.* BCR-ABL1 mutation development during first-line treatment with dasatinib or imatinib for chronic myeloid leukemia in chronic phase. *Leukemia* 2015; **29**(9)**:** 1832-1838.

325. Soverini S, Colarossi S, Gnani A, Castagnetti F, Rosti G, Bosi C*, et al.* Resistance to dasatinib in Philadelphia-positive leukemia patients and the presence or the selection of mutations at residues 315 and 317 in the BCR-ABL kinase domain. *Haematologica* 2007; **92**(3)**:** 401-404.

326. Miller GD, Bruno BJ, Lim CS. Resistant mutations in CML and Ph(+)ALL - role of ponatinib. *Biologics* 2014; **8:** 243-254.

327. Khorashad JS, Kelley TW, Szankasi P, Mason CC, Soverini S, Adrian LT*, et al.* BCR-ABL1 compound mutations in tyrosine kinase inhibitor-resistant CML: frequency and clonal relationships. *Blood* 2013; **121**(3)**:** 489-498.

328. Gibbons DL, Pricl S, Posocco P, Laurini E, Fermeglia M, Sun H*, et al.* Molecular dynamics reveal BCR-ABL1 polymutants as a unique mechanism of resistance to PAN-BCR-ABL1 kinase inhibitor therapy. *Proc Natl Acad Sci U S A* 2014; **111**(9)**:** 3550-3555.

329. Hantschel O, Superti-Furga G. Regulation of the c-Abl and Bcr-Abl tyrosine kinases. *Nat Rev Mol Cell Biol* 2004; **5**(1)**:** 33-44.

330. Branford S, Rudzki Z, Walsh S, Parkinson I, Grigg A, Szer J*, et al.* Detection of BCR-ABL mutations in patients with CML treated with imatinib is virtually always accompanied by clinical resistance, and mutations in the ATP phosphate-binding loop (P-loop) are associated with a poor prognosis. *Blood* 2003; **102**(1)**:** 276-283.

331. Goujon M, McWilliam H, Li W, Valentin F, Squizzato S, Paern J*, et al.* A new bioinformatics analysis tools framework at EMBL-EBI. *Nucleic Acids Res* 2010; **38**(Web Server issue)**:** W695-699.

332. Sievers F, Wilm A, Dineen D, Gibson TJ, Karplus K, Li W*, et al.* Fast, scalable generation of high-quality protein multiple sequence alignments using Clustal Omega. *Mol Syst Biol* 2011; **7:** 539.

333. Leguay T, Desplat V, Lagarde V, Marit G, Reiffers J, Mahon FX. An amino-acid switch in the BCR-ABL kinase domain modifies sensitivity to imatinib mesylate. *Leukemia* 2005; **19**(9)**:** 1671-1673.

334. Reva B, Antipin Y, Sander C. Predicting the functional impact of protein mutations: application to cancer genomics. *Nucleic Acids Res* 2011; **39**(17)**:** e118.

335. Shah NP, Skaggs BJ, Branford S, Hughes TP, Nicoll JM, Paquette RL*, et al.* Sequential ABL kinase inhibitor therapy selects for compound drug-resistant BCR-ABL mutations with altered oncogenic potency. *J Clin Invest* 2007; **117**(9)**:** 2562-2569.

336. O'Hare T, Deininger MW, Eide CA, Clackson T, Druker BJ. Targeting the BCR-ABL signaling pathway in therapy-resistant Philadelphia chromosome-positive leukemia. *Clin Cancer Res* 2011; **17**(2)**:** 212-221.

337. Redaelli S, Mologni L, Rostagno R, Piazza R, Magistroni V, Ceccon M*, et al.* Three novel patient-derived BCR/ABL mutants show different sensitivity to second and third generation tyrosine kinase inhibitors. *Am J Hematol* 2012; **87**(11)**:** E125-128.

338. Edwards SL, Brough R, Lord CJ, Natrajan R, Vatcheva R, Levine DA*, et al.* Resistance to therapy caused by intragenic deletion in BRCA2. *Nature* 2008; **451**(7182)**:** 1111-1115.

339. Komp Lindgren P, Karlsson A, Hughes D. Mutation rate and evolution of fluoroquinolone resistance in Escherichia coli isolates from patients with urinary tract infections. *Antimicrob Agents Chemother* 2003; **47**(10)**:** 3222-3232.

340. Linde HJ, Notka F, Metz M, Kochanowski B, Heisig P, Lehn N. In vivo increase in resistance to ciprofloxacin in Escherichia coli associated with deletion of the C-terminal part of MarR. *Antimicrob Agents Chemother* 2000; **44**(7)**:** 1865-1868.

341. Johnson N, Johnson SF, Yao W, Li YC, Choi YE, Bernhardy AJ*, et al.* Stabilization of mutant BRCA1 protein confers PARP inhibitor and platinum resistance. *Proc Natl Acad Sci U S A* 2013; **110**(42)**:** 17041-17046.

342. Okuda K, D'Andrea A, Van Etten RA, Griffin JD. The C-terminus of c-ABL is required for proliferation and viability signaling in a c-ABL/erythropoietin receptor fusion protein. *Blood* 1998; **92**(10)**:** 3848-3856.

343. Underhill-Day N, Pierce A, Thompson SE, Xenaki D, Whetton AD, Owen-Lynch PJ. Role of the C-terminal actin binding domain in BCR/ABL-mediated survival and drug resistance. *Br J Haematol* 2006; **132**(6)**:** 774-783.

344. Heisterkamp N, Voncken JW, Senadheera D, Gonzalez-Gomez I, Reichert A, Haataja L*, et al.* Reduced oncogenicity of p190 Bcr/Abl F-actin-binding domain mutants. *Blood* 2000; **96**(6)**:** 2226-2232.

345. Wertheim JA, Perera SA, Hammer DA, Ren R, Boettiger D, Pear WS. Localization of BCR-ABL to F-actin regulates cell adhesion but does not attenuate CML development. *Blood* 2003; **102**(6)**:** 2220-2228.

346. Hong A, Moriceau G, Sun L, Lomeli S, Piva M, Damoiseaux R*, et al.* Exploiting drug addiction mechanisms to select against MAPKi-resistant melanoma. *Cancer Discovery* 2017.

347. Sherman-Baust CA, Becker KG, Wood Iii WH, Zhang Y, Morin PJ. Gene expression and pathway analysis of ovarian cancer cells selected for resistance to cisplatin, paclitaxel, or doxorubicin. *J Ovarian Res* 2011; **4**(1)**:** 21.

348. Robertson G, Schein J, Chiu R, Corbett R, Field M, Jackman SD*, et al.* De novo assembly and analysis of RNA-seq data. *Nat Methods* 2010; **7**(11)**:** 909-912.

349. Hoang VLT, Tom LN, Quek XC, Tan JM, Payne EJ, Lin LL*, et al.* RNA-seq reveals more consistent reference genes for gene expression studies in human non-melanoma skin cancers. *PeerJ* 2017; **5:** e3631.

350. Rajkumar AP, Qvist P, Lazarus R, Lescai F, Ju J, Nyegaard M*, et al.* Experimental validation of methods for differential gene expression analysis and sample pooling in RNA-seq. *BMC Genomics* 2015; **16:** 548.

351. Decaillot FM, Rozenfeld R, Gupta A, Devi LA. Cell surface targeting of mu-delta opioid receptor heterodimers by RTP4. *Proc Natl Acad Sci U S A* 2008; **105**(41)**:** 16045-16050.

352. Colicelli J. Human RAS superfamily proteins and related GTPases. *Sci STKE* 2004; **2004**(250)**:** RE13.

353. Mushinski JF, Nguyen P, Stevens LM, Khanna C, Lee S, Chung EJ*, et al.* Inhibition of tumor cell motility by the interferon-inducible GTPase MxA. *J Biol Chem* 2009; **284**(22)**:** 15206-15214.

354. Kreit M, Vertommen D, Gillet L, Michiels T. The Interferon-Inducible Mouse Apolipoprotein L9 and Prohibitins Cooperate to Restrict Theiler's Virus Replication. *PLoS One* 2015; **10**(7)**:** e0133190.

355. Carrero JA, Calderon B, Towfic F, Artyomov MN, Unanue ER. Defining the transcriptional and cellular landscape of type 1 diabetes in the NOD mouse. *PLoS One* 2013; **8**(3)**:** e59701.

356. Ghosh A, Sampath P, Zhu J, Hornung V, Thorne S, Sarkar SN. Modulation of cellular immune response by 2′-5′ Oligoadenylate Synthetase - like (OASL) proteins during DNA virus infection. *The Journal of Immunology* 2016; **196**(1 Supplement)**:** 61.66-61.66.

357. Hanada T, Yoshida H, Kato S, Tanaka K, Masutani K, Tsukada J*, et al.* Suppressor of cytokine signaling-1 is essential for suppressing dendritic cell activation and systemic autoimmunity. *Immunity* 2003; **19**(3)**:** 437-450.

358. Platanias LC. Mechanisms of type-I- and type-II-interferon-mediated signalling. *Nat Rev Immunol* 2005; **5**(5)**:** 375-386.

359. Hervas-Stubbs S, Perez-Gracia JL, Rouzaut A, Sanmamed MF, Le Bon A, Melero I. Direct effects of type I interferons on cells of the immune system. *Clin Cancer Res* 2011; **17**(9)**:** 2619-2627.

360. Suvas S, Singh V, Sahdev S, Vohra H, Agrewala JN. Distinct role of CD80 and CD86 in the regulation of the activation of B cell and B cell lymphoma. *J Biol Chem* 2002; **277**(10)**:** 7766-7775.

361. Maj T, Slawek A, Chelmonska-Soyta A. CD80 and CD86 costimulatory molecules differentially regulate OT-II CD4(+) T lymphocyte proliferation and cytokine response in cocultures with antigen-presenting cells derived from pregnant and pseudopregnant mice. *Mediators Inflamm* 2014; **2014:** 769239.

362. Tessema M, Yingling CM, Grimes MJ, Thomas CL, Liu Y, Leng S*, et al.* Differential epigenetic regulation of TOX subfamily high mobility group box genes in lung and breast cancers. *PLoS One* 2012; **7**(4)**:** e34850.

363. Miura Y, Kataoka H, Joh T, Tada T, Asai K, Nakanishi M*, et al.* Susceptibility to killer T cells of gastric cancer cells enhanced by Mitomycin-C involves induction of ATBF1 and activation of p21 (Waf1/Cip1) promoter. *Microbiol Immunol* 2004; **48**(2)**:** 137-145.

364. Spencer SL, Cappell SD, Tsai FC, Overton KW, Wang CL, Meyer T. The proliferation-quiescence decision is controlled by a bifurcation in CDK2 activity at mitotic exit. *Cell* 2013; **155**(2)**:** 369-383.

365. Sun X, Xing C, Fu X, Li J, Zhang B, Frierson HF, Jr.*, et al.* Additive Effect of Zfhx3/Atbf1 and Pten Deletion on Mouse Prostatic Tumorigenesis. *J Genet Genomics* 2015; **42**(7)**:** 373-382.

366. Fisher FM, Chui PC, Antonellis PJ, Bina HA, Kharitonenkov A, Flier JS*, et al.* Obesity is a fibroblast growth factor 21 (FGF21)-resistant state. *Diabetes* 2010; **59**(11)**:** 2781-2789.

367. Ge X, Chen C, Hui X, Wang Y, Lam KS, Xu A. Fibroblast growth factor 21 induces glucose transporter-1 expression through activation of the serum response factor/Ets-like protein-1 in adipocytes. *J Biol Chem* 2011; **286**(40)**:** 34533-34541.

368. Hardwick JP. Cytochrome P450 omega hydroxylase (CYP4) function in fatty acid metabolism and metabolic diseases. *Biochem Pharmacol* 2008; **75**(12)**:** 2263-2275.

369. Massey KA, Nicolaou A. Lipidomics of polyunsaturated-fatty-acid-derived oxygenated metabolites. *Biochem Soc Trans* 2011; **39**(5)**:** 1240-1246.

370. Cui JY, Renaud HJ, Klaassen CD. Ontogeny of novel cytochrome P450 gene isoforms during postnatal liver maturation in mice. *Drug Metab Dispos* 2012; **40**(6)**:** 1226-1237.

371. Sampath D, Cortes J, Estrov Z, Du M, Shi Z, Andreeff M*, et al.* Pharmacodynamics of cytarabine alone and in combination with 7-hydroxystaurosporine (UCN-01) in AML blasts in vitro and during a clinical trial. *Blood* 2006; **107**(6)**:** 2517-2524.

372. Housman G, Byler S, Heerboth S, Lapinska K, Longacre M, Snyder N*, et al.* Drug resistance in cancer: an overview. *Cancers (Basel)* 2014; **6**(3)**:** 1769-1792.

373. Lewis-Tuffin LJ, Cidlowski JA. The physiology of human glucocorticoid receptor beta (hGRbeta) and glucocorticoid resistance. *Ann N Y Acad Sci* 2006; **1069:** 1-9.

374. Pace TW, Hu F, Miller AH. Cytokine-effects on glucocorticoid receptor function: relevance to glucocorticoid resistance and the pathophysiology and treatment of major depression. *Brain Behav Immun* 2007; **21**(1)**:** 9-19.

375. Kordes U, Krappmann D, Heissmeyer V, Ludwig WD, Scheidereit C. Transcription factor NF-kappaB is constitutively activated in acute lymphoblastic leukemia cells. *Leukemia* 2000; **14**(3)**:** 399-402.

376. Hornakova T, Staerk J, Royer Y, Flex E, Tartaglia M, Constantinescu SN*, et al.* Acute lymphoblastic leukemia-associated JAK1 mutants activate the Janus kinase/STAT pathway via interleukin-9 receptor alpha homodimers. *J Biol Chem* 2009; **284**(11)**:** 6773-6781.

377. Knight T, Irving JA. Ras/Raf/MEK/ERK Pathway Activation in Childhood Acute Lymphoblastic Leukemia and Its Therapeutic Targeting. *Front Oncol* 2014; **4:** 160.

378. Vainchenker W, Constantinescu SN. JAK/STAT signaling in hematological malignancies. *Oncogene* 2013; **32**(21)**:** 2601-2613.

379. Mullighan CG, Zhang J, Harvey RC, Collins-Underwood JR, Schulman BA, Phillips LA*, et al.* JAK mutations in high-risk childhood acute lymphoblastic leukemia. *Proc Natl Acad Sci U S A* 2009; **106**(23)**:** 9414-9418.

380. Rahman M, Hasan MR. Cancer Metabolism and Drug Resistance. *Metabolites* 2015; **5**(4)**:** 571-600.

381. Ponnusamy S, Meyers-Needham M, Senkal CE, Saddoughi SA, Sentelle D, Selvam SP*, et al.* Sphingolipids and cancer: ceramide and sphingosine-1-phosphate in the regulation of cell death and drug resistance. *Future Oncol* 2010; **6**(10)**:** 1603-1624.

382. Chesney RW. Interactions of vitamin D and the proximal tubule. *Pediatr Nephrol* 2016; **31**(1)**:** 7-14.

383. Moestrup SK, Kozyraki R. Cubilin, a high-density lipoprotein receptor. *Curr Opin Lipidol* 2000; **11**(2)**:** 133-140.

384. Gremel G, Djureinovic D, Niinivirta M, Laird A, Ljungqvist O, Johannesson H*, et al.* A systematic search strategy identifies cubilin as independent prognostic marker for renal cell carcinoma. *BMC Cancer* 2017; **17**(1)**:** 9.

385. Murphy AB, Nyame Y, Martin IK, Catalona WJ, Hollowell CM, Nadler RB*, et al.* Vitamin D deficiency predicts prostate biopsy outcomes. *Clin Cancer Res* 2014; **20**(9)**:** 2289-2299.

386. Salehi-Tabar R, Nguyen-Yamamoto L, Tavera-Mendoza LE, Quail T, Dimitrov V, An BS*, et al.* Vitamin D receptor as a master regulator of the c-MYC/MXD1 network. *Proc Natl Acad Sci U S A* 2012; **109**(46)**:** 18827-18832.

387. Eadie LN, Dang P, Saunders VA, Yeung DT, Osborn MP, Grigg AP*, et al.* The clinical significance of ABCB1 overexpression in predicting outcome of CML patients undergoing first-line imatinib treatment. *Leukemia* 2017; **31**(1)**:** 75-82.

388. Svirnovski AI, Shman TV, Serhiyenka TF, Savitski VP, Smolnikova VV, Fedasenka UU. ABCB1 and ABCG2 proteins, their functional activity and gene expression in concert with drug sensitivity of leukemia cells. *Hematology* 2009; **14**(4)**:** 204-212.

389. De Iudicibus S, De Pellegrin A, Stocco G, Bartoli F, Bussani R, Decorti G. ABCB1 gene polymorphisms and expression of P-glycoprotein and long-term prognosis in colorectal cancer. *Anticancer Res* 2008; **28**(6B)**:** 3921-3928.

390. Hlavata I, Mohelnikova-Duchonova B, Vaclavikova R, Liska V, Pitule P, Novak P*, et al.* The role of ABC transporters in progression and clinical outcome of colorectal cancer. *Mutagenesis* 2012; **27**(2)**:** 187-196.

391. Demidenko R, Razanauskas D, Daniunaite K, Lazutka JR, Jankevicius F, Jarmalaite S. Frequent down-regulation of ABC transporter genes in prostate cancer. *BMC Cancer* 2015; **15:** 683.

392. Metzgeroth G, Schwaab J, Gosenca D, Fabarius A, Haferlach C, Hochhaus A*, et al.* Long-term follow-up of treatment with imatinib in eosinophilia-associated myeloid/lymphoid neoplasms with PDGFR rearrangements in blast phase. *Leukemia* 2013; **27**(11)**:** 2254.

393. Huh WK, Sill MW, Darcy KM, Elias KM, Hoffman JS, Boggess JF*, et al.* Efficacy and safety of imatinib mesylate (Gleevec®) and immunohistochemical expression of c-Kit and PDGFR-β in a Gynecologic Oncology Group Phase II Trial in women with recurrent or persistent carcinosarcomas of the uterus. *Gynecologic oncology* 2010; **117**(2)**:** 248-254.

394. Cristofanilli M, Morandi P, Krishnamurthy S, Reuben JM, Lee BN, Francis D*, et al.* Imatinib mesylate (Gleevec®) in advanced breast cancer-expressing C-Kit or PDGFR-β: clinical activity and biological correlations. *Annals of Oncology* 2008; **19**(10)**:** 1713-1719.

395. Guo J, Si L, Kong Y, Flaherty KT, Xu X, Zhu Y*, et al.* Phase II, open-label, single-arm trial of imatinib mesylate in patients with metastatic melanoma harboring c-Kit mutation or amplification. *Journal of Clinical Oncology* 2011; **29**(21)**:** 2904-2909.

396. Dewar AL, Cambareri AC, Zannettino ACW, Miller BL, Doherty KV, Hughes TP*, et al.* Macrophage colony-stimulating factor receptor c-fms is a novel target of imatinib. *Cell* 2005; **105**(8).

397. Dewar AL, Zannettino AC, Hughes TP, Lyons AB. Inhibition of c-fms by imatinib: expanding the spectrum of treatment. *Cell Cycle* 2005; **4**(7)**:** 851-853.

398. Schwab C, Andrews R, Chilton L, Elliott A, Richardson S, Ryan SL*, et al.* SSBP2-CSF1R is a Recurrent Fusion in B-Other Acute Lymphoblastic Leukaemia with Variable Clinical Outcome. *Blood* 2014; **124**(21)**:** 3773-3773.

399. Liang H, Samanta S, Nagarajan L. SSBP2, a candidate tumor suppressor gene, induces growth arrest and differentiation of myeloid leukemia cells. *Oncogene* 2005; **24:** 2625.

400. Geissmann F, Manz MG, Jung S, Sieweke MH, Merad M, Ley K. Development of Monocytes, Macrophages, and Dendritic Cells. *Science* 2010; **327:** 656-661.

401. Hume DA. Differentiation and heterogeneity in the mononuclear phagocyte system. *Mucosal Immunology* 2008; **1:** 432.

402. MacDonald KPA, Palmer JS, Cronau S, Seppanen E, Olver S, Raffelt NC*, et al.* An antibody against the colony-stimulating factor 1 receptor depletes the resident subset of monocytes and tissue- and tumor-associated macrophages but does not inhibit inflammation. *Blood* 2010; **116:** 3955-3963.

403. Kitagawa D, Gouda M, Kirii Y, Sugiyama N, Ishihama Y, Fujii I*, et al.* Characterization of kinase inhibitors using different phosphorylation states of colony stimulating factor-1 receptor tyrosine kinase. *J Biochem* 2012; **151**(1)**:** 47-55.

404. Mashkani B, Griffith R, Ashman LK. Colony stimulating factor-1 receptor as a target for small molecule inhibitors. *Bioorg Med Chem* 2010; **18**(5)**:** 1789-1797.

405. Uitdehaag JC, Sunnen CM, van Doornmalen AM, de Rouw N, Oubrie A, Azevedo R*, et al.* Multidimensional profiling of CSF1R screening hits and inhibitors: assessing cellular activity, target residence time, and selectivity in a higher throughput way. *J Biomol Screen* 2011; **16**(9)**:** 1007-1017.

406. Lilljebjörn H, Ågerstam H, Orsmark-Pietras C, Rissler M, Ehrencrona H, Nilsson L*, et al.* RNA-seq identifies clinically relevant fusion genes in leukemia including a novel MEF2D/CSF1R fusion responsive to imatinib. *Leukemia* 2013; **28:** 977.

407. Gu T-l, Mercher T, Tyner JW, Goss VL, Walters DK, Cornejo MG*, et al.* A novel fusion of RBM6 to CSF1R in acute megakaryoblastic leukemia. *Blood* 2007; **110:** 323-333.

408. Chase A, Schultheis B, Kreil S, Baxter J, Hidalgo-Curtis C, Jones A*, et al.* Imatinib sensitivity as a consequence of a CSF1R-Y571D mutation and CSF1/CSF1R signaling abnormalities in the cell line GDM1. *Leukemia* 2009; **23**(2)**:** 358-364.

409. Taylor JR, Brownlow N, Domin J, Dibb NJ. FMS receptor for M-CSF (CSF-1) is sensitive to the kinase inhibitor imatinib and mutation of Asp-802 to Val confers resistance. *Oncogene* 2006; **25**(1)**:** 147-151.

410. Larkin MA, Blackshields G, Brown NP, Chenna R, McGettigan PA, McWilliam H*, et al.* Clustal W and Clustal X version 2.0. *Bioinformatics* 2007; **23**(21)**:** 2947-2948.

411. Zhao Z, Wu H, Wang L, Liu Y, Knapp S, Liu Q*, et al.* Exploration of type II binding mode: a privileged approach for kinase inhibitor focused drug discovery? *ACS chemical biology* 2014; **9**(6)**:** 1230-1241.

412. Stanley ER, Chitu V. CSF-1 receptor signaling in myeloid cells. *Cold Spring Harb Perspect Biol* 2014; **6**(6).

413. Gangoiti P, Granado MH, Wang SW, Kong JY, Steinbrecher UP, Gómez-Muñoz A. Ceramide 1-phosphate stimulates macrophage proliferation through activation of the PI3-kinase/PKB, JNK and ERK1/2 pathways. *Cellular Signalling* 2008; **20**(4)**:** 726-736.

414. Mouchemore KA, Pixley FJ. CSF-1 signaling in macrophages: pleiotrophy through phosphotyrosine-based signaling pathways. *Critical Reviews in Clinical Laboratory Sciences* 2012; **49**(2)**:** 49-61.

415. Mahon F-X, Hayette S, Lagarde V, Belloc F, Turcq B, Nicolini F*, et al.* Evidence that Resistance to Nilotinib May Be Due to BCR-ABL, Pgp, or Src Kinase Overexpression. *Cancer Research* 2008; **68:** 9809-9816.

416. Gorre ME, Mohammed M, Ellwood K, Hsu N, Paquette R, Rao PN*, et al.* Clinical resistance to STI-571 cancer therapy caused by BCR-ABL gene mutation or amplification. *Science* 2001; **293**(5531)**:** 876-880.

417. Engelman JA, Zejnullahu K, Mitsudomi T, Song Y, Hyland C, Park JO*, et al.* MET Amplification Leads to Gefitinib Resistance in Lung Cancer by Activating ERBB3 Signaling. *Science* 2007; **316:** 1039-1043.

418. Forbes SA, Beare D, Boutselakis H, Bamford S, Bindal N, Tate J*, et al.* COSMIC: somatic cancer genetics at high-resolution. *Nucleic Acids Res* 2017; **45**(D1)**:** D777-D783.

419. Pao W, Miller VA, Politi KA, Riely GJ, Somwar R, Zakowski MF*, et al.* Acquired resistance of lung adenocarcinomas to gefitinib or erlotinib is associated with a second mutation in the EGFR kinase domain. *PLoS medicine* 2005; **2**(3)**:** e73.

420. Heidel F, Solem FK, Breitenbuecher F, Lipka DB, Kasper S, Thiede MH*, et al.* Clinical resistance to the kinase inhibitor PKC412 in acute myeloid leukemia by mutation of Asn-676 in the FLT3 tyrosine kinase domain. *Blood* 2006; **107**(1)**:** 293-300.

421. Rose AS, Hildebrand PW. NGL Viewer: a web application for molecular visualization. *Nucleic Acids Research* 2015; **43**(W1)**:** W576-W579.

422. Tap WD, Wainberg ZA, Anthony SP, Ibrahim PN, Zhang C, Healey JH*, et al.* Structure-Guided Blockade of CSF1R Kinase in Tenosynovial Giant-Cell Tumor. *N Engl J Med* 2015; **373**(5)**:** 428-437.

423. Moriceau G, Hugo W, Hong A, Shi H, Kong X, Clarissa CY*, et al.* Tunable-combinatorial mechanisms of acquired resistance limit the efficacy of BRAF/MEK cotargeting but result in melanoma drug addiction. *Cancer cell* 2015; **27**(2)**:** 240-256.

424. Suda K, Tomizawa K, Osada H, Maehara Y, Yatabe Y, Sekido Y*, et al.* Conversion from the “oncogene addiction” to “drug addiction” by intensive inhibition of the EGFR and MET in lung cancer with activating EGFR mutation. *Lung Cancer* 2012; **76**(3)**:** 292-299.

425. Kong X, Kuilman T, Shahrabi A, Boshuizen J, Kemper K, Song JY*, et al.* Cancer drug addiction is relayed by an ERK2-dependent phenotype switch. *Nature* 2017.

426. Otero K, Turnbull IR, Poliani PL, Vermi W, Cerutti E, Aoshi T*, et al.* Macrophage colony-stimulating factor induces the proliferation and survival of macrophages via a pathway involving DAP12 and β-catenin. *Nature immunology* 2009; **10**(7)**:** 734-743.

427. Knowlton ML. *Analysis of CSF-1R and SRC-induced tyrosine phosphorylation in breast epithelial cells*. Harvard University, 2010.

428. McVicar DW, Trinchieri G. CSF-1R, DAP12 and beta-catenin: a menage a trois. *Nat Immunol* 2009; **10**(7)**:** 681-683.

429. Rademakers R, Baker M, Nicholson AM, Rutherford NJ, Finch N, Soto-Ortolaza A*, et al.* Mutations in the colony stimulating factor 1 receptor (CSF1R) gene cause hereditary diffuse leukoencephalopathy with spheroids. *Nature Genetics* 2011; **44:** 200.

430. Schubert C, Schalk-Hihi C, Struble GT, Ma H-C, Petrounia IP, Brandt B*, et al.* Crystal structure of the tyrosine kinase domain of colony-stimulating factor-1 receptor (cFMS) in complex with two inhibitors. *Journal of Biological Chemistry* 2007; **282**(6)**:** 4094-4101.

431. Brownlow N, Mol C, Hayford C, Ghaem-Maghami S, Dibb N. Dasatinib is a potent inhibitor of tumour-associated macrophages, osteoclasts and the FMS receptor. *Leukemia* 2009; **23**(3)**:** 590-595.

432. Bradeen HA, Eide CA, O'Hare T, Johnson KJ, Willis SG, Lee FY*, et al.* Comparison of imatinib mesylate, dasatinib (BMS-354825), and nilotinib (AMN107) in an N-ethyl-N-nitrosourea (ENU)-based mutagenesis screen: high efficacy of drug combinations. *Blood* 2006; **108**(7)**:** 2332-2338.

433. van Montfort RLM, Workman P. Structure-based design of molecular cancer therapeutics. *Trends in Biotechnology* 2009; **27**(5)**:** 315-328.

434. Lamprecht B, Walter K, Kreher S, Kumar R, Hummel M, Lenze D*, et al.* Derepression of an endogenous long terminal repeat activates the CSF1R proto-oncogene in human lymphoma. *Nature Medicine* 2010; **16:** 571.

435. Walter M, Lucet IS, Patel O, Broughton SE, Bamert R, Williams NK*, et al.* The 2.7 Å crystal structure of the autoinhibited human c-Fms kinase domain. *Journal of molecular biology* 2007; **367**(3)**:** 839-847.

436. Pridans C, Sauter KA, Baer K, Kissel H, Hume DA. CSF1R mutations in hereditary diffuse leukoencephalopathy with spheroids are loss of function. *Sci Rep* 2013; **3:** 3013.

437. Moorman AV. New and emerging prognostic and predictive genetic biomarkers in B-cell precursor acute lymphoblastic leukemia. *Haematologica* 2016; **101**(4)**:** 407-416.

438. Guo J, Marcotte PA, McCall JO, Dai Y, Pease LJ, Michaelides MR*, et al.* Inhibition of phosphorylation of the colony-stimulating factor-1 receptor (c-Fms) tyrosine kinase in transfected cells by ABT-869 and other tyrosine kinase inhibitors. *Mol Cancer Ther* 2006; **5**(4)**:** 1007-1013.

439. Taipale M, Krykbaeva I, Koeva M, Kayatekin C, Westover KD, Karras GI*, et al.* Quantitative analysis of HSP90-client interactions reveals principles of substrate recognition. *Cell* 2012; **150**(5)**:** 987-1001.

440. Isaacs J, Whitesell L. *Hsp90 in Cancer: Beyond the Usual Suspects*. Elsevier Science, 2016.

441. Raedler LA. Jakafi (Ruxolitinib): First FDA-Approved Medication for the Treatment of Patients with Polycythemia Vera. *Am Health Drug Benefits* 2015; **8**(Spec Feature)**:** 75-79.

442. Leroy E, Constantinescu SN. Rethinking JAK2 inhibition: towards novel strategies of more specific and versatile janus kinase inhibition. *Leukemia* 2017; **31**(5)**:** 1023-1038.

443. Silvennoinen O, Hubbard SR. Targeting the Inactive Conformation of JAK2 in Hematological Malignancies. *Cancer Cell* 2015; **28**(1)**:** 1-2.

444. Wan H, Schroeder GM, Hart AC, Inghrim J, Grebinski J, Tokarski JS*, et al.* Discovery of a Highly Selective JAK2 Inhibitor, BMS-911543, for the Treatment of Myeloproliferative Neoplasms. *ACS Med Chem Lett* 2015; **6**(8)**:** 850-855.

445. Purandare AV, McDevitt TM, Wan H, You D, Penhallow B, Han X*, et al.* Characterization of BMS-911543, a functionally selective small-molecule inhibitor of JAK2. *Leukemia* 2012; **26**(2)**:** 280-288.

446. Harrison CN, Schaap N, Vannucchi AM, Kiladjian JJ, Tiu RV, Zachee P*, et al.* Janus kinase-2 inhibitor fedratinib in patients with myelofibrosis previously treated with ruxolitinib (JAKARTA-2): a single-arm, open-label, non-randomised, phase 2, multicentre study. *The Lancet Haematology* 2017; **4**(7)**:** e317-e324.

447. Pardanani A, Tefferi A, Jamieson C, Gabrail NY, Lebedinsky C, Gao G*, et al.* A phase 2 randomized dose-ranging study of the JAK2-selective inhibitor fedratinib (SAR302503) in patients with myelofibrosis. *Blood Cancer J* 2015; **5:** e335.

448. Kesarwani M, Huber E, Azam M. Overcoming AC220 resistance of FLT3-ITD by SAR302503. *Blood Cancer J* 2013; **3:** e138.

449. Zhang Q, Zhang Y, Diamond S, Boer J, Harris JJ, Li Y*, et al.* The Janus kinase 2 inhibitor fedratinib inhibits thiamine uptake: a putative mechanism for the onset of Wernicke's encephalopathy. *Drug Metab Dispos* 2014; **42**(10)**:** 1656-1662.

450. Monaghan KA, Khong T, Burns CJ, Spencer A. The novel JAK inhibitor CYT387 suppresses multiple signalling pathways, prevents proliferation and induces apoptosis in phenotypically diverse myeloma cells. *Leukemia* 2011; **25**(12)**:** 1891-1899.

451. Asshoff M, Petzer V, Warr MR, Haschka D, Tymoszuk P, Demetz E*, et al.* Momelotinib inhibits ACVR1/ALK2, decreases hepcidin production, and ameliorates anemia of chronic disease in rodents. *Blood* 2017; **129**(13)**:** 1823-1830.

452. Gupta V, Mesa RA, Deininger MW, Rivera CE, Sirhan S, Brachmann CB*, et al.* A phase 1/2, open-label study evaluating twice-daily administration of momelotinib in myelofibrosis. *Haematologica* 2017; **102**(1)**:** 94-102.

453. Pardanani A, Gotlib J, Gupta V, Roberts AW, Wadleigh M, Sirhan S*, et al.* Phase I/II Study of CYT387, a JAK1/JAK2 Inhibitor for the Treatment of Myelofibrosis. *Blood* 2012; **120:** 178-178.

454. Verstovsek S, Courby S, Griesshammer M, Mesa RA, Brachmann CB, Kawashima J*, et al.* A phase 2 study of momelotinib, a potent JAK1 and JAK2 inhibitor, in patients with polycythemia vera or essential thrombocythemia. *Leuk Res* 2017; **60:** 11-17.

455. Zhong J, Sharma J, Raju R, Palapetta SM, Prasad TS, Huang TC*, et al.* TSLP signaling pathway map: a platform for analysis of TSLP-mediated signaling. *Database (Oxford)* 2014; **2014:** bau007.

456. Waters MJ, Brooks AJ. JAK2 activation by growth hormone and other cytokines. *Biochem J* 2015; **466**(1)**:** 1-11.

457. Brooks AJ, Dai W, O'Mara ML, Abankwa D, Chhabra Y, Pelekanos RA*, et al.* Mechanism of activation of protein kinase JAK2 by the growth hormone receptor. *Science* 2014; **344**(6185)**:** 1249783.

458. Waters MJ, Brooks AJ, Chhabra Y. A new mechanism for growth hormone receptor activation of JAK2, and implications for related cytokine receptors. *JAKSTAT* 2014; **3:** e29569.

459. Babon JJ, Lucet IS, Murphy JM, Nicola NA, Varghese LN. The molecular regulation of Janus kinase (JAK) activation. *Biochem J* 2014; **462**(1)**:** 1-13.

460. Shudo E, Yang J, Yoshimura A, Iwasa Y. Robustness of the signal transduction system of the mammalian JAK/STAT pathway and dimerization steps. *J Theor Biol* 2007; **246**(1)**:** 1-9.

461. McNally R, Toms AV, Eck MJ. Crystal Structure of the FERM-SH2 Module of Human Jak2. *PLoS One* 2016; **11**(5)**:** e0156218.

462. Saharinen P, Silvennoinen O. The Janus Kinase Protein Family. In: Sehgal PB, Levy DE, Hirano T (eds). *Signal Transducers and Activators of Transcription (STATs): Activation and Biology*. Springer Netherlands: Dordrecht, 2003, pp 27-42.

463. Shan Y, Gnanasambandan K, Ungureanu D, Kim ET, Hammaren H, Yamashita K*, et al.* Molecular basis for pseudokinase-dependent autoinhibition of JAK2 tyrosine kinase. *Nat Struct Mol Biol* 2014; **21**(7)**:** 579-584.

464. Hammaren HM, Ungureanu D, Grisouard J, Skoda RC, Hubbard SR, Silvennoinen O. ATP binding to the pseudokinase domain of JAK2 is critical for pathogenic activation. *Proc Natl Acad Sci USA* 2015; **112**(15)**:** 4642-4647.

465. Saharinen P, Takaluoma K, Silvennoinen O. Regulation of the Jak2 tyrosine kinase by its pseudokinase domain. *Mol Cell Biol* 2000; **20**(10)**:** 3387-3395.

466. Pieri L, Pancrazzi A, Pacilli A, Rabuzzi C, Rotunno G, Fanelli T*, et al.* JAK2V617F complete molecular remission in polycythemia vera/essential thrombocythemia patients treated with ruxolitinib. *Blood* 2015; **125**(21)**:** 3352-3353.

467. Vannucchi AM, Verstovsek S, Guglielmelli P, Griesshammer M, Burn TC, Naim A*, et al.* Ruxolitinib reduces JAK2 p.V617F allele burden in patients with polycythemia vera enrolled in the RESPONSE study. *Ann Hematol* 2017; **96**(7)**:** 1113-1120.

468. Marty C, Saint-Martin C, Pecquet C, Grosjean S, Saliba J, Mouton C*, et al.* Germline JAK2 mutations in the kinase domain are responsible for hereditary thrombocytosis and are resistant to JAK2 and HSP90 inhibitors. *Blood* 2014; **123**(9)**:** 1372-1383.

469. Meyer SC. Mechanisms of Resistance to JAK2 Inhibitors in Myeloproliferative Neoplasms. *Hematol Oncol Clin North Am* 2017; **31**(4)**:** 627-642.

470. Corporation I, Group CsO. A Phase 2 Study of Ruxolitinib With Chemotherapy in Children With Acute Lymphoblastic Leukemia. https://ClinicalTrials.gov/show/NCT02723994; 2016.

471. Center MDAC, Corporation I. Ruxolitinib or Dasatinib With Chemotherapy in Patients With Philadelphia Chromosome (Ph)-Like Acute Lymphoblastic Leukemia (ALL). https://ClinicalTrials.gov/show/NCT02420717; 2015.

472. Xia J, Gill EE, Hancock RE. NetworkAnalyst for statistical, visual and network-based meta-analysis of gene expression data. *Nat Protoc* 2015; **10**(6)**:** 823-844.

473. Ploner A. Heatplus: Heatmaps with row and/or column covariates and colored clusters. . R package version 2.22.0. ed; 2015.

474. Orchard S, Kerrien S, Abbani S, Aranda B, Bhate J, Bidwell S*, et al.* Protein interaction data curation: the International Molecular Exchange (IMEx) consortium. *Nat Methods* 2012; **9**(4)**:** 345-350.

475. Zotenko E, Mestre J, O'Leary DP, Przytycka TM. Why do hubs in the yeast protein interaction network tend to be essential: reexamining the connection between the network topology and essentiality. *PLoS Comput Biol* 2008; **4**(8)**:** e1000140.

476. Charitou T, Bryan K, Lynn DJ. Using biological networks to integrate, visualize and analyze genomics data. *Genet Sel Evol* 2016; **48**(1)**:** 27.

477. Tamamyan G, Shi C, Roberts K, Ma H, Mullighan C, Konopleva M. Targeting of JAK-STAT signaling pathway and BCL-2 family proteins in Ph-like acute lymphoblastic leukemia. *Clinical Lymphoma Myeloma and Leukemia* 2015; **15:** S4.

478. Nguyen K, Devidas M, Cheng SC, La M, Raetz EA, Carroll WL*, et al.* Factors influencing survival after relapse from acute lymphoblastic leukemia: a Children's Oncology Group study. *Leukemia* 2008; **22**(12)**:** 2142-2150.

479. Holleman A, Cheok MH, den Boer ML, Yang W, Veerman AJ, Kazemier KM*, et al.* Gene-expression patterns in drug-resistant acute lymphoblastic leukemia cells and response to treatment. *N Engl J Med* 2004; **351**(6)**:** 533-542.

480. Bhojwani D, Pui CH. Relapsed childhood acute lymphoblastic leukaemia. *Lancet Oncol* 2013; **14**(6)**:** e205-217.

481. University Health Network T, Novartis. Phase I/II Study of Nilotinib/Ruxolitinb Therapy for TKI Resistant Ph-Leukemia. https://ClinicalTrials.gov/show/NCT01914484; 2013.

482. Vera J, Rateitschak K, Lange F, Kossow C, Wolkenhauer O, Jaster R. Systems biology of JAK-STAT signalling in human malignancies. *Prog Biophys Mol Biol* 2011; **106**(2)**:** 426-434.

483. Warsch W, Walz C, Sexl V. JAK of all trades: JAK2-STAT5 as novel therapeutic targets in BCR-ABL1+ chronic myeloid leukemia. *Blood* 2013; **122**(13)**:** 2167-2175.

484. Stark GR, Darnell JE, Jr. The JAK-STAT pathway at twenty. *Immunity* 2012; **36**(4)**:** 503-514.

485. Andraos R, Qian Z, Bonenfant D, Rubert J, Vangrevelinghe E, Scheufler C*, et al.* Modulation of activation-loop phosphorylation by JAK inhibitors is binding mode dependent. *Cancer Discov* 2012; **2**(6)**:** 512-523.

486. Zhao L, Dong H, Zhang CC, Kinch L, Osawa M, Iacovino M*, et al.* A JAK2 interdomain linker relays Epo receptor engagement signals to kinase activation. *J Biol Chem* 2009; **284**(39)**:** 26988-26998.

487. Gillinder KR, Tuckey H, Bell CC, Magor GW, Huang S, Ilsley MD*, et al.* Direct targets of pSTAT5 signalling in erythropoiesis. *PLoS One* 2017; **12**(7)**:** e0180922.

488. Hansen G, Hercus TR, McClure BJ, Stomski FC, Dottore M, Powell J*, et al.* The structure of the GM-CSF receptor complex reveals a distinct mode of cytokine receptor activation. *Cell* 2008; **134**(3)**:** 496-507.

489. Schinnerl D, Fortschegger K, Kauer M, Marchante JR, Kofler R, Den Boer ML*, et al.* The role of the Janus-faced transcription factor PAX5-JAK2 in acute lymphoblastic leukemia. *Blood* 2015; **125**(8)**:** 1282-1291.

490. Lucet IS, Fantino E, Styles M, Bamert R, Patel O, Broughton SE*, et al.* The structural basis of Janus kinase 2 inhibition by a potent and specific pan-Janus kinase inhibitor. *Blood* 2006; **107**(1)**:** 176-183.

491. Kesarwani M, Huber E, Kincaid Z, Evelyn CR, Biesiada J, Rance M*, et al.* Targeting substrate-site in Jak2 kinase prevents emergence of genetic resistance. *Sci Rep* 2015; **5:** 14538.

492. Tipping AJ, Baluch S, Barnes DJ, Veach DR, Clarkson BM, Bornmann WG*, et al.* Efficacy of dual-specific Bcr-Abl and Src-family kinase inhibitors in cells sensitive and resistant to imatinib mesylate. *Leukemia* 2004; **18**(8)**:** 1352-1356.

493. Oxnard GR, Arcila ME, Sima CS, Riely GJ, Chmielecki J, Kris MG*, et al.* Acquired resistance to EGFR tyrosine kinase inhibitors in EGFR-mutant lung cancer: distinct natural history of patients with tumors harboring the T790M mutation. *Clin Cancer Res* 2011; **17**(6)**:** 1616-1622.

494. Cong J, Geng W, He B, Liu J, Charlton J, Adler PN. The furry gene of Drosophila is important for maintaining the integrity of cellular extensions during morphogenesis. *Development* 2001; **128**(14)**:** 2793-2802.

495. Hayette S, Cornillet-Lefebvre P, Tigaud I, Struski S, Forissier S, Berchet A*, et al.* AF4p12, a human homologue to the furry gene of Drosophila, as a novel MLL fusion partner. *Cancer Res* 2005; **65**(15)**:** 6521-6525.

496. Gentry T, Foster S, Winstead L, Deibert E, Fiordalisi M, Balber A. Simultaneous isolation of human BM hematopoietic, endothelial and mesenchymal progenitor cells by flow sorting based on aldehyde dehydrogenase activity: implications for cell therapy. *Cytotherapy* 2007; **9**(3)**:** 259-274.

497. Rodriguez-Torres M, Allan AL. Aldehyde dehydrogenase as a marker and functional mediator of metastasis in solid tumors. *Clin Exp Metastasis* 2016; **33**(1)**:** 97-113.

498. Tomita H, Tanaka K, Tanaka T, Hara A. Aldehyde dehydrogenase 1A1 in stem cells and cancer. *Oncotarget* 2016; **7**(10)**:** 11018-11032.

499. Javelaud D, Pierrat MJ, Mauviel A. Crosstalk between TGF-beta and hedgehog signaling in cancer. *FEBS Lett* 2012; **586**(14)**:** 2016-2025.

500. Javelaud D, Alexaki VI, Dennler S, Mohammad KS, Guise TA, Mauviel A. TGF-beta/SMAD/GLI2 signaling axis in cancer progression and metastasis. *Cancer Res* 2011; **71**(17)**:** 5606-5610.

501. Scales SJ, de Sauvage FJ. Mechanisms of Hedgehog pathway activation in cancer and implications for therapy. *Trends Pharmacol Sci* 2009; **30**(6)**:** 303-312.

502. Akaogi K, Nakajima Y, Ito I, Kawasaki S, Oie SH, Murayama A*, et al.* KLF4 suppresses estrogen-dependent breast cancer growth by inhibiting the transcriptional activity of ERalpha. *Oncogene* 2009; **28**(32)**:** 2894-2902.

503. Nakatake Y, Fukui N, Iwamatsu Y, Masui S, Takahashi K, Yagi R*, et al.* Klf4 cooperates with Oct3/4 and Sox2 to activate the Lefty1 core promoter in embryonic stem cells. *Mol Cell Biol* 2006; **26**(20)**:** 7772-7782.

504. Khaled WT, Choon Lee S, Stingl J, Chen X, Raza Ali H, Rueda OM*, et al.* BCL11A is a triple-negative breast cancer gene with critical functions in stem and progenitor cells. *Nat Commun* 2015; **6:** 5987.

505. Satterwhite E, Sonoki T, Willis TG, Harder L, Nowak R, Arriola EL*, et al.* The BCL11 gene family: involvement of BCL11A in lymphoid malignancies. *Blood* 2001; **98**(12)**:** 3413-3420.

506. Manzanares M, Blanco MJ, Nieto MA. Snail3 orthologues in vertebrates: divergent members of the Snail zinc-finger gene family. *Dev Genes Evol* 2004; **214**(1)**:** 47-53.

507. Katoh M, Katoh M. Identification and characterization of human SNAIL3 (SNAI3) gene in silico. *Int J Mol Med* 2003; **11**(3)**:** 383-388.

508. Barrallo-Gimeno A, Nieto MA. The Snail genes as inducers of cell movement and survival: implications in development and cancer. *Development* 2005; **132**(14)**:** 3151-3161.

509. Hollinger S, Hepler JR. Cellular regulation of RGS proteins: modulators and integrators of G protein signaling. *Pharmacol Rev* 2002; **54**(3)**:** 527-559.

510. Huang G, Song H, Wang R, Han X, Chen L. The relationship between RGS5 expression and cancer differentiation and metastasis in non-small cell lung cancer. *J Surg Oncol* 2012; **105**(4)**:** 420-424.

511. Xu Z, Zuo Y, Wang J, Yu Z, Peng F, Chen Y*, et al.* Overexpression of the regulator of G-protein signaling 5 reduces the survival rate and enhances the radiation response of human lung cancer cells. *Oncol Rep* 2015; **33**(6)**:** 2899-2907.

512. Formica V, Cereda V, Nardecchia A, Tesauro M, Roselli M. Immune reaction and colorectal cancer: friends or foes? *World J Gastroenterol* 2014; **20**(35)**:** 12407-12419.

513. Dupaul-Chicoine J, Yeretssian G, Doiron K, Bergstrom KS, McIntire CR, LeBlanc PM*, et al.* Control of intestinal homeostasis, colitis, and colitis-associated colorectal cancer by the inflammatory caspases. *Immunity* 2010; **32**(3)**:** 367-378.

514. Saito H, Kubota M, Roberts RW, Chi Q, Matsunami H. RTP family members induce functional expression of mammalian odorant receptors. *Cell* 2004; **119**(5)**:** 679-691.

515. Li VS, Yuen ST, Chan TL, Yan HH, Law WL, Yeung BH*, et al.* Frequent inactivation of axon guidance molecule RGMA in human colon cancer through genetic and epigenetic mechanisms. *Gastroenterology* 2009; **137**(1)**:** 176-187.

516. Bujko M, Kober P, Mikula M, Ligaj M, Ostrowski J, Siedlecki JA. Expression changes of cell-cell adhesion-related genes in colorectal tumors. *Oncol Lett* 2015; **9**(6)**:** 2463-2470.

517. Patel M, Lu L, Zander DS, Sreerama L, Coco D, Moreb JS. ALDH1A1 and ALDH3A1 expression in lung cancers: correlation with histologic type and potential precursors. *Lung Cancer* 2008; **59**(3)**:** 340-349.

518. Dylla SJ, Beviglia L, Park IK, Chartier C, Raval J, Ngan L*, et al.* Colorectal cancer stem cells are enriched in xenogeneic tumors following chemotherapy. *PLoS One* 2008; **3**(6)**:** e2428.

519. Sladek NE, Kollander R, Sreerama L, Kiang DT. Cellular levels of aldehyde dehydrogenases (ALDH1A1 and ALDH3A1) as predictors of therapeutic responses to cyclophosphamide-based chemotherapy of breast cancer: a retrospective study. Rational individualization of oxazaphosphorine-based cancer chemotherapeutic regimens. *Cancer Chemother Pharmacol* 2002; **49**(4)**:** 309-321.

520. Vasiliou V, Pappa A, Estey T. Role of human aldehyde dehydrogenases in endobiotic and xenobiotic metabolism. *Drug metabolism reviews* 2004; **36**(2)**:** 279-299.

521. Garber K. Energy boost: the Warburg effect returns in a new theory of cancer. *J Natl Cancer Inst* 2004; **96**(24)**:** 1805-1806.

522. Kim JW, Dang CV. Cancer's molecular sweet tooth and the Warburg effect. *Cancer Res* 2006; **66**(18)**:** 8927-8930.

523. Vander Heiden MG, Cantley LC, Thompson CB. Understanding the Warburg effect: the metabolic requirements of cell proliferation. *Science* 2009; **324**(5930)**:** 1029-1033.

524. Ito K, Suda T. Metabolic requirements for the maintenance of self-renewing stem cells. *Nat Rev Mol Cell Biol* 2014; **15**(4)**:** 243-256.

525. Bouker KB, Skaar TC, Riggins RB, Harburger DS, Fernandez DR, Zwart A*, et al.* Interferon regulatory factor-1 (IRF-1) exhibits tumor suppressor activities in breast cancer associated with caspase activation and induction of apoptosis. *Carcinogenesis* 2005; **26**(9)**:** 1527-1535.

526. Kim PK, Armstrong M, Liu Y, Yan P, Bucher B, Zuckerbraun BS*, et al.* IRF-1 expression induces apoptosis and inhibits tumor growth in mouse mammary cancer cells in vitro and in vivo. *Oncogene* 2004; **23**(5)**:** 1125-1135.

527. Croker BA, Kiu H, Nicholson SE. SOCS regulation of the JAK/STAT signalling pathway. *Semin Cell Dev Biol* 2008; **19**(4)**:** 414-422.

528. Kershaw NJ, Murphy JM, Liau NP, Varghese LN, Laktyushin A, Whitlock EL*, et al.* SOCS3 binds specific receptor-JAK complexes to control cytokine signaling by direct kinase inhibition. *Nat Struct Mol Biol* 2013; **20**(4)**:** 469-476.

529. Niwa Y, Kanda H, Shikauchi Y, Saiura A, Matsubara K, Kitagawa T*, et al.* Methylation silencing of SOCS-3 promotes cell growth and migration by enhancing JAK/STAT and FAK signalings in human hepatocellular carcinoma. *Oncogene* 2005; **24**(42)**:** 6406-6417.

530. Pierconti F, Martini M, Pinto F, Cenci T, Capodimonti S, Calarco A*, et al.* Epigenetic silencing of SOCS3 identifies a subset of prostate cancer with an aggressive behavior. *Prostate* 2011; **71**(3)**:** 318-325.

531. Shang AQ, Wu J, Bi F, Zhang YJ, Xu LR, Li LL*, et al.* Relationship between HER2 and JAK/STAT-SOCS3 signaling pathway and clinicopathological features and prognosis of ovarian cancer. *Cancer Biol Ther* 2017; **18**(5)**:** 314-322.

532. Alderton WK, Cooper CE, Knowles RG. Nitric oxide synthases: structure, function and inhibition. *Biochem J* 2001; **357**(Pt 3)**:** 593-615.

533. Chen K, Popel AS. Vascular and perivascular nitric oxide release and transport: biochemical pathways of neuronal nitric oxide synthase (NOS1) and endothelial nitric oxide synthase (NOS3). *Free Radic Biol Med* 2007; **42**(6)**:** 811-822.

534. Choudhari SK, Chaudhary M, Bagde S, Gadbail AR, Joshi V. Nitric oxide and cancer: a review. *World J Surg Oncol* 2013; **11:** 118.

535. Renaudin K, Denis MG, Karam G, Vallette G, Buzelin F, Laboisse CL*, et al.* Loss of NOS1 expression in high-grade renal cell carcinoma associated with a shift of NO signalling. *Br J Cancer* 2004; **90**(12)**:** 2364-2369.

536. Seiden-Long I, Navab R, Shih W, Li M, Chow J, Zhu CQ*, et al.* Gab1 but not Grb2 mediates tumor progression in Met overexpressing colorectal cancer cells. *Carcinogenesis* 2008; **29**(3)**:** 647-655.

537. Meng S, Chen Z, Munoz-Antonia T, Wu J. Participation of both Gab1 and Gab2 in the activation of the ERK/MAPK pathway by epidermal growth factor. *Biochem J* 2005; **391**(Pt 1)**:** 143-151.

538. Mirzoeva OK, Das D, Heiser LM, Bhattacharya S, Siwak D, Gendelman R*, et al.* Basal Subtype and MAPK/ERK Kinase (MEK)-Phosphoinositide 3-Kinase Feedback Signaling Determine Susceptibility of Breast Cancer Cells to MEK Inhibition. *Cancer Research* 2009; **69:** 565-572.

539. Roy SK, Srivastava RK, Shankar S. Inhibition of PI3K/AKT and MAPK/ERK pathways causes activation of FOXO transcription factor, leading to cell cycle arrest and apoptosis in pancreatic cancer. *Journal of molecular signaling* 2010; **5**(1)**:** 10.

540. Chow S, Minden MD, Hedley DW. Constitutive phosphorylation of the S6 ribosomal protein via mTOR and ERK signaling in the peripheral blasts of acute leukemia patients. *Experimental hematology* 2006; **34**(9)**:** 1182-1190.

541. Gregorj C, Ricciardi MR, Petrucci MT, Scerpa MC, De Cave F, Fazi P*, et al.* ERK1/2 phosphorylation is an independent predictor of complete remission in newly diagnosed adult acute lymphoblastic leukemia. *Blood* 2007; **109**(12)**:** 5473-5476.

542. Ramadan E, Alinsaif S, Hassan MR. Network topology measures for identifying disease-gene association in breast cancer. *BMC Bioinformatics* 2016; **17 Suppl 7:** 274.

543. Carter H, Hofree M, Ideker T. Genotype to phenotype via network analysis. *Curr Opin Genet Dev* 2013; **23**(6)**:** 611-621.

544. Salminen A, Kaarniranta K. Insulin/IGF-1 paradox of aging: regulation via AKT/IKK/NF-kappaB signaling. *Cell Signal* 2010; **22**(4)**:** 573-577.

545. Grady WM, Parkin RK, Mitchell PS, Lee JH, Kim YH, Tsuchiya KD*, et al.* Epigenetic silencing of the intronic microRNA hsa-miR-342 and its host gene EVL in colorectal cancer. *Oncogene* 2008; **27**(27)**:** 3880-3888.

546. Booth V, Keizer DW, Kamphuis MB, Clark-Lewis I, Sykes BD. The CXCR3 binding chemokine IP-10/CXCL10: structure and receptor interactions. *Biochemistry* 2002; **41**(33)**:** 10418-10425.

547. Campanella GS, Tager AM, El Khoury JK, Thomas SY, Abrazinski TA, Manice LA*, et al.* Chemokine receptor CXCR3 and its ligands CXCL9 and CXCL10 are required for the development of murine cerebral malaria. *Proc Natl Acad Sci U S A* 2008; **105**(12)**:** 4814-4819.

548. Zipin-Roitman A, Meshel T, Sagi-Assif O, Shalmon B, Avivi C, Pfeffer RM*, et al.* CXCL10 promotes invasion-related properties in human colorectal carcinoma cells. *Cancer Res* 2007; **67**(7)**:** 3396-3405.

549. Monteagudo C, Martin JM, Jorda E, Llombart-Bosch A. CXCR3 chemokine receptor immunoreactivity in primary cutaneous malignant melanoma: correlation with clinicopathological prognostic factors. *J Clin Pathol* 2007; **60**(6)**:** 596-599.

550. Piper KP, Horlock C, Curnow SJ, Arrazi J, Nicholls S, Mahendra P*, et al.* CXCL10-CXCR3 interactions play an important role in the pathogenesis of acute graft-versus-host disease in the skin following allogeneic stem-cell transplantation. *Blood* 2007; **110**(12)**:** 3827-3832.

551. Duffner U, Lu B, Hildebrandt GC, Teshima T, Williams DL, Reddy P*, et al.* Role of CXCR3-induced donor T-cell migration in acute GVHD. *Exp Hematol* 2003; **31**(10)**:** 897-902.

552. Kundu M, Roy A, Pahan K. Selective neutralization of IL-12 p40 monomer induces death in prostate cancer cells via IL-12-IFN-gamma. *Proc Natl Acad Sci U S A* 2017; **114**(43)**:** 11482-11487.

553. Razaghi A, Villacres C, Jung V, Mashkour N, Butler M, Owens L*, et al.* Improved therapeutic efficacy of mammalian expressed-recombinant interferon gamma against ovarian cancer cells. *Exp Cell Res* 2017; **359**(1)**:** 20-29.

554. Mittal D, Gubin MM, Schreiber RD, Smyth MJ. New insights into cancer immunoediting and its three component phases--elimination, equilibrium and escape. *Curr Opin Immunol* 2014; **27:** 16-25.

555. Cho HI, Lee YR, Celis E. Interferon gamma limits the effectiveness of melanoma peptide vaccines. *Blood* 2011; **117**(1)**:** 135-144.

556. Zaidi MR, Merlino G. The two faces of interferon-gamma in cancer. *Clin Cancer Res* 2011; **17**(19)**:** 6118-6124.

557. Dimitrakopoulos CM, Beerenwinkel N. Computational approaches for the identification of cancer genes and pathways. *Wiley Interdiscip Rev Syst Biol Med* 2017; **9**(1).

558. Merid SK, Goranskaya D, Alexeyenko A. Distinguishing between driver and passenger mutations in individual cancer genomes by network enrichment analysis. *BMC Bioinformatics* 2014; **15:** 308.

559. Lilljebjorn H, Fioretos T. New oncogenic subtypes in pediatric B-cell precursor acute lymphoblastic leukemia. *Blood* 2017; **130**(12)**:** 1395-1401.

560. Skorski T. Chronic myeloid leukemia cells refractory/resistant to tyrosine kinase inhibitors are genetically unstable and may cause relapse and malignant progression to the terminal disease state. *Leukemia & Lymphoma* 2011; **52**(sup1)**:** 23-29.

561. Cortes J, Goldman JM, Hughes T. Current issues in chronic myeloid leukemia: monitoring, resistance, and functional cure. *Journal of the National Comprehensive Cancer Network* 2012; **10**(Suppl 3)**:** S-1-S-13.

562. Chang BH, Willis SG, Stork L, Hunger SP, Carroll WL, Camitta BM*, et al.* Imatinib resistant BCR-ABL1 mutations at relapse in children with Ph+ ALL: a Children's Oncology Group (COG) study. *British journal of haematology* 2012; **157**(4)**:** 507-510.

563. Nicolini FE, Mauro MJ, Martinelli G, Kim D-W, Soverini S, Müller MC*, et al.* Epidemiologic study on survival of chronic myeloid leukemia and Ph+ acute lymphoblastic leukemia patients with BCR-ABL T315I mutation. *Blood* 2009; **114**(26)**:** 5271-5278.

564. Katayama R, Shaw AT, Khan TM, Mino-Kenudson M, Solomon BJ, Halmos B*, et al.* Mechanisms of acquired crizotinib resistance in ALK-rearranged lung cancers. *Science translational medicine* 2012; **4**(120)**:** 120ra117-120ra117.

565. Camidge DR, Pao W, Sequist LV. Acquired resistance to TKIs in solid tumours: learning from lung cancer. *Nat Rev Clin Oncol* 2014; **11**(8)**:** 473-481.

566. Gounder MM, Maki RG. Molecular basis for primary and secondary tyrosine kinase inhibitor resistance in gastrointestinal stromal tumor. *Cancer chemotherapy and Pharmacology* 2011; **67**(1)**:** 25-43.

567. Planchard D, Loriot Y, Andre F, Gobert A, Auger N, Lacroix L*, et al.* EGFR-independent mechanisms of acquired resistance to AZD9291 in EGFR T790M-positive NSCLC patients. *Annals of Oncology* 2015; **26**(10)**:** 2073-2078.

568. Salomoni P, Calabretta B. Targeted therapies and autophagy: new insights from chronic myeloid leukemia. *Autophagy* 2009; **5**(7)**:** 1050-1051.

569. Tran TH, Nguyen JV, Smith CC, Roberts KG, Mullighan CG, Shah NP*, et al.* Identifying Drug-Resistant Mutations in Ebf1-Pdgfrb Ph-like Acute Lymphoblastic Leukemia. American Society of Haematology (ASH) 57th Annual Meeting & Exposition. Orlando FL, USA; 2015.

570. Aparicio S, Caldas C. The Implications of Clonal Genome Evolution for Cancer Medicine. *New England Journal of Medicine* 2013; **368**(9)**:** 842-851.

571. Turke AB, Zejnullahu K, Wu Y-L, Song Y, Dias-Santagata D, Lifshits E*, et al.* Preexistence and Clonal Selection of MET Amplification in EGFR Mutant NSCLC. *Cancer Cell* 2010; **17**(1)**:** 77-88.

572. Alliance NMCC. Acute Lymphoblastic Leukemia Therapies Informed by Genomic Analyses. https://ClinicalTrials.gov/show/NCT02580981.

573. Institute NC. Combination Chemotherapy in Treating Young Patients With Newly Diagnosed High-Risk B Acute Lymphoblastic Leukemia and Ph-Like TKI Sensitive Mutations. https://ClinicalTrials.gov/show/NCT02883049; 2012.

574. Quintas-Cardama A, Cortes J. Molecular biology of bcr-abl1-positive chronic myeloid leukemia. *Blood* 2009; **113**(8)**:** 1619-1630.

575. Poehlmann A, Kuester D, Meyer F, Lippert H, Roessner A, Schneider-Stock R. K-ras mutation detection in colorectal cancer using the Pyrosequencing technique. *Pathology - Research and Practice* 2007; **203**(7)**:** 489-497.

576. Zlobec I, Bihl MP, Schwarb H, Terracciano L, Lugli A. Clinicopathological and protein characterization of BRAF-and K-RAS-mutated colorectal cancer and implications for prognosis. *International journal of cancer* 2010; **127**(2)**:** 367-380.

577. Sharma SV, Bell DW, Settleman J, Haber DA. Epidermal growth factor receptor mutations in lung cancer. *Nature Reviews Cancer* 2007; **7:** 169.

578. Tsao M-S, Aviel-Ronen S, Ding K, Lau D, Liu N, Sakurada A*, et al.* Prognostic and Predictive Importance of p53 and RAS for Adjuvant Chemotherapy in Non–Small-Cell Lung Cancer. *Journal of Clinical Oncology* 2007; **25**(33)**:** 5240-5247.

579. Nazarian R, Shi H, Wang Q, Kong X, Koya RC, Lee H*, et al.* Melanomas acquire resistance to B-RAF (V600E) inhibition by RTK or N-RAS upregulation. *Nature* 2010; **468**(7326)**:** 973-977.

580. Chng WJ, Gonzalez-Paz N, Price-Troska T, Jacobus S, Rajkumar SV, Oken MM*, et al.* Clinical and biological significance of RAS mutations in multiple myeloma. *Leukemia* 2008; **22**(12)**:** 10.1038/leu.2008.1142.

581. Tyner JW, Erickson H, Deininger MW, Willis SG, Eide CA, Levine RL*, et al.* High-throughput sequencing screen reveals novel, transforming RAS mutations in myeloid leukemia patients. *Blood* 2009; **113**(8)**:** 1749-1755.

582. Case M, Matheson E, Minto L, Hassan R, Harrison CJ, Bown N*, et al.* Mutation of Genes Affecting the RAS Pathway Is Common in Childhood Acute Lymphoblastic Leukemia. *Cancer Research* 2008; **68:** 6803-6809.

583. Piloto O, Wright M, Brown P, Kim K-T, Levis M, Small D. Prolonged exposure to FLT3 inhibitors leads to resistance via activation of parallel signaling pathways. *Blood* 2007; **109:** 1643-1652.

584. Suzuki M, Abe A, Imagama S, Nomura Y, Tanizaki R, Minami Y*, et al.* BCR-ABL-independent and RAS/MAPK pathway-dependent form of imatinib resistance in Ph-positive acute lymphoblastic leukemia cell line with activation of EphB4. *European Journal of Haematology* 2010; **84**(3)**:** 229-238.

585. Melo JV, Chuah C. Resistance to imatinib mesylate in chronic myeloid leukaemia. *Cancer letters* 2007; **249**(2)**:** 121-132.

586. Mian AA, Schull M, Zhao Z, Oancea C, Hundertmark A, Beissert T*, et al.* The gatekeeper mutation T315I confers resistance against small molecules by increasing or restoring the ABL-kinase activity accompanied by aberrant transphosphorylation of endogenous BCR, even in loss-of-function mutants of BCR/ABL. *Leukemia* 2009; **23**(9)**:** 1614-1621.

587. Engelman JA, Settleman J. Acquired resistance to tyrosine kinase inhibitors during cancer therapy. *Curr Opin Genet Dev* 2008; **18**(1)**:** 73-79.

588. Deininger MW, Hodgson JG, Shah NP, Cortes JE, Kim DW, Nicolini FE*, et al.* Compound mutations in BCR-ABL1 are not major drivers of primary or secondary resistance to ponatinib in CP-CML patients. *Blood* 2016; **127**(6)**:** 703-712.

589. Schrock A, Chen T-H, Clackson T, Rivera VM. Comprehensive analysis of the in vitro potency of ponatinib, and all other approved BCR-ABL tyrosine kinase inhibitors (TKIs), against a panel of single and compound BCR-ABL mutants. Am Soc Hematology; 2013.

590. Pricl S, Posocco P, Laurini E, Fermeglia M, Talpaz M, Cortes JE*, et al.* Acquisition Of Compound BCR-ABL1 Alleles As A Mechanism Of Resistance To Ponatinib In Chronic Myeloid Leukemia. Am Soc Hematology; 2013.

591. Deeb KK, Trump DL, Johnson CS. Vitamin D signalling pathways in cancer: potential for anticancer therapeutics. *Nat Rev Cancer* 2007; **7**(9)**:** 684-700.

592. Jingwi EY, Abbas M, Ricks-Santi L, Winchester D, Beyene D, Day A*, et al.* Vitamin D receptor genetic polymorphisms are associated with PSA level, Gleason score and prostate cancer risk in African-American men. *Anticancer Res* 2015; **35**(3)**:** 1549-1558.

593. Gorham ED, Garland CF, Garland FC, Grant WB, Mohr SB, Lipkin M*, et al.* Optimal Vitamin D Status for Colorectal Cancer Prevention: A Quantitative Meta Analysis. *American Journal of Preventive Medicine* 2007; **32**(3)**:** 210-216.

594. Khodarev NN, Roizman B, Weichselbaum RR. Molecular pathways: interferon/stat1 pathway: role in the tumor resistance to genotoxic stress and aggressive growth. *Clinical cancer research* 2012; **18**(11)**:** 3015-3021.

595. Fryknäs M, Dhar S, Öberg F, Rickardson L, Rydåker M, Göransson H*, et al.* STAT1 signaling is associated with acquired crossresistance to doxorubicin and radiation in myeloma cell lines. *International journal of cancer* 2007; **120**(1)**:** 189-195.

596. Stronach EA, Alfraidi A, Rama N, Datler C, Studd JB, Agarwal R*, et al.* HDAC4-regulated STAT1 activation mediates platinum resistance in ovarian cancer. *Cancer research* 2011; **71**(13)**:** 4412-4422.

597. Khodarev NN, Roach P, Pitroda SP, Golden DW, Bhayani M, Shao MY*, et al.* STAT1 pathway mediates amplification of metastatic potential and resistance to therapy. *PloS one* 2009; **4**(6)**:** e5821.

598. Rios JJ, Perelygin AA, Long MT, Lear TL, Zharkikh AA, Brinton MA*, et al.* Characterization of the equine 2'-5'oligoadenylate synthetase 1 (OAS1) and ribonuclease L (RNASEL) innate immunity genes. *BMC genomics* 2007; **8**(1)**:** 313.

599. Kwon Y-C, Kang J-I, Hwang SB, Ahn B-Y. The ribonuclease L-dependent antiviral roles of human 2′, 5′-oligoadenylate synthetase family members against hepatitis C virus. *FEBS letters* 2013; **587**(2)**:** 156-164.

600. Chakrabarti A, Jha BK, Silverman RH. New insights into the role of RNase L in innate immunity. *Journal of Interferon & Cytokine Research* 2011; **31**(1)**:** 49-57.

601. Murphy AM, Besmer DM, Moerdyk-Schauwecker M, Moestl N, Ornelles DA, Mukherjee P*, et al.* Vesicular stomatitis virus as an oncolytic agent against pancreatic ductal adenocarcinoma. *Journal of virology* 2012; **86**(6)**:** 3073-3087.

602. Moerdyk-Schauwecker M, Shah NR, Murphy AM, Hastie E, Mukherjee P, Grdzelishvili VZ. Resistance of pancreatic cancer cells to oncolytic vesicular stomatitis virus: role of type I interferon signaling. *Virology* 2013; **436**(1)**:** 221-234.

603. Mandal S, Abebe F, Chaudhary J. 2′-5′ oligoadenylate synthetase 1 polymorphism is associated with prostate cancer. *Cancer* 2011; **117**(24)**:** 5509-5518.

604. Sava GP, Speedy HE, Di Bernardo MC, Dyer MJS, Holroyd A, Sunter NJ*, et al.* Common variation at 12q24.13 (OAS3) influences chronic lymphocytic leukemia risk. *Leukemia* 2014; **29:** 748.

605. Brownlow N. Kinase inhibitors of the FMS receptor for macrophage colony stimulating factor. 2008.

606. De Melo VAS, Milojkovic D, Marin D, Apperley JF, Nacheva EP, Reid AG. Deletions adjacent to BCR and ABL1 breakpoints occur in a substantial minority of chronic myeloid leukemia patients with masked Philadelphia rearrangements. *Cancer Genetics and Cytogenetics* 2008; **182**(2)**:** 111-115.

607. Lee YK, Kim YR, Min HC, Oh BR, Kim TY, Kim YS*, et al.* Deletion of any part of the BCR or ABL gene on the derivative chromosome 9 is a poor prognostic marker in chronic myelogenous leukemia. *Cancer Genetics and Cytogenetics* 2006; **166**(1)**:** 65-73.

608. Faccio R, Takeshita S, Colaianni G, Chappel J, Zallone A, Teitelbaum SL*, et al.* M-CSF regulates the cytoskeleton via recruitment of a multimeric signaling complex to c-Fms Tyr-559/697/721. *J Biol Chem* 2007; **282**(26)**:** 18991-18999.

609. Choi Y, Faccio R, Teitelbaum SL, Takayanagi H. Chapter 4 - Osteoclast Biology: Regulation of Formation and Function. *Osteoimmunology (Second edition)*. Academic Press: San Diego, 2016, pp 41-70.

610. Takeshita S, Faccio R, Chappel J, Zheng L, Feng X, Weber JD*, et al.* c-Fms Tyrosine 559 Is a Major Mediator of M-CSF-induced Proliferation of Primary Macrophages. *Journal of Biological Chemistry* 2007; **282**(26)**:** 18980-18990.

611. Sun J, Pedersen M, Bengtsson S, Rönnstrand L. Grb2 mediates negative regulation of stem cell factor receptor/c-Kit signaling by recruitment of Cbl. *Experimental Cell Research* 2007; **313**(18)**:** 3935-3942.

612. Mahankali M, Peng H-J, Cox D, Gomez-Cambronero J. The mechanism of cell membrane ruffling relies on a phospholipase D2 (PLD2), Grb2 and Rac2 association. *Cellular Signalling* 2011; **23**(8)**:** 1291-1298.

613. Kholodenko BN. Four-dimensional organization of protein kinase signaling cascades: the roles of diffusion, endocytosis and molecular motors. *Journal of Experimental Biology* 2003; **206:** 2073-2082.

614. Martelli AM, Evangelisti C, Chiarini F, Grimaldi C, Cappellini A, Ognibene A*, et al.* The emerging role of the phosphatidylinositol 3-kinase/Akt/mammalian target of rapamycin signaling network in normal myelopoiesis and leukemogenesis. *Biochimica et Biophysica Acta (BBA) - Molecular Cell Research* 2010; **1803**(9)**:** 991-1002.

615. Martelli AM, Evangelisti C, Chiarini F, Grimaldi C, Manzoli L, McCubrey JA. Targeting the PI3K/AKT/mTOR signaling network in acute myelogenous leukemia. *Expert Opinion on Investigational Drugs* 2009; **18**(9)**:** 1333-1349.

616. Droin N, Solary E. Editorial: CSF1R, CSF-1, and IL-34, a "menage a trois" conserved across vertebrates. *Journal of leukocyte biology* 2010; **87**(5)**:** 745-747.

617. Zhou L, Ercolano E, Ammoun S, Schmid MC, Barczyk MA, Hanemann CO. Merlin-deficient human tumors show loss of contact inhibition and activation of Wnt/β-catenin signaling linked to the PDGFR/Src and Rac/PAK pathways. *Neoplasia* 2011; **13**(12)**:** 1101IN1101-1112IN1102.

618. Rangaswami H, Schwappacher R, Tran T, Chan GC, Zhuang S, Boss GR*, et al.* Protein kinase G and focal adhesion kinase converge on Src/Akt/β-catenin signaling module in osteoblast mechanotransduction. *Journal of Biological Chemistry* 2012; **287**(25)**:** 21509-21519.

619. Wang Y, Krivtsov AV, Sinha AU, North TE, Goessling W, Feng Z*, et al.* The Wnt/β-catenin pathway is required for the development of leukemia stem cells in AML. *Science* 2010; **327**(5973)**:** 1650-1653.

620. Moriceau G, Hugo W, Hong A, Shi H, Kong X, Yu CC*, et al.* Tunable-combinatorial mechanisms of acquired resistance limit the efficacy of BRAF/MEK cotargeting but result in melanoma drug addiction. *Cancer Cell* 2015; **27**(2)**:** 240-256.

621. Das Thakur M, Salangsang F, Landman AS, Sellers WR, Pryer NK, Levesque MP*, et al.* Modelling vemurafenib resistance in melanoma reveals a strategy to forestall drug resistance. *Nature* 2013; **494:** 251.

622. Fridman JS, Sarlis NJ. The interplay between inhibition of JAK2 and HSP90. *JAK-STAT* 2012; **1**(2)**:** 77-79.

623. Vander Heiden MG, Cantley LC, Thompson CB. Understanding the Warburg Effect: The Metabolic Requirements of Cell Proliferation. *Science* 2009; **324:** 1029-1033.

624. Bongaerts GPA, van Halteren HK, Verhagen CAM, Wagener DJT. Cancer cachexia demonstrates the energetic impact of gluconeogenesis in human metabolism. *Medical Hypotheses* 2006; **67**(5)**:** 1213-1222.

625. Lu J, Tan M, Cai Q. The Warburg effect in tumor progression: Mitochondrial oxidative metabolism as an anti-metastasis mechanism. *Cancer Letters* 2015; **356**(2, Part A)**:** 156-164.

626. Herst PM, Howman RA, Neeson PJ, Berridge MV, Ritchie DS. The level of glycolytic metabolism in acute myeloid leukemia blasts at diagnosis is prognostic for clinical outcome. *Journal of leukocyte biology* 2011; **89**(1)**:** 51-55.

627. Chen W-L, Wang J-H, Zhao A-H, Xu X, Wang Y-H, Chen T-L*, et al.* A distinct glucose metabolism signature of acute myeloid leukemia with prognostic value. *Blood* 2014; **124:** 1645-1654.

628. Boag JM, Beesley AH, Firth MJ, Freitas JR, Ford J, Hoffmann K*, et al.* Altered glucose metabolism in childhood pre-B acute lymphoblastic leukaemia. *Leukemia* 2006; **20**(10)**:** 1731-1737.

629. Suganuma K, Miwa H, Imai N, Shikami M, Gotou M, Goto M*, et al.* Energy metabolism of leukemia cells: glycolysis versus oxidative phosphorylation. *Leuk Lymphoma* 2010; **51**(11)**:** 2112-2119.

630. Viale A, Pettazzoni P, Lyssiotis CA, Ying H, Sánchez N, Marchesini M*, et al.* Oncogene ablation-resistant pancreatic cancer cells depend on mitochondrial function. *Nature* 2014; **514**(7524)**:** 628-632.

631. Andersen P, Pedersen MW, Woetmann A, Villingshøj M, Stockhausen MT, Ødum N*, et al.* EGFR induces expression of IRF-1 via STAT1 and STAT3 activation leading to growth arrest of human cancer cells. *International journal of cancer* 2008; **122**(2)**:** 342-349.

632. Gao J, Senthil M, Ren B, Yan J, Xing Q, Yu J*, et al.* IRF-1 transcriptionally upregulates PUMA, which mediates the mitochondrial apoptotic pathway in IRF-1-induced apoptosis in cancer cells. *Cell Death & Differentiation* 2010; **17**(4)**:** 699-709.

633. Ekhart C, Doodeman VD, Rodenhuis S, Smits PH, Beijnen JH, Huitema AD. Influence of polymorphisms of drug metabolizing enzymes (CYP2B6, CYP2C9, CYP2C19, CYP3A4, CYP3A5, GSTA1, GSTP1, ALDH1A1 and ALDH3A1) on the pharmacokinetics of cyclophosphamide and 4-hydroxycyclophosphamide. *Pharmacogenetics and genomics* 2008; **18**(6)**:** 515-523.

634. Yang Y, Zhou W, Xia J, Gu Z, Wendlandt E, Zhan X*, et al.* NEK2 mediates ALDH1A1-dependent drug resistance in multiple myeloma. *Oncotarget* 2014; **5**(23)**:** 11986.

635. Akca H, Demiray A, Tokgun O, Yokota J. Invasiveness and anchorage independent growth ability augmented by PTEN inactivation through the PI3K/AKT/NFkB pathway in lung cancer cells. *Lung Cancer* 2011; **73**(3)**:** 302-309.

636. Ho H-H, Chang C-S, Ho W-C, Liao S-Y, Wu C-H, Wang C-J. Anti-metastasis effects of gallic acid on gastric cancer cells involves inhibition of NF-κB activity and downregulation of PI3K/AKT/small GTPase signals. *Food and Chemical Toxicology* 2010; **48**(8)**:** 2508-2516.

637. Li B, Cheung PY, Wang X, Tsao SW, Ling MT, Wong YC*, et al.* Id-1 activation of PI3K/Akt/NFκB signaling pathway and its significance in promoting survival of esophageal cancer cells. *Carcinogenesis* 2007; **28**(11)**:** 2313-2320.

638. Wang T, Wang X-g, Xu J-h, Wu X-P, Qiu H-l, Yi H*, et al.* Overexpression of the human ZNF300 gene enhances growth and metastasis of cancer cells through activating NF-kB pathway. *Journal of Cellular and Molecular Medicine* 2012; **16**(5)**:** 1134-1145.

639. Grivennikov S, Karin M. Dangerous liaisons: STAT3 and NF-κB collaboration and crosstalk in cancer. *Cytokine & growth factor reviews* 2010; **21**(1)**:** 11-19.

640. Jazirehi AR, Vega MI, Bonavida B. Development of Rituximab-Resistant Lymphoma Clones with Altered Cell Signaling and Cross-Resistance to Chemotherapy. *Cancer Research* 2007; **67**(3)**:** 1270-1281.

641. Demchenko YN, Kuehl WM. A critical role for the NFkB pathway in multiple myeloma. *Oncotarget* 2010; **1**(1)**:** 59.

642. Breccia M, Alimena G. NF-κB as a potential therapeutic target in myelodysplastic syndromes and acute myeloid leukemia. *Expert opinion on therapeutic targets* 2010; **14**(11)**:** 1157-1176.

643. Horie R. NF-κ B in Pathogenesis and Treatment of Adult T-Cell Leukemia/Lymphoma. *International reviews of immunology* 2007; **26**(5-6)**:** 269-281.

644. Meyer SC, Keller MD, Chiu S, Koppikar P, Guryanova OA, Rapaport F*, et al.* CHZ868, a Type II JAK2 Inhibitor, Reverses Type I JAK Inhibitor Persistence and Demonstrates Efficacy in Myeloproliferative Neoplasms. *Cancer cell* 2015; **28**(1)**:** 15-28.

645. Agarwal E, Brattain MG, Chowdhury S. Cell survival and metastasis regulation by Akt signaling in colorectal cancer. *Cellular signalling* 2013; **25**(8)**:** 1711-1719.

646. Bhatt AP, Bhende PM, Sin S-H, Roy D, Dittmer DP, Damania B. Dual inhibition of PI3K and mTOR inhibits autocrine and paracrine proliferative loops in PI3K/Akt/mTOR-addicted lymphomas. *Blood* 2010; **115:** 4455-4463.

647. Thomas SJ, Snowden JA, Zeidler MP, Danson SJ. The role of JAK/STAT signalling in the pathogenesis, prognosis and treatment of solid tumours. *British Journal Of Cancer* 2015; **113:** 365.

648. Beebe K, Lee W-C, Micchelli CA. JAK/STAT signaling coordinates stem cell proliferation and multilineage differentiation in the Drosophila intestinal stem cell lineage. *Developmental Biology* 2010; **338**(1)**:** 28-37.

649. Chung E, Kondo M. Role of Ras/Raf/MEK/ERK signaling in physiological hematopoiesis and leukemia development. *Immunologic Research* 2011; **49**(1)**:** 248-268.

650. McCubrey JA, Steelman LS, Chappell WH, Abrams SL, Wong EWT, Chang F*, et al.* Roles of the Raf/MEK/ERK pathway in cell growth, malignant transformation and drug resistance. *Biochimica et Biophysica Acta (BBA) - Molecular Cell Research* 2007; **1773**(8)**:** 1263-1284.

651. Fang D, Hawke D, Zheng Y, Xia Y, Meisenhelder J, Nika H*, et al.* Phosphorylation of β-Catenin by AKT Promotes β-Catenin Transcriptional Activity. *Journal of Biological Chemistry* 2007; **282**(15)**:** 11221-11229.

652. Saha B, Arase A, Imam SS, Tsao-Wei D, Naritoku WY, Groshen S*, et al.* Overexpression of E-cadherin and β-Catenin proteins in metastatic prostate cancer cells in bone. *The Prostate* 2008; **68**(1)**:** 78-84.

653. Noordhuis MG, Fehrmann RSN, Wisman GBA, Nijhuis ER, van Zanden JJ, Moerland PD*, et al.* Involvement of the TGF-β and β-Catenin Pathways in Pelvic Lymph Node Metastasis in Early-Stage Cervical Cancer. *Clinical Cancer Research* 2011.

654. Schmalhofer O, Brabletz S, Brabletz T. E-cadherin, β-catenin, and ZEB1 in malignant progression of cancer. *Cancer and Metastasis Reviews* 2009; **28**(1)**:** 151-166.

655. Paul I, Bhattacharya S, Chatterjee A, Ghosh MK. Current Understanding on EGFR and Wnt/β-Catenin Signaling in Glioma and Their Possible Crosstalk. *Genes & Cancer* 2013; **4**(11-12)**:** 427-446.

656. Sidhu J, Venkateswaran G, Persad S. Melanoma Progression to Metastatic Disease: The Role of the PI3K/Akt and Wnt/B-catening Pathways. *International Journal of Cancer Research and Prevention* 2014; **7**(3/4)**:** 249.

657. Aksamitiene E, Kiyatkin A, Kholodenko Boris N. Cross-talk between mitogenic Ras/MAPK and survival PI3K/Akt pathways: a fine balance. *Biochemical Society Transactions* 2012; **40:** 139-146.

658. Oeckinghaus A, Hayden MS, Ghosh S. Crosstalk in NF-κB signaling pathways. *Nature Immunology* 2011; **12:** 695.

659. Mendoza MC, Er EE, Blenis J. The Ras-ERK and PI3K-mTOR pathways: cross-talk and compensation. *Trends in Biochemical Sciences* 2011; **36**(6)**:** 320-328.

660. Boettcher M, McManus MT. Choosing the Right Tool for the Job: RNAi, TALEN or CRISPR. *Molecular cell* 2015; **58**(4)**:** 575-585.

661. Wang B, Xu Y-F, He B-S, Pan Y-Q, Zhang L-R, Zhu C*, et al.* RNAi-mediated silencing of CD147 inhibits tumor cell proliferation, invasion and increases chemosensitivity to cisplatin in SGC7901 cells in vitro. *Journal of Experimental & Clinical Cancer Research* 2010; **29**(1)**:** 61.

662. Vainio P, Mpindi J-P, Kohonen P, Fey V, Mirtti T, Alanen KA*, et al.* High-throughput transcriptomic and RNAi analysis identifies AIM1, ERGIC1, TMED3 and TPX2 as potential drug targets in prostate cancer. *PloS one* 2012; **7**(6)**:** e39801.

663. Zang S, Chen F, Dai J, Guo D, Tse W, Qu X*, et al.* RNAi-mediated knockdown of Notch-1 leads to cell growth inhibition and enhanced chemosensitivity in human breast cancer. *Oncology reports* 2010; **23**(4)**:** 893-899.

664. Smith C, Gore A, Yan W, Abalde-Atristain L, Li Z, He C*, et al.* Whole-Genome Sequencing Analysis Reveals High Specificity of CRISPR/Cas9 and TALEN-Based Genome Editing in Human iPSCs. *Cell Stem Cell* 2014; **15**(1)**:** 12-13.

665. Bedell VM, Wang Y, Campbell JM, Poshusta TL, Starker CG, Krug Ii RG*, et al.* In vivo genome editing using a high-efficiency TALEN system. *Nature* 2012; **491:** 114.

666. Dow LE, Fisher J, O'Rourke KP, Muley A, Kastenhuber ER, Livshits G*, et al.* Inducible in vivo genome editing with CRISPR-Cas9. *Nature Biotechnology* 2015; **33:** 390.

667. Zhang F, Cox DBT, Marraffini L, Bikard DO, Jiang W, Sanjana NE. Crispr-cas component systems, methods and compositions for sequence manipulation. Google Patents; 2016.

668. Forés M, Papagianni A, Rodríguez-Muñoz L, Jiménez G. Using CRISPR-Cas9 to Study ERK Signaling in Drosophila. In: Jimenez G (ed). *ERK Signaling: Methods and Protocols*. Springer New York: New York, NY, 2017, pp 353-365.

669. Hulleman E, Kazemier KM, Holleman A, VanderWeele DJ, Rudin CM, Broekhuis MJC*, et al.* Inhibition of glycolysis modulates prednisolone resistance in acute lymphoblastic leukemia cells. *Blood* 2009; **113:** 2014-2021.

670. Kominsky DJ, Klawitter J, Brown JL, Boros LG, Melo JV, Eckhardt SG*, et al.* Abnormalities in Glucose Uptake and Metabolism in Imatinib-Resistant Human BCR-ABL–Positive Cells. *Clinical Cancer Research* 2009; **15:** 3442-3450.

671. Moreno-Sánchez R, Rodríguez-Enríquez S, Marín-Hernández A, Saavedra E. Energy metabolism in tumor cells. *FEBS Journal* 2007; **274**(6)**:** 1393-1418.

672. Warmuth M, Kim S, Gu X-j, Xia G, Adrián F. Ba/F3 cells and their use in kinase drug discovery. *Current opinion in oncology* 2007; **19**(1)**:** 55-60.

673. Soda M, Choi YL, Enomoto M, Takada S, Yamashita Y, Ishikawa S*, et al.* Identification of the transforming EML4–ALK fusion gene in non-small-cell lung cancer. *Nature* 2007; **448**(7153)**:** 561.

674. Mulloy JC, Wunderlich M, Zheng Y, Wei J. Transforming human blood stem and progenitor cells: A new way forward in leukemia modeling. *Cell Cycle* 2008; **7**(21)**:** 3314-3319.

675. Drexler HG. Establishment and Culture of Leukemia–Lymphoma Cell Lines. In: Cree IA (ed). *Cancer Cell Culture: Methods and Protocols*. Humana Press: Totowa, NJ, 2011, pp 181-200.

676. Irfan Maqsood M, Matin MM, Bahrami AR, Ghasroldasht MM. Immortality of cell lines: challenges and advantages of establishment. *Cell biology international* 2013; **37**(10)**:** 1038-1045.

677. Lodhia KA, Hadley A, Haluska P, Scott CL. Prioritizing therapeutic targets using patient-derived xenograft models. *Biochimica et biophysica acta* 2015; **1855**(2)**:** 223-234.

678. Goodspeed A, Heiser LM, Gray JW, Costello JC. Tumor-Derived Cell Lines as Molecular Models of Cancer Pharmacogenomics. *Molecular cancer research : MCR* 2016; **14**(1)**:** 3-13.

679. Morotti A, Panuzzo C, Fava C, Saglio G. Kinase-inhibitor–insensitive cancer stem cells in chronic myeloid leukemia. *Expert Opinion on Biological Therapy* 2014; **14**(3)**:** 287-299.

680. Hermann PC, Huber SL, Herrler T, Aicher A, Ellwart JW, Guba M*, et al.* Distinct Populations of Cancer Stem Cells Determine Tumor Growth and Metastatic Activity in Human Pancreatic Cancer. *Cell Stem Cell* 2007; **1**(3)**:** 313-323.

681. Loo E, De Abreu FB, Kaur P, Ornstein D, Tsongalis GJ. How Genomic Data Are Changing the Leukemia Treatment Landscape. *Oncology Times* 2016; **38**(5)**:** 16-18.

682. Mullighan CG. Abstract IA02: Precision medicine in acute lymphoblastic leukemia. *Clinical Cancer Research* 2016; **22:** IA02-IA02.

683. Deng X, Nakamura Y. Cancer Precision Medicine: From Cancer Screening to Drug Selection and Personalized Immunotherapy. *Trends in Pharmacological Sciences* 2017; **38**(1)**:** 15-24.

684. Fischer U, Forster M, Rinaldi A, Risch T, Sungalee S, Warnatz H-J*, et al.* Genomics and drug profiling of fatal TCF3-HLF−positive acute lymphoblastic leukemia identifies recurrent mutation patterns and therapeutic options. *Nature Genetics* 2015; **47:** 1020.

685. Badura S, Tesanovic T, Pfeifer H, Wystub S, Nijmeijer BA, Liebermann M*, et al.* Differential effects of selective inhibitors targeting the PI3K/AKT/mTOR pathway in acute lymphoblastic leukemia. *PloS one* 2013; **8**(11)**:** e80070.

686. Willems L, Tamburini J, Chapuis N, Lacombe C, Mayeux P, Bouscary D. PI3K and mTOR signaling pathways in cancer: new data on targeted therapies. *Current oncology reports* 2012; **14**(2)**:** 129-138.

687. Delbridge ARD, Strasser A. The BCL-2 protein family, BH3-mimetics and cancer therapy. *Cell Death And Differentiation* 2015; **22:** 1071.

688. Iacovelli S, Ricciardi MR, Allegretti M, Mirabilii S, Licchetta R, Bergamo P*, et al.* Co-targeting of Bcl-2 and mTOR pathway triggers synergistic apoptosis in BH3 mimetics resistant acute lymphoblastic leukemia. *Oncotarget* 2015; **6**(31)**:** 32089-32103.

689. Davila ML, Riviere I, Wang X, Bartido S, Park J, Curran K*, et al.* Efficacy and Toxicity Management of 19-28z CAR T Cell Therapy in B Cell Acute Lymphoblastic Leukemia. *Science Translational Medicine* 2014; **6:** 224ra225-224ra225.

690. Brentjens RJ, Davila ML, Riviere I, Park J, Wang X, Cowell LG*, et al.* CD19-Targeted T Cells Rapidly Induce Molecular Remissions in Adults with Chemotherapy-Refractory Acute Lymphoblastic Leukemia. *Science Translational Medicine* 2013; **5:** 177ra138-177ra138.

691. Turtle CJ, Hanafi L-A, Berger C, Gooley TA, Cherian S, Hudecek M*, et al.* CD19 CAR–T cells of defined CD4(+):CD8(+) composition in adult B cell ALL patients. *The Journal of Clinical Investigation* 2016; **126**(6)**:** 2123-2138.